Springer Proceedings in Complexity

Clemens Mensink
George Kallos *Editors*

Air Pollution Modeling and its Application XXV

Springer

Springer Proceedings in Complexity

Springer Complexity

Springer Complexity is an interdisciplinary program publishing the best research and academic-level teaching on both fundamental and applied aspects of complex systems—cutting across all traditional disciplines of the natural and life sciences, engineering, economics, medicine, neuroscience, social, and computer science.

Complex Systems are systems that comprise many interacting parts with the ability to generate a new quality of macroscopic collective behavior the manifestations of which are the spontaneous formation of distinctive temporal, spatial, or functional structures. Models of such systems can be successfully mapped onto quite diverse "real-life" situations like the climate, the coherent emission of light from lasers, chemical reaction–diffusion systems, biological cellular networks, the dynamics of stock markets and of the Internet, earthquake statistics and prediction, freeway traffic, the human brain, or the formation of opinions in social systems, to name just some of the popular applications.

Although their scope and methodologies overlap somewhat, one can distinguish the following main concepts and tools: self-organization, nonlinear dynamics, synergetics, turbulence, dynamical systems, catastrophes, instabilities, stochastic processes, chaos, graphs and networks, cellular automata, adaptive systems, genetic algorithms, and computational intelligence.

The three major book publication platforms of the Springer Complexity program are the monograph series "Understanding Complex Systems" focusing on the various applications of complexity, the "Springer Series in Synergetics", which is devoted to the quantitative theoretical and methodological foundations, and the "SpringerBriefs in Complexity" which are concise and topical working reports, case-studies, surveys, essays, and lecture notes of relevance to the field. In addition to the books in these two core series, the program also incorporates individual titles ranging from textbooks to major reference works.

More information about this series at http://www.springer.com/series/11637

Clemens Mensink · George Kallos
Editors

Air Pollution Modeling and its Application XXV

Springer

Editors
Clemens Mensink
VITO NV
Mol
Belgium

George Kallos
School of Physics, Division of Environment and Meteorology
University of Athens
Athens
Greece

ISSN 2213-8684 ISSN 2213-8692 (electronic)
Springer Proceedings in Complexity
ISBN 978-3-319-57644-2 ISBN 978-3-319-57645-9 (eBook)
DOI 10.1007/978-3-319-57645-9

Library of Congress Control Number: 2017941472

Printed on acid-free paper

This Springer imprint is published by Springer Nature
The registered company is Springer International Publishing AG
The registered company address is: Gewerbestrasse 11, 6330 Cham, Switzerland

Preface

In 1969, the North Atlantic Treaty Organization (NATO) established the Committee on Challenges of Modern Society (CCMS). As air pollution was one of its main priorities, the committee supported the periodic organization of a conference series called ***International Technical Meeting on Air Pollution Modeling and its Application (ITM)***. This activity continued until 2013, under the successor of ITM/CCMS, the NATO Committee on Science for Peace and Security (NATO/SPS). However, since 2013 the ITM organization continues its meeting series independently of NATO/SPS.

This volume contains the abstracts and papers presented at the 35th ITM, held in Chania (Crete), Greece, from October 3, 2016 to October 7, 2016. The 35th ITM was organized by the National and Kapodistrian University of Athens (Host Country) and VITO (Pilot Country). Key topics presented at this ITM correspond to the sections in this book and include: long-term modeling and trend analysis; model assessment and verification; interactions between air quality and climate change; data assimilation and air quality forecasting; local and urban scale modeling; regional and intercontinental modeling; air quality effects on human health and ecology; and aerosols in the atmosphere.

The ITM was attended by 118 participants representing 31 countries. Invited papers were presented by Douw Steyn, Canada (Long-term modeling and trend analysis), Maria Kanakidou, Greece (Aerosols in the atmosphere), Silvana Di Sabatino, Italy (Local and urban scale modeling), and Athanasios Nenes, USA (Interactions between air quality and climate change).

On behalf of the ITM Scientific Committee and as organizers and editors, we would like to thank all the participants who contributed to the success of the meeting and its high scientific level. We especially recognize the organizational and support efforts of the chairpersons and rapporteurs. Special thanks to the sponsoring

institutions: the National and Kapodistrian University of Athens, Greece, VITO (Belgium), the Federal Public Planning Service Science Policy of Belgium, and the European Association for the Science of Air Pollution (EURASAP). The National and Kapodistrian University of Athens gave a special grant to award prizes to early career researchers for the best paper or poster presentations.

The next meeting will be held in May 2018 in Ottawa, Canada.

Mol, Belgium — Clemens Mensink
Scientific Committee Chair

Athens, Greece — George Kallos
Local Conference Organizer

Organizing Committee

Members of the Scientific Committee for the 35th International Technical Meeting on Air Pollution Modeling and its Application

Clemens Mensink, Belgium
Ekaterina Batchvarova, Bulgaria
Wanmin Gong, Canada
Ari Karppinen, Finland
Laurent Deguillaume, France
Heinke Schluenzen, Germany
George Kallos, Greece
Silvia Trini Castelli, Italy
Hilde Fagerli, Norway
Ana Isabel Miranda, Portugal
Oriol Jorba, Spain
Renske Timmermans, The Netherlands
Selahattin Incecik, Turkey
Tony Dore, UK
Rohit Mathur, USA

Honorary Life Members

Chris De Wispelaere, Belgium
Douw Steyn, Canada
Sven-Erik Gryning, Denmark
Werner Klug, Germany
Carlos Borego, Portugal
Han van Dop, The Netherlands
S.T. Rao, USA
Frank Schiermeier, USA

History of the International Technical Meeting (ITM) on Air Pollution Modeling and Its Application

Pilot Studies

1969–1974	Air Pollution Pilot Study (*Pilot Country: United States of America*)
1975–1979	Air Pollution Assessment Methodology and Modeling (*Pilot Country: Germany*)
1980–1984	Air Pollution Control strategies and Impact Modeling (*Pilot Country: Germany*)

Pilot Follow-Up Meetings

Pilot Country—United States of America (R.A. McCormick, L.E. Niemeyer)

February 1971	Eindhoven, The Netherlands	First Conference on Low Pollution Power Systems Development
July 1971	Paris, France	Second Meeting of the Expert Panel on Air Pollution Modeling

NATO/CCMS International Technical Meetings (ITM) on Air Pollution Modeling and Its Application

Subsequent meetings were supported by the NATO Committee for Challenges to Modern Society and were designated NATO/CCMS International Technical Meetings (ITM) on Air Pollution Modeling and its Application.

October	1972	Paris, France	3rd	ITM
May	1973	Oberursel, Federal Republic of Germany	4th	ITM
June	1974	Roskilde, Denmark	5th	ITM

Pilot Country—Germany (Erich Weber)

September	1975	Frankfurt, Federal Republic of Germany	6th	ITM
September	1976	Airlie House, USA	7th	ITM
September	1977	Louvain-la-Neuve, Belgium	8th	ITM
August	1978	Toronto, Canada	9th	ITM
October	1979	Rome, Italy	10th	ITM

Pilot Country—Belgium (Chris De Wispelaere)

November	1980	Amsterdam, The Netherlands	11th	ITM
September	1981	Menlo Park, California, USA	12th	ITM
September	1982	Ile des Embiez, France	13th	ITM
September	1983	Copenhagen, Denmark	14th	ITM
April	1985	St. Louis, Missouri, USA	15th	ITM

Pilot Country—The Netherlands (Han van Dop)

April	1987	Lindau, Federal Republic of Germany	16th	ITM
September	1988	Cambridge, United Kingdom	17th	ITM
May	1990	Vancouver, BC, Canada	18th	ITM
September	1991	Ierapetra, Greece	19th	ITM

Pilot Country—Denmark (Sven-Erik Gryning)

November	1993	Valencia, Spain	20th	ITM
November	1995	Baltimore, Maryland, USA	21st	ITM
May	1997	Clermont-Ferrand, France	22nd	ITM
September	1998	Varna, Bulgaria	23rd	ITM
May	2000	Boulder, Colorado, USA	24th	ITM

Pilot Country—Portugal (Carlos Borrego)

September	2001	Louvain-la-Neuve, Belgium	25th	ITM
May	2003	Istanbul, Turkey	26th	ITM
October	2004	Banff, Canada	27th	ITM
May	2006	Leipzig, Germany	28th	ITM

NATO/SPS International Technical Meetings (ITM) on Air Pollution Modeling and Its Application

In 2007, NATO's Committee for Challenges to Modern Society was disbanded and replaced by NATO's Committee on Science for Peace and Security (NATO/SPS), which continued its support for the ITM.

September	2007	Aveiro, Portugal	29th	ITM

Pilot Country—Canada (Douw Steyn)

May	2009	San Francisco, California, USA	30th	ITM
September	2010	Torino, Italy	31st	ITM
May	2012	Utrecht, The Netherlands	32nd	ITM

International Technical Meetings (ITM) on Air Pollution Modeling and Its Application

In 2012, the NATO Committee on Science for Peace and Security refocused its mandate, and the ITM became independent of NATO/SPS support.

September	2013	Miami, USA	33rd	ITM
May	2015	Montpellier, France	34th	ITM

Pilot Country—Belgium (Clemens Mensink)

October	2016	Chania (Crete), Greece	35th	ITM

List of Participants

The 35th International Technical Meeting on Air Pollution Modeling and Its Application, Chania (Crete), Greece, October 3–7, 2016.

Austria

Philipp Anne
University of Vienna
Department of Meteorology and Geophysics
Althanstraße 14 (UZAII)
1090 Vienna

Belgium

Bultynck Katrien
VITO NV
Boeretang 200
B-2400 Mol

De Meutter Pieter
SCK•CEN
Boeretang 200
B-2400 Mol

Delcloo Andy
Royal Meteorological Institute of Belgium
Ringlaan 3
B-1180 Ukkel

Lefebvre Wouter
VITO NV
Boeretang 200
B-2400 Mol

Lenartz Fabian
ISSeP Air Quality
Rue du Chéra 200
B-4000 Liège

Mensink Clemens
VITO NV
Boeretang 200
B-2400 Mol

Viaene Peter
VITO NV
Boeretang 200
B-2400 Mol

Bulgaria

Batchvarova Ekaterina
National Institute of Meteorology and Hydrology
Atmospheric Physics and Ecology
66, Blvd Tzarigradsko chaussee
1784 Sofia

Canada

Gong Wanmin
Environment and Climate Change Canada
4905 Dufferin Street
M3H 5T4 Toronto

Makar Paul
Environment and Climate Change Canada
4905 Dufferin Street
M3H 5T4 Toronto

Ménard Richard
Environment and Climate Change Canada
Air Quality Research Division
2121 Transcanada Highway
H9P 1J3 Dorval (QC)

Moran Mike
Environment and Climate Change Canada
Air Quality Research Division
4905 Dufferin Street
M3H 5T4 Toronto, Ontario

Steyn Douw
The University of British Columbia
Earth, Ocean and Atmospheric Sciences
2207 Main Mall
V6T 1Z4 Vancouver, BC

Chili

Sanhueza Pedro
GEOAIRE AMBIENTAL SpA
Atmospheric modeling
La Concepcion 191 of 508
Providencia 7500010 Santiago

Torreblanca Monica
GEOAIRE AMBIENTAL SpA
Atmospheric modeling
La Concepcion 191 of 508
Providencia 7500010 Santiago

Croatia

Gašparac Goran
Gekom—Geophysical and Ecological Modeling Ltd.
Fallerovo šetalište 22
10000 Zagreb

Denmark

Geels Camilla
Aarhus University
Department of Environmental Science
Frederiksborgvej 399
P.O. Box. 358
DK-4000 Roskilde

Gryning Sven-Erik
Technical University of Denmark
DTU Wind Energy, Risø campus
Fredeiksborgvej 399
DK-4000 Roskilde

Hansen Kaj Mantzius
Aarhus University
Department of Environmental Science
Frederiksborgvej 399
Postboks 358
DK-4000 Roskilde

Im Ulas
Aarhus University
Department of Environmental Science
Frederiksborgvej 399
DK-4000 Roskilde

Estonia

Reis Ketlin
Tartu Observatory
Observatooriumi 1
61602 Tõravere

Finland

Aarnio Mia
Finnish Meteorological Institute
Atmospheric Composition Research
Erik Palménin Aukio 1
P.O. Box 503
FI-00101 Helsinki

Backman John
Finnish Meteorological Institute
Erik Palménin Aukio 1
FI-00560 Helsinki

Hellsten Antti
Finnish Meteorological Institute
Erik Palménin Aukio 1
FI-00101 Helsinki

Johansson Lasse
The Finnish Meteorological Institute
Vallikallionkuja 1 c 41
F-02650 Espoo

Karppinen Ari
Finnish Meteorological Institute
Erik Palménin Aukio 1
P.O. Box 503
FI-00101 Helsinki

Kukkonen Jaakko
Finnish Meteorological Institute
Hannukselantie 11b
FI-00750 Helsinki

Paunu Ville-Veikko
Finnish Environment Institute
P.O. Box 140
FI-00251 Helsinki

Prank Marje
Finnish Meteorological Institute
Erik Palménin Aukio 1
FI-00101 Helsinki

Savolahti Mikko
Finnish Environment Institute
Mechelininkatu 34a
FI-00251 Helsinki

Soares Joana
Finnish Meteorological Institute
Erik Palménin Aukio 1
FI-00101 Helsinki

Sofiev Mikhail
Finnish Meteorological Institute
Atmospheric Composition Research
Erik Palménin Aukio 1
FI-00101 Helsinki

Zilitinkevich Sergej
Finnish Meteorological Institute
Luotsikatu 13 A 5
FI-00160 Helsinki

France

Colette Augustin
INERIS
BP2
60550 Verneuil-en-Halatte

Guth Jonathan
Météo-france, CNRM
42 Avenue G. Coriolis
31057 Toulouse

Patryl Luc
CEA
5 rue Alphonse Réault
91310 Leuville sur Orge

Raffort Valentin
CEREA
6-8 avenue Blaise Pascal,
Cité Descartes Champs-sur-Marne
77455 Marne la Vallée Cedex 2

Germany

Gatzsche Kathrin
Leibniz Institute for Tropospheric Research
Permoserstr. 15
04318 Leipzig

Bieser Johannes
Helmholtz Zentrum Geesthacht
Max-Planck-Strasse 1
21502 Geesthacht

Ramacher Martin
Helmholtz Zentrum Geesthacht
Max-Planck-Strasse 1
21502 Geesthacht

Schluenzen K. Heinke
Meteorol. Inst., CEN
University of Hamburg
Bundesstr. 55
20146 Hamburg

Volker Matthias
Helmholtz-Zentrum Geesthacht
Chemistry Transport Modelling
Max-Planck-Strasse 1
21502 Geesthacht

Wolke Ralf
Leibniz Institute for Tropospheric Research
Permoserstr. 15
04318 Leipzig

Greece

Efthimiou George
NCSR Demokritos
Riga Feraiou 41
15351 Pallini

Drakaki Eleni
University of Athens
Department of Physics
Panepistimioupoli Zografou
15784 Athens

Kallos George
University of Athens
Department of Physics
University of Athens Campus, Bldg PHYS-5
15784 Athens

Kanakidou Maria
Department of Chemistry
University of Crete
P.O. Box 2208
Voutes Campus
71003 Heraklion, Crete

Koukoula Marika
University of Athens
Department of Physics
University of Athens Campus, Bldg PHYS-5
15784 Athens

Marougianni Garyfalia
Aristotle University of Thessaloniki
Physics Smirnis 10 Pylaia
55525 Thessaloniki

Methymaki Georgia
National and Kapodistrian University of Athens
Department of Physics
Panepistimioupoli Zografou
15784 Athens

Patlakas Platon
National and Kapodistrian University of Athens
School of Physics
University Campus, Building PHYSICS V
15784 Athens

Tsegas Georgios
Aristotle University of Thessaloniki
Department of Mechanical Engineering
Box 483, Aristotle University Thessaloniki
54124 Thessaloniki

Hungary

Ferenczi Zita
Hungarian Meteorological Service
Division for Analysis of Atmospheric Environment
Kitaibel P. u. 1.
1024 Budapest

Israel

Haikin Nitsa
NRCN
P.O. Box 9001
84190 Beer-Sheva

Kishcha (Kichtcha) Pavel
Tel-Aviv University
Geosciences
Ramat Aviv
69978 Tel Aviv

Italy

Carnevale Claudio
Università degli Studi di Brescia
Dipartimento di Ingegneria Meccanica e Industriale
Via Branze 38
25123 Brescia

Cesari Rita
CNR-ISAC
Strada Prov. Lecce-Monteroni, Km 1.2
73100 Lecce

Di Sabatino Silvana
University of Bologna
Department of Physics and Astronomy
Viale Berti Pichat 6/2
40126 Bologna

Ferrero Enrico
Università del Piemonte Orientale
Dipartimento di Scienze e Innovazione Tecnologica
viale Teresa Michel 11
15121 Alessandria

Galmarini Stefano
EC/JRC
Via Enrico Fermi 2749
21027 Ispra

Hernández-Ceballos Miguel A.
European Commission, Joint Research Centre (JRC)
Institute for Transuranium Elements (ITU)
21027 Ispra

Tomasi Elena
University of Trento
via Mesiano 77
38123 Trento

Trini Castelli Silvia
Institute of Atmospheric Sciences and Climate
ISAC National Research Council
CNR Corso Fiume 4
10133 Torino

Japan

Nakayama Hiromasa
Japan Atomic Energy Agency
2-4 Shirakata-shirane
Tokai-mura, Naka-gun
319-1195 Ibaraki

Lithuania

Aukse Miskinyte
Vytautas Magnus University
Department of Environmental Sciences
Vileikos Street 8
LT-44404 Kaunas

Dedele Audrius
Vytautas Magnus University
Department of Environmental Sciences
Vileikos str. 8-223
LT-44404 Kaunas

Norway

Bartnicki Jerzy
Norwegian Meteorological Institute
P.O. Box 46 Blindern
NO-0313 Oslo

Guerreiro Cristina
NILU—Norwegian Institute for Air Research
P.O. Box 100
NO-2027 Kjeller

Poland

Kryza Maciej
Wroclaw University
Department of Climatology and Atmosphere Protection
ul. Kosiby 8
51-621 Wroclaw

Werner Malgorzata
University of Wroclaw
pl. Uniwersytecki 1
50-137 Wroclaw

Portugal

Borrego Carlos
University of Aveiro
Department of Environment and Planning
Campus Universitário
3810-193 Aveiro

Miranda Ana Isabel
University of Aveiro
Department of Environment and Planning
Campus Universitário
3810-193 Aveiro

Qatar

Alnaimi Haya
Civil avation
Meteorology Doha Qatar
Doha

Romania

David Elena
Institute for Cryogenic and Isotopic Technologies Research
Uzinei street No. 4
P.O. Box Râureni 7
240050 Rm.Valcea

Saudi Arabia

Al-Binali Khalid
Saudi Aramco
P.O. Box 10758
31311 Dhahran

Slovenia

Božnar Marija Zlata
MEIS
Mali Vrh pri Smarju 78
1293 Šmarje-Sap

Mlakar Primož
MEIS
Mali Vrh pri Smarju 78
1293 Šmarje-Sap

Spain

Alonso Alonso Lucio
University of the Basque Country UPV/EHU
Alameda Urquijo s/n
48013 Bilbao

Gangoiti Bengoa
University of the Basque Country UPV/EHU
Alameda Urquijo s/n
48013 Bilbao

Jorba Oriol
Barcelona Supercomputing Center
Calle Jordi Girona 31
8034 Barcelona

Palacios-Peña Laura
University of Murcia
Department of Physics Facultad de Química
Campus de Espinardo
30100 Murcia

Saez de Camara Estibaliz
University of the Basque Country UPV/EHU
Alameda Urquijo s/n
48013 Bilbao

Valdenebro Villar Veronica
University of the Basque Country UPV/EHU
Alameda Urquijo s/n
48013 Bilbao

Sweden

Schrödner Roland
Lund University Centre for Environmental and Climate Research
Sölvegatan 37
223 62 Lund

Switzerland

Aksoyoglu Sebnem
Paul Scherrer Institute
5232 Villigen PSI

Oikonomakis Emmanouil
Paul Scherrer Institut
Eichbuhlstrasse 27
8004 Zurich

The Netherlands

Kranenburg Richard
TNO
Princetonlaan 6
3584 CB Utrecht

Sterk Marina
RIVM
Eykmanstraat 6-III
6706JV Wageningen

Timmermans Renske
TNO
Princetonlaan 6
3584 CB Utrecht

van der Swaluw Eric
RIVM
Antonie van Leeuwenhoeklaan 9
3721 MA Bilthoven

Turkey

Tuna Tuygun Gizem
Dokuz Eylul University
Environmental Engineering
35390 Izmir

United Kingdom

Aleksankina Ksenia
University of Edinburgh 275
Joseph Black Building
David Brewster Road
EH9 3FJ Edinburgh

Derwent Richard
Rdscientific
18 Kingsland Grange
RG14 6LH Newbury

Dore Tony
Centre for Ecology and Hydrology
Bush Estate, Penicuik
EH26 9HF Midlothian

USA

Alessandrini Stefano
National Center for Atmospheric Research
Research Applications Lab
3450 Mitchell Lane
80301 Boulder

Appel Wyat
US EPA National Exposure Research Laboratory
109 TW Alexander Drive
27711 Durham

Arunachalam Sarav
University of North Carolina at Chapel Hill
Institute for the Environment
100 Europa Drive, Suite 490
27517 Chapel Hill

Astitha Marina
University of Connecticut
261 Glenbrook Road, U-3037
06269 Storrs

Bates Josephine
Georgia Institute of Technology
Civil and Environmental Engineering
116 Ponce de Leon Ave NE
30308 Atlanta

Delle Monache Luca
National Center for Atmospheric Research
P.O. Box 3000
80307-3000 Boulder, Colorado

Foroutan Hosein
EPA/NERL/CED Atmospheric Model Development
109 TW Alexander Drive
27711 Research Triangle Park

Hogrefe Christian
US EPA National Exposure Research Laboratory
109 TW Alexander Drive
27711 Durham

Huang Ran
Georgia Institute of Technology
100 10TH ST NW 505a
30309 Atlanta

Kang Daiwen
US EPA National Exposure Research Laboratory
109 TW Alexander Drive
27711 Durham

Lee Pius
NOAA Air Resources Laboratory (NCWCP)
5830 University Research Court
20740 College Park

Mathur Rohit
US EPA National Exposure Research Laboratory
109 TW Alexander Drive
27711 Durham

Moutinho Jennifer
Georgia Institute of Technology
144 Ponce de Leon Ave NE Apt 1203
30308 Atlanta

Nenes Athanasios
School of Earth and Atmospheric Sciences
Georgia Institute of Technology
311 Ferst Drive
30332-0340 Atlanta

Nolte Chris
US EPA National Exposure Research Laboratory
109 TW Alexander Drive
27711 Durham

Pandis Spyros
Carnegie Mellon University
Chemical Engineering
5000 Forbes Avenue PA
15213 Pittsburgh

Rao S.T.
North Carolina State University
Marine, Earth, and Atmospheric Sciences
2316 Heartley Drive
27615 Raleigh

Russell Armistead (Ted)
Georgia Institute of Technology
311 Ferst Drive
30340 Atlanta

Sarwar Golam
US EPA National Exposure Research Laboratory
109 TW Alexander Drive
27711 Durham

Sedefian Leon
SEDEFIAN Consulting
81 Wake Robin Road
12020 Malta

Weil Jeff
National Center for Atmospheric Research
3090 Center Green Dr
80301 Boulder

Wong David
US EPA National Exposure Research Laboratory
109 TW Alexander Drive
27711 Durham

Yarwood Greg
Ramboll Environ
Air Sciences
773 San Marin Drive, Suite 2115
94998 Novato

Contents

Contributors

A.J.A. Aarnink Wageningen Livestock Research, Wageningen, The Netherlands

Mia A. Aarnio Finnish Meteorological Institute, Helsinki, Finland

Jon Abbatt Department of Chemistry, University of Toronto, Toronto, Canada

Jan Aben RIVM, Bilthoven, The Netherlands

Joseph Abrams Department of Environmental Health, Rollins School of Public Health, Emory University, Atlanta, GA, USA

Sandy Adriaenssens IRCEL/CELINE, Brussels, Belgium

A. Akingunola Air Quality Research Division, Environment and Climate Change Canada, Toronto, ON, Canada

Sebnem Aksoyoglu Laboratory of Atmospheric Chemistry, Paul Scherrer Institute, Villigen, Switzerland

J. Al Qahtani Saudi Aramco, Dhahran, Saudi Arabia

Ksenia Aleksankina School of Chemistry, University of Edinburgh, Edinburgh, UK; ERC Centre for Ecology and Hydrology, Penicuik, UK

Stefano Alessandrini National Center for Atmospheric Research (NCAR), Boulder, CO, USA

I. Alexiou Saudi Aramco, Dhahran, Saudi Arabia

Amir A. Aliabadi Air Quality Research Division, Environment and Climate Change Canada, Toronto, Canada; Now at Environmental Engineering, University of Guelph, Guelph, Canada

Lucio Alonso Faculty of Engineering Bilbao, University of the Basque Country UPV/EHU, Bilbao, Spain

Pinhas Alpert Department of Geosciences, Tel-Aviv University, Tel-Aviv, Israel

Hans Estrup Andersen Department of Bioscience, Aarhus University, Aarhus, Denmark

Spyros Andronopoulos Environmental Research Laboratory, INRASTES, NCSR Demokritos, Aghia Paraskevi, Greece

Domenico Anfossi Institute of Atmospheric Sciences and Climate, National Research Council, Turin, Italy

Gianluca Antonacci CISMA—Centro di Ingegneria e Sviluppo Modelli per l'Ambiente, Bolzano, Italy

Christos D. Argyropoulos Department of Chemical Engineering, Mary Kay 'O Connor Processes Safety Center, Texas A&M University at Qatar, Doha, Qatar

P. Armand CEA, DAM, DIF, Arpajon, France

J.A. Arndt Helmholtz-Zentrum Geesthacht, Geesthacht, Germany

Joaquim Arteta Météo-France CNRM-GAME, Toulouse, France

Saravanan Arunachalam The University of North Carolina, Chapel Hill, NC, USA

Marina Astitha Department of Civil and Environmental Engineering, University of Connecticut, Storrs, CT, USA

Armin Aulinger Helmholtz-Zentrum Geesthacht, Institute of Coastal Research, Geesthacht, Germany

Mikko Auvinen Finnish Meteorological Institute, Helsinki, Finland; University of Helsinki, Helsinki, Finland

Anna M. Backes Helmholtz-Zentrum Geesthacht, Institute of Coastal Research, Geesthacht, Germany

John Backman Finnish Meteorological Institute, Helsinki, Finland

Jianhui Bai Institute of Atmospheric Physics, Chinese Academy of Sciences, Beijing, China

Barry Baker NOAA Air Resources Air Resource Laboratory (ARL), NCWCP, College Park, MD, USA; Cooperative Institutes for Satellite and Climate, University of Maryland, College Park, MD, USA

Urs Baltensperger Laboratory of Atmospheric Chemistry, Paul Scherrer Institute, Villigen, Switzerland

Damyan Barantiev National Institute of Meteorology and Hydrology-Bulgarian Academy of Sciences, Sofia, Bulgaria

Fotios Barmpas Aristotle University Thessaloniki, Thessaloniki, Greece

Jerzy Bartnicki Norwegian Meteorological Institute, Oslo, Norway; Centre of Excellence for Environmental Radioactivity, Ås, Norway

Rocio Baró Department of Physics, Regional Campus of International Excellence Campus Mare Nostrum, University of Murcia, Murcia, Spain

N. Bartsotas School of Physics, University of Athens, Athens, Greece

Jesse Bash National Exposure Research Laboratory, Computational Exposure Division, U.S. Environmental Protection Agency, Durham, NC, USA

Ekaterina Batchvarova National Institute of Meteorology and Hydrology-Bulgarian Academy of Sciences, Sofia, Bulgaria

Josephine T. Bates School of Civil and Environmental Engineering, Georgia Institute of Technology, Atlanta, GA, USA

Stephen Beagley Air Quality Research Division, Environment and Climate Change Canada, Toronto, Canada

J. Berckmans Plant and Vegetation Ecology (PLECO), University of Antwerp, Antwerp, Belgium

T. Berndt Leibniz Institute for Tropospheric Research (TROPOS), Leipzig, Germany

Johannes Bieser Helmholtz-Zentrum Geesthacht, Institute of Coastal Research, Geesthacht, Germany

Andrea Bisignano Department of Scienze e Innovazione Tecnologica, University of Piemonte Orientale, Alessandria, Italy

G. Biskos Energy Environment and Water Research Center, The Cyprus Institute, Nicosia, Cyprus; Faculty of Civil Engineering and Geosciences, Delft University of Technology, Delft, The Netherlands

Marco Boetti Department of Physics, University of Torino, Turin, Italy

Karsten Bolding Department of Bioscience, Aarhus University, Aarhus, Denmark

C. Borrego Department of Environment and Planning, CESAM, University of Aveiro, Aveiro, Portugal

E. Bossioli Faculty of Physics, Department of Environmental Physics and Meteorology, National and Kapodistrian University of Athens, Athens, Greece

A. Bougiatioti School of Earth and Atmospheric Sciences, Georgia Institute of Technology, Atlanta, GA, USA; Environmental Chemical Processes Lab, Department of Chemistry, University of Crete, Heraklion, Greece

Heiko Bozem Institute for Atmospheric Physics, Johannes Gutenberg University of Mainz, Mainz, Germany

László Bozó Hungarian Meteorological Service, Budapest, Hungary

Jørgen Brandt Department of Environmental Science, Aarhus University, Aarhus, Denmark

Olivier Brasseur Brussels Environment, Brussels, Belgium

Bert Brunekreef Institute for Risk Assessment Sciences (IRAS), Utrecht, Netherlands

Riccardo Buccolieri Dipartimento di Scienze e Tecnologie Biologiche ed Ambientali, University of Salento, Lecce, Italy

Julia Burkart Department of Chemistry, University of Toronto, Toronto, Canada

Johan Camps Belgian Nuclear Research Institute, Mol, Belgium

Giuseppe Carlino Simularia S.r.l., Turin, Italy

Claudio Carnevale UNIBS, Brescia, Italy

D. Carvalho Department of Environment and Planning, CESAM, University of Aveiro, Aveiro, Portugal

Silvia Trini Castelli Institute of Atmospheric Sciences and Climate, National Research Council, Turin, Italy

Mark Cave British Geological Survey, Nottingham, UK

Rita Cesari Institute of Atmospheric Sciences and Climate, National Research Council, Lecce, Italy

Howard H. Chang Department of Biostatistics and Bioinformatics, Rollins School of Public Health, Emory University, Atlanta, GA, USA

N. Chaumerliac Laboratoire de Météorologie Physique (LaMP), CNRS/Université Blaise Pascal, Aubière Cedex, France

P. Cheung Air Quality Research Division, Environment and Climate Change Canada, Toronto, ON, Canada

Jesper H. Christensen Department of Environmental Science, Aarhus University, Roskilde, Denmark

G. Ciarelli Laboratory of Atmospheric Chemistry, Paul Scherrer Institute (PSI), Villigen, Switzerland

Kevin Civerolo New York State Department of Environmental Conservation, Albany, NY, USA

A. Dandou Department of Environmental Physics and Meteorology, Faculty of Physics, National and Kapodistrian University of Athens, Athens, Greece

N. Daskalakis Environmental Chemical Processes Laboratory, Chemistry Department, University of Crete, Heraklion, Greece; LATMOS/IPSL, CNRS, Paris, France

Estíbaliz Sáez de Cámara Faculty of Engineering Bilbao, University of the Basque Country UPV/EHU, Bilbao, Spain

Pieter De Meutter Belgian Nuclear Research Institute, Mol, Belgium; Royal Meteorological Institute of Belgium, Brussels, Belgium; Department of Physics and Astronomy, Ghent University, Ghent, Belgium

Wilco de Vries RIVM, Bilthoven, The Netherlands

A. Deckmyn Royal Meteorological Institute of Belgium, Brussels, Belgium

Priscilla Declerck Brussels Environment, Brussels, Belgium

L. Deguillaume Laboratoire de Météorologie Physique (LaMP), CNRS/Université Blaise Pascal, Aubière Cedex, France

Andy Delcloo Royal Meteorological Institute of Belgium, Brussels, Belgium

R.G. Derwent rdscientific, Newbury, UK

Martin Deshaies-Jacques Air Quality Research Division, Environment and Climate Change Canada, Dorval, QC, Canada

Felix Deutsch VITO, Mol, Belgium

Silvana Di Sabatino Department of Physics and Astronomy, ALMA MATER STUDIORUM - University of Bologna, Bologna, Italy

Adelaide Dinoi Institute of Atmospheric Sciences and Climate, National Research Council, Lecce, Italy

Ludovic Donnat TOTAL Raffinage Chimie, Centre de Recherche TOTAL, Solaize, France

Anthony J. Dore Centre for Ecology and Hydrology, Edinburgh, UK

Eleni Drakaki Atmospheric Modeling and Weather Forecasting Group, School of Physic, University of Athens, University Campus, Athens, Greece

F. Duchêne Royal Meteorological Institute of Belgium, Brussels, Belgium

Olivier Duclaux TOTAL Raffinage Chimie, Centre de Recherche TOTAL, Solaize, France

J. Duyzer TNO, Department of Climate, Air and Sustainability, Utrecht, The Netherlands

M. Ealo Institute of Environmental Assessment and Water Research (IDAEA-CSIC), Barcelona, Spain; Department of Astronomy and Meteorology, Faculty of Physics, University of Barcelona, Barcelona, Spain

George C. Efthimiou Environmental Research Laboratory, INRASTES, NCSR Demokritos, Aghia Paraskevi, Greece

I. El-Haddad Laboratory of Atmospheric Chemistry, Paul Scherrer Institute (PSI), Villigen, Switzerland

Thomas Ellermann Department of Environmental Science, Aarhus University, Roskilde, Denmark

Timo Elolähde Helsinki Region Transport (HSL), Helsinki, Finland

Hilde Fagerli EMEP MSC-W, Norwegian Meteorological Institute, Oslo, Norway

Kathleen Fahey National Exposure Research Laboratory, Environmental Protection Agency, RTP, NC, USA

Marco Falocchi Atmospheric Physics Group, Department of Civil, Environmental and Mechanical Engineering, University of Trento, Trento, Italy

Ting Fang School of Earth and Atmospheric Sciences, Georgia Institute of Technology, Atlanta, GA, USA

Zita Ferenczi Hungarian Meteorological Service, Budapest, Hungary

A.P. Fernandes Department of Environment and Planning, CESAM, University of Aveiro, Aveiro, Portugal

J. Ferreira Department of Environment and Planning, CESAM, University of Aveiro, Aveiro, Portugal

Enrico Ferrero Department of Scienze e Innovazione Tecnologica, University of Piemonte Orientale, Alessandria, Italy

Frans Fierens IRCEL/CELINE, Brussels, Belgium

G. Finzi University of Brescia, Brescia, Italy

Kristen M. Foley Computational Exposure Division, National Exposure Research Laboratory, U.S. Environmental Protection Agency, Research Triangle Park, NC, USA

Fiona Fordyce British Geological Survey, Edinburgh, UK

Hosein Foroutan Computational Exposure Division, National Exposure Research Laboratory, U.S. Environmental Protection Agency, Research Triangle Park, NC, USA

S. Freitas Department of Environment and Planning, CESAM, University of Aveiro, Aveiro, Portugal

Mariel D. Friberg School of Civil and Environmental Engineering, Georgia Institute of Technology, Atlanta, GA, USA

Qingyan Fu Shanghai Environmental Monitoring Center, Shanghai, China

J.-C. Gallet Norwegian Polar Institute, Tromsø, Norway

Stefano Galmarini European Commission Joint Research Centre, Ispra, Italy

Chuen Meei Gan CSC Government Solutions, RTP, NC, USA

Gotzon Gangoiti Faculty of Engineering Bilbao, University of the Basque Country UPV/EHU, Bilbao, Spain

Brett Gantt Office of Air Quality Planning and Standards, Environmental Protection Agency, NC, RTP, USA

N. García-Borreguero Basque Government, Environment Administration Directorate, Vitoria-Gasteiz, Spain

J.A. García Faculty of Engineering, University of the Basque Country UPV/EHU, Bilbao, Spain

K. Gatzsche Leibniz Institute for Tropospheric Research (TROPOS), Leipzig, Germany

Camilla Geels Department of Environmental Science, Aarhus University, Aarhus, Denmark

B. Geyer Helmholtz-Zentrum Geesthacht, Geesthacht, Germany

Roberta Gianfreda TerrAria s.r.l., Milan, Italy

Lorenzo Giovannini Atmospheric Physics Group, Department of Civil, Environmental and Mechanical Engineering, University of Trento, Trento, Italy

Wanmin Gong Air Quality Research Division, Environment and Climate Change Canada, Toronto, Canada

Dimitrios Gounaridis Department of Geography, University of the Aegean, Mytilene, Lesvos, Greece

Sylvie Gravel Air Quality Research Division, Environment and Climate Change Canada, Montreal, QC, Canada

Diego Guizzardi EC, Joint Research Center, Ispra, Italy

H. Guo School of Earth and Atmospheric Sciences, Georgia Institute of Technology, Atlanta, GA, USA

Jonathan Guth Météo-France CNRM-GAME, Toulouse, France

Jakub Guzikowski Wrocław University, Wrocław, Poland

Steen Gyldenkærne Department of Environmental Science, Aarhus University, Aarhus, Denmark

R. Hamdi Royal Meteorological Institute of Belgium, Brussels, Belgium; Department of Physics and Astronomy, Ghent University, Ghent, Belgium

Kaj M. Hansen Department of Environmental Science, Aarhus University, Aarhus, Denmark

Winston Hao New York State Department of Environmental Conservation, Albany, NY, USA

Harry Harmens Centre for Ecology and Hydrology, Bangor, UK

Berit Hasler Department of Environmental Science, Aarhus University, Aarhus, Denmark

Mathew R. Heal School of Chemistry, University of Edinburgh, Edinburgh, UK

Nicholas Heath Computational Exposure Division, National Exposure Research Laboratory, U.S. Environmental Protection Agency, Research Triangle Park, NC, USA

Antti Hellsten Atmospheric Composition Research, Finnish Meteorological Institute, Helsinki, Finland

Carlijn Hendriks Organisation for Applied Scientific Research (TNO), The Hague, Netherlands

Andreas Herber Alfred Wegener Institute Helmholtz-Center for Polar and Marine Research Bremerhaven, Bremerhaven, Germany

Hartmut Herrmann Leibniz Institute for Tropospheric Research (TROPOS), Leipzig, Germany

Ole Hertel Department of Environmental Science, Aarhus University, Roskilde, Denmark

Gerald Hoek Institute for Risk Assessment Sciences (IRAS), Utrecht, Netherlands

Christian Hogrefe National Exposure Research Laboratory, Computational Exposure Division, U.S. Environmental Protection Agency, Research Triangle Park, NC, USA

Heather A. Holmes Department of Physics, University of Nevada Reno, Reno, NV, USA

Hans Hooyberghs VITO, Mol, Belgium

Xuefei Hu Rollins School of Public Health, Emory University, Atlanta, GA, USA

Jiaoyan Huang The University of North Carolina, Chapel Hill, NC, USA

Ran Huang School of Civil and Environmental Engineering, Georgia Institute of Technology, Atlanta, GA, USA

Y. Iinuma Instrumental Analysis Section, Okinawa Institute of Science and Technology Graduate University (OIST), Onna-son, Kunigami, Okinawa, Japan

Ilia Ilyin EMEP/MSC-East, Moscow, Russia

Ulas Im Department of Environmental Science, Aarhus University, Aarhus, Denmark

Kornélia Imre MTA-PE Air Chemistry Research Group, Veszprém, Hungary

Marian-Daniel Iordache VITO, Mol, Belgium

Mark Iredell NCEP Environmental Modelling Centers, NCWCP, College Park, MD, USA

Cesunica E. Ivey School of Civil and Environmental Engineering, Georgia Institute of Technology, Atlanta, GA, USA

Erko Jakobson Tartu Observatory, Tartu, Estonia

Jukka-Pekka Jalkanen Finnish Meteorological Institute (FMI), Helsinki, Finland

I. Janse RIVM (National Institute for Public Health and the Environment), Bilthoven, The Netherlands

Greet Janssens-Maenhout EC, Joint Research Center, Ispra, Italy

Sonia Jerez Department of Physics, Regional Campus of International Excellence Campus Mare Nostrum, University of Murcia, Murcia, Spain

Pedro Jiménez-Guerrero Department of Physics, Regional Campus of International Excellence Campus Mare Nostrum, University of Murcia, Murcia, Spain

Lasse Johansson The Finnish Meteorological Institute (FMI), Helsinki, Finland

O. Jorba Earth Sciences Department of Barcelona Supercomputing Center (BSC-ES), Nexus II Building, Barcelona, Spain

Béatrice Josse Météo-France CNRM-GAME, Toulouse, France

Dusan Jovic NCEP Environmental Modelling Centers, NCWCP, College Park, MD, USA

Catherine Juery TOTAL Raffinage Chimie, Centre de Recherche TOTAL, Solaize, France

Marko Kaasik University of Tartu, Tartu, Estonia

Konstantinos Kakosimos Department of Chemical Engineering, Mary Kay 'O Connor Processes Safety Center, Texas A&M University at Qatar, Doha, Qatar

George Kallos Atmospheric Modeling and Weather Forecasting Group, School of Physics, University of Athens, University Campus, Athens, Greece

J. Kalogiros Institute of Environmental Research and Sustainable Development, National Observatory of Athens, Athens, Greece

M. Kanakidou Environmental Chemical Processes Laboratory, Chemistry Department, University of Crete, Heraklion, Greece

Daiwen Kang National Exposure Research Laboratory, Computational Exposure Division, U.S. Environmental Protection Agency, Durham, NC, USA

Leena Kangas Finnish Meteorological Institute, Helsinki, Finland

Matthias Karl Helmholtz-Zentrum Geesthacht, Institute of Coastal Research, Geesthacht, Germany

Ari Karppinen Finnish Meteorological Institute, Helsinki, Finland

Niko Karvosenoja Finnish Environment Institute SYKE, Helsinki, Finland

Mari Kauhaniemi Finnish Meteorological Institute, Helsinki, Finland

Klaus Ketelsen Private Software Consultant, Berlin, Germany

Matthias Ketzel Department of Environmental Science, Aarhus University, Roskilde, Denmark

S.K. Kharol Air Quality Research Division, Environment and Climate Change Canada, Toronto, ON, Canada

Youngseob Kim CEREA, Joint Laboratory École des Ponts ParisTech/EDF R&D, Université Paris-Est, Champs-sur-Marne, France

Hristina Kirova National Institute of Meteorology and Hydrology-Bulgarian Academy of Sciences, Sofia, Bulgaria

Pavel Kishcha Department of Geosciences, Tel-Aviv University, Tel-Aviv, Israel

Heiko Klein Norwegian Meteorological Institute, Oslo, Norway; entre of Excellence for Environmental Radioactivity, Ås, Norway

Mitchel Klein Department of Environmental Health, Rollins School of Public Health, Emory University, Atlanta, GA, USA

Franziska Koellner Particle Chemistry Department, Max Planck Institute for Chemistry, Mainz, Germany

M. Koukoula School of Physics, University Campus, University of Athens, Athens, Greece

Anu Kousa Helsinki Region Environmental Services Authority (HSY), Helsinki, Finland

R. Kouznetsov Finnish Meteorological Institute, Helsinki, Finland

Ivan V. Kovalets Department of Environmental Modelling, Institute of Mathematical Machine and System Problems, National Academy of Sciences of Ukraine, Kiev, Ukraine

R. Kranenburg Department of Climate, Air and Sustainability, TNO, Utrecht, The Netherlands

Maciej Kryza Department of Climatology and Atmosphere Protection, University of Wrocław, Wrocław, Poland

Michael Ku New York State Department of Environmental Conservation, Albany, NY, USA

J. Kuenen TNO, Department of Climate, Air and Sustainability, Utrecht, The Netherlands

Jaakko Kukkonen Finnish Meteorological Institute, Helsinki, Finland

Naresh Kumar EPRI, Palo Alto, CA, USA

Kaarle Kupiainen Finnish Environment Institute SYKE, Helsinki, Finland

A. Kurganskiy Niels Bohr Institute, University of Copenhagen, København, Denmark

Jonilda Kushta Atmospheric Modeling and Weather Forecasting Group, School of Physics, University of Athens, University Campus, Athens, Greece

Roger Kwok California Air Resources Board, Sacramento, CA, USA

Tony Christian Landi Institute of Atmospheric Sciences and Climate, National Research Council, Bologna, Italy

J. Langner Swedish Meteorological and Hydrological Institute, Norrköping, Sweden

Timo Lanki Finnish National Institute for Health and Welfare, Helsinki, Finland

J. Lavín Sociedad Española de Abastecimientos, S.A., Valencia, Spain

Pius Lee NOAA Air Resources Air Resource Laboratory (ARL), NCWCP, College Park, MD, USA

Wouter Lefebvre VITO, Mol, Belgium

Fabian Lenartz ISSeP, Liège, Belgium

Donghai Liang Emory University, Atlanta, GA, USA

Cong Liu School of Civil and Environmental Engineering, Georgia Institute of Technology, Atlanta, GA, USA; School of Energy and Environment, Southeast University, Nanjing, China

Peng Liu Computational Exposure Division, National Exposure Research Laboratory, U.S. Environmental Protection Agency, Research Triangle Park, NC, USA

Yang Liu Rollins School of Public Health, Emory University, Atlanta, GA, USA

Jose Maria López-Romero Department of Physics, Regional Campus of International Excellence Campus Mare Nostrum, University of Murcia, Murcia, Spain

Agustín López-Villagra Department of Physics, Regional Campus of International Excellence Campus Mare Nostrum, University of Murcia, Murcia, Spain

Huiying Luo Department of Civil and Environmental Engineering, University of Connecticut, Storrs-Mansfield, CT, USA

Alexandru Lupu Air Quality Research Division, Environment and Climate Change Canada, Toronto, ON, Canada

Guiseppe Maffeis TerrAria s.r.l., Milan, Italy

Bino Maiheu VITO, Mol, Belgium

P.A. Makar Air Quality Research Division, Environment and Climate Change Canada, Toronto, ON, Canada

Heath Malcolm Centre for Ecology and Hydrology, Penicuik, Midlothian, UK

Virginie Marécal Météo-France CNRM-GAME, Toulouse, France

H. Martins Department of Environment and Planning, CESAM, University of Aveiro, Aveiro, Portugal

Rohit Mathur National Exposure Research Laboratory, Computational Exposure Division, U.S. Environmental Protection Agency, Durham, NC, USA

Volker Matthias Helmholtz-Zentrum Geesthacht, Institute of Coastal Research, Geesthacht, Germany

Maija Mattinen Finnish Environment Institute SYKE, Helsinki, Finland

Alberto Maurizi Institute of Atmospheric Sciences and Climate, National Research Council, Bologna, Italy

C. McLinden Air Quality Research Division, Environment and Climate Change Canada, Toronto, ON, Canada

Richard Ménard Air Quality Research Division, Environment and Climate Change Canada, Dorval, QC, Canada

Clemens Mensink VITO, Mol, Belgium

Alexis Merlaud BIRA/IASB, Royal Belgian Institute for Space Aeronomy, Brussels, Belgium

G. Methymaki Department of Environmental Physics and Meteorology, Faculty of Physics, National and Kapodistrian University of Athens, Athens, Greece

Koen Meuleman VITO, Mol, Belgium

N. Mihalopoulos Environmental Chemical Processes Lab., Department of Chemistry, University of Crete, Heraklion, Greece

A.I. Miranda Department of Environment and Planning, CESAM, University of Aveiro, Aveiro, Portugal

Juan Pedro Montávez Department of Physics, Regional Campus of International Excellence Campus Mare Nostrum, University of Murcia, Murcia, Spain

A. Monteiro Department of Environment and Planning, CESAM, University of Aveiro, Aveiro, Portugal

Michael D. Moran Air Quality Research Division, Environment and Climate Change Canada, Toronto, ON, Canada

Luca Mortarini Institute of Atmospheric Sciences and Climate, National Research Council, Turin, Italy

Nicolas Moussiopoulos Laboratory of Heat Transfer and Environmental Engineering, Aristotle University, Thessaloniki, Greece

Jennifer L. Moutinho School of Civil and Environmental Engineering, Georgia Institute of Technology, Atlanta, GA, USA

James A. Mulholland School of Civil and Environmental Engineering, Georgia Institute of Technology, Atlanta, GA, USA

Benjamin Murphy National Exposure Research Laboratory, Computational Exposure Division, U.S. Environmental Protection Agency, Research Triangle Park, NC, USA

Jennifer Murphy Department of Chemistry, University of Toronto, Toronto, Canada

A. Mutzel Leibniz Institute for Tropospheric Research (TROPOS), Leipzig, Germany

S. Myriokefalitakis Environmental Chemical Processes Laboratory, Chemistry Department, University of Crete, Heraklion, Greece; Department of Physics and Astronomy, Institute for Marine and Atmospheric Research (IMAU), Utrecht University, Utrecht, The Netherlands

Sergey Napelenok Computational Exposure Division, National Exposure Research Laboratory, U.S. Environmental Protection Agency, Research Triangle Park, NC, USA

A. Nenes Department of Earth and Atmospheric Sciences, Georgia Institute of Technology, Atlanta, GA, USA

Ole-Kenneth Nielsen Department of Environmental Science, Aarhus University, Roskilde, Denmark

Theodoros Nitis Laboratory of Heat Transfer and Environmental Engineering, Aristotle University, Thessaloniki, Greece; Laboratory of Environmental Quality and Geospatial Applications, Department of Marine Sciences, University of the Aegean, Mytilene, Lesvos, Greece

Tavs Nyord Department of Engineering, Aarhus University, Aarhus, Denmark

V. Obiso Earth Sciences Department of Barcelona Supercomputing Center (BSC-ES), Nexus II Building, Barcelona, Spain

Emmanouil Oikonomakis Laboratory of Atmospheric Chemistry, Paul Scherrer Institute PSI, Villigen, Switzerland

Mohammad Omary The University of North Carolina, Chapel Hill, NC, USA

Riinu Ots School of Chemistry, University of Edinburgh, Edinburgh, UK

B. Pabla Air Quality Research Division, Environment and Climate Change Canada, Toronto, ON, Canada

Laura Palacios-Peña Department of Physics, Regional Campus of International Excellence Campus Mare Nostrum, University of Murcia, Murcia, Spain

Li Pan NOAA Air Resources Air Resource Laboratory (ARL), NCWCP, College Park, USA; Cooperative Institutes for Satellite and Climate, University of Maryland, College Park, USA

M. Pandolfi Institute of Environmental Assessment and Water Research (IDAEA-CSIC), Barcelona, Spain

P. Patlakas School of Physics, University Campus, University of Athens, Athens, Greece

L. Patryl CEA, DAM, DIF, Arpajon, France

Edward Patton National Center for Atmospheric Research, Boulder, CO, USA

Ville-Veikko Paunu Finnish Environment Institute SYKE, Helsinki, Finland

A. Pederzoli University of Brescia, Brescia, Italy

Olav Peeters IRCEL/CELINE, Brussels, Belgium

Anne Philipp Department of Meteorology and Geophysics, Faculty of Earth Sciences, Geography and Astronomy, University of Vienna, Vienna, Austria

V. Phillips Department of Physical Geography and Ecosystem Science, Lund University, Lund, Sweden

Jonathan E. Pleim Computational Exposure Division, National Exposure Research Laboratory, U.S. Environmental Protection Agency, Research Triangle Park, NC, USA

Marlene S. Plejdrup Department of Environmental Science, Aarhus University, Roskilde, Denmark

L. Poulain Leibniz Institute for Tropospheric Research (TROPOS), Leipzig, Germany

George Pouliot National Exposure Research Laboratory, Computational Exposure Division, U.S. Environmental Protection Agency, RTP, NC, USA

Cristina Pozzi Arianet S.r.l., Milan, Italy

Marje Prank Finnish Meteorological Institute, Helsinki, Finland

André S.H. Prévôt Laboratory of Atmospheric Chemistry, Paul Scherrer Institute, Villigen, Switzerland

Havala O.T. Pye Computational Exposure Division, National Exposure Research Laboratory, U.S. Environmental Protection Agency, Research Triangle Park, NC, USA

Markus Quante Helmholtz-Zentrum Geesthacht, Institute of Coastal Research, Geesthacht, Germany

Siegfried Raasch Leibniz Universität Hannover, Hannover, Germany

Paola Radice Arianet S.r.l., Milan, Italy

S. Rafael Department of Environment and Planning, CESAM, University of Aveiro, Aveiro, Portugal

Valentin Raffort CEREA, Joint Laboratory École des Ponts ParisTech/EDF R&D, Université Paris-Est, Champs-sur-Marne, France

Martin Otto Paul Ramacher Helmholtz-Zentrum Geesthacht, Institute of Coastal Research, Geesthacht, Germany

Limei Ran Computational Exposure Division, National Exposure Research Laboratory, U.S. Environmental Protection Agency, Research Triangle Park, NC, USA

Ketlin Reis University of Tartu, Tartu, Estonia

Stefan Reis NERC Centre for Ecology and Hydrology, Penicuik, UK

W. Richard Leaitch Climate Research Division, Environment and Climate Change Canada, Toronto, Canada

C. Rose Laboratoire de Météorologie Physique (LaMP), CNRS/Université Blaise Pascal, Aubière Cedex, France

Shawn J. Roselle Computational Exposure Division, National Exposure Research Laboratory, U.S. Environmental Protection Agency, Research Triangle Park, NC, USA

D. Rosenfeld Institute of Earth Sciences, The Hebrew University of Jerusalem, Jerusalem, Israel

Yelva Roustan CEREA, Joint Laboratory École des Ponts ParisTech/EDF R&D, Université Paris-Est, Champs-sur-Marne, France

M. Ruppel Department of Environmental Sciences, University of Helsinki, Helsinki, Finland

Armistead G. Russell School of Civil and Environmental Engineering, Georgia Institute of Technology, Atlanta, GA, USA

E. Sá Department of Environment and Planning, CESAM, University of Aveiro, Aveiro, Portugal

Jeremy Sarnat Emory University, Atlanta, GA, USA

Stefanie E. Sarnat Department of Environmental Health, Rollins School of Public Health, Emory University, Atlanta, GA, USA

Golam Sarwar National Exposure Research Laboratory, Environmental Protection Agency, RTP, NC, USA

Minna-Kristiina Sassi Finnish Environment Institute SYKE, Helsinki, Finland

Ferd Sauter RIVM, Bilthoven, The Netherlands

Verica Savic-Jovcic Air Quality Research Division, Environment and Climate Change Canada, Toronto, ON, Canada

Mikko Savolahti Finnish Environment Institute SYKE, Helsinki, Finland

M. Schaap TNO, Department of Climate, Air and Sustainability, Utrecht, The Netherlands

J.F. Schijven RIVM (National Institute for Public Health and the Environment), Bilthoven, The Netherlands

Johannes Schneider Particle Chemistry Department, Max Planck Institute for Chemistry, Mainz, Germany

Roland Schrödner Leibniz Institute for Tropospheric Research (TROPOS), Leipzig, Germany; Centre for Environmental and Climate Research, Lund University, Lund, Sweden

Corinna Schrum Helmholtz-Zentrum Geesthacht, Institute of Coastal Research, Geesthacht, Germany

Leon Sedefian SEDEFIAN Consulting, Malta, NY, USA

A. Segers TNO, Department of Climate, Air and Sustainability, Utrecht, The Netherlands

Petra Seibert Institute of Meteorology, University of Natural Resources and Life Sciences, Vienna, Austria

Christian Seigneur CEREA, Joint Laboratory École des Ponts ParisTech/EDF R&D, Université Paris-Est, Champs-sur-Marne, France

Sangeeta Sharma Climate Research Division, Environment and Climate Change Canada, Toronto, Canada

Raquel A. Silva The University of North Carolina, Chapel Hill, NC, USA

Heather Simon Office of Air Quality Planning and Standards, Environmental Protection Agency, NC, RTP, USA

Carsten A. Skjøth National Pollen and Aerobiological Research Unit, Institute of Science and the Environment, University of Worcester, Worcester, UK

J. Soares Finnish Meteorological Institute, Helsinki, Finland

Mikhail Sofiev Finnish Meteorological Institute, Helsinki, Finland

V. Sofieva Finnish Meteorological Institute, Helsinki, Finland

Efisio Solazzo European Commission Joint Research Centre, Ispra, Italy

Stavros Solomos National Observatory of Athens, IAASARS, Panteli, Greece

Christos Spyrou Atmospheric Modeling and Weather Forecasting Group, School of Physics, University of Athens, University Campus, Athens, Greece

Ralf Staebler Air Quality Research Division, Environment and Climate Change Canada, Toronto, Canada

Boris Starobinets Department of Geosciences, Tel-Aviv University, Tel-Aviv, Israel

H.A.M. Sterk RIVM (National Institute for Public Health and the Environment), Bilthoven, The Netherlands

Douw G. Steyn Department of Earth, Ocean and Atmospheric Sciences, The University of British Columbia, Vancouver, Canada

Matthew J. Strickland Department of Environmental Health, Rollins School of Public Health, Emory University, Atlanta, GA, USA

J. Ström Department of Environmental Science and Analytical, Stockholm University, Stockholm, Sweden

Peter Sullivan National Center for Atmospheric Research, Boulder, CO, USA

A.N. Swart RIVM (National Institute for Public Health and the Environment), Bilthoven, The Netherlands

E. Swietlicki Division of Nuclear Physics, Lund University, Lund, Sweden

Mariusz Szymanowski Wrocław University, Wrocław, Poland

Frederick Tack BIRA/IASB, Royal Belgian Institute for Space Aeronomy, Brussels, Belgium

Youhua Tang NOAA Air Resources Air Resource Laboratory (ARL), NCWCP, College Park, USA; Cooperative Institutes for Satellite and Climate, University of Maryland, College Park, USA

David Tarasick Air Quality Research Division, Environment and Climate Change Canada, Toronto, Canada

V. Tarvainen Finnish Meteorological Institute, Helsinki, Finland

Piet Termonia Royal Meteorological Institute of Belgium, Brussels, Belgium; Department of Physics and Astronomy, Ghent University, Ghent, Belgium

Hans Thodsen Department of Bioscience, Aarhus University, Aarhus, Denmark

Andreas Tilgner Leibniz Institute for Tropospheric Research (TROPOS), Leipzig, Germany

Karen Timmermann Department of Bioscience, Aarhus University, Aarhus, Denmark

R. Timmermans Department of Climate, Air and Sustainability, TNO, Utrecht, The Netherlands

Gianni Tinarelli Arianet S.r.l., Milan, Italy

Paige E. Tolbert Department of Environmental Health, Rollins School of Public Health, Emory University, Atlanta, GA, USA

Elena Tomasi Atmospheric Physics Group, Department of Civil, Environmental and Mechanical Engineering, University of Trento, Trento, Italy

M. Tombrou Faculty of Physics, Department of Environmental Physics and Meteorology, National and Kapodistrian University of Athens, Athens, Greece

Daniel Tong NOAA Air Resources Air Resource Laboratory (ARL), NCWCP, College Park, MD, USA; Cooperative Institutes for Satellite and Climate, University of Maryland, College Park, MD, USA

S. Trivikrama Rao Department of Civil and Environmental Engineering, University of Connecticut, Storrs, CT, USA

Dennis Trolle Department of Bioscience, Aarhus University, Aarhus, Denmark

Charles Troupin SOCIB, Parc Bit, Naorte, Palma de Mallorca, Spain

Giorgios Tsegas Aristotle University Thessaloniki, Thessaloniki, Greece

S. Tsyro EMEP MSC-W, Norwegian Meteorological Institute, Oslo, Norway

E. Turrini University of Brescia, Brescia, Italy

P. Uriarte Factor CO2, Bilbao, Spain

Verónica Valdenebro Faculty of Engineering Bilbao, University of the Basque Country UPV/EHU, Bilbao, Spain

Alejandro Valencia The University of North Carolina, Chapel Hill, NC, USA

J. Valente Department of Environment and Planning, CESAM, University of Aveiro, Aveiro, Portugal

Pieter Valkering VITO, Mol, Belgium

Eric van der Swaluw RIVM, Bilthoven, The Netherlands

J.P.G. van Leuken RIVM (National Institute for Public Health and the Environment), Bilthoven, The Netherlands

Dominik van Pinxteren Leibniz Institute for Tropospheric Research (TROPOS), Leipzig, Germany

Addo van Pul RIVM, Bilthoven, The Netherlands

Michel van Roozendael BIRA/IASB, Royal Belgian Institute for Space Aeronomy, Brussels, Belgium

Shari van Wittenberghe IRCEL/CELINE, Brussels, Belgium

Francois Vandenberghe National Center for Atmospheric Research (NCAR), Boulder, CO, USA

Charlotte Vanpoucke IRCEL/CELINE, Brussels, Belgium

P. Vasilakos School of Chemical and Biomolecular Engineering, Georgia Institute of Technology, Atlanta, GA, USA

Guus Velders RIVM, Bilthoven, The Netherlands

Alexandros Venetsanos Environmental Research Laboratory, INRASTES, NCSR Demokritos, Aghia Paraskevi, Greece

Lakshmi Pradeepa Vennam The University of North Carolina, Chapel Hill, NC, USA

Vishal Verma Department of Civil and Environmental Engineering, University of Illinois at Urbana-Champaign, Champaign, IL, USA

Peter Viaene VITO, Mol, Belgium

Massimo Vieno Centre for Ecology and Hydrology, Penicuik, UK

Julius Vira Finnish Meteorological Institute, Helsinki, Finland

Marialuisa Volta UNIBS, Brescia, Italy

Lili Wang Institute of Atmospheric Physics, Chinese Academy of Sciences, Beijing, China

Qian Wang Shanghai Environmental Monitoring Center, Shanghai, China

Kinga Wałaszek Department of Climatology and Atmosphere Protection, University of Wroclaw, Wrocław, Poland

Rodney J. Weber School of Earth and Atmospheric Sciences, Georgia Institute of Technology, Atlanta, GA, USA

Jeffrey Weil National Center for Atmospheric Research, Boulder, CO, USA

Greg Wentworth Department of Chemistry, University of Toronto, Toronto, Canada

Małgorzata Werner Department of Climatology and Atmosphere Protection, University of Wroclaw, Wrocław, Poland

Roy J. Wichink Kruit RIVM (National Institute for Public Health and the Environment), Bilthoven, The Netherlands

Megan Willis Department of Chemistry, University of Toronto, Toronto, Canada

Wilfried Winiwarter IIASA—International Institute for Applied Systems Analysis, Laxenburg, Austria

Ralf Wolke Leibniz Institute for Tropospheric Research (TROPOS), Leipzig, Germany

David C. Wong Computational Exposure Division, National Exposure Laboratory, US EPA, Washington, D.C., USA

Curtis Wood Finnish Meteorological Institute, Helsinki, Finland

I.M. Wouters IRAS (Institute for Risk Assessment Sciences, Utrecht University), Utrecht, The Netherlands

Jianbin Wu Shanghai Meteorological Bureau, Shanghai, China

K. Wyat Appel Computational Exposure Division, National Exposure Research Laboratory, U.S. Environmental Protection Agency, Research Triangle Park, NC, USA

Andrezj Wyszogrodski Polish Bureau of Meteorology, Warsaw, Poland

Jia Xing State Key Joint Laboratory of Environmental Simulation and Pollution Control, School of Environment, Tsinghua University, Beijing, China

Tarja Yli-Tuomi Finnish National Institute for Health and Welfare, Helsinki, Finland

Heather Yorston Edinburgh Parallel Computing Centre, Edinburgh University, Edinburgh, UK

Jeff Young Computational Exposure Division, National Exposure Research Laboratory, U.S. Environmental Protection Agency, Research Triangle Park, NC, USA

Haofei Yu School of Civil and Environmental Engineering, Georgia Institute of Technology, Atlanta, GA, USA

Eric Zalewsky New York State Department of Environmental Conservation, Albany, NY, USA

Dino Zardi Atmospheric Physics Group, Department of Civil, Environmental and Mechanical Engineering, University of Trento, Trento, Italy

Limin Zeng Peking University, Beijing, China

Xinxin Zhai School of Civil and Environmental Engineering, Georgia Institute of Technology, Atlanta, GA, USA

Junhua Zhang Air Quality Research Division, Environment and Climate Change Canada, Toronto, ON, Canada

Q. Zheng Air Quality Research Division, Environment and Climate Change Canada, Toronto, ON, Canada

Part I
Long Term Modeling and Trend Analysis

Chapter 1
The Intellectual History of Air Pollution Modelling as Represented by the ITM Meeting Series

Douw G. Steyn

Abstract I review the development of ideas in air pollution modelling by tracing the sequence of ideas presented in the 35 past instances of International Technical Meetings (ITM) on Air Pollution Modelling and its Application. My review reveals a healthy evolution of ideas presented at the ITMs, and confirms my impression that the ITM series is one of, if not *the* leading air pollution modelling conference series.

1.1 Introduction

I must start off by admitting that this was my idea, so blame me, not the ITM Scientific Committee if I waste your time with what might appear to be the meandering ruminations of an old scientist who is "past it".

On a number of occasions, as Chair of the ITM Scientific Committee over a span of 7 years, I was asked to justify the continued existence (and funding) of the ITM series of meetings. My answer every time was that the papers presented at these meetings, and the resultant ITM books, traced all important developments in the science of air pollution modelling from the late 1960s onwards, and that these books represented the intellectual history of our field. I felt that it was important to share this perspective with you, and thank the present Scientific Committee for giving me the opportunity to do so.

I must emphasize that this is not a history of the meeting and its organization. That you can read on the ITM web site at https://www.itm.marvin.vito.be. It is also not a history of the people involved in the ITM. You might then ask, "So what is this?" Well, it is an intellectual history, which aims to understand ideas from the past by understanding them in context, and like all history, it is just a matter of "one damned thing after the another ...". Professional historians will insist that "ideas do not develop in isolation from the people who create and use them, and that one must study ideas not as abstract propositions but in terms of the culture, lives, and

D.G. Steyn (✉)
Department of Earth, Ocean and Atmospheric Sciences,
The University of British Columbia, Vancouver, Canada
e-mail: dsteyn@eos.ubc.ca

C. Mensink and G. Kallos (eds.), *Air Pollution Modeling and its Application XXV*,
Springer Proceedings in Complexity, DOI 10.1007/978-3-319-57645-9_1

historical contexts that produced them" https://www.en.wikipedia.org/wiki/Intellectual_history. I accept that this is an idea imbedded in the humanities, where humans and their doings are paramount. I am a scientist, and so leave that approach for someone else. This is because I am primarily interested in the nature and evolution of the ideas themselves. I also avoid discussing people because I fear that would descend into anecdotes, or worse, gossip, and anyway, to do that would expose me to the risk of offending some of my friends and colleagues. I make one notable exception to this in Sect. 1.5.2.

The ITM proceedings over the past 40 years were published as books from the 6th ITM onward, with the Roman numbered volumes starting at the 11th ITM. I will refer to the *pre-Roman* volumes as ITM 1 (1972) for example, and the current series as ITM XXIV (2015) for example, which is of course: Steyn et al. (2016). You are now attending the 35th named ITM.

It might be argued that all one has to do is read through the sequence of meeting themes or topics to develop a comprehensive view of important ideas. This is true in that the various ITM Scientific Committees have worked to keep the meeting series relevant and up-to-date by slowly evolving the theme topics. For my purposes, this is rather too coarse-grained an approach, so I had no choice but to delve into both indices and paper details in the ITM proceedings volumes.

I must acknowledge my debt to my colleague, and frequent ITM attendee, Peter Builtjes, who in ITM XIV (2000) presented a retrospective paper titled *Major Twentieth Century Milestones in Air Pollution Modelling and its Application* and also to Akula Venkatram, who, also in ITM XIV (2000) presented a forward looking paper titled *Challenges of Air Pollution Modelling and its Application in the next Millennium*. In many ways, I am simply providing an update on Peter's work, and a review of the first 15 years of Akula's predictions (see Sect. 1.6).

1.2 Air Pollution Modelling: The State of the Art in 1969

I would like to start with a very brief introduction to the origins of the subject of air pollution modelling, so as to bring you up to about 1970, when the ITM series began. The origins of the subject of applied air pollution modelling lay in the need to understand dispersion of chemical munitions following their use in the 1st world war. Much of the early work on atmospheric diffusion modelling was done using data generated at the Porton Down military research establishment in the UK. Early work concentrated on atmospheric diffusion from isolated, elevated pollution sources in effectively flat topography. The question of plume rise due to buoyancy and momentum effects was approached using data from (among other studies), large thermal electricity generating plants operated by the Tennessee Valley Authority in the USA. This work was lead by scientists at the Oak Ridge National (USA) Laboratories. It was soon realized that turbulent diffusion was (and still remains) a theoretically intractable problem. The "work-around" solution was to avoid theoretical difficulties that arose from "first principles" approaches (of which quite a few existed)

and to inject a sweeping, empirical (but theoretically supportable) assumption at the outset—this resulted in the Gaussian Plume Model (GPM), whose plume parameters were derived from observations, and whose stability dependence was captured by the Pasquill-Gifford stability classes.

In the late 1960s, concern about dispersion of fissionable materials from nuclear power plants, and developing air quality control legislation in North America and Western Europe invigorated research (by making additional funding available, and by the need to develop science to support regulatory requirements) into atmospheric dispersion modelling. An important book from this era is Slade (1968), which carries the fascinating title *Meteorology and Atomic Energy*. These developments defined what came to be called *First Generation Air Pollution Models*.

1.3 *First Generation* Air Pollution Models in Early ITMs

Work presented in ITM 1 (1972) to ITM VII (1988) report applications of the GPM in a wide variety of specific regional settings. Through this period, a substantial number of papers covered development of plume parameter schemes, plume rise parameterizations and boundary layer depth schemes, all used in applications of the GPM. One recurring theme in these meetings was the wide range of approaches to GPM model application in European regulatory settings, and the need to harmonize these approaches. This eventually resulted in the spin-off series of meetings starting in 1991 which came to be know as the *Harmonization Meeting* http://www.harmo.org/. By ITM X (1993) GPM work was effectively absent from the ITMs, as research interest shifted to second generation air pollution modelling. Around this time, the ITM Scientific Committee began actively discouraging submission of papers dealing with simple GPM applications. A recurrent theme in subsequent ITMs (up to about ITM XIII (1998)) was the development, performance assessment and application of Gaussian Puff models, exemplified by the CALPUFF model, which was first presented at ITM XI (1995). While the performance is markedly superior to simple GPMs, CALPUFF in approach and theoretical foundations remains a first generation model. In many regulatory contexts, CALPUFF has come to replace the simple GPM.

1.3.1 Analytical Modelling Continues

The GPM circumvents the very complex (and in formal terms, unsolved) nature of turbulent diffusion by injecting a sweeping, empirically based, assumption at an early stage of the analysis. There continued to be a small, though active, community of scientists within the ITM community who study turbulent diffusion using more-or-less theoretically based approaches that avoided the early-stage empiricism of the GPM. This work includes Lagrangian particle dispersion modelling, and diffusion based on stochastic differential equations (usually the Langevin equation). All of this

work attempts to achieve progress using analytical techniques to develop models that ultimately must rely on numerical solution techniques. This style of work is evident as early as ITM IX (1992), though it appears less frequently after ITM XV (2002).

1.4 Development of *Second Generation* Air Pollution Models

As early as 1982, McRae, Goodin and Seinfeld McRae et al. (1982) used the term *Second Generation Air Pollution Model*, by which they meant ".... a comprehensive modelling system for urban air pollution, including three-dimensional, grid-based as well as Lagrangian trajectory, vertically integrated and single cell formulations". Characteristics of *Second Generation* air pollution models are:

- A gridded Eulerian or Lagrangian approach, based on numerical solution of (simplified) Navier-Stokes equations,
- The ability to incorporate sophisticated atmospheric boundary later turbulence schemes into the model,
- The ability to incorporate chemical transformation into the model,
- The ability to explicitly include spatially variable land-use characteristics and topography,
- Applicability to (much) larger scales than the 10 or so *km* over which GMPs operate,
- A greatly increased complexity and computational demand.

As is obvious, these are substantial development beyond the GPM. The characteristics listed above are all substantially new in their intellectual content. While the initial impetus for the development of these models was the need to understand urban scale air pollution, the models themselves imposed no particular restriction on scale of application.

Research on the development and application of second generation air pollution models first appears in the ITM during ITM IV (1983). At that stage the idea was no more a hint that air pollution at the regional scale was an important consideration, and that it should be approached using a mesoscale meteorological model with an imbedded chemical transformation model (or module). The topic grew in complexity and number of papers until ITM XII (1997) by which stage it was a fully-developed ITM topic that attracted a substantial number of papers. The slow adoption of third generation models is surely a reflection of the greatly increased complexity and resource (mainly computational) demands when compared with first generation models. From ITM XII (1997) onwards, work involving second generation models as applied to regional, national and ultimately global air pollution questions has become a regular feature of ITM activity. Furthermore, such models have become the central focus of the *Air Quality Model Evaluation International Initiative, (AQMEII)* discussed in Sect. 1.5.1.

It may be argued that the class of air pollution models exemplified by the integrated *Weather Research and Forecasting, (WRF)* meteorological model and *Community Multiscale Air Quality, (CMAQ)* air quality modelling system constitutes the third generation of air quality models. Arguments for this position are the multiscale capability, modular nature and coupled meteorology and chemistry processes incorporated in these models. I believe these unquestionably important features are technical developments, rather than a fundamentally new approach. I therefore do not present them as a new idea.

It is interesting to note that while fundamental research on approaches to chemical modelling, and the development of chemical mechanisms, as demanded by second generation models are of fundamental importance in these models, very little of that work is presented at ITMs. This is probably because atmospheric chemists tend not to attend ITMs, where most attendees have a meteorological background.

1.4.1 Long-Range Transport of Air Pollution

Growing concern with acid rain in Western Europe and North America in the 1970s and 1980s and the realization that the problem was intimately tied to the long range transport of air pollution provided strong motivation (and funding) for the development of second generation air pollution models. These models were generalizations that went beyond the initial urban focus of second generation models, and provided easy extension to regional, and eventually global, modelling capability. This capability found ready application to problems of Arctic Pollution, and eventually in the 1980s and 1990s with growing concern over global dispersion of air pollution. The change of scale from local to global is more than a mere refocussing, but constitutes a real shift in ideas, and is therefore a notable step in this intellectual history of air pollution modelling.

ITM IV (1983) was the first meeting at which the subject appears as both a theme topic, and as work presented at the meeting. Following this meeting, the topic of regional to global scale air pollution modelling became a fixed feature of the ITM series, and continues to be that to the present meeting.

1.4.2 Chernobyl and Its "fallout"

In late April, 1986 the Nuclear power plant in Chernobyl, Ukraine exploded, releasing at least 5% of the radioactive reactor core (about 2×10^{18} Bq of ^{131}I equivalent) into the atmosphere. This radioactive effluent dispersed in the atmosphere over the following weeks, resulting in radiation exposure to downwind regions. By 8 days after the explosion, there was detectable radioactivity over much of Europe, from Greece to the United Kingdom, and from southern Sweden to much of the Ukraine and southern Russia.

ITM VI (1987) carried a special topic on the Chernobyl accident, and contains two papers reporting on attempts to model dispersion of the radioactive plume. Similar work was reported in ITM volumes VII (1988), VIII (1990) and IX (1992). In the latter two meetings, a 21 model inter-comparison exercise (called ATMES) was reported. While overall modelling results were deemed acceptable, uncertainties related to source strength and release height introduced considerable uncertainty. It was noted that a core group of eight models showed consistently reliable ability to predict the arrival of the plume. These two findings had consequences that came to play significant roles in future ITMs. In order to reduce model uncertainty due to lack of source information, a controlled release of a tracer substance was recommended. This eventually resulted in the *European Tracer Experiment (ETEX)*, which provided an exceptional model testing data set for long range dispersion of any pollutants, but especially those from accidental releases of radioactive materials. Subsequent ITM volumes provided a venue for reporting of major ETEX findings, and were an important part of a growing interest in model evaluation that still is an important theme topic in the ITM (see Sect. 1.5). The second consequence (notably because of the discovery of a core of consistent models) was the development of ensemble modelling of air pollution (see Sect. 1.5.3). In my opinion, the new ideas and initiatives that arose out of the Chernobyl explosion are wide-ranging enough to constitute a shift in fundamental thinking about air pollution modelling.

1.5 Miscellany

1.5.1 Model Evaluation and AQMEII

Model evaluation is a (largely statistical) exercise in which output from a model is compared with observations (and sometimes the output of a theoretical model) in an attempt to show how much useful information is captured by the model. This has been a topic of great interest to the ITM community since the very earliest ITMs, when the term "model accuracy" was used. By ITM 5 (1976), the term "model validation" was used, which came to be slowly replaced by the more logically neutral term "model evaluation". During ITM XX (2009) the *Air Quality Model Evaluation International Initiative, (AQMEII)* was announced. This initiative arose directly out of the ITM community, and focussed on evaluation of regional photochemistry models http://www.ensemble2.jrc.ec.europa.eu/aqmeii/. This initiative operated through collaborative modelling exercises, independent meetings, and joint meetings at ITM XX (2009) to ITM XXVI (2015). A core idea arising out of AQMEII is that model evaluation can take one of four possible approaches: *operational, diagnostic, dynamic, and probabilistic*. Ideas arising out of the AQMEII constitute a substantial advance in our understanding of, and approaches to air pollution modelling.

1.5.2 Large Eddy Simulation and Direct Numerical Simulation

In a remarkably forward looking paper presented at ITM VI (1987), Frans Nieuwstadt reported on a study of pollutant dispersion in a convective atmospheric boundary layer using *Large Eddy Simulation (LES)* modelling. This technique circumvents the computationally impossible task (at least with presently available computing capability) of *Direct Numerical Simulation, (DNS)* of a real atmosphere. Research into a variety of LES applications to turbulent diffusion in the atmosphere have appeared regularly in subsequent ITM volumes. This approach represents a completely new approach to understanding and quantifying atmospheric turbulent diffusion, and steps aside of earlier reliance on field observational studies.

1.5.3 Ensemble Modelling

The idea of creating a weather forecast from an ensemble of models or runs of the same model has been well-established in the meteorological forecasting community. Following on from the ATMES exercise, the use of an ensemble approach to air pollution modelling was presented at ITM XVII (2004) by two separate groups. This has developed into a steady sequence of works at the ITM which demonstrate the clear superiority of ensemble forecasts of air pollution over single-model exercises. This approach constitutes a sharp change in approaches to modelling of air pollutant dispersion, at least at regional and possibly global scales.

1.5.4 Reduced Equation Set Chemical Modelling

Air pollution chemical transformation models are generally developed by atmospheric chemists specializing in chemical kinetics. The resulting modelling schemes often consist of at least many tens of chemical species and the resulting larger set of chemical reactions. Of necessity, the resulting computer code consumes substantial computing resources and hence results in long execution times. An interesting solution that can be used in broad-brush or screening-level modelling is to utilize a Generic, or Reduced reaction set. Work of this kind first appeared in ITM XIV (2000) and subsequently has been represented by a slow trickle of papers. I believe this idea could only arise from a community of meteorological (rather than chemical) modellers, and constitutes a new idea in air pollution modelling.

1.6 What Comes Next?

I am acutely aware of the dangers inherent in ignoring Nils Bohr who said: *"Prediction is very difficult, especially if it's about the future"*. I will not make a prediction, but rather hide behind the term extrapolation, which specifies the process, if not the result!

I believe regional to global modelling of a variety of pollutants will dominate the science of air pollution modelling in the near term. This will be expressed in both more detailed modelling studies, and more comprehensive model evaluation exercises.

I believe also that the topics of Sects. 1.5.2, 1.5.3 and 1.5.4 will become important themes in air pollution modelling, and hence the ITM series of meetings. Specifically, I believe LES/DNS modelling holds promise for developing insights into atmospheric dispersion, especially at a fine scale such as in urban settings. This topic is of particular concern with growing fears of deliberate releases of biological or radioactive materials in cities. While operational prediction at fine scales using LES modelling is not yet feasible, growth in computing capacity could one day make this a reality.

1.7 Conclusion

The development of ideas in air pollution modelling is not unique to the ITM series of meetings, but it can be easily argued that work presented at this series through the past has tracked, if not lead developments in the field. Air pollution modelling is a strongly applied field, being driven by needs in the regulatory and environmental sectors. These needs have provided funds and motivation to conduct the research, but have only been met by the creativity, ingenuity and industry of the small group of scientists who make up the ITM community.

Questions and Answers

Questioner: Peter Builtjes (question put in e-mail to speaker)
Question: Why did you not include data-assimilation as an important topic for the future?
Answer: I accept fully your idea that data assimilation will be an important topic in future. Thank you for pointing out my omission.

Questioner: Stefano Galmarini
Question: Given that air pollution modelling does not seem to improve comparably to the effort put in, what are the next steps in model development that would allow us to talk about third generation models?

Answer: We should not assume that there will be a third generation! If there is to be one, I believe it will be in the area of fully coupled LES flow and chemistry models. I believe your PhD work pointed in this direction.

Questioner: Silvia Trini-Castelli
Question: Your suggestion is to move to global scales since physical processes are cross-scale. However, when considering global modelling, physical processes that are fundamental for atmospheric boundary layers are not properly solved and described. This means that, since the atmosphere is characterized by multi-scale processes, properly modelling them would remain an unresolved and unfolded problem. Can you comment on this?
Answer: I believe this is another way of expressing the idea that turbulence remains a fundamentally unsolved problem in physics. I say this because one of the defining characteristics of turbulent flows is that flow features exist on multiple scales.

Questioner: Heinke Schlunzen
Question 1: Why was local scale and urban scale modelling not mentioned as future developments, keeping in mind that we have the highest concentration values within urban areas (within the canopy layer), and very large spatial and temporal gradients? should seamless models include the local scale?
Answer 1: I agree that matters on urban and local scales are vitally important, mainly because of human population distribution. However, I must point out that the urban scale is a forced scale imposed on the atmosphere, and is therefore not a fundamental (free) scale. I view it as a scale important in the administrative and political realm, but not so in the physical and chemical realm.
Question 2: What do you expect from political pressures on scientists to decide on one model? How can we explain that the one answer wanted by decision makers might not be sufficient?
Answer 2: This is a fundamental problem that we all face, but try to avoid. It all boils down to the politician's dislike of (or inability at) probabilistic thinking. I have no wisdom to offer you, I am ashamed to admit.

Questioner: Jaakko Kukkonen
Question: Do you think that there could be a major breakthrough related to the use of advanced NWP models? There has been substantial progress on those models regarding their functioning on meso- and micro-scales, the treatment of surface processes, etc?
Answer: I think the breakthrough is slowly coming, in the form of operational air pollution modelling. When it comes we will see air pollution forecasts imbedded in weather forecasts, not as after-the-fact add ons, but as part of the entire product.

Questioner: Silvana DiSabatini
Question 1: What is/are the most "striking" contribution(s) of the ITM conferences in terms of impact in advancing science?
Answer 1: I believe the linked activities of ETEX and AQMEII, which arose through the ITM meetings and the ITM community are both striking and unique to the ITM series.

Question 2: Is it possible to talk of a "measurable" effect of these meetings?
Answer 2: The problem is how to "measure". I suppose one could count the number of papers, or citations but both of these approaches are flawed. An additional problem is that ITM presentation does not formally constitute publication so the most notable work in ITM volumes is generally published in the open literature as well.

Questioner: Wouter Lefebvre
Question: How do we bridge the gap between the regulatory "regional scale" with measurement at point locations and discussion about export/import of air pollution on one hand and global scale modelling on the other?
Answer: Your question is closely related to those of both Silvia and Heinke. I am encouraged to hear that we all recognize the fundamental difficulties that arise from the multi-scale nature of atmospheric processes. I wish that I had an encouraging answer to give you, but must admit that I do not.

Questioner: Sven-Erik Gryning
Question: The introduction of data assimilation (linked closely to measurement) resulted in major progress in weather forecasting. How do you see the use of assimilation techniques (also ensemble assimilation) and the fast development in observations (for example remote sensing) in the future of air pollution modelling?
Answer: Peter also mentioned the importance of data assimilation. I agree with him that it is an extremely important approach, and that it will become a substantial part of air pollution modelling in future. My answer to Jaakko implies that data assimilation will be part of the science in future since NWP use this approach.

Questioner: S.T. Rao
Question: Given that NATO is no longer the sponsor of ITMs, what are your suggestions on where ITM should be going in the future in terms of scientific development and global participation?
Answer: I believe the Scientific Committee should expand its membership to include representatives from Asia, South-East Asia, South America and Africa.

Questioner: Clemens Mensink
Question: Did you find any interest in integrated assessment modelling through the history of the ITM?
Answer: Well, this topic does exist in one of our key topics, but we see very few presentations on such work. I suspect that people working in integrated assessment are not aware of the ITM series, and so do not submit their work.

References

McRae GJ, Goodin WR, Seinfeld JH (1982) Development of a second-generation mathematical model for urban air pollution part I. Model formulation. Atmos Environ 16(4):679–696
Slade D (ed) (1968) Meteorology and atomic energy, USAEC,' Hep. No. TID-24190, p 44.5
Steyn DG, Chaumerliac N (eds) (2016) Air pollution modelling and its application XXIV. Springer, Switzerland, p 640. doi:10.1007/978-3-319-24478-5

Chapter 2
A Modeling Study of the Influence of Hemispheric Transport on Trends in O_3 Distributions Over North America

Rohit Mathur, Daiwen Kang, Sergey Napelenok, Jia Xing and Christian Hogrefe

Abstract Changing emission patterns across the globe are resulting in heterogeneous changes in tropospheric chemical composition and likely altering the long-range transport of air pollutants and their impact at receptor regions. In this study, we combine results from multi-decadal simulations with the WRF-CMAQ model with source-region sensitivity information derived with the Decoupled Direct Method (DDM) to examine trends in long-range transport contributions to background O_3 concentrations at receptor regions.

2.1 Introduction

Strategies for reduction in pollution levels of surface air over a region are complicated not only by the interplay of local emission sources and complex physical, chemical, dynamical processes in the atmosphere, but also by the hemispheric background levels of pollutants. Contrasting changes in emission patterns across the globe (e.g. declining emissions in North America and Western Europe in response to implementation of control measures and increasing emissions across Asia, Central America, and Eastern Europe due to economic and population growth) are resulting in heterogeneous changes in the tropospheric chemical composition which are likely altering long-range transport impacts and, consequently, background pollution levels at receptor regions. To investigate these issues, the coupled Weather Research and Forecasting—Community Multiscale Air Quality (WRF-CMAQ) model is expanded to hemispheric scales and multi-decadal model

R. Mathur (✉) · D. Kang · S. Napelenok · C. Hogrefe
Computational Exposure Division, National Exposure Research Laboratory, U.S. Environmental Protection Agency, Research Triangle Park, NC, USA
e-mail: mathur.rohit@epa.gov

J. Xing
School of Environment, Tsinghua University, Beijing, China

C. Mensink and G. Kallos (eds.), *Air Pollution Modeling and its Application XXV*, Springer Proceedings in Complexity, DOI 10.1007/978-3-319-57645-9_2

simulations were recently performed for the period spanning 1990–2010 to examine changes in air pollution across the Northern hemisphere resulting from changes in emissions over this period (Xing et al. 2015).

2.2 Model Setup

The coupled WRF-CMAQ modeling system (Wong et al. 2012) was exercised for a 21-year period spanning 1990–2010 to simulate changes in tropospheric ozone (O_3) resulting from changes in anthropogenic emissions during this period. Model simulations were performed over a domain encompassing the entire Northern Hemisphere (Fig. 2.1), set on a polar stereographic projection and discretized with a horizontal grid spacing of 108 km (cf. Mathur et al. 2012, 2014). Year specific emissions for the Northern Hemispheric domain were derived from the EDGARv4.2 global emission inventory (Xing et al. 2015). The CB05 chemical mechanism was used to represent gas-phase photochemistry. In addition, O_3 mixing ratios in the top most model layer (~50 hPa) were modulated based on scaling of the spatially and temporally varying potential vorticity fields to represent possible effects associated with stratosphere-troposphere exchange (Mathur et al. 2008).

The entire Northern Hemisphere modeling domain was divided into seven source regions (see Fig. 2.1) nominally representing: (1) North America (NAM), (2) Europe and Russia (EUR+RUS), (3) East and Southeast Asia (EAS+SEA), (4) South Asia (SAS; the Indian subcontinent), (5) Northern Africa and the Middle East (NAF+MDE), (6) Central America (CAM), and (7) Other (the rest of the

Fig. 2.1 The Northern Hemisphere modeling domain and source region definition

geographic domain). The CMAQ model configured with the decoupled direct method (DDM; Napelenok et al. 2008) was then exercised over an annual cycle for the base year 2006 to estimate the sensitivity (S_j) of O_3 to nitrogen oxides (NO_x) and volatile organic compound (VOC) emissions from each source region, j. The estimated long-range transport of O_3 to a receptor region, m, can then be estimated as $\sum S_j$ for $j \neq m$. Further, if ΔE_j^N is the change in emission for year N relative to the base year and C^N is the simulated concentration for year N, then the receptor region concentration due to long-range transport may be approximated by the Taylor series expansion combining the DDM-based sensitivity estimates and the concentration predictions for each year in the 21-year period as:

$$C_{LRT,m}^N = \left(\sum_{j \neq m} S_j \Delta E_j^N \right) \left(C^N / \sum S_j \Delta E_j^N \right).$$

In the equation above, the first term is the first-order Taylor series approximation, while the second term represents a renormalizing factor acknowledging the challenges in reconstructing a non-linearly evolving field with first-order approximations.

2.3 Results and Discussion

Figure 2.2 presents examples of simulated source-region fractional contributions to boundary layer and seasonal-average O_3 levels for two source regions: North America and East and Southeast Asia. The impact of long-range inter-continental transport of O_3 across the Pacific and Atlantic Oceans are evident from this

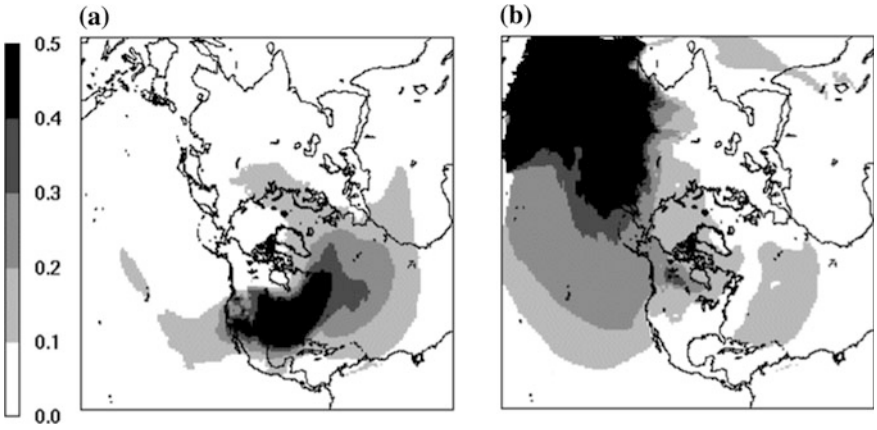

Fig. 2.2 Source region fractional contributions to boundary-layer and seasonal average (Spring) O_3 mixing ratios for **a** North America (NAM), and **b** East and Southeast Asia (EAS+SEA)

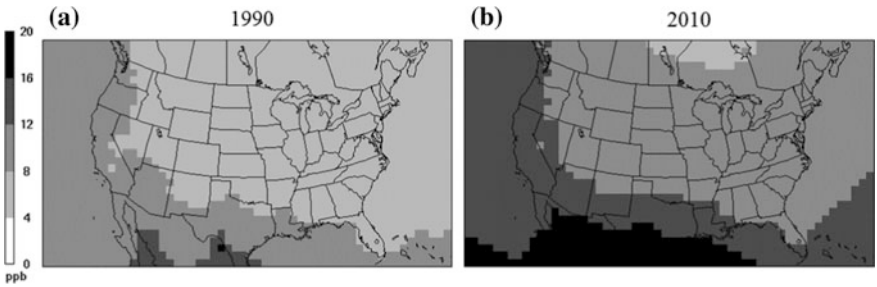

Fig. 2.3 Estimated boundary-layer average O_3 during Spring (March–April–May) from long-range transport during **a** 1990 and **b** 2010

illustration, with emissions from a continent contributing up to several percent to the O_3 mixing ratios in the boundary layer over other continents.

Figure 2.3 presents estimated O_3 over the U.S. attributable to long-range transport using the methodology summarized in Eq. 1 for the years 1990 and 2010. The difference in O_3 mixing ratios between these years is representative of the increasing contributions, over the past two decades, of long-range transport to O_3 within the U.S. boundary layer.

These results emphasize the impact of contrasting changes in emission patterns across the globe on altering long-range transport impacts and consequently background O_3 levels at receptor regions. The expansion of CMAQ to hemispheric scales provides a consistent framework to assess such changes. Additionally, the combination of DDM sensitivity estimates with multi-decadal model calculations enables the examination of both seasonal changes and source region contributions to background pollution levels at receptor regions.

Disclaimer: Although this work has been reviewed and approved for publication by the U.S. Environmental Protection Agency, it does not necessarily reflect the views and policies of the agency.

Questions and Answers

Questioner: S. Aksoyoglu
Question: Was there any change in vegetation and then biogenic emissions between 1990 and 2010 represented in the model?
Answer: The land-use was kept constant during this period as there exists no dataset to consistently represent changes across all the land-use categories used in the model over the multi-decadal period examined here. Thus possible impacts of changes in vegetation were not reflected in the biogenic emission estimates. Biogenic emissions however did change due to changes in temperature and radiation during this period and seasonally to the land cover.

Questioner: S. Galmarini
Question: Can you briefly illustrate the advantages of scaling up the modeling efforts from a more detailed experience (e.g., from regional to global)? What are the advantages?
Answer: Our past attempts at linking regional and global scales models has met with mixed success, in that biases from the larger model often propagate to the regional scale and confound interpretation of results. The primary motivation for scaling up was to have consistency in process representations across all scales. Thus, one now has a consistent modeling framework (in terms of process biases/errors) to enable examination of the effects of long-range transport on regional pollution. Scaling up however did necessitate the inclusion of additional processes to accurately represent longer term processes (e.g., organic nitrate chemistry), new environments (marine emissions), and careful examination of 3-D transport.

Questioner: Kaj Mantzius Hansen
Question: The stratospheric contributions to surface O_3 concentrations appear to be significant. Have you investigated the trends in this contribution over the simulated period?
Answer: Stratospheric contributions to surface and boundary layer O_3 are not limited only to episodic and local deep intrusion events. Our results support the notion that some fraction of the O_3 in the mid-lower troposphere originated in the stratosphere, and is gradually transported downwards through synoptic features and deep clouds and eventually entrained to the boundary layer. Thus O_3 in air masses entering North America likely have both an inter-continental anthropogenic components and a stratospheric contribution. We use a potential-vorticity scaling to specify O_3 at our model top (50 mb)—thus the modeled stratospheric contribution responds to changing dynamics over the two decade period but not say to any plausible effects associated with the recovery of the ozone hole. Trends in the stratospheric contribution is intriguing and should be investigated—unfortunately the current simulations do not allow for a detailed investigation of this nature.

References

Mathur R, Lin H-M, McKeen S, Kang D, Wong D (2008) Three-dimensional model studies of exchange processes in the troposphere: use of potential vorticity to specify aloft O_3 in regional models. In: 2008 CMAS conference. http://www.cmascenter.org

Mathur R, Gilliam R, Bullock OR, Roselle S, Pleim J, Wong D, Binkowski F, Streets D (2012) In: Steyn DG, Trini Castelli S (eds) Extending the applicability of the community multiscale air quality model to hemispheric scales: motivation, challenges, and progress, air pollution modeling and its applications, vol XXI. Springer, pp 175–179

Mathur R, Roselle S, Young J, Kang D (2014) Representing the effects of long-range transport and lateral boundary conditions in regional air pollution models. In: Steyn DG et al (eds) Air pollution modeling and its application, vol XXII. doi:10.1007/978-94-007-5572-2_51. Springer, pp 303–308

Napelenok S, Cohan D, Odman MT, Tonse S (2008) Extension and evaluation of sensitivity analysis capabilities in a photochemical model. Environ Model Softw 23(8):994–999

Wong DC, Pleim J, Mathur R, Binkowski F, Otte T, Gilliam R, Pouliot G, Xiu A, Young JO, Kang D (2012) WRF-CMAQ two-way coupled system with aerosol feedback: software development and preliminary results. Geosci Model Dev 5:299–312. doi:10.5194/gmd-5-299-2012

Xing J, Mathur R, Pleim J, Hogrefe C, Gan C-M, Wong DC, Wei C, Gilliam R, Pouliot G (2015) Observations and modeling of air quality trends over 1990–2010 across the Northern Hemisphere: China, the United States and Europe. Atmos Chem Phys 15:2723–2747. doi:10.5194/acp-15-2723-2015

Chapter 3
Dynamic Evaluation of Two Decades of CMAQ Simulations over the Continental United States

Marina Astitha, Huiying Luo, S. Trivikrama Rao, Christian Hogrefe, Rohit Mathur and Naresh Kumar

Abstract This paper focuses on dynamic evaluation of the CMAQ model over the continental United States using multi-decadal simulations for the period from 1990 to 2010 to examine how well the changes in observed ozone air quality induced by variations in meteorology and/or emissions are simulated by the model. We applied the anomalies method where changes in observed and modeled 4th highest, 95th, 90th and 85th percentile of summertime (May–September) daily maximum 8-h (DM8HR) ozone concentrations are compared for all monitoring stations in the USA. We also applied spectral decomposition of ozone time-series using the KZ filter to assess variations in the strengths of synoptic (weather-induced variations) and baseline (long-term variation forcings), embedded in the simulated and observed concentrations. The results reveal that CMAQ captured the year-to-year variability (more so in the later years than the earlier years) and the synoptic forcing in accordance with what the observations are showing. We examine methods to identify the strengths of the model in representing the changes in simulated O_3 air quality over this period that can guide the development of approaches for a more robust analysis of emission reduction scenarios.

3.1 Introduction

There have been numerous studies focusing on the operational evaluation of regional air quality models and less on the other three components of the model evaluation framework recommended by Dennis et al. (2010). Despite the substantial

M. Astitha (✉) · H. Luo · S. Trivikrama Rao
Department of Civil & Environmental Engineering, University of Connecticut, Storrs-Mansfield, CT, USA
e-mail: marina.astitha@uconn.edu

C. Hogrefe · R. Mathur
U.S. Environmental Protection Agency, Research Triangle Park, NC, USA

N. Kumar
EPRI, Palo Alto, CA, USA

C. Mensink and G. Kallos (eds.), *Air Pollution Modeling and its Application XXV*, Springer Proceedings in Complexity, DOI 10.1007/978-3-319-57645-9_3

improvement in our understanding of the atmospheric physics and chemistry and availability of high-quality model input data, the common model performance metrics such as correlation, mean bias, and root mean square error are still in use over the past two decades. The assessment of a model's ability to reproduce changes in observed air quality conditions is known as the dynamic evaluation and is one of the key components for building confidence in model's use for policy analysis. This paper presents the dynamic evaluation of the CMAQ model over the continental United States for previously conducted multi-decadal simulations for the period from 1990 to 2010 (Gan et al. 2015). The methodology and discussion section include concluding remarks on how well the changes in observed ozone air quality induced by variations in meteorology and/or emissions are simulated by the model.

3.2 Methodology

3.2.1 Data and Models

Time series of the summertime (May–September) DM8HR ozone observations and CMAQ-simulated concentrations covering the continental US from 1990 to 2010 were used in this work. The observations were selected based on quality-assured ozone measurements that have at least 80% data coverage at each monitoring location using EPA's AQS database (186 stations). The simulated concentrations originate from the coupled WRF-CMAQ (Version 5.0.1) with 36-km grid cells over the USA driven with internally consistent historic emission inventories and boundary conditions derived from the hemispheric CMAQ model (Gan et al. 2015).

3.2.2 Data Analysis Techniques

The KZ filter (Rao et al. 1997) was utilized for the spectral decomposition of the DM8HR ozone time series into short-term (synoptic reflecting weather-induced variation) and long-term (baseline reflecting seasonality, emissions loading, policy, and trend) components. The scale separation reveals important information about the components embedded in observed and modeled time series of air pollutant concentrations as to understand the driving forces that control the exceedances. Changes in DM8HR and 4th highest ozone concentrations are estimated for 5-year and 10-year intervals, using all possible combinations within the 21-year period. The observed changes are compared against the modeled changes to determine the model's skill in capturing the changes that occur in the ozone concentration.

3.3 Results and Discussion

The correlation between observed and modeled components (synoptic and baseline) indicates how capable the model is in reproducing the observed patterns. The baseline component is controlled by the changes in emissions, whereas the synoptic component indicates weather-induced effects in the concentrations. The comparison showed that CMAQ better reproduces the baseline and synoptic components in the later year (2010) than in the earlier year (1990), possibly reflecting the use of bet-ter emissions inventory (Fig. 3.1). The synoptic component is reproduced better than the baseline in both years, which is expected since the retrospective model simulations were configured using 4-D data assimilation for the weather variables. Similar results highlighted for NE US were also found for the other sub-regions.

The year-by-year changes in the 4th highest ozone concentration for NE US present a larger scatter and variability in the earlier years (Fig. 3.2, left plot, blue colors) that becomes reduced when looking at the changes in the most recent years during the 21-y framework (Fig. 3.2, left plot, red colors).

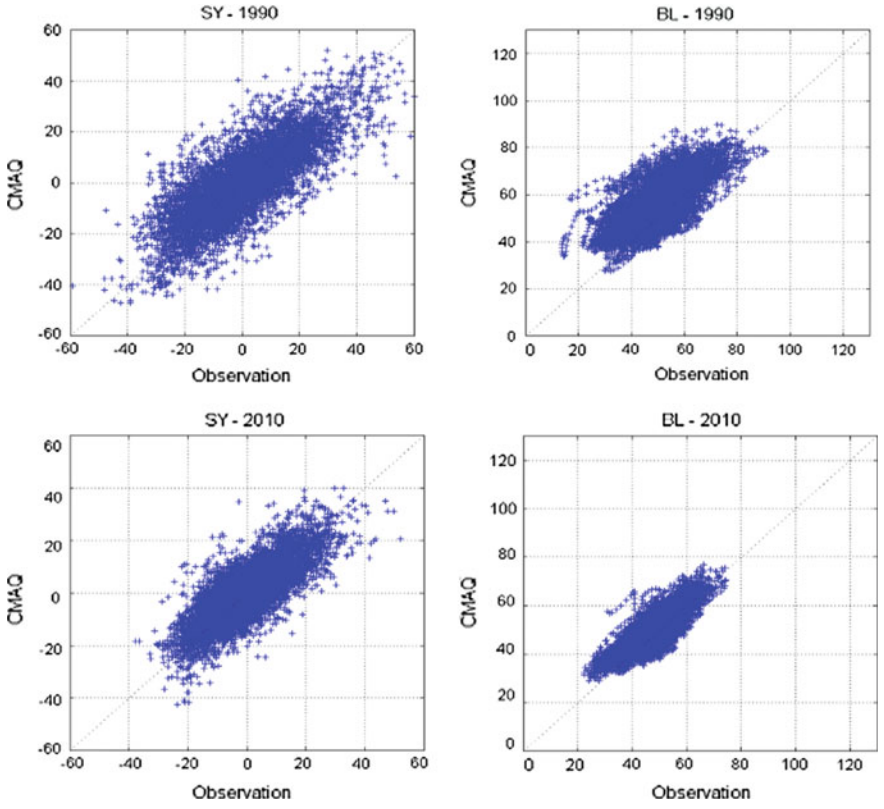

Fig. 3.1 Spectral decomposition of the DM8HR ozone concentrations at 63 stations in NE US. Synoptic component (SY) on the *left plots* and baseline component (BL) on the *right plots*

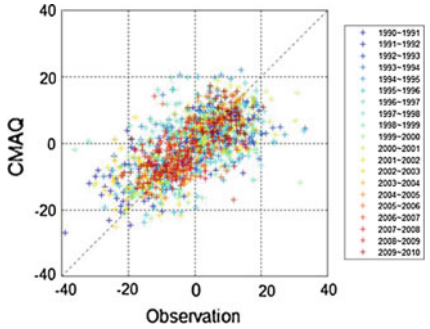

Metrics	R	IA	RMSE
4th highest	0.63	0.78	8.82
95 percentile	0.69	0.81	7.35
90 percentile	0.74	0.84	6.06
85 percentile	0.76	0.85	5.36
median	0.72	0.82	3.91
Inter-quantile	0.39	0.64	4.09
average of top10	0.70	0.82	7.42

Fig. 3.2 *Left plot* Year-by-year changes in CMAQ versus observed 4th highest ozone concentration for NE US. *Right table* Statistical results for the entire dataset shown in the *left plot* (correlation R, Index of Agreement IA, RMSE) for NE US

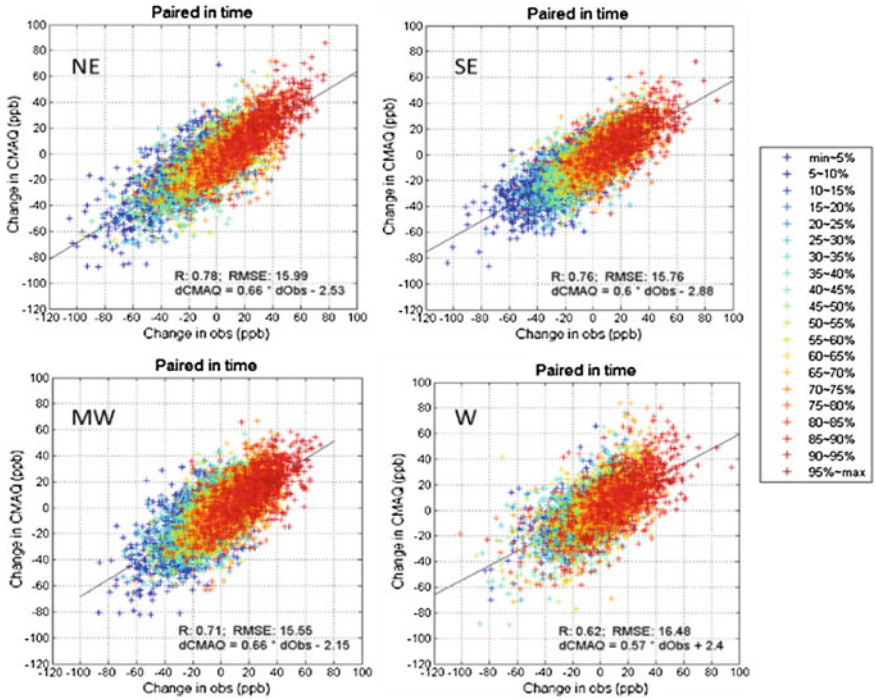

Fig. 3.3 Percentiles of the changes in CMAQ compared to changes in observed DM8HR ozone concentration for each sub-region (color coded based on observations for 2010). The changes are calculated as the difference 2000–1990

Looking at 2 years with very distinctive emissions, 1990 and 2000, the changes in the modeled DM8HR ozone concentration compare well to changes in the observations for NE, SE and MW. There is a larger scatter in the upper percentiles for the Western region that is shown by higher RMSE and lower R (W in Fig. 3.3).

The dynamic evaluation of 21-years of WRF-CMAQ simulations has provided quantitative metrics about the skillfulness of the model in representing the changes in ozone concentration. One notable conclusion is the dependence of the results on the analyzed region as well as the specific year interval. More details will be presented and discussed at the time of the podium presentation.

Acknowledgements Although this work has been reviewed and approved for publication by the U.S. Environmental Protection Agency, it does not reflect Agency's views and policies. Two of the authors (MA and HL) gratefully acknowledge the support of the Electric Power Research Institute (EPRI) for this research under Contract #00-10005071, 2015–2017.

Questions and Answers

Questioner: Clemens Mensink
Question: Do you have any idea why the Southwest behaves differently? Is there some interesting information hiding in it?
Answer: The meteorology and physical environment of the western part of the domain, and especially California, is challenging. We expect that the coastal stations will not be represented accurately in the 36-km simulations but other locations show also a lower correlation with the measured ozone values. One notable conclusion from our work is that for the recent 10-years (2000–2010), the model predictions are improved in terms of the error, compared to the prior 10-years (1990–2000). We suspect that the emissions might play a significant role in this behaviour and we plan to look into the details of the prediction for this area in the following months.

Questioner: Richard G. Derwent
Question: NOAA Boulder (David Parish) has assembled a long-term time series of baseline ozone at the Trinidad Head station in California. None of the global chemistry transport models in the ACCMIP inter-comparison exercise is able to reproduce the observed time trend and seasonal cycle at this baseline station. How well does your CMAQ implementation perform against this dataset?
Answer: Thank you for mentioning this dataset. We have only used surface measurements from the AQS network so far. It is a great opportunity to look at the Trinidad Head time series when we perform a more detailed analysis for California and understand the model behaviour over the 21-year framework.

Questioner: Sarav Arunachalam
Question: Instead of grouping 186 monitors by 4 regions of the country, have you considered looking at the rural versus urban locations and looking at how synoptic scales (BL vs. SY) are affected in your dynamic evaluation?
Answer: Kristen Foley of EPA has done this type of urban versus rural analysis (presented at the A&WMA 108th Annual Conference) with the same dataset, looking at all percentiles of the ozone distribution. It would be interesting to look at

the baseline versus synoptic forcing of the ozone decomposition in the same way but we haven't worked on that to avoid duplicating previous work.

Questioner: Peter Viaene
Question: Extend of the domain? Seems there are boundary condition effects in the results.
Answer: The boundary conditions were derived from the hemispheric CMAQ model ensuring compatibility with the regional simulations. We cannot conclude at this point that the boundary conditions significantly affect the correlation with the observations since some of the poor-performing stations are not directly located near the boundaries. Our future work will reveal these relationships in a more robust way.

References

Dennis R, Fox T, Fuentes M, Gilliland A, Hanna S, Hogrefe C, Irwin J, Rao ST, Scheffe R, Schere K, Steyn D, Venkatram A (2010) A framework for evaluating regional-scale numerical photochemical modeling systems. Environ Fluid Mech 10(4):471–489

Gan CM et al (2015) Assessment of long-term WRF–CMAQ simulations for understanding direct aerosol effects on radiation "brightening" in the United States. Atmos Chem Phys 15:12193–12209. doi:10.5194/acp-15-12193-2015

Rao ST, Zurbenko I, Neagu R, Porter PS, Ku JY, Henry R (1997) Space and time scales in ambient ozone data. Bull Am Meteor Soc 78(10):2153–2166

U.S. EPA (2014) Modeling guidance for demonstrating attainment of air quality goals for ozone, PM2.5, and regional haze—December 2014 DRAFT. http://www.epa.gov/scram001/guidance/guide/Draft_O3-PM-RH_Modeling_Guidance-2014.pdf

Chapter 4
On Regional Modeling to Support Air Quality Policies

S. Trivikrama Rao, Huiying Luo, Marina Astitha, Christian Hogrefe, Rohit Mathur and Naresh Kumar

Abstract We examine the use of the Community Multiscale Air Quality (CMAQ) model in simulating the **changes** in the extreme values of air quality that are of interest to the regulatory agencies. Year-to-year changes in ozone air quality are attributable to variations in the prevailing meteorology and emissions loading over the contiguous United States. To this end, we spectrally decomposed the daily maximum 8-h (MDA8) ozone time-series for the period from 1990 to 2010 using the Kolmogorov-Zurbenk (KZ) filter to examine the variability in the relative strengths of the synoptic forcing (i.e., short-term variation induced by weather fluctuations) and the baseline forcing (i.e., long-term variation induced by emissions, policy, and trends) embedded in model output and observations. Using the information extracted from the synoptic and baseline forcings in ozone observations over the 21-year period, we present a new method for applying regional ozone air quality models in the regulatory setting. The new method provides the confidence limits for the 4th highest MDA8 ozone value and number of ozone exceedances for a given emission reduction scenario. This information is useful to policy-makers in deciding upon the emission control policy that can help meet and maintain the ozone National Ambient Air Quality Standard.

S. Trivikrama Rao (✉) · H. Luo · M. Astitha
Department of Civil & Environmental Engineering, University of Connecticut, Storrs, CT, USA
e-mail: strao@ncsu.edu

C. Hogrefe · R. Mathur
U.S. Environmental Protection Agency, Research Triangle Park, Durham, NC, USA

N. Kumar
EPRI, Palo Alto, CA, USA

C. Mensink and G. Kallos (eds.), *Air Pollution Modeling and its Application XXV*, Springer Proceedings in Complexity, DOI 10.1007/978-3-319-57645-9_4

4.1 Introduction

Regional-scale air pollution models are being used by environmental agencies world-wide for determining compliance with the air quality standards. In the United States, regional air quality models are being used to design emission controls needed to comply with the ozone standard (i.e., the 4th highest daily maximum 8-h ozone concentration in each year averaged over a consecutive 3-year period to be at a specified level). Confidence in model estimates of air pollutant distributions and their changes is often established through comparison with corresponding observations made at discrete locations for the base case simulation. Because of the uncertainties in model inputs and parameters and disparities associated with comparing volume-averaged model estimates with point measurements, accurate simulation of observed concentrations or their changes cannot always be expected (Dennis et al. 2010). Thus, comparisons of modeled and observed concentrations paired in space and time often reveal biases in the ability of models to reproduce the absolute concentration levels or observed changes. This is particularly true at the upper tail of the concentration cumulative frequency distribution, which can raise concerns regarding the use of the model to quantify the effectiveness of emission reductions in reducing the 4th highest ozone concentration to the level of the standard.

In an effort to improve upon the current method for using regional air quality models in the regulatory context (USEPA 2014), we analyzed 21-years of ozone observations and CMAQ model outputs for the contiguous United States. We examined the variability in the extreme values stemming from changes in emissions and meteorology during the 1990–2010 period, and present a potential new method for building confidence in using regional air quality models for policy support.

4.2 Data and Method of Analysis

Ozone data covering the contiguous United States (CONUS) were extracted from the U.S. Environmental Agency's (US EPA) AQS. Only those monitoring stations that had 80% of data coverage during May–September for the 1990–2010 period are analyzed in this study. Air quality modeling simulations were performed for the years 1990–2010 with the in-line coupled Weather Research and Forecasting (WRF)—CMAQ v.5.0. The model domain covered the CONUS at horizontal grid spacing 36 km and with 35 vertical layers between the surface and 100 mb. Emissions for the 36 km CONUS simulations incorporated information from US EPA's National Emissions Inventory for the years 1990, 1995, 1996, 1999, 2001, 2002 and 2005 and information on trends of activity data and emission controls that have been implemented over the entire period. Biogenic emissions were estimated in-line during the WRF-CMAQ simulation using BEIS, with effects of meteorology on emissions.

Ozone can be thought of as the baseline of pollution formed by the emitting sources and is modulated by the prevailing meteorology. The combination of the baseline level and associated synoptic forcing controls extreme ozone concentration levels. Hence, time series of observed and modeled daily maximum 8-h ozone concentrations for the 1990–2010 period have been spectrally-decomposed into the short-term (weather-induced variations) and long-term (variations attributable to the seasonality, policy, and trends) components using the KZ filter (Rao et al. 1997).

4.3 Results and Discussion

In this study, we evaluate the year-to-year variability in the strengths of the short-term (synoptic forcing) and long-term (baseline forcing) components during these two decades. Figure 4.1 displays the observed (a and c) and modeled (b and d) ozone time series along with the embedded baseline concentration during May through October in 1994 and 2009, respectively, at Essex, MD. Because of the implementation of emission control programs on the utility and mobile source sectors, there has been a substantial improvement in ozone air quality from 1994 to 2009. While the 4th highest ozone was 94 ppb in 1994, it was reduced to 76 ppb in 2009; the number of

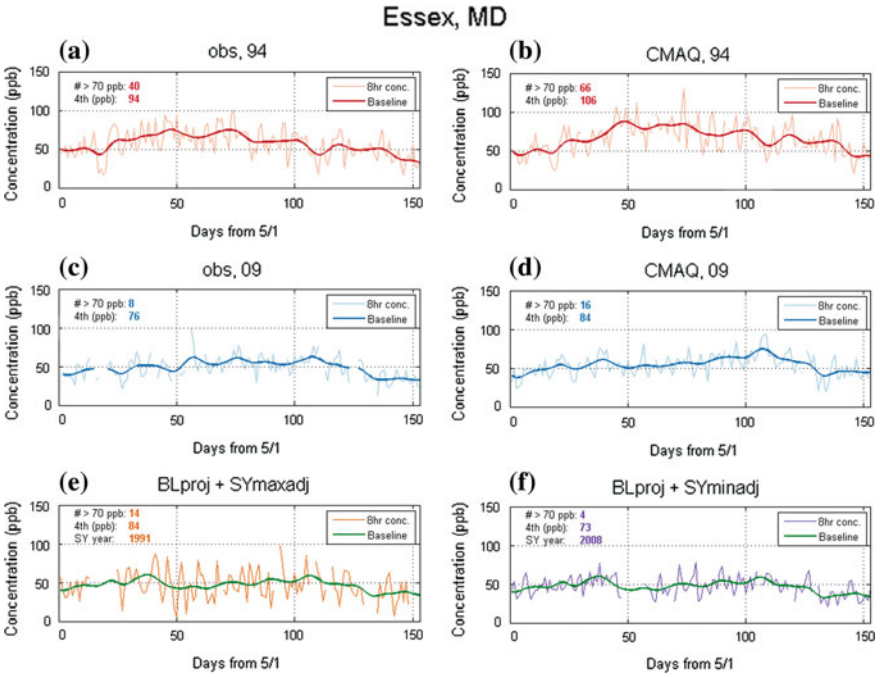

Fig. 4.1 Observed (**a**) and modeled (**b**) ozone time series in 1994 and in 2009 (**c** and **d**). The upper and lower bounds for the ozone time series projected to 2009 using the CMAQ results are presented in (**e**) and (**f**), respectively

days exceeding 70 ppb was 40 in 1994, but only 8 in 2009. At this site, CMAQ overestimated these variables of concern to the regulatory agencies in both years. Astitha et al. (2016) have demonstrated that CMAQ is better at simulating year-to-year changes in ozone levels than the absolute concentration levels.

In the following, we present an approach to estimate the ozone levels that would be expected with changing emissions by determining the change in the baseline concentration between 1994 and 2009 as predicted by CMAQ, and adding this change to the observed 1994 baseline level to project the baseline concentration to be expected in 2009. Then, we superimposed the strongest and weakest synoptic forcings that prevailed in observed ozone time series during the 1990–2010 period upon the projected baseline level to determine the upper (Fig. 4.1e) and lower bounds (Fig. 4.1f) for the ozone concentration time series. The results reveal that observed 4th highest ozone and number of exceedances in Fig. 4.1c are contained within the projected time series (Fig. 4.1e, f). Similar results have been found at many sites in the eastern United States (Fig. 4.2), indicating the appropriateness of this method to estimate confidence bounds for the 4th highest ozone concentration and the number of ozone exceedances for a given emission reduction scenario. With CMAQ's 36-km grid cell size, it is difficult to capture the variability observed in ozone near large water bodies, coastal and urban core areas, and complex terrains (see red dots in Fig. 4.2).

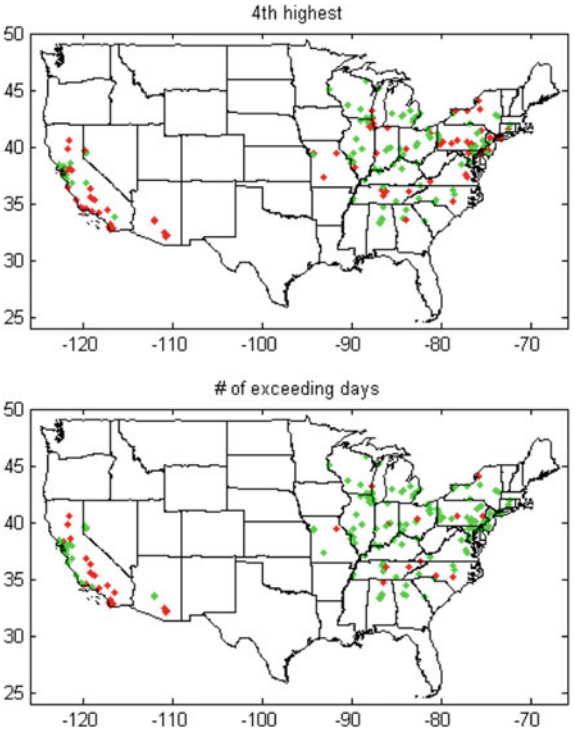

Fig. 4.2 *Green dots* represent the locations where the observed 4th highest ozone and exceedances are within the confidence bounds for the estimated values

4.4 Summary

Capturing the extreme values is challenging for regional models given uncertainties in input data and model physics and chemistry, but our analysis revealed that there is greater confidence in model estimates of the changes in the baseline concentration stemming from changes in emissions. Given the linkage between the baseline concentration level and extreme values, we can estimate the associated 4th highest value and number of ozone exceedances and determine their confidence bounds by superposing stronger versus weaker synoptic forcing acting on the baseline concentration. Thus, model-based assessments that focus on the impact of emission changes on the baseline concentration level could provide greater confidence in policy inferences.

Acknowledgements Although this work has been reviewed and approved for publication by the U.S. Environmental Protection Agency, it does not necessarily reflect the Agency's views and policies. Two of the authors (MA and HL) gratefully acknowledge the support of this work by the Electric Power Research Institute (EPRI) Contract #00-10005071, 2015–2017.

References

Astitha M, Luo H, Rao ST, Hogrefe C, Mathur R, Kumar N (2016) Dynamic evaluation of two decades of CMAQ simulations over the continental United States. ITM, Chania

Dennis R, Fox T, Fuentes M, Gilliland A, Hanna S, Hogrefe C, Irwin J, Rao ST, Scheffe R, Schere K, Steyn D, Venkatram A (2010) A framework for evaluating regional-scale numerical photochemical modeling systems. Environ Fluid Mech 10(4):471–489

Gan CM et al (2015) Assessment of long-term WRF–CMAQ simulations for understanding direct aerosol effects on radiation "brightening" in the United States. Atmos Chem Phys 15:12193–12209. doi:10.5194/acp-15-12193-2015

Rao ST, Zurbenko I, Neagu R, Porter PS, Ku JY, Henry R (1997) Space and time scales in ambient ozone data. Bull Am Meteor Soc 78(10):2153–2166

U.S. EPA (2014) Modeling guidance for demonstrating attainment of air quality goals for ozone, PM2.5, and regional haze—December 2014 DRAFT. http://www.epa.gov/scram001/guidance/guide/Draft_O3-PM-RH_Modeling_Guidance-2014.pdf

Chapter 5
The Impact of "Brightening" on Surface O_3 Concentrations over Europe Between 1990 and 2010

Emmanouil Oikonomakis, Sebnem Aksoyoglu, Urs Baltensperger and André S.H. Prévôt

Abstract Since 1990 the O_3 precursor emissions (NO_x, VOC) have been reduced in Europe. Observations of O_3 concentrations, however, don't match the expected changes based on emission reductions. An increasing trend in surface solar radiation (SSR) ("brightening") has been detected since the mid-80s as a result of decreased particulate matter (PM) concentrations. In this study we use the regional air quality model, CAMx (Comprehensive Air Quality Model with extensions) to simulate and quantify the effect of increased radiation on photochemistry and surface O_3 concentrations over Europe between 1990 and 2010. The year 2010 was used as the base case. Two sensitivity runs were performed to investigate the effect of radiation on photolysis rates and biogenic emissions as they affect surface O_3. The first scenario examined the effect of a 50% increase in PM_{10} (corresponding to PM_{10} in Europe in summer of 1990) applied only to the calculation of photolysis rates. This isolated the radiative effect of PM on tropospheric O_3 chemistry from other influences. The PM_{10} adjustment factor is based on a trend analysis of observational data from the literature. In the second scenario, we reduced the SSR by 5% (keeping plant cover and temperature the same), based on a similar observational trend analysis, re-calculated the biogenic emissions and re-ran the base case simulations with the new biogenic emissions. Preliminary results for the summer show that increasing PM_{10} has a significant effect on surface O_3, leading to a difference between base case and first scenario of up to 0.7 ppb in the afternoon average. The largest hourly difference was up to 3 ppb. The second scenario had a negligible effect on afternoon average surface O_3 (up to 0.1 ppb) as the change in biogenic emissions was small; the largest hourly difference was up to 2 ppb.

E. Oikonomakis · S. Aksoyoglu (✉) · U. Baltensperger · A.S.H. Prévôt
Laboratory of Atmospheric Chemistry, Paul Scherrer Institute, 5232 Villigen, Switzerland
e-mail: sebnem.aksoyoglu@psi.ch

C. Mensink and G. Kallos (eds.), *Air Pollution Modeling and its Application XXV*,
Springer Proceedings in Complexity, DOI 10.1007/978-3-319-57645-9_5

5.1 Introduction

Efforts to improve air quality led to decreases in precursor emissions over Europe in the last 20 years. However, observed changes in ozone concentrations do not match the predicted levels based on reductions in precursor (NO_x, VOC) emissions (Wilson et al. 2012; Aksoyoglu et al. 2014). Although there is a number of possible factors (e.g., intercontinental transport, stratosphere—troposphere exchange, underestimation of emissions reductions) responsible for this, studies on the impact of solar radiation are scarce. Observations show an increase in the surface solar radiation (SSR) at various European sites after 1980s ("brightening", due to decreased PM concentrations) following the "dimming" period, which took place between the 1950s and 1980s (Wild 2009; Allen et al. 2013). The changes in solar radiation might have an effect on photochemistry and biogenic emissions. In this study we applied the CAMx model to investigate and quantify the Direct Aerosol Effect (DAE) of the PM decreasing trends on the photochemistry and surface ozone concentrations.

5.2 Model Setup

The simulations with CAMx (version 6.3) were performed for the entire year of 2010 using the last two weeks of 2009 as spin up period. The model domain covered Europe in lat/lon coordinates with a horizontal resolution of 0.125° and 0.25° respectively and extended from 35°N to 70°N and 15°W to 35°E with a total number of 14 sigma layers. The meteorological data was calculated by the Weather Research and Forecasting model (WRF-ARW), version 3.7.1, with European Centre for Medium-Range Weather Forecasts (ECMWF) data assimilation. We generated the hourly, gridded anthropogenic emissions for our domain using the TNO-MACIII emission inventory provided by TNO. The biogenic emissions were calculated according to the method described by Andreani-Aksoyoglu and Keller (1995) using meteorological input from WRF-ARW. The initial and boundary conditions were obtained from the MOZART global model data for 2010. The photochemistry in CAMx is performed in two steps. First, clear-sky photolysis rates are calculated externally by the Tropospheric Ultraviolet and Visible (TUV) radiation model and then used as input into CAMx, where they are internally adjusted (using an in-line version of TUV) for clouds, aerosols, pressure and temperature for each time step and each grid cell. In addition, Total Ozone Mapping Spectrometer (TOMS) data were obtained by National Aeronautics and Space Administration (NASA) and served as total ozone column input for both TUV and CAMx. Finally, three simulations were performed for this study. In the first simulation the aforementioned parameterization was used and served as the base case representing the year 2010. In first scenario we changed the source code of in-line TUV inside the CAMx model so that the PM_{10} concentrations in the calculation of Aerosol Optical

Depth (AOD) were considered to be 50% higher as in summer of 1990. This isolated the radiative effect of PM on the photolysis rates. The adjustment factor was based on trend analysis we performed using European air quality database (Airbase) and Swiss National Air Pollution Monitoring Network (NABEL) data for the period 1990 and 2010 and in line with other studies in similar time periods over Europe (Barmpadimos et al. 2011; Xing et al. 2015). In the second scenario we decreased the SSR by 5% (according to Turnock et al. 2015) in our biogenic emission model in order to quantify the impact on the biogenic emissions and we ran CAMx with the new emissions and base case model configuration.

5.3 Results

Model results are shown here for summer which is more relevant for surface O_3 production due to high SSR and temperature. Results for the first scenario show that the afternoon average O_3 concentrations increased by about 0.3 ppb over continental Europe and by up to 0.7 ppb over the Mediterranean Sea (Fig. 5.1). Furthermore, we quantified the maximum impact of the DAE for 50% PM_{10} reduction, where the maximum difference in hourly O_3 concentrations showed an increase up to 1–2 ppb over continental Europe and up to 3 ppb in the Mediterranean Sea (Fig. 5.1). In the second scenario, the impact of 5% increase in SSR had a small effect on biogenic emissions (2–5% for isoprene and 1.5–2.5% for terpenes) and therefore had a negligible effect on surface O_3 concentrations. The difference on afternoon average O_3 concentration was generally lower than 0.05 ppb, while the maximum hourly difference is 0.4–1 ppb (Fig. 5.2). In this sensitivity test, we only considered the direct effect of SSR on biogenic emissions and not the long-term, indirect one that might be important for the plant photosynthesis and growth.

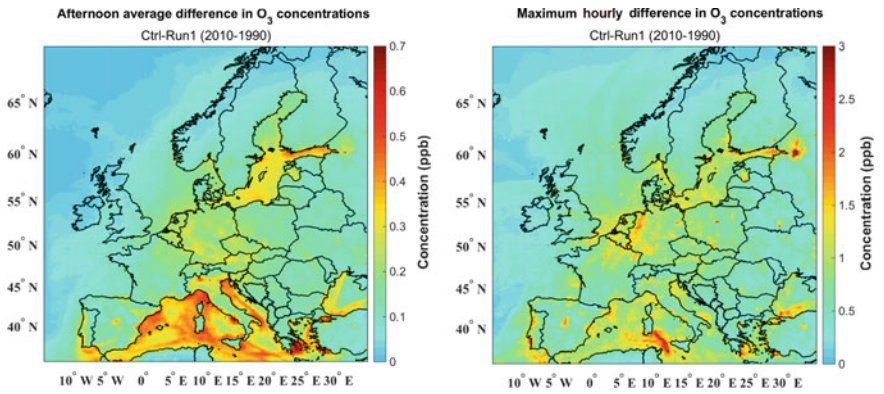

Fig. 5.1 Afternoon average difference (*left*) and maximum hourly difference (*right*) in surface O_3 concentrations for summer 2010 between the base case and the first scenario (DAE of 50% PM_{10} increase)

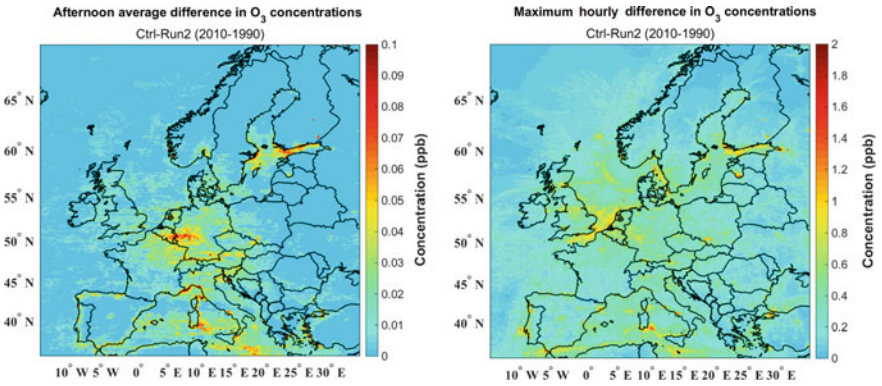

Fig. 5.2 Afternoon average difference (*left*) and maximum hourly difference (*right*) in surface O_3 concentrations for summer 2010 between the base case and the second scenario (effect of 5% SSR decrease on biogenic emissions)

5.4 Conclusions

Two sensitivity runs were performed with the CAMx model to investigate the DAE effect of 50% PM_{10} increase and the biogenic emissions effect due to 5% SSR decrease on ozone. The results of the first scenario indicated that on average the impact is not large on surface O_3 concentrations, but it can be quite significant on specific days and hours in the order of 1–2 ppb over continental Europe. In addition, we expect this impact to be higher by increasing our model's ability to reproduce better the afternoon surface O_3 concentrations (currently it is underestimated). The second scenario suggested a small impact of the 5% SSR decrease in biogenic emissions and the effect on surface O_3 concentrations was also small with the largest difference at some regions being 1–2 ppb. Further sensitivities studies are planned to improve the investigation and quantification of the possible effects of the "brightening" over Europe between 1990 and 2010.

Acknowledgements This work was financially supported by the Swiss Federal Office for the Environment (FOEN). We are grateful to the following people and institutions for providing us with models as well as weather, emission and air quality data: RAMBOLL ENVIRON, University Corporation for Atmospheric Research (UCAR), ECMWF, NASA, European Environment Agency (EEA), NABEL, TNO and Swiss National Supercomputing Centre (CSCS).

Questions and Answers

Questioner: C. Hogrefe
Question: In your approach, the largest photolysis changes occur over areas with the highest PM loading in 2010 (e.g. in areas of large shipping emissions). Do you

have plans to extend the analysis to account for changes in the spatial distribution of aerosol loadings between 1990 and 2010 and how this would impact photolysis rates?
Answer: We examine different ideas for better representation of 1990 conditions for the PM (e.g. spatial distribution, species composition). One idea would be to run CAMx model with the 1990 emission inventory (keeping 2010 meteorology) and use those simulated PM in the sensitivity test mentioned in this study, instead of adjusting by a factor the PM of 2010. This way we take into account the spatial distribution and species composition of the PM as in the year 1990. We don't expect a significant difference in the magnitude of the photolysis rates change, but its spatial distribution will be different as it will follow the new PM spatial distribution.

Questioner: P. Kishcha
Question: The solar brightening phenomenon has a different rate (changes with time) over rural and urban areas in Europe. Was your modeled ozone concentrations trends sensitive to these signal differences in surface solar radiation?
Answer: For the sensitivity test we performed, we adjusted the PM concentration contribution to the calculation of AOD by a relative factor (50%). This implies that the absolute change in solar radiation and thus photolysis rates will be higher in urban areas. Since urban areas have also higher NOx emissions, the impact of solar radiation difference on ozone chemistry might have been larger compared to the rural areas.

Questioner: M. Astitha
Question: I have one clarifying question and one suggestion. For the 1990 simulation did you use the 1990 meteorology and emissions? If not, what would the implications be in your results if the actual year 1990 was simulated and compared to 2010? The suggestion is to present the results using relative instead of absolute changes, given the uncertainties associated with the calculations and assumptions in the design of the sensitivity tests.
Answer: For the 1990 year simulation we used the emissions and meteorology of 2010 and we adjusted the PM concentrations contribution to the calculation of the AOD to represent the PM concentrations in 1990. If we modelled the actual year 1990 with its respective emissions and meteorology, then we wouldn't be able to distinguish the impact of the direct aerosol effect (due to PM reductions) from meteorological or emission inventory changes on the surface ozone concentration differences between 1990 and 2010. Regarding your suggestion, most of the times relative numbers can be misleading. For example in the North Sea the relative maximum change in surface ozone concentrations was 10% but the absolute one was up to 1 ppb, while in the Mediterranean Sea the respective relative change was 5% or less and the absolute change was up to 3 ppb. So I wouldn't replace the absolute changes with relative ones, but instead report both.

References

Aksoyoglu S, Keller J, Ciarelli G, Prévôt ASH, Baltensperger U (2014) A model study on changes of European and Swiss particulate matter, ozone and nitrogen deposition between 1990 and 2020 due to the revised Gothenburg protocol. Atmos Chem Phys 14:13081–13095

Allen RJ, Norris JR, Wild M (2013) Evaluation of multidecadal variability in CMIP5 surface solar radiation and inferred underestimation of aerosol direct effects over Europe, China, Japan and India. J Geophys Res 118:633–6311

Andreani-Aksoyoglu S, Keller J (1995) Estimates of monoterpene and isoprene emissions from the forests in Switzerland. J Atmos Chem 20:71–87

Barmpadimos I, Hueglin C, Keller J, Henne S, Prévôt ASH (2011) Influence of meteorology on PM10 trends and variability in Switzerland from 1991 to 2008. Atmos Chem Phys 11:1813–1835

Turnock ST, Spracklen DV, Carslaw KS, Mann GW, Woodhouse MT, Forster PM, Haywood J, Johnson CE, Dalvi M, Bellouin N, Sanchez-Lorenzo A (2015) Modelled and observed changes in aerosols and surface solar radiation over Europe between 1960 and 2009. Atmos Chem Phys 15:9477–9500

Wild M (2009) Global dimming and brightening: a review. J Geophys Res 114

Wilson RC, Fleming ZL, Monks PS, Clain G, Henne S, Konovalov IB, Szopa S, Menut L (2012) Have primary emission reduction measures reduced ozone across Europe? An analysis of European rural background ozone trends 1996–2005. Atmos Chem Phys 12:437–454

Xing J, Mathur R, Pleim J, Hogrefe C, Gan C-M, Wong DC, Wei C, Gilliam R, Pouliot G (2015) Observations and modeling of air quality trends over 1990–2010 across the Northern Hemisphere: China, the United States and Europe. Atmos Chem Phys 15:2723–2747

Chapter 6
An Analysis of Modelled Long-Term Trends of Sulphur in the Atmosphere

J. A. Arndt, A. Aulinger, J. Bieser, B. Geyer, V. Matthias and M. Quante

Abstract Sulphur emissions have significantly decreased in Europe since the 1980s. Consequently, atmospheric concentrations of sulphur dioxide and particle bound sulphate have decreased, too, but not to the same extent. The oxidation of sulphur dioxide has become more efficient over time, leading to an increased sulphate to sulphur dioxide ratio. The reasons for this were investigated in a long term CMAQ model run covering the period 1985–2007. Observations and model results show the same non-linear relation between sulphur dioxide and particle bound sulphate concentrations. An analysis of the sulphur dioxide oxidation pathways was performed in a box-model simulation using the same algorithms as implemented in the CMAQ model. The oxidation was accelerated over time due to an increase in the hydrogen peroxide concentrations. This was mainly caused by a reduction of the sulphur dioxide concentrations, themselves.

6.1 Introduction

Sulphur compounds belong to the most important air pollutants causing respiratory diseases and acid rain. They mainly stem from combustion of sulphur containing fossil fuels like coal and oil as well as from wood burning. In Europe, sulphur dioxide emissions peaked in the 1980s and have since then decreased a lot. Most of the emissions appear in the form of sulphur dioxide (SO_2, S of oxidation state IV, S(IV)) which is then oxidised in the atmosphere to form sulphuric acid (H_2SO_4, S(VI)) and particle bound sulphate SO_4^{2-} (S(VI)). In the gas phase, OH is the most important oxidant, however, the largest part of the SO_2 oxidation takes place in the wet phase inside cloud droplets. Here, O_3, H_2O_2 and methylhydroperoxide (CH_3OOH) play a role as well as catalytic and non-catalytic reactions with O_2, involving Fe and Mn as catalysts. Reaction rates depend, besides meteorological conditions, on the cloud water pH.

J.A. Arndt · A. Aulinger · J. Bieser · B. Geyer · V. Matthias (✉) · M. Quante
Helmholtz-Zentrum Geesthacht, Max-Planck-Straße 1, 21502 Geesthacht, Germany
e-mail: volker.matthias@hzg.de

C. Mensink and G. Kallos (eds.), *Air Pollution Modeling and its Application XXV*,
Springer Proceedings in Complexity, DOI 10.1007/978-3-319-57645-9_6

Sulphur emission reductions in Europe led to a similar decrease of the SO_2 and SO_4^{2-} concentrations in the atmosphere, however, it has been observed that SO_4^{2-} concentrations decreased to a lower extent than SO_2 concentrations. Jones and Harrison (2011) investigated the relation between SO_2 and SO_4^{2-} concentrations at several EMEP measurement stations between 1999 and 2006 and found a non-linear relation between them for annual means. These observations indicate that more SO_2 is converted to SO_4^{2-} at low SO_2 concentrations. The question why this is the case has been investigated by means of multi-annual CMAQ simulations for entire Europe. Subsequent box-model experiments using parts of the CMAQ code to test different oxidation pathways were set up to investigate the oxidation processes.

6.2 Model Description

The model chain consists of three main model systems, the mesoscale meteorological model COSMO-CLM (Doms and Schättler 2002), the chemistry transport model CMAQ (Byun and Ching 1999) and the emission model SMOKE for Europe (Bieser et al. 2011).

CMAQ was set up in its version 4.6 on a 72×72 km^2 grid for Europe, covering the entire continent. Thirty vertical layers up to 20 hPa were implemented. The CMAQ setup included the CBIV chemistry mechanism and the so called aero4 module for the aerosol phase. CMAQ was run for a period from 15 December 1984 until 31 December 2007. Boundary conditions stem from monthly averages calculated with the global atmospheric chemistry models TM4 (until 2000) and TM5 (from 2001 to 2008) (Huijnen et al. 2010).

For COSMO-CLM the simulation was once initialized in 1948 and then done continuously with a resolution of 0.22°, and 40 vertical levels up to a height of about 27 km (Geyer 2014). The NCEP-NCAR reanalysis I (Kalnay et al. 1996) with a resolution of T62 (approx. 210 km) was used as initial and boundary condition.

The emission data used in this study is based on the CEIP emission inventory. Annual national totals were distributed onto a 5×5 km^2 grid using proxies like population density, road and rail networks as well as land use, depending on emission sector. Large point sources were taken from the point source emission register PRTR and considered individually. The emissions were then accumulated in order to match the coarse grid. The species considered are CO, NO_x, NMVOC, NH_3, and SO_2 as well as PM_{10} and $PM_{2.5}$. PM emissions were split into sector specific chemical compounds, including, among others, SO_4^{2-}, NO_3^- and black carbon.

6.3 Results

First, annual averages of modelled SO_2 and SO_4^{2-} concentrations are compared to observations at selected EMEP stations. Afterwards, in-cloud oxidation pathways were tested with a box model. Figure 6.1 shows the temporal development of the

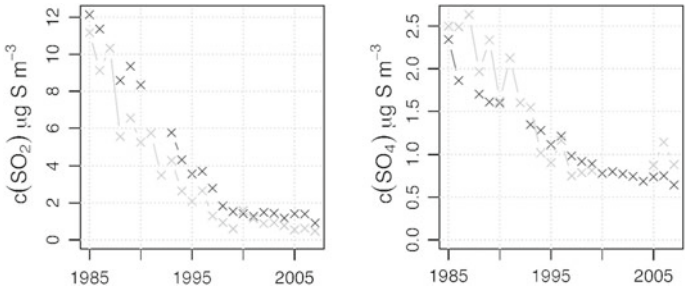

Fig. 6.1 Annual average concentrations of SO_2 (*left*) and SO_4^{2-} (*right*) at Waldhof, Germany, between 1985 and 2007. Modelled values are in *black*, EMEP observations in *grey*

SO_2 and SO_4^{2-} concentrations at Waldhof, Germany, between 1985 and 2007. Model data was not available for 1987, 1991 and 1992 due to a failure in the archive system. Particle bound sulphate observations were not available at Waldhof between 2000 and 2004. At Waldhof, CMAQ was able to reproduce the decreasing concentrations quite well, although SO_2 concentrations were too high ($+1.2\,\mu g/m^3$ S) and SO_4^{2-} concentrations too low ($-0.1\,\mu g/m^3$ S). This was even more pronounced at Jarczew, Poland (not shown). This station is located in an area with high sulphur emissions. Therefore, it is likely that the total emissions are underestimated and the split of the emissions into gaseous SO_2 and particle bound SO_4^{2-} is too much shifted to SO_2.

The relation between SO_2 and SO_4^{2-} concentrations at Jarczew could best be represented by a linear function. At Waldhof the relationship became non-linear in summer, pointing to more efficient oxidation of SO_2 during times with low SO_2 concentrations. These relationships were the same for both, model and observations, and in agreement with the analysis by Jones and Harrison (2011).

A box model has been set up in order to investigate the SO_2 oxidation pathways represented in CMAQ and how they changed over time. The CMAQ model code was extracted and transferred into a R-program. Only the more important wet-phase oxidation was considered. The model was fed with 24-h-average meteorological and concentration data from 90 grid cells in cloud heights over the time period from 1985 to 2007.

Figure 6.2 shows the long-term trends for the conversion rate (per time unit) of S(IV) into S(VI) when the effect of the reduction of SO_2 concentrations is already subtracted. In Fig. 6.2(a) all relevant processes are included. Then they are further split into the dependence on pH (b), concentration of oxidising substances (c) and meteorological conditions (d).

It could be shown that the oxidation of S(IV) into S(VI) accelerated over time. The pH value had a small contribution to this effect, much more important was the increase in the concentration of oxidising substances. Looking in detail into this, it could be shown that H_2O_2 had the highest contribution to the more efficient oxidation rate. O_3, Fe and Mn and other hydroperoxides were of minor importance.

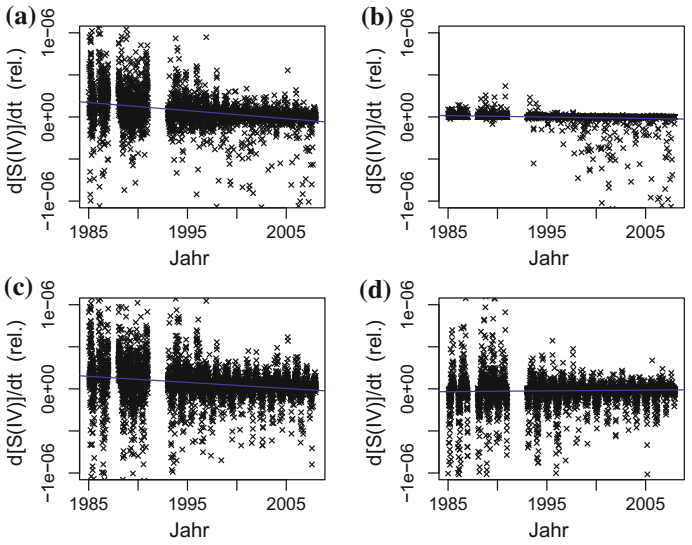

Fig. 6.2 Oxidation rates of S(IV) calculated with the box model OXI-BOX between 1985 and 2007 (**a**) and their dependence on pH (**b**), concentration of oxidising substances (**c**) and meteorological conditions (**d**)

6.4 Conclusions

Decreasing concentrations of oxidised sulphur compounds since the 1980s in Europe could be reproduced with a long-term CMAQ run. The observed non-linear relationship between SO_2 and SO_4^{2-} concentrations was reproduced by the model, too. Box model simulations using the CMAQ algorithms demonstrated that the process that contributed most to the more efficient oxidation of S(IV) in recent years was the increase in H_2O_2 concentrations. This was caused by a significant decrease in the concentration of reaction partners, in particular SO_2 concentrations, themselves.

Questions and Answers

Questioner: Tony Dore
Question: Your presentation showed a change in the balance between the gas phase (SO_2) and the particulate phase (SO_4). How could this affect the local range/long range effects of acid deposition?
Answer: Particles typically have longer lifetimes in the atmosphere and therefore they will be transported over longer distances. Consequently, one can expect that sulphur deposition will be spread over a larger area but with less pronounced peak values in the vicinity of a source.

Questioner: Sebnem Aksoyoglu
Question: In southern Poland, people living around coal mines use coal in residential heating. Are they included in your emission inventory?
Answer: The emission inventory is based on official EMEP country totals for the years 1980–2007. Poland has high SO_2 emissions in the SNAP2 sector for residential heating, therefore coal combustion is certainly considered. Comparing different countries, it can be seen that the decrease of emissions in this sector is less pronounced in Poland compared to e.g. Germany.

Questioner: Heinke Schlünzen
Question: You stated that emission data for SO_4 are uncertain compared to SO_2 emissions. Is this the real reason or doesn't the 72×72 km^2 grid need other emission data than e.g. a 10×10 km^2 grid? Or said differently: Shouldn't emission inventories be scale dependent and thereby consider chemical reactions within the grid?
Answer: This is certainly true, emission inventories should consider the chemical conversion of emissions that takes place between the source and a place somewhere within the grid. However, until today this is not yet state of the art. We stated the uncertainty in the SO_2/SO_4 emission split in connection with the underestimation of sulphate concentrations in Poland. Considering in-grid conversion of SO_2/SO_4 would reduce this deviation between model and observations. Our attempt to investigate this is to repeat the simulations on a much finer grid. Despite this, the split of the emissions into SO_2 and SO_4 remains a large source of uncertainty because it is hardly anywhere reported.

References

Bieser J, Aulinger A, Matthias V, Quante M, Denier van der Gon HAC (2011) Vertical emission profiles for Europe based on plume rise calculations. Environ Pollut 159(10):2935–2946

Byun D, Ching J (1999) Science algorithms of the EPA models-3 community multiscale air quality modeling system. Epa/600/r-99/030, US Environmental Protection Agency, Office of Research and Development, Washington DC

Doms G, Schättler U (2002) A description of the nonhydrostatic regional model LM. Part I: dynamics and numerics. Technical report, Deutscher Wetterdienst

Geyer B (2014) High-resolution atmospheric reconstruction for Europe 1948–2012: coastDat2. Earth Syst Sci Data 6(1):147–164

Huijnen V, Williams J, van Weele M, van Noije T, Krol M, Dentener F, Segers A, Houweling S, Peters W, de Laat J, Boersma F, Bergamaschi P, van Velthoven P, Le Sager P, Eskes H, Alkemade F, Scheele R, Nedelec P, Paetz HW (2010) The global chemistry transport model TM5: description and evaluation of the tropospheric chemistry version 3.0. Geosci Model Dev 3(2):445–473

Jones AM, Harrison RM (2011) Temporal trends in sulphate concentrations at European sites and relationships to sulphur dioxide. Atmos Environ 45(4):873–882

Kalnay E, Kanamitsu M, Kistler R, Collins W, Deaven D, Gandin L, Iredell M, Saha S, White G, Woollen J, Zhu Y, Chelliah M, Ebisuzaki W, Higgins W, Janowiak J, Mo KC, Ropelewski C, Wang J, Leetmaa A, Reynolds R, Jenne R, Joseph D (1996) The NCEP/NCAR 40-year reanalysis project. Bull Am Meteorol Soc 77(3):437–471

Chapter 7
Modelling Concentrations and Trends of Atmospheric Pollutants in the Arctic over a 37 Years Period

Kaj M. Hansen, Camilla Geels, Ulas Im, Jørgen Brandt and Jesper H. Christensen

Abstract We have simulated air pollution levels over the Arctic for a 37 years period from 1979 to 2015 using a 3D hemispheric chemistry-transport model, the Danish Eulerian Hemispheric Model (DEHM). The observed and simulated trends have been analysed at a number of sites in the Arctic. The levels of SO_2 are decreasing over the simulated period, which follows the decreased anthropogenic emission in source areas. Differences in trends between sites can be explained by the influence from different source areas. The levels of O_3 are almost constant over the 37 year period and no difference in trends between sites can be seen.

7.1 Introduction and Study Setup

The Arctic is a pristine area with no or few local sources to air pollution. Most air pollution is transported to the Arctic via long-range atmospheric transport from Europe, Asia and North America. We have applied the 3D chemistry-transport model DEHM (the Danish Eulerian Hemispheric Model) to study the concentrations of air pollution in the Arctic over three and a half decades. DEHM was

K.M. Hansen (✉) · C. Geels · U. Im · J. Brandt · J.H. Christensen
Department of Environmental Science, Aarhus University, Aarhus, Denmark
e-mail: kmh@envs.au.dk

C. Geels
e-mail: cag@envs.au.dk

U. Im
e-mail: ulas@envs.au.dk

J. Brandt
e-mail: jbr@envs.au.dk

J.H. Christensen
e-mail: jc@envs.au.dk

K.M. Hansen · J.H. Christensen
Arctic Research Centre, Aarhus University, Aarhus, Denmark

C. Mensink and G. Kallos (eds.), *Air Pollution Modeling and its Application XXV*,
Springer Proceedings in Complexity, DOI 10.1007/978-3-319-57645-9_7

originally developed to study atmospheric transport of sulphur and sulphate to the Arctic and is set-up using a polar stereographic projection with a 150 km grid resolution over the Northern Hemisphere with the Arctic in the centre (Christensen 1997). Further development has resulted in the implementation of e.g. full ozone chemistry and nesting capabilities (Brandt et al. 2012). The model domain includes the most important source areas for the Arctic and is therefore ideally suited to study atmospheric pollution in the Arctic. Air pollution levels have been monitored in the Arctic for the past about 25 years. In this study we have made a simulation that extends approximately 10 years further back in time covering a 37 years period from 1979 to 2015. The model is driven by meteorological data from the WRF model and anthropogenic emissions from ECLIPSEv5.0 for the Northern Hemisphere, EMEP emissions for the European domains and national emission inventory with a high spatial resolution for the domain over Denmark.

7.2 Results and Discussion

The simulated concentrations have been evaluated against measurements from monitoring stations in the European EMEP network and are in fair agreement with observations for a range of pollutants. This is also the case for the few monitoring sites in the high Arctic, e.g. Ny Aalesund at Svalbard (Fig. 7.1).

The annual averaged simulated concentrations of SO_2 at Ny Aalesund are reduced with 80% over the simulated period (Fig. 7.2). The annual averaged simulated concentration of SO_2 is reduced with 50% at Alert, Nunavut, Canada. The annual averaged simulated concentrations of O_3 at both sites are almost constant through the 37 year period.

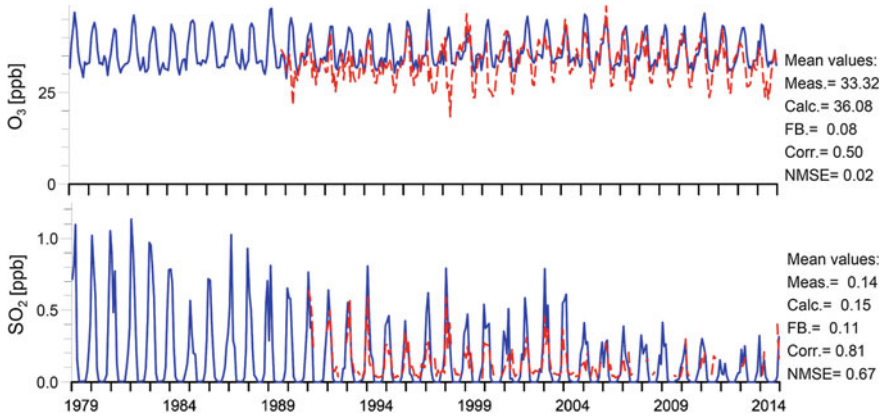

Fig. 7.1 Measured (*red*) and simulated (*blue*) mixing ratios of O_3, and SO_2 at Ny Aalesund, Svalbard (78.9°N, 11.9°E)

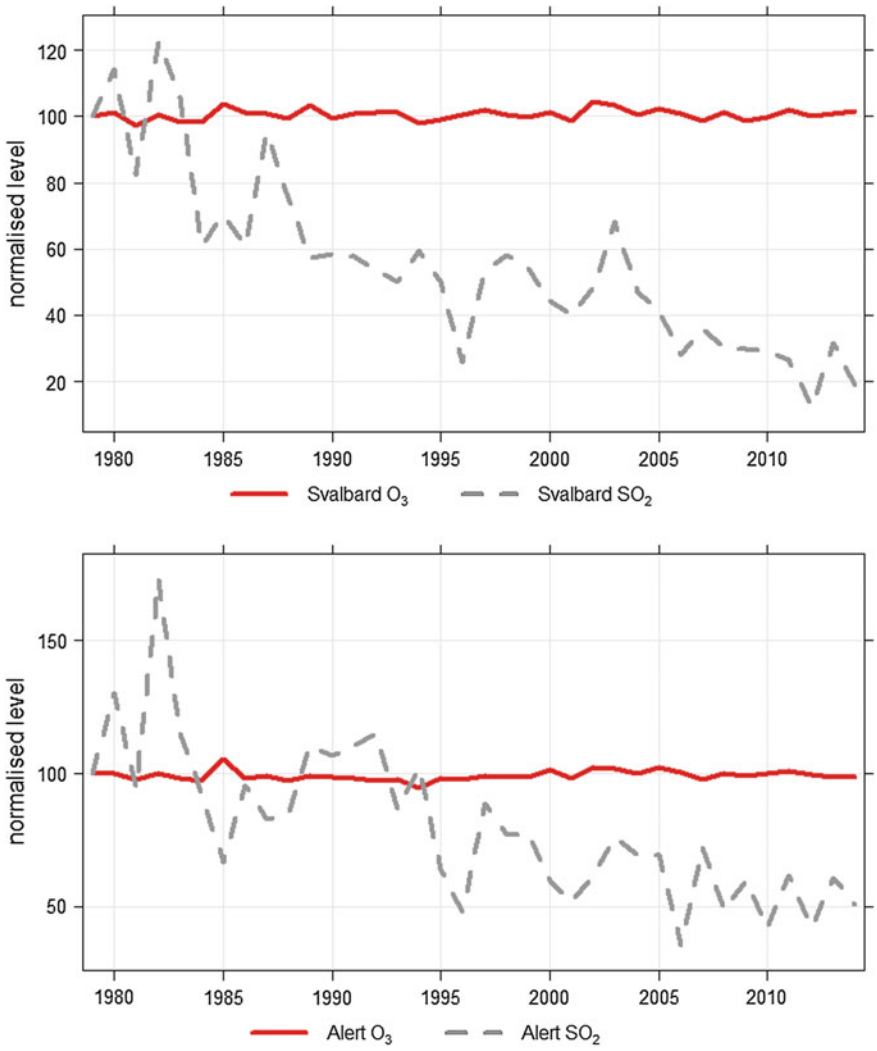

Fig. 7.2 Simulated concentrations of O_3 and SO_2 at Ny Aalesund, Svalbard (78.9°N, 11.9°E; *top*) and at Alert, Nunavut, Canada (82.5°N, 62.3°W; *bottom*), normalised to the 1979 concentrations

Differences in concentrations between the two sites can arise due to the influence of different source areas. Ny Aalesund is expected to be dominated by emissions from Europe, while the source areas at Alert are expected to be more mixed. We have compared the predicted trends in concentrations with trends in the applied emission estimates from different source areas: Europe, North America and Asia. The total emissions of SO_2 in the model domain decrease with 40% in the modelled period, the emissions in Europe and North America decrease with approximately 75% and 60%, while the emissions in Asia increase with 35%. The reduction in

predicted SO_2 levels at Ny Aalesund follows closely the large reduction in European emissions over the simulated period, which reflects the large influence from this source area at the site. The development in SO_2 at Alert is closer to the developments in the total emissions reflecting that the air masses at Alert are not directly influenced by a single source area.

Monitoring data from the Canadian Arctic supports the almost constant development of O_3 concentrations since the early 1980s (Oltmans et al. 2015). Concentrations of O_3 from monitoring sites in the mid-latitudes of the Northern Hemisphere have increased since the early 1980s despite decreasing emissions of precursors in Europe and North America (Oltmans et al. 2015). Increasing emissions of O_3 precursors in China as well as increased downward transport of stratospheric ozone is shown to lead to a large increase in tropospheric ozone in China, and this affects ozone concentrations at the US west coast and may contribute to the increasing background concentration (Verstraeten et al. 2015). The increase in background concentrations may be counteracted by climatic changes in the Arctic resulting in the lack of trends in this region.

7.3 Conclusion

We have investigated the spatial and temporal variability of O_3 and SO_2 concentrations in the Arctic over a 37 years period from 1979 to 2015 simulated by the Danish Eulerian Hemispheric Model. The concentrations of SO_2 have decreased following reductions in emissions from source areas. Differences in trends between sites can be explained by the influence from different source areas. This confirms our general understanding that concentrations of SO_2 in the Arctic are governed by direct transport. There are no clear trends in the annual averaged simulated O_3 concentrations in the Arctic through the simulated 37 years period and no difference in trends between sites. This indicates that O_3 in the Arctic is governed by background concentrations and stratospheric intrusion and to a less degree by direct transport of precursors from the source areas.

Acknowledgements We gratefully acknowledge the contributions of Arctic Research Centre (ARC), Aarhus University. The research leading to these results has received funding from the Danish Environmental Protection Agency as part of the environmental support program Dancea—Danish Cooperation for Environment in the Arctic. The authors are solely responsible for all results and conclusions presented in the paper; these do not necessarily reflect the position of the Danish Environmental Protection Agency. This work is a contribution to the Arctic Science Partnership (ASP).

Questions and Answers

Questioner: Emmanouil Oikonomakis
Question: Have you investigated trends in the sub-periods of the total period, because it seems that there may be and if they exist are they related to any synoptic meteorological patterns?
Answer: We have not investigated the trends in sub-periods and their relations to synoptic scale meteorological patterns. This will be the subject for further analysis of the data.

Questioner: Wouter Lefebvre
Question: Is sea ice taken into account? And if so, do you see already an effect on for instance SO_x and O_3 deposition, especially in winter?
Answer: Yes, sea ice extent is taken into account in DEHM. We have not investigated the data in detail so we cannot see if there is an effect of changed sea ice cover on the deposition. But an earlier study with the DEHM model coupled to climate data, showed a decrease in the dry deposition of O_3 over the Arctic marine areas following the projected decrease in sea ice towards the end of the 21st century (Hedegaard et al. Atmospheric and Climate Sciences, 2012, 2, 546–561; http://dx.doi.org/10.4236/acs.2012.24050).

Questioner: Heinke Schlünzen
Question: Sea ice has reduced considerably, especially in summer and autumn with minimum extents found more and more. As a hypothesis, might it be possible that ozone concentrations could have increased in the Arctic if the sea ice cover where still the same as several decades ago? Is the main reason for the missing increase in O_3 the lost impact of the reflective sea ice covered areas?
Answer: We will further investigate the relationship between the predicted ozone concentrations and the extent of sea ice so we can test this hypothesis.

Questioner: Mikhail Sofiev
Question: Asian high-emission area is only partly in the domain, which puts substantially challenges to boundary conditions arrangements. What did you use for the boundaries?
Answer: The boundary conditions on O_3 are from a 3D climatological O_3 field based on radiosonde data (Logan, J. Geophys. Res., 104, 16115–16149, 1999). That the Asian high-emission area is only partly in the domain will introduce some uncertainty into the contribution to the Arctic from this area. However, the influence from Southeast Asian sources on surface concentrations in the Arctic is not expected to be as large as to the concentrations in mid-latitudes. This will be included in a further analysis of the data.

References

Brandt et al (2012) An integrated model study for Europe and North America using the Danish Eulerian hemispheric model with focus on intercontinental transport. Atmos Environ 53:156–176

Christensen JH (1997) The Danish Eulerian hemispheric model—a three-dimensional air pollution model used for the Arctic. Atmos Environ 31:4169–4191

Oltmans SJ, Lefohn AS, Shadwick D, Harris JM et al (2015) Recent tropospheric ozone changes—a pattern dominated by slow or no growth. Atmos Environ 67:331–351

Verstraeten WW, Neu JL, Williams JE, Bowman KW, Worden JR, Folkert Boersma K (2015) Rapid increases in tropospheric ozone production and export from China. Nat Geosci 8:690–695

Chapter 8
Air Pollutant Trends over Denmark over the Last 37 Years as Simulated by the Integrated Model System THOR

Ulas Im, Jesper H. Christensen, Matthias Ketzel, Thomas Ellermann, Camilla Geels, Kaj M. Hansen, Ole Hertel, Ole-Kenneth Nielsen, Marlene S. Plejdrup and Jørgen Brandt

Abstract Air pollutant levels over Denmark are simulated using the high resolution THOR model system for the years 1979–2015. The system employs the Danish Eulerian Hemispheric Model (DEHM), coupled to the Urban Background Model (UBM) that covers the whole of Denmark on a 1 km spatial resolution. This study evaluates the performance of the model system in simulating hourly, daily, monthly and yearly mean ozone (O_3), nitrogen oxides (NOx) and particulate matter (PM_{10} and $PM_{2.5}$) concentrations using surface measurements from eight Danish

U. Im (✉) · J.H. Christensen · M. Ketzel · T. Ellermann · C. Geels · K.M. Hansen · O. Hertel · O.-K. Nielsen · M.S. Plejdrup · J. Brandt
Department of Environmental Science, Aarhus University, Roskilde, Denmark
e-mail: ulas@envs.au.dk

J.H. Christensen
e-mail: jc@envs.au.dk

M. Ketzel
e-mail: mke@dmu.dk

T. Ellermann
e-mail: tel@envs.au.dk

C. Geels
e-mail: cag@envs.au.dk

K.M. Hansen
e-mail: kmh@envs.au.dk

O. Hertel
e-mail: oh@envs.au.dk

O.-K. Nielsen
e-mail: okn@envs.au.dk

M.S. Plejdrup
e-mail: msp@envs.au.dk

J. Brandt
e-mail: jbr@envs.au.dk

C. Mensink and G. Kallos (eds.), *Air Pollution Modeling and its Application XXV*,
Springer Proceedings in Complexity, DOI 10.1007/978-3-319-57645-9_8

monitoring stations between 1990 and 2015. The spatial and temporal variability of air pollutants and emissions are also investigated to better understand the air pollution trends over Denmark during this 37 year period.

8.1 Introduction

Integrated model systems couple several models that represent different geographical scales with appropriate complexity. The coupling of models over different scales makes it possible to account for contributions from local, near-local as well as remote emission sources in order to describe the air quality at a specific location —e.g. in a street canyon or in a sub-urban area. These integrated systems can be very valuable in air quality assessments over cities, where regional models would computationally suffer due to resolution and complexity issues.

In Denmark such an integrated system exists and has been operational since 1999 (Ellermann et al. 2015). The THOR system is a highly integrated model system, capable of forecasting meteorological and chemical variables for the general public as well as providing a tool for assessment and management for decision-makers in general. The aim of this study is to validate the THOR system over Denmark using available long term surface observations and to assess the trends in emissions and air pollutant concentrations from 1979 to 2015.

8.2 Materials and Methods

THOR model system employs the Danish Eulerian Hemispheric Model (DEHM: Brandt et al. 2012) running on a 150 km × 150 km resolution over the Northern Hemisphere, with nesting capability for higher resolutions over Europe, Northern Europe and Denmark on 50 km × 50 km, 16.7 km × 16.7 km and 5.6 km 5.6 km resolutions, respectively. DEHM is coupled to the Urban Background Model (UBM: Berkowicz 2000) that covers the whole of Denmark on a 1 km 1 km spatial resolution. Over Denmark, the 1 km × 1 km resolution SPREAD emissions are used (Plejdrup and Gyldenkærne 2011).

The surface observations are obtained from the Danish monitoring network operated by Department of Environmental Science, Aarhus University. In this study, we have used eight urban-background monitoring stations to validate the THOR system for the period 1990–2015, and all 28 stations (rural, urban and street stations) as well as the domain-mean levels to assess the trends over the full simulation period.

8.3 Results and Conclusions

Simulated annual O_3 values agree with the observations temporally (r = ~0.8–0.9), with a 2–4% error (*NMB* < 1%). Simulated annual PM_{10} and $PM_{2.5}$ levels also compare well with the observations temporally (r = ~0.7–0.9), but with a general underestimation of up to ~40%, with the larger underestimations for PM_{10} compared to $PM_{2.5}$ (*NMB* = −10% to −30%). Table 8.1 summarizes the model performance based on the annual observed and simulated surface concentrations. Figure 8.1 presents the same statistics as Taylor diagrams.

Observations show that O_3 levels have increased over the last 25 years by $0.8 \pm 0.9\%yr^{-1}$ while NOx, PM_{10} and $PM_{2.5}$ levels decreased by -2.0 ± 3.4, -3.3 ± 1.1 and $-3.2 \pm 3.2\%yr^{-1}$, respectively. The model system was able to simulate these observed trends over the monitoring stations reasonably well for O_3 ($0.7 \pm 0.6\%yr^{-1}$) while it simulated a slightly larger decrease for NOx ($-3.4 \pm 2.7\%yr^{-1}$) and a smaller decreases in PM_{10} ($-1.0 \pm 1.1\%yr^{-1}$) and $PM_{2.5}$ ($-1.4 \pm 2.5\%yr^{-1}$).

Over the 37 years, the Danish emissions of all pollutants decreased (Fig. 8.2a), with the gaseous pollutants decreasing more than the particulate emissions. The 37 year simulation over all receptors in Denmark showed a decreasing trend for all pollutants except for ozone (Fig. 8.2b). NOx emissions in Denmark experienced a larger decrease over the 37 years ($-2.0\%yr^{-1}$) compared to the surface concentrations ($-0.60\%yr^{-1}$) suggesting the local impact of emission reductions in

Table 8.1 Statistics for the annual surface mean concentrations at each urban background and rural monitoring station

		Anholt	HCØ	Keldsnor	Odense	Risø	Ulborg	Aalborg	Aarhus
NOx	*NMB*	0.10	−0.02	0.45	0.43	2.60	0.34	0.17	0.07
	NMGE	0.71	0.33	0.77	0.68	2.73	0.63	0.76	0.52
	RMSE	4.71	7.63	7.31	21.07	18.92	2.59	23.97	14.16
	r	0.30	0.70	0.39	0.57	0.29	0.47	0.46	0.56
O_3	*NMB*		0.02	0.07	−0.01	−0.09	0.10	0.07	0.02
	NMGE		0.18	0.20	0.19	0.21	0.16	0.17	0.21
	RMSE		6.04	7.40	6.50	7.80	6.35	6.04	6.46
	r		0.83	0.70	0.81	0.75	0.78	0.81	0.77
PM_{10}	*NMB*		−0.41	−0.23		−0.19			
	NMGE		0.43	0.35		0.37			
	RMSE		12.93	10.82		8.44			
	r		0.65	0.66		0.59			
$PM_{2.5}$	*NMB*		−0.19			−0.02		−0.30	−0.10
	NMGE		0.34			0.39		0.40	0.33
	RMSE		6.51			7.08		7.82	6.20
	r		0.71			0.66		0.70	0.71

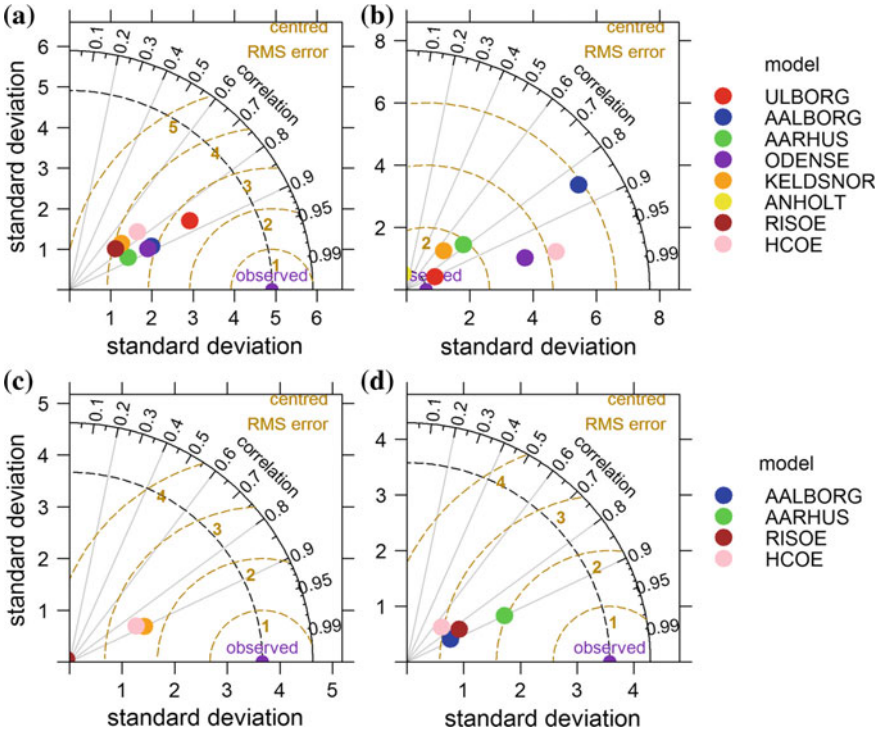

Fig. 8.1 Taylor diagrams for **a** O_3, **b** NOx, **c** PM_{10} and **d** $PM_{2.5}$ over all monitoring stations

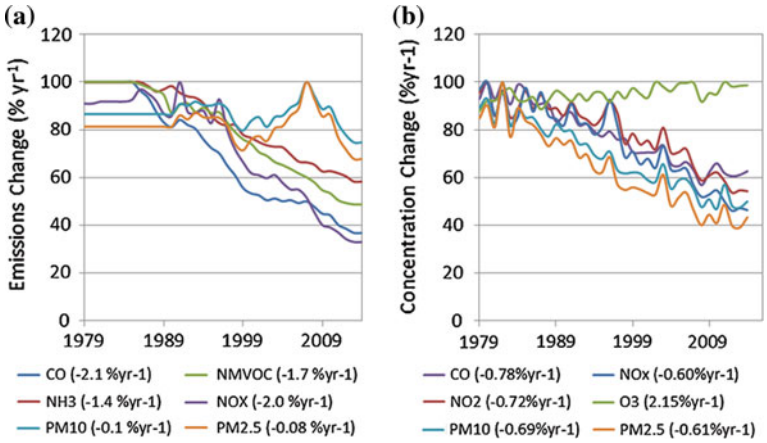

Fig. 8.2 37-year trends of **a** emissions and **b** surface concentrations over the Danish domain

Denmark, while $PM_{2.5}$ emissions had smaller decreases ($-0.08\%yr^{-1}$) compared to the surface levels ($-0.61\%yr^{-1}$) suggesting larger influence of regional emissions on $PM_{2.5}$ levels compared to reductions in local emissions.

The results show that the THOR system is capable of reasonably simulating the observed levels and trends of the air pollutants over Denmark. The trend analyses suggest that PM levels over Denmark are controlled largely by regional transport from source regions, while NOx is originating from local sources.

Acknowledgements This work is funded by the Danish Center for Energy and Environment, Aarhus University and NordForsk under the Nordic Programme on Health and Welfare. Project #75007: Understanding the link between air pollution and distribution of related health impacts and welfare in the Nordic countries (NordicWelfAir).

Questions and Answers

Questioner 1: Greg Yardwood
Question: How do you avoid double counting the air quality impacts (e.g. on NO_2 or O_3 concentrations in Aarhus) of Danish emissions if they are included both in the DEHM and UBM models?
Answer: THE DEHM model provides the boundary conditions to the UBM model and these two models run separately. UBM takes into account the emissions up to 30 km upwind from all the individual receptor points and at the end of the 30 km trajectory, the boundary conditions are given by DEHM.

Questioner 2: Peter Viaene
Question: Don't you commit an error by removing the Danish emissions from your domain to calculate the background?
Answer: We do not remove the Danish emission from our DEHM model, we replace the EMEP emissions over Denmark with the SPREAD emission for Denmark in order to have consistent emissions in both DEHM and UBM models and to aply the best available emission data on a high resolution.

Questioner 3: George Tsegas
Question: Which particular measures are taken in order to avoid multiple counting of emissions in finer-scale model?
Answer: The UBM model is run using background concentrations from the DEHM model. In order to avoid double counting, for each grid cell in the UBM model, the background value is calculated using the concentration value of the DEHM grid cell that corresponds to the 30 km upwind to the particular UBM grid cell (see also question 1).

References

Berkowicz R (2000) A simple model for urban background pollution. Environ Monit Assess 65 (1/2):259–267

Brandt et al (2012) An integrated model study for Europe and North America using the Danish Eulerian hemispheric model with focus on intercontinental transport. Atmos Environ 53:156–176

Ellermann et al (2015) The Danish air quality monitoring programme annual summary for 2013. Scientific Report from DCE—Danish centre for environment and energy No 134

Plejdrup MS, Gyldenkærne S (2011) Spatial distribution of emissions to air—the SPREAD model. National Environmental Research Institute, Aarhus University, Denmark. NERI Technical Report no. FR823, 72 pp

Chapter 9
A Long-Term Re-Analysis of Atmospheric Composition and Air Quality

M. Sofiev, R. Kouznetsov, M. Prank, J. Soares, J. Vira, V. Tarvainen and V. Sofieva

Abstract The paper presents a global-to-mesoscale model re-analysis of atmospheric composition for the period of 1980–2014 and the first outcome of the evaluation. The goals of the re-analysis were to assess the multi-decade evolution of atmospheric composition and air quality at several spatial scales and to evaluate the performance of SILAM dispersion model in this large-scale exercise. The dataset covered troposphere and the stratosphere, main anthropogenic pollutants and had a special line for natural constituents, such as sea salt and pollen. This dataset forms the starting point for episodic and meso-to-local-scale studies, which will refine its predictions.

9.1 The Re-Analysis Goals and Setup

The re-analysis has been produced within the scope of the APTA project (The Influence of Air Pollution, Pollen and Ambient Temperature on Asthma and Allergies in Changing Climate), aiming at providing the lifetime exposure data for several patient cohorts in Finland and abroad. The other targets were to assess the multi-decadal atmospheric composition trends and the extent the SILAM chemistry-transport model can reproduce them.

The re-analysis was made with SILAM model v.5.5 (Sofiev et al. 2015) at three spatial scales: global (the troposphere and the stratosphere), European (troposphere), and Northern Europe (troposphere)—see Table 9.1.

The emission information was compiled from the MACCITY (Granier et al. 2011) and EDGAR (EDGAR 2014) anthropogenic, GEIA lightning (Price et al.

M. Sofiev (✉) · R. Kouznetsov · M. Prank · J. Soares · J. Vira · V. Tarvainen · V. Sofieva
Finnish Meteorological Institute, Helsinki, Finland
e-mail: mikhail.sofiev@fmi.fi

M. Prank
e-mail: marje.prank@fmi.fi

J. Soares
e-mail: joana.soares@fmi.fi

C. Mensink and G. Kallos (eds.), *Air Pollution Modeling and its Application XXV*,
Springer Proceedings in Complexity, DOI 10.1007/978-3-319-57645-9_9

Table 9.1 Setup of three scales of the model re-analysis

	Globe	Europe	Northern Europe
Period	1980–2015	1980–2015	1980–2015
Output resolution	1.44° × 1.44° × 20 lyrs up to ~60 km alt × 1 h	0.5° × 0.5° × 13 lyrs up to ~8 km alt × 1 h	0.1° × 0.1° × 10 lyrs up to ~5 km alt × 1 h
Meteo input	ERA-Interim, 0.72° × 0.72° × 61 lyrs up to ~65 km alt × 3 h	ERA-Interim, 0.72° × 0.72° × 61 lyrs up to ~65 km alt × 3 h	BaltAn 1980–2005, 0.1° × 0.1° × 60 lyrs up to ~31 km alt × 6 h ECMWF IFS, 2006–2015, resolution (0.36° − 0.09°) × (61–137) lyrs × 3 h
Input emission	MACCity, ACCMIP fires, MEGAN BVOC, GEIA lightning and aircraft	MACCity, ACCMIP fires, GEIA lightning and aircraft	EDGAR, ACCMIP fires, GEIA lightning and aircraft
Online emission	Wind-blown dust, DMS, sea salt	Wind-blown dust, DMS, sea salt, BVOC	Sea salt, BVOC
Chemical setup	CB4 gas-phase + halogens, PSC, SIA and SOA formation	CB4 gas-phase, SIA and SOA formation	CB4 gas-phase, SIA and SOA formation

1997) and aircraft, ACCMIP biomass-burning (Lamarque et al. 2010), and MEGAN biogenic (used for global domain only, (Guenther et al. 2006)) emission inventories. The emission of sea salt (Sofiev et al. 2011), wind-blown dust, and biogenic VOCs (European and Northern Europe domains, (Poupkou et al. 2010)) is computed with the embedded SILAM modules. The driving meteorological datasets were the ERA-Interim re-analysis (global and European domains, (Dee et al. 2011; Simmons et al. 2010)) and BaltAn HIRLAM re-analysis combined with operational ECMWF archives for the Northern European domain.

The in-depth analysis and evaluation of the dataset is only starting but the first outlook showed that the obtained patterns match the historical developments of air pollution (Fig. 9.1): gradual decrease of concentrations in Europe (including Northern Europe) and Northern America, whereas a huge rise of concentrations is seen in Asia. At finer temporal scale (days/hours), individual episodes connected with the synoptic-scale meteorological processes, fire seasons, and storms are visible and can be related to the observed time series and satellite retrievals.

An interesting exception from the above tendency is ozone, which combined small reduction in some part of the US and Europe with substantial rise of the concentrations in remote areas. As a result, if in 1980 ozone was rather a regional pollutant then in 2015 one has to talk about hemispheric scale of its distribution. This tendency, however, is yet to be evaluated against observations, which are limited in the remote areas and difficult to obtain for historical times.

The evaluation of the re-analysis has started from the global-scale phenomena: the model was tested to reproduce the major patterns and events, such as vertical

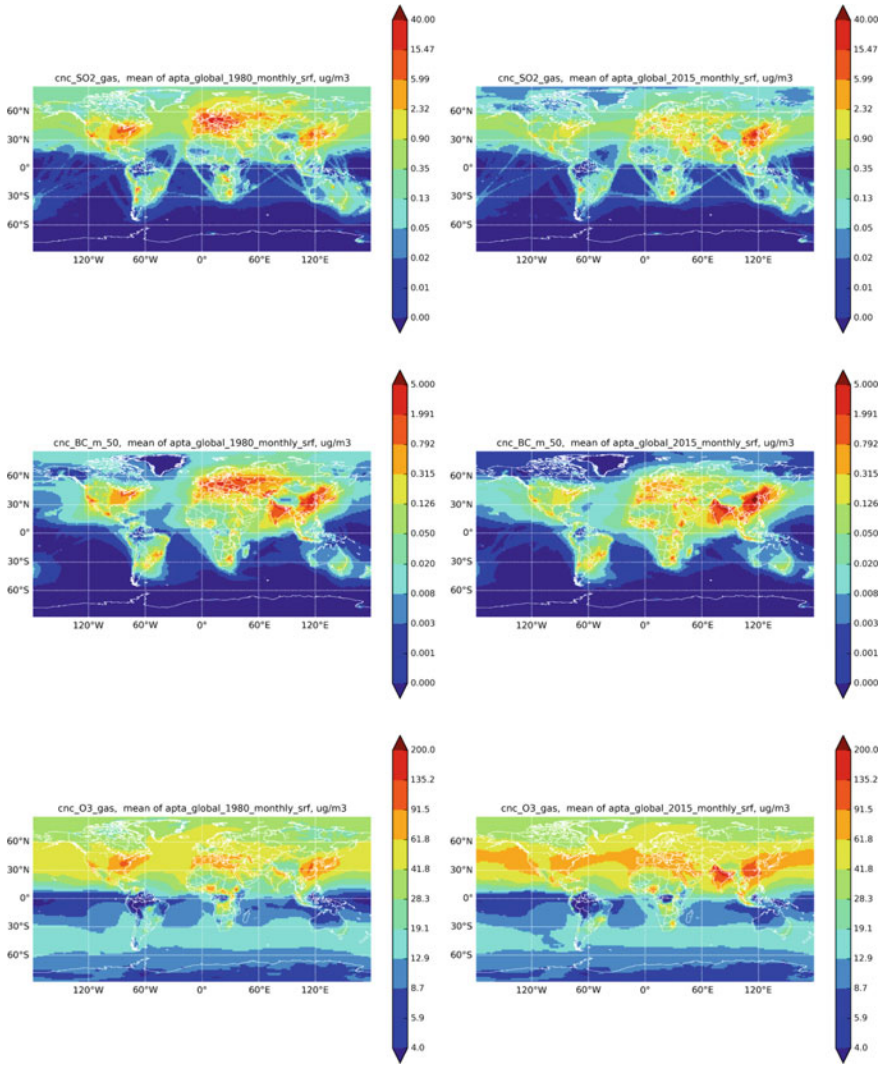

Fig. 9.1 Example of changes in annual concentrations for SO_2 (*upper row*), BC (*middle row*), and O_3 (*lower row*) between 1980 (*left*) and 2014 (*right*). Unit = [μg of species m^{-3}]

distribution of the main stratospheric constituents, the effect of Asian monsoon, vertical and zonal distributions of the age of air, etc. An example of the evaluation is given in Fig. 9.2 for the main reactive constituents in the stratosphere. The comparison is made against GOMOS satellite observations in 2010.

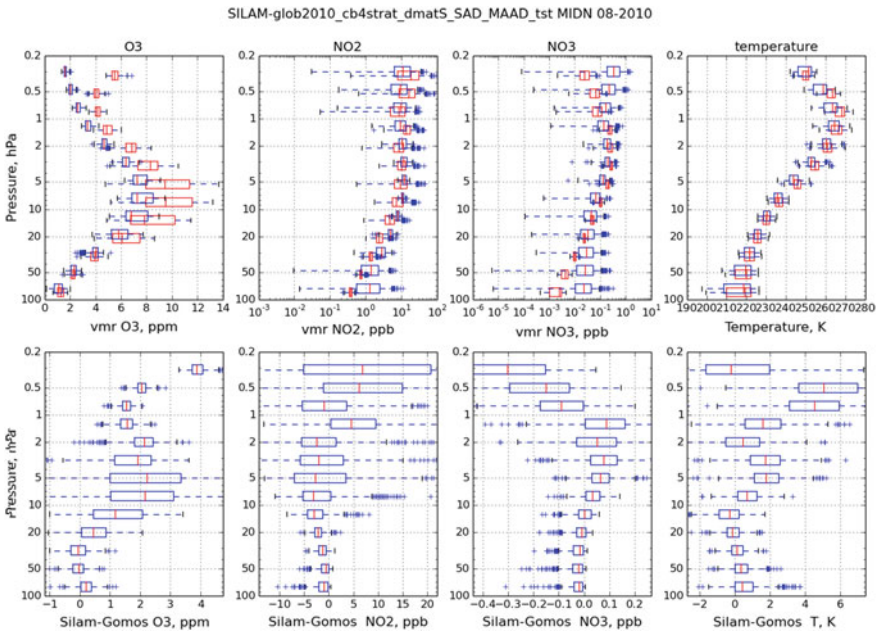

Fig. 9.2 Evaluation of vertical zonal-mean profiles of the main stratospheric constituents: O_3 (*left*, unit = ppm), NO_2 (*second left*, unit = ppb), NO_3 (*second right*, unit = ppb), and temperature (*right*, unit = K, taken from the ERA-Interim data). Absolute profiles (*upper row*) and deviations (*lower row*) are shown

Questions and Answers

Question (P. Kishcha): For initialization, you used the meteorological fields from ERA-Interim, which were produced without taking into consideration the aerosol effects on meteorological parameters. The SILAM model probably included these aerosol effects on meteorology (i.e. on radiation budget, temperature, etc.). How could these effects influence your results?

Answer: SILAM is an offline chemistry transport model, i.e. we did not compute the meteorology, instead using the ERA-Interim/BaltAn/IFS fields as they are. Therefore, our aerosols did not influence the meteorology during the computations. However, both ERA-Interim and IFS heavily use data assimilation to nudge their predictions to the actual situation. Therefore, I would expect that the main parts of the aerosol impact are indirectly summoned in the meteorological data through the assimilation of the actual observations.

References

Dee DP, Uppala SM, Simmons AJ, Berrisford P, Poli P, Kobayashi S, Andrae U, Balmaseda MA, Balsamo G, Bauer P, Bechtold P, Beljaars ACM, van de Berg L, Bidlot J, Bormann N, Delsol C, Dragani R, Fuentes M, Geer AJ, Haimberger L, Healy SB, Hersbach H, Hólm EV, Isaksen L, Kållberg P, Köhler M, Matricardi M, McNally AP, Monge-Sanz BM, Morcrette J-J, Park B-K, Peubey C, de Rosnay P, Tavolato C, Thépaut J-N, Vitart F (2011) The ERA-Interim reanalysis: configuration and performance of the data assimilation system. Q J R Meteorol Soc 137:553–597. doi:10.1002/qj.828

EDGAR (2014) Emission Database for Global Atmospheric Research (EDGAR). http://edgar.jrc.ec.europa.eu/. Accessed 26 Jun 2017

Granier C, Bessagnet B, Bond T, D'Angiola A, Denier van der Gon H, Frost GJ, Heil A, Kaiser JW, Kinne S, Klimont Z, Kloster S, Lamarque J-F, Liousse C, Masui T, Meleux F, Mieville A, Ohara T, Raut J-C, Riahi K, Schultz MG, Smith SJ, Thompson A, Aardenne J, Werf GR, Vuuren DP (2011) Evolution of anthropogenic and biomass burning emissions of air pollutants at global and regional scales during the 1980–2010 period. Clim Change 109:163–190. doi:10.1007/s10584-011-0154-1

Guenther A, Karl T, Harley P, Wiedinmyer C, Palmer PI, Geron C (2006) Estimates of global terrestrial isoprene emissions using MEGAN (Model of Emissions of Gases and Aerosols from Nature). Atmos Chem Phys 6:3181–3210. doi:10.5194/acpd-6-107-2006

Lamarque J-F, Bond TC, Eyring V, Granier C, Heil A, Klimont Z, Lee D, Liousse C, Mieville A, Owen B, Schultz MG, Shindell D, Smith SJ, Stehfest E, Van Aardenne J, Cooper OR, Kainuma M, Mahowald N, McConnell JC, Naik V, Riahi K, van Vuuren DP (2010) Historical (1850–2000) gridded anthropogenic and biomass burning emissions of reactive gases and aerosols: methodology and application. Atmos Chem Phys 10:7017–7039. doi:10.5194/acp-10-7017-2010

Poupkou A, Giannaros T, Markakis K, Kioutsioukis I, Curci G, Melas D, Zerefos C (2010) A model for European Biogenic Volatile Organic Compound emissions: Software development and first validation. Environ Model Softw 25:1845–1856. doi:10.1016/j.envsoft.2010.05.004

Price C, Penner J, Prather M (1997) NOx from lightning: 1. Global distribution based on lightning physics. J Geophys Res 102:5929. doi:10.1029/96JD03504

Simmons AJ, Willett KM, Jones PD, Thorne PW, Dee DP (2010) Low-frequency variations in surface atmospheric humidity, temperature, and precipitation: inferences from reanalyses and monthly gridded observational data sets. J Geophys Res Atmos 115:1–21. doi:10.1029/2009JD012442

Sofiev M, Soares J, Prank M, de Leeuw G, Kukkonen J (2011) A regional-to-global model of emission and transport of sea salt particles in the atmosphere. J Geophys Res 116. doi:10.1029/2010JD014713

Sofiev M, Vira J, Kouznetsov R, Prank M, Soares J, Genikhovich E (2015) Construction of the SILAM Eulerian atmospheric dispersion model based on the advection algorithm of Michael Galperin. Geosci Model Dev 8:3497–3522. doi:10.5194/gmd-8-3497-2015

Part II
Model Assessment and Verification

Chapter 10
Intercomparison of Chemical Mechanisms for European Air Quality Policy Formulation and Assessment

R.G. Derwent

Abstract An intercomparison and evaluation of nine chemical mechanisms has been made for their suitability for European air quality policy formulation and assessment. Box modelling techniques were employed using a range of background environmental conditions across Europe. Although the chemical mechanisms gave strikingly similar base case ozone production rates, their responses to 30% NO_x and VOC reductions showed significant dispersion. These 30% reductions in NO_x and VOCs also produced changes in the hydroxyl radical number densities which were again chemical mechanism dependent.

10.1 Techniques

A zero-dimensional box model was set up to provide a framework for the intercomparison and evaluation of the nine chemical mechanisms listed in Table 10.1. The chemical mechanisms varied markedly in complexity from the highly detailed explicit Master Chemical Mechanism (MCMv3.3) to the highly condensed and parameterised Carbon Bond and SAPRC mechanisms. The mechanisms were harmonised and standardised by using a common set of inorganic reactions representing the fast photochemical balance of the lower atmosphere involving: OH, HO_2, O_3, NO_x, O^1D, O^3P, H_2O, CO, H_2, SO_2 and HNO_3, a common set of photolysis rate coefficients and a common description of PAN chemistry, taken from the MCM website: http://mcm.leeds.ac.uk/mcm. To draw attention to the harmonisation and standardisation steps, the names of the mechanisms have been printed in *italics* to indicate that they have not been implemented as originally developed.

An intercomparison of chemical mechanisms requires some input data and background environmental conditions to set up appropriate chemical regimes to

R.G. Derwent (✉)
rdscientific, Newbury, UK
e-mail: r.derwent@btopenworld.com

C. Mensink and G. Kallos (eds.), *Air Pollution Modeling and its Application XXV*,
Springer Proceedings in Complexity, DOI 10.1007/978-3-319-57645-9_10

Table 10.1 Summary of the nine chemical mechanisms employed, together with their 5-day time-averaged ozone production rates with base case emissions and averaged over all 32 sets of background environmental conditions. Also shown are the percentage responses in the ozone production rates to 30% reductions in NO_x and VOCs

Chemical mechanism	5-day averaged ozone production rate, ppb hr^{-1}	Percentage response in ozone production rate to 30% NO_x reduction	Percentage response in ozone production rate to 30% VOC reduction
CBM4[a]	4.45	−29.2	−6.1
CB05[b]	4.46	−27.1	−6.3
CB6[c]	4.49	−26.7	−5.8
CRIv2[d]	4.47	−26.2	−7.1
EMEP[e]	4.47	−27.9	−6.6
GEOS-CHEM[f]	4.47	−27.6	−5.1
MCMv3.3[g]	4.47	−27.2	−6.7
SAPRC-99[h]	4.48	−26.6	−7.9
SAPRC-07[i]	4.47	−27.4	−6.9

Notes
[a]Gery et al. (1989)
[b]CAMx mechanism 6: CB05 gas-phase chemistry, Appendix C, Environ International Corporation (2015)
[c]CAMx mechanism 2: CBr6 gas-phase chemistry, Appendix A, Environ International Corporation (2015)
[d]Jenkin et al. (2008)
[e]Default chemical mechanism, EmChem09, Table S11, Simpson et al. (2012)
[f]GEOS-Chemv9-02f (accepted 07 Feb 2013): downloaded from http://wiki.seas.harvard.edu/geos-chem/index.php/updating_standard_chemistry_with_JPL_10-6#Species. This is the version reviewed by Emmerson and Evans (2009)
[g]Jenkin et al. (2015)
[h]CAMx mechanism 5: SAPRC99 gas-phase chemistry, Appendix D, Environ International Corporation (2015)
[i]CS07A is the most highly condensed version of SAPRC-07: Carter (2010)

frame the evaluation. In this study, output was taken from a global Lagrangian chemistry-transport model (STOCHEM-CRI) (Derwent et al. 2015) to provide realistic mixing ratios for 30 trace gases with atmospheric lifetimes of minutes and longer for 32 locations at the centres of $5^{\circ} \times 5^{\circ}$ latitude-longitude grid boxes covering 55°–30°N and 10°W–30°E. The mixing ratios of the 30 trace gases were constrained to the background conditions by the addition or subtraction of a flux of that species at each time step of the 5-day integration. The time-integrated fluxes over the 5-day period, together with the box model concentrations of the unconstrained free radical species averaged over the same period, provided the necessary box model output. Atmospheric number densities, temperatures and water vapour number densities were taken from STOCHEM-CRI. Time-dependent solar photolysis rate coefficients were estimated for 1st July conditions.

10.2 Results

Table 10.1 presents the 5-day time-averaged ozone production rates required to keep the ozone mixing ratios at their constraints, averaged over all 32 sets of background environmental conditions for the nine chemical mechanisms under base case conditions. The dispersion in the ozone production rates between the nine chemical mechanisms was vanishingly small (within ±0.5%), showing that the standardisation and harmonisation procedures had not introduced significant bias between the chemical mechanisms.

Despite the excellent agreement between the base case ozone production rates, there were significant differences in the responses of the ozone production rates to 30% reductions in NO_x and VOCs. Ozone production rates decreased by between 26.2–29.2% in response to 30% NO_x controls and by 5.8–7.9% in response to 30% VOC controls. The ozone production rates predicted with the *CBM4* mechanism were the most responsive to NO_x controls and with the CRIv2 mechanism, the least. The *SAPRC-99* mechanism was the most responsive to VOC controls and the *CB6* mechanism, the least. Because the NO_x responses were more negative than the corresponding VOC responses, it was concluded that the ozone production regime was NO_x–limited.

Table 10.2 presents the 5-day average hydroxyl radical number densities under base case conditions, averaged over the 32 sets of background environmental conditions with the nine chemical mechanisms. The dispersion in the hydroxyl radical number densities was significant, between 3.09–3.69 $\times$ 10^6 molecule cm^{-3}, despite the small dispersion in the base case ozone production rates in Table 10.1 above. This dispersion was significantly more marked when background environmental conditions gave NO_x levels below about 1.5 ppb.

Table 10.2 Summary of the 5-day averaged hydroxyl number densities predicted with each mechanism under base case conditions, averaged over all 32 sets of environmental conditions. Also shown are the percentage responses in hydroxyl radical number densities to 30% reductions in NO_x and VOCs

Chemical mechanism	5-day average OH number densities, 10^6 molecule cm^{-3}	Percentage response in OH to 30% NO_x reduction	Percentage response in OH to 30% VOC reduction
CBM4	3.68	−6.93	+6.89
CB05	3.63	−8.89	+6.94
CB6	3.09	−8.66	+6.41
CRIv2	3.24	−9.77	+7.87
EMEP	3.62	−8.03	+7.31
GEOS-CHEM	3.69	−8.35	+5.49
MCMv3.3	3.39	−8.74	+7.46
SAPRC-99	3.35	−9.25	+8.74
SAPRC-07	3.52	−8.44	+7.57

In response to 30% reductions in NO_x, 5-day averaged hydroxyl number densities decreased by 6.93–9.77%. Whereas in response to 30% reductions in VOCs, hydroxyl radical number densities increased by 5.40–8.74%, see Table 10.2. The hydroxyl radical number densities predicted with the CRIv2 mechanism were the most responsive to NO_x, with *CBM4* the least. *SAPRC-99* was the most responsive to VOCs with *GEOS-CHEM*, the least. The large ranges in the OH responses to 30% reductions in NO_x and VOCs between the mechanisms will mean that there are uncertainties in the knock-on predictions for the responses in the deposition of acidic species which are mechanism dependent. This is because the OH radical number density fixes the production of gaseous nitric acid from NO_x and the oxidation of sulphur dioxide by OH and hydrogen peroxide.

10.3 Conclusions

The good agreement found between the mechanisms for ozone and its responses to NO_x and VOC reductions should give confidence to policy-makers in formulating efficient control strategies based on them, despite there being significant differences in detail between them. The predictions of OH radical number densities were significantly more mechanism dependent than those of ozone and this greater variability will be reflected in the predicted responses of acidic deposition species to NO_x and VOC reductions.

Acknowledgements The authors of the chemical mechanisms are gratefully thanked for their help and advice with the implementation of the mechanisms.

Questions and Answers

Questioner: Emmanouil Oikonomakis
Question: Why do the ozone production rates and OH radical number densities diverge in low NO_x conditions for the different chemical mechanisms but in high NO_x conditions they do not?
Answer: Under high NO_x situations, the reactions of OH with VOCs generate HO_2 and RO_2 radicals which are efficiently recycled back to OH to continue the fast photochemistry. However, as NO_x levels fall, HO_2 and RO_2 radicals increasingly react amongst themselves to form organic hydroperoxides and terminate the free radical chain reactions and reduce photochemical ozone production. These reactions have not been well studied in smog chamber systems so there are large divergences between the chemical mechanism under these conditions.

Questioner: Johannes Bieser
Question: Based on your analysis, can you give a ranking of the different chemical mechanism?
Answer: Which is the best mechanism to use depends on the implementation and application. If the application describes ozone production on the regional scale from largely man-made VOC precursors, then mechanism choice is not an important issue and all the tested mechanisms will work satisfactorily. However, if the application deals with individual VOCs, then the choice of mechanism will be crucial. Such applications include situations with large emissions of biogenic VOCs such as isoprene, the fate and behaviour of air toxics, studies of local ozone formation from highly reactive VOCs and the generation of VOC reactivity scales. For these applications, explicit mechanism such as the Master Chemical Mechanism are recommended.

References

Carter WPL (2010) Development of a condensed SAPRC-07 chemical mechanism. Atmos Environ 44:5336–5345

Derwent RG, Utembe SR, Jenkin ME, Shallcross DE (2015) Tropospheric ozone production regions and the intercontinental origins of surface ozone over Europe. Atmos Environ 112:216–224

Emmerson KM, Evans MJ (2009) Comparison of tropospheric gas-phase chemistry schemes for use within global models. Atmos Chem Phys 9:1831–1845

Environ International Corporation (2015) CAMx user's guide version 6.2, Novato, California

Gery MW, Whitten GZ, Killus JP, Dodge MC (1989) A photochemical kinetics mechanism for urban and regional scale computer modelling. J Geophys Res 94:12925–12956

Jenkin ME, Watson LA, Utembe SR, Shallcross DE (2008) A Common Representative Intermediates (CRI) mechanism for VOC degradation. Part 1: gas phase mechanism development. Atmos Environ 42:7185–7195

Jenkin ME, Young JC, Rickard AR (2015) The MCM v3.3 degradation scheme for isoprene. Atmos Chem Phys Discuss 15:9709–9766

Simpson D, Benedictow A, Berg H, Bergstrom R, Emberson LD, Fagerli H, Flechard CR, Hayman GD, Gauss M, Jonson JE, Jenkin ME, Nyiri A, Richter C, Semeena VS, Tsyro S, Tuovinen J-P, Valdebenito A, Wind P (2012) The EMEP MSC-W chemical transport model—technical description. Atmos Chem Phys 12:7825–7865

Chapter 11
Overview and Evaluation of the Community Multiscale Air Quality (CMAQ) Modeling System Version 5.2

K. Wyat Appel, Sergey Napelenok, Christian Hogrefe, George Pouliot, Kristen M. Foley, Shawn J. Roselle, Jonathan E. Pleim, Jesse Bash, Havala O.T. Pye, Nicholas Heath, Benjamin Murphy and Rohit Mathur

Abstract A new version of the Community Multiscale Air Quality (CMAQ) model, version 5.2 (CMAQv5.2), is currently being developed, with a planned release date in 2017. The new model includes numerous updates from the previous version of the model (CMAQv5.1). Specific updates include a new windblown dust scheme; updates to the organic aerosol treatment; updates to the atmospheric chemistry, including the Carbon-Bond 6 chemical mechanism; and various updates to the cloud treatment in the model. In addition, a new lightning assimilation scheme has been implemented in WRF, the meteorological driver for the CMAQ simulations, which greatly improves the placement and intensity of precipitation, which in turn results in improved CMAQ performance. Comparisons between CMAQv5.1 and v5.2 show that ozone (O_3) mixing ratios generally increase in the summer with CMAQv5.2, which results in increased bias, while fine particulate matter ($PM_{2.5}$) concentrations also increase in the summer, which results in decreased bias.

11.1 Introduction

A number of important science updates are in development and will be available in the next release of CMAQ (version 5.2) which update or correct known issues in v5.1 (Appel et al. 2017), and improve upon the existing science in the model. These

K. Wyat Appel (✉) · S. Napelenok · C. Hogrefe · G. Pouliot · K.M. Foley · S.J. Roselle · J.E. Pleim · J. Bash · H.O.T. Pye · N. Heath · B. Murphy · R. Mathur
Computational Exposure Division, National Exposure Research Laboratory, U.S. Environmental Protection Agency, Research Triangle Park, NC 27711, USA
e-mail: appel.wyat@epa.gov

C. Hogrefe
e-mail: hogrefe.christian@epa.gov

R. Mathur
e-mail: mathur.rohit@epa.gov

C. Mensink and G. Kallos (eds.), *Air Pollution Modeling and its Application XXV*, Springer Proceedings in Complexity, DOI 10.1007/978-3-319-57645-9_11

updates include a new version of the windblown dust (WBD) treatment, the Carbon-Bond 6 (CB6) chemical mechanism, enhancements to the calculation of semi-volatile Primary Organic Aerosol (POA) and Secondary Organic Aerosol (SOA) from combustion sources in CMAQ, and additional updates to the calculation of clouds. In addition to the model updates, a number of instrumented versions of the model (e.g. decoupled direct method, sulfur tracking) will also be released with v5.2. These updates represent potentially significant improvements over the current options in v5.1 (specifically the updated WBD treatment) and therefore are being made available to the community more quickly than they might have in the past. Below is a brief description of several of the major planned updates for v5.2.

11.2 CMAQv5.2 Updates

A physics-based windblown dust emission parameterization was developed and implemented into v5.2. This model formulates the dust emission due to saltation (sandblasting). A distinct feature of this implementation of the windblown dust treatment is that it includes the incorporation of a newly developed dynamic relation for the surface roughness length, which is important in correctly predicting both the friction velocity and its threshold value used in the dust emission model. Using this new relation, the effects of larger solids (such as pebbles) and vegetative non-erodible elements in local wind acceleration, drag partitioning, and protective coverage is formulated in a consistent manner. The fraction of absorbed photosynthetically active radiation (PAR) from the Moderate Resolution Imaging Spectroradiometer (MODIS) is used to represent more realistic time-varying vegetation coverage in this model. Additionally, the threshold friction velocity for dust emission is updated to reflect the dependency on soil grain size. The idea behind this approach is that the soil particles with diameters from 60 to 200 μm are most likely to be picked up by the wind, resulting in saltation and vertical dust emission. For smaller particles, cohesive forces prevent the saltation, while larger particles are harder to move due to the gravitational force.

Updates for v5.2 also include a semivolatile POA treatment, an empirical representation of anthropogenic combustion SOA, and improved SOA species properties (e.g. ratio of aerosol organic mass to aerosol organic carbon, density, Henry's law coefficient). The goal of these updates is to provide a more realistic representation of aerosol in terms of volatility and primary versus secondary partitioning and to provide a meaningful characterization of the organic aerosol for future work in the area of aqueous-organic interactions. CMAQv5.2 now includes support for the CB6r3 chemical mechanism. While similar to CB05 in the general condensation approach, CB6r3 has some important improvements. It includes additional explicit and model species to represent longer-lived but abundant organics, such as acetone, benzene, propane and acetylene, additional radicals to represent low-NOx radical reactions, explicit glyoxal and analogs. In CB6, many reaction rates and products

have been updated to be consistent with recent research, including reactions of isoprene, aromatic hydrocarbons, and reactions of peroxy radicals with HO_2. While several of the reaction rate and product updates are present in both CB6r3 and CB05e51, CB6r3 has a much more comprehensive updating.

The cloud parametrization in CMAQ v5.1 overestimated the cloud fraction over large bodies of water, the Great Lakes and ocean in the domain considered here when compared to WRF output and GOES satellite observation. This overestimation was found to be due to the relative humidity function in CMAQ's sub-grid cell shallow convective cloud parameterizations. The CMAQ sub-grid cell shallow convective cloud parameterization in v5.2 is being made more consistent with WRF v3.7. This results in a reduction of the estimated cloud fractions in v5.2 over large bodies of water, and the estimates are closer to those of WRF v3.7 and the GOES satellite observations. This impacts the vertical mixing of pollutants in clouds in CMAQ and photolysis rates, with a general reduction in the mean O_3 in most coastal areas on the order of 1.0 ppbv due to a larger reduction in mixing from aloft than increases from photolysis.

11.3 Results and Discussion

CMAQ simulations were performed for January and July, 2011 using both CMAQv5.1 and v5.2 in order to assess the impact that the updates to the modeling system had on the model performance for maximum 8-hr average (MDA8) O_3 and $PM_{2.5}$. Shown in Fig. 11.1 is the difference in absolute bias between CMAQv5.1 and v5.2 (v5.2–v5.1) for July, where cool colors indicate a decrease in bias in v5.2, while warm colors indicate an increase in bias. For $PM_{2.5}$, the bias decreases across almost the entire domain (nearly 80% of the sites report a decrease in bias), as $PM_{2.5}$ is typically underestimated by CMAQ in the summer and $PM_{2.5}$ increases in the summer in v5.2. For MDA8 O_3, the change in bias is mixed across the domain (45% of the sites report a decrease in bias), with decreased O_3 bias in the northeast, southeast, and along the west coast, and increased bias in the Great Lakes region and in the San Joaquin Valley of California. Overall, the science updates incorporated into WRF and CMAQv5.2 should result in improved model performance, particularly for $PM_{2.5}$.

11.4 Disclaimer

Although this work has been reviewed and approved for publication by the U.S. Environmental Protection Agency, it does not necessarily reflect the views and policies of the agency.

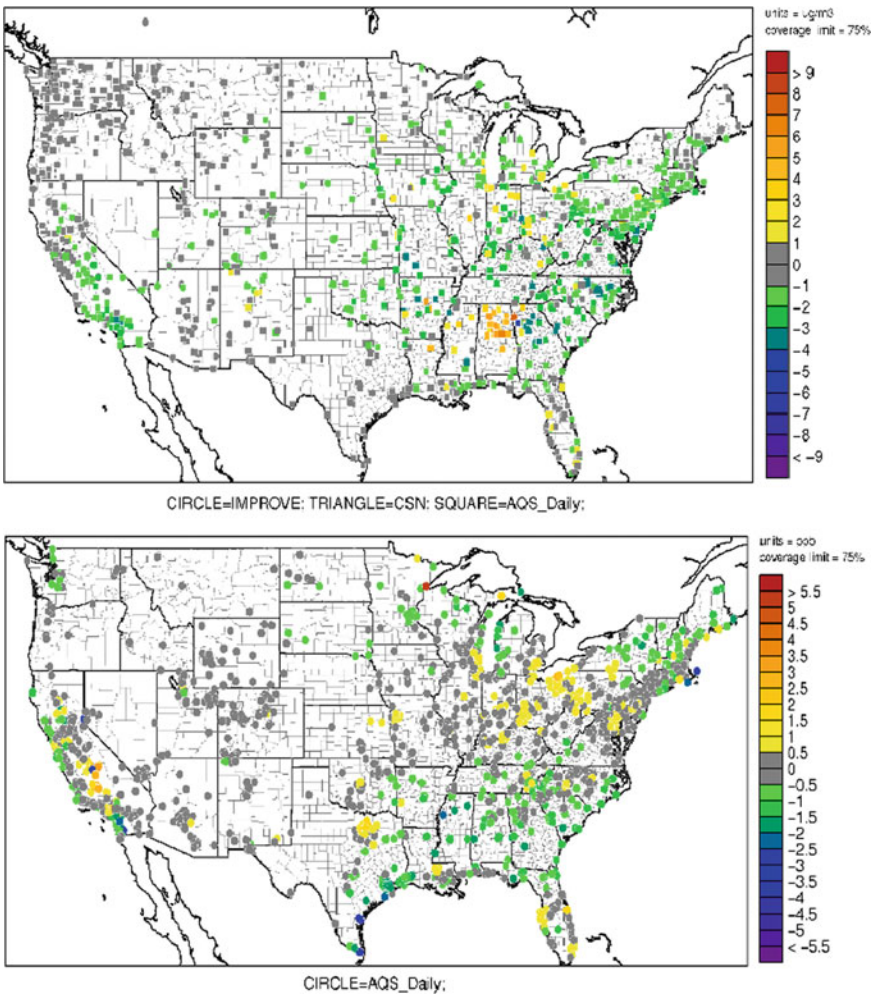

Fig. 11.1 Change in absolute bias for $PM_{2.5}$ (*top*, μgm^{-3}) and MDA8 O_3 (*bottom*, ppbv) for July 2011

Questions and Answers

Questioner: Chris Nolte

Question: The change in ozone during summer between CMAQv5.1 and CMAQv5.2 is very dramatic. The largest contribution to that decreases appears to be the change in how boundary conditions are generated. Has any work been done to determine why these differences exist? Is GEOS-Chem ozone that much higher than hemispheric CMAQ? Are there important differences in ozone precursors in

the later boundaries? And is the potential vorticity scaling approach used in the CONUS 12-km domain, or only for the hemispheric domain?
Answer: Since the hemispheric CMAQ simulations are relatively new, work is ongoing to evaluate why differences exist between hemispheric CMAQ and GEOS-Chem, which includes examining precursors. I don't believe the PV scaling approach was applied in the 12-km domain.

Questioner: S. Aksoyoglu
Question: Was the improvement in $PM_{2.5}$ due to inclusion of semi-volatile POA the same in winter and summer.
Answer: $PM_{2.5}$ is reduced in both summer and winter due to the semi-volatile POA. However, the addition of SOA from assumed combustible sources contributes more to $PM_{2.5}$ in the summer than the semi-volatile POA reduces $PM_{2.5}$. The overall result is a reduction in $PM_{2.5}$ in the winter and an increase in $PM_{2.5}$ in the summer.

Questioner: Silvia Trini Castelli
Question: What is the reason, and your interpretation, for the worse-error cases after the model changes and improvements?
Answer: We actually saw large reductions in error in both $PM_{2.5}$ and ozone in CMAQv5.2. There are some isolated areas where $PM_{2.5}$/ozone error increased, but overall both species were largely improved.

Questioner: Clemens Mensink
Question: Based on your analysis, can you advise on where further model improvements are needed?
Answer: Work still needs to be done to improve the representation of meteorology, particularly in coastal areas and regions with complex terrain. In addition, emissions inventories can always benefit from improvement.

Reference

Appel KW, Napelenok SL, Foley KM, Pye HOT, Hogrefe C, Luecken DJ, Bash JO, Roselle SJ, Pleim JE, Foroutan H, Hutzell WT, Pouliot GA, Sarwar G, Fahey KM, Gantt B, Gilliam RC, Kang D, Mathur R, Schwede DB, Spero TL, Wong DC, Young JO (2017) Overview and evaluation of the Community Multiscale Air Quality (CMAQ) model version 5.1. Geosci Model Dev. doi:10.5194/gmd-1703-2017

Chapter 12
A Comprehensive Performance Evaluation of the Next Generation of the Canadian Operational Regional Air Quality Deterministic Prediction System

Michael D. Moran, Alexandru Lupu, Junhua Zhang, Verica Savic-Jovcic and Sylvie Gravel

Abstract The core of the Environment and Climate Change Canada (ECCC) operational Regional Air Quality Deterministic Prediction System (RAQDPS) is the GEM-MACH air quality model, which consists of an on-line chemical transport model embedded within the GEM model, ECCC's multi-scale operational weather forecast model. A new version of GEM-MACH, version 2, which is based on the next-generation version of GEM, became operational earlier this year (2016) after 4 years of development and testing. A comprehensive evaluation of the performance of GEM-MACH version 2 for a 2010 annual simulation on a 10-km North American continental grid was performed as part of this implementation effort using measurements from multiple Canadian and U.S. air-chemistry and precipitation-chemistry surface networks. One evaluation metric considered was skill in predicting annual mean values of a number of gas- and particle-phase species, including $PM_{2.5}$ chemical components such as elemental carbon and crustal material. Such an analysis of time-averaged spatial fields is useful to check for systematic errors in input emissions fields, in chemical lateral boundary conditions, and in the representation of atmospheric dispersion, chemistry, and removal processes by the model. Spatial R values for NO_2, O_3, and $PM_{2.5}$ mean annual concentrations in air for all networks were 0.84, 0.76, and 0.58, and for $PM_{2.5}$ chemical components SO_4, NO_3, NH_4, EC, OM, and CM the corresponding R values were 0.95, 0.88, 0.78, 0.77, 0.54, and 0.41. For $SO_4^{=}$, NO_3^{-}, and NH_4^{+} mean annual concentrations in precipitation the R values were 0.79, 0.80, and 0.92.

M.D. Moran (✉) · A. Lupu · J. Zhang · V. Savic-Jovcic
Air Quality Research Division, Environment and Climate Change Canada, Toronto, ON, Canada
e-mail: Mike.Moran@canada.ca

S. Gravel
Air Quality Research Division, Environment and Climate Change Canada, Montreal, QC, Canada

C. Mensink and G. Kallos (eds.), *Air Pollution Modeling and its Application XXV*, Springer Proceedings in Complexity, DOI 10.1007/978-3-319-57645-9_12

12.1 Introduction

Version 1 of the Global Environmental Multiscale–Modelling Air quality and CHemistry (GEM-MACH) chemical weather model has served as the core of the ECCC operational regional air quality (AQ) forecasting system known as the RAQDPS since 2009 (Moran et al. 2014; Pavlovic et al. 2016). A next-generation version, GEM-MACH v2, became operational in 2016 (Moran et al. 2016).

RAQDPS performance is monitored routinely at ECCC using near-real-time hourly AQ measurements of a handful of chemical species, in particular O_3, NO_2, and $PM_{2.5}$, made by multiple North American air-chemistry networks. However, if model predictions are evaluated for an extended past period (e.g., an entire year), then it is possible to consider a much larger set of *quality-controlled* measurements for a larger number of species from both air- and precipitation-chemistry networks than is possible in real time due to the delay of months or even years associated with the process of sample collection, transport, analysis, checking, and delivery that must be followed by many AQ networks.

This paper presents selected results from a comprehensive performance evaluation for such an extended past period, in this case a 1-year simulation of North American atmospheric chemistry for the year 2010 made using GEM-MACH v2. One reason to choose the year 2010 for this evaluation was that two AQ field studies, the California Nexus study (CalNex) and the Whistler Atmospheric Chemistry Study (WACS 2010), took place that year in North America, which allows access to special non-network AQ data sets (e.g., Ryerson et al. 2013; Wainwright et al. 2012). A second reason was that 2010 had already been chosen as the simulation period for two international AQ model intercomparison initiatives (AQMEII-2, HTAP2), which allows GEM-MACH v2 performance for 2010 to be compared with that of a number of peer models (e.g., Im et al. 2015; Stjern et al. 2016).

12.2 Model Description and Application

For this 2010 annual evaluation GEM-MACH v2 was run for a 13-month period from 1 Dec. 2009 to 31 Dec. 2010 on a North American latitude-longitude grid with 10-km horizontal grid spacing and 80 hybrid sigma-pressure levels extending from the Earth's surface to 0.1 hPa. The first month was treated as a chemistry spin-up period. Following ECCC operational practice 48-h runs were launched every 12-h during this period beginning at 00 and 12 UTC. Initial chemical fields were obtained from the 12th-hour fields of the preceding run. Spatially- and seasonally-varying chemical lateral boundary conditions (LBC) were specified using 3-month mean fields (Dec.–Feb., etc.) based on 6-h fields from a 1-year simulation for 2009 with the MOZART4 global chemical transport model run on a 1.9° by 2.5° grid. Initial meteorological fields were obtained from Canadian

Meteorological Centre analyses and hourly meteorological LBC fields were obtained from a GEMv4.7 annual run on a global 15-km Yin-Yang grid. The GEM-MACH runs used the same physics configuration as the global GEM run. Input emissions were based on a 2010 Canadian national emissions inventory, a 2011 U.S. inventory, and a 1999 Mexican inventory (Moran et al. 2015).

12.3 Evaluation Data and Results

An updated version of the 2010 AQ measurement data base for North America used in the AQMEII2 model intercomparison was used for this study (Im et al. 2015). Quality-assured AQ measurement data sets for 2010 were obtained from six North American air-chemistry networks for gas-phase and/or particle-phase species (AQS, CAPMoN, CASTNet, CSN, IMPROVE, NAPS) and five precipitation-chemistry networks (AIRMoN, CAPMoN, NBPMN, NSPSN, NTN). Sampling periods varied from network to network and species to species and included hourly, 24-h every day, 24-h every third or sixth day, and weekly periods.

Four evaluation processing steps were then carried out to compare model predictions with measurements. The first step was to match modelled and measured species. For example, GEM-MACH considers nine particulate-matter (PM) chemical components: p-SO_4 (particle sulphate); p-NH_4 (ammonium); p-NO_3 (nitrate); p-EC (elemental carbon); p-POM (primary organic matter); p-SOM (secondary organic matter); p-CM (crustal material); p-SS (sea salt); and p-WA (particle-bound water). Since $PM_{2.5}$ speciation networks (CSN, IMPROVE, NAPS) measure organic carbon (OC), model p-POM and p-SOM components must be summed to obtain p-OM values while measured OC values must be converted to OM values by applying a scaling factor. An OM: OC scaling factor of 1.8 was used, although other values suggested in the literature (1.4, 2.1) were tested. In the case of p-CM the well-known IMPROVE formula was used to estimate measured p-CM based on measured elemental concentrations of Al, Ca, Fe, Si, and Ti.

The second step was to match model predictions with the hourly, daily, or weekly measurement sampling periods by averaging (concentration) or accumulating (wet deposition) hourly grid-cell values, noting that measurement start time varies by network. The third step, if required, was to aggregate model-measurement data pairs in time to longer periods, including daily, weekly, monthly, seasonal, and annual periods. This step is necessary in order to perform multi-network analyses when sampling period varies between networks. Finally, the fourth step was to ensure representativeness by imposing a data-completeness threshold of 75% for concentration measurements for each temporal aggregation period and remove data pairs below this threshold. For wet concentration and wet deposition measurements, the corresponding completeness threshold was to require that the total precipitation associated with valid chemistry data must be at least 85% of the aggregation period's total precipitation.

Statistical analyses were then performed on the resulting model-measurement data pairs for all measured species for both individual networks separately and for combined networks, and for the network sampling period (e.g., hourly, daily) and for longer aggregated time periods (e.g., monthly, seasonally). Temporal aggregation reduces the number of available data points but has the benefit of reducing temporal variability and focussing on model prediction of spatial patterns (Schaap et al. 2015), which is useful for assessing correctness and impact of input emissions, chemical lateral boundary conditions, representation of atmospheric dispersion, and overall representation of chemistry and removal processes.

Here we show 2010 annual results for selected species. Figure 12.1 shows the locations of all stations measuring NO_2, O_3, and $PM_{2.5}$ together with scatterplots of predicted versus measured annual abundances of these three species for stations with complete annual records. Pearson's correlation coefficient (R) values were 0.84, 0.76, and 0.58 for NO_2, O_3, and $PM_{2.5}$ and normalized mean bias (NMB) values were 19, 1, and −1% across 481, 896, and 1199 stations. Note that the many U.S. stations that measure O_3 only during the ozone season were excluded.

Corresponding scatterplots of annual concentrations for six $PM_{2.5}$ chemical components are shown in Fig. 12.2. The statistics for these species have a wider range, with R values of 0.95, 0.88, 0.78, 0.77, 0.54, and 0.41 and NMB values of

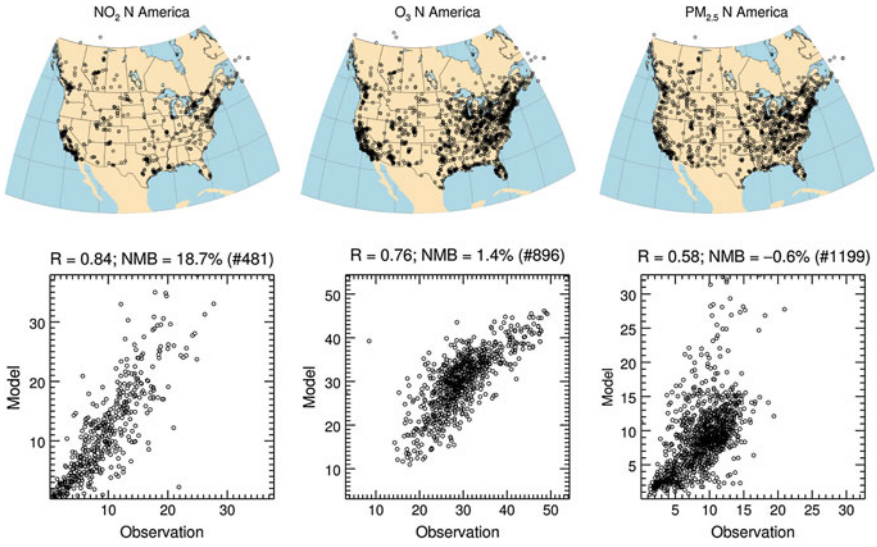

Fig. 12.1 (*Upper row*) Locations of North American stations measuring (*left*) NO_2, (*centre*) O_3, and (*right*) $PM_{2.5}$; (*lower row*) scatterplots of predicted versus measured annual abundances of (*left*) NO_2 [ppbv], (*centre*) O_3 [ppbv], and (*right*) $PM_{2.5}$ [ug m^{-3}] for AQS, CASTNet, and NAPS stations with 75% annual completeness

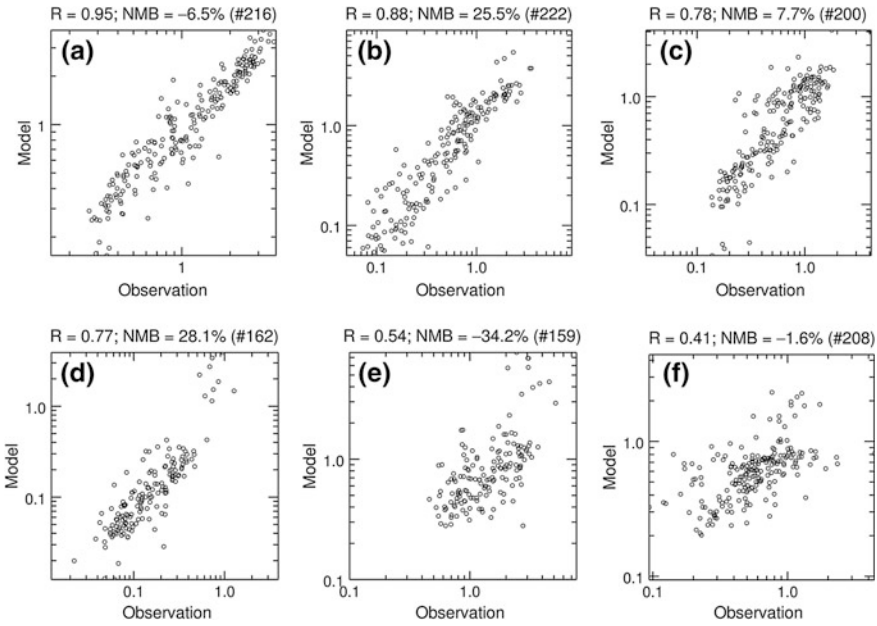

Fig. 12.2 Scatterplots of predicted versus measured annual concentrations [ug m^{-3}] of $PM_{2.5}$ chemical components **a** SO_4, **b** NO_3, **c** NH_4, **d** EC, **e** OM, and **f** CM for CSN, IMPROVE, and NAPS stations with 75% annual completeness

−7, 26, 8, 28, −34, and −2% for 216, 222, 200, 162, 159, and 208 stations (same order as figure). Model performance is best for SO_4, NO_3, and NH_4. The quite good results for EC and CM, which are effectively passive tracers, suggest that the emissions used for these species are reasonable. OM has the largest NMB value (−34%): one possible explanation for this general low bias is that SOM concentrations are underpredicted by the model. It is also worth noting that in the AQMEII2 model intercomparison for 2010, GEM-MACH v1 was found to strongly overpredict $PM_{2.5}$-SO_4 (Im et al. 2015). The introduction of a mass-conserving tracer advection scheme in version 2 likely helped to correct this problem.

The use of precipitation-chemistry measurements for evaluation provides a useful complement to the air-chemistry measurements. Consistent with the speciated $PM_{2.5}$ results from Fig. 12.2, performance for the three major inorganic species is good. R values for $SO_4^{=}$, NO_3^{-}, and NH_4^{+} mean annual concentrations in precipitation were 0.79, 0.80, and 0.92, respectively, while NMB values were 14, −4, and 16% for 208 stations. One inconsistency, however, is the small negative NMB value for nitrate in precipitation (−4%) versus the positive values of 26% for p-NO_3 in air and 76% for HNO_3 in air (but R of 0.83) based on annual measurements from the CAPMoN and CASTNet networks. Overall, the above results suggest that systematic errors are not a major issue for this new model version.

Questions and Answers

Questioner: Sebnem Aksoyoglu
Question: The performance for annual nitrate looks quite good. Is it good also in winter?
Answer: The winter performance for $PM_{2.5}$-NO_3 was actually slightly better than the annual performance (n = 208, R = 0.90, NMB = 5%). By contrast, autumn performance was the least good (n = 212, R = 0.87, NMB = 80%).

Questioner: Jeff Weil
Question: Many of the plots showing predicted versus observed concentrations showed very large scatter (factor of 10–100) and thus the concentration variance is a very big problem. Do you, your group, or others in the modeling community attempt to model or predict this concentration variance? Such modeling would seem to be a problem worthy of attention.
Answer: Large scatter between model predictions and measurements is always of concern, but for regional chemical transport models (CTMs) there are many sources of such statistical dispersion, including measurement errors and uncertainties in numerical representations of emissions, meteorology, transport and diffusion, chemical transformation, and removal processes. An additional source of scatter arises from the inherent incommensurability between point measurements and model grid-volume predictions. I believe that the focus of the CTM community has been to reduce such scatter rather than trying to model or predict it.

References

Im U et al (2015) Evaluation of operational online-coupled regional air quality models over Europe and North America in the context of AQMEII phase 2 Part II: Particulate matter. Atmos Environ 115:421–441. doi:10.1016/j.atmosenv.2014.08.072

Moran MD et al (2014) Recent advances in Canada's national operational AQ forecasting system. In: Steyn DG, Builtjes PJH, Timmermans RMA (eds) Air pollution modeling and its application XXII, pp 215–220. Springer, Dordrecht. doi:10.1007/978-94-007-5577-2_4

Moran M, Zheng Q, Zhang J, Pavlovic R (2015) RAQDPS version 013: upgrades to the CMC operational regional air quality deterministic prediction system released in June 2015. Technical note, Nov., Canadian Meteorological Centre, Montreal, p 54. http://collaboration.cmc.ec.gc.ca/cmc/cmoi/product_guide/docs/lib/op_systems/doc_opchanges/Technical_Note_GEM-MACH10_v1.5.3+SET2.1.1_Emissions_9Nov2015.pdf

Moran M, Gravel S, Savic-Jovcic V, Pavlovic R, Lupu A (2016) RAQDPS versions 015 and 016: migration of the CMC operational regional air quality deterministic prediction system to the next generation of the GEM numerical weather prediction model. Technical note, Dec., Canadian Meteorological Centre, Montreal [In preparation]

Pavlovic R, Chen J, Anderson K, Moran MD, Beaulieu P-A, Davignon D, Cousineau S (2016) The FireWork air quality forecast system with near-real-time biomass burning emissions: recent developments and evaluation of performance for the 2015 North American wildfire season. J Air Waste Manag Assoc. doi:10.1080/10962247.2016.1158214

Ryerson TB et al (2013) The 2010 California research at the Nexus of air quality and climate change (CalNex) field study. J Geophys Res 118:5830–5866

Schaap M et al (2015) Performance of European chemistry transport models as function of horizontal resolution. Atmos Environ 112:90–105

Stjern CW et al (2016) Global and regional radiative forcing from 20% reductions in BC, OC and SO_4—an HTAP2 multi-model study. Atmos Chem Phys 16:13579–13599. doi:10.5194/acp-16-13579-20

Wainwright CD, Pierce JR, Liggio J, Strawbridge KB, Macdonald AM, Leaitch RW (2012) The effect of model spatial resolution on Secondary Organic Aerosol predictions: a case study at Whistler, BC, Canada. Atmos Chem Phys 12:10911–10923

Chapter 13
Assessment of Black Carbon in Arctic: Current Status and Potential Improvements

J. Soares, C. Geels, J. Langner, S. Tsyro, A. Kurganskiy, J. Ström, J.-C. Gallet, M. Ruppel and M. Sofiev

Abstract This multi-model study discusses how physical characteristics of black carbon (BC) and removal processes are influencing BC concentrations and depositions in the Arctic and how trends for concentration and depositions are important to understand BC as a short-term climate forcer.

13.1 Introduction

BC is an important short-term climate forcer, in particular over the Arctic. The absorption of radiation caused by BC-containing aerosols over a highly reflective surface, such as snow, will result in a warming at high-altitudes and at the surface

J. Soares (✉) · M. Sofiev
Finnish Meteorological Institute, Helsinki, Finland
e-mail: joana.soares@fmi.fi

C. Geels
Department of Environmental Science, Aarhus University, Aarhus, Denmark
e-mail: cag@envs.au.dk

J. Langner
Swedish Meteorological and Hydrological Institute, Norrköping, Sweden

S. Tsyro
EMEP MSC-W, Norwegian Meteorological Institute, Oslo, Norway

A. Kurganskiy
Niels Bohr Institute, University of Copenhagen, København, Denmark

J. Ström
Department of Environmental Science and Analytical, Stockholm University, Stockholm, Sweden

J.-C. Gallet
Norwegian Polar Institute, 9296 Tromsø, Norway

M. Ruppel
Department of Environmental Sciences, University of Helsinki, Helsinki, Finland

C. Mensink and G. Kallos (eds.), *Air Pollution Modeling and its Application XXV*,
Springer Proceedings in Complexity, DOI 10.1007/978-3-319-57645-9_13

due to an increase of the downward longwave radiation. In snow, BC will intensify the melting of the snow pack. Based on observations and model results, atmospheric BC concentrations have declined in the Arctic, during the last decades (AMAP 2011). With BC being mainly wet-deposited in the Arctic (Wang et al. 2011), the warming of the atmosphere in the last decades resulted in an increasing of wet deposition and, consequently, increasing BC concentration in snow as reported in core measurements in Svalbard, Norway (Ruppel et al. 2014). Multi-model studies show a discrepancy between models towards northern latitudes (e.g. Eckhardt et al. 2015). Stohl et al. (2013) shows a misrepresentation of emissions for atmospheric composition in the Arctic.

13.2 Methods

This modelling study includes long-term results (1980–2014) from SILAM model, and a study involving several CTMs (DEHM, Enviro-HIRLAM, EMEP, MATCH and SILAM) for 2010, to analyse predicted surface concentration and deposition in snow. The models set-up is shown in Table 13.1.

For the long term runs, SILAM was driven by ERA-Interim meteorological ields (Dee et al. 2011) and emissions from MACCity (Granier et al. 2011) with flaring emissions from ECLIPSE (Klimont et al. 2013). The validation of the models via concentration and deposition measurements, close to BC sources and in remote places (Arctic sites) was done for 2010, with measurement data obtained from http://www.ebbas.nilu.no.

Table 13.1 model setting for the run for 2010

Model	Meteorological fields	Emissions	Resolution	Ageing
DEHM	ERA-INTERIM	ECLIPSE (Klimont et al. 2013) shipping: RCP6 (Fujino et al. 2006); STEAM (Jalkanen et al. 2012) fires: IS4FIRES (Soares et al. 2015	1.5 × 1.5	OH oxidation (Liu et al. 2011)
EMEP	ERA-INTERIM		0.72 × 0.72	Hydrocopicity (Riemer et al. 2004)
Enviro-HIRLAM	Internal		0.72 × 0.72	aerosol microphysics and dynamics (Vignati et al. 2011)
MATCH	ERA-INTERIM		0.72 × 0.72	OH oxidation (Liu et al. 2011)
SILAM	ERA-INTERIM		0.72 × 0.72	–

13.3 Results and Discussion

The results for 2010 show that the CTMs can represent BC atmospheric concentrations very differently, especially towards the Arctic (Fig. 13.1).

Evaluation of the models show that correlation coefficients are relatively good over Europe (up-to 70) but poor for Arctic sites (<40) and bias is low over Europe (all models) but high for SILAM, EMEP, ENVIRO-HIRLAM; low for DEHM and MATCH for Arctic sites. SILAM ageing was not introduced to compare the models with and without BC ageing. It is clear that is not due to ageing that models show a striking difference. Adding ageing of the aerosol to SILAM does not bring further improving to the model results (Fig. 13.2); changing particle size distribution seems

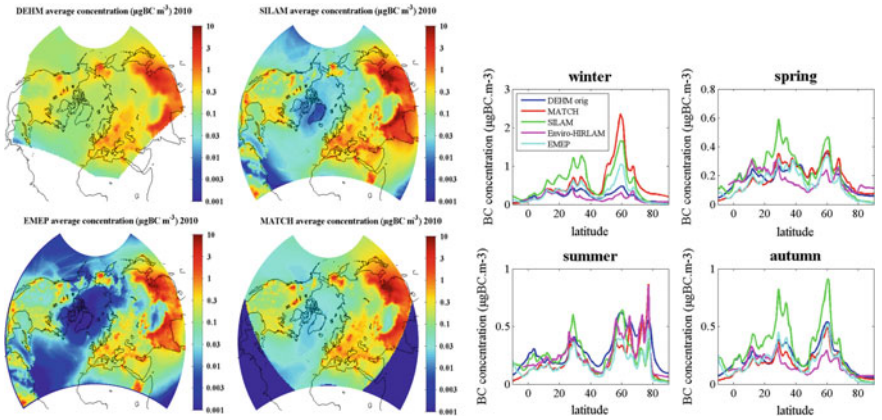

Fig. 13.1 BC surface concentrations (μg m^{-3}). *Left*, spatial distribution for offline models (DEHM, SILAM, EMEP and MATCH); *right*, longitude-wise averaged for all the models

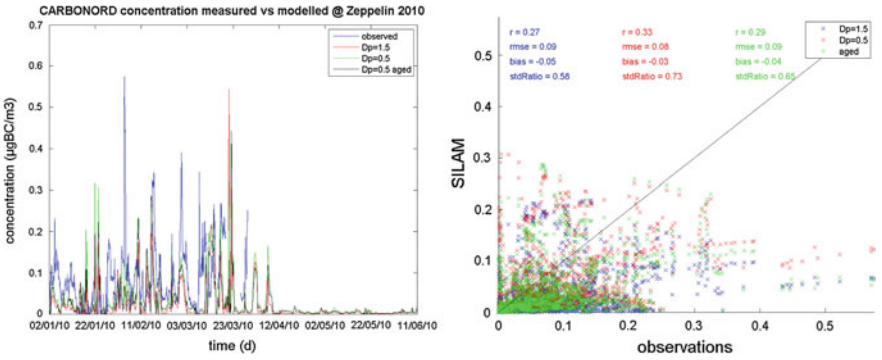

Fig. 13.2 Validation of model results with surface concentration observations (μg m^{-3}) at Zeppelin, Norway, for 2010: timeseries and scatter plot assuming different size distributions and ageing

to be the most relevant parameter, e.g. mean *Dp* from 1.5 to 0.5 μm results that the transport of BC is lengthier and increases surface concentrations predicted by the model. Nevertheless, it can have the opposite effect, in very specific cases such as when the plume hitting the station is due to domestic heating.

Long-term modeling work with SILAM has the potential of renewing the general conception of meteorological processes driving BC deposition trends. Preliminary model results prepared for the Holtedahlfonna glacier show that while both modelled and observed atmospheric BC concentrations declined at the site, the modelled wet deposition and observed ice core deposition increased between 1980 and 2000, most likely due to increasing temperatures increasing the cloud water content and the wash-out ratio of BC at the site. This finding highlights that BC scavenging efficiency may vary irrespective of atmospheric concentrations, for example with varying temperatures during cloud formation. Thus, temporal trends in atmospheric BC concentrations and wet deposition may diverge. Also it was found that dry deposition is not following the same trend as atmospheric concentrations in specific places, as it would be expected, particularly in sites that are further to anthropogenic sources.

13.4 Conclusions

The current work shows that the representation of BC in CTM is too simplistic to represent the concentrations measures at Arctic sites. This could be due to misrepresentation of the aerosol dynamics but also improving emissions for in the Arctic is needed. Complement current emission inventories with accurate estimates of flaring and shipping and small wood combustion is needed. Scavenging seems to be the key process for BC models: problems reproducing the Arctic haze could be related to in-cloud scavenging, e.g. rimming processes not taking into consideration.

Acknowledgements This work was supported by the NordForsk NCoE CRAICC, Academy of Finland project 257903 and NordFork CARBONORD.

References

AMAP (2011) The impact of black carbon on arctic climate. AMAP, Oslo, Norway 72

Eckhardt S, Quennehen B, Olivié DJL, Berntsen TK, Cherian et al (2015) Current model capabilities for simulating black carbon and sulfate concentrations in the Arctic atmosphere: a multi-model evaluation using a comprehensive measurement data set, vol 15. ACP, pp 9413–9433. doi:10.5194/acp-15-9413-2015

Granier C, Bessagnet B, Bond T, D'Angiola A, van der Gon HD, Frost GJ, Heil A, Kaiser JW et al (2011) Evolution of anthropogenic and biomass burning emissions of air pollutants at global and regional scales during the 1980–2010 period. Clim Change 109:163–190. doi:10.1007/s10584-011-0154-1

Klimont Z, Smith SJ, Cofal J (2013) The last decade of global anthropogenic sulfur dioxide: 2000–2011 emissions. Environ Res Lett 8(1):014003. doi:10.1088/1748-9326/8/1/014003

Liu J, Fan S, Horowitz LW, Levy II H (2011) Evaluation of factors controlling long-range transport of black carbon to the Arctic. JGR. 116:D04307. doi:10.1029/2010JD015145

Ruppel MM, Isaksson E, Ström J, Beaudon E, Svensson J, Pedersen CA, Korhola A (2014) Increase in elemental carbon values between 1970 and 2004 observed in a 300-year ice core from Holtedahlfonna (Svalbard). ACP 14:11447–11460

Stohl A, Klimont Z, Eckhardt S, Kupiainen K, Shevchenko VP, Kopeikin VM, Novigatsky AN (2013) Black carbon in the Arctic: the underestimated role of gas flaring and residential combustion emissions. ACP 13:8833–8855. doi:10.5194/acp-13-8833-2013

Wang Q, Jacob DJ, Fisher JA, Mao J, Leibensperger EM, Carouge CC, Le Sager P, Kondo Y, Jimenez JL, Cubison MJ, Doherty SJ (2011) Sources of carbonaceous aerosols and deposited black carbon in the Arctic in winter-spring: implications for radiative forcing. ACP 11:12453–12473

Chapter 14
The Sensitivity of the Predictions of a Roadside Dispersion Model to Meteorological Variables: Evaluation Using Algorithmic Differentiation

John Backman, Curtis Wood, Mikko Auvinen, Leena Kangas, Ari Karppinen and Jaakko Kukkonen

Abstract Dispersion and transformation of air pollution originated from a network of vehicular sources can be evaluated using the CAR-FMI model, combined with a meteorological pre-processor, MPP-FMI. The aim of this study is to analyse the sensitivities of both the meteorological pre-processor and the roadside dispersion model to the variations of model input values, taking especially into account the meteorological variables. Comprehensive and systematic analyses of the sensitivities of atmospheric dispersion models have been scarce in the literature. Such sensitivity analyses can be used in the refinement of both categories of models. The sensitivity analyses have been performed using an algorithmic differentiation (AD) tool called TAPENADE. We present selected illustrative results on the sensitivities of the meteorological pre-processing model MPP-FMI and the roadside dispersion

J. Backman (✉) · C. Wood · M. Auvinen · L. Kangas · A. Karppinen · J. Kukkonen
Finnish Meteorological Institute, Erik Palménin aukio 1, Helsinki, Finland
e-mail: John.Backman@fmi.fi

C. Wood
e-mail: Curtis.Wood@fmi.fi

L. Kangas
e-mail: Leena.Kangas@fmi.fi

A. Karppinen
e-mail: Ari.Karppinen@fmi.fi

J. Kukkonen
e-mail: Jaakko.Kukkonen@fmi.fi

M. Auvinen
University of Helsinki, Erik Palménin aukio 1, Helsinki, Finland
e-mail: Mikko.Auvinen@fmi.fi; Mikko.Auvinen@helsinki.fi

C. Mensink and G. Kallos (eds.), *Air Pollution Modeling and its Application XXV*,
Springer Proceedings in Complexity, DOI 10.1007/978-3-319-57645-9_14

model CAR-FMI on the model input variables. However, the AD method in general could also be applied for analysing the sensitivities of any other atmospheric modelling system.

14.1 Introduction

A model developed at the Finnish Meteorological Institute (FMI) is used to model the emissions, dispersion, and transformation of pollution from an open road network (CAR-FMI). The model is a Gaussian finite line source model where the road network comprises the emission sources (Kukkonen et al. 2001). Like any short-range urban dispersion model, CAR-FMI requires that information about the state of the atmospheric boundary layer is provided to it externally. This information is generated by a meteorological pre-processor MPP-FMI (Karppinen et al. 1997), which uses meteorological observations to derive the necessary quantities describing the atmospheric state required by CAR-FMI. These evaluations are done by applying an energy-flux method that estimates turbulent heat and momentum fluxes in the boundary layer.

The sensitivity of this meteorological pre-processor has not previously been investigated, nor the combination of the models MPP-FMI and CAR-FMI. The sensitivity analysis of the model combination is studied using an algorithmic differentiation (AD) tool called TAPENADE (Hascoët and Pascual V 2013).

14.2 Methods

14.2.1 Meteorological Pre-processor

The meteorological pre-processor (MPP-FMI) is used to estimate turbulent fluxes, atmospheric stability, and boundary-layer scaling parameters from routine observations. These meteorological observations comprise temperature (T_2), wind speed (U), wind direction, amount of predominant clouds (C_C), cloud height (C_Z), incoming solar radiation (R_S), state of the ground (wet, dry, snow, ice etc.), and precipitation. These are the key inputs needed by the pre-processor in order to model boundary-layer scaling parameters required by the Gaussian dispersion model CAR-FMI.

The MPP-FMI is based on previous work found in literature with modifications that makes the parametrisation more suitable for high latitudes (Karppinen et al. 1997; van Ulden and Holtslag 1985). The core of the method is the surface heat budget equation $Q^* - Q_G = Q_H + Q_E$ where Q^* is the net surface radiation, Q_G is the heat flux into the soil, Q_H is the sensible heat flux, and Q_E is the latent heat flux. The meteorological observations are decomposed into components, namely to estimate the terms $Q^* - Q_G$.

The estimation then exploits that, according to surface-layer similarity theory, both friction velocity (u_*) and temperature scale for turbulent heat transfer (θ^*) can be written as a function of vertical profiles of wind speed (van Ulden and Holtslag 1985). Then the Obukhov-length L is changed, which impacts both u_* and θ^*, until θ^* calculated using a modified Penman-Monteith equation matches θ^* calculated using stability profiles (Karppinen et al. 1997; van Ulden and Holtslag 1985).

14.2.2 Roadside Dispersion Model

The roadside dispersion model (CAR-FMI) investigated in this work is a Gaussian finite line source model. The model comprise an emission model, a dispersion model, and finally statistical analysis of the obtained time series of the model results. In the model, the road network comprise a network of line sources where the source strength of the line sources are modelled as a function of traffic intensity and traffic type.

In the model, the analytical dispersion equation for finite line sources is derived from a Gaussian plume dispersion equation (Luhar and Patil 1989). The lateral and vertical dispersion parameters of the Gaussian dispersion equation requires boundary layer scaling parameters; which are provided by MPP-FMI. These scaling parameters include u_*, L, and mixing layer height z_i.

14.2.3 Algorithmic Differentiation

AD is a branch of computer science that deals with the numerical evaluation of derivatives of functions that are implemented in a computer programme, in this case MPP-FMI and CAR-FMI. Any computer program, no matter how complex, performs a sequence arithmetic operations ($+, -, /, \ldots$) or elementary functions (*exp*, *sin*, *log*, …) whose derivatives are known. AD exploits this fact by applying the chain rule of differentiation to the entire sequence of operations within the program (Griewank and Walter 2008). This systematic approach yields numerical derivative values at machine-precision, which describe how the program outputs depend on the input parameters.

Here the discussion will be limited to the forward mode of AD, which has been employed in this study. As a starting point, consider an arbitrary computer program that takes n input variables and returns m outputs. It can be described as a vector-valued function $\mathbf{y} = F(\mathbf{x})$ such that, the function F maps $\mathbb{R}^n \rightarrow \mathbb{R}^m$ where $\mathbf{x} \in \mathbb{R}^n$ defines the input and $\mathbf{y} \in \mathbb{R}^m$ the output vectors. Application of the forward mode AD to a vector valued function yields a new implementation of the program, which, in addition to the original function evaluation, evaluates its differential

Table 14.1 Range of parameters used for studying the sensitivity of the boundary-layer scaling parameters modelled by MPP-FMI. For each range, six points were linearly spaced within the range. This amounts to 6^8 combinations of input variables to be evaluated; resulting in 6^8 Jacobian matrices. The input variables are surface roughness length (z_0), albedo r, temperature at 2 metres (T_2), cloud cover C_C, cloud height C_Z, Priestley-Taylor moisture parameter (α) (Karppinen et al. 1997), and solar radiation (R_S)

Inputs	z_0	r	T_2 (C°)	C_C	C_Z (m)	U (m s^{-1})	α	R_S (Wm^{-2})
Range	0.3–1.3	0.05–0.7	−20–30	0–1	30–6000	1–20	0.5–1.0	0–900

$$\dot{\mathbf{y}} = F'(\mathbf{x})\dot{\mathbf{x}}_{\mathbf{k}} \tag{14.1}$$

where $F'(\mathbf{x}) \in \mathbb{R}^{m \times n}$ defines the Jacobian matrix which contains which contains all first-order partial derivatives $\partial \mathbf{y}/\partial \mathbf{x}$ and $\mathbf{x}_\mathbf{k}$ is the seeding vector used to construct the Jacobian. In this way, AD was used to construct a complete Jacobian matrix from the input into MPP-FMI to the output of CAR-FMI.

14.3 Results

The range of values in Table 14.1 were then used to construct a Jacobian (i.e. sensitivity information) for every combination of the meteorological input variables. The rows of interest for this work are those rows in the Jacobian containing the sensitivity information of L and u_* since these are further needed in CAR-FMI. In addition to L and u_*, the Jacobian comprise sensitivity of Q_H, Q_E, Q^*, and θ^* to the input variables listed in Table 14.1.

The sensitivity analysis showed that both u_* and inverse Obukhov-length L^{-1} are very sensitive to wind speed (U). For L^{-1}, the sensitivity to U is most pronounced at low values of U; i.e. when $U \approx 1$ [m s^{-1}]. For unstable conditions, when $L^{-1} \ll 0$, an increase in U will cause the stability to become more neutral ($L^{-1} \approx 0$). Moreover, for initially stable conditions ($L^{-1} \gg 0$) an increase in U will also neutral conditions; i.e. L^{-1} will drop towards $L^{-1} \approx 0$.

The sensitivity study also showed that u_* is sensitive to U and even more so when U is low. Moreover, the greatest sensitivity of u_* to U is when L^{-1} is in the range $0 < L^{-1} < 0.1$.

These sensitivities will impact the modelled dispersion of pollutants from the road network using CAR-FMI. To which extent remains to be investigated.

Acknowledgements Maj and Tor Nessling foundation is acknowledged for financially supporting this work under grants 2014044 and 201600449.

Questions and Answers

Questioner: Heinke Schluenzen
Question: The approach assumes linear relations which are not true for the real atmosphere. What is the conclusion for modelling based on this analysis?
Answer: The method of algorithmic differentiations (AD) does not assume linear relations. However, in this work, to be able to inter-compare the sensitivity of the output parameters of the model to the input data, the partial derivatives needed to be scaled according to the range of the respective input data; thus assuming a linear relationship. The scaling, which assumes a linear relationship, is not a problem specific for AD. The issue raised can be minimised with confidence using AD by increasing the number of data points. The conclusion concerning this sensitivity study is that the most fundamental input parameter to the model combination of MPP-FMI and CAR-FMI is wind speed (U). The second most important is solar radiation (R_S).

Questioner: Peter Viaene
Question: How difficult was it to apply TAPENADE to your code?
Answer: To apply TAPENADE to the code was not that difficult. The main work was to make the computer programs into a FORTRAN subroutine that takes the independent input variables of interest and outputs the dependent output variables. This subroutine is then the top routine that TAPENADE needs to know and the subsequent code will undergo source transformation. Then TAPENADE is told which are independent and dependent variables of interest. The next step was to write a wrapper subroutine to handle the differentiated code which was used construct all the Jacobians (column by column in the forward mode).

Questioner: Emmanouil Oikonomakis
Question: According to your talk, the 2nd most sensitive parameter on the stability (L^{-1}) is solar radiation. Does that mean that a consistent trend in solar radiation have a systematic effect on the stability L^{-1}?
Answer: For the meteorological pre-processor (MPP-FMI) that was investigated in this study, an increase in solar radiation (R_S) will always favour unstable conditions. This behaviour of the model is systematic. However, in the study, artificial data was used. When using measured data as model input it is highly likely that the many input parameters are likely to be, at least to some degree, interdependent. This interdependency is not possible to study with MPP-FMI but would have to be studied with a boundary layer dynamics model.

References

Griewank A, Walter A (2008) Evaluating derivatives principles and techniques of algorithmic differentiation. SIAM, Philadelphia

Hascoët L, Pascual V (2013) The Tapenade automatic differentiation tool: principles, model, and specification. ACM Trans Math Softw. doi:10.1145/2450153.2450158

Karppinen A, Joffre SM, Vaajama P (1997) Boundary-layer parameterization for finnish regulatory dispersion models. Int J Environ Pollut. doi:10.1504/IJEP.1997.028206

Kukkonen J, Härkönen J, Walden J, Karppinen A, Lusa K (2001) Evaluation of the CAR-FMI model against measurements near a major road. Atmos Envriron. doi:10.1016/S1352-2310(00)00337-X

Luhar AK, Patil RS (1989) A general finite line source model for vehicular pollution prediction. Atmos Environ. doi:10.1016/0004-6981(89)90004-8

van Ulden AP, Holtslag AAM (1985) Estimation of atmospheric boundary layer parameters for diffusion applications. J Clim Appl Meteorol. doi:10.1175/1520-0450(1985)0241196:EOABLP2.0.CO2

Chapter 15
Validation of PM2.5 Concentrations Based on Finnish Emission—Source-Receptor Scenario Model

Ville-Veikko Paunu, Niko Karvosenoja, Kaarle Kupiainen, Leena Kangas, Mikko Savolahti and Minna-Kristiina Sassi

Abstract Atmospheric fine particulate matter (PM2.5) is a major health risk in both developing and developed countries. Health impact assessments utilize often air quality models, consisting of emission and atmospheric dispersion and meteorological models. For policy purposes, there is often a need to assess the air quality impact of large number of alternative emission reduction measures. For such assessments at high spatial resolution for regional scale domains, e.g. the area of a whole country, simplified linear source-receptor relationships can be used to substitute more laborious atmospheric models. In this study we compared PM2.5 concentrations calculated with our policy analysis emission model with available measurement data. The PM2.5 concentrations were modelled using the Finnish Regional Emission Scenario (FRES) model coupled with source-receptor matrices at various resolutions. The measurement data for comparisons were taken from several monitoring stations across Finland, and represented different site types i.e. rural and urban background and traffic dominated environments. In general the model overestimated the PM2.5 concentrations in urban locations and underestimated in rural stations. One possible reason for the overestimation is that emissions from some sectors may have inaccurate spatial disaggregation. Especially the use of population density as a spatial proxy for the distribution of emissions often poorly represents the polluting activity and results in too high modelled concentrations in densely populated areas. In rural regions the omission of sea traffic emissions and natural sources might explain some of the underestimation. The results highlight the importance of the quality of the emission data used as input in dispersion modelling and the need for reliable spatial representation of emissions in the model.

V.-V. Paunu (✉) · N. Karvosenoja · K. Kupiainen · M. Savolahti · M.-K. Sassi
Finnish Environment Institute SYKE, P.O. Box 140, FI-00251 Helsinki, Finland
e-mail: ville-veikko.paunu@ymparisto.fi

M. Savolahti
e-mail: mikko.savolahti@ymparisto.fi

L. Kangas
Finnish Meteorological Institute, P.O. Box 503, FI-00101 Helsinki, Finland

C. Mensink and G. Kallos (eds.), *Air Pollution Modeling and its Application XXV*,
Springer Proceedings in Complexity, DOI 10.1007/978-3-319-57645-9_15

15.1 Introduction

Air pollution continues to be one of the main environmental risks for human health. Especially adverse health effects of particulate matter, including fine particle matter (PM2.5), have been proven in several studies (WHO 2013). No evidence has been found on any threshold below which no short- or long-term health effects could be seen. Thus, air quality modelling is important even in areas where concentrations of air pollutants are close to legislative limit values. Local air quality is usually affected by not only local emissions, but also pollution originating further away, for example from different countries. Therefore, taking transboundary pollution into account is important for comprehensive impact assessment.

Assessing multiple different emission reduction scenarios across several source sectors is resource intensive, especially at high spatial resolution. Simplified linear source-receptor matrices based on actual atmospheric models offer an efficient tool for such an assessment. The resolution of the matrices has an important impact on the results of the modelling. If the resolution if coarse, say kilometers, local phenomenon might not be captured well. Also, validation by comparing the results to measurements might be difficult, as measurements are done in a specific point, as opposed to modelling results which represent an average in a grid cell. If the resolution is sufficiently high, comparison to measurements may offer possibilities to identify the parts for improvement in the emissions model.

In this study we compared the PM2.5 concentrations calculated with our policy analysis emission model to measurements. The measured annual averages were from several monitoring stations across Finland, representing both urban and less urban locations. The research questions were: (1) How well the calculated concentrations compare to the measured values, and (2) does under- or overestimation of the emissions at high spatial resolution from some source sectors explain the possible differences?

15.2 Methods

PM2.5 concentrations were calculated in two parts with the Finnish Regional Emission Scenario (FRES) model (Karvosenoja 2008). Primary PM2.5 from Finnish sources were modelled using simplified linear source-receptor matrices developed using Gaussian UDM-FMI dispersion model at 1 × 1 km resolution (Karvosenoja et al. 2011). Transboundary PM2.5 and Finnish secondary PM2.5 were modelled using matrices adopted from the Greenhouse Gas and Air Pollution Interactions and Synergies (GAINS)-Model developed at the International Institute for Applied Systems Analysis (IIASA) (Amann et al. 2011). Concentrations were calculated in 1 × 1 km grid (FRES grid) and 0.5° × 0.25° grid (GAINS grid). The emissions were calculated for the year 2010. Natural sources were not taken into account.

Table 15.1 Measured and calculated PM2.5 concentrations (μg/m^3). GAINS-grid is 0.5° × 0.25° and FRES-grid 1 × 1 km

		Station type	Measured	GAINS-grid	FRES-grid
Helsinki metropolitan area	Mannerheimintie	Traffic, urban	10.9	7.2	15.7
	Kallio	Background, urban	8.9	7.2	19.1
	Vartiokylä	Background, suburban	8.1	5.7	11.0
	Luukki	Background, rural	8.2	6.5	5.5
	Tikkurila	Traffic, suburban	9.4	7.0	11.5
Other	Lohja	Background, urban	7.2	5.4	7.9
	Virolahti	Background, rural	8.7	4.7	4.8
	Turku	Traffic, urban	10.5	6.5	10.0
	Joensuu	Background, urban	2.5	4.6	9.0
	Vaasa	Traffic/background, urban	7.0	4.5	13.3
	Kittilä	Background, rural	3.8	2.1	2.2

The measurements were annual averages of PM2.5 in 2010 and were from several monitoring stations across Finland representing different site types. The stations and their type are presented in Table 15.1. The data was gathered from Air Quality In Finland-portal (http://www.ilmanlaatu.fi).

The calculated concentrations were compared to the measured values in each monitoring station. Modelled values are averages within the 1 × 1 km and 0.5° × 0.25° grid cell, and measurements are concentrations at the station, i.e. at that point. Contribution of main source sectors to the concentrations was broken down to identify the biggest contributors. Sectors with known uncertainties were assessed in more detail in the Helsinki region to explain differences between measurements and calculated values. Sensitivity of emission from these sectors to the concentrations was analyzed.

15.3 Results and Discussion

Calculated and measured PM2.5 concentrations are presented in Table 15.1. Map of concentrations is also presented in Fig. 15.1. In general, concentrations in the FRES-grid in urban sites, especially in Helsinki metropolitan area, were overestimates. In contrast rural concentrations tend to be underestimates. Especially in Kallio the calculated value was significantly higher than the measured one. One reason for this is that FRES model doesn't capture urban background measurements well, as it gives average concentration in the grid cell, not concentrations in single points. i.e. very fine local variations are not captured. Measurement in Joensuu in 2010 was a clear outlier when compared to the values from different years, and, therefore, likely caused by some kind of measurement error.

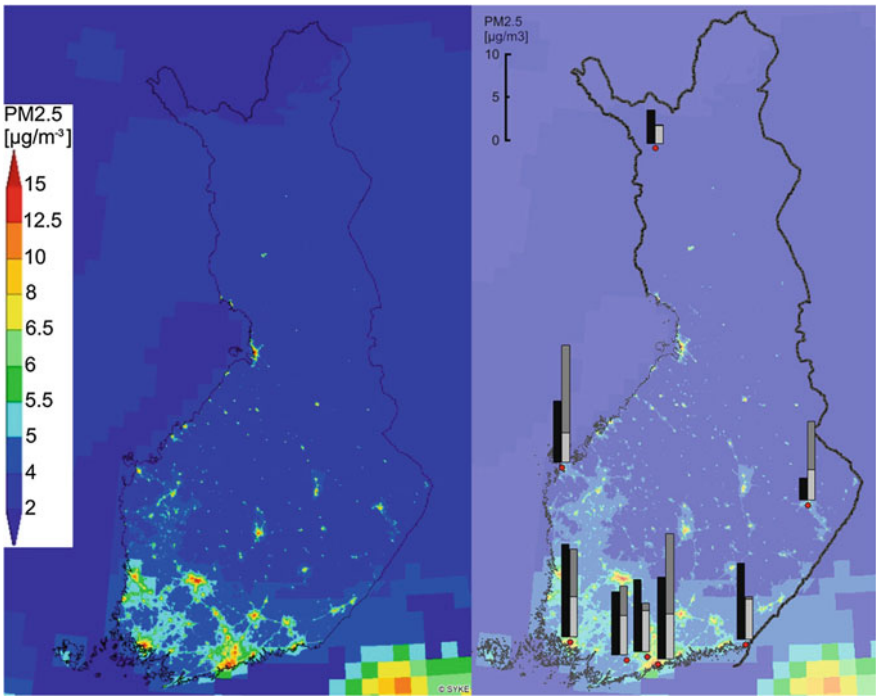

Fig. 15.1 On the *left* calculated PM2.5 concentrations and on the *right* comparison of measured (*black bars*) and calculated concentrations (with primary PM2.5 in *dark grey* and secondary and transboundary PM2.5 in *light grey bars*). Measurement stations clockwise from the *top* Kittilä, Joensuu, Virolahti, Helsinki (average of four stations), Luukki, Lohja, Turku, and Vaasa

In rural areas, natural sources and sea traffic are not taken into account, which might explain some of the difference. Rural station at Luukki is stationed next to a gravel road, which could explain the relatively high concentration for a rural site.

Calculated values in the coarser GAINS-grid were lower than the values in the finer FRES-grid, except in rural background station in Luukki. The smaller resolution of the GAINS-grid doesn't capture the contribution of local PM2.5 sources as well as the higher resolution grid. This highlights the need for higher spatial resolution in population exposure studies.

Emissions from some sectors were thought to be overestimated or suboptimally spatially represented in the FRES model. These inaccuracies in emissions will be analyzed and the calculation developed further in the near future in NordicWelfAir (http://projects.au.dk/nordicwelfair/) and BATMAN projects. As a first step for the analysis, sensitivity of the most obvious errors in emissions were roughly investigated in this paper. Sectors taken into assessment were traffic resuspension, maintenance and construction machinery, and barbeque emission. In revised calculation, traffic resuspension emissions were decreased 50% based on comparison to recent emissions measurements. Maintenance and construction machinery emissions use

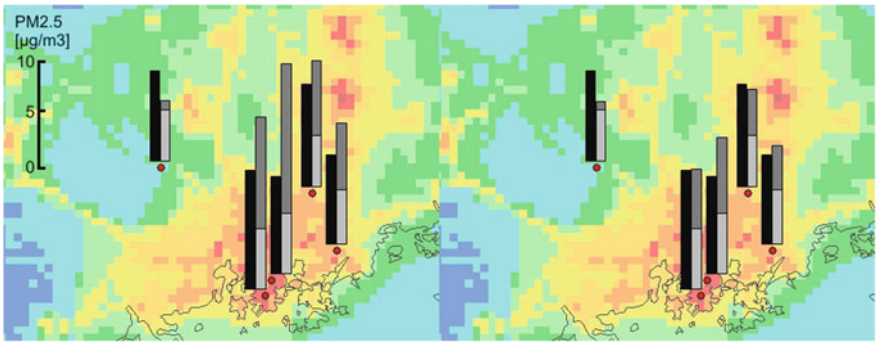

Fig. 15.2 Measured (*black bars*) and calculated (primary particles in *dark grey* and secondary and transboundary in *light grey*) PM2.5 concentrations in Helsinki metropolitan area. On the *left* are the original calculations, and on the *right* revised numbers. Stations from *left* to *right* Luukki, Mannerheimintie, Kallio, Tikkurila, and Vartiokylä

population as spatial proxy in the FRES model. This creates an overestimation of non-urban machinery within cities. Their emissions were reduced 50% based on an estimate on the fraction of non-urban machinery from the total. Barbeque emissions use population as a proxy as well. Furthermore, the emission factors are based on a study made in the US and their values are high. This was thought to cause overestimation of barbeque emissions, especially in areas with high population density. Barbeque emissions were therefore decreased by 70% in the revised calculations.

The results of the original and revised calculations for Helsinki region in the FRES-grid are compared in Fig. 15.2. In the revised calculation, average difference between the measured and calculated PM2.5 concentrations were diminished from 50 to 18%. The analysis shows that revising the sectors with higher uncertainties in the model will correct urban concentrations closer to the measurement values, and that the identified sectors are likely to be the ones that explain most of the difference between the measured and calculated values.

15.4 Conclusion

In this study we compared results from comprehensive PM2.5 concentration modelling to measurements in Finland. In general, urban concentrations tended to be overestimated by the model, whereas rural concentrations were underestimated. Some source sectors (traffic resuspension, maintenance and construction machinery, and barbeque emission) were thought to have inaccurate emission or spatial representations. These sectors will be revised soon to enhance the modelling. The study highlights the importance of the quality of the emission data in air quality modelling. Furthermore, the study emphasizes the significance of representative spatial proxies for the emissions.

Acknowledgements This study was funded by: NordForsk under the Nordic Programme on Health and Welfare Project #75007: Understanding the link between air pollution and distribution of related health impacts and welfare in the Nordic countries (NordicWelfAir); and Environmental impact assessment of airborne particulate matter: the effects of abatement and management strategies (BATMAN)-project funded by the Academy of Finland.

Questions and Answers

Session 2, Talk 2.7, Ville-Veikko Paunu

Questioner: Peter Viane
Question: Why is wood burning missing from your analysis? Road resuspension are normally associated with the coarse fraction.
Answer: Wood burning is an important source of PM2.5. We have done a lot of work on wood combustion emissions, so we know there is more work to be done in other sectors in which we know some overestimation is done. These sectors were looked into more closely in this study. While most particles emitted by resuspension fall within the coarse fraction, resuspension still contributes to the PM2.5 concentrations as well.

Questioner: Richard Derwent
Question: Have you performed any evaluation of the PM input into Finland by long-range transport from the GAINS model? My understanding is that this model does not include organic aerosol. This may be a major cause of your rural PM2.5 underestimation.
Answer: We haven't performed such an evaluation. The GAINS model includes primary organic carbon and VOC's, but not as speciated.

Questioner: Johannes Bieser
Question: On what scientific basis did you decide to reduce these particular emission sectors? Did you validate your assumptions e.g. by looking at fingerprints in the speciated PM2.5 composition? Could your revised emission estimate lead to the right results for the wrong reasons? (E.g. uncertainties in meteorological parameters like PBL height could also explain the observed bias.)
Answer: We did not have speciated PM2.5 measurement results in this study. However, it would be really interesting to have them and get an idea of the source division of the PM2.5 in each measurement point. The choosing of sectors was based on our knowledge of sources which have thought overestimations in our model, as expressed in the presentation and the extended abstract. Of course, these sources don't explain all of the difference between measured and calculated concentrations. The revisions done for these sectors in this study were rather crude, and more sophisticated revisions are planned for the near future. In other words, revisions of these sectors will not be based on this study, but more comprehensive evaluation of our emission model.

References

Amann M, Bertok I, Borken-Kleefeld J, Cofala J, Heyes C, Hglund-Isaksson L, Klimont Z, Nguyen B, Posch M, Rafaj P, Sandler R, Schpp W, Wagner F, Winiwarter W (2011) Cost-effective control of air quality and greenhouse gases in Europe: modeling and policy applications. Environ Model Softw 26(12):1489–1501

Karvosenoja N (2008) Emission scenario model for regional air pollution. Monographs Boreal Environ Res 32

Karvosenoja N, Kangas L, Kupiainen K, Kukkonen J, Karppinen A, Sofiev M, Tainio M, Paunu V-V, Ahtoniemi P, Tuomisto JT, Porvari P (2011) Integrated modeling assessments of the population exposure in Finland to primary PM2.5 from traffic and domestic wood combustion on the resolutions of 1 and 10 km. Air Qual Atmos Health 4:179–188

WHO (2013) Review of evidence on health aspects of air pollution—REVIHAAP project. Technical report. The WHO European Centre for Environment and Health, Bonn, WHO Regional Office for Europe, pp 302

Chapter 16
A Model Evaluation Strategy Applied to Modelling of PM in the Helsinki Metropolitan Area

Mia A. Aarnio, Jaakko Kukkonen, Leena Kangas, Mari Kauhaniemi, Anu Kousa, Carlijn Hendriks, Tarja Yli-Tuomi, Timo Lanki, Gerald Hoek, Bert Brunekreef, Timo Elolähde and Ari Karppinen

Abstract We have developed a deterministic urban scale dispersion modelling system further by adding a road dust suspension model. The system includes both vehicular exhaust emissions and suspended road dust. The modelling system was combined with a regional scale chemical transport model for calculations of concentrations in an urban area for the year 2008, and for the year 2010 measured regional background concentration was used. The time series' were modelled for a spatial area more extensive than before using the FORE road dust suspension model. The predictions were compared against observed concentrations of $PM_{2.5}$ and PM_{10}. The use of the index of determination (r^2) is discussed. We criticize the use of r^2 alone as well as in addition to an index of agreement—type measure of

M.A. Aarnio (✉) · J. Kukkonen · L. Kangas · M. Kauhaniemi · A. Karppinen
Finnish Meteorological Institute, Erik Palmenin Aukio 1, P.O. Box 503,
00101 Helsinki, Finland
e-mail: mia.aarnio@fmi.fi

J. Kukkonen
e-mail: Jaakko.Kukkonen@fmi.fi

A. Karppinen
e-mail: ari.karppinen@fmi.fi

A. Kousa
Helsinki Region Environmental Services Authority (HSY), Helsinki, Finland

C. Hendriks
Organisation for Applied Scientific Research (TNO), The Hague, Netherlands

T. Yli-Tuomi · T. Lanki
Finnish National Institute for Health and Welfare, Helsinki, Finland

G. Hoek · B. Brunekreef
Institute for Risk Assessment Sciences (IRAS), Utrecht, Netherlands

T. Elolähde
Helsinki Region Transport (HSL), Helsinki, Finland

C. Mensink and G. Kallos (eds.), *Air Pollution Modeling and its Application XXV*,
Springer Proceedings in Complexity, DOI 10.1007/978-3-319-57645-9_16

agreement, and review the underlying data assumptions for the use of both measures. We then suggest a strategy to develop model evaluation statistical understanding, practice and nomenclature.

16.1 Introduction

The Helsinki Metropolitan Area (HMA) comprises four cities; Helsinki, Espoo, Vantaa and Kauniainen. The total population in the HMA in 2010 was approximately 1.1 million, while the population of Helsinki alone is about 0.6 million inhabitants. The most important anthropogenic local source of the PM mass fractions is road traffic. Other significant sources include shipping and harbor operations, industry, small-scale combustion (residential) and aviation.

16.2 Methods

For the years 2008 and 2010, the synoptic weather observations from the stations at the Helsinki-Vantaa airport (18 km north of the Helsinki city centre) and Kumpula (5 km north of the city centre), and sounding observations from Jokioinen (90 km northwest of Helsinki) were the input for the meteorological pre-processing model MPP-FMI.

The local PM emission inventory included exhaust emissions from vehicular traffic for the network of roads and streets in the HMA, including about 4300 road and street links. The traffic volumes and average travel speeds for each traffic link were calculated with the EMME/2 transportation planning system (INRO 1994).

The FORE model (Forecasting of Road Suspension Emissions) produces emission factors for suspension. The emission factor for the suspension of road dust is a product of the so-called reference emission factors, the reduction factor for the road surface moisture content, and a weighted sum of the contributions originated from particles from the wear of pavement and from traction sand.

The urban-scale dispersion of vehicular emissions was evaluated with the CAR-FMI model (Contaminants in the Air from a Road, Finnish Meteorological Institute). Street canyon dispersion modelling and modelling of aerosol transformation processes were not included in the calculations, as very few streets in the study area are street canyons, and the dispersion model does not include particle number concentration. The receptor grid intervals ranged from 20 m near major roads to 500 m on the fringes of the modelled area. The concentration values were computed at more than 18 and 24 thousand receptor points for 2008 and 2010, respectively (Aarnio et al. 2016).

For the estimation of the regional background concentration values for the year 2008 we used the LOTOS-EUROS chemical transport model predictions time series' of hourly $PM_{2.5}$ and PM_{10} concentrations from the 7 × 7 km^2 grid square where the regional background station at Luukki was located.

In the evaluation of the regionally- and long range transported $PM_{2.5}$ background concentrations for the year 2010, we used the concentrations observed at the regional background station of Luukki (PM_{10} was not included in calculations for this year, as no observations of it were available from the Luukki station).

We used the hourly time series observed by the HSY air quality measurement network for the evaluation of the modelling of both PM fractions.

16.3 Statistical Analysis

The use of the coefficient of determination (r^2) in comparisons of observed and theoretically deduced values of a variable for the purpose of model evaluation has been criticized since long ago, e.g. (Robinson 1957; Wilmott 1981), as it measures the degree to which paired values of two variables X_1 and X_2 are proportional ($X_1 = a + bX_2$) rather than identical ($X_1 = X_2$) to each other. There are two underlying assumptions regarding the significance test associated with the coefficient of determination. First, both variables must be normally distributed, as otherwise nothing can be said about the significance of the correlation between the variables. Second, the data must be a random sample. If these qualities apply to the data, then the use of r^2 is correct. Then the size of the sample should be reported, as well as the possible exclusion of any data points (such as missing observed values). The significance level and the name of the used test should also be given.

Our observed and predicted daily averaged time series data (non-normality verified at http://contchart.com/goodness-of-fit.aspx) resemble the log-normal distribution. On the other hand, our aim was to study the AQ modelling system predicted data exactness with the observed data, **not to build a regression model**. In place of the coefficient of determination, Willmott (1981) suggested the use of a root mean squared error (RMSE) and an index of agreement (d). They first defined the **index of agreement** as

$$d_2 = 1 - \frac{\sum_{i=1}^{n} (P_i - O_i)^2}{\sum_{i=1}^{n} \left(\left| P_i - \bar{O} \right| + \left| O_i - \bar{O} \right| \right)^2}, \tag{16.1}$$

where n is the sample size, P is the predicted quantity, P_i is the value of P at time i, O is the observed quantity, O_i is the value of O at time i, and $\bar{O}$ is the mean value of the time series O_i (i = 1, …, n). d_2 is dimensionless and has the range of 0–1.

The better-known **RMSE** is defined as

$$RMSE = \left[\frac{1}{n}\sum_{i=1}^{n}(P_i - O_i)^2\right]^{0.5}. \tag{16.2}$$

The RMSE has the same metric as the observed and predicted values. Later, Willmott et al. (2011) developed the concept further, as they felt that the Eq. 16.1 over-weighted the influence of the squaring errors. Therefore, they introduced the **modified index of agreement**, defined as

$$d_1 = 1 - \frac{\sum_{i=1}^{n}|P_i - O_i|}{\sum_{i=1}^{n}\left(|P_i - \bar{O}| + |O_i - \bar{O}|\right)}, \tag{16.3}$$

where d_1 is dimensionless and also has the range of 0–1.

Index of agreement-type statistic metrics are not measures of correlation or association between two series of variables in the formal sense. Instead, they provide a measure of the degree to which the model predictions are exact matches with no proportionality.

In modeling evaluation, one should not rely on only one statistical metric, but a group of well thought out metrics that describe the data sets and their agreement from many different points of view but with a minimum of overlap.

We decided to choose d_1 for use instead of r^2 for the evaluation of our modelling work. We studied the behaviour of d_1 with some data sets containing the natural logarithms of observed daily-averaged time series versus random time series with the same means and standard deviations as the observed time series. In these comparisons d_1 was between 0.28 and 0.32. Regarding d_2, it has been previously stated that "Numerical experiments have shown that a totally random predicted time series having the same range of variability as the measured time series, would result in an index of agreement value equal to approximately 0.4." Standard deviation is a common measure of variability (dispersion) of the data. d_1 and d_2 approach the value 1 with increasing agreement of observed and predicted time series, while d_1 approaches 1 slower than d_2. In comparison with the coefficient of determination, the d_1 and d_2 indices of agreement are especially sensitive to the difference of the mean values of the observed and predicted data sets. The d_2 index of agreement has more often been used in recent air quality modelling studies but has usually been denoted there as IA. RMSE is a relevant measure of the model error to be used with d_2, but Willmott et al. (2011) introduced two more error statistics to be used with d_1: these are the mean-absolute error MAE and mean-absolute deviation MAD, defined as

$$MAE = \frac{1}{n}\sum_{i=1}^{n}|P_i - O_i|, \tag{16.4}$$

$$MAD = \frac{1}{n}\sum_{i=1}^{n}\left|O_i - \bar{O}\right|. \tag{16.5}$$

The other statistical metrics we used are a Fractional Bias, given by

$$FB = \frac{2(\bar{P} - \bar{O})}{\bar{P} + \bar{O}}, \tag{16.6}$$

where $\bar{P}$ is the mean value of the time series P_i (i = 1, …, n), and the Fraction of Two, defined as

$$\text{F2} = \text{fraction of data for which } 0.5 \leq \text{P/O} \leq 2. \tag{16.7}$$

16.4 Results and Discussion

The numerical values of the predicted annual average PM concentrations in 2008 ranged from 6.4 to 14.4 μg m^{-3} for $PM_{2.5}$ within the study area, and from 7.4 to 33.9 μg m^{-3} for PM_{10}.

The values of statistical metrics indicate that the agreement of the measured and predicted hourly time-series can be considered to be fairly good for the modelling system including the LOTOS-EUROS model, and good when using measured regional background concentration values at the available measurement sites. For instance, the modified indices of agreement (d_1) in 2008 varied from 0.53 to 0.57 (MAE 3.24. 4.47, MAD 3.39.. 4.31, F2 0.69.. 0.72, FB −0.32.. −0.12) for $PM_{2.5,}$ and from 0.47 to 0.51 (MAE 6.90.. 15.07, MAD 6.38.. 12.4, F2 0.45. 0.61, FB −0.65.. −0.45) for PM_{10}.

Both the $PM_{2.5}$ and PM_{10} concentrations were under-predicted in 2008 (more pronounced for PM_{10}, compared with that for $PM_{2.5}$), as indicated by the negative FB values. We suspect this was caused mainly by the under-predictions of the biogenic organics by the LOTOS-EUROS model and maybe of the suspended dust by the model FORE (Kauhaniemi et al. 2014). There was no systematic under- or over-prediction of the $PM_{2.5}$ values for the year 2010 for which observed regional background data was used; this points to the modelled background as one source of the under-prediction.

Suspended road dust has become important in practically all road traffic environments, as vehicular traffic intensities continuously increase and exhaust emissions per vehicle decrease. Also, electric vehicles' growing success in becoming part of the vehicle fleets has been estimated to increase the relative importance of suspended road dust. Detailed road suspension emission models have previously been applied only to modelling of specific street segments, not extensive urban areas. This has been due to such areas' complexity and also due to scarcity of measurement data.

Acknowledgements This study has been a part of the research projects APTA (The Influence of Air Pollution, Pollen and Ambient Temperature on Asthma and Allergies in Changing Climate), and NordicWelfAir (Project #75007: Understanding the link between Air pollution and Distribution of related Health Impacts and Welfare in the Nordic countries). The funding from the Academy of Finland and the Nordforsk Nordic Programme on Health and Welfare is gratefully acknowledged.

Questions and Answers

Questioner name: Sebnem Aksoyoghi
Question: LOTOS-EUROS did not have SOA in the past. Did you have them in your application? Did you have biogenic emissions?
Answer: Secondary Organic Aerosols were included in the LOTOS-EUROS calculations of this work, but biogenic emissions were not included.

Questioner name: Antti Hellsten
Question/comment: Always use more than one or two metrics in model evaluation. Different metrics measure different kind of disagreements. E.g. FAC2 tells nothing about possible bias, use e.g. FB, too.
Answer: Yes, exactly. One should report several metrics of statistic analysis, but a consistent set of them. The use of the coefficient of determination, r^2, however is not a good one to use with data sets that are not normally distributed. But, even more importantly, **a danger of misuse comes from when the r^2 for a linear regression model equation determined with some kind of least residual sum fitting to a set of data points, e.g. (Co_{bs}, C_{pred}) is used as a measure of the goodness of the model used to calculate the C_{pred} data**. This is what, for example, the Excel software produces when one makes a scatter plot of the (C_{obs}, C_{pred}) data with added "trendline" and "coefficient of correlation".

A consistent set of statistic parameters could include the number of data points, the means and standard deviations of C_{obs} and C_{pred}, a measure of the bias (e.g. FB), a measure of the spread of the data(e.g. F2), a measure of the exactness of $C_{obs,i} = C_{pred,i}$ for the whole data set (e.g. an index of agreement), and a statistic that would involve estimates for the measurement uncertainty.

Questioner name: Heinke Schluenzen
Question: Thanks for an elaboration on the quality measures. Why don't you aim at an index Ia measure that considers measurement uncertainty (e.g. hit rate)?
Answer: The Helsinki Metropolitan Area Council, the source for the observed data that we used in this work, has now stated that "the measurement uncertainty <25%". This information was not available before. Hit rate represents the fraction of (P_i, O_i)-points from the whole evaluation data set that differ within an allowed range from the diagonal of the P, O-space. The range definition can be then done using the measurement uncertainty, if it is known. (Reference: COST 732 Model Evaluation Case Studies: Approach and Results. Edited by: Schatzmann, M.,

Olesen H., Franke J., 2010. COST Office, Avenue Louise 149, 1050 Brussels, Belgium. 121 pp.

Questioner name: Pius Lee
Question: In your presentation of the index of agreement:

$$\mathbf{d}_2 = 1 - \frac{\sum_{i=1}^{n} (P_i - O_i)^2}{\sum_{i=1}^{n} \left(\left|P_i - \bar{O}\right| + \left|O_i - \bar{O}\right|\right)^2}, \quad \mathbf{d}_1 = 1 - \frac{\sum_{i=1}^{n} |P_i - O_i|}{\sum_{i=1}^{n} \left(\left|P_i - \bar{O}\right| + \left|O_i - \bar{O}\right|\right)}$$

Given that both formulations attempted to quantify the variance (or uncertainty) in each of the observation. Also now the sample size n can be much more since hand-held devices are getting attention of environmental agencies and may soon be deployed as viable observations. Would d_2, d_1 be still a good measure of model performance when n is ten or 100 times more numerous than the current conventional "fixed regulatory monitors". The crux of the difficulty may also lie in the fact that there the variances are large as hand-held devices are much less well standardized and their performance is expected to vary over a much larger range.
Answer: The index of agreement statistic attempts to quantify the "exactness" of the predicted variable time series compared to the observed time series. The index of agreement—statistic is always calculated for a pair of data sets that includes observed and predicted concentrations for a specific point in space, as a time series. So in the analysis of the hourly data for e.g. a year, n would always be around 8860 (or 8884 for a leap year) for a location, regardless of the number of measurement devices. If the measurement devices were mobile, then the data set of the predicted concentrations would have to be interpolated with the movement data combined with calculation point data, but each data set to be analysed would still have the standard length of the chosen study period. But this statistic, in any of its reported incarnations, would not quantify the uncertainty of the measurements in any way.

References

Aarnio MA, Kukkonen J, Kangas L, Kauhaniemi M, Kousa A, Hendriks C, Yli-Tuomi T, Hoek G. Brunekreef B, Elolähde T, Karppinen A (2016) Modelling of particulate matter concentrations in the Helsinki metropolitan area in 2008 and 2010. Boreal Env Res 21: 445–460

INRO (1994). EMME/2 User's Manual. INRO Consultants Inc. Montreal, Canada.

Kauhaniemi M, Stojiljkovic A, Pirjola L, Karppinen A, Härkönen J, Kupiainen K, Kangas L, Aarnio MA, Omstedt G, Denby BR, Kukkonen J (2014) Comparison of the predictions of two road dust emission models with the measurements of a mobile van. Atmos Chem Phys Discuss 14(4):4263–4301

Robinson WS (1957) The statistical measurement of agreement. ASR 22(1):17–25. http://www.jstor.org/stable/2088760

Willmott CJ (1981) On the validation of models. Phys Geogr 2(2):184–194

Willmott CJ, Robeson SM, Matsuura K (2011) A refined index of model performance. Int J Climatol 32:2088–2094

Chapter 17
Assessing the Effect of Uncertainty in Input Emissions on Atmospheric Chemistry Transport Model Outputs

Ksenia Aleksankina, Mathew R. Heal, Anthony J. Dore, Massimo Vieno and Stefan Reis

Abstract Atmospheric Chemistry Transport Models (CTMs) provide important scientific support for effective policy development. It is therefore important to have a quantitative understanding of the level of uncertainty associated with model outputs. Conventionally, model assessment studies direct attention to uncertainties in parameter values and model-specific structural and computational errors. Here, we investigate uncertainty in model outputs as a function of the uncertainty in model inputs, such as emissions of primary pollutants. The Fine Resolution Atmospheric Multi-pollutant Exchange (FRAME) model provides the basis for the development of an uncertainty estimation framework. The study utilises local and global sensitivity analysis techniques. The impact on model outputs of variation in the input emissions of SO_2, NO_x, and NH_3 individually within a $\pm 30\%$ range is assessed using sensitivity coefficients (local method). The propagation of uncertainty in all emissions together is investigated using a Latin hypercube sampling (LHS) global sensitivity analysis. Preliminary results show variability in the uncertainty ranges for different output species and different spatial distribution of these ranges. We present further detail on the development and application of the sensitivity analysis framework for assessment of the effect of input uncertainties on CTMs used for policy support.

17.1 Introduction and Model Description

FRAME is a Lagrangian model used to calculate annual average surface concentrations of SO_2, NO_x, NH_3, and HNO_3, particulate NH_4^+, SO_4^{2-}, and NO_3^-, and dry and wet deposition of oxidised sulphur (SO_y), oxidised (NO_y), and reduced (NH_x) nitrogen. Its main policy-support applications include estimation of critical

K. Aleksankina (✉) · M. R. Heal
School of Chemistry, University of Edinburgh, Edinburgh, UK
e-mail: K.Aleksankina@sms.ed.ac.uk; s0950577@sms.ed.ac.uk

K. Aleksankina · A. J. Dore · M. Vieno · S. Reis
NERC Centre for Ecology and Hydrology, Penicuik, UK

C. Mensink and G. Kallos (eds.), *Air Pollution Modeling and its Application XXV*,
Springer Proceedings in Complexity, DOI 10.1007/978-3-319-57645-9_17

load exceedances and generation of SRR matrices for the UK Integrated Assessment Model, which directly underpins UK air pollution control policies (Oxley et al. 2013).

The FRAME model has a 5 km × 5 km horizontal resolution over the UK with all processes being simulated in an air column divided into 33 vertical layers of varying thickness from 1 m at the surface to 100 m at the top of the vertical domain. The movement of the air columns is defined by averaged wind speed and direction generated from the output of the Weather Research and Forecast model. The chemical scheme in FRAME includes gas and aqueous phase interactions between NH_3, SO_2, and NO_x. Modelled dry deposition is land-cover dependent and calculated using a canopy resistance model. Wet deposition is calculated using scavenging coefficients and driven by rainfall, which is modelled using a constant drizzle approach based on annual average rainfall data with assumption of enhanced washout rate over elevated areas (Dore et al. 2012; Matejko et al. 2009).

Gridded emissions of SO_2, NO_x, and NH_3 from the UK national atmospheric emissions inventory (UK NAEI) at 1 km × 1 km spatial resolution are used. The emissions are injected into the air column at different heights based on a classification of emission sources. A detailed evaluation of model outputs with annually averaged measurements of in air and precipitation concentrations of pollutants is discussed elsewhere (Dore et al. 2015). In this study all model runs were performed using emissions and meteorology data for 2012.

17.2 Sensitivity Coefficients

Sensitivity coefficients, S, represent the effect of the relative variation of model output (y) when perturbing input emissions (x) by a fixed fraction of the baseline value (Eq. 17.1). Resulting sensitivity coefficients are normalised, therefore $S = 1$ indicates a unit change in output due to the unit change in input, $S = 0$ indicates no response to change in the model input, and negative values of S indicate inverse correlation between changes in model input and output.

$$S = \frac{x}{y}\frac{\partial x}{\partial y} \tag{17.1}$$

To create sensitivity coefficient maps for all FRAME model output variables, input emissions of SO_2, NO_x, and NH_3 were perturbed one-at-a-time with reductions ranging from −10 to −30%. Sensitivity coefficients were calculated for each grid square of the model output. The spatial pattern and the magnitude of sensitivity coefficients observed for all output variables remained the same within the applied emission reduction range, which indicates a linear model response to emission reductions within the ±30% range.

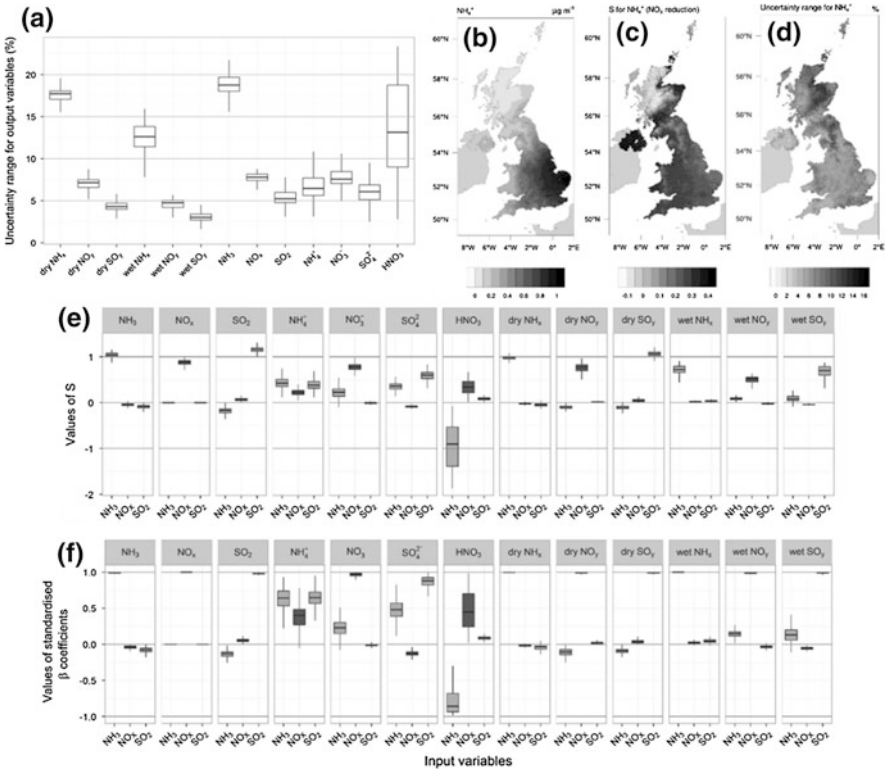

Fig. 17.1 **a** Distributions for uncertainty ranges derived from total input uncertainty for all FRAME output variables, **b** annual average concentration of particulate ammonium over the UK in (range of values 0–1 μg m^{-3}), **c** spatial distribution of sensitivity coefficients for particulate ammonium in response to a 30% reduction in NO_x emissions (−0.1 to 0.4 range), **d** spatial distribution of the uncertainty ranges for particulate ammonium (0–20% range), **e** distribution of sensitivity coefficient values for each output variable given a 30% reduction in each input variable, **f** distribution of β coefficients resulting from multiple regression model fitted for all FRAME outputs

Figure 17.1c shows an example of the spatial distribution of sensitivity coefficient for ammonium (NH_4^+) air concentrations given a 30% reduction in NO_x emissions. It can be noted that spatial patterns of NH_4^+ air concentration (Fig. 17.1b) and NH_4^+ sensitivity coefficients (Fig. 17.1c) differ; areas with the highest concentrations of NH_4^+ do not show the strongest response to changes in NO_x emissions. Additionally concentrations of NH_4^+ in the North of Scotland show a weak inverse response. Low levels of NO_x emission are initially available for chemical reaction with NH_3 in that area, therefore reduced NO_x concentrations lead to increased availability of NH_3, which reacts with SO_x to form $(NH_4)_2SO_4$. Figure 17.1e shows the distributions of sensitivity coefficient values for each output variable given a 30% reduction in emissions of SO_2, NO_x, or NH_3. The bar chart

allows to identify output variables that are most sensitive to reductions in the input emissions. For example NO_x air concentration only responds to changes in NO_x emissions, unlike NH_4^+ which is affected by changes in all input variables.

17.3 Overall Uncertainty in Model Outputs

The propagation of overall uncertainty in the FRAME model input emissions to uncertainty about the output variables was performed using a sampling based approach. Probability distributions of model input emissions were chosen based on overall uncertainty values for SO_2 (±4%), NO_x (±10%) and NH_3 (±20%) emissions estimated for the inventory values reported by UK NAEI (Misra et al. 2015). The input sample space was created based on those distributions and LHS was used to sample the scaling factors that were later applied to perturb input emissions and calculate corresponding model outputs. The uncertainty ranges for each output variable were calculated by taking values of 5th and 95th percentiles for an output distribution for each grid square. The study was conducted for 50 and 100 samples. The results showed no significant difference for ranges obtained with different sample sizes, hence it was concluded that increasing sample size did not yield improved results.

The spatial pattern of uncertainty ranges for the output variables was found to differ from the spatial distribution of the variables themselves. This can be explained by the complex combination of parameters affecting the uncertainty, such as location and absolute values of the input emissions. Uncertainty range distributions for all FRAME output variables are shown in Fig. 17.1a. The results show higher ranges of uncertainty for variables derived from input emissions of NH_3, which was the most uncertain model input.

17.4 Global Sensitivity Analysis

For global sensitivity analysis the LHS space was extended to a ±40% range for each input emission variable and 100 model runs were performed. The data from the model runs was used to perform multiple linear regression analysis for all output variables. Given the relative simplicity of the FRAME model (mostly linear and monotonic response to emission perturbations), the standardised regression, β, coefficients were chosen to provide a measure of input variable importance. Figure 17.1f shows distribution of β coefficients for each model output variable; it can be seen that in most cases variation in the model output is dominated by the variation in a single input variable. Additionally both sensitivity coefficients and β coefficients provide the same importance ranking for the effect of input variables on the model output.

17.5 Conclusions

- Spatial distributions of model output variables (concentrations and depositions) differ from spatial distributions of both sensitivity coefficient and uncertainty ranges.
- Linearity in the model response to the one-at-a-time emission perturbations within a ±30% region was observed, therefore sensitivity coefficient maps can be used as a quick tool to identify areas that will benefit from reduction in the levels of particular pollutant according to FRAME model.
- LHS has proven to be a successful and efficient method for the uncertainty propagation from multiple inputs.
- Sensitivity coefficients and β coefficients show the same importance ranking for the effect of an input variable on a model output. In most cases variation in a single input has significant effect on the variation in the output variable.

Acknowledgements KA thanks the University of Edinburgh School of Chemistry and NERC Centre for Ecology and Hydrology (project number NEC05006) for PhD studentship funding. The authors are also acknowledge use of R and its packages.

Questions and Answers

Questioner: Heinke Schlünzen
Question: Can you comment on the impact of the NO-NO_2 mixing ratio on the model results? What uncertainty is in that mixing ratio?
Answer: Uncertainty in the NO–NO_2 ratio was not investigated in this study. NO to NO_2 conversion rate in the FRAME model is relatively quick compared to the timescale of the model outputs (annual average concentration and deposition), hence this source of uncertainty was not considered to be influential.

Questioner: Mikhail Sofiev
Question: FRAME model has been described as the Lagrangian model. Such kind of models are linear with regard to emissions (usually). What was the origin of non-linearities mentioned in the outcome of the analysis?
Answer: The non-liniarities in the FRAME model response to emission perturbation resulted from the chemical scheme implemented in the model, in particular the formation of ammonium nitrite aerosol by the equilibrium reaction between HNO_3 and NH_3, and ammonium sulphite aerosol by the reaction between H_2SO_4 and NH_3. Both reactions are dependent on the availability of NH_3, SO_2, and NH_3.

References

Dore AJ, Kryza M, Hall JR, et al (2012) The influence of model grid resolution on estimation of national scale nitrogen deposition and exceedance of critical loads. Biogeosciences 9:1597–1609

Dore AJ, Carslaw DC, Braban C et al (2015) Evaluation of the performance of different atmospheric chemical transport models and inter-comparison of nitrogen and sulphur deposition estimates for the UK. Atmos Environ 119:131–143

Matejko M, Dore AJ, Hall J et al (2009) The influence of long term trends in pollutant emissions on deposition of sulphur and nitrogen and exceedance of critical loads in the United Kingdom. Environ Sci Policy 12:882–896

Misra A, Passant NR, Murrells TP et al (2015) UK informative inventory report (1990 to 2013)

Oxley T, Dore AJ, ApSimon H et al (2013) Modelling future impacts of air pollution using the multi-scale UK Integrated Assessment Model (UKIAM). Environ Int 61:17–35

Chapter 18
EMEP4PL and WRF-Chem—Evaluation of the Modelling Results

Małgorzata Werner, Maciej Kryza, Kinga Wałaszek, Massimo Vieno and Anthony J. Dore

Abstract We used two different Eulerian atmospheric transport models—the Weather Research and Forecasting (WRF) coupled online with chemistry (WRF-Chem) and EMEP4PL coupled offline with meteorology from WRF-Chem. The models were run for Poland, which is characterized by a relatively poor air quality, especially during winter seasons. The simulations were run for 2 months—January and July 2015 and modelled concentrations of PM_{10}, $PM_{2.5}$, SO_2 and NO_2 were compared with measurements available at a one hour resolution. Both models give better results for the winter period than for summer. For July the WRF-Chem results for particulate matters are improved after inclusion of boundary conditions from the MOZART model. In general WRF-Chem gives higher FAC2 and lower NMB for both months in comparison to EMEP4PL. For EMEP4PL correlations with observations are higher in comparison to WRF-Chem.

M. Werner (✉) · M. Kryza · K. Wałaszek
Department of Climatology and Atmosphere Protection, University of Wroclaw, Wrocław, Poland
e-mail: malgorzata.werner@uwr.edu.pl

M. Kryza
e-mail: maciej.kryza@uwr.edu.pl

K. Wałaszek
e-mail: kinga.walaszek@uwr.edu.pl

M. Vieno · A. J. Dore
Centre for Ecology and Hydrology, Edinburgh, UK
e-mail: mvi@ceh.ac.uk

A. J. Dore
e-mail: todo@ceh.ac.uk

C. Mensink and G. Kallos (eds.), *Air Pollution Modeling and its Application XXV*,
Springer Proceedings in Complexity, DOI 10.1007/978-3-319-57645-9_18

18.1 Introduction

Increased computing capacity in the last decade enables closer coupling of meteorological models with atmospheric chemical transport models (CTM) either offline or online. Offline modelling implies that the CTM is run after the meteorological simulation is completed, while online modelling allows for coupling and integration of some of the physical and chemical components to various degrees (Baklanov et al. 2014). It is well recognized that weather is of decisive importance for air quality and that chemical species influence the weather by changing the atmospheric radiation budget and through cloud formation (Grell and Baklanov 2011). However, the computational costs are still relevant and offline models, which are more computationally efficient, are widely used for different purposes. In this study we used two different Eulerian models—the Weather Research and Forecasting (WRF) coupled online with chemistry (WRF-Chem) and EMEP4PL coupled offline with meteorology from WRF-Chem. The models were run for Poland, which is characterized by relatively poor air quality, especially during winter seasons. The simulations were run for 2 months—January and July 2015 and modeled concentrations of PM_{10}, $PM_{2.5}$, SO_2 and NO_2 were compared with measurements available at a 1 h resolution.

18.2 Data and Methods

We used the online WRF-Chem model version 3.5.1 (Grell et al. 2005) with the physical options described in Werner et al. (2017). Here, the model was run with the RADM2 gas phase chemistry and the MADE/SORGAM aerosol chemistry. The second model applied in this study was Open Source EMEP/MSC-W model version 4.8 (Simpson et al. 2012) with the meteorological fields provided by the WRF-Chem simulation (called EMEP4PL). The default chemical scheme EmChem09 was used (Simpson et al. 2012) in the simulations. Both models were run with the same domain setups—mother domain over Europe (12 km × 12 km) and the inner domain focused on Poland (4 km × 4 km) for January and July 2015 with a 7 days spin up for each simulation. We used the TNO MACC III data set at 1/8° × 1/16° spatial resolution. The EMEP temporal emissions profile was applied to the emissions data (with degree-days factors for daily emission switched off) and used in the WRF-Chem simulations. Emission was distributed to vertical layers according to the SNAP sectors. We used the standard option available in the EMEP4PL model (emissions provided to 5 vertical layers, Simpson et al. 2012) and developed the vertical distribution for the WRF-Chem emissions based on Bieser et al. (2011).

The WRF-Chem model was run two times. In the first simulation boundary conditions were provided from the MOZART model (Emmons et al. 2010), and the second simulation was fed by a default boundary profile (Grell et al. 2005).

For EMEP4PL, default boundary conditions for the outermost domain were used. For the nested model run, the mother domain results were used as boundary conditions.

The modeled concentrations of PM_{10}, $PM_{2.5}$, NO_2 and SO_2 were compared with observations available at 1 h temporal resolution, provided by the Chief Inspectorate of Environmental Protection. This included 111 (PM_{10}, 89 background stations), 41 ($PM_{2.5}$, 34 background), 141 (NO_2, 113 background), 136 (SO_2, 109 background) stations.

18.3 Results

The results are presented as follows: (1) WRF-Chem with MOZART and EMEP4PL for January, (2) WRF-Chem with MOZART and EMEP4PL for July, (3) comparison of WRF-Chem results with and without boundary conditions from MOZART.

Mean monthly observed concentrations of PM_{10}, $PM_{2.5}$, SO_2 and NO_2 in January were respectively: 33.0, 28.0, 9.0, 18.2 μg m^{-3}. Two low air quality episodes were observed in this period, with PM_{10} concentrations above 100 μg m^{-3} at most of the stations. WRF-Chem has a tendency to overestimate concentrations of most species (NO_2, PM_{10} and $PM_{2.5}$), whereas EMEP4PL underestimates concentrations of all of them (Table 18.1). For all the species the absolute value of NMB is lower for WRF-Chem. However correlation coefficients are higher for EMEP4PL (Table 18.1, Fig. 18.1). For NO_2 and particulate matter FAC2 is above 0.60 for WRF-Chem and for all components is higher for WRF-Chem than for EMEP4PL. For NO_2 and PM_{10} NMGE is slightly better for EMEP4PL than for WRF-Chem. Taylor diagrams indicate that there is too low variability of modeled values in comparison to measurements. It is especially noticed for EMEP4PL but also for SO_2 and PM_{10} from WRF-Chem (Fig. 18.1). There is no large difference in the

Table 18.1 Comparison of WRF-Chem (with MOZART) and EMEP4PL results with observations for Poland

		January					July				
		FAC2	MB	NMB	NMGE	R	FAC2	MB	NMB	NMGE	R
	SO_2	0.48	−1.58	−0.18	0.71	0.29	0.26	−2.36	−0.62	0.79	0.19
WRF-Chem	NO_2	0.66	2.74	0.15	0.62	0.42	0.45	−2.51	−0.17	0.70	0.37
MOZART	PM_{10}	0.62	7.95	0.24	0.64	0.36	0.64	0.36	0.02	0.60	0.20
	$PM_{2.5}$	0.66	6.46	0.23	0.58	0.46	0.58	7.18	0.63	0.92	0.32
	SO_2	0.26	−6.19	−0.67	0.75	0.33	0.38	−1.95	−0.51	0.72	0.21
EMEP4PL	NO_2	0.53	−8.93	−0.48	0.56	0.45	0.20	−11.68	−0.77	0.79	0.37
	PM_{10}	0.41	−20.14	−0.58	0.62	0.39	0.32	−12.44	−0.61	0.62	0.38
	$PM_{2.5}$	0.35	−16.88	−0.60	0.62	0.48	0.51	−5.00	−0.43	0.53	0.45

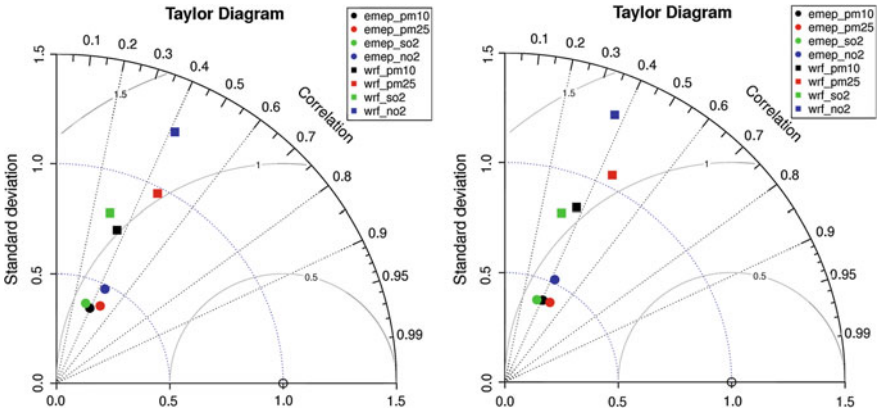

Fig. 18.1 Taylor plot based on all available stations (*left*) and based on background stations (*right*)

Table 18.2 Comparison of WRF-Chem results with default boundary profile with observations for Poland

		January					July				
		FAC2	MB	NMB	NMGE	R	FAC2	MB	NMB	NMGE	R
	SO_2	0.45	−2.07	−0.23	0.72	0.29	0.26	−2.35	−0.62	0.79	0.19
WRF-Chem	NO_2	0.65	2.73	0.15	0.62	0.41	0.43	−2.46	−0.17	0.71	0.37
	PM_{10}	0.67	2.70	0.08	0.56	0.36	0.35	−10.30	−0.51	0.67	0.05
	$PM_{2.5}$	0.72	1.90	0.07	0.50	0.49	0.44	−2.46	−0.22	0.67	0.21

models performance when all type of stations and only background stations are taken for the verification (Fig. 18.1).

In July, mean monthly observed concentrations were lower than in winter and equal to 20.0, 11.4, 3.5 and 14.5 μg m^{-3} respectively for PM_{10}, $PM_{2.5}$, SO_2 and NO_2. In general, WRF-Chem results for July are worse than the results for January with lower FAC2 and R and higher NMGE. In the case of EMEP4PL correlation coefficients were lower for all compounds and FAC2 and NMGE poorer for NO_2 and PM_{10} in July in comparison to winter. Similarly as for January, for July EMEP4PL underestimates measured concentrations of all compounds and WRF-Chem underestimates concentrations of SO_2 and NO_2.

When we compare the WRF-Chem simulations with two different setups of boundary conditions: (1) from the MOZART model, (2) default boundary profile, it shows that application of MOZART improves especially the results for the summer period (higher FAC2 and R, lower NMGE) (Tables 18.1 and 18.2). For July the WRF-Chem results with default boundary conditions are more similar to the EMEP4PL model results in comparison to the WRF-Chem simulation with MOZART.

18.4 Summary

- Two Eulerian models—online WRF-Chem and offline EMEP4PL were run for Poland for January and July 2015. The basic version of the EMEP4PL model includes hourly temporal profile and vertical profile of anthropogenic emissions. These profiles had to be introduced into the emissions data before running WRF-Chem, which is very time consuming. WRF-Chem requires more effort in preparation of input data compared to EMEP4PL. Due to the fact that each simulation of WRF-Chem is related with modelling of meteorological parameters, the model is more time and resources demanding. Thus, EMEP4PL seems to be better suited for tasks which require many simulations for the same period, like e.g. source-receptor matrices.
- Both models give better results for the winter period than for summer. For July the WRF-Chem results for particles are improved after inclusion of MOZART boundary conditions, which is not the case in January. Both these aspects could be related with the fact that winter period concentrations are mainly affected by relatively well represented anthropogenic emissions from local sources. High particulate matter concentrations in summer can be related to a long range transport of natural dust. These episodes could be reproduced by the boundary conditions provided with the MOZART data.
- In general WRF-Chem gives higher FAC2 and lower NMB for both months in comparison to EMEP4PL. However EMEP4PL correlates better with observations in comparison to WRF-Chem. It is difficult to distinguish what is the main reason of the differences in correlation coefficients as i.e. both models use the same temporal emission profiles. More studies are required to find out the reasons for the differences.

Acknowledgements The study was supported by the Polish National Science Centre project no. UMO-2013/09/B/ST10/00594.

Questions and Answers

Questioner: Heinke Schluenzen
Question: Did you use grid average values for comparison with the 2m values or did you apply some vertical interpolation method to determine concentration values at e.g. 2m?
Answer: We used the grid averaged values for comparison with measurements.

Questioner: Johannes Bieser
Question: How do the model values compare if you integrate over similar vertical layers? (either integrate WRF-Chem over 90 m or apply a gradient based on dry deposition velocity on the EMEP lowest layer).
Answer: We have not done this yet. Thank you for your suggestion.
Questioner: Ari Karppinen
Question: Did you compare your modelling results with any other available model results, e.g. from Copernicus Model Ensamble?
Answer: The results have not been compared with other models, yet.

References

Baklanov A, Schlünzen K, Suppan P, Baldasano J, Brunner D, Aksoyoglu S, Carmichael G, Douros J, Flemming J, Forkel R, Galmarini S, Gauss M, Grell G, Hirtl M, Joffre S, Jorba O, Kaas E, Kaasik M, Kallos G, Kong X, Korsholm U, Kurganskiy A, Kushta J, Lohmann U, Mahura A, Manders-Groot A, Maurizi A, Moussiopoulos N, Rao ST, Savage N, Seigneur C, Sokhi RS, Solazzo E, Solomos S, Sørensen B, Tsegas G, Vignati E, Vogel B, Zhang Y (2014) Online coupled regional meteorology chemistry models in Europe: current status and prospects. Atmos Chem Phys 14(1):317–398. doi:10.5194/acp-14-317-2014

Bieser J, Aulinger A, Matthias V, Quante M, Denier Van Der Gon HAC (2011) Vertical emission profiles for Europe based on plume rise calculations. Environ Pollut 159(10):2935–2946. doi:10.1016/j.envpol.2011.04.030

Emmons LK, Walters S, Hess PG, Lamarque J-F, Pfister GG, Fillmore D, Granier C, Guenther A, Kinnison D, Laepple T, Orlando J, Tie X, Tyndall G, Wiedinmyer C, Baughcum SL, Kloster S (2010) Description and evaluation of the Model for Ozone and Related chemical Tracers, version 4 (MOZART-4). Geosci Model Dev 3(1):43–67. doi:10.5194/gmd-3-43-2010

Grell G, Baklanov A (2011) Integrated modeling for forecasting weather and air quality: a call for fully coupled approaches. Atmos Environ 45(38):6845–6851. doi:10.1016/j.atmosenv.2011.01.017

Grell G, Peckham SE, Schmitz R, McKeen SA, Stuart Frost G, Skamarock WC, Eder B (2005) Fully coupled "online" chemistry within the WRF model. Atmos Environ 39(37):6957–6975. doi:10.1016/j.atmosenv.2005.04.027

Simpson D, Benedictow A, Berge H, Bergström R, Emberson LD, Fagerli H, Flechard CR, Hayman GD, Gauss M, Jonson JE, Jenkin ME, Nyíri A, Richter C, Semeena VS, Tsyro S, Tuovinen J-P, Valdebenito Á, Wind P (2012) The EMEP MSC-W chemical transport model—technical description. Atmos Chem Phys 12(16):7825–7865. doi:10.5194/acp-12-7825-2012

Werner M, Kryza M, Skjøth CA, Wałaszek K, Dore AJ, Ojrzyńska H (2017) Aerosol-radiation feedback and PM10 air concentrations over Poland. Pure Appl Geophys 174:551. doi:10.1007/s00024-016-1267-2

Chapter 19
Climatological Modelled and Measured AOD in Baltic Sea Region

Ketlin Reis, Mikhail Sofiev, Marje Prank, Erko Jakobson and Marko Kaasik

Abstract This study is based on AOD values from long-term re-analysis of atmospheric composition and air quality performed with SILAM model in Finnish Meteorological Institute. This study uses two spatial scales: global (1.44° Resolution, ERA-Interim re-analysis meteo data) and Northern Europe (0.1°, BaltAn65+ meteo). The emission information is compiled from the MACCITY and EDGAR anthropogenic, GEIA lightning and aircraft, MACCity-ACCMIP biomass-burning, and MEGAN biogenic emission inventories. The emission of sea salt and wind-blown dust is computed with embedded SILAM modules. Comparison of AOD from global run for 2008–2014 with 13 Aeronet stations in the Baltic Sea region (54 to 63° N and 8 to 38° E) show underestimation of station-wise average AOD-s by factor of 1.5–2.6, whereas the predicted and measured values are well correlated: linear correlation coefficients based on hourly values in different stations range from 0.46 to 0.85 (average 0.59). Nordic run made for only year 2010 show underestimation by factor of 1.6–4.1 with linear coefficients ranging from 0.33 to 0.73. Thus, the underestimation was a bit lower in the global run. A reason of underestimation may be missing local ground dust emissions and long-term realistic fire emissions that are only available until 2008 Granier et al. (Clim Change 109:163, 2011). Also, AOD measurements made with sun photometer like it is done in Aeronet stations tend to give higher AOD values than actinometric measurements do. The analysis based on longer time series (since 1990) is in progress.

K. Reis (✉) · M. Kaasik
University of Tartu, Tartu, Estonia
e-mail: ketlin.reis@ut.ee; ketlinpiir@gmail.com

M. Sofiev · M. Prank
Finnish Meteorological Institute, Helsinki, Finland

E. Jakobson
Tartu Observatory, Tartu, Estonia

C. Mensink and G. Kallos (eds.), *Air Pollution Modeling and its Application XXV*,
Springer Proceedings in Complexity, DOI 10.1007/978-3-319-57645-9_19

19.1 Introduction

This study is based on AOD values from long-term re-analysis of atmospheric composition and air quality performed with SILAM model in Finnish Meteorological Institute, see Sofiev et al. (2017). The further aim of this study is to investigate the climate change in the Baltic Sea region by detecting linkages between temporal variability of aerosols using System for Integrated modeLling of Atmospheric coMposition (SILAM) model. Therefore, validation of input data from SILAM is necessary.

19.2 Methods

AOD 550 was simulated with chemistry-transport model SILAM (http://silam.fmi.fi/). SILAM output was compared with measured hourly average AOD in Baltic Sea region. Thirteen AERONET (http://aeronet.gsfc.nasa.gov/) AOD monitoring stations were included in the comparison (Fig. 19.1).

This study uses two spatial scales: global (1.44° Resolution, ERA-Interim re-analysis meteo data) and Northern Europe (0.1°, BaltAn65+ meteo). The emission information is compiled from the MACCITY and EDGAR anthropogenic, GEIA lightning and aircraft, MACCity-ACCMIP biomass-burning, and MEGAN biogenic emission inventories. The emission of sea salt and wind-blown dust is computed with embedded SILAM modules.

Fig. 19.1 AOD monitoring stations in Baltic Sea region chosen for this study

19.3 Results and Discussion

Comparison of AOD from global run for 2008–2014 with 13 Aeronet stations in the Baltic Sea region (54 to 63° N and 8 to 38° E) show underestimation of station-wise average AOD-s by factor of 1.5–2.6, whereas the predicted and measured values are well correlated: linear correlation coefficients based on hourly values in different stations range from 0.46 to 0.85 (average 0.59). Nordic run made for year 2010 only shows underestimation by factor of 1.6–4.1 with linear correlation coefficients ranging from 0.33 to 0.73. Thus the underestimation was slightly smaller in the global run (Table 19.1).

In August 2010 there were unusually intensive wildfires in Russia and the plume reached Tõravere station as seen from the measured AOD (Fig. 19.2). Both SILAM runs underestimate these episodes. A reason for underestimation may be missing local ground dust emissions and lack of long-term fire emission inventories that are also available after 2008 Granier et al. (2011). Thus, the 2008 emissions were used also for the following years, missing the extreme 2010 emissions. This is supported by the fact that there is a positive linear trend of ratios of annual mean AOD-s by SILAM in 2000–2014 (Fig. 19.3). Meanwhile, there does not seem to be a remarkable negative trend in annual average correlation. The analysis based on longer time series (since 1990) is in progress.

Also, AOD measurements made with sun photometer in Tõravere Aeronet station tend to give higher AOD values than actinometric measurements made in

Table 19.1 Underestimation factor and correlation with SILAM global and nordic runs compared to measured AOD

Site	Factor of underestimation		Linear correlation coeffficient	
	Aeronet/SILAM global	Aeronet/SILAM nordic	Global run	Nordic run
Birkenes	2.46	2.70	0.55	0.46
Gustav Dalen Tower	**1.45**	**1.63**	0.68	0.69
Hamburg	1.93	2.54	0.67	0.57
Helgoland	1.97	2.57	0.57	0.53
Helsinki	1.73	1.82	0.80	0.66
Helsinki Lighthouse	1.51	1.66	**0.85**	**0.73**
Hyytiälä	2.06	2.05	0.71	0.70
Kuopio	2.60	2.47	0.79	0.68
Minsk	2.02	4.11	0.75	0.46
Moscow	2.53	2.46	0.46	0.33
Palgrunden	1.63	2.05	0.62	0.66
Zvenigorod	1.49	2.80	0.63	0.57
Tõravere	1.83	2.87	0.63	0.63

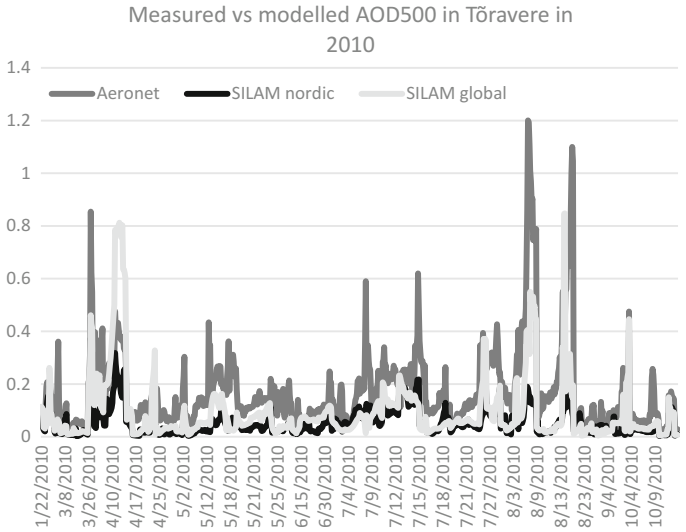

Fig. 19.2 Measured and modelled AOD both global and nordic run in Tõravere station in 2010

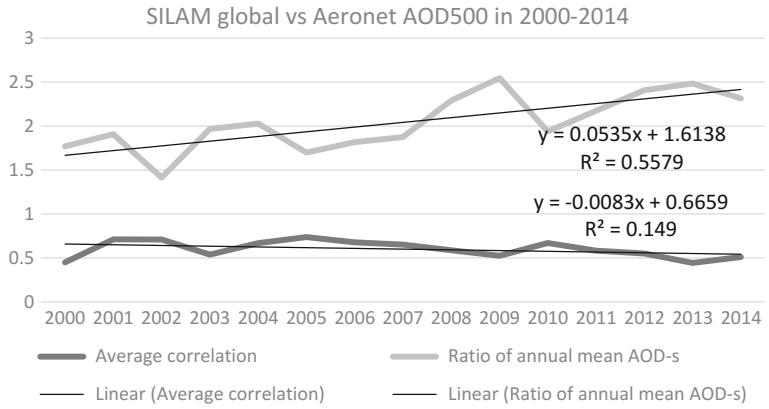

Fig. 19.3 AOD500 average correlation and ratio of annual mean AOD-s of SILAM global run and Aeronet measurements in 2000–2014

Tõravere station Kannel et al. (2012). This might enhance the difference between measured and modelled AOD values.

Acknowledgements This study was funded by Estonian Research Council research projects PUT645 and IUT20-11.

Questions and Answers

Questioner: Ulas Im
Question: Have you done any comparison with satellite observations?
Answer: No, only with ground measurements.

Questioner: V. Matthias
Question: Could you explain how the AOD is calculated in the model? In particular, do you take aerosol growth with humidity into account?
Answer: Yes

Questioner: Paul Makar
Question: Is SILAM an online or offline model? If offline—the AQMEII-2 special issue in Atmospheric Environment has several papers examining the Russian fires of 2010. These online model papers showed that the cloud of particles from the fires reduced downward shortwave radiation flux by 80 W/m^2. This resulted in reduced PBL heights and higher concentrations. Part of the AOD underestimation you have might be due to the PBL height too high, hence not as much horizontal dispersion due to lower wind speeds, hence higher AOD values than simulated by SILAM. You could try comparing SILAM's PBL heights to those simulated in the AQMEII-2 papers to check this.
Answer: SILAM is an offline model. There is a paper in Atmospheric Environment about SILAM as well: Toll, V.; Reis, K.; Ots, R.; Kaasik, M.; Männik, A.; Prank, M.; Sofiev, M. (2015). SILAM and MACC reanalysis aerosol data used for simulating the aerosol direct radiative effect with the NWP model HARMONIE for summer 2010 wildfire case in Russia. Atmospheric Environment, 121, 75–85, j.atmosenv.2015.06.007.

References

Granier C, Bessagnet B, Bond T et al (2011) Clim Change 109:163. doi:10.1007/s10584-011-0154-1

Kannel M, Ohvril H, Okulov O (2012) A shortcut from broadband to spectral aerosol optical depth. Proc Est Acad Sci 61(4):266–278

Sofiev M, Kouznetsov R, Prank M, Soares J, Vira J, Tarvainen V (2017) A long-term re-analysis of atmospheric composition and air quality (in this volume)

Chapter 20
Comparison of WRF PBL Models in Low-Wind Speed Conditions Against Measured Data

Enrico Ferrero, Francois Vandenberghe, Stefano Alessandrini and Luca Mortarini

Abstract In a previous work (Ferrero et al. 2016) we have tested the WRF PBL models during two different months (January and July) of the experimental campaign. Here, we are particularly interested in low-wind conditions (wind speed less then 1.5 ms^{-1}), which are frequent in the Po Valley were the mast is located. Thus, we selected these cases and compared the model results with measurements. Some results of the comparison are presented here in term of 2D histograms and marginal rug plots between measured and simulated quantities for the month of July 2007.

20.1 Introduction

We run different PBL models in the Weather Research and Forecasting model (WRF) and perform a validation with measurements of wind profiles, temperature and turbulent kinetic energy. We used the UTP (Urban Turbulence Project, Mortarini et al. 2013) dataset measured in the outskirts of Turin (Italy). It provides measurements performed by sonic anemometers at three different heights (5, 9, 25 m). The data refer to mean wind, temperature and standard deviations of the

E. Ferrero (✉)
Department of Science and Technological Innovation, University of Piemonte Orientale, Viale Teresa Michel, 11, Alessandria, Italy
e-mail: enrico.ferrero@uniupo.it

F. Vandenberghe · S. Alessandrini
National Center for Atmospheric Research (NCAR), PO Box 3000, Boulder, CO 80307-3000, USA
e-mail: vandenb@ucar.edu

S. Alessandrini
e-mail: alessand@ucar.edu

E. Ferrero · L. Mortarini
Institute of Atmospheric Sciences and Climate, National Research Council, Corso Fiume, 4, Turin, Italy
e-mail: l.mortarini@isac.cnr.it

C. Mensink and G. Kallos (eds.), *Air Pollution Modeling and its Application XXV*, Springer Proceedings in Complexity, DOI 10.1007/978-3-319-57645-9_20

wind velocity components continuously collected for 15 months. PBL models can be classified as local/non-local model depending whether the flux-gradient relationship is modified or not. The model can include the turbulent kinetic energy equation. All the cases provide a diffusion coefficient, which depends on a velocity scale and a length scale. Each model differs from the others in the way it calculates these two quantities. WRF also offers an urban model, able to simulate the effects of vertical (walls) and horizontal (streets and roofs) surfaces on momentum (drag force), turbulent kinetic energy and potential temperature.

20.2 The PBL Models in WRF

In WRF are embedded many different PBL models that can be divided in local and nonlocal models (YSU; Hong et al. 2006 and ACM2; Pleim 2007a, b). Some of them also entail a turbulent kinetic energy (TKE) equation (MYJ; Mellor and Yamada 1974, 1982; Janjic 1990, 2002; BOULAC; Bougeault and Lacarrere 1989; QNSE; Sukoriansky et al. 2005 and MYNN25; Nakanishi and Niino 2004).

20.3 The UTP Dataset

In this work we considered an urban environment of a large city located in the Po Valley (Italy). It is remarkable that the site is characterized by frequent cases of low-wind speed and calm conditions. This fact leads to high convection during summer and strong inversion in wintertime. The UTP dataset (Mortarini et al. 2013) includes measurements of wind, temperature and turbulence at three different levels within and just above the canopy layer. This allows us to compare the quantities and their differences at the three heights.

20.4 Numerical Simulations Against Experimental Data

We show some preliminary results of the comparison between the model simulations and the UTP data set. We consider the 25 m anemometer, which corresponds at about the top of the roughness layer. For the PBL we chose the BOULAC model (Bougeault and Lacarrere 1989) in WRF with the coupled urban model BEP + BEM (Martilli et al. 2002; Salamanca and Martilli 2010).

Figure 20.1 shows the 2D histograms with marginal rug plots for the four quantities, wind speed and direction, temperature and TKE at 25 m for the entire month of July 2007. Generally speaking the model results are satisfactory. The wind speed is slightly overestimated and the TKE is underestimated at the highest

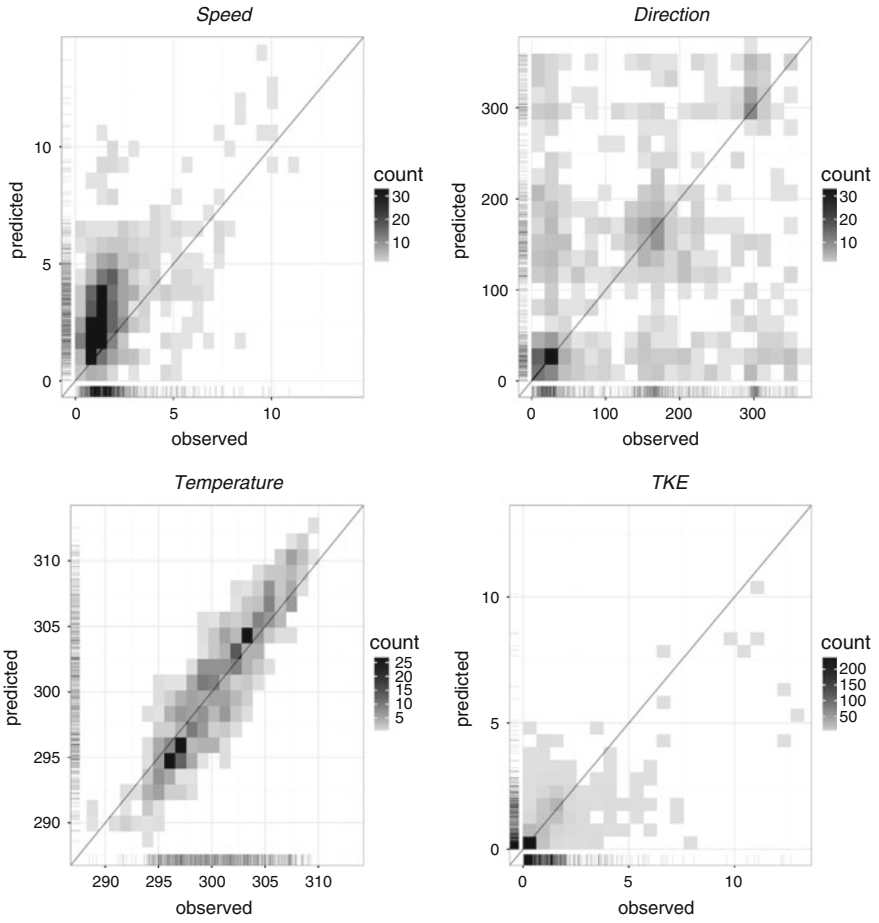

Fig. 20.1 2D Histograms and marginal rug plots between measured and simulated quantities for the month of July 2007

values. Figure 20.2 shows the same plots but in the case of low-wind speed (<1.5 ms^{-1}). While temperature is still satisfactorily reproduced, wind speed is dramatically overestimated. On the opposite of the previous case turbulence is well simulated with a slight overestimation at the highest values.

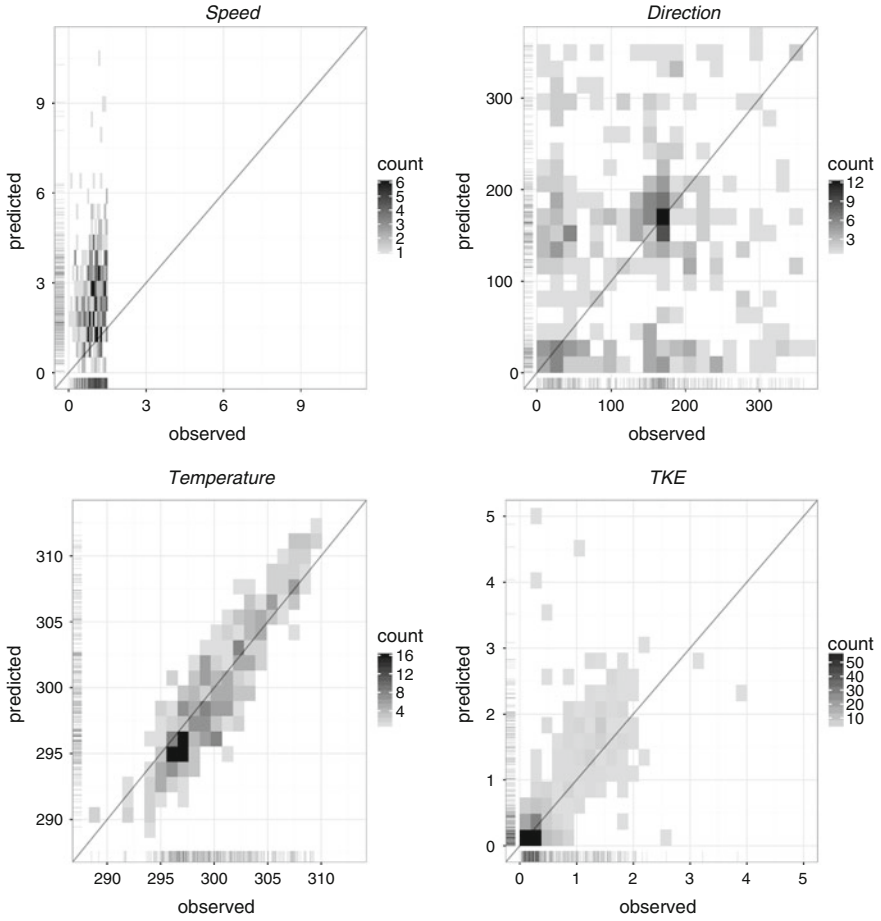

Fig. 20.2 2D Histograms and marginal rug plots between measured and simulated quantities for the month of July 2007. The values refer to the low-wind cases (<1.5 ms^{-1})

Questions and Answers

Questioner: Jeff Weil
Question: For low winds in stable conditions, you might try the Brost and Wyngaard (1978) K-profile parameterization to improve the wind speed prediction; i.e., to reduce the wind speed overprediction.
Answer: Thank you for your suggestion, we will try to implement this module in the future.

Questioner: Silvana Di Sabatino
Question: Did you differentiate between day-time and night time conditions. Perhaps your grid resolution for the urban model was too coarse. You are not

comparing models considering the purpose they were formulated for. (Perhaps you should comment on this on your paper)
Answer: We did not differentiate between day-time and night-time nor between different stability conditions but we plan to do this in a future work. I believe that the grid resolution in our simulation is fine enough for the purpose, which is not to simulate urban canyon flow but urban boundary layer flow. It should be stressed that the boundary layer models in WRF are designed also for urban environment, accounting for the land-use and not for the urban morphology. I apologize but due to limitation in the pages I cannot add this comment in the paper.

Questioner: Heinke Schlünzen
Question: For the test cases without the urban scheme, was the roughness length z_0 reduced to ensure $z \gg z_0$? How was it done for the urban scheme?
Answer: We did not modify z_0 neither for the urban scheme nor for the case without urban scheme. In fact, we aim to test WRF and the boundary layer models as they are implemented in the WRF. In the future we may plan to modify them to better reproduce the measured data.

Questioner: Sven-Erik Gryning
Question: How did you determine the wind speed from the sonic anemometer at the low wind speed conditions. The wind direction can be very variable on a large directional sector (about 180°). The resulting vector speed can be very low but if the wind speed is measured with a cup-anemometer it will be much higher.
Answer: We considered all the cases in which the wind speed was less than 1.5 m/s on the basis of hourly mean data. The data were collected by using sonic anemometers.

References

Bougeault P, Lacarrere P (1989) Parameterization of orography-induced turbulence in a mesobeta-scale model. Mon Weather Rev 117(8):1872–1890

Brost RA, Wyngaard JC (1978) A model study of the stably stratified planetary boundary layer. J Atmos Sci 35:1427–1440

Ferrero E, Alessandrini S, Vandenberghe F (2016) WRF PBL models comparison against data measured in a urban environment. In: 10th international conference on air quality—science and application, 14–18 Mar 2016, Milan, Italy

Hong S, Noh Y, Dudhia J (2006) A new vertical diffusion package with an explicit treatment of entrainment processes. Mon Weather Rev 134(9):2318–2341

Janjic ZI (1990) The step-mountain coordinate: physical package. Mon Weather Rev 118(7): 1429–1443

Janjic ZI (2002) Nonsingular implementation of the Mellor-Yamada level 2.5 scheme in the NCEP meso model. Technical report, NCEP

Martilli A, Clappier A, Rotach MW (2002) An urban surface exchange parameterization for mesoscale models. Bound-Layer Meteorol. 104:261–304

Mellor GL, Yamada T (1974) A hierarchy of turbulence closure models for planetary boundary layers. J Atmos Sci 31:1791–1806

Mellor GL, Yamada T (1982) Development of a turbulence closure model for geophysical fluid problems. Rev Geophys 20(4):851–875

Mortarini L, Ferrero E, Falabino S, Trini Castelli S, Richiardone R, Anfossi D (2013) Low-frequency processes and turbulence structure in a perturbed boundary layer. Q J R Meteorol Soc 139:1059–1072

Nakanishi M, Niino H (2004) An improved Mellor–Yamada level-3 model with condensation physics: its design and verification. Bound-Layer Meteorol 112(1):1–31

Pleim JE (2007a) A combined local and nonlocal closure model for the atmospheric boundary layer. Part I: model description and testing. J Appl Meteorol Climatol 46(9):1383–1395

Pleim JE (2007b) A combined local and nonlocal closure model for the atmospheric boundary layer. Part II: application and evaluation in a mesoscale meteorological model. J Appl Meteorol Climatol 46(9):1396–1409

Salamanca F, Martilli A (2010) A new building energy model coupled with an urban canopy parameterization for urban climate simulations—part II. Validation with one dimension off-line simulations. Theoret Appl Climatol 99:345–356

Sukoriansky S, Galperin B, Perov V (2005) Application of a new spectral theory of stably stratified turbulence to the atmospheric boundary layer over sea ice. Bound-Layer Meteorol 117(2): 231–257

Chapter 21
Sensitivity of the WRF-Chem Modelled Particulate Matter Concentrations to Microphysics, Planetary Boundary Layer and Radiation Schemes: A Case Study for Poland

Maciej Kryza, Jakub Guzikowski, Małgorzata Werner, Mariusz Szymanowski, Kinga Wałaszek and Anthony J. Dore

Abstract The Weather Research and Forecasting (WRF) model has been used to assess the role of parameterisation applied for the planetary boundary layer (PBL) and surface layer, microphysics and radiation on modelled surface air temperature and wind speed. The best model—measurements agreement, in terms of bias and index of agreement statistics, is found for the combination of Goddard microphysics, Yonsei University PBL and the MM5 similarity surface layer schemes, together with the RRTMG and RRTM options for shortwave and longwave radiation, respectively. With this configuration, the model results meet the benchmark values for bias and index of agreement for air temperature. Finally, we have used two configurations that resulted in the best and the worst performance for the meteorological model WRF to run the WRF-Chem model for high PM10 concentration episode of 05–10.01.2015. The WRF-Chem model performance for PM10 concentration is better if optimal meteorological configuration is applied.

21.1 Introduction

Meteorological information is vital for regional air quality modelling, as meteorology is responsible for transport and removal of atmospheric pollutants (Borge et al. 2008; Seaman 2000; Skjøth et al. 2011). Meteorological models, such as the

M. Kryza (✉) · J. Guzikowski · M. Werner · M. Szymanowski · K. Wałaszek
Wrocław University, Wrocław, Poland
e-mail: maciej.kryza@uwr.edu.pl

M. Werner
e-mail: malgorzata.werner@uwr.edu.pl

A.J. Dore
Centre for Ecology and Hydrology, Edinburgh, UK

C. Mensink and G. Kallos (eds.), *Air Pollution Modeling and its Application XXV*,
Springer Proceedings in Complexity, DOI 10.1007/978-3-319-57645-9_21

Advanced Research Weather Research and Forecasting (WRF) model (Skamarock et al. 2008) used in this study, provide the meteorological fields required by the atmospheric transport and chemistry models, as well as for emission pre-processing. Here we compare the performance of the meteorological model WRF with different configurations of microphysics, planetary boundary layer and radiation for air temperature and wind speed. Secondly, we select two meteorological model configurations, the one with the largest and with the smallest errors for wind speed and air temperature, and use them to run the WRF model with chemistry (WRF-Chem), to check the significance of the meteorological model configuration on the performance of the WRF-Chem model.

21.2 Data and Methods

The WRF model version 3.5 was configured using two nested domains with spatial resolutions of 50 km × 50 km for Europe and 10 km × 10 km for the area of Poland (Central Europe). The model was run 24 times for the test period of January 2009, using different physics options (Table 21.1). For the base run (BaseR, Table 21.1) we applied the configuration presented by Kryza et al. (2012). The second group used various parameterizations of boundary and surface layer, while the microphysics, short and longwave radiation schemes are kept the same. Third group of model runs used different options of microphysics, and for fourth group various radiation schemes were used (Table 21.1). The best model configuration was determined by selecting the microphysics, PBL and radiation schemes that resulted in the smallest error values for air temperature and wind speed in groups 1–4. The best model configuration was included in group 5, and the WRF model was run for January 2009 and January 2010. The results were compared with air temperature and wind speed measurements available from 69 meteorological stations operated by the Institute of Meteorology and Water Management in Poland.

The WRF model configuration with the smallest (OS run) and the largest (pbl4 run) errors for air temperature and wind speed were used to run the WRF model with chemistry (WRF-Chem). Thus, WRF-Chem was run twice (pbl4_chem and os_chem run), using two different meteorological configurations, for the high PM10 concentration episode observed on 05–10 January 2015. The modelled hourly PM10 concentrations were compared with measurements gathered at 87 air quality stations. The WRF-Chem model was configured using two nested domains with spatial resolution of 12 km × 12 km for Europe and 4 km × 4 km for Poland. Emissions data were taken from the TNO MACC III database, and were included in the model every hour. The SNAP sector dependent emission profile was applied using the approach proposed by Bieser et al. (2011).

The model performance, in terms of both meteorology and PM10 air concentrations, was summarized using two error statistics: mean bias (MB) and index of agreement (IOA).

Table 21.1 Summary of the WRF model runs

Group	Simulation id	Microphysics	Boundary layer	Surface layer	Short-wave radiation	Long-wave radiation
1. Base run	BaseR	Thompson	ACM2	Pleim-Xiu	Dudhia	RRTM
2. Boundary layer and surface model runs	pbl1	Lin	YSU	MM5	Dudhia	RRTM
	pbl2	Lin	ACM2	Pleim-Xiu	Dudhia	RRTM
	pbl3	Lin	MYJ	Eta	Dudhia	RRTM
	pbl4	Lin	QNSE	QNSE	Dudhia	RRTM
	pbl5	Lin	MYNN2	MYNN	Dudhia	RRTM
	pbl6	Lin	MYNN3	MYNN	Dudhia	RRTM
	pbl7	Lin	MYNN2	MM5	Dudhia	RRTM
	pbl8	Lin	MYNN2	Janic Eta	Dudhia	RRTM
	pbl9	Lin	MYNN3	MM5	Dudhia	RRTM
	pbl10	Lin	ACM2	MM5	Dudhia	RRTM
3. Microphysics model runs	mp1	WSM3	YSU	MM5	Dudhia	RRTM
	mp2	WSM5	YSU	MM5	Dudhia	RRTM
	mp3	Eta (Ferrier)	YSU	MM5	Dudhia	RRTM
	mp4	WSM6	YSU	MM5	Dudhia	RRTM
	mp5	Goddard	YSU	MM5	Dudhia	RRTM
	mp6	Thompson	YSU	MM5	Dudhia	RRTM
	mp7	Milbrand 2	YSU	MM5	Dudhia	RRTM
	mp8	Morrison 2	YSU	MM5	Dudhia	RRTM
	mp9	WDM5	YSU	MM5	Dudhia	RRTM
	mp10	WDM6	YSU	MM5	Dudhia	RRTM
4. SW and LW model runs	rd1	Lin	YSU	MM5	Dudhia	RRTMG
	rd2	Lin	YSU	MM5	RRTMG	RRTM
	rd3	Lin	YSU	MM5	RRTMG	RRTMG
5. Optimal settings	OS09	Goddard	YSU	MM5	RRTMG	RRTM
	OS10	Goddard	YSU	MM5	RRTMG	RRTM

21.3 Results

The WRF model performance for temperature for each model run is presented in Fig. 21.1. For all the model runs, air temperature at 2 m is underestimated, but this underestimation can be significantly reduced, if compared to BaseR, by selecting different schemes of PBL, microphysics or radiation (Fig. 21.1). The wind speed is overestimated for all the model runs, and the impact of different model configurations is smaller if compared to air temperature. Mean bias is 0.57, 0.67 and 0.57 m s^{-1} for BaseR, OS9 and OS10 runs, respectively, and IOA is 0.74 for all three model runs.

We have found that the changes in meteorological settings of the WRF-Chem model affect the model performance in terms of PM10 concentrations significantly. Both pbl4_chem and os_chem runs overestimated mean PM10 concentrations for

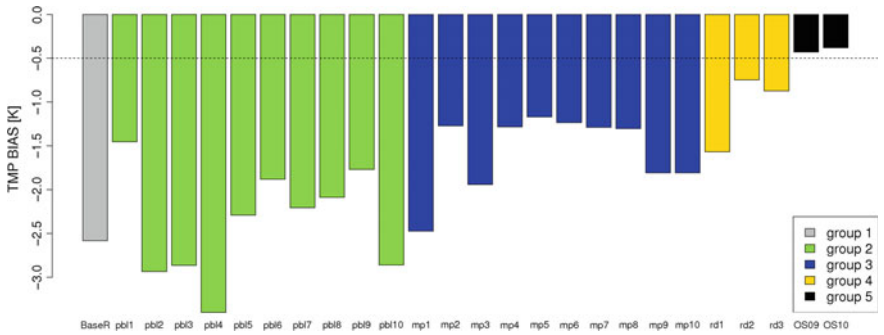

Fig. 21.1 Mean bias for air temperature at 2 m (*dashed line*—acceptance criterion after Emery et al. 2001)

this period, with MB at 6.9 and 7.6 μg m^{-3}, respectively. Index of agreement was higher for os_chem run (0.54) if compared with pbl4_chem (0.48). The maximum hourly PM10 concentration, calculated with the os_chem run is 375 μg m^{-3}, and this is closer to measured value (448 μg m^{-3}) if compared to pbl4_chem (250 μg m^{-3}).

Temporal changes in observed and modelled hourly PM10 air concentrations are presented in Fig. 21.2 using Kraków air quality station as an example. During the nighttime, observed PM10 concentrations were very high, reaching 250 μg m^{-3} on 07.01.2016. Both model runs were capable of reproducing some of the peak values, including the highest peak. However, the pbl14_chem run missed the peak on

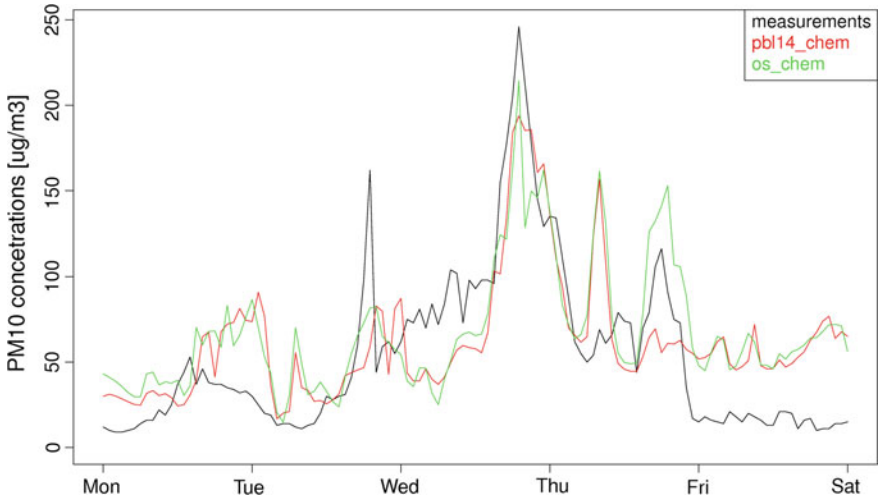

Fig. 21.2 Observed and modelled hourly PM10 air concentrations for Kraków station for 05–10.01.2016

08.01.2016. The difference in modelled PM10 concentrations between the pbl14_chem and os_chem runs for this peak exceeded 100 μg m^{-3} and this is mainly attributed to differences in PBL height. Both WRF-Chem runs show unrealistically high PM10 concentrations during morning hours on 08.01.2016.

21.4 Conclusion

In this work we have shown that the configuration of the meteorological model WRF in terms of physics: boundary layer scheme, radiation and microphysics, may significantly affect the model performance in terms of basic meteorological variables like surface air temperature or wind speed. The model error can be reduced significantly by selection of the appropriate model configuration. Further, model configuration in terms of meteorology also affects the model performance if chemistry transport is turned on (WRF-Chem model). For one selected case of severe air pollution we have shown that the differences in modelled hourly PM10 concentrations between the two runs with different meteorological configuration may reach 100 μg m^{-3}.

Acknowledgements The project was supported by the Polish National Science Centre project no. UMO-2013/09/B/ST10/00594. Calculations have been carried out using resources provided by Wroclaw Centre for Networking and Supercomputing (http://wcss.pl), grant No. 170.

References

Bieser J, Aulinger A, Matthias V, Quante M, Denier van der Gon H (2011) Vertical emission profiles for Europe based on plume rise calculations. Environ Pollut 159:2935–2946. doi:10.1016/j.envpol.2011.04.030

Borge R, Alexandrov V, del Vas JJ, Lumbreras J, Rodriguez E (2008) A comprehensive sensitivity analysis of the WRF model for air quality applications over the Iberian Peninsula Atmos. Environ. 42:8560–8574

Emery C, Tai E, Greg Y (2001) Enhanced meteorological modeling and performance evaluation for two Texas Ozone episodes. Report to the Texas Natural Resource Conservation Commission, College Station, TX, USA

Kryza M, Werner M, Dore AJ, Vieno M, Błaś M, Drzeniecka-Osiadacz A, Netzel P (2012) Modelling meteorological conditions for the episode (December 2009) of measured high PM10 air concentrations in SW Poland—application of the WRF model. Int J Environ Pollut 50:41–52

Seaman NL (2000) Meteorological modeling for air-quality assessments. Atmos Environ 34:2231–2259

Skamarock WC, Klemp JB, Dudhia J, Gill DO, Baker DM, Duda MG, Huang X, Wei W, Powers JG (2008) A description of the advanced research WRF version 3. NCAR Technical Note. National Center for Atmospheric Research, Boulder, Colorado, USA

Skjøth CA, Geels C, Berge H, Gyldenkaerne S, Fagerli H, Ellermann T, Frohn LM, Christensen J, Hansen KM, Hansen K, Hertel O (2011) Spatial and temporal variations in ammonia emissions —a freely accessible model code for Europe. Atmos Chem Phys 11:5221–5236

Chapter 22
Solar Irradiance Prediction over the Aegean Sea: Shortwave Parameterization Schemes and Aerosol Radiation Feedback

G. Methymaki, E. Bossioli, A. Dandou, J. Kalogiros, G. Biskos, N. Mihalopoulos, A. Nenes and M. Tombrou

Abstract In order to study the solar irradiance's prediction over Greece, WRF-Chem model is applied, using three shortwave radiation parameterization schemes: Dudhia, Goddard and RRTMG which simulate differently the aerosol-radiation interaction. This study focuses on a typical summertime wind pattern, the Etesian outbreaks, during which polluted air masses are transported in Greek territory and therefore they affect incoming solar irradiance. The results indicate that schemes overall overestimate solar irradiance reaching the ground;

G. Methymaki (✉) · E. Bossioli · A. Dandou · M. Tombrou
Faculty of Physics, Department of Environmental Physics and Meteorology, National and Kapodistrian University of Athens, Athens, Greece
e-mail: gmethymaki@phys.uoa.gr

J. Kalogiros
Institute of Environmental Research & Sustainable Development, National Observatory of Athens, Athens, Greece

G. Biskos
Energy Environment and Water Research Center, The Cyprus Institute, Nicosia 2121, Cyprus

G. Biskos
Faculty of Civil Engineering and Geosciences, Delft University of Technology, 2628CN Delft, The Netherlands

N. Mihalopoulos
Environmental Chemical Processes Lab., Department of Chemistry, University of Crete, Heraklion, Greece

A. Nenes
School of Earth and Atmospheric Sciences, Georgia Institute of Technology, Atlanta, GA, USA
e-mail: athanasios.nenes@gatech.edu

A. Nenes
School of Chemical & Biomolecular Engineering, Georgia Institute of Technology, Atlanta, GA, USA

C. Mensink and G. Kallos (eds.), *Air Pollution Modeling and its Application XXV*, Springer Proceedings in Complexity, DOI 10.1007/978-3-319-57645-9_22

Dudhia scheme by 9%, RRTMG by 13%, and Goddard by 17%. The performance of all schemes is improved when the aerosol-radiation interaction is considered at least by 1.5%, while local temperature changes, by up to 1.5°, are noticed.

22.1 Introduction

Aerosols scatter and absorb solar radiation ("direct effect"), hence reduce the flux reaching the ground (Charlson et al. 1992). Meanwhile, absorption below, within, and above clouds influences the atmospheric conditions thus, differentiates the cloudiness ("semi-direct effect") (Hansen et al. 1997). Greece receives one of the highest budgets of solar irradiance (SI) among European countries. We present a modeling study that focuses on SI prediction over Greece, during an Etesian outbreak using the non-hydrostatic Advanced Research WRF (ARW) meso-scale meteorological model fully coupled with chemistry (WRF-Chem) (Grell et al. 2005). During the Etesian outbreaks polluted air masses, originating from north-eastern Europe, Russia and the Black Sea are transported in the greater area of Greece (Lelieveld et al. 2002; Bossioli et al. 2016). Simulations considering and ignoring the direct effect are performed.

22.2 Methodology and Data

WRF-Chem is applied, using three shortwave parameterization schemes. Dudhia scheme (Dudhia 1989) performs a simple downward calculation for the fluxes, taking into account water vapor and stratospheric ozone absorption, cloud albedo and absorption, as well as Rayleigh scattering by applying a constant reduction; when solved with aerosol chemistry it also considers the $PM_{2.5}$ scattering. Goddard scheme (Chou 1975) applies a spectral method for flux calculation, interacts with resolved clouds, takes into account aerosol and all the major atmospheric gases' absorption, except for water vapor, and incorporates Rayleigh and multiple scattering. RRTMG (Iacono et al. 2008), also, incorporates the aerosols and the trace gases, including water vapor absorption, Rayleigh and multiple scattering, while it uses a different spectral band technique. Goddard considers aerosol-radiation feedback only in solar but RRTMG both in solar and terrestrial radiation. The model set-up is identical to Bossioli et al. (2016). Two simulations are performed for each scheme, one with (WF) and one without (WOF) aerosol-radiation feedback for Goddard and RRTMG schemes, and one with (WC) and one without aerosol emissions and chemistry (WOC) for Dudhia. The simulations cover a 2-week period (i.e., from 29/8 to 9/9 2011) and are evaluated against airborne observations over the Aegean Sea (AEGEAN-GAME campaign) and routine measurements from Finokalia station (Tombrou et al. 2015).

22.3 Results

In all simulations, SI reaching the ground is overestimated (Table 22.1), except for Dudhia WC. This overall overestimation could be attributed to the underprediction of atmospheric gases and particles by the model (Bossioli et al. 2016). On days with high pollution levels (3/9, 4/9, 7–9/9 (Athanasopoulou et al. 2015)) all simulations predict lower values of SI reaching the ground comparing with other days, while on days with high biomass burning activity (2/9, 4/9, 7/9 (Bossioli et al. 2016, Fig. S6)), the direct effect is more pronounced (Fig. 22.1).

When the interaction between radiation and aerosols is not taken into account, the water vapor absorption is the major factor that determines the performance of the schemes over Aegean Sea. Therefore, as Dudhia and RRTMG schemes employ this physical procedure, their biases are much lower. Moreover, although Dudhia scheme is brief in the representation of the rest of the absorbers, it seems to follow more proximately the data, outputting smaller SI values, which is more obvious during the sunrise and sunset (Zempila et al. 2015). This performance could be explained by the fact that it disregards the phenomenon of multiple scattering.

Table 22.1 Model statistical evaluation for all schemes. The measurements refer to the low-level flights' legs (~150 m) of Aegean-GAME (AG) and ground measurements at Finokalia station (FS)

	Mean bias (W/m^2)		Gross error (W/m^2)		Normalized mean bias (%)		Correlation coefficient	
	AG	FS	AG	FS	AG	FS	AG	FS
Dudhia WOC	23	40	56	49	3.2	9.0	0.89	0.99
Dudhia WC	−4	12	50	35	−0.6	2.7	0.92	0.99
Goddard WOF	56	74	67	79	8.0	16.5	0.90	0.99
Goddard WF	46	66	61	71	6.5	14.7	0.90	0.99
RRTMG WOF	35	57	58	62	5.0	12.7	0.90	0.99
RRTMG WF	24	47	54	53	3.4	10.5	0.91	0.99

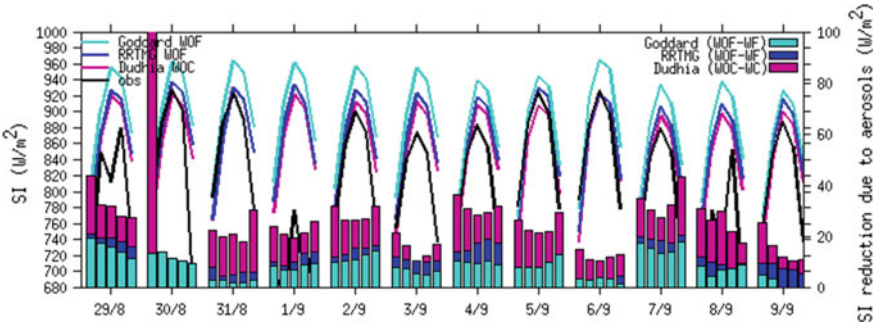

Fig. 22.1 The simulated and measured SI timeseries (*lines*) from 8:00 to 12:00 UTC at Finokalia station during the 2-week period. *Bars* show the irradiance reduction due to aerosols

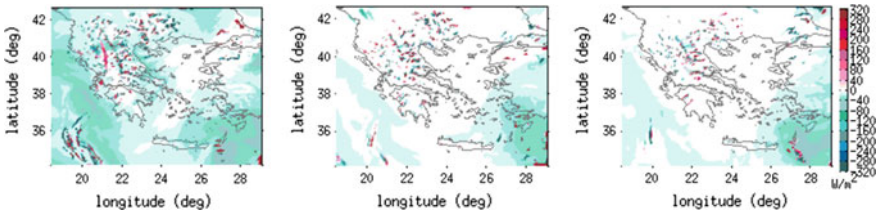

Fig. 22.2 The direct effect with Dudhia (*left*), Goddard (*center*) and RRTMG (*right*) schemes on 4/9/2011 at 10:00 UTC (differences greater than 320 W/m^2 are not presented because they are related to clouds)

Despite its simpler assumptions, the impact of aerosols is more profound in the Dudhia scheme (Fig. 22.2). This result is probably associated with the different aerosol predefined levels considered in the WOC/WOF simulations. In particular, Dudhia considers a constant low aerosol optical depth value (AOD = 0.1) (Zamora et al. 2005) while Goddard and RRTMG take as input a climatological profile of aerosols. The mean reduction of IR for the 2-week period in the modeling domain is 31 W/m^2 for Dudhia and 11 W/m^2 for Goddard and RRTMG. In areas with high aerosol load, e.g. above SE Aegean Sea (Fig. 22.3), the latter two schemes predict more than 40 W/m^2 decrease (Fig. 22.2).

The scattering and/or absorption of SI by aerosols alter the air temperature up to 1.5° (Fig. 22.4). In Dudhia WC simulation, where only scattering is considered, the SI reaching the ground decreases thus, the surface temperatures become lower, which then are transported over sea. An analogous procedure is observed both in Goddard and RRTMG schemes (Fig. 22.4) but with a different response over the areas with high concentration of absorbing aerosols (elemental carbon and dust).

This local heating below and within clouds creates less appropriate conditions for the formation and evolution of clouds. In this particular event the cloud reduction for Goddard and RRTMG is 50% and 10%, accordingly.

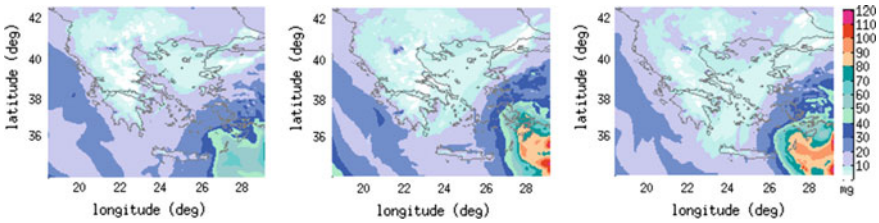

Fig. 22.3 The total mass of $PM_{2.5}$ integrated in a column with 1 m^2 cross-sectional area as simulated by Dudhia (*left*), Goddard (*center*), and RRTMG (*right*) schemes on 4/9/2011 at 10:00 UTC

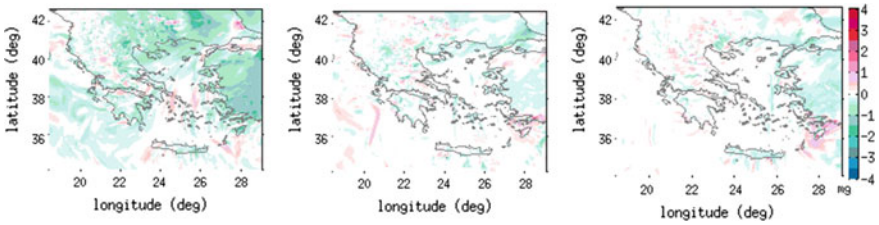

Fig. 22.4 The temperature difference (°C) with Dudhia (WC-WOC) (*left*), Goddard (WF-WOF) (*center*), and RRTMG scheme (WF-WOF) (*right*) on 4/9/2011 at 10:00 UTC

Acknowledgements This work was supported by the Cy-Tera Project (NEA ΥΠΟΔΟΜΗ/ΣΤΡΑΤΗ/0308/31), which is co-funded by the European Regional Development Fund and the Republic of Cyprus through the Research Promotion Foundation.

References

Athanasopoulou E et al (2015) Aerosol chemistry above an extended archipelago of the eastern Mediterranean basin during strong northern winds. Atmos Chem Phys 15:8401–8421

Bossioli E et al (2016) Atmospheric composition in the Eastern Mediterranean: Influence of biomass burning during summertime using the WRF-Chem model. Atmos Environ 132:317–331

Charlson RJ et al (1992) Climate forcing by anthropogenic aerosols. Science 255:423–430

Chou MD (1975) A solar radiation model for use in climate studies. J Atmos Sci 49:762–772

Dudhia J (1989) Numerical study of convection observed during the winter monsoon experiment using a mesoscale two-dimensional model. J Atmos Sci 46:3077–3107

Grell GA et al (2005) Fully coupled "online" chemistry within the WRF model. Atmos Environ 39:6957–6975

Hansen J et al (1997) Radiative forcing and climate response. J Geophys Res 102:6831–6864. doi:10.1029/96JD03436

Iacono MJ et al (2008) Radiative forcing by long-lived greenhouse gases: calculations with the AER radiative transfer model. J Geophys Res, 113(D13103):1609

Lelieveld J et al (2002) Global air pollution crossroads over the Mediterranean. Science 298:794. doi:10.1126/science.1075457

Tombrou M et al (2015) Physical and chemical processes of air masses in the Aegean Sea during Etesians: Aegean-Game airborne campaign. Sci Total Environ 506–507:201–216

Zamora RJ et al (2005) The accuracy of solar irradiance calculations used in mesoscale numerical weather prediction. Mon Weather Rev 86(133):783–792

Zempila M-M et al (2015) Evaluation of WRF shortwave radiation parameterizations in predicting global horizontal irradiance in Greece. Renew Energy 86:831–840

Chapter 23
Backtracking Radioxenon in Europe Using Ensemble Transport and Dispersion Modelling

Pieter De Meutter, Johan Camps, Andy Delcloo and Piet Termonia

Abstract The Comprehensive nuclear Test-Ban-Treaty bans nuclear explosions by everyone, everywhere. Radioxenon monitoring by the International Monitoring System is a key component of the verification of the Treaty. Atmospheric transport modelling can be used to determine the sources of radioxenon plumes. The Flexpart model is used to backtrack radioxenon observations in Europe to determine their source. An ensemble is used to quantify uncertainty.

23.1 Introduction

Certain radioactive xenon isotopes (^{131m}Xe, ^{133}Xe, ^{133m}Xe, ^{135}Xe; further on called radioxenon) are monitored by the International Monitoring System (IMS), with the purpose of verifying compliance with the Comprehensive Nuclear-Test-Ban Treaty. If such radioxenon is measured at an IMS station, atmospheric transport models can be used to determine its source. These atmospheric transport models are, however, prone to errors. Therefore it is important to know the uncertainties on the analysis of nuclear explosion signals picked-up by the IMS.

Civil sources such as medical isotope production facilities and nuclear power plants also emit radioxenon. In this paper we backtrack episodes of high ^{133}Xe con-

P. De Meutter (✉) · J. Camps
Belgian Nuclear Research Institute, Boeretang 200, 2400 Mol, Belgium
e-mail: pieter.de.meutter@sckcen.be

J. Camps
e-mail: johan.camps@sckcen.be

P. De Meutter · A. Delcloo · P. Termonia
Royal Meteorological Institute of Belgium, Ringlaan 3, 1180 Brussels, Belgium
e-mail: andy.delcloo@meteo.be

P. Termonia
e-mail: piet.termonia@meteo.be

P. De Meutter · P. Termonia
Department of Physics and Astronomy, Ghent University,
Krijgslaan 281, 9000 Ghent, Belgium

C. Mensink and G. Kallos (eds.), *Air Pollution Modeling and its Application XXV*,
Springer Proceedings in Complexity, DOI 10.1007/978-3-319-57645-9_23

centration at the IMS station *RN33* in Schauinsland (Germany) to see whether we can link these to the medical isotope production facility *Institute for Radioelements* (IRE) at Fleurus (Belgium), which is the largest regional ^{133}Xe emitter. An ensemble of 50 + 1 members is used to quantify uncertainty from the meteorological data.

23.2 Data and Methods

The atmospheric transport and dispersion simulations have been realized with the Lagrangian particle model Flexpart Stohl et al. (2005). Flexpart can be used to calculate the source-receptor-sensitivity in backward mode Seibert and Frank (2004).

The Ensemble Data Assimilation product of the European Centre for Medium-Range Weather Forecasts Buizza et al. (2008) has been used for the backtracking simulations. The spread between the individual realizations or members contains information about the uncertainty of the simulation.

The measured concentration at a receptor can be reconstructed by multiplying a source field $Q(x, y, z, t)$ with the source-receptor-sensitivity field $SRS(x, y, z, t)$, outputted by Flexpart, and by summing over all grid boxes and times (x, y, z, t):

$$obs = \sum_{x,y,z,t} Q(x, y, z, t)\, SRS(x, y, z, t) \tag{23.1}$$

If we assume time independent point sources, we can readily calculate Q for every grid point.

23.3 Results

23.3.1 Case Study

We consider four consecutive days of elevated ^{133}Xe concentration at *RN33* in July 2014 (Table 23.1). For each measurement we calculate the SRS fields, from which we can calculate a corresponding source term. If the calculated source term is below $10^{13}\ Bq/day$, which is the maximum expected ^{133}Xe release from civil sources Saey (2009), we consider that grid point as a possible source area. The possible sources for the four measurements are shown in Fig. 23.1 (left).

We assume that all four ^{133}Xe samples originates from the same source, and therefore plot the overlap of possible source areas in Fig. 23.1 (right). There are three areas where all four possible source regions overlap: the first area extends from the detector RN33 to the northeast part of France, Belgium, Luxembourg and the Netherlands and a large part of the North Sea. The second area is located south-west of Denmark. The third area is located at the border of Poland and Ukraine.

Table 23.1 Elevated activity concentration measurements at RN33 in July 2014

Receptor	Collection start	Collection stop	Act. conc. (mBq/m^3)
RN33	10 Jul 2014 0600 UTC	11 Jul 2014 0600 UTC	4.5
RN33	11 Jul 2014 0600 UTC	12 Jul 2014 0600 UTC	5.3
RN33	12 Jul 2014 0600 UTC	13 Jul 2014 0600 UTC	6.1
RN33	13 Jul 2014 0600 UTC	14 Jul 2014 0600 UTC	1.4

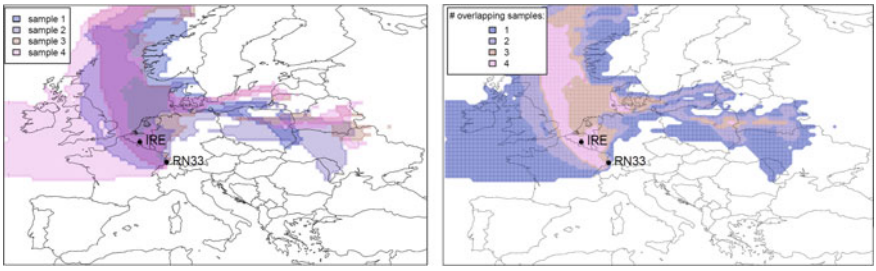

Fig. 23.1 *Left* for each sample, the area of possible sources is shown in *transparent colors* (assuming a source term below 10^{13} Bq/day). *Right* overlap of the areas of possible sources shown *left*

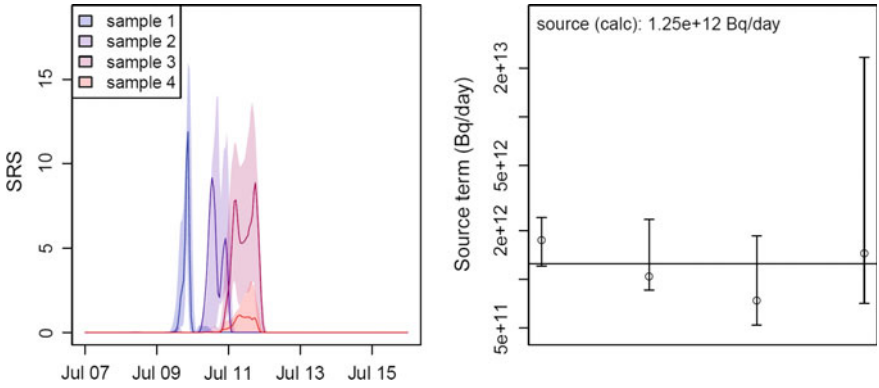

Fig. 23.2 *Left* SRS at IRE. *Right* source term for sample 1 (most *left*) to sample 4 (most *right*). Shaded areas (*left*) and error bars (*right*) represent 95% confidence interval

If we exclude grid points where the release exceeds 10^{11} Bq/day (which can be considered as the maximal release from nuclear power plants in that region), only a very small area around RN33 remains (not shown). We therefore consider IRE as the most likely source.

To determine the ^{133}Xe release, we have interpolated the SRS fields to the location of IRE. Figure 23.2 (left) shows the time series of the SRS of the four samples. The corresponding source term for each measurement is shown in Fig. 23.2 (right). We see that all four source terms are similar and the uncertainty depends on the flow.

23.3.2 Ten Highest ^{133}Xe episodes at RN33

We have selected the ten highest ^{133}Xe episodes at RN33 in 2014 and have calculated the corresponding source term (not shown), assuming IRE as dominant source. Nine out of ten gave a realistic source term. However, for one case we were not able to attribute the observed ^{133}Xe to IRE, suggesting that nearby nuclear power plants can also significantly contribute to the ^{133}Xe concentration at RN33.

23.4 Summary

ATM is a valuable tool for the Comprehensive nuclear Test-Ban-Treaty verification regime since it allows to calculate possible source regions and to estimate, for a specific location, when releases could have occurred, and what amount of radioxenon should have been released under different release duration assumptions.

We have selected elevated ^{133}Xe concentrations at RN33 and have calculated the corresponding source term assuming that IRE was the dominant source. Nine out of ten observations could be attributed to the IRE. The use of an ensemble allows to quantify uncertainty of the calculated source term.

Acknowledgements One of the authors (P De Meutter) acknowledges funding from Engie under contract number JUR2015-28-00.

References

Buizza R, Leutbecher M, Isaksen L (2008) Potential use of an ensemble of analyses in the ECMWF Ensemble Prediction System. Q J R Meteor Soc 134:2051–2066. doi:10.1002/qj.346

Saey PR (2009) The influence of radiopharmaceutical isotope production on the global radioxenon background. J Environ Radioactiv. doi:10.1016/j.jenvrad.2009.01.004

Seibert P, Frank A (2004) Source-receptor matrix calculation with a Lagrangian particle dispersion model in backward mode. Atmos Chem Phys. doi:10.5194/acp-4-51-2004

Stohl A, Forster C, Frank A, Seibert P, Wotawa G (2005) Technical note: the Lagrangian particle dispersion model FLEXPART version 6.2. Atmos Chem Phys. doi:10.5194/acp-5-2461-2005

Chapter 24
Evaluation of Mesoscale Modelling of a Closed Breeze Cell Against Sodar Data

Hristina Kirova, Damyan Barantiev and Ekaterina Batchvarova

Abstract Simulating a closed breeze cell is a challenging task for mesoscale models, but very important for air quality modelling in coastal areas. The occurrence, the vertical and temporal scales of the phenomenon "closed breeze cell" and the magnitude of wind-speed field depend on the synoptic situation, the difference in surface temperature of sea and soil and from the configuration of the coast. In this study we show results of about 4 years of sodar data analysis at Ahtopol on the Bulgarian Black sea coast. We chose cases when the vertical extend of the local circulation fell within the range of the sodar. We present the results of simulations with Weather Research and Forecasting (WRF) model. The model performed with different success from case to case. The simulated closed breeze cells are with smaller vertical extend and lower values for wind speed. There is also a shift of the onset of the sea breeze and the duration of the phenomenon.

24.1 Observations

The near surface observations are taken at 2 m height for temperature and at 10 m height for wind at standard synoptic station Ahtopol, southern part of the Bulgarian Black Sea coast, with resolution 3 h. At the same site, a SCINTEC MFAS sodar has been in operation since 19 July 2008 with 10 m vertical resolution and 10 min temporal resolution of 20 min moving average values for mean and turbulent wind parameters. The sodar data are used for studies of the wind regime and characterisation of the vertical structure of the coastal boundary layer. The effective range of the sodar (about 700 m) allows to detect closed breeze cells with distinguished time of onset of the daytime sea breeze both in wind speed (WS) and wind direction

H. Kirova (✉) · D. Barantiev · E. Batchvarova
National Institute of Meteorology and Hydrology-Bulgarian Academy of Sciences, Sofia, Bulgaria
e-mail: Hristina.Kirova@meteo.bg

E. Batchvarova
e-mail: ekaterina.batchvarova@meteo.bg

C. Mensink and G. Kallos (eds.), *Air Pollution Modeling and its Application XXV*, Springer Proceedings in Complexity, DOI 10.1007/978-3-319-57645-9_24

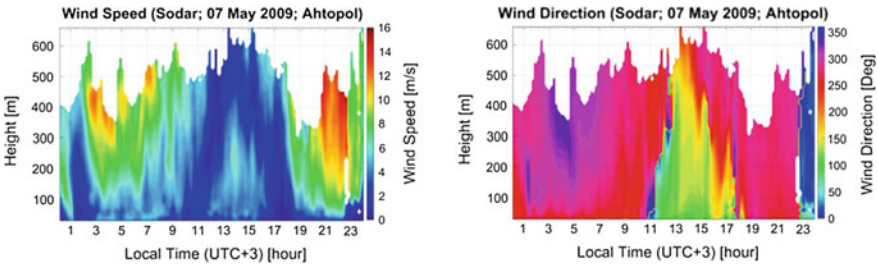

Fig. 24.1 Observed closed sea breeze cell at Ahtopol on 7 May 2009—wind speed (*left*) and wind direction (*right*)

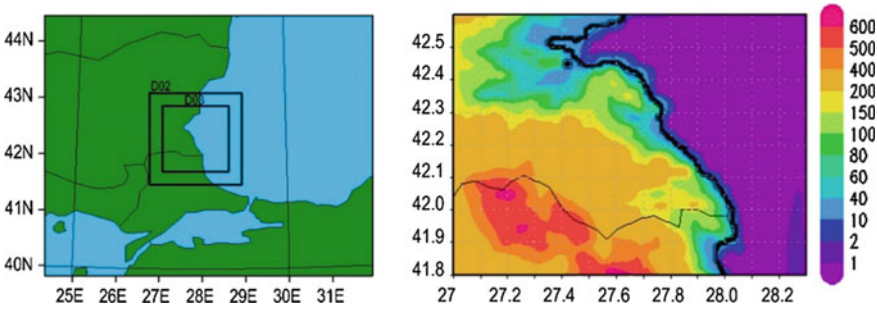

Fig. 24.2 Model domains configuration (*left*) and topography [m] of the innermost domain (*right*)

(WD), zones of high winds in the flow from the sea (WD from 0 to 120° at Ahtopol), calm zones before, aloft and after the flow from the sea and a reverse flow from the land higher up, Fig. 24.1. The analysis of 4 years of data (2008–2012) indicates that such clear closed breeze cells appear in about 6% of all days. Here, three cases are used for modelling and analysis—5 August 2008, 5 September 2008 and 7 May 2009 (Barantiev et al. 2011).

24.2 Model Setup

The Advanced Research WRF (ARW) Version 3.3.1 (Skamarock et al. 2008) was initialized with US National Center for Environmental Prediction Final Analyses (FNL) of 1° × 1° spatial and 6 h temporal resolution. Two-way nesting was applied on three model domains of grid size 25, 5 and 1 km and number of grid points 26 × 21, 36 × 36, 111 × 111, respectively (Fig. 24.2). A Lambert projection with truelat1 = 30°, truelat2 = 60° and coordinates of the centre of the outermost domain 42.084°N, 27.951°E was used. 24 categories for land surface according USGS (US Geological Survey) were taken. The choice of the physical

Table 24.1 Physical processes' parameterizations as defined in (Skamarock et al. 2008)

Physical process	Scheme
Microphysics	8 (MO2 и 3) = Thompson graupel scheme; 4(MO1) = WSM 5-class scheme
Longwave radiation	1 = RRTM: rapid radiative transfer model
Shortwave radiation	2 = Goddard
Surface layer	2 = Eta similarity
Surface	2 = Noah LSM
Planetary boundary layer	2 = MYJ: mellor-yamada-janjic TKE
Cumulus parameterization	5 (only for domains 1 and 2) = Grell3D

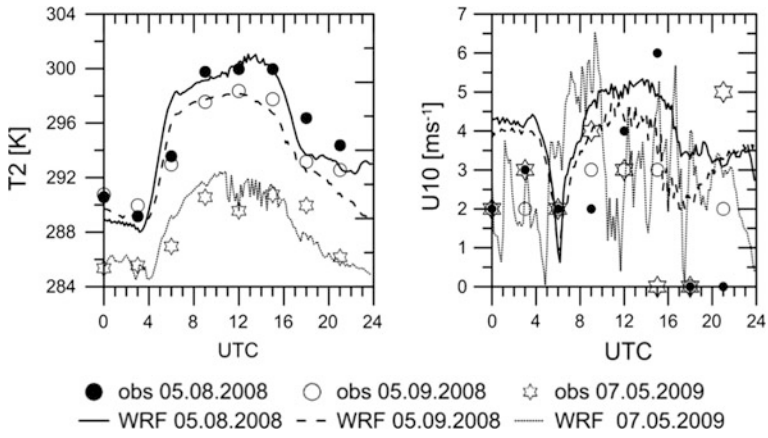

Fig. 24.3 Diurnal change of temperature (*left*) and U10 (*right*) at the measuring site (42.084 N, 27.951 E)

processes' parameterizations is listed in Table 24.1. The upper boundary of the model domains was set at 50 hPa and 43 vertical levels were defined, 30 of which below 2000 m. For each case, a 36 h simulation was performed and the first 12 h were used for model spin-up. The model data were extracted with 10 min temporal resolution to correspond to the time resolution of the sodar data.

24.3 Evaluation of Model Results

The modelled diurnal change of temperature at 2 m (T2) and wind speed at 10 m (U10) as well as synoptic observations are shown in Fig. 24.3. Because of the 3-h temporal resolution, standard measurements miss the onset of the sea breeze which happens typically around 9:30–10 a.m. The agreement between model and

observations for T2 is very good. Concerning U10, the discrepancy between modelled and measured diurnal change is larger.

Analysing the model results for the entire vertical domain, covered by the sodar measurements, revealed that WRF simulated closed breeze cells on the chosen days, but shifted in time and space and with smaller than observed values for wind speed. The model results, differences observations-model and change of correlation coefficients in height and time for 7 May 2009 (in order to compare with the observations in Fig. 24.1) are illustrated in Fig. 24.4. Highest (>0.6) correlation coefficients for wind speed are obtained when comparing the modelled and measured profiles at each time interval during night hours before sunrise and above 500 m in the profile of the correlation coefficient for all modelled and measured data during the day. Similar results are obtained for wind direction.

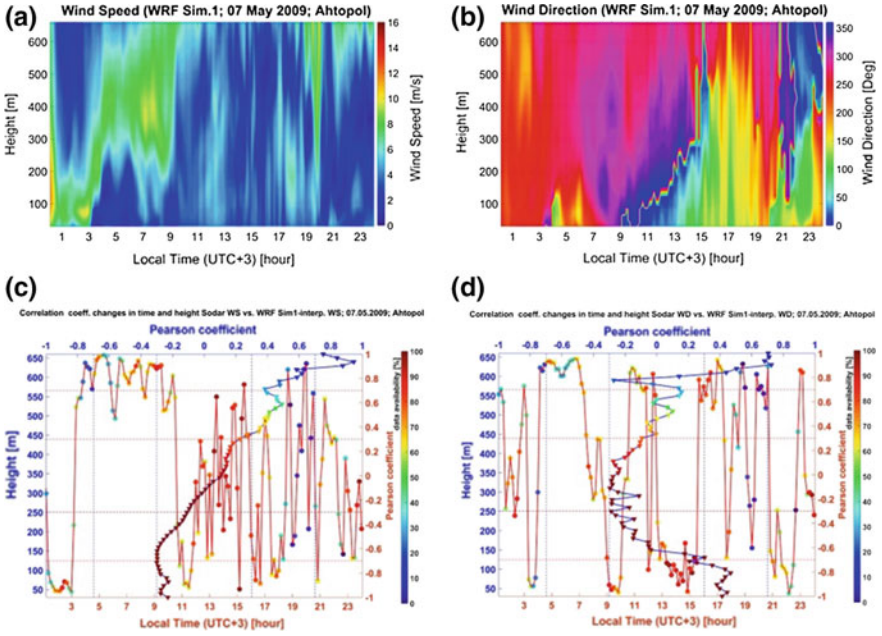

Fig. 24.4 Space-time cross-sections for wind speed (**a**) and wind direction (**b**); change of correlation coefficients for all time periods with height (*blue line*, *blue* x-axis and colored according data availability *triangles*) and change of correlation coefficient for all heights with time (*red line*, *red* y-axis and colored according data availability *circles*) for wind speed (**c**) and wind direction (**d**) on 7 May 2009

24.4 Conclusions

WRF simulated qualitatively the phenomenon "closed breeze cell", but with differences in space and time for the specific features, such as time of onset, magnitude of the wind speed, position of the zone with maximal wind speed in the flow from the sea, duration of the sea breeze, etc.

References

Barantiev D, Novitsky M, Batchvarova E (2011) Meteorological observations of the coastal boundary layer structure at the Bulgarian Black Sea coast. Adv Sci Res 6(1):251–259. doi:10.5194/asr-6-251-2011

Skamarock W, Klemp JB, Dudhia J, Gill DO, Barker DM, Duda MG. Huang X-Y, Wang W, Powers JG (2008) A description of advanced research WRF version3. http://www.mmm.ucar.edu/wrf/users/docs. Accessed 1 Nov 2016

Chapter 25
Dispersion Modeling Over Complex Terrain in the Bolzano Basin (IT): Preliminary Results from a WRF-CALPUFF Modeling System

Elena Tomasi, Lorenzo Giovannini, Marco Falocchi, Dino Zardi, Gianluca Antonacci, Enrico Ferrero, Andrea Bisignano, Stefano Alessandrini and Luca Mortarini

Abstract This chapter presents preliminary results obtained from a WRF-CALPUFF modeling system applied at a local scale, over complex terrain, in order to reproduce the dispersion of a tracer gas released from an incinerator stack.

25.1 Introduction

Air quality scenarios provided by coupled meteorological and dispersion models play a key role in supporting policies for monitoring air pollutants, but their reliability is still uncertain, especially when models are applied over very complex terrains. Indeed, a complex orography introduces additional difficulties in reproducing both atmospheric and dispersion processes. In this work, preliminary results from a project carried out in the Bolzano basin, in the Central Italian Alps,

E. Tomasi (✉) · L. Giovannini · M. Falocchi · D. Zardi
Atmospheric Physics Group, Department of Civil, Environmental and Mechanical Engineering, University of Trento, Trento, Italy
e-mail: elena.tomasi@unitn.it

G. Antonacci
CISMA - Centro di Ingegneria e Sviluppo Modelli per l'Ambiente, Bolzano, Italy

E. Ferrero · A. Bisignano
Department of Scienze e Innovazione Tecnologica, University of Piemonte Orientale, Alessandria, Italy

S. Alessandrini
National Center for Atmospheric Research (NCAR), Boulder, CO, USA

L. Mortarini
Institute of Atmospheric Sciences and Climate, National Research Council (ISAC-CNR), Turin, Italy

C. Mensink and G. Kallos (eds.), *Air Pollution Modeling and its Application XXV*, Springer Proceedings in Complexity, DOI 10.1007/978-3-319-57645-9_25

are presented. In July 2013, a new waste incinerator became operative 2 km Southwest of the city of Bolzano, requiring policy makers to improve the forecast of dispersion processes in the area (Ragazzi et al. 2013). Accordingly, a trustful modelling chain to provide emission-impact scenarios was needed. The CALMET/CALPUFF modelling chain (Scire et al. 2000a, b) was therefore tested for application in the area, by means of short-term simulations of tracer releases, under meteorological situations conducive to critical air pollution episodes, e.g. strong ground-based thermal inversion and calm conditions. In order to minimize uncertainties on the input meteorological fields, high resolution simulations were run with the Weather Research and Forecasting (WRF) model (Skamarock et al. 2008), with observational nudging. These simulations provided reliable fields, and captured the development of ground-based thermal inversions and of valley winds. CALPUFF simulations are analysed and simulations with the SPRAYWEB model (Tinarelli et al. 2000; Alessandrini and Ferrero 2009) are planned.

25.2 Case Study

The city of Bolzano (262 m a.s.l.) lies in the middle of a wide basin at the junction of the Isarco Valley and of the Sarentino Valley with the Adige Valley (Fig. 25.1). Wind regimes are dominated by terrain effects (Dosio et al. 2001), developing thermally-driven winds (de Franceschi et al. 2009), which however are mostly absent or very weak during wintertime (de Franceschi and Zardi 2009). This aspect, in connection with the frequent occurrence of ground-based inversions at the bottom of the valley, determines frequent critical conditions for air quality. Figure 25.1 shows the study area in the Bolzano basin, its tributary valleys and all the available measurement stations. The 27th of January 2016 was chosen as the reference day for the dispersion simulations, covering a period of 7 h, from 04 to 10 LST (UTC + 1). Indeed, this day presented most of the typical wintertime meteorological conditions relevant for the stagnation of locally emitted atmospheric pollutants: a strong ground-based thermal inversion, up to 700 m above the valley floor, and weak wind speeds.

25.3 Meteorological Simulations

High-resolution numerical simulations with the WRF model were performed with four nested domains, reaching a horizontal resolution of 333 m in the inner domain, centred in the Bolzano basin. In the inner domain, the observational nudging technique was applied in order to assimilate measurements recorded within the area. Namely, surface data from 8 different weather stations and wind and temperature profiles from a SODAR and a thermal profiler were assimilated during the simulation on an hourly basis. A 30 m resolved Digital Terrain Model and a 100 m land use map were used in order to properly describe the characteristics of the inner domain.

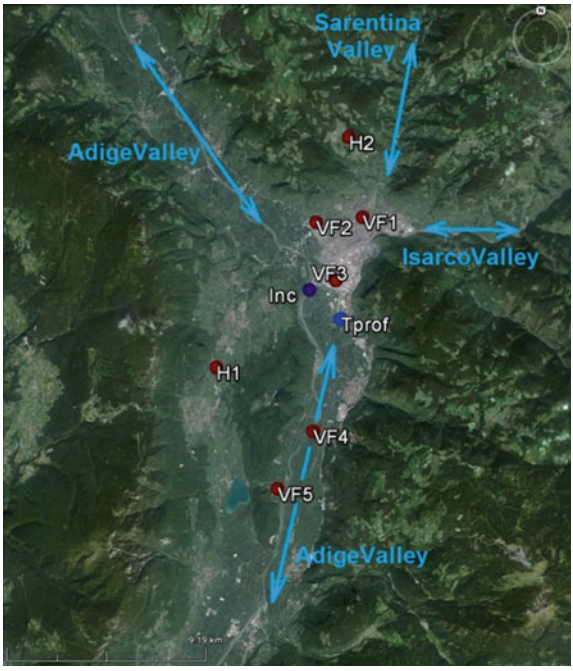

Fig. 25.1 The Bolzano basin with available weather stations: "Inc" incinerator; "Tprof" thermal profiler; "VF#" valley floor and "H#" sidewalls stations (background from GoogleEarth)

WRF simulations properly reproduce the complex flow field in the Bolzano area, capturing the shift of up- and down-valley winds flowing in the valleys which join into the basin. In particular, simulations highlight the occurrence of a low-level nocturnal jet at the exit of the narrow canyon-like Isarco Valley (Fig. 25.2). This specific local phenomenon is very relevant for the fate of pollutants released from the incinerator, as the jet stream flows exactly over the plant: this fact is also well captured by the wind profile measurements, showing that the wind direction at upper layers is reversed with respect to the lower ones. Properly reproducing this flow feature within the meteorological fields is a necessary but not sufficient condition to guarantee the correct pattern of the tracer released from the chimney: in these conditions, indeed, the calculation of the effective release height made by the dispersion model also plays a key role in the assessment of the dispersion pattern direction.

25.4 CALPUFF Simulations

Short-term (7 h) simulations with the CALMET/CALPUFF model are run with a horizontal resolution of 200 m over a 20 × 20 km^2 domain, and with 10 vertical levels from the ground up to 2400 m. The dispersion module is set up to simulate a tracer release from the incinerator chimney starting at 7 LST and lasting 40 min.

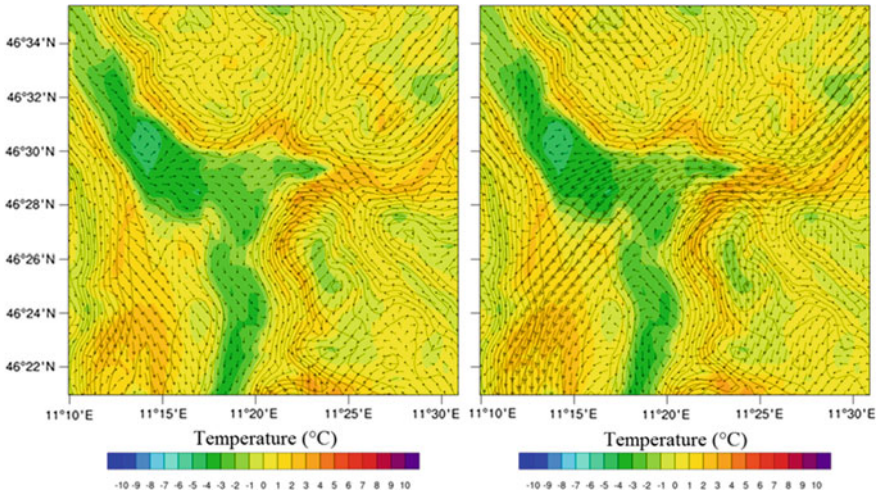

Fig. 25.2 Temperature and wind at 7 LST near the ground (*left*) and at 300 m AGL (*right*)

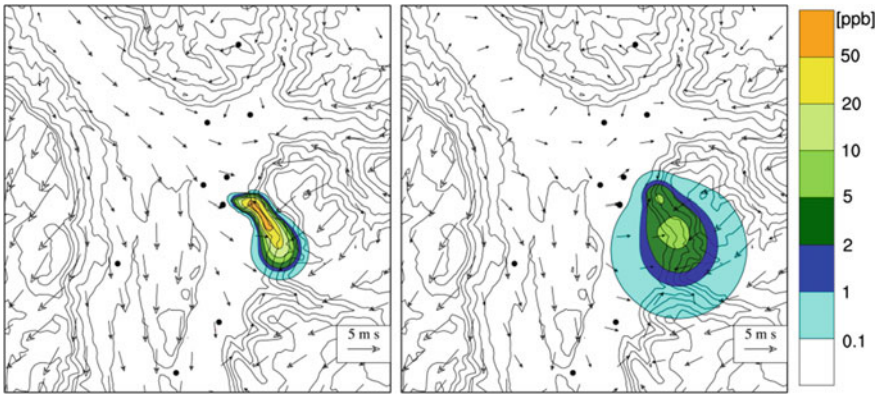

Fig. 25.3 Near ground concentration in the CALPUFF domain at 8:20 (*left*) 9:00 LST (*right*)

As CALMET pre-processor is used in order to increase horizontal resolution from 333 to 200 m, the wind field is slightly modified with respect to the original WRF output. CALPUFF dispersion pattern is shown in Fig. 25.3, where near-ground concentrations are shown at two different times of the simulation. It is clear that the effective release height calculated by the model is lower than the height of the nocturnal low level jet, as the tracer is transported southwest, according to the wind direction of the layers near the ground. The lack of measurements of ground concentrations prevents a formal validation of obtained results and they are hence affected by uncertainties.

25.5 Future Work

Simulations with the SPRAYWEB model are under test to reproduce the same case study. Results from these simulations will allow a direct comparison of two different approaches to dispersion modelling: the CALPUFF mixed lagrangian-gaussian puff approach and the SPRAYWEB purely lagrangian stochastic particle approach. The comparison turns out to be of great interest, as the present case study puts these models to the test in extreme conditions, both in terms of complex orography and of the variability of meteorological conditions. Moreover, the two models can be fed with the same meteorological input, as an interface between SPRAYWEB and WRF is under test and development (Bisignano et al. 2016). Furthermore, measurements to validate numerical simulations are of fundamental importance, and therefore releases of a tracer from the incinerator chimney are planned for the next winter season.

References

Alessandrini S, Ferrero E (2009) A hybrid Lagrangian-Eulerian particle model for reacting pollutant dispersion in non-homogeneous non-isotropic turbulence. Physica A Stat Mech Appl 388(8):1375–1387

Bisignano A, Mortarini L, Ferrero E, Alessandrini S (2016) Model chain for buoyant plume dispersion. Submitted to Int J Environ Pollut

de Franceschi M, Zardi D (2009) Study of wintertime high pollution episodes during the Brenner-South ALPNAP measurement campaign. Meteor Atmos Phys 103:237–250

de Franceschi M, Zardi D, Tagliazucca M, Tampieri F (2009) Analysis of second order moments in the surface layer turbulence in an Alpine valley. Quart J R Meteor Soc 135:1750–1765

Dosio A, Emeis S, Graziani G, Junkermann W, Levy A (2001) Assessing the meteorological conditions of a deep Italian Alpine valley system by means of a measuring campaign and simulations with two models during a summer smog episode. Atmos Environ 35:5441–5454

Ragazzi M, Tirler W, Angelucci G, Zardi D, Rada EC (2013) Management of atmospheric pollutant from waste incineration processes: the case of Bozen. Waste Manag Res 31:235–240

Scire JS, Robe FR, Fernau ME, Yamartino RJ (2000a) A user's guide for the CALMET meteorological model. Earth Tech Inc, Concord, MA

Scire JS, Strimaitis DG, Yamartino RJ (2000b) A user's guide for the CALPUFF dispersion model. Earth Tech Inc, Concord, MA

Skamarock WC, Klemp JB, Dudhia J, Gill DO, Barker DM, Duda MG, Huang X-Y, Wang W, Powers JG (2008) A description of the advanced research WRF version 3. NCAR Technical Note TN-475 + STR, 125

Tinarelli G, Anfossi D, Bider M, Ferrero E, Trini Castelli S (2000) A new high performance version of the Lagrangian particle dispersion model SPRAY, some case studies. Air Pollut Model Appl XIII, vol 23. Plenum Press, New York, pp 499–506

Chapter 26
Can Aircraft-Based Remote-Sensing NO_2 Measurements Combined with High Resolution Model Data Improve NO_2 Exposure Estimates over Urban Areas?

Wouter Lefebvre, Hans Hooyberghs, Felix Deutsch, Frederick Tack, Michel van Roozendael, Marian-Daniel Iordache, Frans Fierens, Charlotte Vanpoucke, Sandy Adriaenssens, Shari van Wittenberghe, Peter Viaene, Koen Meuleman, Olav Peeters and Alexis Merlaud

Abstract As part of the STEREO-III BUMBA (Belgian Urban NO_2 Monitoring Based on APEX hyperspectral data) project, we try to exploit the synergy between NO_2 column measurements derived from the aircraft-based APEX hyperspectral imaging system and high-resolution model data from a combined land use regression-Gaussian plume model system for the complex city-port region of Antwerp (Belgium). The resulting model maps are then used to determine the NO_2-exposure of the population of the region.

Several difficulties are encountered when attempting to reconcile measurements and model results. These stem from four main different reasons:

(1) The APEX remote-sensing measurements provide integrated NO_2 columns, while the modelled data are focused on ground-level concentrations.
(2) The model data typically represent hourly averages, while measurements are instantaneous.
(3) The model uses time factors in determining the amount of emissions from traffic, industry, etc.
(4) Additional sources of uncertainties in both the model and the measurements.

In conclusion, our study shows that the use of APEX data to constrain NO_2-exposure estimations is a complex process involving a number of uncertainties that

W. Lefebvre (✉) · H. Hooyberghs · F. Deutsch · M.-D. Iordache · P. Viaene · K. Meuleman
VITO, Boeretang 200, 2400 Mol, Belgium
e-mail: wouter.lefebvre@vito.be

F. Fierens · C. Vanpoucke · S. Adriaenssens · S. van Wittenberghe · O. Peeters
IRCEL/CELINE, Kunstlaan 10-11, 1210 Brussels, Belgium

F. Tack · M. van Roozendael · A. Merlaud
BIRA/IASB, Royal Belgian Institute for Space Aeronomy, Avenue Circulaire 3, 1180 Brussels, Belgium

C. Mensink and G. Kallos (eds.), *Air Pollution Modeling and its Application XXV*, Springer Proceedings in Complexity, DOI 10.1007/978-3-319-57645-9_26

need to be properly characterised. In particular we find that a robust methodology for relating concentration profiles to surface concentrations is needed before aircraft data can eventually help improving the model input data (e.g. time factors). This is further studied in the project.

26.1 Introduction

In this paper, we describe the results of part of the STEREO-III BUMBA (Belgian Urban NO_2 Monitoring Based on APEX hyperspectral data) project, in which we try to exploit the synergy between NO_2 column measurements derived from the aircraft-based APEX hyperspectral imaging system and high-resolution model data from a combined land use regression-Gaussian plume model system for the complex city-port region of Antwerp. We plan to use the resulting model maps to determine the NO_2-exposure of the population of the region.

While the systematic use of APEX measurements in combination with modelled concentrations for determining exposure is not envisaged in this project due to aircraft operational costs limiting the number of flights, our study concentrates on exploring the potential of remote-sensing NO_2 mapping observations as an input for model validation. We primarily focus on the Antwerp area, but the BUMBA project also targets Brussels and Liège, and these cities will be addressed in a second step of the project.

26.2 Methodologies: APEX-Based NO_2 Column Retrieval

The APEX instrument (Schaepman et al. 2015) is a push broom hyperspectral imager with high spatial resolution (3 m), a swath width of 3000 m and high spectral performance (3 nm). APEX was mounted in a Dornier DO-228 airplane, operated by Deutsches Zentrum für Luft- und Raumfahrt (DLR) at an altitude of 6.1 km. APEX spectra has been acquired under clear sky conditions over the three largest and most heavily polluted Belgian cities, i.e. Brussels, Antwerp and Liège, on April 14 and 15, and June 30, 2015.

The NO_2 column retrieval algorithm based on APEX spectra, being solar radiation backscattered by the atmosphere or ground surface, consists of the following main steps: (1) spatial aggregation of the observed radiance spectra in order to increase the signal-to-noise ratio (SNR), (2) spectral calibration based on a high resolution solar spectrum (425–600 nm), (3) DOAS analysis (Danckaert et al. 2015) of the pre-processed spectra in the visible wavelength region (470–510 nm), with reference spectra containing low NO_2 absorption, (4) air mass factor calculations based on the VLIDORT 2.6 radiative transfer model, accounting for albedo, aerosol and NO_2 profile shapes and viewing and sun geometry, in order to convert slant to vertical columns, and (5) georeferencing and visualization of the NO_2

spatial distribution in a GIS environment. The NO_2 levels in the city-port region of Antwerp range between 3 and 35×10^{15} molec cm^{-2}, with a mean of 1.6×10^{16} molec cm^{-2}. The detection limit has a typical value between 1.7 and 2.2×10^{15} molec cm^{-2} on the vertical column.

26.3 Methodologies: High-Resolution Air Quality Modelling

An integrated model chain has been set up to assess the air quality at the local (street level) scale, including both regional variability as well as local variation in sources of air pollution. The FASTRACE (Veldeman et al. 2016) emission model, distributing emissions based on the COPERT-model (Gkatzoflias et al. 2012) on the road network, is used to calculate local road traffic emissions. The resulting spatially and temporally distributed emissions are used in the bi-Gaussian model IFDM (Lefebvre et al. 2011a, b). These results are coupled to output of the land-use regression model RIO (Hooyberghs et al. 2006; Janssen et al. 2008). A method to avoid double counting of the (local) emissions by the different models is applied (Lefebvre et al. 2011b).

The integrated model chain has been used to perform simulations for the city of Antwerp, using meteo-rological data of a local meteo station, situated in the northern part of the city. Simulations are performed using the meteorology for the hours for which the APEX flight was done. Yearly emissions are distributed over the different hours of the year by using time factors per SNAP-sector (EEA 2013). For traffic time factors per road type are available.

26.4 Preliminary Findings

Figure 26.1 shows two maps. At the left hand side the modelled ground level concentrations are shown over the city of Antwerp. At the right hand side, the APEX-measured integrated vertical columns are shown.

Several difficulties (Fig. 26.1) are encountered when attempting to reconcile measurements and model results. These stem from four main different reasons:

(1) The APEX remote-sensing measurements provide integrated NO_2 vertical columns, while the modelled data are primarily focused on ground-level concentrations. We try to solve this by modelling vertical profiles, which show that the 3D-concentration field above the Antwerp city and the port is very complex due to the different sources involved in both areas of the city. This renders the data interpretation complicated, requiring to account for the vertically-dependent sensitivity of the APEX observations.

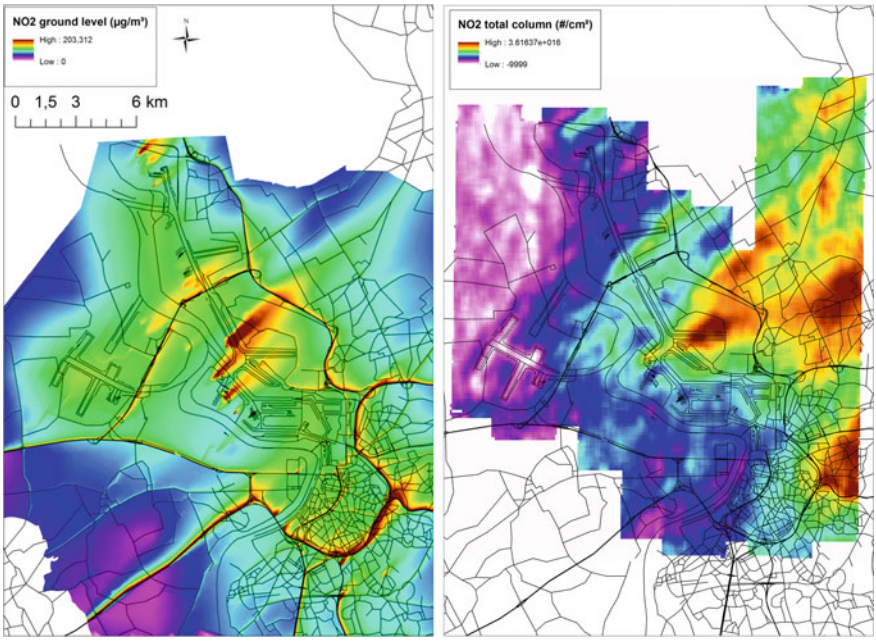

Fig. 26.1 RIO-IFDM model NO_2 surface concentrations (*left*) and APEX-derived total columns (*right*). *Black lines* major NOx emissions line sources. The location of the major point sources could not be shown due to confidentiality issues. (low = −9999 is not the lowest NO_2 value but the background layer)

(2) The model data typically represent hourly averages, while measurements are instantaneous. This introduces additional sources of uncertainties related to the small-scale spatial and temporal variability of the NO_2 concentration fields.
(3) The model uses time factors in determining the amount of emissions from traffic, industry, etc. However, in reality, emission time profiles are more complex, due to for instance downtime of industrial installations, timing and length of traffic jams on the roads, etc.
(4) Additional sources of uncertainties in both the model and the measurements. For instance, the airborne APEX instrument is measuring the NO_2 dynamic field in swaths over the city, where the swaths are recorded one after the other. In total, one and a half hour of flight is needed to cover the entire area. During flight time meteorological conditions such as the height of the boundary layer changed significantly while in the model the same meteorology is assumed for the entire model domain. On the contrary, one meteorological situation is used in the model for all locations, whereas in reality the height of the boundary layer increased quite strongly during the flight.

26.5 Conclusions

In conclusion, our study shows that the use of APEX data to constrain NO_2-exposure estimations is a complex process involving a number of uncertainties that need to be properly characterised. In particular we find that a robust methodology for relating concentration profiles to surface concentrations is needed before aircraft data can eventually help improving the model input data (e.g. time factors). This is further studied in the project.

Acknowledgements Financial support from Belspo for the BUMBA project is gratefully acknowledged by all authors.

References

Danckaert T, Fayt C, van Roozendael M (2015) QDOAS software user manual 2.108, IASB/BIRA, Uccle, Belgium. http://uv-vis.aeronomie.be/software/QDOAS/QDOAS_manual.pdf 2015. Accessed 12 Dec 2015

EEA (2013) EMEP/EEA air pollutant emission inventory guidebook. http://www.eea.europa.eu/publications/emep-eea-guidebook-2013

Gkatzoflias D, Kouridis C, Ntziachristos L, Samaras Z (2012) COPERT 4 computer programme to calculate emissions from road transport—user's manual, ETC-ACC

Hooyberghs J, Mensink C, Dumont G, Fierens F (2006) Spatial interpolation of ambient ozone concentrations from sparse monitoring points in Belgium. J Environ Monit 8:1129–1135. doi:10.1039/b612607n

Janssen S, Dumont G, Fierens F, Mensink C (2008) Spatial interpolation of air pollution measurements using CORINE land cover data. Atm Env 42(20):4884–4903. doi:10.1016/j.atmosenv.2008.02.043

Lefebvre W, Fierens F, Trimpeneers E, Janssen S, van de Vel K, Deutsch F, Viaene P, Vankerkom J, Dumont G, Vanpoucke C, Mensink C, Peelaerts W, Vliegen J (2011a) Modeling the effects of a speed limit reduction on traffic-related elemental carbon (EC) concentrations and population exposure to EC. Atmos Environ 45:197–207. doi:10.1016/j.atmosenv.2010.09.026

Lefebvre W, Vercauteren J, Schrooten L, Janssen S, Degraeuwe B, Maenhaut W, de Vlieger I, Vankerkom J, Cosemans G, Mensink C, Veldeman N, Deutsch F, Van Looy S, Peelaerts W, Lefebre F (2011b) Validation of the MIMOSA-AURORA-IFDM model chain for policy support: modeling concentrations of elemental carbon in Flanders. Atm Env 45(37):6705–6713. doi:10.1016/j.atmosenv.2011.08.033

Schaepman ME, Jehle M, Hueni A, D'Odorico P, Damm A, Weyermann J, Schneider FD, Laurent V, Popp C, Seidel FC, Lenhard K, Gege P, Küchler C, Brazile J, Kohler P, De Vos L, Meuleman K, Meynart R, Schläpfer D, Kneubühler M, Itten KI (2015) Advanced radiometry measurements and Earth science applications with the airborne prism experiment (APEX). Remote Sens Environ 158:207–219

Veldeman N, Maiheu B, Lefebvre W, Viaene P, Deutsch F, Janssen S, Vanhulsel M, Janssen L, Peelaerts W, Driesen G, Van Looy S, Hooyberghs H (2016) Rapport activiteiten in 2015 uitgevoerd in kader van de referentietaak 12 "Kenniscentrum Luchtkwaliteitmodellering", 2016/RMA/R/0582, April 2016

Part III
Interactions Between Air Quality and Climate Change

Chapter 27
High Aerosol Acidity Despite Declining Atmospheric Sulfate Concentrations: Lessons from Observations and Implications for Models

A. Nenes, R.J. Weber, H. Guo, P. Vasilakos, A. Russell, A. Bougiatioti and N. Mihalopoulos

Abstract Particle acidity affects aerosol concentrations, chemical composition, toxicity and nutrient bioavailability. We present a summary of thermodynamic analysis of comprehensive observations of ambient aerosol collected over the US and E.Mediterranean to understand the levels and drivers of aerosol pH. We find that acidic aerosol in the fine mode is ubiquitous, with levels that range between 0 and 2 throughout most of the data examined. The strong acidity is largely from the large difference in volatility between sulfate (the main acidic compound, which resides completely in the aerosol phase) and ammonia (the main neutralizing agent, which partitions between aerosol and gas-phase). This counterintuitive, but thermodynamically consistent finding explains why aerosol acidity in the southeastern

A. Nenes (✉) · R.J. Weber · H. Guo · A. Bougiatioti
School of Earth and Atmospheric Sciences, Georgia Institute of Technology, Atlanta, GA, USA
e-mail: athanasios.nenes@gatech.edu

A. Nenes · P. Vasilakos
School of Chemical & Biomolecular Engineering, Georgia Institute of Technology, Atlanta, GA, USA

A. Nenes · N. Mihalopoulos
Institute of Environmental Research & Sustainable Development, National Observatory of Athens, Athens, Greece

A. Nenes
Institute of Chemical Engineering Sciences, Foundation for Research and Technology-Hellas, Patras, Greece

A. Russell
School of Civil & Environmental Engineering, Georgia Institute of Technology, Atlanta, GA, USA
e-mail: ar70@ce.gatech.edu

A. Bougiatioti · N. Mihalopoulos
Environmental Chemical Processes Lab, Department of Chemistry, University of Crete, Heraklion, Greece

C. Mensink and G. Kallos (eds.), *Air Pollution Modeling and its Application XXV*, Springer Proceedings in Complexity, DOI 10.1007/978-3-319-57645-9_27

United States has not decreased over the last decades, despite a 70% reduction in sulfates and a constant ammonia background. We then demonstrate that evaluation of model-predicted pH is critical for model predictions of semi-volatile species, e.g., nitrate.

27.1 Acidic Fine Mode Aerosol Is Ubiquitous

Particle acidity affects aerosol concentrations, chemical composition, toxicity and nutrient bioavailability. Aerosol acidity depends on particle composition, concentration, humidity levels, and temperature. Sulfate is the primary strong acid found in the fine mode and is neutralized throughout most of the atmosphere by volatile gas phase ammonia; regionally, non-volatile cations found in seasalt and dust (such as K, Na, Ca and Mg) also neutralize sulfate. Understanding the levels and drivers of acidity as a function of particle size, location and time is critical for understanding many aerosol processes that depend on pH.

In situ particle pH measurement is not possible for complex ambient aerosol, and so-called "pH proxies" (cation-anion molar ratios, ion balances) are largely inaccurate for determining pH (Guo et al. 2015; Hennigan et al. 2015; Guo et al. 2016; Weber et al. 2016). Application of thermodynamic equilibrium models, such as ISORROPIA-II (Fountoukis and Nenes 2007) however yield plausible pH predictions that can largely reproduce observed aerosol liquid water content and semi-volatile partitioning of NH_3, HNO_3 and HCl (Guo et al. 2015, 2016, 2017; Bougiatioti et al. 2016, 2017). When applied to comprehensive observations of ambient aerosol collected over the US and E.Mediterranean, thermodynamic analysis reveals that acidic aerosol in the fine mode is ubiquitous, with levels that range between 0 and 2 throughout most of the data examined (Table 27.1). This behavior arises primarily from the large difference in volatility between sulfate, which resides exclusively in the aerosol, and ammonium which always needs to partition with the gas phase to attain equilibrium. For this reason (and as long as non-volatile cations are not present in large quantity), acidity tends to slightly increase with decreasing sulfate levels—even if total ammonia remains about constant. This highly intuitive, but thermodynamic consistent behavior, explains why aerosol acidity has not reduced over time in regions like the southeastern United States, where sulfate has decreased by 70%, but ammonia concentrations have not changed (Weber et al. 2016).

27.2 Importance of Aerosol pH for Model Simulations

Regional and global aerosol models are routinely used to predict aerosol formation for air quality, climate and other studies. The large uncertainty of aerosol simulations can only be reduced if the sensitivity of predicted aerosol to emissions is

Table 27.1 Comparisons between different studies for particle pH, and meteorological conditions. All pH calculations carried out with the ISORROPIA-II thermodynamic model (Fountoukis and Nenes 2007), as described in the respective references

Campaign	CalNex	SOAS	SENEX	WINTER	FAME-12	NOA-13
Altitude	Ground	Ground	Aircraft	Aircraft	Ground	Ground
PM size cut	1 (2.5) μm	2.5 μm	1 μm	1 μm	1 μm	1 μm
Year	2010	2013	2013	2015	2012	2013
Season	Summer	Summer	Summer	Winter	Summer-Autumn	Winter
Location	SW US	SE US	SE US	NE US	Finokalia, Greece	Athens, Greece
RH, %	79 ± 17 (87 ± 9)	74 ± 16	72 ± 9	58 ± 19	57 ± 11	80 ± 9
T, °C	18 ± 4 (18 ± 3)	25 ± 3	22 ± 3	0 ± 8	27 ± 3	12 ± 3
pH	1.9 ± 0.5 (2.7 ± 0.3)	0.9 ± 0.6	1.1 ± 0.4	0.8 ± 1.0	1.3 ± 1.1	2.4 ± 0.8
Reference	Guo et al. (2017)	Guo et al. (2015)	Xu et al. (2016)	Guo et al. (2016)	Bougiatioti et al. (2016)	Bougiatioti et al. (2017)

correctly captured. A good representation of aerosol pH is critical for this, given that many aerosol processes and the semivolatile partitioning of compounds like nitrate and chloride can be strongly impacted by pH biases. Models are never evaluated in terms of their ability to predict pH, so we advocate strongly for such evaluations be carried out in future modeling studies—especially since aerosol pH distributions from ambient data analysis is becoming increasingly available in the literature. To illustrate the importance of pH bias, we focus on aerosol inorganic nitrate predictions—an aerosol species that historically has been very difficult to capture in models and regionally important for air quality and climate forcing.

Meskhidze et al. (2003) and Guo et al. (2016) showed that there is "window" of pH values (that depends on the temperature and the amount of liquid water, but typically between 1.5 and 3; Guo et al. 2017; Bougiatioti et al. 2017), within which aerosol inorganic nitrate concentration is susceptible to shifts and uncertainties in pH. As a consequence, aerosol nitrate concentrations can increase considerably when the pH shifts within this "window", so that aerosol pH prediction biases may precondition the model to be positively (if pH is too high) or low (if pH is too low) biased in terms of nitrate prediction skill. When below this "pH sensitivity window", aerosol nitrate is almost nonexistent and relatively insensitive to emissions (and pH biases); when above the window, almost all nitrate resides in the aerosol phase, and directly responds to emissions.

To demonstrate the influence of pH prediction biases, we analyze CMAQ simulations over the continental US, for "current day" (2011) emissions (Vasilakos et al. 2017; Fig. 27.1) by comparing pH predictions against the observational dataset presented in Table 27.1. pH values predicted by CMAQ agree relatively well with observations, but tend to overpredict pH during the winter. We then

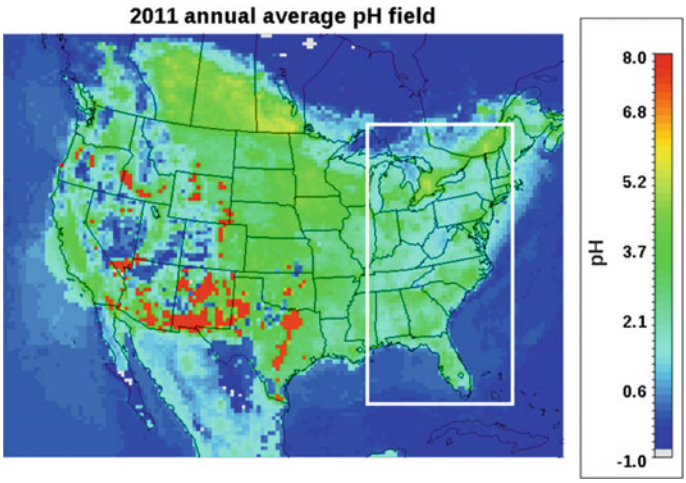

Fig. 27.1 Simulated annual average pH with CMAQ for "current day" emissions (Vasilakos et al. 2017). The rectangle defines the region for nitrate prediction bias analysis shown in Figs. 27.2 and 27.3

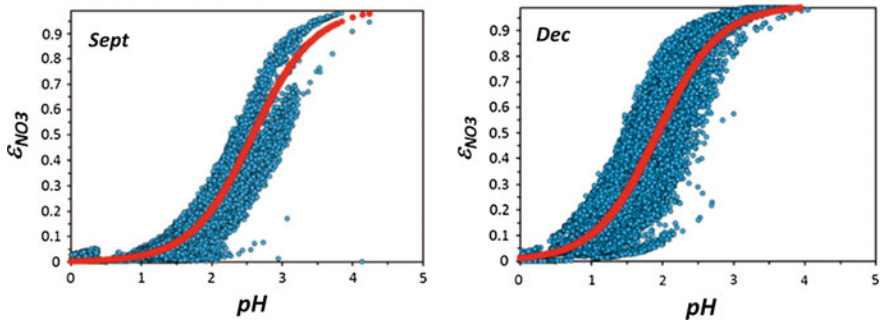

Fig. 27.2 CMAQ-simulated partitioning fraction for nitrate, ε_{NO3}, against pH for the month of September (*left panel*) and December (*right panel*), with "current day" emissions (Vasilakos et al. 2017). *Blue symbols* represent model simulations, while the *red curve* corresponds to the sigmoid fit. The *yellow square symbols* on each subplot denote the average pH for the month and domain

express the partitioning fraction, ε_{NO3} (i.e., molar ratio of aerosol to gas + aerosol) for nitrate on a monthly basis for the CMAQ cells over the Eastern US (white rectangle in Fig. 27.1). Given that T conditions do not change significantly over one month, most of the partitioning fraction data closely follows a "sigmoid", that has a functional form given by Meskhidze et al. (2003) (Fig. 27.2).

Once the sigmoidal fits are obtained for each simulated month, we then determine the uncertainty in ε_{NO3}, $\Delta\varepsilon_{NO3}$, that corresponds to a given uncertainty in aerosol pH from the sigmoids. Here, we arbitrarily pick the pH uncertainty, ΔpH, to be 0.5 units around the average pH of the month. The uncertainty in ε_{NO3} is then

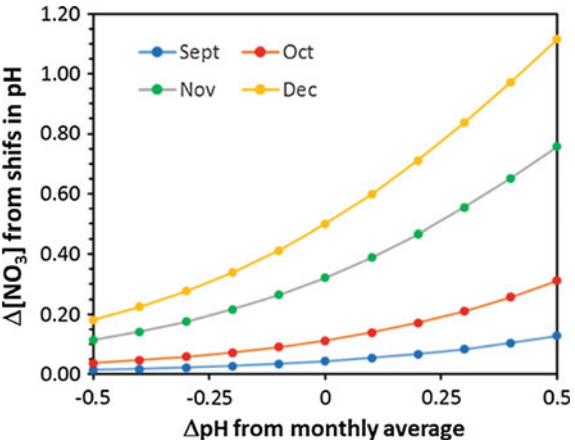

Fig. 27.3 The simulated partitioning fraction for nitrate, ε_{NO3}, against pH with CMAQ for the month of September (*left panel*) and December (*right panel*), with 2011 emissions (Vasilakos et al. 2017). *Blue symbols* represent model simulations, while the *red curve* corresponds to the sigmoid fit. The *black square* symbols on each subplot denote the average pH for the month and domain

expressed as uncertainty in aerosol nitrate, by multiplying the $\Delta\varepsilon_{NO3}$ with the total monthly average nitrate (aerosol + gas) from CMAQ. The results of this analysis is shown in Fig. 27.3, which shows the uncertainty in aerosol nitrate, $\Delta[NO_3]$, as a function of the pH uncertainty. From the figure it becomes clear that pH uncertainties during summertime or early fall (September) lead to minor impacts on aerosol nitrate levels, because the sensitivity of ε_{NO3} for the September-average pH is very low (Fig. 27.2a). Wintertime nitrate levels, however, can be quite sensitive to pH shifts (Fig. 27.2b), giving up to ~1 μg m^{-3} aerosol nitrate uncertainty in December for $\Delta pH = \pm 0.5$ units around the monthly average (Fig. 27.3). The regional responses can be larger, depending on where you are on the partitioning "sigmoid" (the maximum sensitivity to pH biases occurs around where $\varepsilon_{NO3} = 0.5$) and the total amount of nitrate in the gridcell.

27.3 Conclusions

Thermodynamic analysis of ambient observations show that acidic fine mode aerosol is ubiquitous in many regions of the globe, and a consequence of the thermodynamic partitioning of the major neutralizing agent, ammonia, between the aerosol and gas phase. As a consequence, the expectation that aerosol nitrate will increase as sulfate levels drop may be unfounded for many regions of the globe. We show that aerosol pH, never evaluated in models, needs to be considered for models to correctly capture aerosol responses to precursor emissions. Otherwise, important biases in predictions (here, demonstrated for inorganic nitrate) will result if pH levels are biased in models.

Acknowledgements This work was supported by the Electric Power Research Institute, Phillips 66 Company, the US NSF grants AGS-0931492 and AGS-0802237, the European Union (European Social Fund—ESF) and Greek national funds through the Operational Program

"Education and Lifelong Learning" of the National Strategic Reference Framework (NSRF)—Research Funding Program ARISTEIA I—PANOPLY, US EPA STAR grant R835410, and NOAA CPO Award NA10OAR4310102.

References

Bougiatioti A, Nenes A, Paraskevopoulou D, Fourtziou L, Stavroulas I, Liakakou E, Myriokefalitakis S, Daskalakis N, Weber R, Gerasopoulos E, Nikolaou P, Mihalopoulos N (2017) The unappreciated effects of biomass burning on fine mode aerosol acidity, in review

Bougiatioti A, Nikolaou P, Stavroulas I, Kouvarakis G, Weber R, Nenes A, Kanakidou M, Mihalopoulos N (2016) Particle water and pH in the Eastern Mediterranean: Sources variability and implications for nutrients availability. Atmos Chem Phys 16:4579–4591. doi:10.5194/acp-16-4579-2016

Fountoukis C, Nenes A (2007) ISORROPIA II: a computationally efficient thermodynamic equilibrium model for K^+-Ca^{2+}-Mg^{2+}-NH_+^4-Na^+-SO_4^{2-}-NO_3^--Cl^--H_2O aerosols. Atmos Chem Phys 7:4639–4659

Guo H, Xu L, Bougiatioti A, Cerully KM, Capps SL, Hite JR, Carlton AG, Lee SH, Bergin MH, Ng NL, Nenes A, Weber RJ (2015) Fine-particle water and pH in the southeastern United States. Atmos Chem Phys 15:5211–5228. doi:10.5194/acp-15-5211-2015

Guo H, Sullivan AP, Campuzano-Jost P, Schroder JC, Lopez-Hilfiker FD, Dibb JE, Jimenez JL, Thornton JA, Brown SS, Nenes A, Weber RJ (2016) Fine particle pH and the partitioning of nitric acid during winter in the northeastern United States. J Geophys Res Atmos 121(10):355–310, 376. doi:10.1002/2016jd025311

Guo H, Liu J, Froyd KD, Roberts JM, Veres PR, Hayes PL, Jimenez JL, Nenes A, Weber RJ (2017) Fine particle pH and gas-particle phase partitioning of inorganic species in Pasadena, California, during the 2010 CalNex campaign, in review

Hennigan CJ, Izumi J, Sullivan AP, Weber RJ, Nenes A (2015) A critical evaluation of proxy methods used to estimate the acidity of atmospheric particles. Atmos Chem Phys 15:2775–2790. doi:10.5194/acp-15-2775-2015

Meskhidze N, Chameides W, Nenes A, Chen G (2003) Iron mobilization in mineral dust: can anthropogenic SO_2 emissions affect ocean productivity? Geophys Res Lett 30(21):2085. doi:10.1029/2003GL018035

Vasilakos P, Russell A, Nenes A (2017) Aerosol pH and its effect on nitrate over a decade (2001–2011) in the United States, in preparation

Weber RJ, Guo H, Russell AG, Nenes A (2016) High aerosol acidity despite declining atmospheric sulfate concentrations over the past 15 years. Nat Geosci 9:282–285. doi:10.1038/ngeo2665

Xu L, Middlebrook AM, Liao J, de Gouw JA, Guo H, Weber RJ, Nenes A, Lopez-Hilfiker FD, Lee BH, Thornton JA, Brock CA, Neuman JA, Nowak JB, Pollack IB, Welti A, Graus M, Warneke C, Ng NL (2016) Enhanced formation of isoprene-derived organic aerosol in sulfur-rich power plant plumes during Southeast Nexus. J Geophys Res Atmos 121(11):137–111, 153. doi:10.1002/2016jd025156

Chapter 28
Modelling Resilient Measures to Climate Change Impacts on Urban Air Quality

E. Sá, A. Monteiro, A.P. Fernandes, J. Valente, D. Carvalho, J. Ferreira, S. Freitas, S. Rafael, H. Martins, A.I. Miranda and C. Borrego

Abstract Considering different resilience measures such as the increase of urban green areas and the application of white roofs, a set of resilience scenarios were evaluated with a cascade of numerical models (MPI-ESM-LR/WRF/CAMx) using as case study a future heat wave occurring in Porto (Portugal) urban area. Meteorological forcing and boundary data was derived from the CMIP5 earth system model MPI-ESM (Representative Concentration Pathway RCP 8.5) downscaled to Porto urban area. The influence of different resilience scenarios on the air quality was quantified and compared for the different scenarios. The results show that all tested measures lead to an increased resilience to CC impacts, promoting the reduction of ozone concentrations. The application of green roofs was the measure that shows more benefits to air quality.

28.1 Introduction

Urban areas are home to over half of the world people and are at the forefront of the climate change issue. The challenges related to continuous growth of world population and the atmospheric emissions highlight the need for cities to rethink how climate will affect long-term growth and development plans, how infrastructure investments are prioritized, and how assets are deployed and people protected (EEA 2010). Additionally, despite urban areas are highly vulnerable to climate change they have great potential to lead adaptation efforts.

The concept of urban resilience is associated with the vulnerability to climate change (CC), reflecting the ability of urban areas to quickly recover from the

E. Sá · A. Monteiro · A.P. Fernandes · J. Valente · D. Carvalho · J. Ferreira · S. Freitas · S. Rafael · H. Martins · A.I. Miranda · C. Borrego (✉)
CESAM & Department of Environment and Planning, University of Aveiro, 3810-193 Aveiro, Portugal
e-mail: cborrego@ua.pt

A.I. Miranda
e-mail: miranda@ua.pt

C. Mensink and G. Kallos (eds.), *Air Pollution Modeling and its Application XXV*,
Springer Proceedings in Complexity, DOI 10.1007/978-3-319-57645-9_28

disturbances related to climate change (e.g. extreme events like heat waves). The CLICURB-Urban Atmospheric Quality, Climate Change and Resilience project (http://www.ua.pt/clicurb/) addressed risks and studied solutions to CC challenges in cities, with a particular focus on the urban area of Porto (Northern Portugal). An integrated analysis of CC, air quality and resilience measures was developed, applied and assessed through the use of an air quality modelling system, considering the inclusion of adaptation strategies in the city's planning and in the decision making process. The inclusion of green areas, the use of green roofs and surfaces with high levels of solar reflection in buildings, have been cited as the most effective measures for reducing the temperature in urban areas (Bell et al. 2008). In this sense, a set of scenarios were developed to evaluate the impact of these resilience measures on urban air quality, through a specific modelling setup. A cascade of numerical models (MPI-ESM-LR/WRF/CAMx), from the global to the urban scale (200 m resolution), was applied to a heat wave centred on 2050, from July, 24 until July, 26, to study the impacts of the resilience measures on surface temperature and air quality under a CC scenario (RCP8.5).

28.2 Methodology

The WRF model, one of the most robust models to simulate European climate (Brands et al. 2013), was used to downscale global climate simulations, performed by the Earth Systems Model MPI-ESM-LR that runs freely, only constrained by the greenhouse gases concentrations. Three nested domains covering part of the North Atlantic and Europe were used, with resolutions of 81, 27 and 9 km for the innermost domain covering the Iberian Peninsula. Two simulation periods were studied: (i) historical (1986–2005) and (ii) medium-term future (2046–2065). For the future simulations, the IPCC greenhouse gas concentration scenario RCP8.5 was adopted. For validation purposes, an additional simulation for the year 2011, forced by ERA-INTERIM data, was performed (Marta-Almeida et al. 2016).

The meteorological outputs for the 9 km resolution domain from the WRF application with ERA-INTERIM or MPI-ESM-LR are used as meteorological forcing for the chemistry-transport model CAMxv6.0. CAMx is an Eulerian photochemical dispersion model that considers the emission, dispersion, chemical reaction, and removal of pollutants in the troposphere by solving the pollutant continuity equation for each chemical species on a system of nested three-dimensional grids (Morris et al. 2004). From regional to urban scale, CAMx was applied with the flexi-nesting capability enabled, which is an algorithm that interpolates the missing fields from the parent grid, in this case meteorological fields into the other nesting grids. For CAMx validation purposes, a simulation for the year 2011 was performed (Sá et al. 2015).

The air quality simulations considered three domains: D1 with a 9 km spatial resolution, covering Portugal, D2 with a 3 km spatial resolution, covering the Northern Region and D3 with a 1 km spatial resolution, covering the Porto urban

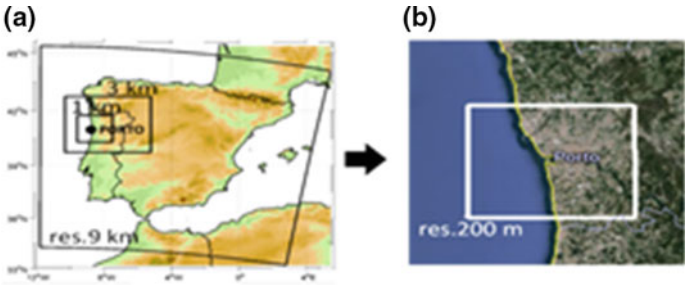

Fig. 28.1 **a** model domain used in the regional CAMx implementation. Model ran in flexi-nesting mode with increasing domain resolutions of 9, 3 and 1 km. **b** Innermost simulation domain for the selected heat wave, with a horizontal resolution of 200 m

area (Fig. 28.1a). In order to assess the impacts of including resilience factors on air quality, the CAMx model was then applied at a 200 m spatial resolution over Porto urban area (Fig. 28.1b), using as input the CAMx results for D3, to the heat wave (24–26 of July 2049) for the base scenario and for five scenarios: (i) Scenario 1: duplication of the existing green urban areas; (ii) Scenario 2: introduction of green roofs at 75% of the urban area; (iii) Scenario 3: introduction of white roofs in areas with high residential density; (iv) Scenario 4: duplication of the existing green areas plus the introduction of green roofs at 75% of the urban area (combination of scenarios 1 and 2); (v) Scenario 5: duplication of the existing green areas plus the introduction of white roofs in areas with high residential density (combination of scenarios1 and 3).

28.3 Results

To assess the impacts of the resilience factors on air quality under climate change, the CAMx model was applied to the selected heat wave for the base scenario (without resilience measures) and for the five scenarios previously described. The analysis of the simulation results was focused on the difference of the maximum hourly concentration of ozone (maximum value of the episode days) between each resilience scenario and the base scenario (Fig. 28.2).

Figure 28.2 shows that the application of the selected resilience measures produced at least a reduction of 10 μg m^{-3} in the ozone maximum hourly concentration. The highest impact on air quality was achieved in scenarios 2 and 4. However, since the latter was a combination of scenario 1 and 2, the resilience measure with the highest impact is the application of green roofs; it allows obtaining a maximum reduction of almost 30 μg m^{-3} over the study domain. Moreover, the expected reduction on temperature will lead to a lower photochemical ozone production during the precursors' transport (follows the flow

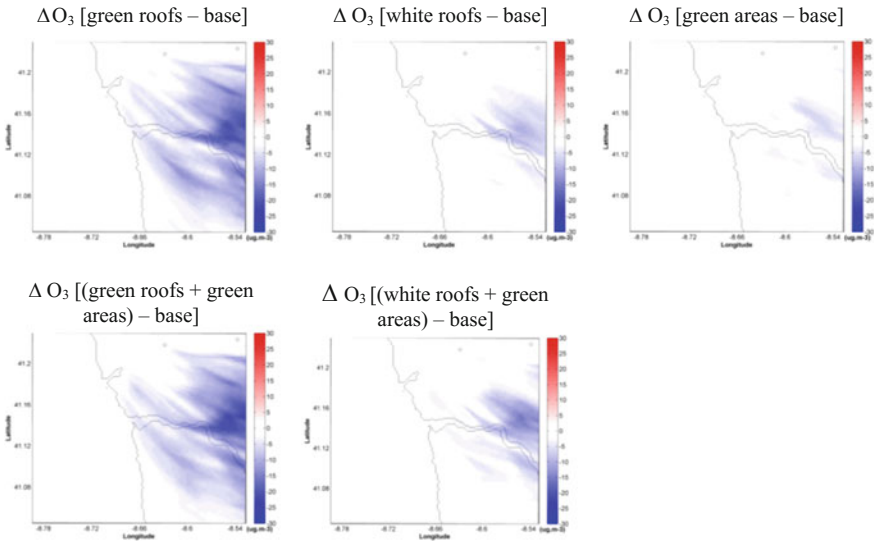

Fig. 28.2 Difference between each of the five resilience scenarios and the base scenario for ozone maximum hourly concentration (μg m^{-3})

direction), which justifies why the most significant O_3 reduction happens in the eastern part of the domain.

28.4 Conclusions

The application of the WRF-CAMx modelling system to Porto urban area revealed that all tested scenarios lead to increased resilience of the city to CC, with benefits in terms of air quality, and, consequently, to an improvement of the quality of life. The application of green roofs to 75% of the buildings in the Porto urban area is responsible for the higher reductions in ozone maximum hourly concentrations (around 30 μg m^{-3}). As a result, these findings are particularly relevant, since an increase of severity and magnitude of heat waves is expected in the future. Future work will be developed to assess the influence of these resilience measures on particulate matter concentrations, one of the main pollutants of concern regarding the air quality in Porto urban area.

Acknowledgements The authors acknowledge the financial support of CLICURB project (EXCL/AAG-MAA/0383/2012), supported in the scope of the European Funds through COMPETE and by National Funds through the Portuguese Science Foundation (FCT) within project PEst-C/MAR/LA0017/2013. An acknowledgement to the Portuguese 'Ministério da Educação e Ciência' and POHP/FSE funding program for the PhD grant of S. Rafael (SFRH/BD/103184/2014) and A Fernandes (SFRH/BD/86307/2012), and for the Post-doc grant of J. Ferreira (SFRH/BPD/100346/2014).

Questions and Answers

Questioner: Stefano Alessandrini
Question: In a similar study over the city of Chicago they observed a negative feedback over air pollution due to introduction of green roofs. In fact, the sea-land temperature gradient tend to decrease, reducing the sea breeze. Why you didn't observe such an effect?
Answer: It is a fact that the sea-breeze affect part of the days over the study region. Nevertheless, this thermal circulation does not prevail during the heat wave study period, so it was not possible to conclude about it influence on this particular study.
Questioner: Sebnem Aksoyoğlu
Question: Did you take into account the change in biogenic emissions in your green roof, green park scenarios?
Answer: No, we didn't. But we are now presently considering it in our modeling tests.
Questioner: V. Kallos
Question: I wonder about the large decrease on ozone on the green roof scenario by more than 30%. Did you look into the main mechanisms that are responsible for this decrease?
Answer: The objective of this study was to analyze the differences obtained by our (extensively validated) modeling system when different type of resilient measures is considered in order to select the most appropriated to be studied. In this sense, it was not yet performed a detailed analysis about the mechanism responsible for such behavior. This will be the next phase after selecting the most efficient and resilient measures to be adopted.
Questioner: Jaakko Kukkonen
Question: Have you considered the potential increased allergenic pollen concentrations? Many tree and grass species cause adverse health effects for humans, due to allergenicity. It would therefore be important to select the plant species carefully, also allowing for this issue.
Answer: No, the associated pollen concentrations were not considered in the present work. Nevertheless, we agree that this should be taken into account when selecting the plants of the green roof/parks. We intend to include the pollen simulation in our dispersion models, but first this requires several tests and validation procedures, still under development.
Questioner: Heinke Schlünzen
Question: How is the green roof considered in the modelling? Is evaporating "solucing" the available water reservoir and eventually can the green on the roof dry out?
Answer: The green roof was considered in the same way as the green areas existent in the rest of the domain.
Question: Are the albedo values changed in the meteorology model consistently used in the chemistry part (lower for green, higher for white)? Is the neglected radiation considered in the photochemical reactions leading to ozone formation?

Answer: Yes, the change in albedo was considered in the simulation, but the role of the neglected radiation was not quantified.

References

Bell R, Cole D, Deangelo B, Desaultes L, Dickerhoff E, Estes M, Heisler G, Hitchcock D, Klunich K, Kollin C, Lewis M, Magee J, Mcpherson G, Nowak D, Rodbell P, Rosenthal J, Sarkovich M, Wolf K, Yarbrough J, Zalph B (2008) Trees and vegetation—reducing urban heat islands: compendium of strategies. EPA, US (Chapter 2, p 32)

Brands S, Herrera S, Fernandez J, Gutierrez JM (2013) How well do CMIP5 Earth system models simulate present climate conditions in Europe and Africa? A performance comparison for the downscaling community. Clim Dyn 41:803–817

EEA (European Environment Agency) (2010) The European environment: state and outlook 2010. Publications Office of the European Union, Luxembourg. ISBN: 78-92-9213-151-7

Marta-Almeida M, Teixeira J, Carvalho M, Melo-Gonçalves P, Rocha A (2016) High resolution climatic simulations for the Iberian Peninsula: model validation. Phys Chem Earth (in press)

Morris RE, Yarwood G, Emery C, Koo B (2004) Development and application of the CAMx regional one-atmosphere model to treat ozone, particulate matter, visibility, air toxics and mercury. Presented in 97th annual conference and exhibition of the A&WMA, June 2004, Indianapolis

Sá E, Ferreira J, Carvalho A, Borrego C (2015) Development of current and future pollutant emissions for Portugal. Atmos Pollut Res 6:849–857

Chapter 29
Assessment of Aerosol-Radiation (ARI) and Aerosol-Cloud (ACI) Interactions from Dust: Modelled Dust Optical Properties and Remote Sensing Observations

Laura Palacios-Peña, Rocio Baró, Jose Maria López-Romero, Agustín López-Villagra, Sonia Jerez, Juan Pedro Montávez and Pedro Jiménez-Guerrero

Abstract Dust is a natural aerosol with an important influence over the Mediterranean basin from a climatic perspective. WRF-Chem simulations have been evaluated over Europe for an October 2010 dust episode. Three modeling scenarios differ in the inclusion or not of aerosol-radiation-cloud interactions.The evaluation of the aerosol optical depth (AOD) indicates a slight improvement of simulations when evaluated against MODIS when including the aerosol radiative feedbacks (RF). For the and Angström exponent (AE), the model tends to underestimate the variability of this variable, and a much more limited improvement when including RF.

29.1 Introduction

Atmospheric aerosols affect the Earth's climate through their radiative feedbacks (RF), being one of the most uncertain areas in climate modelling. RF depend mainly on the aerosol optical properties and can be divided into aerosol-radiation (ARI) and aerosol-cloud (ACI) interactions (Boucher et al. 2013). With the aim of reducing this uncertainty and estimating the radiative forcing, the use of coupled chemistry-climate models is demanded. Dust plays an important role in global climate because of its impact, which may go beyond desert regions. The Mediterranean basin, due to its proximity to a major dust source like the Saharan desert, is frequently affected by transported high dust loads referred to as episodes or events.

L. Palacios-Peña · R. Baró · J.M. López-Romero · A. López-Villagra · S. Jerez · J.P. Montávez · P. Jiménez-Guerrero (✉)
Department of Physics, Regional Campus of International Excellence Campus Mare Nostrum, University of Murcia, Murcia, Spain
e-mail: pedro.jimenezguerrero@um.es

C. Mensink and G. Kallos (eds.), *Air Pollution Modeling and its Application XXV*,
Springer Proceedings in Complexity, DOI 10.1007/978-3-319-57645-9_29

For all these reason, the main objective of this work is to assess the representation of dust optical properties by an online-coupled chemistry-climate model and to determine whether the inclusion of aerosol RF in this type of models improves or not the modelling outputs over Europe, including the Mediterranean basin.

29.2 Methodology

The evaluated data comes from regional air quality-climate simulations performed using the WRF-Chem model (Grell et al. 2005), under the umbrella of the EuMetChem Cost Action ES1004. A detailed description of the simulations can be found in Palacios-Peña et al. (2016). The case study consists on a desert dust outbreak with enhanced cloud and rain (from 2 to 15 October 2010). The simulations are run for three different feedbacks: (1) a base-case with No Radiative Feedbacks (NRF); (2) Aerosol-Radiation Interactions (ARI); and (3) Aerosol-Radiation and Aerosol-Clouds Interactions (ARI + ACI). The model outputs have a resolution of 23 km and are interpolated to 0.1°, covering a domain between 25° and 55° north and −10° and 30° east, according to EuMetChem specifications.

The observational data chosen to carry out the evaluation come from the MODIS (Moderate Resolution Imaging) sensor, on-board Aqua satellite (MYD04_L2). The data used is the Level 2 of Atmospheric Aerosol Product from the collection 6 with a resolution of 10 km. The variables used are: a combined variable of Dark Target (DT) (estimated error (EE) over ocean $-(+)0.02(0.04) \pm 10\%$ and land $\pm(0.05 + 15\%)$) and Deep Blue (EE $0.05 + 20\%$) algorithms of AOD at 0.55 μm and AE (DT algorithm) between 0.55 and 0.86 μm over the ocean (EE 0.45 on pixels with an AOD > 0.2).

Further discussions on the methodology used for evaluation can be found in Palacios-Peña et al. (2016).

29.3 Results

Figure 29.1 shows the results for AOD, while Fig. 29.2 depicts AE levels. For AOD, the temporal mean shows high levels (above 0.4) over the south and the east of the domain, due to the shape of the dust outbreak. The model underestimates MODIS AOD (mean bias error -MBE- minimum values for NRF, ARI and $ARI + ACI$ simulations, respectively, −0.58, −0.58 and −0.57) over the locations with important dust loads (high AOD). In spite of this underestimation, the $ARI + ACI$ scenario shows an improvement in AOD representation, estimated as the percentual difference in the mean absolute error -MAE- of the different simulations (maximum values of improvement > 75%). This improvement is noticeable over the locations with impor-

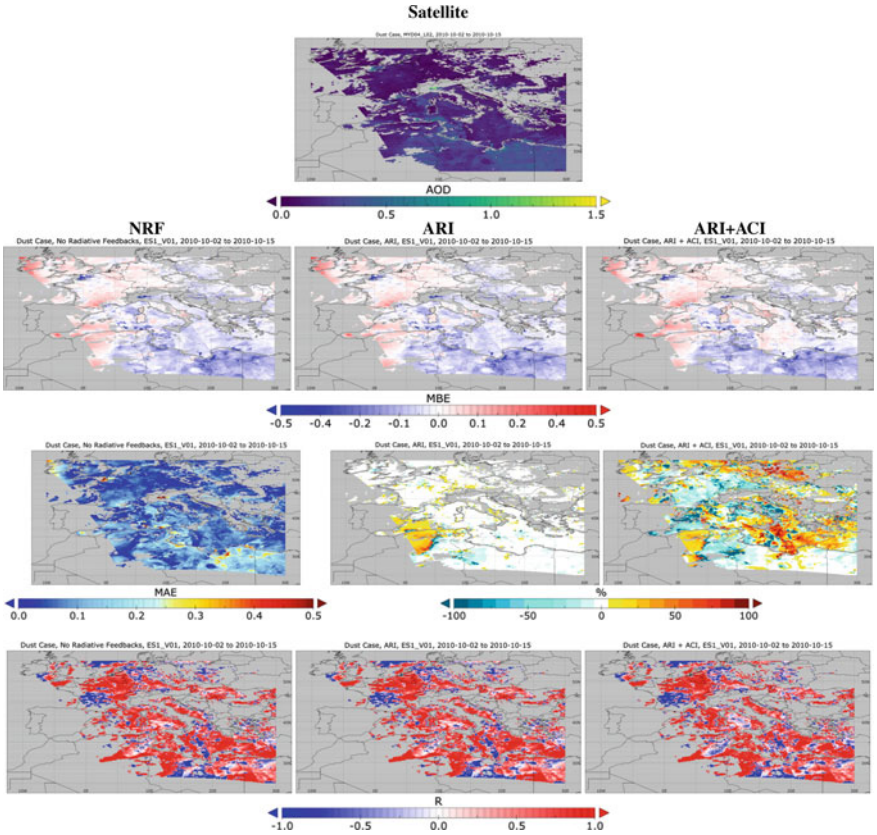

Fig. 29.1 Results for AOD. From *top* to *bottom* satellite mean values, MBE, MAE and their improvements and correlation coefficients. From *left* to *right* NRF, ARI and ARI + ACI scenarios

tant dust loads and hence high AOD levels. Regarding the correlation coefficient, all feedbacks show high values (around 0.9) of this statistical figure.

For AE, temporal mean values below 0.5 are found over the Mediterranean basin. Low values of this variable indicate the presence of coarse particulates as mineral dust. Generally, for all feedbacks, the model underestimates high values of AE and overestimates low values. Thus, the variability of AE is under predicted in general. There is not a clear improvement on this variable when the RF are taken into account. Concerning the correlation coefficient for all feedbacks, the value of this statistic is lower than for AOD.

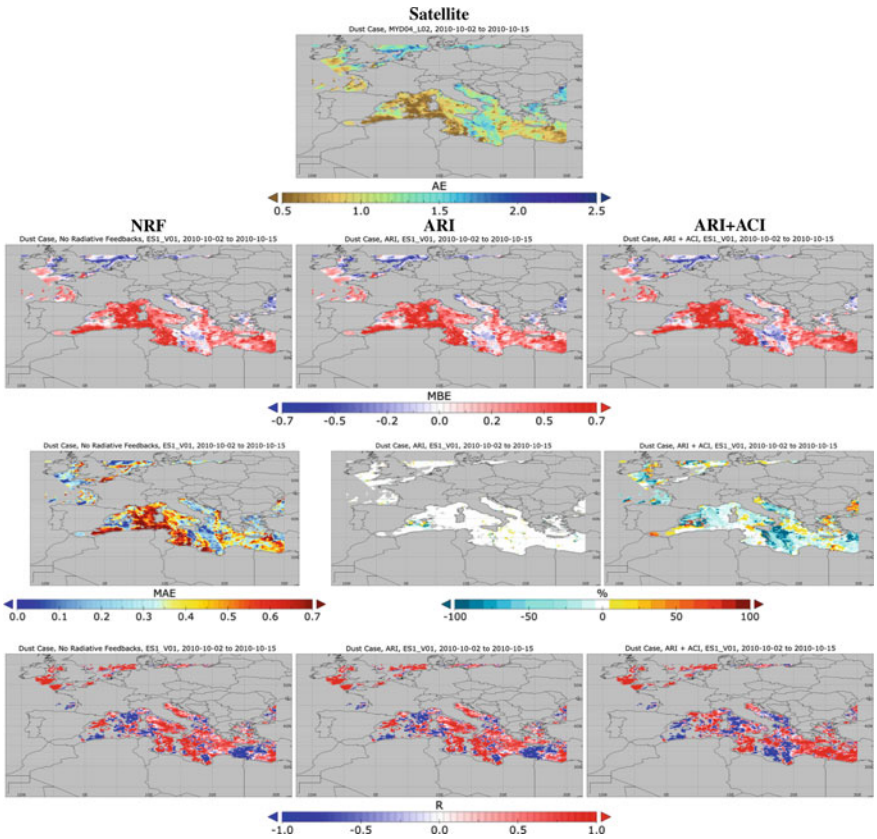

Fig. 29.2 Results for AE. Description idem as Fig. 29.1

29.4 Conclusion

The best-represented variable is AOD and there is a general improvement of AOD when including the aerosol RF in the model. Correlation coefficients show higher values for AOD than for the AE. Generally, for the latter, the model tends to underestimate the variability of this variable. However, the improvement in the representation of AOD may be of essential importance for a better description of ARI and ACI in online regional coupled models.

Acknowledgements Thanks to the *REPAIR-CGL2014-59677-R* project (Spanish Ministry of Economy and Innovation, also funded by the FEDER programme of the European Union), Fundacin Séneca-Agencia de Ciencia y Tecnología de la Región de Murcia—Programme Jiménez de la Espada de Movilidad, Cooperación e Internacionalización, in the framework of II PCTIRM 2011–2014 *EuMetChem COST ACTION ES1004* and the *AQMEII initiative* are also acknowledged.

Questions and Answers

Questioner: Pavel Kisheha
Question: MODIS AOD includes contributions not only from mineral dust but also from other aerosol species such as sea salt, industrial pollution, ship emissions, etc. Could it be that the model underestimation of MODIS AOD could be explained by the contribution of non-dust aerosol instead of radiation effects of dust?
Answer: Non-dust aerosol species are included in the model. Anthropogenic emissions, as industrial pollution, are obtained from a recent update of the TNO MACC emissions inventory (http://www.gmes-atmosphere.eu/; Pouliot et al. 2012, 2015; Kuenen et al. 2014). Biomass burning emission, such as black carbon have been calculated from global fire emission data that have been supplied from the integrated monitoring and modelling system for wild-land fires (IS4FIRES) project (Sofiev et al. 2009) with $0.1 \times 0.1°$ spatial resolution. Biogenic emissions are based on the Model of Emissions of Gases and Aerosols from Nature (MEGAN) model (Guenther 2006) which is on-line coupled with WRF-Chem and makes use of simulated temperature and solar radiation. Moreover, dust and sea salt emissions are estimated online by WRF-Chem from the meteorological parameters.

References

Boucher O, Randall D, Artaxo P, Bretherton C, Feingold G, Forster P, Kerminen V-M, Kondo Y, Liao H, Lohmann U, et al (2013). Clouds and aerosols. In: Climate change 2013: the physical science basis. Contribution of working group I to the fifth assessment report of the intergovernmental panel on climate change. Cambridge University Press, pp 571–657

Grell GA, Peckham SE, Schmitz R, McKeen SA, Frost G, Skamarock WC, Eder B (2005) Fully coupled online chemistry within the WRF model. Atmos Environ 39(37):6957–6975

Guenther C (2006) Estimates of global terrestrial isoprene emissions using megan (model of emissions of gases and aerosols from nature). Atmos Chem Phys, 6

Kuenen J, Visschedijk A, Jozwicka M, Denier Van der Gon H (2014) Tno-macc_ii emission inventory; a multi-year (2003–2009) consistent high-resolution european emission inventory for air quality modelling. Atmos Chem Phys 14(20):10963–10976

Palacios-Peña L, Baró R, Guerrero-Rascado JL, Alados-Arboledas L, Brunner D, Jiménez-Guerrero P (2016) Assessment of the radiative effects of aerosols in an on-line coupled model over the Iberian Peninsula. Atmos Chem Phys Discuss 2016:1–29

Pouliot G, Pierce T, van der Gon HD, Schaap M, Moran M, Nopmongcol U (2012) Comparing emission inventories and model-ready emission datasets between Europe and North America for the AQMEII project. Atmos Environ 53:4–14

Pouliot G, van der Gon HAD, Kuenen J, Zhang J, Moran MD, Makar PA (2015) Analysis of the emission inventories and model-ready emission datasets of Europe and North America for phase 2 of the AQMEII project. Atmos Environ 115:345–360

Sofiev M, Vankevich R, Lotjonen M, Prank M, Petukhov V, Ermakova T, Koskinen J, Kukkonen J (2009) An operational system for the assimilation of the satellite information on wild-land fires for the needs of air quality modelling and forecasting. Atmos Chem Phys 9(18):6833–6847

Chapter 30
The Impact of Heat Waves and Urban Heat Island on the Production of Ozone Concentrations Under Present and Future Climate Conditions for the Belgian Domain

A.W. Delcloo, F. Duchêne, R. Hamdi, J. Berckmans, A. Deckmyn and P. Termonia

Abstract Due to a strong urbanization in Belgium, a lot of areas can be considered as particularly vulnerable to heat waves due to the urban heat island (UHI) effect. However, little information exists on the interaction between the urban heat island effects during heat waves and their interactions under present and future conditions. The heat wave definition and heat stress index chosen in this study are based upon the warnings issued by the Public Health of Belgium for the Brussels Capital Region. For this study, regional simulations were performed using the limited area model ALARO, coupled with the Town Energy Balance scheme. The offline air quality simulations are calculated using the CHIMERE model. Results from our observations and climate simulations indicate that for the present climate conditions night time UHI is enhanced during heat waves which affects also urban and rural surface energy balance differently. The projected climate change under scenario A1B for 2050 leads to an increase of the number and duration of heat waves. More specifically, for rural (urban) areas, climate change increases the intensity of heat waves more during the day (night). We will also look more closely to the effect these changes have on air quality when taking the present and future climate scenarios under consideration. There is a significant increase in the number of days for which ozone concentrations exceed the warning threshold during heat waves. Besides the urban scale we will also investigate the impact of this configuration on air quality for the rural scale under present and future climate conditions.

A.W. Delcloo (✉) · F. Duchêne · R. Hamdi · A. Deckmyn · P. Termonia
Royal Meteorological Institute of Belgium, Brussels, Belgium
e-mail: Andy.Delcloo@meteo.be

R. Hamdi · P. Termonia
Department of Physics and Astronomy, Ghent University, Ghent, Belgium

J. Berckmans
Plant and Vegetation Ecology (PLECO), University of Antwerp, Antwerp, Belgium

C. Mensink and G. Kallos (eds.), *Air Pollution Modeling and its Application XXV*,
Springer Proceedings in Complexity, DOI 10.1007/978-3-319-57645-9_30

30.1 Introduction

Previous research indicates that human mortality is impacted by both meteorological conditions and atmospheric pollutant levels, such as the high temperatures and high levels of ozone experienced during the 2003 heat wave that had a substantial effect on human health (Vautard et al. 2005). Stedman (2004) suggests that between 21 and 38% of the excess deaths observed during the summer 2003 European heat wave were attributed to ozone and PM10 pollutants. In this study, the chemical transport model (CTM) CHIMERE (Vautard et al. 2001) has been coupled to the climate simulations.

Three different simulations were considered as following: (i) 4 years with ERA-INTERIM driven experiment (2005–2008), (ii) current climate (1990–1999), and (iii) future climate (2046–2055), following the A1B scenario. For all the simulations, the same emissions from TNO/GEMS (2004) were used (Visschedijck et al. 2007). This will allow us to verify if the changes in climate conditions will actually lead to a change in ozone concentration, especially during heat wave events.

To validate the skills of our ALARO-CHIMERE system, the simulations for the time period 2005–2008 have been validated using observational data (PM10 and O3) from IRCELINE. In Delcloo et al. (2014a), it has already been shown that the use of the Town Energy Balance parameterization in the land surface scheme of ALARO have significantly improved the modelling of PM10 and ozone in the urban areas. When comparing the time series of observed and modelled PM10 data for the station of Uccle during the time period 2005–2008, a correlation coefficient (R) of 0.72 and a bias of 1.7 $\mu g/m^3$ are found. The intercomparison statistics for ozone show a negative bias of -9.3 $\mu g/m^3$ with a correlation of 0.86, which elucidates that the model underestimates some of the observed ozone peaks. Since the station of Uccle is situated in a suburban area, the observed ozone time series show more elevated maximum ozone concentrations during ozone peaks, due to less influence by titration by NO. This chemical reaction favors the destruction of ozone and happens typically on locations which are much more exposed to traffic emissions (Beekmann and Vautard 2010).

30.2 Results and Discussion

30.2.1 Urban Micro-climate

From previous work it is shown that while the Brussels Capital Region warms substantially for the 2050s horizon, climate change will have a neutral impact on the annual mean urban heat island (UHI) intensity. The biggest and statistically significant change of nocturnal (daytime) UHI is noted during winter (summer) season with an increase (decrease) of +0.2 °C (−0.1 °C). During summer, the decrease in daytime UHI is directly connected to soil drying over rural areas, while

the increase in nocturnal UHI during the winter can be explained by the projected decrease of wind speed (Hamdi et al. 2014).

The projected climate change under scenario A1B for 2050 leads to an increase of the number and duration of heat waves. More specifically, for rural (urban) areas, climate change increases the intensity of heat waves more during the day (night).

30.2.2 Air Quality

For the policy maker, it is interesting to know how these changes in heat wave intensity/events will have an impact on air quality by looking at how the number of exceedances will evolve in the future climate scenarios. To evaluate these changes, we have verified the number of days in which ozone concentrations exceed the warning thresholds of 180 μg/m^3 during a heat wave event in the present and future climate simulations.

Table 30.1 shows results for some stations, which clearly indicate an increase in exceeding the warning threshold for ozone in the future climate. It is important for the interpretation of these results to take into account that the emissions that have been used are more representative for the first half of the time period 2000–2010 instead of the 90s. A strong reduction in NOx and NMVOCs has been observed since then (Wilson et al. 2012). From the results in Table 30.1 we can deduce that for the city climate, the increase is higher when compared with the results from stations, located in a more rural area. However, we also observe that for stations, located in more forested area (Vezin, Offagne), the increase in ozone concentrations is even more elevated.

Table 30.1 The relative change in number of days in which ozone concentrations exceed the warning threshold of 180 μg/m^3 for the future climate simulations compared to the present climate simulations for some stations under consideration

Station	Type	Relative change in number of exceedances (%)
Ukkel	Suburban	138
Destelbergen	Suburban	110
Houtem	Rural	58
Moerkerke	Rural	60
Offagne	Rural	453
Vezin	Rural	360
Dessel	Rural	142

30.3 Conclusions

The projected climate change simulations under scenario A1B for 2050 show that this will lead to an increase of the number and duration of heat waves. More specifically, for rural (urban) areas, climate change increases the intensity of heat waves more during the day (night).

The effects of these changes on air quality elucidate that in the future climate more exceedances of the warning threshold for ozone will take place. Especially for the suburban and more forested regions this seems to be the case. Since the intensity of the heat waves will increase for the future climate, a significant impact on the ozone burden is to be expected.

Acknowledgements The authors would like to thank IRCELINE for providing the observational data.

Question and Answer

Questioner: Richard Derwent
Question: You did not provide any projections of future ozone levels for the Offagne station in the forested region of Southern Belgium. Have you any results?
Answer: New results have been added for the Offagne and Vezin station in the Southern part of Belgium within this work.

References

Beekmann M, Vautard R (2010) A modelling study of photochemical regimes over Europe: robustness and variability. Atmos Chem Phys 10: 10067–10084. doi:10.5194/acp-10-10067-2010

Delcloo A, Hamdi R, Deckmyn A, De Backer H, Forêt G, Termonia P, Van Langenhove H (2014a) A one year evaluation of the CTM CHIMERE using SURFEX/TEB within the high resolution NWP models ALARO and ALADIN for Belgium. In: Air pollution modeling and its application XXIII, NATO science for peace and security series C: environmental security, pp 495–498. doi:10.1007/978-3-319-04379-1_81

Hamdi R, Van de Vyver H, De Troch R, Termonia P (2014) Assessment of three dynamical urban climate downscaling methods: Brussels's future urban heat island under an A1B emission scenario. Int J Clim 34(4):978–999. doi:10.1002/joc.3734

Stedman JR (2004) The predicted number of air pollution related deaths in the UK during the August 2003 heatwave. Atmos Environ 38:1087–1090

Vautard R, Beekmann M, Roux J, Gombert D (2001) Validation of a deterministic forecasting system for the ozone concentrations over the Paris area. Atmos Environ 35:2449–2461

Vautard R, Bessagnet B, Chin M, Menut L (2005) On the contribution of natural Aeolian sources to particulate matter concentrations in Europe: testing hypotheses with a modelling approach. Atmos Environ 39:3291–3303

Visschedijk AJH, Zandveld PYJ, Denier van der Gon HAC (2007) A high resolution gridded European database for the EU integrate project GEMS, TNO-report 2007-A-R0233/B

Wilson RC, Fleming ZL, Monks PS, Clain G, Henne S, Konovalov IB, Szopa S, Menut L (2012) Have primary emission reduction measures reduced ozone across Europe? An analysis of European rural background ozone trends 1996–2005. Atmos Chem Phys 12(437–454):2012. doi:10.5194/acp-12-437-2012

Chapter 31
Dynamic Coupling of the NMMB and CMAQ Models Through the U.S. National Unified Operational Prediction Capability (NUOPC)

Pius Lee, Barry Baker, Daniel Tong, Li Pan, Dusan Jovic, Mark Iredell and Youhua Tang

Abstract An earth system modeling framework (ESMF) that enables unprecedented insight into the various aspects of the geophysical sciences of Planet Earth in an integrated and holistic manner is needed to study the physical phenomena of weather and climate. The ESMF concept has recently been promoted and elevated by multiple governmental agencies and institutions in the U.S.A. to unify a standard engineering practice and coding protocol in building geophysical model interfaces towards efficient dynamic coupling of earth models and deployment of earth modeling systems for operational services. This new capability is called the National Unified Operational Prediction Capability (NUOPC) (available at http://www.nws.noaa.gov/nuopc/). This project demonstrates the efficacy of using NUOPC as the software package to efficiently in-line, or 2-way couple at every synchronization time-step, the dust prediction capability of the U.S. National Air Quality Forecasting Capability (NAQFC). The NAQFC in the National Centers for Environmental Prediction (NCEP) operations comprises of an off-line coupled National Weather Service (NWS) North American Mesoscale-model (NAM) and the U.S. EPA Community Air Quality Multiscale Model (CMAQ). The limitation of the off-line coupled NAM-CMAQ is that NAM gives meteorological prediction to CMAQ hourly and uni-directionally. This project attempted a new coupling paradigm allowing NAM and CMAQ communicate with one another per synchronization time-step at roughly 5 min intervals uni-directionally or bi-directionally. In this project, the NUOPC protocol was tightly followed and the

P. Lee (✉) · B. Baker · D. Tong · L. Pan · Y. Tang
NOAA Air Resources Air Resource Laboratory (ARL), NCWCP, College Park, MD 20740, USA
e-mail: pius.lee@noaa.gov

B. Baker · D. Tong · L. Pan · Y. Tang
Cooperative Institutes for Satellite and Climate, University of Maryland, College Park, MD, USA

D. Jovic · M. Iredell
NCEP Environmental Modelling Centers, NCWCP, College Park, MD 20740, USA

C. Mensink and G. Kallos (eds.), *Air Pollution Modeling and its Application XXV*, Springer Proceedings in Complexity, DOI 10.1007/978-3-319-57645-9_31

in-line NAM-CMAQ ability tested to forecast fine mode particulates concentration with earth-crustal origin. A strong dust storm occurred in the South Western U.S. on May 11 2014 was used as a test case for the NUOPC in-line NAM-CMAQ forecasting capability. The forecast performance for the test case was evaluated against measured surface concentration of fine particulate smaller than 2.5 μm in diameter ($PM_{2.5}$).

31.1 Introduction

Customarily earth modeling is disciplinary centric. The disciplinary centric paradigm envisions a numerical earth model to simulate in isolation of one another addressing only one of the five spheres of the Planet Earth: Atmosphere, Biosphere, Cryosphere, Hydrosphere and Lithosphere. Each earth model does not feedback or does not feedback frequently enough with other earth models simulating the other earth spheres. The conventional approach is to use climatological averaged values of the properties from the other earth sphere(s) as static or quasi-static variables for the earth model under consideration. This can be a severe shortcoming making feedback from other earth models too slow, sparse and unidirectional.

The Earth System Modeling Framework (ESMF) approach represented a paradigm change in allowing meaningful and frequent enough feedback from earth models of different disciplines to communicate and constrain one another in concurrent executions of the models (Hill et al. 2004; Black et al. 2009) (available at https://earthsystemcog.org/projects/esmf/). In the past few years NOAA and a few governmental agencies and institutions played the role of lead developers and users of a set of the-state-of-science climate and weather models who collectively optimized a subset of the ESMF package. This optimized subset of the ESMF software system is called the National Unified Operational Prediction Capability (NUOPC) (available at http://www.nws.noaa.gov/nuopc/).

31.2 Dynamic Coupling Between NMMB and CMAQ

The NWS chose the U.S. EPA CMAQ as the regional chemical transport model (CTM) and the NWS NAM numerical weather prediction model (NWP) as the regional meteorological model as the two center-piece components for the U.S. NAQFC in 2003. The NAM refers to the NWS operational regional meteorological forecasting modeling system. In term of the NWP, NAM comprises of the Non-hydrostatic Meso-scale Model with B-grid staggering (NMMB) (Janjic and Gall 2012). The CMAQ and NMMB models are currently coupled in an off-line manner under the auspices of the operational NAQFC in NCEP. The NAQFC forecast is well utilized by local health and air quality forecasters. NAQFC is a

typical disciplinary centric earth modeling application where data exchange from NAM to CMAQ is infrequent and unidirectional.

This work aims to prove the efficacy of building an integrated earth modeling system by dynamically coupling NMMB with CMAQ to allow data-exchange per synchronization time-step between them, or at roughly every 5 min (effectively in-lining NMMB with CMAQ) via the NUOPC. Under the resource constraint of the project only the dust forecasting capability from CMAQ is considered due to its representativeness in reflecting a successful in-line system yet simple enough not to be implicated by anthropogenic emissions and chemical transformation calculations. Another important consideration of focusing on dust forecasting first is the minimum number of state variables CMAQ is required of NMMB for emission, transport, and the removal calculation for the wind-blown dust.

This project couples dynamically per synchronization time-step, i.e., effectively in-line, NMMB and CMAQ for dust forecasting. We take a NUOPC approach (available at: https://www.earthsystemcog.org/projects/nuopc/). The progress in the NUOPC has realized an in-line earth modeling system that can first couple ocean, meteorological and hydrological models so that severe weather forecasts such as those for hurricane track and intensity can begin to see the fruition of such an integrated earth modeling approach. We leverage this progress to demonstrate a NUOPC in-lined NMMB-CMAQ (Table 31.1).

Table 31.1 Description of the NUOPC generic functional components

Components	Primary functions
Driver	A NUOPC driver steers the initialization and run-sequence of an earth modeling system. The initialization step is defined by an overarching file called the "initialization phase definition". Similarly the run sequence is defined by a "user-defined run-sequence" file. The driver depends on the clock definition defined in the model component to control the run sequence
Connector	A NUOPC connector is invoked by the driver to implement field matching based on an application specific standard metadata. The connector also executes map-projection transforms and re-gridding interpolation. The connector links an earth model to either another earth model or to a mediator. In a modeling system with only two earth models the connector can be the sole linking component between the earth models
Model	A NUOPC model is a slight expansion of the stand-alone version of the corresponding earth model. The expansion includes internal clock definition for time steps for the major physical and chemical processes and wrapper codes to allow invocation by the driver
Mediator	A NUOPC mediator functions as a communication hub among earth models especially there are three or more earth models in the modeling system. The mediator performs customized calculations for flux rates and spatial and/or temporal averages needed by one or multiple other earth models in the earth modeling system

31.3 Test Case and Evaluation

The FENGSHA wind-blown dust emission module is rather sensitive to the threshold friction velocity and the land surface texture conditions. We analyzed a readily available prediction results from the FENGSHA enabled NAQFC system that has been implemented into NCEP operations in February 2016. We studied the May 11 2014 dust case basing on the standard NAQFC 12 km horizontal grid (See Fig. 31.1). The NAQFC derives wind and soil moisture fields from the NCEP 12 km NAM from NCEP. NAM conducts 6 hourly data assimilation at 00, 06, 12 and 18 UTC. NAM generates hourly meteorological fields for CMAQ where the full hour values from NAM are interpolated linearly into instantaneous values correspond to the advection time steps in CMAQ. Therefore there was inherent smoothing and losing of transient features in the meteorological fields by virtue of temporal interpolation. Moreover, at 12 km horizontal resolution NAQFC is too coarse in describing local wind and surface texture in adequate details critical for dust modeling. However, the operational NAQFC is a good first cut test to dive deeper into the initial uptake and suspension of the dust particles—the first two important processes in the chain of events defining the wind-blown dust. We evaluated the NAQFC predicted $PM_{2.5}$ forecasting skill during this dust storm and assessed the impact of dust emission on the regional air quality.

Figure 31.1 shows an instantaneous depiction of the elevated surface $PM_{2.5}$ concentration at 12 UTC May 11 2014. The predicted spatial distribution of the surface $PM_{2.5}$ concentration is roughly corresponding to what was illustrated by the satellite imagery shown in Fig. 31.1. An AIRNow monitor or monitor-cluster specific verification time series tracking the evolution of predicted concentration versus measured $PM_{2.5}$ was pursued.

As another candidate wind-blown dust forecast potentially to be implemented as the next DFC, we leverage the superior meteorology from HRRR to couple it with the FENGSHA dust emission module and the dust transport and removal capability

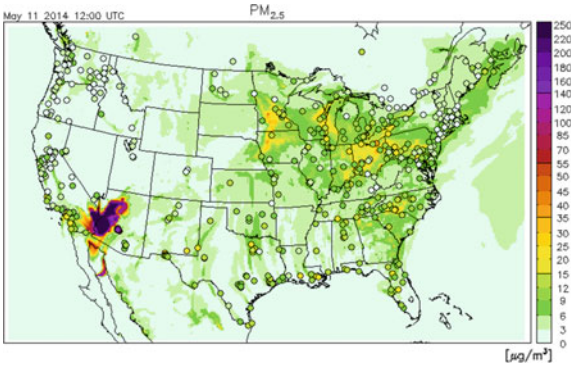

Fig. 31.1 Surface $PM_{2.5}$ ($\mu g\ m^{-3}$) at 12 UTC May 11 2014 depicted by a color scheme as shown in the *right-side* color bar for: Prediction by the offline coupled NMMB and CMAQ as in NAQFC operations in background shading, and measurement by the EPA AIRNow monitoring network in *filled circles*

of CMAQ. In order to directly quantify the benefit of leveraging the 3 km resolution and the rapid hourly cycles of data assimilation in HRRR against the NAM input with a coarse grid at 12 km and 6 hourly data assimilation we also couple HRRR with FENGSHA-CMAQ offline. Again the full hour HRRR meteorological fields are used in input for CMAQ. Similarly, the full hour HRRR fields were interpolated linearly into instantaneous values correspond to the advection time steps in FENGSHA-CMAQ. This offline coupled HRRR-FENGSHA-CMAQ system was tested and evaluated for the May 11 2014 case. The NUOPC driver prescribes a NUOPC-synchronization time and a universal clock for the earth modeling system. The two quantities allow the NMMB and CMAQ see a common NUOPC "clock" time. The NMMB and CMAQ exchange data values at the NUOPC synchronization times. Output is produced and written-out and accumulated hourly to a result file at the "outputting" times. The earth model system simulation terminates at the prescribed finishing time. Chronologically the NMMB terminates first and then the CMAQ. Finally, a restart file is written as the finishing time.

31.4 Summary and Future Work

Figure 31.2 shows the schematic on the time advancement of the NUOPC dynamically coupled NMMB-CMAQ simulation. The NUOPC driver prescribes a NUOPC-synchronization time and a universal clock for the earth modeling system. The two quantities allow the NMMB and CMAQ see a common NUOPC "synchronization", "outputting" and "finishing" time. The NMMB and CMAQ exchange data values at the NUOPC synchronization times. Output is produced and written-out and accumulated hourly to a result file at the "outputting" times. The earth model system simulation terminates at the prescribed finishing time. Chronologically the NMMB terminates first and then the CMAQ. Finally, a separate CMAQ restart file is written-out as the last step at the finishing time.

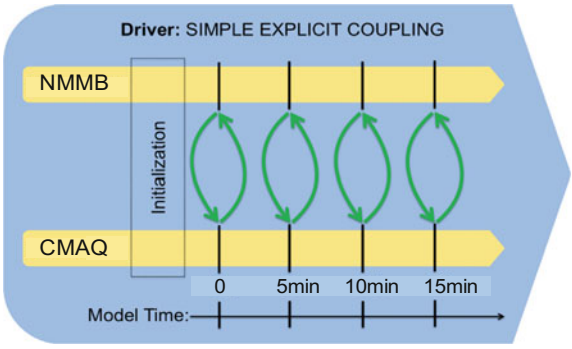

Fig. 31.2 A schematic on the time advancement of the NUOPC dynamically coupled NMMB-CMAQ simulation

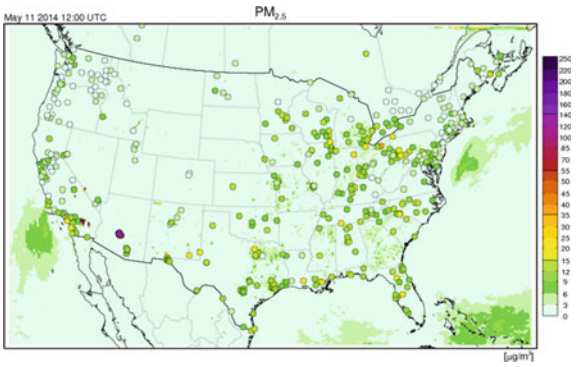

Fig. 31.3 Same as Fig. 31.1 but for the model prediction generated by the NUOPC dynamically coupled NMMB-CMAQ

Figure 31.2 shows the schematic on the time advancement of the NUOPC dynamically coupled NMMB-CMAQ simulation. Figure 31.3 shows the same depiction as in Fig. 31.1 except for the HRRR meteorology.

References

Black T, Juang HMH, Iredell M (2009) The NOAA environmental modeling system at NCEP. Proc 23rd Conference on Weather Analysis and Forecasting/19th Conference on Numerical Weather Prediction, American Meteorological Society, Omaha, NE

Janjic Z, Gall R (2012) Scientific documentation of the NCEP nonhydrostatic multiscale model on B grid (NMMB). Part 1 Dynamics. NCAR Technical Note NCAR/TN-489+STR 80 pp

Hill C, DeLuca C, Balaji V, Suarez M, da Silva A (2004) The architecture of the earth system model ing framework. IEEE Comput Sci Eng 6:18–28. doi:10.1109/MCISE.2004.1255817

Chapter 32
Impact of Climate on Air Quality in the Mediterranean Basin: Present Climate

Jonathan Guth, Virginie Marécal, Béatrice Josse and Joaquim Arteta

32.1 Introduction

Atmospheric pollution is an environmental problem our modern societies have to face with. The Mediterranean basin is a sensible region to atmospheric pollution, especially for air quality issues. Moreover, this region is also especially vulnerable to global climate change leading to dryer and warmer conditions especially during the summer.

Associated to the strong population density on the Mediterranean coast, one can wonder what will be the composition of the atmosphere in the future in a context of climate change, and what will the impact on the air quality be. The aim of this work is to use the Chemistry Transport Model MOCAGE in order to address this question. To do this we run several simulations using the CTM MOCAGE. The aim of this first part is to characterize the air quality in the near past and the present climate conditions using air quality indicators such as PM concentrations, or gaseous compounds concentrations.

J. Guth (✉) · V. Marécal · B. Josse · J. Arteta
Météo-France CNRM-GAME, Toulouse, France
e-mail: jonathan.guth@meteo.fr

V. Marécal
e-mail: virginie.marecal@meteo.fr

B. Josse
e-mail: beatrice.josse@meteo.fr

J. Arteta
e-mail: joaquim.arteta@meteo.fr

C. Mensink and G. Kallos (eds.), *Air Pollution Modeling and its Application XXV*,
Springer Proceedings in Complexity, DOI 10.1007/978-3-319-57645-9_32

32.2 MOCAGE Chemistry Transport Model

MOCAGE is the 3D global off-line chemistry transport model (CTM) run at Météo-France since 2005 for air quality operational forecasts. Its latest version includes tropospheric and stratospheric chemistry, and primary and secondary inorganic aerosols (Guth et al. 2016). It is set with 47 vertical levels (from the surface to 5 hPa) and has a grid nesting capability. The model MOCAGE is also able to simulate long period, using climate simulation or reanalysis, in order to evaluate the impact of climate and climate change on atmospheric composition.

32.3 Experimental Set Up

Here the aim is to characterize the air quality in the near past and the present climate conditions using air quality indicators. To do this the model is forced using ERA-Interim meteorological fields. A 10 years simulation, between 2000 and 2010, is run using the Chemistry-Transport Model MOCAGE (Guth et al. 2016). To focus on the Mediterranean basin, we use a 0.5° × 0.5° resolution domain including North Africa, western Europe up to the Benelux and Israel to the East. The domain simulated is represented in Fig. 32.1. Emission used are MACCity for the anthropogenic part and MEGAN-MACC for the biogenic part. Biomass burning and aircraft emissions are taken into account with ACCMIP emissions.

32.4 Evaluation and Results

Before going into the results of the simulation, we make an evaluation of the simulation. A dense European measurement network is used for air quality monitoring. The network data are gathered into a database named AIRBASE which is used here to evaluate the simulation.

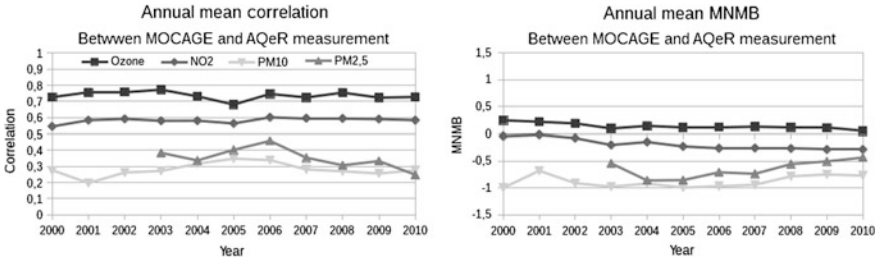

Fig. 32.1 Time series of annual correlation (*left*) and MNMB (*right*) from the MOCAGE simulation against the AIRBASE database measurements between 2000 and 2010

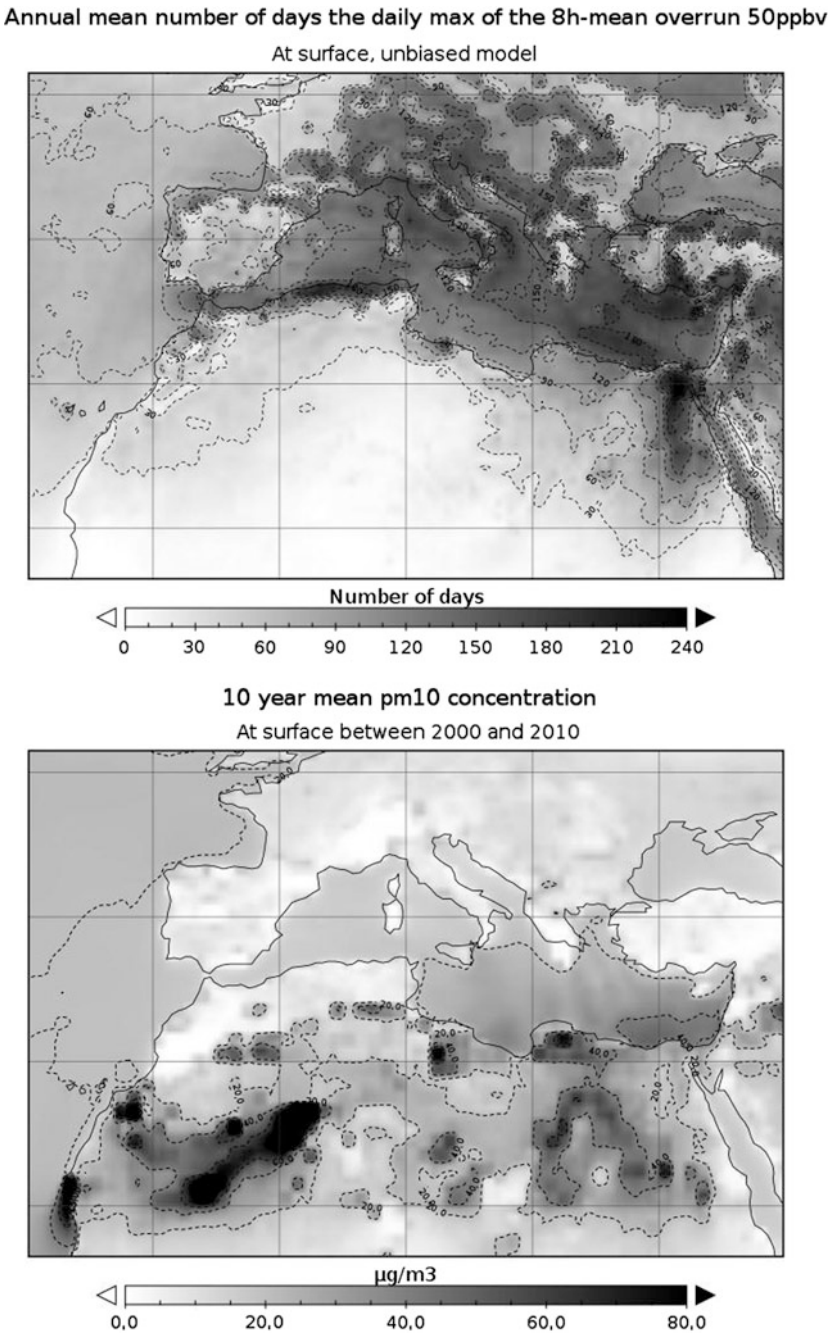

Fig. 32.2 Maps of annual mean number of days of the 50 ppbv exceedance for the daily maximum of the 8 h-mean ozone concentration (*top*) and annual mean surface concentration of PM_{10} (*bottom*)

Stations are located on various sites being representative of rural, suburban or urban conditions. To compare the model to the observations, we select stations representative of the model resolutions using the Joly and Peuch (2012) classification. The Fig. 32.1 presents the time series of the annual Modified Normalized Mean Bias (MNMB, varying between −2 and 2) and the correlation between 2000 and 2010 for O_3, NO_2, PM_{10} and $PM_{2.5}$. The model shows an underestimation of the PM, mainly due to a lack of secondary organic aerosols in the model. This 10-year long simulation was used to study the air quality over the Mediterranean basin during this period. We examine in particular the ozone and particulate matter concentration at surface.

For ozone, we relied on the World Health Organization (WHO) guidelines which indicates that the daily maximum of the 8 h ozone mean concentration should not overrun 50 ppbv (100 μg/m^3). Moreover, for ozone we firstly unbiased the model by simply subtracting the mean bias found when comparing the simulation with the AIRBASE database. The top panel in Fig. 32.2 presents the mean annual number of days where this 50 ppbv threshold is overrun. One can see that some regions presents more than 150 days per year of ozone related polluted air such as North Africa. For particulate matter, we also relied on the WHO guidelines who claims that annual mean PM_{10} concentrations should not overrun the 20 μg/m^3 limit value. The bottom panel in Fig. 32.2 presents the mean annual surface concentrations of PM_{10}. This figure shows that a large part of the southern half of the domain presents particulate matter concentrations above the WHO threshold.

32.5 Conclusion and Future Work

This first 10 years simulation of the recent climate allow us to evaluate the model performances in a climate long duration mode forced by ERA-Interim and to evaluate the air quality over the Mediterranean basin. The second step will be to run the same period using a climate simulation from model ARPEGE, developed at CNRM. This simulation will serve to evaluate the performance of the model MOCAGE using the ARPEGE climate forcing to represent the air quality during the 2000s against observations and the MOCAGE/ERA-Interim simulation. Then we will simulate the future, around 2050, using ARPEGE climate-forcing fields to assess the air quality in the next decades.

References

Guth J, Josse B, Marécal V, Joly M, Hamer P (2016) First implementation of secondary inorganic aerosols in the MOCAGE version R2. 15.0 chemistry transport model. Geosci Model Dev 9(1):137–160

Joly M, Peuch VH (2012) Objective classification of air quality monitoring sites over Europe. Atmos Environ 47:111–123

Part IV
Data Assimilation and Air Quality Forecasting

Chapter 33
Using Air Quality Model-Data Fusion Methods for Developing Air Pollutant Exposure Fields and Comparison with Satellite AOD-Derived Fields: Application over North Carolina, USA

Ran Huang, Xinxin Zhai, Cesunica E. Ivey, Mariel D. Friberg, Xuefei Hu, Yang Liu, James A. Mulholland and Armistead G. Russell

Abstract A data fusion approach is developed to blend ground-based observations and simulated data from the Community Multiscale Air Quality (CMAQ) model. Spatiotemporal information and finer temporal scale variations have been captured by the resulting fields that are provided by both air quality modeling and observations. The approach is applied to daily $PM_{2.5}$ total mass, five major particulate species (OC, EC, SO_4^{2-}, NO_3^-, and NH_4^+), and three gaseous pollutants (CO, NO_x, NO_2) during 2006–2008 over North Carolina (USA). Applying the data fusion method significantly reduces biases in CMAQ fields to almost zero at monitor locations. The results show improvements in capturing spatial and temporal variability with observations, which is important to health and planning studies. The correlation for the cross-validation test decreased from 0.98 (no withholding) to 0.91 (10% random data withholding) when comparing modeled results to observations. If 10% monitor-based withholding is used, the correlation is 0.91 (random 10% of monitors withheld), and the correlation is 0.88 if spatially-specific withholding is used (10% of monitors withheld are grouped spatially). Results from a satellite-retrieved aerosol optical depth (AOD) method were compared with $PM_{2.5}$ total mass concentration from data fusion, and the data-fusion fields have slightly less overall error; an R^2 of 0.95 compared to 0.81 (AOD). Comparing results from an application of the Integrated Mobile Source Indicator method shows that the data fusion fields can be used to estimate mobile source impacts. Overall, the data fusion

R. Huang · X. Zhai · C.E. Ivey · M.D. Friberg · J.A. Mulholland · A.G. Russell (✉)
School of Civil and Environmental Engineering, Georgia Institute of Technology, Atlanta, GA 30332, USA
e-mail: ted.russell@ce.gatech.edu

X. Hu · Y. Liu
Rollins School of Public Health, Emory University, Atlanta, GA 30322, USA

C. Mensink and G. Kallos (eds.), *Air Pollution Modeling and its Application XXV*, Springer Proceedings in Complexity, DOI 10.1007/978-3-319-57645-9_33

approach is attractive for providing spatiotemporal pollutant fields for speciated particulate pollutants, as the demand for accurate, fused, air quality model fields is growing.

33.1 Introduction

Estimating population exposure to $PM_{2.5}$ has traditionally been done by assigning measurements of a central ground monitor to people living within the region (Kanaroglou et al. 2005). However, studies have shown that there are limitations of using central ground monitor data as the exposure metric (Wade et al. 2006), as monitoring sites in national regulatory networks are relatively sparse across broad regions of the country, and the concentration of pollutants can be impacted by emissions, leading to local variations. Methods are being developed that use a variety of modeling approaches to better estimate pollutant concentration variations not captured by observations (Johnson et al. 2010). One approach involves using chemical transport models (CTMs) to calculate air quality fields using that account for local variations affected by emissions and meteorology (Pleim et al. 2016). In order to develop fields that more accurately represent the actual concentrations, a novel data fusion (DF) approach was developed that blends measured data from ambient monitors and data from CMAQ. The DF approach better estimates ground-level air pollutant concentration fields, which improves exposure estimates (Friberg et al. 2016).

33.2 Methods

Three data assimilation methods are compared here. The DF method (Friberg et al. 2016) employed here combines pollutant observations and modeled pollutant fields, and is being applied to the 2006–2008 time period over North Carolina for daily $PM_{2.5}$ total mass, five major particulate species (OC, EC, SO_4^{2-}, NO_3^-, and NH_4^+), and three gaseous pollutants (CO, NO_x, NO_2). $PM_{2.5}$ fields are also developed using a method that combines satellite aerosol optical depth (AOD) retrievals (Hu et al. 2014) and ordinary kriging (Cressie et al. 1988).

In order to evaluate the performance of the DF method, cross-validation (CV) has been used in several approaches. For one CV approach, 10% of random observations were withheld without replacement (10 groups of randomly selected data points are removed without being linked to specific monitors). The observational data are applied, and the DF method is then repeated 10 times, withholding one group each time. This 10% random data withholding is applied for all species. For the second CV approach, the entire set of $PM_{2.5}$ monitors (60) was randomly (random-monitor-based) and spatially (spatial-based) split into ten subsets with 6 monitors in each subset. Following the split, the DF method is repeated 10 times.

In each round of CV, one subset (10% of monitors) was selected as the testing sample and the remaining nine subsets (90% of the monitors) were used to reapply the DF method. Then the predictions of the withheld monitors' values were compared with the initial monitors' values. The random subset removal was repeated twice in order to check the stability of this evaluation. For CO, considering the limited number of monitors, leave-one-monitor-out (LOO) has been applied in each test, where only one monitor has been removed.

33.3 Results

Spatial plots of the seasonal averages for $PM_{2.5}$ show high concentrations in major urban centers and highways (Fig. 33.1). Concentrations at the eastern and western boundaries are much lower than the other areas because these areas are forest and coastal areas. DF concentrations are higher than CMAQ concentrations in winter and lower than CMAQ in summer (Table 33.1).

The mean concentration from CMAQ is lower than observations, especially in summer. Both CMAQ and DF perform better for summer months than for winter months, but DF performance is better overall ($R^2 = 0.94$ in summer, $R^2 = 0.90$ in winter). The 10% random data withholding may overestimate the performance of the method compared with the spatial monitor-based data withholding. RMSE from 10% data withholding is 2.32 μg/m^3, which is lower than the spatial monitor-based

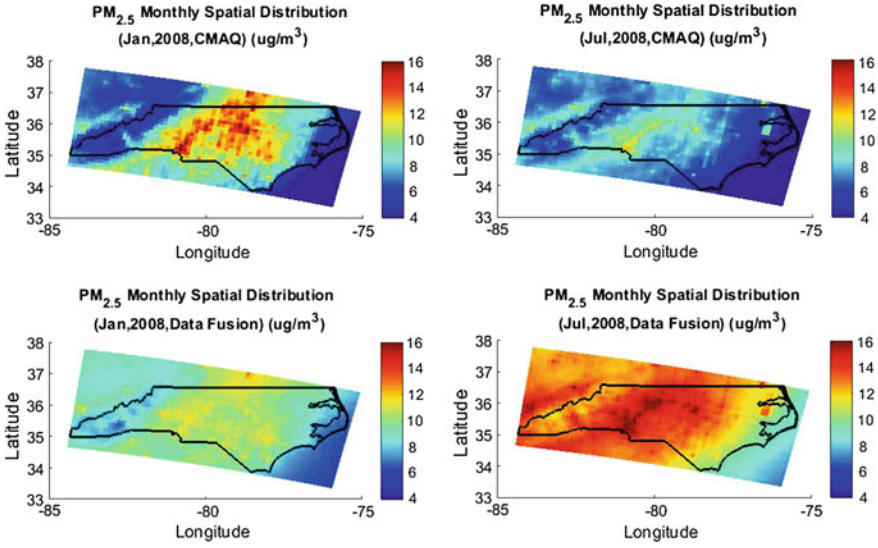

Fig. 33.1 Seasonally averaged spatial fields for $PM_{2.5}$ concentration estimated by CMAQ (*top row*) and the data fusion approach (*bottom row*); January 2008 (*left column*) and July 2008 (*right column*)

Table 33.1 Performance evaluation for observations and simulations of $PM_{2.5}$ concentrations (2006–2008): annual, January (winter), and July (summer) average for all 3 years

	Mean (μg/m^3)			NME			R^2		
	Annual	Jan	Jul	Annual	Jan	Jul	Annual	Jan	Jul
Observations	12.7	9.4	17.6	0	0	0	1	1	1
CMAQ	10.9	10.8	10.7	0.38	0.42	0.42	0.32	0.23	0.40
Data fusion	11.8	8.9	15.2	0.10	0.11	0.11	0.95	0.90	0.94
10% Random data withholding	11.7	9.2	15.4	0.16	0.21	0.15	0.82	0.56	0.86
Random 10% monitors withholding (first time)	12.0	8.9	15.7	0.16	0.20	0.14	0.82	0.58	0.86
Random 10% monitors withholding (second time)	12.3	9.0	15.0	0.17	0.21	0.15	0.81	0.57	0.83
Spatial 10% monitors withholding	12.3	9.1	14.8	0.19	0.25	0.18	0.73	0.48	0.76
Interpolation(ordinary kriging)	12.7	9.7	17.9	0.02	0.04	0.02	0.99	0.96	0.99
Ordinary kriging: random 10% monitors withholding (first time)	12.8	9.7	18.0	0.13	0.21	0.09	0.83	0.55	0.87
Ordinary kriging: random 10% monitors withholding (second time)	12.7	9.7	17.9	0.14	0.22	0.11	0.81	0.54	0.84
Ordinary kriging: spatial 10% monitors withholding	12.6	9.6	17.8	0.19	0.25	0.15	0.71	0.44	0.73
AOD	12.8	8.9	20.0	0.15	1.32	0.74	0.81	0.60	0.83

data withholding (2.81 μg/m^3 (annual), 2.58 μg/m^3 (winter), and 2.56 μg/m^3 (summer)). Although ordinary kriging performs well at the monitor location (R^2 = 0.99 (annual), 0.96 (winter), 0.99 (summer)), the monitor-based data withholding shows the uncertainty at the location without observations (averaged R^2 = 0.82 (annual), 0.51 (winter), 0.81 (summer)). AOD method performs well with a NME equals to 0.15 but still not good enough compared to data fusion method at the monitor locations (NME = 0.10).

Linear regression between DF and AOD data for $PM_{2.5}$ simulations is conducted for monitor sites and for all research grids, and the slope for analysis that includes all grids is closer to 1 (slope = 0.91 for monitor sites and slope = 1.01 for all grids) (Fig. 33.2). Most monitor sites are located in urban areas, the data fusion and AOD methods capture the urban area $PM_{2.5}$ concentrations well. The relatively higher concentrations of AOD come from the coastal area, considering that AOD method can overestimate concentrations in the coastal areas of eastern NC because of the high relative humidity (Hu et al. 2013).

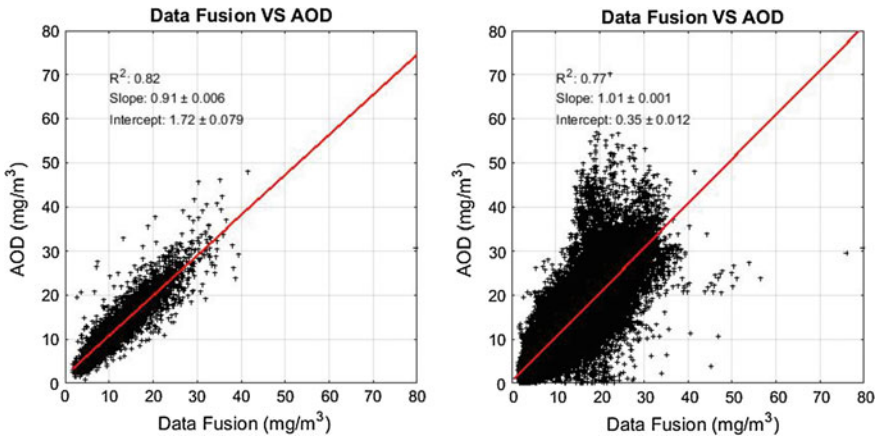

Fig. 33.2 Linear regression between data fusion and AOD at monitor site (*left*) and all research grids (*right*)

Acknowledgements This publication was made possible by USEPA grant R834799. The work of X. Hu and Y. Liu was supported by NASA Applied Sciences Program (grant numbers NNX11AI53G and NNX14AG01G, Principal Investigator: Liu). Its contents are solely the responsibility of the grantee and do not necessarily represent the official views of the US government. Further, US government does not endorse the purchase of any commercial products or services mentioned in the publication.

Question and Answer

Questioner: Sofiev
Question: You mentioned issues in AOD retrievals over coastal areas due to humidity impact. So what is the issue?
Answer: The AOD method is 10 km resolution which is difficult to handle the grid that mix the land and water (coastal areas). The method retrieval doesn't include RH, although they calibrate during the following steps. RH is related to sea salt aerosol which is important to $PM_{2.5}$ concentration in coastal areas. Also, the data is incomplete in the day and areas that they can't retrieve from satellite.

References

Cressie N (1988) Spatial prediction and ordinary kriging. Math Geol 20:405–421
Friberg MD, Zhai X, Holmes HA, et al (2016) Method for fusing observational data and chemical transport model simulations to estimate spatiotemporally resolved ambient air pollution. Environ Sci Technol

Hu X, Waller LA, Al-Hamdan MZ et al (2013) Estimating ground-level PM(2.5) concentrations in the southeastern U.S. using geographically weighted regression. Environ Res 121:1–10

Hu X, Waller LA, Lyapustin A et al (2014) Estimating ground-level PM2.5 concentrations in the Southeastern United States using MAIAC AOD retrievals and a two-stage model. Remote Sens Environ 140:220–232

Johnson M, Isakov V, Touma JS et al (2010) Evaluation of land-use regression models used to predict air quality concentrations in an urban area. Atmos Environ 44:3660–3668

Kanaroglou PS, Jerrett M, Morrison J et al (2005) Establishing an air pollution monitoring network for intra-urban population exposure assessment: a location-allocation approach. Atmos Environ 39:2399–2409

Pleim J, Gilliam R, Appel W, Ran L (2016) Recent advances in modeling of the atmospheric boundary layer and land surface in the coupled WRF-CMAQ model. Springer International Publishing, pp 391–396

Wade KS, Mulholland JA, Marmur A et al (2006) Effects of instrument precision and spatial variability on the assessment of the temporal variation of ambient air pollution in Atlanta, Georgia. J Air Waste Manage Assoc 56:876–888

Chapter 34
Fusion of Air Quality Information: Evaluation of the Enfuser-Methdoology in Finland and a Case Study in China

Ari Karppinen and Lasse Johansson

Abstract We describe a modelling system (FMI-ENFUSER), which fuses environmental information for the assessment of urban air quality in a high resolution based on local sensor network, meteorological data and a collection of GIS-datasets. With this combination of techniques the hourly concentration of particle matter ($PM_{2.5}$ and PM_{10}) and NO_2 can be accurately predicted in several selected urban test sites in Finland. We also show and discuss the first results from test sites in China and India. The methodology can be used in any region where a proper training dataset and GIS-information exists.

34.1 Introduction

The amount of environmental information that can be used for the assessment of air quality in urban areas has increased substantially during the recent years. Sensor network are becoming denser and regional air quality forecasts are freely available online. However, for a citizen that is interested in the urban air quality the measurements of a single sensor, even the closest one, may require interpretation and expertise. The pollutant concentrations in urban areas show great geographical variability to the extent that even the close by buildings, roads and measurement height can significantly affect the pollutant concentrations measured by the sensors. It therefore makes sense to fuse all the available information with methods that can take the above mentioned aspects into account and assess the air quality in the whole city. Given that weather forecasts and regional air quality forecasts are available, it is also possible to forecast the air quality in the near future based on the current state, future meteorology and modelled long range transportation of

A. Karppinen (✉) · L. Johansson
The Finnish Meteorological Institute (FMI), Erik Palménin aukio 1,
00101 Helsinki, Finland
e-mail: ari.karppinen@fmi.fi

L. Johansson
e-mail: lasse.johansson@fmi.fi

C. Mensink and G. Kallos (eds.), *Air Pollution Modeling and its Application XXV*,
Springer Proceedings in Complexity, DOI 10.1007/978-3-319-57645-9_34

pollutants. The fusion of measured air quality data is especially demanding, since each data point is also subject to meteorological conditions, human activities and background concentrations. Furthermore, the individual sensor quality must be considered and if modelled air quality data is also included the fusion the limitations and imprecision of the included modelled data must be taken into account.

34.2 Methods

The FMI-ENFUSER is a hybrid model that combines statistical air quality modelling, Gaussian dispersion modelling techniques and information fusion algorithms (Johansson et al. 2015a, b). The main components of the modelling system have been illustrated in Fig. 34.1.

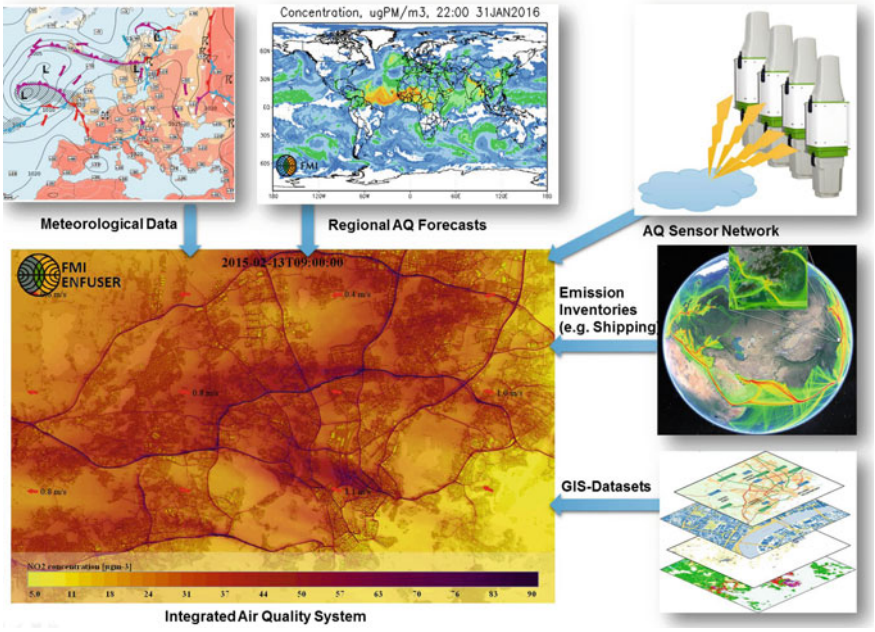

Fig. 34.1 The core components of FMI-ENFUSER modelling system, which utilizes latest sensor observations, meteorological data and regional air quality forecast in the production of high resolution AQ heatmaps for the current and future situation in urban locations. GIS-datasets and emission inventories together with archived concentration time series are used for the calibration of the model (Most of the datasets are open-source and globally available, such as OpenStreetMap and NASA EOSDIS data. In Finland the used GIS-datasets also includes CORINE land cover, population density mapping (2010, 250 × 250 m). For the case-study in Langfang a high resolution land-use GIS-dataset (5 × 5 m) was obtained by the courtesy of local authorities.)

Shortly put, the model is a 'tabula rasa' area source dispersion model without knowledge of local emission sources and their temporal/seasonal variation. With sufficient amount of calibration material including GIS-datasets, sensor measurement time series and weather data, the model detects the key relationships between GIS-properties and observed pollutant concentrations through multivariable regression. Such a key relationship can also be a more complicated sub-model that utilize several GIS-information layers as well as meteorological variables, and these sub-models aim to describe physically realistic emission sources rather than some more abstract GIS-properties that are commonly used in Land Use Regression. For example, individual households can be associated as a significant source for $PM_{2.5}$ through heating and this particular emission source can be dealt with by (i) detecting buildings from land-use data, (ii) assessing physical area of the buildings and (iii) taking into account the observed ambient temperature. In Helsinki Metropolitan Area the model distinguishes close to 100,000 small households that can contribute to $PM_{2.5}$ through this relationship.

After the calibration the model can associate proper emission rates as a function of GIS-properties and time to local area sources, after which the expected pollutant concentration for any given location and meteorological condition can be estimated. Finally, given a set of recent sensor observations the model can compare the observed concentrations with the expected modelled concentrations and adjust to the perceived conditions applying data fusion techniques. Data fusion algorithms makes it possible to fuse the information from multiple sensors and supporting air quality models of variable quality, also taking into account the temporal and spatial separation of data points. In theory, the more data is available the better the model output should become. To address the long range transportation of pollutants and enhance the forecasting capabilities of the model, the globally operational FMI-SILAM regional air quality model is also included in the pool of information (Sofiev et al. 2015).

The main advantages of the combination of techniques can be summarized as follows:

- Dispersion modelling facilitates the inclusion of meteorological variables including wind direction, wind speed, boundary layer height and atmospheric stability parameters. Height differences and topography can be taken into account.
- Statistical LUR methodology allows the model to be calibrated without a priori knowledge of local emission sources, using a large set of historical pollutant concentration time series. However, known emission inventories can be included in the modelling if available (such as the modelled shipping emissions of Fig. 34.1 which are provided by FMI-STEAM model (Jalkanen et al. 2012).
- With data fusion algorithms sensor/model quality can be addressed and modelled data can be fused together with sensor observations.
- Modelling system is computationally light-weight and exportable to other regions.

34.3 Results

As a demonstration for the modelling system in another region, the FMI-ENFUSER model was set up in Langfang, China, 2015 (Johansson et al. 2016). A small sensor network of five $PM_{2.5}$ sensors were installed around the city and the sensors were connected to a cloud data portal, from which the model was able to access the measurement data in near real time.

While most of the sensors were placed near ground level in variable environments, one of the sensors was placed on roof top. The FMI-ENFUSER model can take into account the individual measurement heights of sensors and variable measurement heights will enrich the information content available for the system, which in turn makes it easier to establish a comprehensive picture of the air quality in the city. In Fig. 34.2 the modelled hourly average pollutant concentration based on measurements from 5 sensors in a selected hour in Langfang is presented.

The ENFUSER model was also installed and calibrated in Delhi using the local historical AQ measurement data and meteorological measurements without any detailed emission factors or inventories for Delhi. Hourly concentration

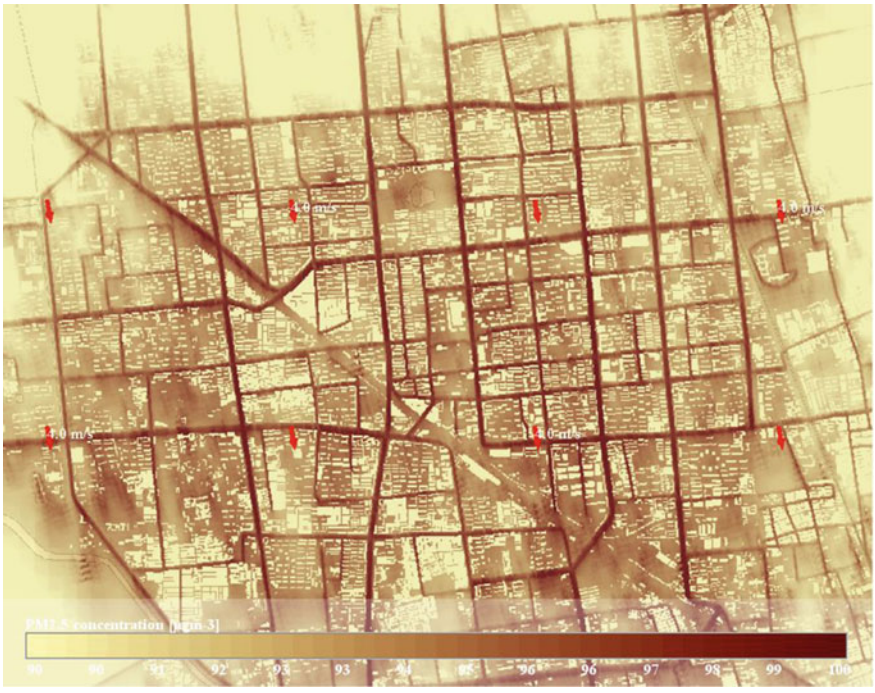

Fig. 34.2 Modelled hourly $PM_{2.5}$ concentration in Langfang based on sensor measurements during 2015-06-20T19:00. Wind conditions (direction, speed) have been illustrated with *red arrows*

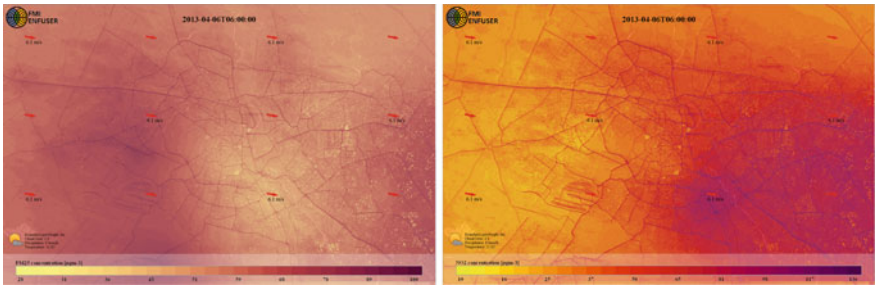

Fig. 34.3 Fused hourly PM2.5 and NO_2 concentration in Delhi in 2013-04-06T06:00 (UTC)

measurements were available for 8 stations in Delhi in 2013 for O_3, NO_2, SO_2, $PM_{2.5}$ and PM_{10}.

Before calibration and use of the model the consistency of available AQ data was also to be studied. This kind of consistency analysis can be done automatically with ENFUSER by launching a series of auto-covariance and variogram analysis routines. While the ultimate goal of these diagnostics was to assess data weighting factors for each station (for each pollutant type separately) and make the model operate more accurately, these diagnostics can also be used for the assessment of measurement data quality and quality control metrics for measurement stations. Figure 34.3 illustrate the modelled $PM_{2.5}$ and NO_2 concentrations in Delhi based on our first installation of ENFUSER there.

34.4 Conclusions

We presented the FMI-ENFUSER system and demonstrated its capability to fuse hourly pollutant concentrations in an urban area. The presented approach that combines statistical air quality modelling, dispersion modelling and data fusion algorithms offers several advantages: a priori emission inventories are not necessary required since the model can be calibrated with historical data. Most important GIS-datasets as well as regional air quality data are openly available globally. And finally, with the modelling system high resolution air quality output can be produced in near real time using relatively low-cost computations.

FMI-ENFUSER was demonstrated in Langfang together with a newly established sensor network. While the pollutant concentrations are generally much larger in China, the same calibration routines can be applied and the model is able to distinguish the relationships between observed pollutant concentrations, meteorological conditions and GIS-properties.

FMI-ENFUSER model was also successfully installed with offline modelling capabilities for Delhi. In the future ENFUSER model could be used also operatively in Delhi, but additional work towards this goal is needed especially for Near Real

Time access of meteorological data (ECMWF or IMD) and FMI-SILAM regional AQ data. Further, it would be highly beneficial to investigate more thoroughly the main sources for local emissions in Delhi. Once identified, a more comprehensive and realistic set of emission source categories can be introduced to the model via various GIS-datasets.

Acknowledgements This work was supported and funded by TEKES SHOK/CLEEN MMEA and INKA-ILMA/EAKR projects.

Question and Answer

Questioner: Peter Viaene
Question: Do you have any plans to extend this system to a planning/scenario tool?
Answer: Yes. That will happen in a near future. The current version of EnFuser is not directly applicable to planning and scenario runs, but adding an option for feeding in artificial/generated data for scenarios will make the model applicable planning too.

References

Jalkanen J-P, Johansson L, Kukkonen J, Brink A, Kalli J, Stipa T (2012) Extension of an assessment model of ship traffic exhaust emissions for particulate matter and carbon monoxide. Atmos Chem Phys 12:2641–2659

Johansson L, Epitropou V, Karatzas K, Karppinen K, Wanner L, Vrochidis S, Bassoukos A, Kukkonen J, Kompatsiaris I (2015a) Fusion of meteorological and air quality data extracted from the web for personalized environmental information services. Environ Model Softw (Elsevier) 64(2015):143–155

Johansson L, Karppinen A, Loven K (2015b) Evaluation of air quality using dynamic land-use regression and fusion of environmental information. In: Proceedings of the 2nd international workshop on environmental multimedia retrieval. ACM New York, NY, USA, pp 33–38. ISBN: 978-1-4503-3558-4

Johansson L, Karppinen A, Dong L (2016) Development of air quality modelling system in Langfang based on sensor measurements and data fusion. In: Lappalainen H, Borisova A, Liang D, Enroth J, Kulmala M (eds) Report series in aerosol science, no 180. Helsinki, pp 205–210

Sofiev M, Vira J, Kouznetsov R, Prank M, Soares J, Alves Antunes J, Genikhovich E (2015) Construction of the SILAM Eulerian atmospheric dispersion model based on the advection algorithm of Michael Galperin. Geosci Model Dev 8:3497–3522. doi:10.5194/gmd-8-3497-2015

Chapter 35
Assimilating Anthropogenic Heat Flux Estimated from Satellite Data in a Mesoscale Flow Model

Theodoros Nitis, George Tsegas, Nicolas Moussiopoulos and Dimitrios Gounaridis

Abstract The need for comprehensive prognostic meteorological models is paramount in various applications related to environmental assessment. The inclusion of urban land cover in the computational domain in mesoscale models introduces new challenges for accurately incorporating the complex interactions related to the dynamical and thermal effects of the urban canopy. Aiming to address these requirements, a new urban surface scheme was introduced in a mesoscale meteorological model incorporating parameterisations of the area-averaged effects of drag and turbulence production as well as an improved representation of the surface heat and moisture fluxes. In addition, an advanced data assimilation module was implemented for enabling the self-consistent estimation of anthropogenic heat fluxes on the basis of representative satellite data, as well as the introduction of resulting forcing in the surface energy budget. The enhanced version of the model was evaluated in two mesoscale applications covering the greater urban areas of Paris, France and Athens, Greece. The model was evaluated over the course of three periods of strong anticyclonic conditions, enabling a better assessment of the influence of urban effects. The results confirmed that the urban surface module enhancements led to a significant improvement of model performance.

T. Nitis (✉) · G. Tsegas · N. Moussiopoulos
Laboratory of Heat Transfer and Environmental Engineering,
Aristotle University, 54124 Thessaloniki, Greece
e-mail: theonitis@aegean.gr

G. Tsegas
e-mail: gtseg@aix.meng.auth.gr

N. Moussiopoulos
e-mail: moussio@eng.auth.gr

T. Nitis
Laboratory of Environmental Quality and Geospatial Applications,
Department of Marine Sciences, University of the Aegean,
81100 Mytilene, Lesvos, Greece

D. Gounaridis
Department of Geography, University of the Aegean, 81100 Mytilene, Lesvos, Greece
e-mail: gounaridis.d@geo.aegean.gr

C. Mensink and G. Kallos (eds.), *Air Pollution Modeling and its Application XXV*,
Springer Proceedings in Complexity, DOI 10.1007/978-3-319-57645-9_35

Finally, the assimilation of anthropogenic heat data in the model provided an improved capability of reproducing the observed spatial and temporal variation of surface temperature.

35.1 Introduction

Human activities and the consequent alterations of the land characteristics which lead to urban growth is a worldwide phenomenon. This rapid increase of urbanization has a significant influence on the surface energy and water moisture balance, affects the local atmosphere boundary layer structure and urban microclimate and has an impact on the quality of urban life (Chen et al. 2009). Anomalies in surface heating, moisture availability and surface roughness could be also induced in distances from several to 100 km, affecting mesoscale circulations and the Atmospheric Boundary Layer (ABL) structure. Urban warming, or the urban heat island (UHI), and the associated circulation is a result of man-made modifications of the surface energy balance (SEB). Anthropogenic heat release is one of the most important causes of the UHI and it impacts urban ABL (Falasca et al. 2016). Several parameterisation schemes of anthropogenic heat release have been suggested for numerical modeling in urban areas. The objective of this paper is to develop a methodology for estimating anthropogenic heat as well as the investigation of the influence of surface parameters appearing in the SEB terms (albedo, thermal inertia, and anthropogenic heat flux) and mechanical parameters (roughness length) on the structure of the ABL over urban areas.

35.2 Surface Parameterisation and Anthropogenic Flux

The Greater Athens and Paris Areas (GAA & GPA) were selected as case studies (Fig. 35.1) for validating the system as typical cases of complex and simple topographical configurations, respectively. The meteorological periods selected were (a) for the GAA: 23–24/6/2002, 29–30/6/2002 and 19–20/9/2002 and (b) for the GPA: 1–2/7/1999, 16–17/7/1999 and 28–29/7/1999. The non-hydrostatic mesoscale meteorological model MEMO was used (Moussiopoulos 1995).

Mesoscale models require a variety of input data whose collection might be inaccurate or costly. Remote sensing data provide a great advantage, due to their high spatial/temporal resolution and rich spectral content. In this study, a comprehensive input database was developed by remote sensing image processing. A detailed orography dataset was derived from the Shuttle Radar Topography Mission—SRTM/90 m database. The landuse dataset originated from the Corine Land Cover 2000 (CLC 2000) database, which includes 44 landuse (LU) types. In this study, the original LU types were reclassified to (a) seven LU types, traditionally used in MEMO applications (scheme-1) and (b) eleven LU types for a more

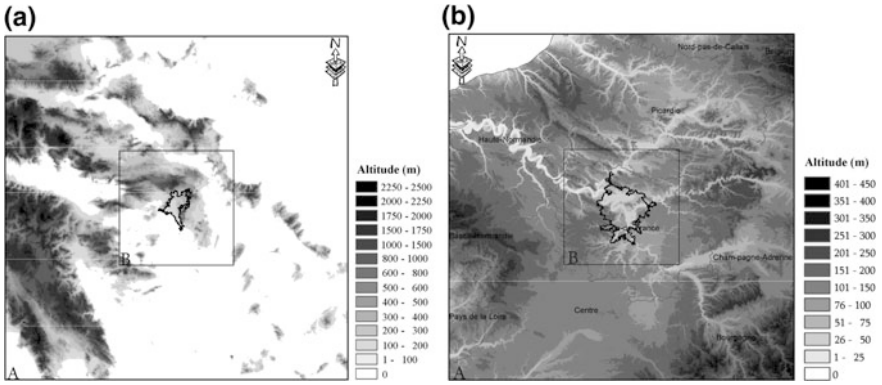

Fig. 35.1 Configuration of nested grids for **a** Greater Athens Area and **b** Greater Paris Area. The outer frame indicates the coarse grid and the inner the fine domain

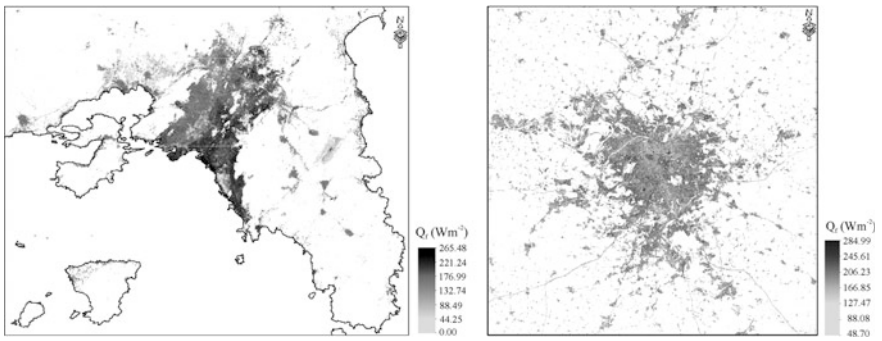

Fig. 35.2 Anthropogenic heat spatial distribution for GAA (26 July 2001) and for GPA (24 August 2000)

accurate representation of the urban environment (scheme-2). Initial night time Land and Sea Surface Temperatures were derived from the Moderate-resolution Imaging Spectro-radiometer (MODIS) instruments. Finally, the roughness length was derived by the application of simple empirical relationships between satellite radiometry and vegetation physiology (Nitis 2016).

Anthropogenic heat (Q_f) and moisture emissions vary significantly both in time and space, and are not readily measured nor calculated. In urban areas, Q_f is difficult to be quantified directly and accurately. In this study, the anthropogenic heat discharge was estimated based on the urban canopy energy balance equation and use of combined advanced spaceborne thermal emission and reflection radiometer remote-sensing data and ground meteorological data (Nitis 2016). The results are shown in Fig. 35.2 for typical summer days with a spatial resolution of 30 m.

In the GAA, values range from 0–265 Wm^{-2} with a mean value of 149 Wm^{-2}. In the GPA, maximum values for Q_f reach 285 Wm^{-2} with a mean value of

197 Wm^{-2}. It should be noted that over dense urban fabric, maximum Q_f values are strongly dependent on the spatial resolution.

35.3 Model Results

The MEMO model performance was evaluated and the two landuse schemes were compared for the wind speed and direction and temperature at specific meteorological stations for the periods under study. A satisfactory performance of the model was shown for all cases. The spatial distribution of the median daily fluctuation of hourly temperature values for GAA is shown in Fig. 35.3 for the entire calculation period and for 29 June 2002. The appearance of a strong temperature differential between the urban and the surrounding rural areas can be noted, which is about 3 K. The spatial maximum of the median calculated hourly temperatures for the entire study period is 302.63 K while its spatial average amounts to 299.13 K, with spatial temperature maxima consistently located in the central and south-central parts of the urban area. Results for the 29 June also indicate a systematic cooling of the Mesogeia area in the eastern part of the Attica peninsula. In contrast, the heavily-industrialised Elefsis bay area in the west appears to be warmer than the domain average.

In Fig. 35.4, the spatial distribution of the median hourly temperature for GPA is shown for the entire calculation period and for 28 July 1999. An increase of the temperature spatial maximum by 3.1 K is observed. Outside the central urban area, several individual maxima can be noted, corresponding to sub-urban centres. On 28 July 1999, a shift of the spatial temperature distribution towards the west-southwest can be seen, reaching even low-Q_f areas of urban green. This trend is consistent with a displacement of the urban plume along the direction of the prevailing

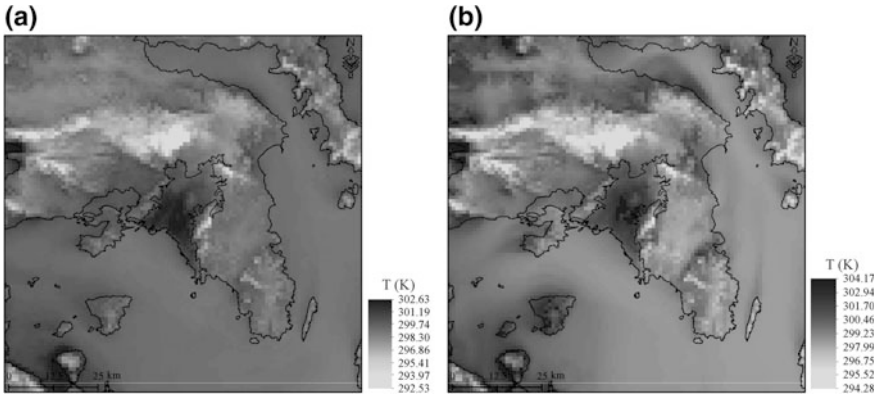

Fig. 35.3 Spatial distribution of the median daily fluctuation of hourly temperature values for the fine domain in GAA **a** for all periods under study and **b** for 29 June 2002 for the scheme-2

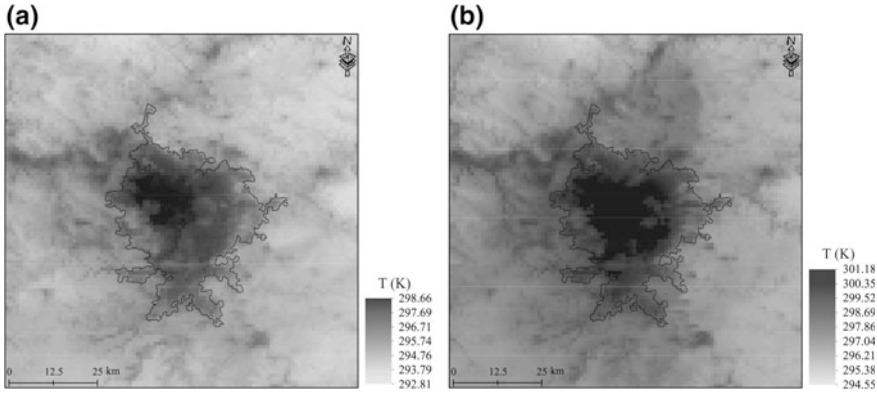

Fig. 35.4 Spatial distribution of the median daily fluctuation of hourly temperature values for the fine domain in the GPA **a** for all the periods under study, **b** for 28 July 1999 for the scheme-2

east-northeast winds during most of this day. The calculated temperature maximum is 301.18 K with a spatial average of 298.98 K for the urban area, corresponding to an average UHI intensity of 3 K.

35.4 Conclusion

The main goal of this study was to describe the effects of the incorporation of Q_f in the model calculations and its impact on the boundary layer structure over high populated areas. The results showed that the model performance is satisfactory in simulating the mesoscale fields reasonably well. The introduction of Q_f in the model calculations indicated a significant improvement in the simulation of nighttime UHI, by consistently predicting an early-nighttime urban-rural temperature differential of 1–4 K. In the case of Paris, however, the lack of an explicit heat storage scheme is considered to prevent an accurate prediction of UHI during the early-morning hours.

Questions and Answers

Questioner: Peter Viaene (VITO)
Question: Did you in some way check/ensure consistency between the data sources use (eg Corine/AVHRR Albedo)?
Answer: The main aim of this paper was to underline the importance of a simple parametrisation and inclusion of thermophysical parameters from satellite data with a high spatial and temporal resolution, which could lead to an improvement of the

performance of the Mesoscale Meteorological Model. Based on this idea we used satellite data originating from the European Environment Agency (EEA), the United States National Aeronautics and Space Administration (NASA) and German Aerospace Center (DLR), who have already carried out extensive quality control of their products.

Questioner: Silvana Di Sabatino (Univ. of Bologna)
Question: Have you compared your method for anthropogenic heat flux with other existing methods? What is new in the method? Does it bring a new insight in the way we deal with Urban Heat Island (UHI)?
Answer: There are many methods in order to estimate the anthropogenic heat flux over urban areas. These can be classified in three basic categories:

(a) In situ measurements. The estimations are based on the surface energy balance equation and depend on field measurements of the energy fluxes.
(b) Inventory approach. This method depends on measuring energy consumptions to estimate the heat emission flux.
(c) Remote-sensing. In this approach, which was adopted in this paper, the anthropogenic heat is estimated as a residual term of the surface energy balance equation. Compared with the previous two methods, this technique can obtain the heat flux as continuous fields of high spatial resolution.

The aim of this work was not the intercomparison of methods for estimating anthropogenic heat. We focused on the introduction of a new method which takes into account all potential sources of anthropogenic heat flux, is of low cost, can be applicable to any urban area around the world and therefore, can be suitable for Mesoscale Meteorological Model applications. Based on the results of the MEMO model application it can be concluded that this method can help in the determination of UHI; however, further research is need in order to assess the accuracy of the method.

References

Chen Y, Jiang WM, Zhang N, He XF, Zhou RW (2009) Numerical simulation of the anthropogenic heat effect on urban boundary layer structure. Theor Appl Climatol 97:123–134

Falasca S, Catalano F, Moroni M (2016) Numerical study of the daytime planetary boundary layer over an idealized urban area: influence of surface properties, anthropogenic heat flux, and geostrophic wind intensity. J Appl Meteorol Climatol 55

Moussiopoulos N (1995) The EUMAC zooming-model, a tool for local-to-regional air-quality studies. Meteorol Atmos Phys 57:115–133

Nitis T (2016) An atmospheric environment management system incorporating the impact of urban areas and using geoinformatics. PhD thesis, Aristotle University Thessaloniki, Thessaloniki, 191 p

Chapter 36
An Integrated Data-Driven/Data Assimilation Approach for the Forecast of PM10 Levels in Northern Italy

C. Carnevale, G. Finzi, A. Pederzoli, E. Turrini and M. Volta

Abstract The EU Air Quality Directive 2008/50/EC recommends member states to ensure that timely information about actual and forecasted levels of pollutant concentrations are provided to the public. In order to follow these guidelines, prevent critical episodes and inform the public, environmental authorities need fast and reliable real time alarm systems. In this work, a performance comparison of different data driven model families has been performed using information provided by more than 100 monitoring stations in Northern Italy. The different models include linear (auto-regressive), non-linear (neural network), time variant (lazy learning) methods and their ensemble. Moreover, their inability to perform forecast where no monitoring stations are available is known as one of the main limitations related to this kind of models. To address this issue, an optimal interpolation technique has been introduced to integrate daily PM10 forecasted concentrations with the results of a deterministic chemical transport model, extending the forecast from the monitoring network sites to the whole area of interest. The validation shows very good performances for all stations, with high agreement in both mean value and 95th percentile computed over the whole year, a correlation coefficient usually higher than 0.7 and small values of root mean square error.

36.1 Introduction

Over recent years, the high level of PM10 concentrations measured across Europe have become an important problem due to its effect on human health. In particular, the effects of PM10 exposure include respiratory diseases, hearth failure and immune disorders (Pope III et al. 2008).

To warn the public about daily levels of pollutant concentration, the EU directive recommends member states to ensure that timely information about actual and forecasted levels of pollutants are provided.

C. Carnevale · G. Finzi · A. Pederzoli · E. Turrini (✉) · M. Volta
University of Brescia, Brescia, Italy
e-mail: enrico.turrini@unibs.it

C. Mensink and G. Kallos (eds.), *Air Pollution Modeling and its Application XXV*,
Springer Proceedings in Complexity, DOI 10.1007/978-3-319-57645-9_36

The forecast of secondary air pollutants concentrations is a challenging task as it involves non-linear relationships and uncertain variables. A possible solution of the problem can be the use of data driven statistical models (Pisoni et al. 2009).

Point-wise data driven statistical models describe a particular phenomenon in terms of a mathematical relationship between input and output, without considering its physics and chemistry processes. They usually require lower computational effort to be run than deterministic models and can reach good performances, but they give information only where data are actually collected, i.e. in the monitoring station locations. In this work, an integrated modelling system for the forecast of daily mean PM10 concentrations is presented. The system integrates data driven models based on artificial neural networks, lazy learning, regression tree and deterministic model simulation results applying an optimal interpolation technique. The methodology has been applied to a Northern Italy domain, known as one of the most polluted and industrialized area in Europe, for year 2008.

36.2 Methodology

The implemented integrated modeling system consists of two main parts:

- A set of data driven models performing the point-wise forecast at each monitoring location;
- A geospatial interpolation algorithm performing the optimal interpolation of the forecasts over a gridded domain.

The data driven models are responsible to provide point-wise forecast at the location X of the monitoring stations:

$$PM10(X,t+1) = f(X, \overline{PM10}(t), \ldots, \overline{PM10}(t-n), \overline{\overline{PM10}}(t), \ldots, \overline{\overline{PM10}}(t-n) \tag{36.1}$$

where $PM10(X,t+1)$ is the forecasted value of PM10 at location X and time t + 1, $\overline{PM10}(t)$ is the measured value of PM10 at location X and time t (autoregressive part), $\overline{\overline{PM10}}(t)$ is the measured value of PM10 at the location closest to X and time t (exogenous part), n is the order of the autoregressive part, m is the order of the exogenous part and f is the data driven model linking input and output.

In this work, the function f is defined using 3 different model family for n and m ranging from 1 to 3 (1) Feedforward Neural Network (Pisoni et al. 2009), (2) Lazy Learning models (Carnevale et al. 2016) and (3) Regression Tree models (Prassad et al. 2006). Moreover, two different ensembles of the models are computed: (1) the average among the forecasts of the models and (2) the weighted average among the forecasts of the models with weights equal to the values of the correlation coefficients on the validation dataset.

The second phase of the forecasting systems is performed through Optimal Interpolation (Carnevale et al. 2014). In this procedure, the re-analyzed fields x_a is computed as the best linear unbiased estimator (BLUE):

$$x_a(\mathrm{t}+1) = \mathrm{x}_b(\mathrm{t}_b) + \mathrm{K}[\mathrm{PM10}(\mathrm{t}+1) - \mathrm{Hx}_b(\mathrm{t}_b)] \tag{36.2}$$

where $x_a(t+1)$ is the analysis field which can be considered as the best possible estimate of a certain pollutant concentration over a certain domain at time t, $x_b(t_b)$ is the raw (model) field that can have a temporal resolution different with respect to the point-wise forecast, $PM10(t+1)$ is the point-wise forecast vector, H is a linear operator mapping the raw model field into the observation space and the gain vector K is computed as:

$$K = BH^T(HBH^T + R)^{-1} \tag{36.3}$$

where B and R are the model and point-wise forecast covariance, respectively.

36.3 The Case Study

The methodology has been applied over a domain covering the whole Northern Italy (Fig. 36.1), with a resolution of 6 × 6 km^2, for the entire 2008 year. This area is often affected by very high PM10 concentrations both in winter and summer seasons. The measurement data of years 2000–2007 (identification/training) and 2008 (validation/test) have been collected from the AIRBASE database (http://acm.eionet.europa.eu/databases/airbase/) for around 200 stations, while the background fields for optimal interpolation are monthly PM10 means computed over the study domain by taking the output of different simulations performed with the TCAM model (Carnevale et al. 2014) in the frame of the POMI exercise (http://ies-webarchive.jrc.ec.europa.eu/POMI/).

Figure 36.2 presents the boxplot of correlation coefficient (a) and rmse (b) values for the models and their ensemble. All tested models present acceptable results both in terms of correlation (median greater than 0.7) and RMSE (around 15 μgm^3). Moreover, the impact of the ensemble is particularly important for the weighted. This ensemble has statistical indexes comparable to those of the best model family in terms of median, a lower variability of the results (actually the differences between 75th and 25th are smaller).

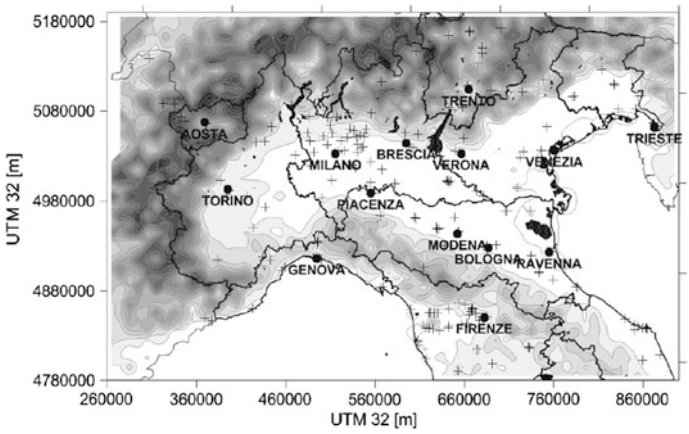

Fig. 36.1 Test case domain, with monitoring stations locations (crosses)

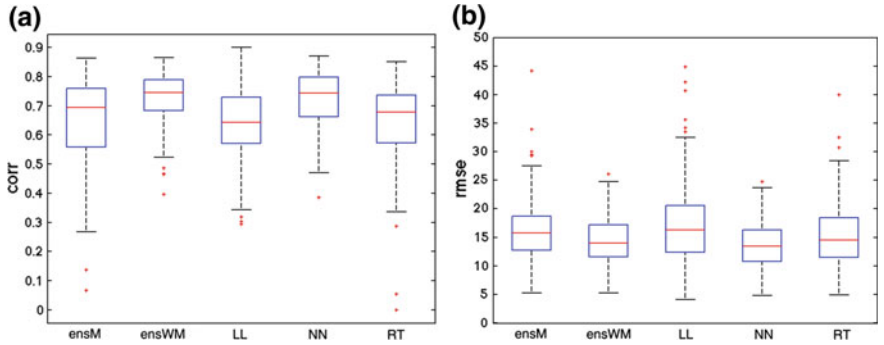

Fig. 36.2 Correlation coefficient (**a**) and RMSE (**b**) boxplot for the tested models and their ensemble

36.4 Conclusions

The paper presents the formalization and the first application of a new technique for the forecast of PM10 levels over a mesoscale domain. The application, performed for a Northern Italy domain for year 2008 shows good performances. Even if a lot of work has still to be carried out, the presented methodology can be considered a fast and acceptable solution for the need of Regional Authorities to provide future pollution levels information to the population.

Questions and Answers

Questioner: Luca Delle Monache
Question: How do you estimate the error covariance matrix B?
Answer: The error covariance matrix B, as well as the matrix R, have not been computed directly, but their ratio have been used to "tune" the model according to the relative reliability that the modeller gives to the forecast and the CTM model results. More work on the sensitivity on this parameter will be performed.

Questioner: Luca Delle Monache
Question: How do you generate the ensemble?
Answer: Two ensemble techniques have been tested. One is the simple mean among the forecasts for year 2008 of all the different Data Driven Models identified. The other one is a weighted mean of the same forecasts, where the weights are equal to the values of the correlation coefficients on the validation dataset.

Questioner: Luca Delle Monache
Question: Have you verified the ensemble also for probabilistic predictions, i.e. not only for the ensemble mean?
Answer: So far, no verification for probabilistic predictions has been performed. The work is the first step of a more comprehensive project where we will surely follow the suggestion.

Questioner: Peter Viaene
Question: How did you select the data for the validation?
Answer: The measurement data for years 2000–2007 have been used for identification/training and 2008 for validation/test.

References

Carnevale C, Finzi G, Pederzoli A, Pisoni E, Thunis P, Turrini E, Volta M (2014) A methodology for the evaluation of re-analyzed PM10 concentration fields: a case study over the PO valley. Air Qual Atmos Health 8(6):533–544

Carnevale C, Finzi G, Pederzoli A, Turrini E, Volta M (2016) Lazy learning based surrogate models for air quality planning. Environ Model Softw 83:47–57

Pisoni E, Farina M, Carnevale C, Piroddi L (2009) Forecasting peak air pollution levels using NARX models. Eng Appl Artif Intell 22(4–5):593–602

Pope CA III, Renlund DG, Kfoury AG, May HT, Horne BD (2008) Relation of heart failure hospitalization to exposure to fine particulate air pollution. Am J Cardiol 102(9):1230–1234

Prasad AM, Iverson LR, Liaw A (2006) Newer classification and regression tree techniques: bagging and random forests for ecological prediction. Ecosystems 9(2):181–199

Chapter 37
Data Interpolating Variational Analysis for the Generation of Atmospheric Pollution Maps at Various Scales

Fabian Lenartz, Charles Troupin and Wouter Lefebvre

Abstract Ordinary kriging is a widely used method to estimate the spatial distribution of atmospheric pollutants at all scales. However, more sophisticated strategies exist. For local mapping, where one often focuses on pollutants with a high spatio-temporal variability, such as nitrogen dioxide or black carbon, land use regression models are commonly used. In epidemiological research, several model reviews have already been published on this topic Hoek et al. (A review of land-use regression models to assess spatial variation of outdoor air pollution. Atmos Environ 42:7561–7578, 2008); Gaines et al. (A review of intraurban variations in particulate air pollution: Implications for epidemiological research. Atmos Environ 39:6444–6462, 2005). For regional mapping, de- and retreading procedures also make use of ancillary variables, such as the population density or the land use, to take into account the local characteristics of the sampling sites before and after the actual interpolation. Due to their low computational cost, these techniques can be implemented operationally Janssen et al. (Spatial interpolation of air pollution measurements using CORINE land cover data. Atmos Environ 42:4884–4903, 2008). In this study we introduce DIVA, a variational inverse method, originally designed for oceanographic applications, that allows one to take into account some new constraints. As it is based on a finite-element approach, physical boundaries such as buildings are naturally taken into account since they actually define the domain of interest. Another useful feature is the possibility to consider an advection field and hence propagate the information in the preferred direction. Finally, this technique also allows one to attribute a different weight to each available measurement, according to the quality of the data, so that heterogeneous data sources, consisting for example of monitoring network, passive sampler and mobile device

F. Lenartz (✉)
ISSeP, Rue Du Chéra 200, 4000 Liège, Belgium
e-mail: f.lenartz@issep.be

C. Troupin
SOCIB, Parc Bit, Naorte, Bloc a 2ºp. Pta. 3, 07121 Palma de Mallorca, Spain

W. Lefebvre
VITO, Boeretang 200, 2400 Mol, Belgium
e-mail: wouter.lefebvre@vito.be

C. Mensink and G. Kallos (eds.), *Air Pollution Modeling and its Application XXV*,
Springer Proceedings in Complexity, DOI 10.1007/978-3-319-57645-9_37

values, can be used simultaneously and consistently. The model will be tested for two situations: the mapping of NO_2 in the Walloon Region and the air pollution assessment of year 2012 in Antwerp. Results will be qualitatively compared with those of operational models: an ordinary kriging method run at AwAC by Bonvalet et al. (Validation of a geostatistical interpolation model using measurement of particulate matter concentration, Matinée des chercheurs à l'Université de Mons 2013) and a detrended kriging run at ISSeP and originally implemented by Merbitz (Untersuchung und Modellierung der raumzeitlichen Variabilität urbaner und regionaler Feinstaubkonzentrationen. Ph.D. thesis 2013) for the first case, and the RIO-IFDM-OSPM modelling system for the second case as implemented by Maiheu et al. (Luchtkwaliteitsmodellering Ringland, Studie uitgevoerd in opdracht van Stramien cvba en Ring genootschap vzw 2015/RMA/R/13 2015).

37.1 Introduction

At this time, geosciences have to take advantage of the numerous real time measurements that become available. In the domain of air quality, the use of mobile devices or monitoring networks of low-cost sensors providing georeferenced data at a high spatio-temporal resolution is already popular for exposure studies or city-scale pollution assessments, and it will probably not be long before most of them are smartphone-based. Nevertheless, to the extent of my knowledge, such dense information is rarely integrated into a model via data assimilation techniques because of the high computational cost, and the visualization of these records usually consists in simply displaying big colored dots at the sampling locations, sometimes superimposed on an interpolated field. Some of the reasons for this limited treatment are that (i) for many methods the number of operations is proportional to the number of data points cubed (N_d^3); (ii) in cities, where one usually sets up close-knit networks or itinerant campaigns, the physical boundaries play an important role in the pollutant dispersion (see Fig. 37.1); (iii) the air quality measurement community often warns about the relatively poor quality of these sensors, in comparison with the official national or regional monitoring networks. In this study, we introduce DIVA, an approximation technique that tackles, at least partly, these problems.

37.2 Material and Method

DIVA, which stands for Data-Interpolating Variational Analysis, is designed to solve 2-D differential or variational problems of elliptic type with a finite-element method. Here we work with the anomaly field φ', obtained by subtraction of the background field φ_b from the original one φ. This allows our data set to be closer

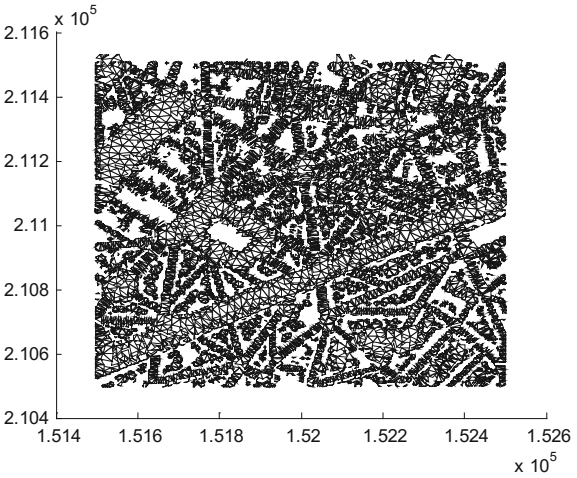

Fig. 37.1 Finite-Element mesh for one of the 1 km × 1 km area of Antwerp in which DIVA operates

from the assumed normal distribution. However, for readability reasons we drop the' superscript from now on. Here is its mathematical formulation:

$$J[\varphi] = \sum_{j=1}^{N_d} \mu_j \left[d_j - \varphi\left(x_j, y_j\right)\right]^2 + \|\varphi\|^2$$

with

$$\|\varphi\| = \int_D \left(\alpha_2 \nabla\nabla\varphi : \nabla\nabla\varphi + \alpha_1 \nabla\varphi . \nabla\varphi + \alpha_0 \varphi^2\right) dD$$

where α_0 penalizes the field itself, α_1 gradients, α_2 variability and μ data-analysis misfits (Troupin et al. 2012; Troupin et al. 2013). The considered data sets are (i) the NO_2 hourly measurements of the Walloon official monitoring network for the years 2010–2015; (ii) the multi-parameter intensive measurement campaign led in the city of Antwerp in 2012 (Lefebvre et al. 2016).

37.3 Results

For Wallonia, results provided by DIVA combined with an a priori land-use regression on one hand, and ordinary kriging on the other hand, display very large differences. However, the latter are mainly due to the proxy, which accounts for the station direct environment fingerprint (Fig. 37.2). For the Antwerp test case, the method was found not to be adequate in its actual set-up. It has shown some limitations due to the high spatial resolution required for the mesh to include the

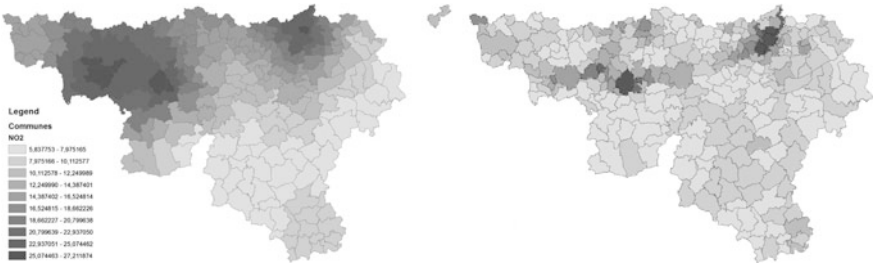

Fig. 37.2 Average NO_2 concentration in Wallonia for the period 2011–2013 obtained via ordinary kriging (*upper panel*) and DIVA combined with land-use regression (*lower panel*)

physical barrier of street canyons. Since DIVA's computational load is proportional to $N_a^{5/2}$ where Na is the number of grid points, working at these scales is problematic, without additional treatments.

Acknowledgements We would like to thank AwAC (Air and Climate Walloon Agency) and VITO (Flemish Institute for Research and Technology) for sharing their data sets with us. We are also grateful to Virginie Hutsemekers who has performed and is going to perform some additional comparison exercises, as well as to Simon Vermeulen who is setting up a new campaign to validate the method.

Question and Answer

Question: Have you considered introducing anisotropic variogram/covariance in order to facilitate preferential propagation of concentrations e.g. along the direction of streets?
Answer: In DIVA, the covariance function is not explicitly defined, but is the result of the minimization of the cost function. In particular case (infinite domain, specific values for the coefficients), it is possible to compute an analytical solution to the problem, which is an isotropic function (modified Bessel function). When the advection constraint is activated, the covariance is indeed increased in the direction of the flow, even though the covariance function doesn't have to be explicitly defined.

References

Bonvalet L, Marijns A, Coussement G, Passlecq C (2013) Validation of a geostatistical interpolation model using measurement of particulate matter concentration, Matinée des chercheurs à l'Université de Mons

Gaines Wilson J, Kingham S, Pearce J, Sturman AP (2005) A review of intraurban variations in particulate air pollution: Implications for epidemiological research. Atmos Environ 39:6444–6462

Hoek G, Beelen R, de Hoogh K, Vienneau D, Gulliver J, Fischer P, Briggs D (2008) A review of land-use regression models to assess spatial variation of outdoor air pollution. Atmos Environ 42:7561–7578

Janssen S, Dumont G, Fierens F, Mensink C (2008) Spatial interpolation of air pollution measurements using CORINE land cover data. Atmos Environ 42:4884–4903

Lefebvre W, Hooyberghs H, Janssen S, Maiheu B (2016) Description of data delivered in the framework of the Fairmode exercise on spatial representativeness—Final report, Study accomplished under the authority of 2016/RMA/R/053

Maiheu B, Vranckx S, Lefebvre W, Janssen S (2015) Luchtkwaliteitsmodellering Ringland, Studie uitgevoerd in opdracht van Stramien cvba en Ring genootschap vzw 2015/RMA/R/13

Merbitz H (2013) Untersuchung und Modellierung der raumzeitlichen Variabilität urbaner und regionaler Feinstaubkonzentrationen. Ph.D. thesis

Troupin C, Sirjacobs D, Rixen M, Brankart J-M, Barth A, Alvera-Azcárate A, Capet A, Ouberdous M, Lenartz F, Toussaint M-E, Beckers J-M (2012) Generation of analysis and consistent error field using the data interpolating variational analysis (Diva). Ocean Model 52–53:90–101. doi:10.1016/j.ocemod.2012.05.002

Troupin C, Ouberdous M, Sirjacobs D, Alvera-Azcárate A, Barth A, Toussaint M-E, Watelet S, Beckers J-M (2013) Diva user guide. http://www.modb.oce.ulg.ac.be/mediawiki/index.php/Diva_documents

Chapter 38
Is the Recent Decrease in Belgian Air Pollution Concentration Levels Due to Meteorology or to Emission Reductions?

Wouter Lefebvre, Bino Maiheu, Hans Hooyberghs and Frans Fierens

Abstract Recent years have shown significant decrease in concentrations levels of particulate matter (PM_{10}) and nitrogen dioxide (NO_2) in Belgium. For ozone (O_3), no such trend is found. Recent years, however, did not feature many periods with unfavourable meteorological dispersion conditions, casting some ambiguity on the underlying reasons for the decrease. This study tries to separate the impact of weather effects from emission reductions in the long-term trend. We build a statistical model explaining the daily averaged concentrations based on 32 meteorological parameters, the day of the week, the month of the year and the year itself, for the period 2004–2014. The 32 meteorological parameters are those considered to train the neural network prediction model OVL. Many of these meteo variables have only a small predictability and are intercorrelated with each other. Therefore, only those meteo parameters are used that have a significant impact on concentration levels. This procedure is applied for the complete time series and for each air quality monitoring location separately. In order to avoid overfitting, the same analysis is done, restricted to the data of even-numbered years, and the regression is then applied to the odd-numbered years. It is shown that the statistical parameters remain reasonably constant, which proves that the amount of overfitting is not significant. The results show, on average over all measurement locations, a range of yearly meteorological effects of 1.9 $\mu g/m^3$ for NO_2, 3.1 $\mu g/m^3$ for PM_{10} and 2.7 $\mu g/m^3$ for O_3. Meteorology combined with the residuals of the statistical fit show a range of 1.2 $\mu g/m^3$ for NO_2, 2.9 $\mu g/m^3$ for PM_{10} and 4.4 $\mu g/m^3$ for O_3. Finally, the long-term trend shows a range of 5.3 $\mu g/m^3$ for NO_2, 11.1 $\mu g/m^3$ for

W. Lefebvre (✉) · B. Maiheu · H. Hooyberghs
VITO, Boeretang 200, 2400 Mol, Belgium
e-mail: wouter.lefebvre@vito.be

F. Fierens
IRCEL/CELINE, Kunstlaan 10-11, 1210 Brussels, Belgium

C. Mensink and G. Kallos (eds.), *Air Pollution Modeling and its Application XXV*,
Springer Proceedings in Complexity, DOI 10.1007/978-3-319-57645-9_38

PM_{10} and 2.3 μg/m^3 for O_3, with clearly decreasing trends for NO_2 and PM_{10}, and an oscillating trend for O_3. Differences between rural, urban background, urban and industrial stations exist but are rather small. We can conclude that the major trend in air pollution (Belgium) is a long-term trend, linked to emission changes, and it can be expected that the concentration decreases of the last years will not suddenly disappear in the near future given unchanged policy. Furthermore, it can be concluded that emission reductions at the local, regional, European and worldwide scale are the dominant factors explaining the improvement of air quality.

38.1 Introduction

Recent years have shown significant decrease in concentrations levels of particulate matter (PM_{10}) and nitrogen dioxide (NO_2) in Belgium. For ozone (O_3), no such trend is found. Recent years, however, did not feature many periods with unfavourable meteorological dispersion conditions, casting some ambiguity on the underlying reasons for the decrease. This study tries to estimate the impact of weather effects on the long-term trend.

38.2 Methodology

We build a statistical model explaining the daily averaged concentrations based on 32 meteorological parameters, the day of the week, the month of the year and the year itself, for the period 2004–2014. The 32 meteorological parameters are those used to train the neural network prediction model OVL (Hooyberghs et al. 2005). The following model equation is used:

$$O_{s,t} = Mean + Meteo + Longterm\ trend + Rest = \overline{O_s} + \sum_{i=1}^{34} b_{i,s} P_{i,s}(m_{i,s,t}) + b_{Ts} P_{Ts}(T_t) + \varepsilon_{s,t}$$

As such, we try to decompose the daily average measurements of NO_2, O_3, PM_{10} and $PM_{2.5}$ in four components:

(1) A component with the long-term average (Mean), calculated based on the measurements;
(2) A component determined by the meteorology (Meteo), found by a linear regression of the measurements on a set of 32 meteorological parameters;
(3) A component explaining the long-term trend (Longterm trend), found by a linear regression of the measurements on the time of the measurement.
(4) A component unexplained by the regression (Rest).

However, many of the meteorological variables have only a small predictability and are intercorrelated with each other. Therefore, only those meteorological parameters are used that have a significant impact on concentration levels. We employed a procedure in which variables for which the regression was not significant were one by one dropped from the regression until all regression coefficients were significantly different from zero. This procedure is applied for the complete time series and for each air quality monitoring location separately. An example for one measurement location and one pollutant is shown in Fig. 38.1. In order to avoid overfitting, the same analysis is done, restricted to the data of even-numbered years, and the regression is then applied to the odd-numbered years. It is shown that the statistical parameters remain reasonably constant, which proves that the amount of overfitting is not significant (Table 38.1).

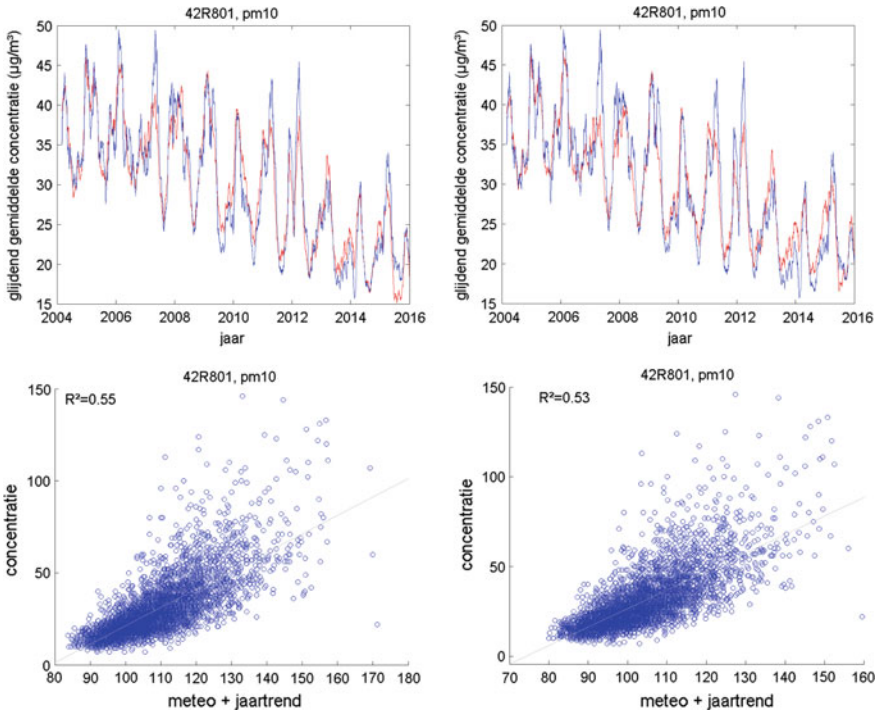

Fig. 38.1 Sixty-day running average measurements (*blue*) and regression (mean + meteorology + long-term trend, *red*) trained on the complete set (*left*) and on the even-numbered years for the measurement location of the urban background location 42R801 for PM_{10}. The lower part of the chart shows the scatter plot of the estimated concentrations on the real concentrations for the same station and the same training sets

Table 38.1 R^2 between daily average model results and measurements. The 'complete dataset' is the column with both training and validation datasets encompassing the complete dataset. The right column ('Validation') uses the even-numbered years as training set and validates on the odd-numbered years

Pollutant	Complete dataset	Validation
NO_2	0.59	0.63
O_3	0.66	0.64
PM_{10}	0.45	0.44
$PM_{2.5}$	0.55	0.51

38.3 Results

A summary of the results is shown in Fig. 38.2.

The meteorology has, for NO_2, a maximal effect of 1.8 μg/m^3. Although the meteorology has a positive effect on the concentration declines during the last years of the analysis, its standard deviation accounts only for 27% of the standard deviation of the measurements, indicating that this component is not of major importance. Including the residues in the meteorological part does not affect these results. The long-term trend for NO_2 is however quite strong, with a total effect of about 6.3 μg/m^3. This shows that the long-term trend of NO_2 is the main driver of the changes in annual concentrations of NO_2.

Similar results are found for PM_{10} with a maximal meteorological effect of 3.6 μg/m^3 and lower concentrations thanks to the meteorology during the more recent years. However, the standard deviation of the meteorology is only 24% of the standard deviation of the measurements. Including the residues, this number increases to 29%. This shows that the meteorological variability is not the main driver of the changes in PM_{10}-concentrations. On the contrary, the long-term trend goes up to 10.5 μg/m^3, explaining most of the variability of PM_{10}.

On the contrary, for O_3 the meteorological effect in the year-to-year variability is important. The effect on the yearly average concentration has a range of 4.3 μg/m^3 (64% of the standard deviation). The year-to year trend is oscillating with a range of at maximum 2.4 μg/m^3 and a standard deviation of only 29% of the total measurement standard deviation.

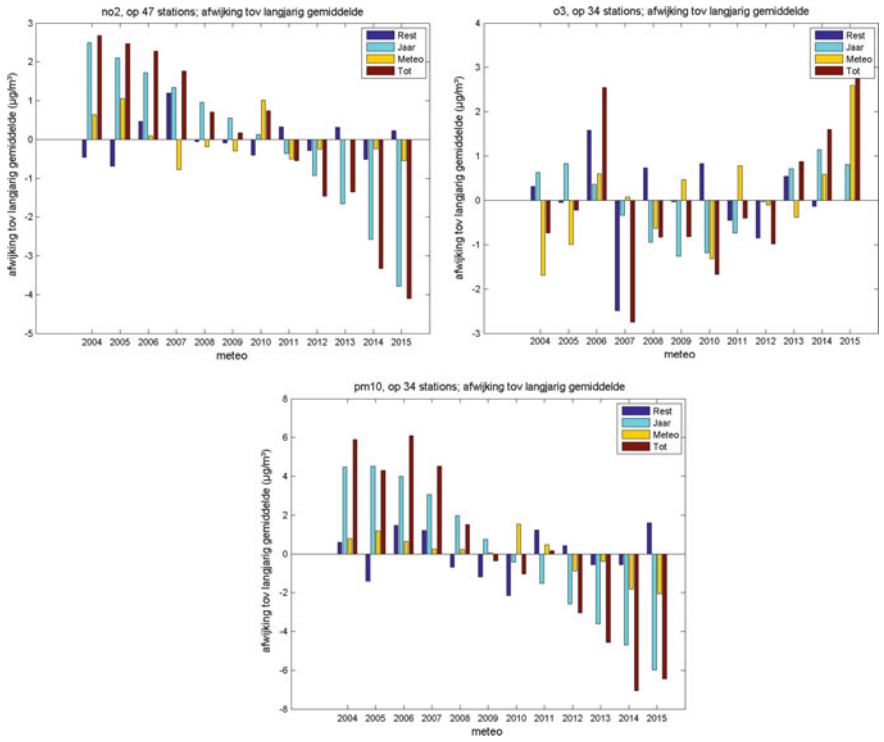

Fig. 38.2 Final results, averaged over all stations with enough data availability (at least 50% of period 2004–2015 available + at least one measurement per year; number of measurement locations is in the title of each figure) for the differet pollutants (NO_2, *upper left*; O_3, *upper right*; PM_{10}, *lower left*). *Light blue* part: due to the long-term trend; *Yellow*: due to meteorology; *Brown*: total trend; *Dark blue*: non-explained by regression. Y-axis in µg/m^3. X-axis: years. The colors in the Figure are linked to the corresponding colors in the equation

38.4 Conclusions

We conclude that most of the trends in air pollution in Belgium are long-term trends and thus emission changes and it can be expected that the concentration decreases will not change given unchanged policy. Furthermore, emission reductions at the local, regional, European and worldwide scale are the dominant factors explaining the improvement of air quality.

Questions and Answers

Questioner: Paul Makar
Question: I was wondering whether clouds, cloud rainfall were included in the set of meteo variables, since they would influence O_3 via photolysis rates?

Answer: The meteovariables (day of the week and month of the year are added later) that were taken into account are shown in the table below:

P1	2-m temperature
P2	30-m temperature
P3	10-m wind velocity
P4	10-m wind direction
P5	30-m wind velocity
P6	30-m wind direction
P7	Boundary layer height (corresponding to critical bulk Richardson = 0.5)
P8	Height of the layer where the transport length < 100 m
P9	Transport length at the first level (about 25-m height)
P10	Mean transport length in the layer 0–50 m (from the surface)
P11	Mean transport length in the layer 0–100 m
P12	Total cloud cover (range0 to 1)
P13	Low cloud cover (range0 to 1)
P14	Medium cloud cover (range0 to 1)
P15	High cloud cover (range0 to 1)
P16	Horizontal transport in the boundary layer
P17	Height of the layer where the transport length < 200 m
P18	Height of the layer where the transport length < 300 m
P19	Height of the layer where the transport length < 500 m
P20	Height of the layer where the transport length < 1000 m
P21	"S parameter" of Bultynck-Malet classification (multiplied by a factor 1000)
P22	"λ parameter" of Bultynck-Malet classificationLambda = LOG10(106 * ABS(S))
P23	Relative humidity (%) at 300-m height
P24	Relative humidity in the layer 0–50 m
P25	Relative humidity at 100-m height (not layer 0–100 m!)
P26	Wind velocity at 50-m height
P27	Wind velocity at 100-m height
P28	Wind velocity at 200-m height
P29	Wind velocity at 300-m height
P30	Wind velocity at 500-m height
P31	Wind velocity at 750-m height
P32	Wind velocity at 1000-m height

Cloud cover is thus taken directly into account, precipitation only with related variables (such as relative humidity).

Questioner: Tony Dore
Question: For analysis of trends, consistency in monitoring techniques is important. Your air concentrations showed more annual variability at the start of the time series. Has there been any change in quality control during the monitoring period?

Answer: There have been changes between monitoring techniques, and thus probably to associated quality control. However, at least for NO_2 and PM_{10}, these changes cannot account for the large trends that have been found in the results.

Reference

Hooyberghs J, Mensink C, Dumont G, Fierens F, Brasseur O (2005) A neural network forecast for daily average PM concentrations in Belgium. Atmos Environ 39:3279–3289. doi:10.1016/j.atmosenv.2005.01.050

Chapter 39
Modelling Air Quality and Deposition at High Resolution in the Netherlands with Plume and Grid Models

Eric van der Swaluw, Wilco de Vries, Massimo Vieno, Ferd Sauter, Jan Aben, Guus Velders, Roy Wichink Kruit, Hilde Fagerli and Addo van Pul

Abstract We present high resolution (1×1 km^2) modelling of air quality and deposition in the Netherlands. We use the OPS model, a combination of a Gaussian plume model for local processes and a Lagrangian trajectory model for long-range transport, to calculate these concentration and deposition maps. Earlier work has shown that the OPS model typically yields better results for precursor gases like NH_3 and NO_x, as compared to a Eulerian model, due to its higher resolution. However, for secondary aerosols Eulerian models perform better because in the OPS model the chemistry is strongly parameterized. Here we elaborate on this work, by making a comparison between the OPS model and the Eulerian model EMEP. The latter is run in an EMEP4NL configuration, in which the horizontal resolution can be increased to the same level as used for the OPS model, i.e. 1 km resolution. This allows for a valid assessment of the state of performance for precursor gases like NH_3 between the OPS model and a state-of-the-art Eulerian model.

39.1 Introduction

Modelling is an efficient and complementary way to measurements, which is necessary in order to maintain an integral air quality monitoring system. In the Netherlands, annual concentration and deposition maps of pollutants at 1 km

E. van der Swaluw (✉) · W. de Vries · F. Sauter · J. Aben · G. Velders · R. Wichink Kruit · A. van Pul
RIVM, PO Box 1, 3720 BA Bilthoven, The Netherlands
e-mail: Eric.van.der.Swaluw@rivm.nl

M. Vieno
Centre for Ecology and Hydrology, Penicuik, UK

H. Fagerli
EMEP MSC-W, Norwegian Meteorological Institute, Oslo, Norway

C. Mensink and G. Kallos (eds.), *Air Pollution Modeling and its Application XXV*,
Springer Proceedings in Complexity, DOI 10.1007/978-3-319-57645-9_39

resolution are produced (Velders et al. 2016) on a yearly basis, using a combination of calculations and measurements. The calculations are performed with the OPS model (Sauter et al. 2016), which is a Gaussian plume model approach for local applications with a Lagrangian trajectory model for long-range transport. Measurements are performed by the Dutch National Air Quality Monitoring Network (LML, Landelijk Meetnet Luchtkwaliteit, http://www.lml.rivm.nl/). The OPS model has a good performance on local scales for gas precursors. This was shown in a recent study, which compares calculations from OPS and the Eulerian chemistry transport model LOTOS-EUROS with measurements (van der Swaluw et al. 2017). It was also shown in this study that chemistry in the OPS model is in general less robust than in a Eulerian model, because it is strongly parameterized. In this paper, we elaborate on our previous study by presenting results of the OPS and EMEP model and their inter-comparison with measurements. The difference with the previous study is that for the results as presented in this project, the OPS and EMEP model will use the same horizontal resolution, i.e. 1 km.

39.2 The Motivation and Set-up for the EMEP and OPS Model Comparison

The EMEP model is the Eulerian atmospheric transport model (Simpson et al. 2012), which has been instrumental to the development of air quality policies in Europe since the late 1970s, and has become the reference tools for atmospheric dispersion calculations as input to the Integrated Assessment Modelling. The latter supports the development of air quality polices in the European Union (http://www.emep.int). Here we want to investigate how the performance of the OPS model for gas precursors compares with results from a Eulerian model, if the latter runs at a similar resolution as the OPS model. In order to make such a comparison, we launch the setup of an EMEP4NL model configuration. This set-up is similar as the one used for the United Kingdom, i.e. the EMEP4UK model, which was already demonstrated to run at high horizontal resolution (see e.g. Vieno et al. 2014). The emission dataset used for both models, OPS and EMEP4NL, is the same as the one used for the yearly production of concentration and deposition maps over the Netherlands (see e.g. Velders et al. 2016). Meteorology is treated in a different way in both models.

39.3 Results of the Comparison for NH_3

We present the first results from simulations with the EMEP4NL model (EMEP model version rv4.8) on a resolution of 2 km over the Netherlands for the months March, April and September 2009. We make a comparison with both OPS model results, and with measurements. The results presented in this paper are for ammonia and ammonium concentrations. The results with the OPS model are statistical,

in the sense that concentration values are calculated, for the different stability classes, and the *monthly averaged* values are obtained by summation of these values, weighted with their relative frequencies of occurrence.

The upper panel of Fig. 39.1 shows the NH_3 concentration for the months March, April and September of the year 2009 as calculated with the OPS model and

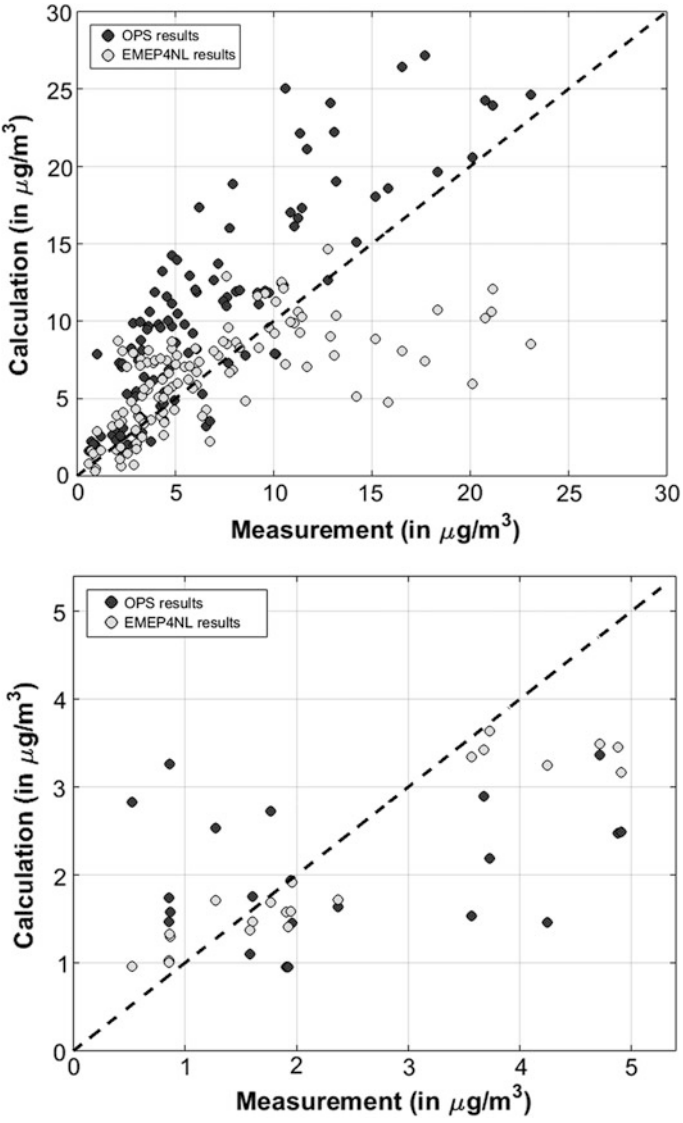

Fig. 39.1 A scatter plot of the measurement and calculation of NH_3 concentrations (*upper panel*) and NH_4 concentrations (*bottom panel*) in the Netherlands for the months March, April and September 2009 for the OPS model and the EMEP4NL model

the EMEP4NL model, compared with measurements. It can be seen that the OPS model is able to represent areas with high emissions of NH_3 (concentrations higher than 10 μg/m^3), whereas the EMEP4NL model is underestimating these areas. The latter is expected to improve if the resolution has been increased to 1 km, and the first vertical layer has been decreased. The OPS model on the other hand slightly overestimates the NH_3 concentrations in the range of 5–10 μg/m^3. The bottom panel of Fig. 39.1 shows the results for the ammonium aerosol: one can see that the EMEP4NL model is representing the measurements much more accurately than the OPS model, due to its better description of the atmospheric chemistry.

39.4 Conclusions and Outlook

A detailed comparison between results from the EMEP4NL and the OPS model at 1 km resolution for a couple of years, enables one to make a valid assessment of the performance of both models for NH_3 concentration and deposition of reduced nitrogen over the Netherlands. A comparison like this is of importance for the Netherlands, because the OPS model is used for policy-oriented applications like AERIUS, in which it serves as the calculation tool of the Integrated Approach to Nitrogen (PAS). The fast calculation times of the OPS model makes it a very efficient and applicable tool for these type of applications. An assessment with a state-of-the-art Eulerian model like EMEP would solidify its status as a valid calculation tool for policy-oriented applications like AERIUS.

References

Sauter F, van Zanten MC, van der Swaluw E, Aben J, van Jaarsveld H (2016) The OPS-model. Description of OPS 4.5.0. http://www.rivm.nl/media/ops/OPS-model.pdf

Simpson D, Benedictow A, Berge H, Bergström R, Emberson LD, Fagerli H, Flechard CR, Hayman GD, Gauss M, Jonson JE, Jenkin ME, Nyíri A, Richter C, Semeena VS, Tsyro S, Tuovinen J-P, Valdebenito Á, Wind P (2012) The EMEP MSC-W chemical transport model—technical description. Atmos Chem Phys 12:7825–7865

van der Swaluw E, de Vries W, Sauter F, Aben J, Velders G, van Pul A (2017) High resolution modelling of air pollution and deposition over the Netherlands with plume, grid and hybrid modelling. Atmospheric Environment 155:140–153 doi:10.1016/j.atmosenv.2017.02.009

Velders GJM, Aben JMM, Geilenkirchen GP, den Hollander HA, Megens L, van der Swaluw E, de Vries WJ, van Zanten MC (2016) Large-scale concentration and deposition maps the Netherlands report 2016, RIVM report 2016–0068

Vieno M, Heal MR, Hallsworth S, Famulari D, Doherty RM, Dore AJ, Tang YS, Braban CF, Leaver D, Sutton MA, Reis S (2014) The role of long-range transport and domestic emissions in determining atmospheric secondary inorganic particle concentrations across the UK. Atmos Chem Phys 14:8435–8447. doi:10.5194/acp-14-8435-2014

Chapter 40
Error Covariance Estimation Methods Based on Analysis Residuals and Its Application to Air Quality Surface Observation Networks

Richard Ménard and Martin Deshaies-Jacques

Abstract We review the method to estimate error variances based on analysis residuals in observation space, also known as the Desroziers method, and combine it with the maximum likelihood method to estimate correlation length scales. The theoretical foundation of this combined approach using a simplified and regular observation network has been studied in Ménard (2016). We then apply this method to the AirNow surface observation network of air quality observations using GEM-MACH as the model prior. In this application the challenge is to estimate spatially varying and non-stationary error statistics with a relatively small sample size. When using the statistics strictly at the station we observe that the scheme is usually non-convergent in the length-scale estimates. However by performing a local average of the analysis residuals statistics in the Desroziers' iterative scheme we resolve this issue. The resulting estimates are also compared with the locally averaged error variance estimates obtained from the Hollingsworth-Lonnberg method.

40.1 Theoretical Foundation of Error Statistics Estimation

40.1.1 Theorem on Error Covariance Estimates in Observation Space

Assuming that the observation and background errors are uncorrelated, the *necessary* and *sufficient* condition for error covariance estimates to be equal to the true observation and background error covariance in observation space is

$$1.\ \widetilde{\mathbf{HK}} = \mathbf{HK} \quad \text{the gain is equal to the Kalman gain in obs space} \tag{40.1}$$

$$2.\ \widetilde{\mathbf{D}} \stackrel{\triangle}{=} \widetilde{\mathbf{HBH}}^T + \widetilde{\mathbf{R}} = \mathbf{D} \quad \text{the } \textit{innovation covariance consistency} \tag{40.2}$$

R. Ménard (✉) · M. Deshaies-Jacques
Air Quality Research Division, Environment and Climate Change Canada,
2121 Transcanada Highway, Dorval, QC H9P 1J3, Canada
e-mail: Richard.Menard@canada.ca

C. Mensink and G. Kallos (eds.), *Air Pollution Modeling and its Application XXV*,
Springer Proceedings in Complexity, DOI 10.1007/978-3-319-57645-9_40

where $\mathbf{K}$ is the *Kalman gain* matrix, $\mathbf{R}$ and $\mathbf{B}$ are the observation and background error covariances, and $\mathbf{D}$ is the *innovation matrix*. The proof is given in Ménard (2016). We stress the fact that having the gain equal to the Kalman gain in observation space or an optimal analysis is not a sufficient condition for the estimates to be equal to the true covariances, one need to have also $\widetilde{\mathbf{D}} = \mathbf{D}$.

40.1.2 Desroziers' Scheme

Desroziers et al. (2005) showed how analysis residuals in observation space, specifically the *observation-minus-analysis* residuals $(O - A)$ and the *analysis-minus-background* residuals $(A - B)$, could be used to obtain estimates of $\widetilde{\mathbf{R}}$ and $\mathbf{H}\widetilde{\mathbf{B}}\mathbf{H}^T$ with an iterative scheme

$$\widetilde{\mathbf{R}}_{i+1} = \langle (O - A_i)(O - B)^T \rangle, \tag{40.3}$$

$$\mathbf{H}\widetilde{\mathbf{B}}_{i+1}\mathbf{H}^T = \langle (A_i - B)(O - B)^T \rangle. \tag{40.4}$$

40.1.3 Properties and Consequences

Property 1 *One step of the full error covariance estimation scheme (3–4) produces new estimates that meet the innovation consistency condition (40.2).*

Property 2 *The estimation of both full covariances* $\widetilde{\mathbf{R}}$ *and* $\widetilde{\mathbf{B}}$ *converges in a single iteration. Doing further iterations of the full covariances will not change the estimates.*

Property 3 *The estimated observation and background error covariance in observation space are equal to the truth* $\widetilde{\mathbf{R}} = \mathbf{R}$ *and* $\mathbf{H}\widetilde{\mathbf{B}}\mathbf{H}^T = \mathbf{H}\mathbf{B}\mathbf{H}^T$ *if and only if the initial gain is the Kalman gain.*

Consequence 1 *The estimation of the both full error covariance* $\mathbf{R}$ *and* $\mathbf{H}\mathbf{B}\mathbf{H}^T$ *is ill-posed with the Desroziers scheme. Feasible estimation is possible only if not all the elements (or simply parameters) of error covariances are estimated.*

Property 4 *The Desroziers' estimation of the error variances is well defined and gives an innovation variance consistency in a single step.*

Remark 1 The iterative variance scheme will converge to the true error variances only if the other elements that makes up the Kalman gain, in particular, the error correlations are correctly specified.

Consequence 2 *A viable option to the estimation of error statistics is to simultaneously estimate the error variance and the correlation lengths.*

40.1.4 Maximum Likelihood Estimation of Correlation Length

In the maximum likelihood method, we assume that the conditional p.d.f. of the innovations for a given parameter value (L_c) (the correlation length) is Gaussian-distributed. It is also usual to define the log-likelihood function $\mathcal{L}(L_c|\mathbf{d}_b^o)$ as $p(\mathbf{d}_b^o|L_c) = \exp[-\mathcal{L}(L_c|\mathbf{d}_b^o)]$, so that the maximum likelihood is equivalent to the minimum of the log-likelihood function,

$$\mathcal{L}(L_c|\mathbf{d}_b^o) \propto \log[\det(\widetilde{\mathbf{D}}(L_c))] + tr(\widetilde{\mathbf{D}}^{-1}(L_c)\mathbf{D}). \tag{40.5}$$

Here the maximum likelihood method and the Desroziers' method are combined. At each iterate new error variances are obtained at each observation station using the Desroziers method, and the maximum likelihood is used to obtain an estimate of the correlation length that fits all the station statistics.

Remark 2 It was found in an earlier study of Ménard (2016) that this algorithm may not converge when the correlation model or other statistical assumptions are inadequate.

40.2 Application to the AirNow Surface Air Quality Observation Network

We now apply the Desroziers method of estimation of error variances with the maximum likelihood estimation of correlation length to the AirNow air quality measurement network over North America. Innovations are obtained with respect to the Canadian operational air quality model, GEM-MACH. There is over 1,300 O_3 (ozone) and nearly 750 $PM_{2.5}$ (fine mode aerosols) measurements reported in real time each hour.

The estimation of the error statistics is challenged by:

- *Significant spatial inhomogeneity*
- *Strong diurnal cycles for photochemical species*

which results in having only a small number of measurements per site per hour (typically 60) to construct these estimates, and while the Desroziers method was developed and tested to estimate a single variance scaling factor for all observation sites.

At each hour at each station, statistics are built from a 60 day (2 months) sample. In a first experiment we use the statistics at each stations to estimate the observation and background error variance as well as the correlation length-scale using all station variance estimates. The result of this first experiment for the estimation of ozone error statistics is illustrated in Fig. 40.1 for two stations in and around Montreal. The results show a lack of convergence in the correlation length estimate but also

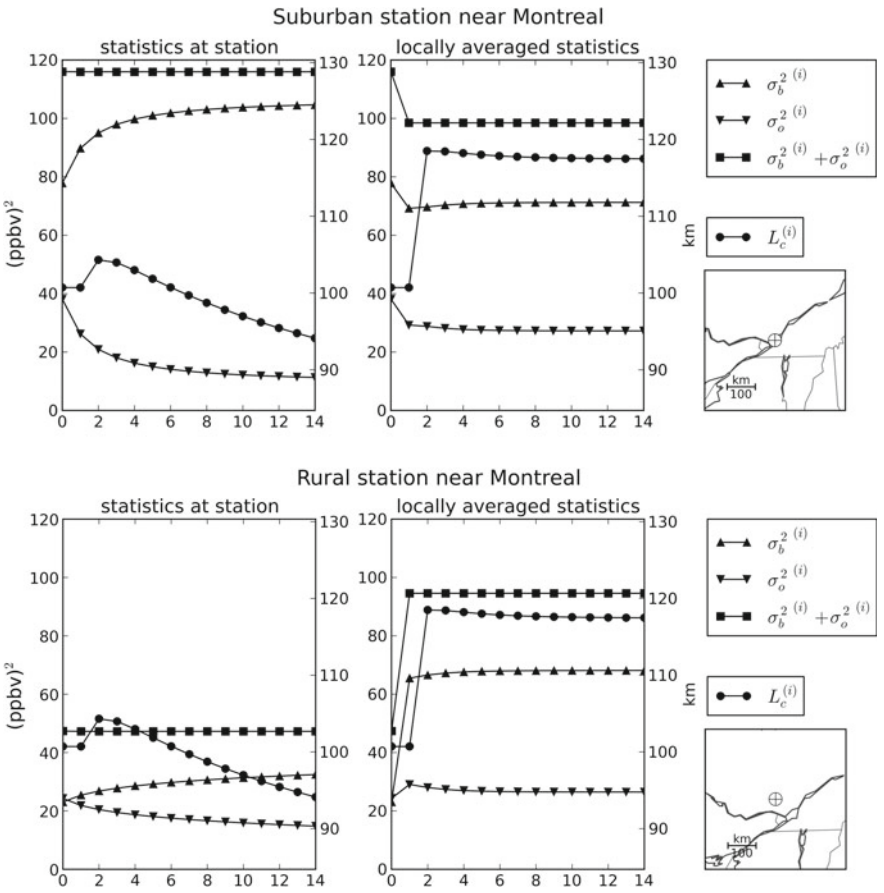

Fig. 40.1 Desroziers iterates using statistics at stations (*left*). Locally averaged with an exponentially decaying function (*right*)

in the variance estimates. If we use instead locally averages of (40.3) and (40.4) we obtain new error statistic estimates that now converge. This spatial averaging was performed by using an exponentially decaying function with a length-scale typical of the background error correlation length (Fig. 40.1).

We observe that although spatial averaging was used to obtain the error estimate the estimated error variance are relatively well organized in smoothly varying pattern (Fig. 40.2).

To validate these estimate we compare them with another method - the *local* Hollingsworth-Lonnberg method described in Ménard et al. (2016). The station variance estimates are then spatially averaged using the same exponential function as used in the Desroziers method. The two estimates are compared in the following figure.

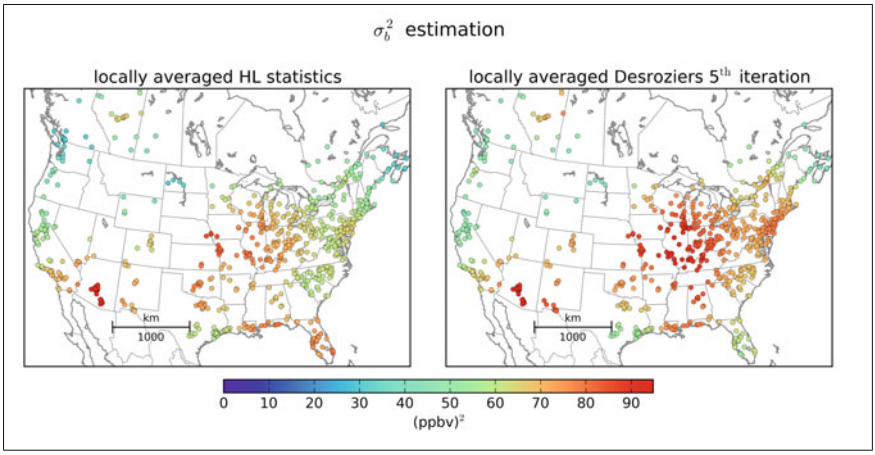

Fig. 40.2 Estimates of the background error variance at each stations. *Left* panel, by locally averaging the H.L. estimates. *Right* panel using the local averaged form of the Desroziers' scheme

40.3 Conclusion

We have applied the Desroziers method to an air quality surface measurements network to obtain non-homogeneous and time-varying estimates with a relatively small sample size. We found that when only the station statistics is used to estimate the error variance at each station then it results in non-convergence of the algorithm. However, when we apply a locally average to the Eqs. (40.3) and (40.4) we get convergent estimates with estimated values that agrees with other estimation methods.

References

Desroziers G, Berre L, Chapnik B, Poli P (2005) Diagnosis of observation, background, and analysis error statistics in observation space. Q J R Meteorol Soc 131:3385–3396

Ménard R (2016) Error covariance estimation methods based on analysis residuals: theoretical foundation and convergence properties derived from simpliéd observation networks. Q J R Meteorol Soc 142:257–273. doi:10.1002/qj.2650

Ménard R, Deshaies-Jacques M, Gasset N (2016) A comparison of correlation-length estimation methods for the objective analysis of surface pollutants at Environment and Climate Change Canada. J Air Waste Manage Assoc. doi:10.1080/10962247.2016.1177620

Part V
Local and Urban Scale Modeling

Chapter 41
Progress in Local Scale Flow and Dispersion Modelling

Silvana Di Sabatino

Abstract This review paper provides an overview of current understanding of local scale flows and dispersion with attention to the urban canopy layer and related spatial and temporal scales. The presence of buildings and topographic features are responsible for a vast number of processes ranging from simple drag and friction effects, wakes, corner vortices, flow separation and reattachment to differential heating leading to local thermal circulation. In highlighting key processes at various spatial-temporal scales, it will be shown lesson learnt from recent laboratory and field experiments. Progress made in understanding physical mechanisms occurring in streets, between groups of buildings and above, has inspired the advance of new conceptual models suitable for operational applications and development of sub-grid parameterizations within "urbanized" mesoscale weather prediction models. Among recent developed conceptual framework the one of city breathability is an example of how integrated knowledge (from physics-based understanding to computational fluid dynamics) can capture salient aspects of ventilation and dispersion in cities. After reviewing the relevant processes, the role of buildings, urban morphology and thermal characteristics are examined in view of delineating future developments and challenges.

41.1 Introduction

Prediction of flow and dispersion at local scale continues to be a vivid area of research especially in consideration of the variety of applications to the urban environment. More precisely, modern societies worldwide pose to the scientific community several questions concerning health, energy, transportation and quality of life in increasingly specific terms. The comprehension of physical mechanisms controlling flow and dispersion in cities including thermally-driven flows (Fernando

S. Di Sabatino (✉)
Department of Physics and Astronomy, ALMA MATER STUDIORUM, University of Bologna, Viale Berti Pichat 6/2, 40127 Bologna, Italy
e-mail: silvana.disabatino@unibo.it

C. Mensink and G. Kallos (eds.), *Air Pollution Modeling and its Application XXV*, Springer Proceedings in Complexity, DOI 10.1007/978-3-319-57645-9_41

et al. 2015) are important topics because of their implications for air quality, building design, pedestrian comfort and emergency response planning (Allegrini et al. 2012; Kwak and Baik 2014). In urban areas, there are usually considerable variations in the types, sizes, and layout of buildings and streets and over larger urban areas there are often also significant variations in the natural topography. The resulting flows are complex and require adoption of approaches that may range from complex numerical simulations to physics-based models tailored to a specific application. Similarly, pollutant dispersion in the built environment is intrinsically a multi-scale problem. Pollutants emitted in the atmosphere are dispersed over a wide range of horizontal length scales, from macro-scale to meso-scale and micro-scale. Pollutant "plumes" reaching the city or pollutants that are locally emitted are dispersed according to the flow dynamics at different scales: street (of order 10–100 m), neighbourhood/city (100 m–10 km) and regional (10–20 km). Their final spatial distribution depends upon several factors, such as morphological characteristics and type, nature and spatial location of sources. Important parameters for dispersion around buildings are building geometry and environment topography, wind speed, wind direction, turbulence, atmospheric stability, temperature, humidity and solar radiation (Blocken 2013), together with the presence of obstacles such as trees, low barriers and parked cars (Gallagher et al. 2015).

As known for over a decade each scale may be treated with its specific scale that determines the relevant dynamics (e.g. number of terms in the governing equations) (Britter and Hanna 2003). Each scale needs to be appropriately understood and related to each other when depicting a picture of the airflow and dispersion with a focus on local scale. Figure 41.1 shows relevant features and scales considered to

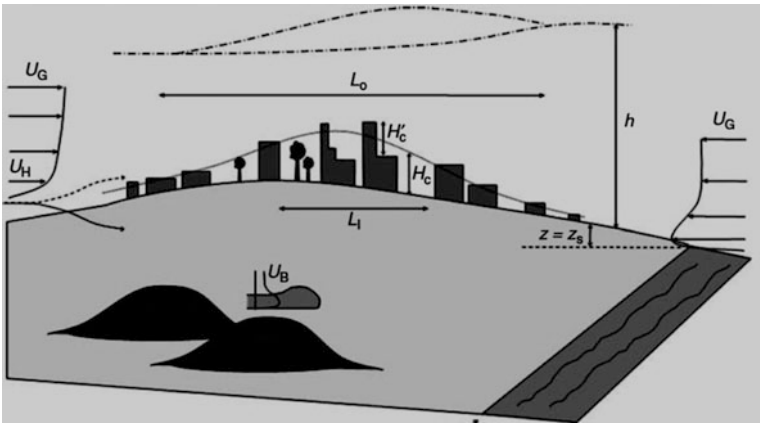

Fig. 41.1 Characteristic features of the terrain, buildings, and meteorology of significance for urban dispersion at local scale. Background flow (meso/regional scale is included as this needs to be used as input in flow and dispersion models). L_O and L_I are the overall and inner city length scales, respectively. U_G is the geostrophic wind, U_B is the typical wind speed associated with local buoyancy effects, for example, downslope winds from nearby mountains. Hc is the canopy height and Hc' is the standard deviation of canopy height (Adapted from Carruthers et al. 2012)

be important as current knowledge. The presence of buildings induces pressure forces (drag term), generates wakes and overall modifies the flow structure and prescribes pollutant dispersion patterns in the near field and affects the far-field. Understanding the relationships between the various scales has been one of the challenges being tackled by several researchers around the world. In the following, we will attempt to highlight some key elements and review some key findings based on our understanding of the problem.

41.2 Relevant Processes

The characteristic features of the airflow and dispersion at local scale (here we choose the neighborhood/city scale L_N of the order 1–10 km) are dependent on the grouping of the buildings/streets (with average building height H, breadth b, width w, and distance between buildings d). In suburban areas or spaciously designed urban centers, the buildings are effectively isolated. However, in dense suburbs and city centers there may be "canyons" with long rows of buildings neighboring streets. The suburban areas or spacious urban centers are essentially porous to the incoming boundary layer flow; the airflow slows down as it passes between the buildings, as a result of both the bulk displacement of the flow over and around the "envelope" or canopy of the buildings and their drag. Downwind of a characteristic adjustment distance L_A, (which is of the order of H ($d^2/w\ b$) or H/β, where $1-\beta$ is the volume occupied by the buildings and β is the volume of air between buildings and therefore a measure of porosity), or typically 10–30 building widths (Belcher et al. 2003), the drag force dominates but is weakened by the sheltering effect of upwind buildings. Over this adjustment distance the air flow above the buildings first accelerates as a result of the vertical displacement by the buildings, and then decelerates as slow moving fluid is expelled from below the level of the building envelope or canopy. Downwind of the adjustment distance, if the neighborhood scale is large enough (i.e., $L_N > L_A \cong 30\,H$), the airflow (having speed U_c) within the canopy is largely driven by turbulent shear stresses generated in the shear layer just above buildings $Hc < z^* < z$ (rather than by the incoming airflow), where z^* is the top of the shear layer of the buildings. Above this height, the airflow is characteristic of a surface layer with displacement height z_d. The displacement height z_d according to Jackson (1981) can be interpreted as the level of mean momentum absorption. Despite the understanding based on both theoretical and experimental investigations, calculations of this quantity revealed to be a non-trivial task. It is emphasized that development of new models has been achieved also through the set-up of sophisticated tools for calculation of geometry related variables such as those based on image processing of Digital Elevation Models (DEMs) as discussed in next sections.

Using urban air quality as an example, "canyons" are naturally associated to the street scale i.e., the smallest scale that encompasses both the source and the receptor and therefore the scale that determines the extreme values of concentration. The street scale flows are mainly straightforward and can be described as those that are

driven by the mixing of high momentum fluid down from above the canopy into the street canyons where the momentum will be lost to forces (normal and shear) on, e.g., the building, vegetation, and street surfaces. Insight on these aspects has been achieved by both laboratory and computational studies. An example is the case of flow in a very long street with no intersections and driven by the wind aloft being in the direction of the street. The fully developed bulk wind velocity in the street is directly linked to the momentum mixed down into the street and the skin friction coefficient of the street canyon walls and floor. Increased mixing due to variability of nearby building heights will tend to increase the wind along the streets while irregularities (building offsets or balconies) will tend to reduce the wind speed. When the wind direction aloft is normal to the street axis the flow is typically viewed as a recirculating eddy within the street canyon driven by the wind flow at the top of the street canyon with a shear layer separating the above canyon flow from that within. If the street canyon has a large depth to width ratio then the recirculation may not reach the canyon floor and the ground level regions may experience little ventilation. What is often overlooked is that such flows are rarely as simple as the idealized one often prescribed in computational modelling. Real flows are nearly always intermittent with the flowing going in the reverse direction for much of the time. There are many variations on realistic flows even in street canyons due to wind directions not parallel or normal to the street axis, the real rather than the simple idealized geometry of the street canyon and the mean flow and turbulence generated by vehicles within the street canyon. Typically, main flows are affected by thermally driven flows arising from incident solar radiation, building heat sources, and the vehicles themselves. Inclusion of all the features into a single model still remains to be addressed. Surely, one of the challenges in future years is to integrate all these aspects. The integration of data derived from new low cost devices into new physical models may inspire applications that are more realistic than currently.

41.3 Method of Analysis

Once a picture of relevant processes have been formed (see, e.g., Fernando et al. 2010; Carruthers et al. 2012; Britter and Di Sabatino 2012; Barlow 2014) the methods of analysis will follow from the specific approach adopted which might be different according to the specific area of expertise being engineering, meteorology, geography, urban climatology, and so on. Historically important has been the use of gross parameterizations of the surface and the flow for neighbourhoods and cities (see early works of Ratti et al. 2002; Di Sabatino et al. 2010). It has been recognized that one way of proceed is to use models in which the urban canopy is replaced with several parameters such as *H,* the aerodynamic roughness z_0 and z_d, the friction velocity u*, and the skin-friction coefficient. These parameters can be determined on both city and neighbourhood scales and are useful for characterizing the flow above and within the urban canopy layer.

Models for the mean flow within the urban canopy such as those developed by Cionco (1965), Macdonald (2000), Bentham and Britter (2003) are essentially similar in that they all assume that the distribution of drag producing elements are uniformly distributed throughout the urban canopy layer. The extension of this approach by Di Sabatino et al. (2008) is to use DEMs to provide the vertical distribution of the drag producing elements within the urban canopy and subsequently predict the spatially averaged mean velocity profile. A remaining important uncertainty is to investigate whether the "underlying viewpoint" should be one based on an array of buildings as in Bentham and Britter (2003) or an array of streets as in Soulhac et al. (2002). In later years, the latter shows to be promising at least for European type cities.

Complementary to the development of physics-based models are Computational Fluid Dynamics (CFD) modelling. The latter has become a major tool for simulating urban canopy flow and dispersion. Urban canopy flows have been widely investigated considering urban-like building arrays and street networks (e.g., Garbero et al. 2010) and in real urban built-up areas (e.g., Xie and Castro 2009). Studies have been carried out comparing CFD results with both field and laboratory experiments. Earlier work typically used Reynolds-averaged Navier–Stokes (RANS) turbulence models including commercially available models and more recently using large-eddy simulation (LES) models. The recent review by Di Sabatino et al. (2013) highlights latest findings in flow and dispersion modelling at various scales. One of the key elements of CFD modelling have being to predict the size of the wakes, the separation as well turbulence levels within the urban canopy layer where buildings, trees and all morhological features are explicitly resolved. CFD has being used in various ways to obtain benchmark data to fill the gaps from laboratory experiments or to verify the essential physics underlying a process. Literature is voluminous but one effective point is (e.g., Lateb et al. 2016) the standard k-ε model within Navier-Stokes equations provides inadequate results for the concentration field, because it cannot reproduce the basic flow structure, such as the reverse flow on both the roof and the wakes. Better results have been achieved by LES with considerable much more computational efforts. Nevertheless, the widespread of CFD modelling exercises and expert applications has been essential to extract "known" physics (in terms of known processes as outlined above) in parameterized form and inspired the development of subgrid parameterizations suitable for meso-scale weather models. Studies by Santiago and Martilli (2010), Gutiérrez et al. (2015) show the use of CFD to quantify the variation of drag coefficients with lambda-parameters (building packing densities), and parameterizations of turbulent length scales and its usefulness in mesoscale models. Of relevance is that the introduction of a drag coefficient that varies with the building plan-area fraction increases the accuracy of a mesoscale model in predicting surface wind speed in complex urban environments particularly in areas with tall buildings. Work is on going for further tests of improved drag coefficients for tall buildings to capture not only wind speed but also wind direction at high resolution for the high-rise and compact city of Hong Kong. Results are very encouraging showing that urban microclimate of coastal high-rise cities can be predicted in a realistic way

if complexity of urban morphology is well described (Wang et al. 2017). The required simple yet robust parameterization of urban morphology within weather prediction models would not have been possible without the large reasearch effort devoted to CFD modelling and companion experimental work undertaken in the last decade.

It is worth mentioning the steady transformation of engineering based codes to include aspects of meteorology (e.g., inclusion of solar radiation) and meteorological codes to include aspects of engineering studies (e.g., treatment of sharp-edged buildings). Many are the examples attempting to do that. We believe that the integration of meteorological and engineering type of models is one of the most useful approaches for applications in air quality as well urban planning. Further progress could be achieved in the formal evaluation of hybrid approaches that could foster robustness and reliability of results for an in increasing number of users and applications. In addition, inclusion of chemistry into CFD models would be beneficial to detailed dispersion studies in streets.

41.4 City Breathability

As an example of a concept, being developed by the author and co-workers that is driven by application we mention city breathability which directly builds upon concepts of exchange velocity (Bentham and Britter 2003). The exchange velocity *Ue,* a surrogate for the exchange processes occurring between the canopy and the atmosphere above, can be interpreted as useful quantity to assess ventilation within the urban canopy. However, it accounts for bulk vertical exchange of air masses but does not account for the effects of spatial variability. The basic underlying idea is that flow entering urban areas from rural environments is a source of clean air that can dilute pollution particularly at street level. An alternative approach to the use of exchange velocity to assess street-level pollutant dilution can be adopted from building ventilation concepts previously used to evaluate indoor exposure. Hang et al. (2009) analyzed the flow being advected into the city from its surrounding rural areas using the concept of the local mean age of air (Etheridge and Sandberg 1996) that represents the time taken for an air parcel to reach a given place after the clean air enters the city. A poorly ventilated region implies a large mean age and this, in turn, means an accumulation of pollutants in the region and larger concentration. The supplying of clean air into the urban area can be thought of as an *inhale* and pollutant removal reminds us of an *exhale*. Buccolieri et al. (2010) used the expression “city breathability” to describe these effects. Wind tunnel and numerical simulations suggested a way to classify cities into three groups: sparse, compact, and very compact cities. The sparse city acts as a collection of obstacles, where reversed flow only occurs behind the individual buildings. The compact city behaves as a unique obstacle with respect to the flow. A single wake, whose size scales with the horizontal dimension of the city, forms behind the building array. In the very compact city, the horizontal flow in the streets at the center of the array is

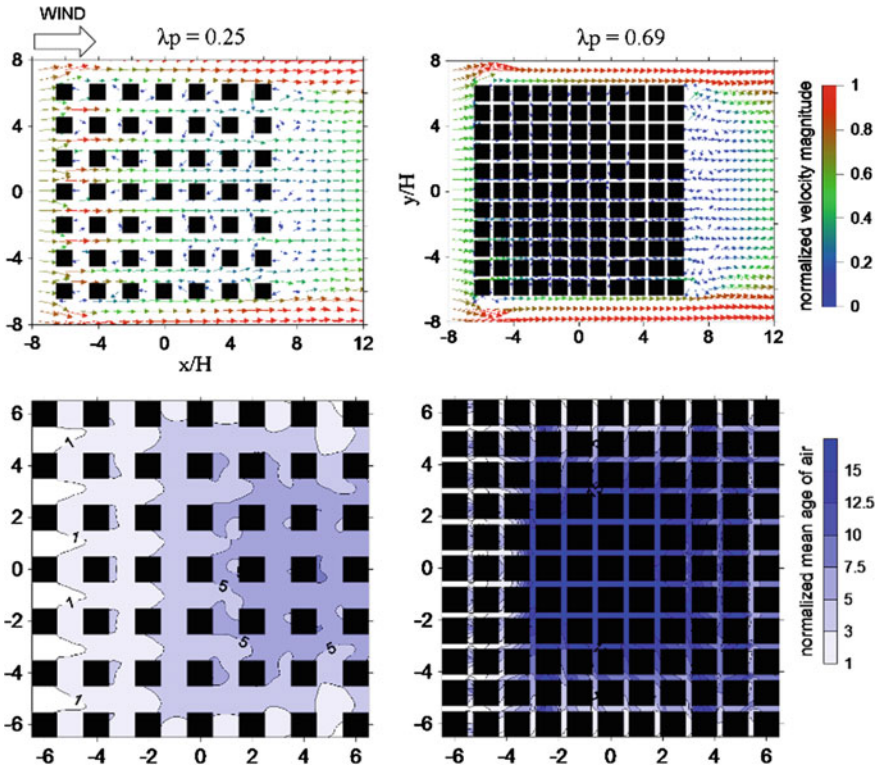

Fig. 41.2 Regular arrays of cubes. Vectors of normalized (by the undisturbed velocity UH at the building height H) velocity magnitude at z = 0.5 H (*top*) and normalized mean age of air at z = 0.06 H (corresponding to the pedestrian level) for a sparse canopy (*left*) and a very compact canopy (*right*)

negative, i.e., opposite of the approaching wind direction. As an example, Fig. 41.2 shows the vectors of normalized velocity U/U_H at z = 0.5 H and the normalized mean age of air at pedestrian level (~0.06 H), where U_H is the undisturbed velocity at the building height H, for a sparse case (λp = 0.25 where is plan area density) and for a very compact case (λp = 0.69) obtained from the general purpose CFD code Fluent ©. The uniform volume source of pollutant was defined over all gaps within the urban building array, from the ground to the street top. Figure 41.2 shows that the age of air was normalized using only a portion of the overall gaps volume. Overall, the mean age of air is large in poorly ventilated recirculation zones and in downstream regions. The air becomes older in the downstream region of the array as the building packing density increases. Pollutants tend to accumulate in the downstream region along the streets, because of the pollutant transport from the street sides in this region and the low vertical air mass through the street top. Local mean age of air is low near the side openings where lower concentrations are found. The figure also shows that the mean age of air is larger close to the middle of the

arrays. Moreover, it increases as building packing density increases, and this occurs both in the middle and at the edge of the array. However, some differences can be observed. In general, it can be argued that the mean age of air increases downstream in the sparse case, while for the compact case it reaches a maximum and then decreases close to the end of the array. The local mean age of air can be considered a useful indirect way to quantify the breathability of a city. Local mean age of air, estimated for a given city and specific meteorological conditions, can be displayed into spatial maps to easily evaluate city breathability and pollutant removal potential. This may be used as a fast way to identify ventilation in a given portion of the city for implementation of mitigation strategies or environmental policies.

Other researchers have investigated city breathability in a series of idealized neighborhood-scale and city-scale models such as round, square, long rectangular cities etc. Overall, the differences in the age of air between round, square and long cities are mainly attributed to the size of wakes behind the city due to the overall shape effect. The analysis for highly-packed cities with tall buildings shows that city-scale high-rise urban areas should be avoided. If sufficiently wide 'urban canyons' are used to separate the city-scale high-rise urban areas into several shorter neighborhoods (for example less than 1 km or shorter) between which the roughness isolated flow regime exists, city breathability is improved even in presence of tall buildings in such urban areas (Hang et al. 2012). In a recent paper by Buccolieri et al. (2015), who studied the ventilation of regular arrays of parallelepipeds representing compact cities of different packing density, a high variability of ventilation conditions was found depending on the incident wind angle and slight modifications of the array geometry. For low wind angles, a clear effect of channelling of pollutants along the street parallel to the wind direction was observed. This effect, combined with relative low exchange (horizontal) at street intersections and with the overlying atmosphere (exchange velocity), resulted in poor ventilation conditions. Conversely, large wind angles were shown to enhance transversal mean transfers at street intersections and vertical exchange with the overlying atmosphere. For increasing incident angles, the vertical transfer increased due to the enhancement of the mean counterpart of the total flux (that typically include the turbulent component). This effect was associated with a stronger interaction between the mean flow developing above the canopy and that within it. All the above examples may be useful in the context of urban planning.

Further Considerations

In this short paper, we have highlighted some key processes in flow and dispersion at local scale and reported on the development of some conceptual frameworks that may be used to advance the use of numerical modelling in practical applications. While our general understanding of the processes is good and this enables us to construct approximate models, it is clear that there is still a paucity of detailed field data and the most detailed numerical models are still not able to resolve all the features of the flow and dispersion. With the availability of faster response and cheaper instrumentation (Kumar et al. 2015), the continuing improvements in calculation capabilities, and the current vivid interest in this topic, it is certain that

more detailed data will increasingly become available, resulting in large data resources. Understanding of such data will continue to rely on the general concepts as partially reported here and available in recent literature (e.g., Fernando et al. 2010; Carruthers et al. 2012; Britter and Di Sabatino 2012; Barlow 2014 and several others).

Also of great relevance to future developments is both the impact of climate change on local scale flow and dispersion and the response of the urban environment to climate change. Some of these issues are being currently addressed in latest funded H2020 projects under SC5 programme call. One example is the just started iSCAPE (Improving the Smart Control of Air Pollution in European Cities) project (2016–2019).

Acknowledgements The author wish to acknowledge gratefully the Scientific Committee and Local Organizers of the 35TH "International Technical Meeting on Air Pollution Modelling and Its Applications (ITM)" Conference for the opportunity to write this contribution and generously support my participation.

The work has been partly supported by iSCAPE (Improving Smart Control of Air Pollution in Europe) project, which is funded through the European Community's H2020 Programme (H2020-SC5-04-2015) under the Grant Agreement No. 689954. Also, the author wishes to gratefully acknowledge the long standing collaboration with Profs. R. Britter, Prof. J. Fernando, Dr. D. Carruthers, Prof. J. Hunt, and the many students and collaborators especially Dr. R. Buccolieri and Dr. L. Leo with whom the author have developed with time several of the ideas and results reported here.

References

Allegrini J, Dorer V, Carmeliet J (2012) Analysis of convective heat transfer at building facades in street canyons and its influence on the predictions of space cooling demand in buildings. J Wind Eng Ind Aerod 104–106:464–473

Barlow JF (2014) Progress in observing and modelling the urban boundary layer. Urban Climate Part 2 10:216–240

Belcher SE, Jerram N, Hunt JCR (2003) Adjustment of a turbulent boundary layer to a canopy of roughness elements. J Fluid Mech 488:369–398

Bentham T, Britter RE (2003) Spatially averaged flow within obstacle arrays. Atmos Environ 37:2037–2043

Blocken B, Tominaga Y, Stathopoulos T (2013) CFD simulation of micro-scale pollutant dispersion in the built environment. Build Environ 64:225–230

Britter RE, Di Sabatino S (2012) Flow through urban canopies. In Fernando HJS (ed) Handbook of environmental fluid dynamics, vol 2. CRC Press, pp 85–96

Britter RE, Hanna SR (2003) Flow and dispersion in urban areas. Annu Rev Fluid Mech 35:469–496

Buccolieri R, Sandberg M, Di Sabatino S (2010) City breathability and its link to pollutant concentration distribution within urban-like geometries. Atmos Environ 44:1894–1903

Buccolieri R, Salizzoni P, Soulhac L, Garbero V, Di Sabatino S (2015) The breathability of compact cities. Urban Climate 13:73–93

Carruthers D, Di Sabatino S, Hunt J (2012) Urban air quality: meteorological processes. In: Meyers R, (ed) Encyclopedia of sustainability science and technology. Springer, pp 11158–11187, Article n. 00427. ISBN: 978-0-387-89469-0

Cionco R (1965) A mathematical model for air flow in a vegetative canopy. J Appl Meteorol 4:517–522

Di Sabatino S, Solazzo E, Paradisi P, Britter RE (2008) A simple model for spatially-averaged wind profiles within and above an urban canopy. Bound-Layer Meteorol 127:131–151

Di Sabatino S, Leo LS, Cataldo R, Ratti C, Britter RE (2010) On the construction of DEMs of a southern European city and a comparative morphological analysis with respect to northern European and North American cities. J Appl Meteorol Climatol 49:1377–1396

Di Sabatino S, Buccolieri R, Salizzoni P (2013) Recent advancements in numerical modelling of flow and dispersion in urban areas: a short review. Int J Environ Pollut 52:172–191

Etheridge D, Sandberg M (1996) Building ventilation: theory and measurement. Wiley, Chichester, U.K

Fernando HJS, Zajic D, Di Sabatino S, Dimitrova R, Hedquist B, Dallman A (2010) Flow, turbulence and pollutant dispersion in the urban atmospheres. Phys Fluids 22:051301–051320

Fernando HJS, Pardyjak E, Di Sabatino S, Chow FK, De Wekker SFJ, Hoch SW, Hacker J, Pace JC, Pratt T, Pu Z, Steenburgh WJ, Whiteman DC, Wang Y, Zajic D, Balsley B, Dimitrova R, Emmitt GD, Higgins CW, Hunt J, Knievel JC, Lawrence D, Liu D, Nadeau DF, Kit E, Blomquist BE, Conry P, Coppersmith RS, Creegan E, Felton M, Grachev A, Gunawardena N, Hang C, Hocut CM, Huynh G, Jeglum ME, Jensen D, Kulandaivelu V, Lehner M, Leo LS, Liberzon D, Massey JD, McEnerney K, Pal S, Price T, Sghiatti M, Silver Z, Thompson M, Zhang H, Zsedrovits T (2015) The MATERHORN: unraveling the intricacies of mountain weather. Bulletin of the American Meteorological Society, November Issue:1946–1968

Gallagher J, Baldauf R, Fuller CH, Kumar P, Gill LW, McNabola A (2015) Passive methods for improving air quality in the built environment: A review of porous and solid barriers. Atmos Environ 120:61–70

Garbero V, Salizzoni P, Soulhac L (2010) Experimental study of pollutant dispersion within a network of streets. Bound-Layer Meteorol 136:457–487

Hang J, Sandberg M, Li Y (2009) Age of air and air exchange efficiency in idealized city models. Build Environ 44:1714–1723

Hang J, Li Y, Buccolieri R, Sandberg M, Di Sabatino S (2012) On the contribution of mean flow and turbulence to city breathability: the case of long streets with tall buildings. Sci Total Environ 416:362–373

Gutiérrez E, Martilli A, Santiago JL, González JE (2015) A mechanical drag coefficient formulation and urban canopy parameter assimilation technique for complex urban environments. Bound-Layer Meteorol 157:333–341

Jackson PS (1981) On the displacement height in the logarithmic velocity profile. J Fluid Mech 111:15–25

Kumar P, Morawska L, Martani C, Biskos G, Neophytou M, Di Sabatino S, Bell M, Norford L, Britter RE (2015) The rise of low-cost sensing for managing air pollution in cities. Environ Int 75:199–205

Kwak K-H, Baik J-J (2014) Diurnal variation of NOx and ozone exchange between a street canyon and the overlying air. Atmos Environ 86:120–128

Lateb M, Meroney RN, Yataghene M, Fellouah H, Saleh F, Boufadel MC (2016) On the use of numerical modelling for near-field pollutant dispersion in urban environments. Rev Environ Pollut 208:271–283

Macdonald RW (2000) Modelling the mean velocity profile in the urban canopy layer. Bound-Layer Meteorol 97:25–45

Ratti C, Di Sabatino S, Caton F, Britter R, Brown M, Burian S (2002) Analysis of 3-D urban databases with respect to pollution dispersion for a number of European and American cities. Water, Air Soil Pollut Focus 2:459–469

Santiago JL, Martilli A (2010) A dynamic urban canopy parameterization for mesoscale Models based on computational fluid dynamics reynolds-averaged navier-stokes microscale simulations. Bound-Layer Meteorol 137:417–439

Soulhac L, Mejean P, Perkins RJ (2002) Modelling transport and dispersion of pollutant in street canyons. Int J Environ Pollut 16:404–416

Wang Y, Di Sabatino S, Martilli A, Li Y, Wong MS, Gutiérrez E, Chan PK (2017) Impact of land surface heterogeneity on urban heat island circulation and sea-land breeze circulation in Hong Kong. J Geophys Res 122:4332–4352

Xie ZT, Castro IP (2009) Large-eddy simulation for flow and dispersion in urban streets. Atmos Environ 43:2174–2185

Chapter 42
Modelling the Dispersion of Ship Emissions in Different Scenarios and Sensitivity Analysis

Silvia Trini Castelli, Gianni Tinarelli, Luca Mortarini, Paola Radice, Giuseppe Carlino, Cristina Pozzi and Domenico Anfossi

Abstract A modelling study, supported by a sensitivity analysis, is proposed for assessing the distinctive features of the dispersion of ship emissions in the Venice Lagoon. The main aspects on which the analysis focuses are the appropriate parameterization of the turbulence variables in the lagoon, the proper treatment of the lagoon-sea surface temperature and the evaluation of different parameterizations for the plume rise to describe the pollutant emissions from moving ships. The results of the study are discussed in the context of the environmental impact assessment of present and future scenarios.

42.1 Introduction

In the framework of an environmental impact assessment study, the dispersion related to ship emissions in the Venice Lagoon has been simulated for a full year. The area considered is rather complex, because of the particular landuse and topography, mixing land, lagoon water and open sea. For this reason, distinctive issues have to be addressed when modelling both the meteorology and the pollutant dispersion. In particular, the turbulence parameterizations need to account for the specific heterogeneity of the site when estimating the surface fluxes. Then, considering that sea-surface temperature databases typically used in atmospheric models are hardly representative of the lagoon conditions, an appropriate approach is needed to properly treat and assimilate the lagoon surface temperature in the model simulation. For the dispersion, in order to properly describe the pollutant

S.T. Castelli (✉) · L. Mortarini · D. Anfossi
Institute of Atmospheric Sciences and Climate, National Research Council, Turin, Italy
e-mail: s.trinicastelli@isac.cnr.it

G. Tinarelli · P. Radice · C. Pozzi
Arianet S.r.l., Milan, Italy

G. Carlino
Simularia S.r.l., Turin, Italy

C. Mensink and G. Kallos (eds.), *Air Pollution Modeling and its Application XXV*,
Springer Proceedings in Complexity, DOI 10.1007/978-3-319-57645-9_42

emissions from moving ships, an adaptation of the plume rise parameterization is essential.

In this work, a modified version of the RMS (RAMS-MIRS-SPRAY) modelling system is applied, integrating it with the meteorological diagnostic code MINERVE/Swift and implementing an ad hoc version of the atmospheric boundary-layer processor. Two different emission scenarios are considered, the present one and one with a possible future variation of the ships' itinerary. One-year-long simulations, for 2013, are performed for both scenarios and the evaluation of the results is carried out by comparisons with both meteorological and pollutant concentration observed data.

42.2 The Case Study and the Simulations

The two scenarios considered are the "present", S0, corresponding to the ship emissions inventory for year 2013, and a possible "future" one, S1, for which the trajectory of the Passenger Ships heavier than 40.000 tons will be moved from the Giudecca Canal to the Malamocco-Marghera Canal, then landing through a new canal and hoteling in the same harbor as S0 (Fig. 42.1).

When dealing with environmental impact assessment, often the due time for delivering the simulation outputs is short and optimization of the numerical modelling is requested. In this case, we adopted and tested a hybrid configuration for the atmospheric model RAMS, combining a prognostic with a diagnostic approach.

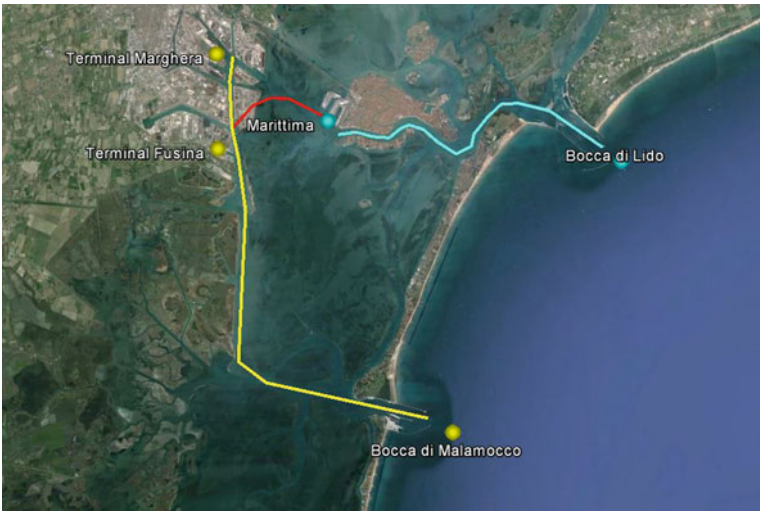

Fig. 42.1 Itinerary of the ships >40 kTon in the Venice Lagoon. *Light blue line* S0 scenario; *yellow* and *red lines* S1 scenario

The meteorological fields were firstly selected from a pre-calculated database including the 2013 outputs from RAMS prognostic simulations on two large nested grids, with a coarse resolution of 48 and 12 km respectively. Then, the ISAN (ISentropic ANalysis package) module of RAMS was used to downscale the output fields over two further nested grids, with resolutions of 4 and 1 km zooming on the lagoon area, at the same time assimilating the meteorological observations available at several measuring stations in the area. A further downscaling was then made with a diagnostic approach, using the mass-consistent MINERVE/Swift code, down to the final computational domain at the target resolution of 200 m. To account for the heterogeneity in the area, in the downscaling procedure, together with a high-resolution (100 m) database for the orography, a refined landuse database was used. The CORINE data have been reformulated in classes that are more representative of the topographical variability of the area, with 200-m resolution. For the SPRAY (Tinarelli et al. 2000) dispersion model simulations, in order to properly account for the spatial heterogeneity when calculating the surface fluxes and turbulence variables, the SST have been calculated from the measured data available at eight stations in the lagoon area. First, hourly 2D fields spatially homogeneous on the grid at 200-m resolution were elaborated from the median values of the measurements. Then, the hourly fields have been spatially re-modulated using the observed data with a data-assimilation technique based on successive corrections (Bratseth 1986). Finally, to reproduce the emission from moving ships, in the source term, besides the geometrical and thermodynamic characteristics of the emission, the speed of the ship is assigned to each released particle. Thus, in the plume rise algorithm the apparent wind velocity seen by the particle during its trajectory will be given by the sum of the wind velocity and the ship velocity. This approach accounts for the source motion and, typically, implies a reduced rising of the plume.

42.3 Results and Conclusions

In Fig. 42.2 an example of the results obtained for the meteorology at a station in Venice city is plotted, showing a good agreement between predicted and observed data. The improvement in the agreement after the downscaling can also be appreciated. The hybrid prognostic/diagnostic approach for the meteorological simulation is presently under verification versus a fully-prognostic simulation for different short-period episodes. Results are presented and discussed.

In Fig. 42.3 an example of SPRAY outputs is shown for the NO_x yearly mean concentration calculated in the two scenarios, considering only the ships that will change their itinerary. As expected, the change in the ship trajectory has consequences on the affected area, which moves from the Venice city center towards inland, in the Marghera-Mestre area. The concentration values do not substantially vary, as it can be seen in Fig. 42.4 showing the differences in NO_x yearly mean concentration between the two scenarios. Through a comparison between data

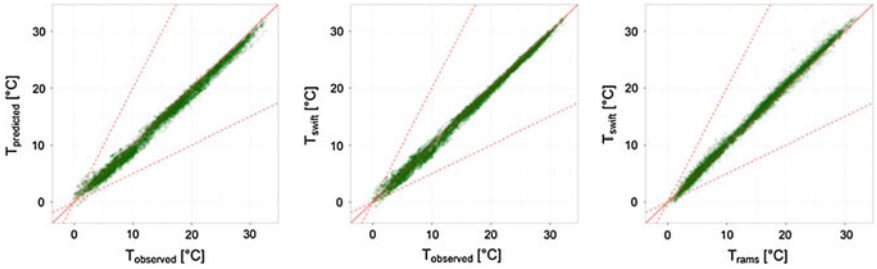

Fig. 42.2 Scatter plots for the temperature at "Venezia Cavanis" station. *Left* RAMS/ISAN predictions versus observations; *center* MINERVE/Swift predictions versus observations; *right* MINERVE/Swift predictions versus RAMS/ISAN predictions

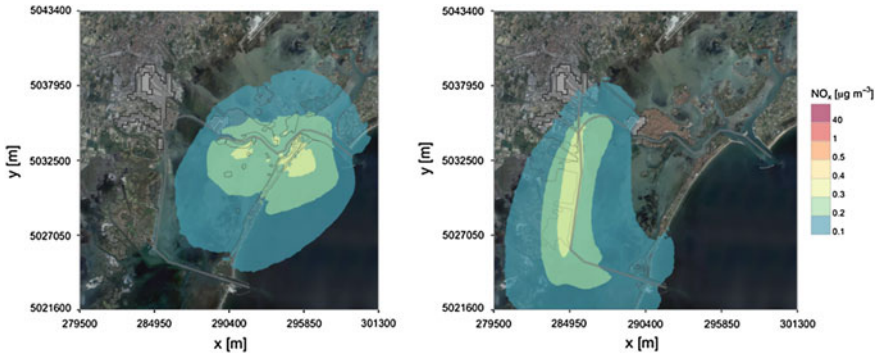

Fig. 42.3 Yearly mean concentration, NO_x. *Left* present scenario S0, *right* future scenario S1

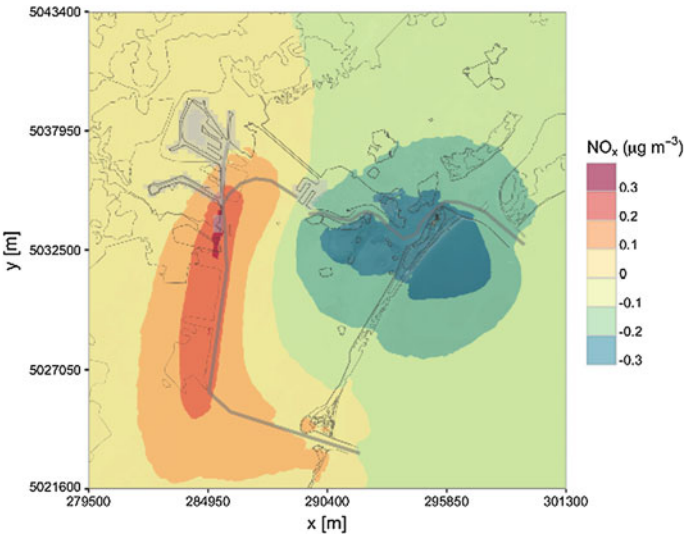

Fig. 42.4 Difference between the yearly mean concentrations, NO_x: future S1—present S0

measured at the stations and predicted values, the increase or decrease in concentration was quantified in the different parts of the domain. In any case, since the contribution of the ships >40 kTon is small with respect to the total ship emissions, at the measuring stations the variation between the two scenarios keeps small, ranging from 0.02 to 0.08 μg/m^3 for the NO_x yearly mean concentration.

Simulations are being repeated using the standard plume-rise algorithm, the results are presented and discussed.

Questions and Answers

Questioner: Jaakko Kukkonen
Question: Which emission model did you use? Was it based on the AIS signals or some other data? There are various models for evaluating ship emissions, and these can provide substantially different results.
Answer: We used the methodology described in the EMEP/EEA Air Pollutant Emission Inventory Guidebook (2013) using the ship characteristics and setting time modulations using the daily ship movements to/from the ports given by the local Port Authority of Venice.

Questioner: Jeff Weil
Question: Did you account for the increased relative velocity on the emission strength as you did for the plume buoyancy and plume rise? The increased relative velocity would also dilute/reduce the mass emission per unit length of the plume as it does for the buoyancy per unit length, $F_b/(u_a + u_{ship})$
Answer: No, we did not. We were not considering the exact position of each moving ship because this information was not available. This means we considered the total emission spread along the entire trajectory for each different ship category, as if the entire trajectory was homogeneously filled by emitting ships. Along the whole trajectory, the total emitted mass had to be conserved and we did not apply any correction to the emission strength.

Questioner: Peter Viaene
Question: You consider the flattening of the plume on your plume rise. Wouldn't the extra turbulence in the wake cause a dilution of the concentration?
Answer: The ships are moving along the canal with a velocity ranging from 12 to 20 km/h, so we do not expect a possible wake turbulence to be significantly effective in diluting the plume. In addition, differently from most vehicles, the plume is emitted from a chimney (on top, in the vertical) and not from an exhaust pipe (at the rear side, in the horizontal).

Questioner: Wouter Lefebvre
Question: How did the public react to the 'small' results, i.e. only difference in NO_x of 0.3 μg/m^3 max, which is not measurable?

Answer: The complete study, including also all other contributions (effects on sediments, lagoon waves, noise etc.) at this time have not yet been presented to the public. The main result for the air pollution is the shift of the impact area from the Venice city centre and surrounding to the industrial and residential areas of Marghera and Mestre, thus affecting a different part of the population. Anyway, we note that considering we are simulating the emission of only a part of a single source category, a contribution of 0.3 $\mu g/m^3$ of NO_x on the yearly average can be regarded as non-negligible.

References

Bratseth AM (1986) Statistical interpolation by means of successive corrections. Tellus 38A:439–447

Tinarelli G, Anfossi D, Bider M, Ferrero E, Trini Castelli S (2000). A new high performance version of the Lagrangian particle dispersion model SPRAY, some case studies. In: Gryning SE, Batchvarova E (eds) Air Pollution modelling and its application XIII, vol 23. Plenum Press, New York, pp 499–506. ISBN: 0-306-46188-9

Chapter 43
Application of a Comprehensive Integrated Assessment Tool for the Brussels Capital Region

Peter Viaene, Enrico Turrini, Claudio Carnevale, Marialuisa Volta, Roberta Gianfreda, Guiseppe Maffeis, Priscilla Declerck, Olivier Brasseur, Pieter Valkering and Clemens Mensink

Abstract While in general air quality has improved in Europe over the past decades, there are still problems with exceedances of ambient air quality limit values in many urban areas. To design efficient Air Quality Plans to face these problems, methodologies and tools are required to assess the effects of possible abatement measures on local air quality. One such tool is RIAT+ (http://www.riatplus.eu) which was designed to help regional decision makers select air pollution reduction policies that will improve the air quality at minimal costs. In this contribution to ITM we present the results obtained as well as the lessons learned for an application of the RIAT+ tool to the Brussels Capital Region. RIAT+ has been previously applied successfully to regions in the Po Valley in Italy and to the Alsace region in France. The application to the BCR however poses specific challenges due to the fact that both the area on which the abatement measures can be applied as the emissions are more limited than in previous cases. Inside the BCR, emissions of nitrogen oxide and particulate matter are mainly from non-industrial combustion and traffic. For these two source categories a list of possible air quality abatement measures was provided by the Brussels Environmental agency. To allow RIAT+ to determine the optimal combination of abatement measures with minimal cost, information was collected on both the emission reduction efficiency and the costs of

P. Viaene (✉) · P. Valkering · C. Mensink
VITO, Boeretang 200, 2400 Mol, Belgium
e-mail: peter.viaene@vito.be

C. Mensink
e-mail: clemens.mensink@vito.be

E. Turrini · C. Carnevale · M. Volta
UNIBS, Via Branze 38, 25123 Brescia, Italy
e-mail: claudio.carnevale@unibs.it

R. Gianfreda · G. Maffeis
TerrAria s.r.l., via Melchiorre Gioia 132, 20125 Milan, Italy

P. Declerck · O. Brasseur
Brussels Environment, Thurn & Taxis Havenlaan 86C/3000, 1000 Brussels, Belgium

C. Mensink and G. Kallos (eds.), *Air Pollution Modeling and its Application XXV*,
Springer Proceedings in Complexity, DOI 10.1007/978-3-319-57645-9_43

each of these measures. RIAT+ efficiently calculates concentration changes from emission changes using a receptor model based on an artificial neural network. Input for this receptor model was obtained from the results of a validated AURORA chemical transport model setup for the BCR. Once the receptor model was validated, RIAT+ was then used to calculate the effect of the different proposed abatement measures on air quality.

43.1 Introduction

Although air quality in Europe has improved significantly in the past decades, exceedances of air quality limit values are still common and member states have to submit Air Quality Plans accordingly as required by the Air Quality Directive 2008/50/EC. To devise such Air Quality Plans integrated assessment modelling (IAM) tools can help to determine cost efficient emission abatement measures. In this contribution to ITM we describe the application of such an IAM to the Brussels Capital Region (BCR). The BCR that encompasses Brussels, the capital of Belgium, is a relatively small region of 161 km^2 that is home to 1.1 million people. The BCR mainly has problems meeting the yearly average NO_2 concentrations limit value of 40 $\mu g/m^3$ as set by the Directive.

43.2 Methodologies

RIAT+ (Carnevale et al. 2012) is an IAM tool that was developed specifically for assisting regional authorities in identifying suitable abatement measures to improve the air quality at a regional/local level. The tool does not only allow its user to assess the effects of different abatement measure scenarios on concentration and health impact but can also automatically through optimization determine the optimal set of abatement measures for a given investment.

To calculate the effect of abatement measures on emissions RIAT+ requires information on the emission reduction efficiency of these measures. Furthermore, in optimization mode, RIAT+ also requires data on abatement measure costs. Such information can for example be sourced from GAINS (Amann et al. 2011). For the BCR it was made clear by Brussels Environment (BIM), that were involved in the project as a stakeholder, that they were only interested in assessing the effects of a set of 14 emission abatement measures that had been agreed on within the Brussels Administration. Inside the BCR more than 90% of the NO_x and PM_{10} emissions can be attributed to traffic and non-industrial combustion, therefore the focus is on measures that will impact the emissions from these two source categories. After a preliminary screening in which abatement measures that also affected sources outside the BCR were excluded, a set of 10 emission abatement measures was retained for which the emission reduction efficiencies were taken from reports provided by

Table 43.1 Emission reduction efficiency relative to the reference emissions (2010) for the different emission abatement measures proposed for the BCR and average yearly NO_2 and PM_{10} concentrations and associated health costs in 2020 for the same domain calculated by RIAT+

	Measures	Emission reduction per pollutant (%)					NO_2 (µg/m3)	PM_{10} (µg/m3)	Health costs (M€)
		NOx	VOC	PM_{10}	$PM_{2.5}$	SO_2			
	Reference	*0.00*	*0.00*	*0.00*	*0.00*	*0.00*	*28.6*	*22.1*	*334*
1	Eco driving	0.62	0.12	2.31	2.43	0.00	28.6	22.1	333
2	Modal shift	0.62	0.12	3.47	3.64	0.00	28.6	22.1	332
3	Transport plan	0.62	0.12	3.47	3.64	0.00	28.6	22.1	332
4	Urban toll	5.61	1.35	17.36	18.22	0.04	28.2	21.0	317
5	Parking places	0.31	0.06	1.16	1.21	0.00	28.6	22.1	333
6	Low Emission Zone	2.00	0.20	19.40	17.2	0.00	28.6	22.0	333
	Σ Traffic	*9.78*	*1.97*	*47.17*	*46.34*	*0.04*	*27.8*	*20.7*	*312*
7	Boiler maintenance	2.20	0.19	2.25	2.50	1.51	28.6	22.0	333
8	Exemplary building	0.14	0.01	0.05	0.06	0.00	28.6	22.1	334
9	Energy efficiency large buildings	0.21	0.02	0.16	0.18	0.08	28.6	22.0	334
10	Energy audits	0.96	0.09	0.54	0.60	0.30	28.6	22.0	333
	Σ Heating	*3.51*	*0.31*	*3.00*	*3.34*	*1.89*	*28.6*	*21.9*	*332*
	All	*13.29*	*2.28*	*50.17*	*49.68*	*1.93*	*27.7*	*20.6*	*310*

BIM (Table 43.1). The reports also provided estimates of costs for some of these measures. Some of these values were however considered rather dubious, more specifically, abatement measures which only implied a change of legislation were considered to incur no cost in these reports. While this may be true for the administration imposing these measures, those that will have to comply will most likely disagree that such measures come for free. It was therefore in the end decided not to retain any of the cost estimates and only use RIAT+ in scenario mode.

The source/receptor relation RIAT+ uses to calculate the effects of emission changes on concentration efficiently, is an artificial neural network (ANN). To train the ANN a set of chemical transport model (CTM) calculations are needed. For the BCR the AURORA (Lauwaet et al. 2013) CTM was set up for a 50 × 50 km grid covering the BCR with a resolution of 1 km nested inside a 4 km resolution run for Belgium. The CTM was run for the reference year 2009, validated and then run for a set of scenarios in which the emissions for the different pollutants were varied individually or in combinations as to cover the range of emission/concentration patterns to be expected. Both the reference run of the CTM and the trained ANN were validated (Fig. 43.1).

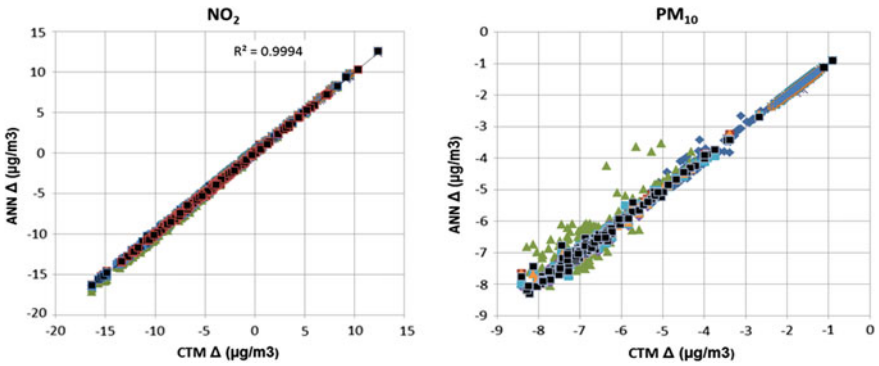

Fig. 43.1 Scatter plots for changes in yearly average NO_2 (*left*) and PM_{10} concentrations calculated with the CTM and the ANN for the training scenarios for a set of grid cells not used in training the ANN

43.3 Results

From Table 43.1 it can be seen that the health cost will be reduced by 7% when all proposed abatement measures are applied. As the BCR emissions for NOx and PM_{10} are respectively only 1.72% and 0.78% of the Belgian emissions and the region's extend is limited, it is not totally unexpected that the effect of the emission abatement measures aimed at reducing only the emissions in the BCR have a rather small impact. For the Low Emission Zone (LEZ) the small effect can be explained by the fact that many of the cars that will not be allowed in the LEZ are expected to have been replaced by newer, higher EURO standard models by 2020. The model resolution in this application is 1 km which is already quite high for a CTM but is still too low to correctly represent street level NO_2 concentrations. The effect of traffic measures on NO_2 concentration is therefore likely to have been underestimated in the current IAM application. One of the rather obvious observations one can also make is that in this case a simple preliminary calculation would probably have been more appropriate to assess the (lack of) impact of the proposed measures at the 1 km resolution than setting up a IAM tool.

43.4 Conclusions

The main lessons learned from this application of RIAT+ to the BCR were:

- Choice of abatement measures is determined and limited by what is deemed politically/socially acceptable. Such considerations should be included in an IAM tool.

- The biggest challenge in applying a tool such as RIAT+ was in this application to determine emission reduction efficiency and costs for the abatement measures;
- When using simplified source receptor relations such as ANN one should test whether dynamic behaviour of the complex model (CTM) is reproduced correctly.
- The effect of the proposed emission abatement measures is small due to the limited extent of the BCR application area and the contribution of local emissions. Effective policy will require targeting emissions outside the BCR as well, something that is outside the jurisdiction of the BCR;
- There is a need for (even) higher resolution modelling to correctly assess the impact of local measures especially for pollutants such as NO_2;
- Applying a full blown IAM system can be overkill in some cases.

Acknowledgements This project received funding from the European Union's Seventh Framework Programme for research, technological development and demonstration under grant agreement number CA 308395.

Questions and Answers

Questioner: Fabian Lenartz
Question: How are the measurement errors for the target plot defined?
Answer: The uncertainty $U_{95}(O_i)$ on the measurements (O_i) is calculated for the target plot according to the following formula

$$U_{95}(O_i) = U_{95,r}^{RV}\sqrt{(1-\alpha^2)O_i^2 + \alpha^2.RV^2}$$

In this formula the

$U_{95,r}^{RV}$	relative uncertainty
α	fraction of the uncertainty that is not proportional to the measured value
RV	reference concentration value for which the uncertainty is determined

The subscript '95' is used to indicate that the 95th percentile highest values among all uncertainty values calculated is used as a representative value of the measurement uncertainty.

Details on how the values for the parameters $U_{95,r}^{RV}$ and α are derived can be found in Pernigotti et al. (2013) and Thunis et al. (2013). For the RV typically the European legislated limit value is taken e.g. 200 µg/m^3 for hourly NO_2 concentration.

Questioner: Heike Schlünzen
Question: Air pollution does not respect political boundaries and there might not be room within one administrative region to reduce concentrations. Do you see a clear possibility to address sources of air pollution upstream so that political trans-boundary action can be taken.
Answer: Absolutely. This case study clearly illustrates the limitations of local action plans for the case of the Brussels Capital Region (BCR). The only effective measures will have to be measures that address the sources outside the BCR.

References

Amann M, Bertok I, Borken-Kleefeld J, Cofala J, Heyes C, Höglund-Isaksson L, Klimont Z, Nguyen B, Posch M, Rafaj P, Sandler R, Schöpp W, Wagner F, Winiwarter W (2011) Cost-effective control of air quality and greenhouse gases in Europe: modelling and policy applications. Environ Model Softw 26(12):1489–1501. ISSN 1364-8152, doi:10.1016/j.envsoft.2011.07.012

Carnevale C, Finzi G, Pisoni E, Volta M, Guariso G, Gianfreda R, Maffeis G, Thunis P, White L, Triacchini G (2012) An integrated assessment tool to define effective air quality policies at regional scale. Environ Model Softw 38:306–315

Lauwaet D, Viaene P, Brisson E, van Noije T, Strunk A, Van Looy S, Maiheu B, Veldeman N, Blyth L, De Ridder K, Janssen S (2013) Impact of nesting resolution jump on dynamical downscaling ozone concentrations over Belgium Atmospheric Environment, vol 67, pp 46–52

Pernigotti D, Thunis P, Belis C, Gerboles M (2013) Model quality objectives based on measurement uncertainty. Part II: PM10 and NO2. Atmos Environ 79:869–878

Thunis P, Pernigotti D, Gerboles M (2013) Model quality objectives based on measurement uncertainty. Part I: ozone. Atmos Environ 79:861–868

Chapter 44
Concentration Fluctuations and Variability at Local and Regional Scales: Use of a Lagrangian Two-Particle Dispersion Model Coupled with LES Fields

Jeffrey Weil, Peter Sullivan, Edward Patton and Andrezj Wyszogrodski

Abstract A Lagrangian two-particle dispersion model (L2PDM) driven by velocity fields from large-eddy simulations (LESs) is used to compute the mean and fluctuating concentrations in a highly convective boundary layer. The model results agree with data from two convection tank experiments.

44.1 Introduction

A striking feature of atmospheric dispersion is its large variability. This is especially true in the convective boundary layer (CBL) where the plume from an elevated source meanders due to the large convective eddies, producing high fluctuations in surface concentrations. The concentration peaks are caused by intermittent transport of plume segments to the surface by CBL downdrafts, where the plume spread about the local centerline is due to small-scale turbulence (Gifford 1959). The concentration fluctuations are characterized by their root-mean-square (rms) value σ_c or the fluctuation intensity σ_c/C, where C is the ensemble-mean concentration. Measurements show that surface σ_c/C can be large ranging from 1 to 10 for short averaging times (<5 min) and downstream distances (<5 km).

In this work, we extend Thomson's (1990) Lagrangian two-particle dispersion model (L2PDM) for concentration fluctuations in homogeneous turbulence to the inhomogeneous conditions of the CBL by coupling it with velocity fields from large-eddy simulations (LES) (e.g., Moeng and Sulllivan, 1994). Thomson's model

J. Weil (✉) · P. Sullivan · E. Patton
National Center for Atmospheric Research, Boulder, CO 80307, USA
e-mail: weil@ucar.edu

A. Wyszogrodski
Polish Bureau of Meteorology, Warsaw, Poland

C. Mensink and G. Kallos (eds.), *Air Pollution Modeling and its Application XXV*,
Springer Proceedings in Complexity, DOI 10.1007/978-3-319-57645-9_44

handles the two-particle motion due to the "unresolved" or LES subfilter-scale (SFS) velocities, whereas the LES "resolved" velocities address particle displacements due to the larger-scale motion.

44.2 Models

In an L2PDM, one tracks the simultaneous motion of two particles that start from a small separation and spread due to inertial-subrange turbulence leading to "relative dispersion" about the plume centerline (Batchelor 1950). Thomson (1990) used stochastic equations to follow the evolution of the six-dimensional position and velocity arrays defining the two-particle system. He produced a relative dispersion (σ_r) with $\sigma_r \propto t^{3/2}$ at short times (t) and $\sigma_r \propto t^{1/2}$ at long times, consistent with Batchelor's (1950) theory, and σ_c results in agreement with wind-tunnel data.

In using LES fields to drive the particles, we decompose the total or Lagrangian velocity ($\boldsymbol{u}_{Lk}$) of particle k (= 1, 2) as $\boldsymbol{u}_{Lk} = \boldsymbol{u}_{Rk}$ ($\boldsymbol{x}_{pk}$, t) + $\boldsymbol{u}_{Sk}$ ($\boldsymbol{x}_{pk}$; $\boldsymbol{x}_{pj}$, t), where the resolved and SFS velocities (subscripts $\boldsymbol{R}$ and $\boldsymbol{S}$) of a particle (subscript p) are superposed as in the 1-particle LPDM (Weil et al. 2004); a bold-faced symbol denotes a vector. The SFS velocity depends on the positions of both particles (k and j) due to the two-point velocity correlation built into the SFS model (Thomson's); the resolved velocity correlation is implicitly included in the computed LES fields.

For a continuous point source (CPS), a one-particle LPDM can be used to find the mean concentration from the probability density function (PDF), p_1, of particle position $\boldsymbol{x}_p$ (Weil et al. 2004). For the two-particle releases, the plume concentration c also is computed from a p_1 but one using both particle positions, which accounts for the relative dispersion. Such dispersion leads to a narrower plume and higher local concentrations c than for the mean dispersion. The C and σ_c fields are obtained from an ensemble of N widely-spaced sources at height z_s in a horizontal plane, creating N "independent" realizations of the c field (see Weil et al. 2012).

The Moeng and Sullivan (1994) LES model was adopted for the 1-particle LPDM (Weil et al. 2004) and served as a reference case. The LES was run for a 5 × 5 2 km^3 domain, 96^3 grid points, a surface heat flux of 0.24 K ms^{-1}, a mean CBL height z_i of 1 km, a convective velocity scale w_* of 2 ms^{-1}, and a mean wind speed U over the CBL of 3 ms^{-1}; thus, $U/w_* = 1.5$. For the two-particle model, the EULAG (EUlerian/semi-LAGrangian) model (Prusa et al. 2008) was adopted and run for the same setup, domain size, and variables as in Weil et al. (2004).

44.3 Results

We performed L2PDM simulations for four release heights: $z_s/z_i = 0.07$, 0.25, 0.49, and 0.8; the first three matched those in the Willis and Deardorff (WD) (1976, 1978, 1981) experiments and all were close to or the same as in Hibberd (2000).

The simulations were driven by LES fields input sequentially from 210 data volumes stored at 10 s intervals. The C and σ_c fields were obtained with $N = 25$ CPS releases, each with 2.1×10^5 particles, whereas the laboratory experiments used an instantaneous line source (ILS). For sufficiently high U/w_* (≥ 1.5), WD (1976) argued that the C fields for the CPS and ILS were equal upon replacing t by x/U in the ILS results; i.e., rms longitudinal velocity fluctuations σ_u would not significantly affect the CPS results. However, no data were given for the σ_c fields.

Figure 44.1 presents L2PDM results of the mean dimensionless crosswind-integrated concentration (CWIC), $C^y U z_i/Q$, at the surface versus the dimensionless downwind distance $X = w^* x/(U z_i)$, the ratio of travel time (x/U) to the eddy turnover time (z_i/w_*). For the lowest source, the L2PDM results agree well with the earlier 1-particle LPDM and the WD (1976) data, establishing consistency between the 1- and 2-particle LPDMs. However, the Hibberd (2000) data has a much lower peak CWIC, which is probably due to the long ILS setup time ($t_s = 0.4 z_i/w_*$) with emissions distributed over t for $t \leq t_s$. The L2PDM generally agrees with the lab data for the other sources showing a systematic variation with z_s and X, although the Hibberd data has a reduced and delayed peak for $z_s/z_i = 0.25$, likely due to the t_s.

Figure 44.2 shows the CWIC fluctuation intensity, σ_{C^y}/C^y, versus X at the surface. The CPS results (solid line) and lab data are consistent at short range, where the σ_{C^y}/C^y is dominated by plume vertical meandering; the large initial drop in σ_{C^y}/C^y is due to the increase of σ_r relative to the rms meander. However, once the decrease in σ_{C^y}/C^y subsides, the CPS results tend to higher values than the data.

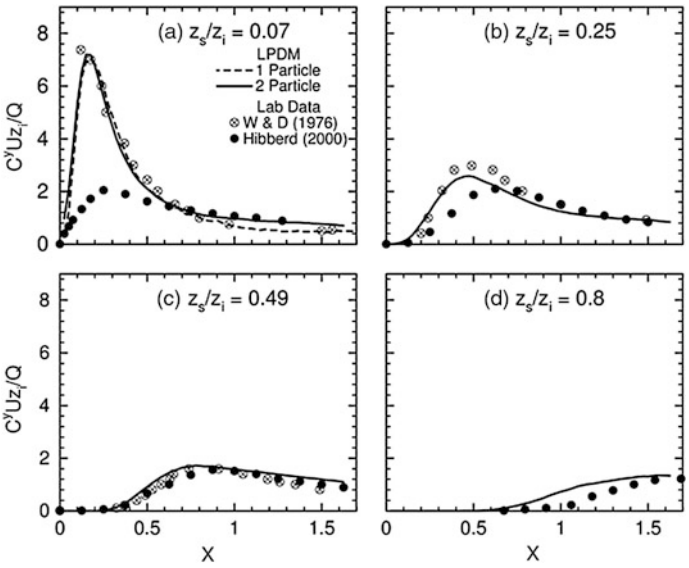

Fig. 44.1 Dimensionless CWIC at surface versus X for 1- and 2-particle LPDMs and comparison to the convection tank experiments of Willis and Deardorff (1976, 1978, 1981) and Hibberd (2000); Weil et al. (2004) only provided the 1-particle LPDM results for $z_s/z_i = 0.07$

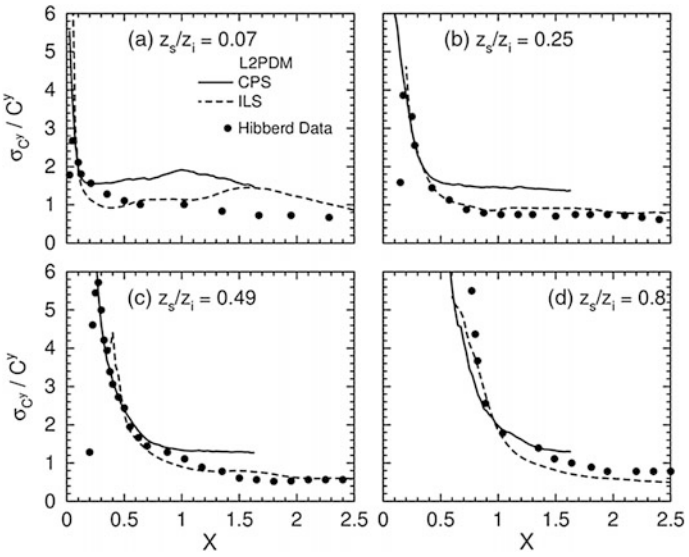

Fig. 44.2 Fluctuation intensity of surface CWIC versus X compared to Hibberd (2000) data

We believe that this is due to the CBL longitudinal variance σ_u^2 generating plume c fluctuations in low winds: U/w_* (~1.5) or equivalently $\sigma_u/U \sim 0.4$. Thus, we modeled the release as an ILS (no σ_u effects), and this result (dashed line) agrees much better with the data. More study is required of the σ_{C^y}/C^y (X) variation with U/w_*.

Overall, these results support the L2PDM-LES approach for modeling mean and fluctuating concentrations due to sources in the CBL, and our contention that the CBL longitudinal variance σ_u^2 affects the rms concentration (σ_c) more than the mean (C) at low values of U/w_*. This contention requires further investigation.

Acknowledgements This work was sponsored by the Defense Threat Reduction Agency and the U.S. Army Research Office (Grant W911NF-09-0572).

Questions and Answers

Question: Peter Viaene: Why do you limit to 2 particles?
Answer: Jeffrey Weil: We restrict the model to 2 particles because it is sufficient to determine both the mean and rms concentrations and it has lower computational demands than models for higher numbers (n) of particles. In principle one needs multi-particle spatial correlations to compute the n–particle relative motions, and these are not readily available; the 2-particle velocity correlations exist and are used in Thomson's (1990) model. Models do exist for tetrads ($n = 4$) (e.g., Toschi, F.,

and E. Bodenschatz, 2009: Lagrangian properties of particles in turbulence. *Ann. Rev. Fluid Mech.*, **41**, 375–404) and clusters of $n = 6$ particles (Sawford, B.L., S.B. Pope, and P.K. Yeung, 2013: Gaussian Lagrangian stochastic models for multi-particle dispersion. *Phys. Fluids*, **25**, 055101-1–055101-19). However, in the latter case ($n = 6$), the model is constrained by the $n = 2$ spatial correlations, and the higher-n spatial correlations are neglected.

Question: Enrico Ferrero: (1) Is there any limitation due to the fact that the two-particle model is valid only for homogeneous isotropic turbulence? (2) Which kind of PDF do you use in the Lagrangian model?

Answer: Jeffrey Weil: (1) Thomson's (1990) 2-particle stochastic model is only used for the subgrid-scale or subfilter-scale treatment, and we believe that the homogeneous isotropic assumption is adequate at this scale and consistent with the LES. The larger-scale inhomogeneous and anisotropic motion of the CBL flow is handled by the LES resolved velocities, which evolve in a natural way in the computed flow field. (2) For Thomson's 2-particle model, the PDF of the random velocity forcing is assumed to be joint normal.

References

Batchelor GB (1950) The application of the similarity theory of turbulence to atmospheric diffusion. Q J R Meteorol Soc 76:133–146

Gifford FA (1959) Statistical properties of a fluctuating plume dispersion model. Adv Geophys 6:117—138. Academic Press

Hibberd M (2000) Vertical dispersion of a passive scalar in the convective boundary layer: new laboratory results. In: Preprints: 11th joint conference on the applications of air pollution meteorology with the A&WMA. American Meteorological Society, Long Beach, CA, pp. 18–23

Moeng C-H, Sullivan PP (1994) A comparison of shear- and buoyancy-driven planetary boundary layer flows. J Atmos Sci 51:999–1022

Prusa JM, Smolarkiewicz PK, Wyszogrodzki AA (2008) EULAG, a computational model for multiscale flows. Comput Fluids 37:1193–1207

Thomson DJ (1990) A stochastic model for the motion of particle pairs in isotropic high Reynolds turbulence, and its application to the problem of concentration variance. J Fluid Mech 210:113–153

Weil JC, Sullivan PP, Moeng C-H (2004) The use of large-eddy simulations in Lagrangian particle dispersion models. J Atmos Sci 61:2877–2887

Weil JC, Sullivan PP, Patton EG, Moeng C-H (2012) Statistical variability of dispersion in the convective boundary layer: ensembles of simulations and observations. Bound.-Layer Meteorol 145:185–210

Willis GE, Deardorff JW (1976) A laboratory model of diffusion into the convective planetary boundary layer. Q J R Meteorol Soc 102:427–445

Willis GE, Deardorff JW (1978) A laboratory study of dispersion from an elevated source within a modeled convective planetary boundary layer. Atmos Environ 12:1305–1312

Willis GE, Deardorff JW (1981) A laboratory study of dispersion from a source in the middle of the convectively mixed layer. Atmos Environ 15:109–117

Chapter 45
Nested Multi-scale System in the PALM Large-Eddy Simulation Model

Antti Hellsten, Klaus Ketelsen, Fotios Barmpas, Giorgios Tsegas, Nicolas Moussiopoulos and Siegfried Raasch

Abstract Large-Eddy Simulation (LES) of atmospheric boundary layer (ABL) is becoming an important research method for urban air-quality studies. Until very recently, it was impossible to include detailed structures, such as buildings in ABL LES. Nowadays, it is possible, but such LES is still limited to a relatively small areas because typically about 1 m resolution is required. However, for several reasons an ABL LES domain should cover a large area leading to huge computational task. A means to overcome this is to concentrate resolution to the primary area of interest by means of model nesting. The idea of nesting is to simultaneously run a series of two or more LES in domains with different sizes and resolutions. In this work, two-way nesting is implemented in the parallelized LES model PALM. The nesting system is tested for several test cases including a convective boundary layer with zero mean wind, several neutral boundary layers over both flat terrain and terrain with an array of obstacles.

45.1 Introduction

Large-Eddy Simulation (LES) of atmospheric boundary layer (ABL) is an important research method. Until very recently, it was impossible to include detailed surface structures, such as buildings or steep complex terrain shapes in ABL LES. Nowadays, it is possible to carry out LES e.g. for complex built areas (Letzel et al. 2008).

A. Hellsten (✉)
Atmospheric Composition Research, Finnish Meteorological Institute, Helsinki, Finland
e-mail: antti.hellsten@fmi.fi

K. Ketelsen
Private Software Consultant, Berlin, Germany

F. Barmpas · G. Tsegas · N. Moussiopoulos
Aristotle University Thessaloniki, Thessaloniki, Greece

S. Raasch
Leibniz Universität Hannover, Hannover, Germany

C. Mensink and G. Kallos (eds.), *Air Pollution Modeling and its Application XXV*, Springer Proceedings in Complexity, DOI 10.1007/978-3-319-57645-9_45

But this is still limited to a relatively small areas because of the high spatial resolution requirement. Xie and Castro (2006) have shown that at least 15–20 grid nodes are needed across street canyons to satisfactorily resolve the most important turbulent structures within the canyons. This requirement typically leads to grid spacings of the order of 1 m. However, the extent of the LES domain should vertically include the whole ABL and the horizontal size should span over several ABL heights. The uncertainty related to the boundary conditions usually decreases as the domain is made larger. Therefore, even larger domains are highly recommendable.

Many numerical solution methods allow variable resolution so that the resolution can be concentrated to the area of principal interest and relaxed elsewhere. However, only unstructured grid systems allow full advantage of spatially variable resolution. Many general-purpose computational fluid dynamics packages offer unstructured grid systems, but such solvers are usually computationally much slower and somewhat less accurate than ABL-tailored LES models, such as PALM (Maronga et al. 2015), that are usually based on structured grid system with constant horizontal resolution. Model nesting approach can be exploited to further speed up ABL LES models or to allow larger domain sizes without compromizing the resolution in the area of primary interest.

The idea of nesting is to simultaneously run a series of two or more LES in model domains with different spatial extents and resolutions. The outermost model is called the root model and it is given boundary conditions on its outer boundaries similarly as in usual LES. The other models are called nest models and their domains are smaller than that of the root and they are nested completely inside the root domain. A nest model can have its own nest models and so on. A nest model obtains boundary conditions from its parent model. In one-way coupled nesting only the nests obtain information from their parents. However, one-way coupled nesting is known to be of little advantage (Clark and Hall 1991). In two-way coupled nesting, also the parents are influenced by their nests (Clark and Farley 1984; Clark and Hall 1991; Sullivan et al. 1996). The latter interaction may be implemented using e.g. the post insertion (PI) approach (Clark and Hall 1991) which means that the parent solution is replaced by the restricted nest solution in the domain of overlap. This procedure is called anterpolation. In practice, some spatial under relaxation is necessary near the nest boundaries in order to avoid growth of unphysical perturbations near the nest boundaries (Moeng et al. 2007). An example of a two-way coupled nesting implemented in the WRF-LES model is given by (Moeng et al. 2007). However, the WRF-LES nesting is limited to horizontal directions, i.e. all the domains have equal height.

45.2 Methods

45.2.1 Numerical Methods

In this work two-way coupled nesting is implemented in the parallelized LES model, PALM (Maronga et al. 2015). PALM is based on the non-hydrostatic, filtered, incompressible Navier-Stokes equations together with a subgrid-scale model according to Deardorff (1980). PALM solves the transport equations in staggered Arakawa C grid with horizontally constant grid spacing. The vertical grid spacing may be stretched. The solution method is a projection method in which a provisional velocity field is first integrated from the momentum equations without the pressure gradient term using three-step Runge-Kutta scheme. Then perturbation pressure is solved from a Poisson equation and the provisional velocity is projected to solenoidal field using pressure gradient. Parallelization of PALM is based on MPI and two-dimensional (horizontal) domain decomposition.

Our nesting approach is a variant of the PI method. In the present implementation, the inter-model communication including interpolations and anterpolations is carried out on each Runge-Kutta substep before the pressure-projection step. This way the mass conservation is enforced in the anterpolated solution. Interpolation scheme is trilinear and the anterpolation is based on top-hat filtering.

45.2.2 Implementation

The nested model system is implemented using two levels of MPI communicators. The inter-model communication is handled by a global communicator using the one-sided communication pattern. The intra-model communication is two-sided and it is handled using a 2-D communicator that has different color for each model. The mapping between each parent and nest model domain decompositions is determined in the initialization phase so that the communication during the time-stepping is straightforward and efficient. Each model inputs and outputs in the same way. The i/o-files are separated from each other by model tags added to their names.

45.3 Test Results

45.3.1 Basic Functional Testing

First, the nested model system was functionally tested in a very simple case with neutral boundary layer over flat ground with no buildings. In this case the system was tested up to three models. First a root model including two parallel nests, and second a root with two cascading nests. The model interfaces are continuous and

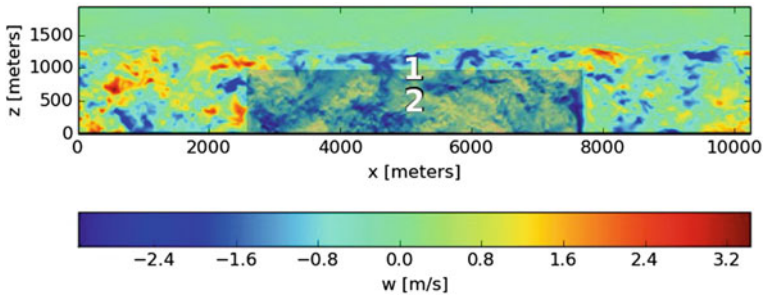

Fig. 45.1 Instantaneous vertical velocity component w in a vertical cut plane through convective boundary layer. Different colormap and transparency is used for the nest solution in order to make the nest boundaries visible

smooth, and the mean profiles in each model domain are consistent with each other. No results from these tests are shown here owing to the space limitation.

45.3.2 Convective Boundary Layer Without Mean Wind

Next, the system was tested in a convective boundary layer with zero mean wind. Also in this case, the ground is flat with no obstacles. The horizontal size of the root domain is 10.24 km × 10.24 km, and its height is 1.92 km. The resolution is 20 m in all directions. The nest domain size is 5.12 km × 5.12 km × 0.96 km with 10 m resolution. Constant kinematic heat flux of 0.15 K m s^{-1} is set on the ground surface and there is a capping inversion starting at height of 1250 m. This test case is described in more detail by Hellsten and Zilitinkevich (2013). Instantaneous vertical velocity component w in an x, z-plane is shown in Fig. 45.1. The figure shows that the solutions are continuous over the nest boundaries. Also vertical profiles are continuous and smooth over the nest top boundary.

45.3.3 Neutral Boundary Layer Over an Array of Obstacles

The next test case is a neutral boundary layer over a uniform non-staggered array of 14 × 8 rectangular obstacles mounted on flat ground. The obstacle size is 32 m 32 m × 24 m and their spacing is 32 m in both directions. The ABL height is about 250 m and the root domain size is 2.048 km × 0.512 km × 0.512 km and resolution is 2 m. The nest domain size is 512 m × 256 m × 128 m and resolution is 1 m. Figure 45.2 shows that the solution is again continuous over the nest boundaries. Also vertical profiles are continuous and smooth over the nest top boundary.

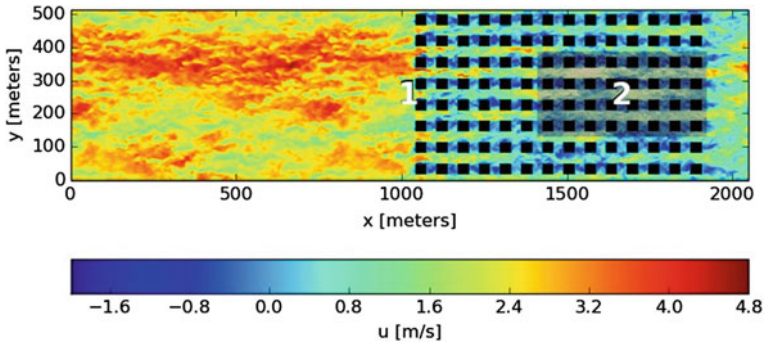

Fig. 45.2 Instantaneous horizontal velocity component u in a horizontal cut plane through the surface layer of a neutral boundary layer over an array of obstacles. Again, different colormap and transparency is used for the nest solution in order to make the nest boundaries visible

45.4 Conclusions

Model nesting functionality based on two-way coupling using post insertion approach is implemented in the parallelized LES model PALM. The implementation is based on two-level parallelism including inter-model and intra-model parallelization by MPI. The nesting system is shown to work well in the test cases considered so far. The next step is to validate the system against measurement data in a realistic urban ABL test case.

Questions and Answers

Questioner: Luca Delle Monache
Question: Can you explain how buildings and topography are treated in fact?
Answer: In the PALM model the terrain topography and buildings are currently taken into account by a simplified masking method. This means that those grid cells, that are located below the surface of the terrain or buildings, are simply excluded from the solution. Surface boundary conditions based on the Monin-Obukhov similarity theory and constant-flux-layer assumption are then applied to the first cells above or adjacent to the surface of the terrain or buildings. However, this arrangement does not allow modelling of buildings with overhanging structures. Therefore, a more general treatment of topograhy is currently being implemented in PALM.

Questioner: Heinke Schlünzen
Question: How do you intend to avoid leaving the LES regime in case of very stable, windles situations as found in some parts of urban areas?

Answer: Such conditions are indeed outside of the range of applicability of the LES approach. In the present example (the oral presentation involved an example of urban LES with stable stratification which is not included in this paper) the degree of stable stratification was kept moderate and there was a considerable geostrophic wind above the ABL. Therefore this case stays within the range of applicability of LES.

References

Clark T, Farley R (1984) Severe downslope windstorm calculations in two and three spatial dimensions using anelastic interactive grid nesting: a possible mechanism for gustiness. J Atmos Sci 41:329–350

Clark T, Hall W (1991) Multi-domain simulations of the time dependent Navier-Stokes equations: benchmark error analysis of some nesting procedures. J Comput Phys 92:456–481

Deardorff JW (1980) Stratocumulus-capped mixed layers derived from a three-dimensional model. Bound-Layer Meteorol 18(4):495–527

Hellsten A, Zilitinkevich S (2013) Role of convective structures and background turbulence in the dry convective boundary layer. Boundary-Layer Meteorol 149:323–353

Letzel M, Krane M, Raasch S (2008) High resolution urban large-eddy simulation studies from street canyon to neighbourhood scale. Atmos Environ 42:8770–8784

Maronga B, Gryschka M, Heinze R, Hoffmann F, Kanani-Sühring F, Keck M, Ketelsen K, Letzel M, Sühring M, Raasch S (2015) The parallelized large-eddy simulation model (palm) version 4.0 for atmospheric and oceanic flows: model formulation, recent developments, and future perspectives. Geosci Model Dev 8:1539–1637

Moeng C, Dudhia J, Klemp J, Sullivan P (2007) Examining two-way grid nesting for large-eddy simulation of the PBL using the WRF model. Mon Weather Rev 135:2295–2311

Sullivan P, McWilliams J, Moeng C-H (1996) A grid nesting method for large-eddy simulation of planetary boundary-layer flow. Bound-Layer Meteorol 80:167–202

Xie Z, Castro I (2006) LES and RANS for turbulent flows over arrays of wall-mounted obstacles. Flow Turbul Combust 76:291–312

Chapter 46
Are CO_2 Emissions from a City Metabolically Consistent with Its Size?

Stefano Galmarini, Greet Janssens-Maenhout and Diego Guizzardi

Abstract Could one speculate a sub-exponential growth of the energy consumption as the city grows in size? In other words *a larger city could require a smaller amount of energy in proportion to its size than a smaller city*, just like for a living creature? CO_2 is a by-product of any animal metabolic activity and human living activities, one could invert the argument and ask: *does a larger city produce less* CO_2 *in proportion to the size difference, than a smaller one?* The paper will address exactly this issue, by analyzing CO_2 emissions of hundreds of city dwellings from middle size towns to megacities, for several countries in the world and across the decades.

46.1 Introduction

The sometimes overstretched analogy that compares a city with a living body is often used in literature to find reasons to justify the agglomeration of people in urban settlements, to relate the advantages of the agglomeration of cells in a body to those of people in a city. A clear example of the latter has been produced with allometric representations by Betancourt et al. (2007), whom without necessarily indulging on the abovementioned analogy show that across the world, positive as well as negatives aspects of social aggregation scale with increasing trends of urban population. Allometric analysis or scaling analysis is a very powerful tool to investigate the correspondence between specific variables especially when the latter span over several orders of magnitudes, such as in the case of city's population and activities. It is well known that the metabolic rate in mammals scales with body mass with a power of ¾. In the case of a city it would be very difficult to measure the metabolic rate as it would depend from a myriad of processes of the most different nature for which there are no data. One could think of metabolic rate in a living creature in terms of metabolic waste resulting from cell respiration, that is

S. Galmarini (✉) · G. Janssens-Maenhout · D. Guizzardi
EC, Joint Research Center, Ispra, Italy
e-mail: Stefano.galmarini@ec.europa.eu

C. Mensink and G. Kallos (eds.), *Air Pollution Modeling and its Application XXV*,
Springer Proceedings in Complexity, DOI 10.1007/978-3-319-57645-9_46

CO_2. Therefore we can assume that there is a direct proportionality between the metabolic rate of mammal, for example, and the amount of CO_2 it produces. By extension of the argument could we try to infer the relationship between the metabolic rate of a city and its size from its CO_2 emissions? Or on a more general level what is the scaling relationship between the size of a city and the CO_2 it emits? As a matter of fact a study already exists that started from the same starting point as this paper but restricted the analysis to the USA (Fragkias et al. 2013). The questions addressed here are: can an urban per capita CO_2 emission level be defined and monitored? How much that depends for equal city sizes on the level of development of the city?

46.2 The Urban CO_2 Emissions from EDGAR and Urban Settlement Identification

The Emissions Database for Global Atmospheric Research (EDGAR) provides for all world countries anthropogenic CO_2 emissions, which are consistently calculated under a bottom-up approach with international activity statistics and emission factors. The latest version EDGARv4.3.1 (EC-JRC/PBL, 2015) provides emissions as time series 1970–2010 and as global emission gridmaps with 0.1 deg $\times$ 0.1 deg $\times$ deg resolution, using the location of point sources or proxies. For more details on the spatial distribution we refer to the EDGAR spatial distribution manual of Janssens-Maenhout et al. (2012). While the CO_2 emissions are spatially unambiguously distributed allocating these to the place of emission, the per capita CO_2 can be allocated also to the place of emission (or human activity) or to the place of living (or population maps). We judge it meaningful to evaluate different per capita CO_2 emissions for a city: (a) either using the average (national) per capita CO_2 and to take the share of the emissions in the city area over the national total; (b) or using the (local) information on the gridded CO_2 and the gridded population data. The latter determines the urban fraction of the emissions in the region. Different urban CO_2 emissions can be defined: either allocating only the CO_2 produced locally in the city area or making the city's population responsible for all CO_2 emissions of activities within, for and around the city. While the production-based approach leads to lower CO_2 per capita values, a consumption-based approach with allocation of emissions from the industry, energy and transport around the city to citizens lifestyle. It was decided to determine the allocation of the CO_2 emissions to the world cities by means of the following methodology. Based on the density of urban occupancy of a grid cell and an algorithm that groups emissions from adjacent cells that have a urban occupancy larger than zero. A shortage of the method is that it may well over estimate the city size. On the one hand we can expect that the density of urban settlements depends largely on the country size but on the other, we cannot expect the same radius of proximity to identify the cells that make a urban settlement in China and in Germany. Ad-hoc radii of proximities have been selected

considering as reference parameter an acceptable value for the number of inhabitant of largest city of the country. The countries analyzed are USA, Germany, Japan, China, India, Brasil and UK for the years 1990 and 2010. The choice of these countries has been based on the fact that: they represent a selection of fully established economies that is reflected on fully developed cities and megacities; there are developing countries with rapidly expanding urban centers. The sectors that are responsible for CO_2 emissions and that are normally accounted for in the EDGAR database are the following: energy production, production/transmission/distribution of fossil fuels, industrial combustion for manufacturing, non-road transport, refineries, small scale combustion for the residential sector (heating/equipping of buildings), road transport sector, fuel transformation sector (fossil fuel + charcoal), solvents manufacturing and use, non-energy use of fossil fuel, chemical process emissions (non-combustion), process emissions of iron and steel production (non-combustion), process emissions of non-ferrous metal industry (non-combustion), process emissions of the non-metallic minerals (cement, lime, bricks, glass, non-combustion), solid waste incineration (not present for all countries because some of the countries go 100% for landfills). A scaling analysis demonstrated that not all sectors scale with populations in every country and only does that do are retained for this analysis.

46.3 Results and Conclusions

The scaling of cities CO_2 emissions as a function of city populations for the years 1990 and 2010 and the considered countries is presented in Table 46.1.

Values clearly reveal that all slopes for all countries except for China 1990 are above 1. For developed countries the tendency seems to be a rather stationarity of the values that either slightly increase or decrease over the 20 years of reference. China shows a remarkable leap forward whereas for India and Brasil the situation is more or less that recorded for developed countries. An interesting characteristic is

Table 46.1 Results of the scaling analysis per country and year, including the national average and the urban average emission

Country	Slope		Nat. average (Tons pc)		Urban average (Tons pc)	
	2010	1990	2010	1990	2010	1990
USA	1.082 ± 0.013	1. 026 ± 0.005	10.97	12.93	9.34	12.12
CHN	1.122 ± 0.029	0.990 ± 0.021	8.56	3.76	10.64	5.01
IND	1.07 ± 0.03	1.108 ± 0.03	2.49	2.41	3.44	1.81
GBR	1.081 ± 0.03	1.08 ± 0.03	7.57	8.58	6.37	6.98
JPN	1.04 ± 0.040	1.07 ± 0.030	9.54	9.26	8.95	7.58
DEU	1.18 ± 0.33	1.17 ± 0.028	11.32	13.95	13.62	16.33
BRA	1.104 ± 0.019	1.102 ± 0.016	4.05	3.67	4.80	4.31

the fact that in all developed countries except for Germany the urban average is constantly lower than the national average, whereas for developing countries the former is larger than the national average emission. The dissonant behavior of Germany from the other developed economies could be attributed to a too coarse resolution of EDGAR and the incapacity to capture the actual city structure. However, past studies conducted for Germany with bottom up approaches on a given city seem to be in line with this out come (H. Schluenzen, private communication).

Questions and Answers

Questioner: G. Weil
Question: In the US, there is a tendency among young people to live in flats within building blocks that are more energy efficient than individual houses. Do you see such a tendency in your analyses?
Answer: Not for the time period analyzed, though if it is a real tendency it could be noticeable within the next decades since CO_2 emissions from housing are a considerable component of a city budget.

References

Bettencourt LMA, Lobo J, Helbing D, Kühnert C, West GB (2007) Growth, innovation, scaling, and the pace of life in cities. PNAS 104 (17):7301–7306; published ahead of print April 16, 2007. doi:10.1073/pnas.0610172104

Fragkias M, Lobo J, Strumsky D, Seto KC (2013) Does size matter? Scaling of CO_2 emissions and U.S. urban areas. PLoS ONE. doi:10.1371/journal.pone.0064727

Janssens-Maenhout et al (2012) EDGAR Gridding manual, JRC report, 2012

Chapter 47
Sensitivity Analysis of Ambient Particulate Matter to Industrial Emissions Using a Plume-in-Grid Approach: Application in the Greater Paris Region

Valentin Raffort, Youngseob Kim, Ludovic Donnat, Catherine Juery, Yelva Roustan, Christian Seigneur and Olivier Duclaux

Abstract The Polyphemus Plume-in-Grid (PinG) model, which is based on a 3D Eulerian model and an imbedded puff model, was developed to represent the dispersion and transformation of air pollutants in industrial plumes. It was later improved to take into account particulate matter (PM) formation and transport in order to evaluate secondary PM formation in refinery plumes. The performance of the PinG model, applied to a refinery in the Greater Paris region, was previously evaluated at the regional scale for July 2009, showing satisfactory results for O_3 and PM. The PinG model is applied here to the same refinery for a different period, April 2013, when local measurements were available. The refinery is located close to a large NH_3 source, which is also treated here using the puff model in order to evaluate the interactions of the plumes of these two industrial sites. Modeled PM is compared here to local measurements in terms of mass concentrations and chemical composition. The measurement sites are located around the refinery and are impacted by the plumes of the two industrial sites. The results show good agreement between measured and modeled PM chemical composition. The sensitivity of the local concentrations to the refinery emissions is evaluated. It is mostly due to primary and secondary inorganic aerosols, emitted and formed in the plumes, and to secondary organic aerosols (SOA) formed from the refinery VOC fugitive emissions.

V. Raffort (✉) · Y. Kim · Y. Roustan · C. Seigneur
CEREA, Joint Laboratory École des Ponts ParisTech/EDF R&D,
Université Paris-Est, 77455 Champs-sur-Marne, France
e-mail: valentin.raffort@enpc.fr

L. Donnat · C. Juery · O. Duclaux
TOTAL Raffinage Chimie, Centre de Recherche TOTAL, 69360 Solaize, France

C. Mensink and G. Kallos (eds.), *Air Pollution Modeling and its Application XXV*,
Springer Proceedings in Complexity, DOI 10.1007/978-3-319-57645-9_47

47.1 Introduction

The Polyphemus Plume-In-Grid model (PinG), coupling an Eulerian 3D model and a Gaussian puff model in subgrid treatment was recently extended to treat PM and volume sources (Kim et al. 2014). This previous study showed that the use of a PinG representation to model industrial point sources leads to a much improved representation of the plume chemical evolution. The PinG model is used here to evaluate the contribution of industrial sources to local PM concentrations. The study focuses on a refinery in the Greater Paris region, in the context of a PM measurement campaign conducted in its vicinity in April 2013. The refinery contribution to local primary and secondary PM concentrations is evaluated, in terms of its impacts on sulfate, nitrate, ammonium, and SOA formation.

47.2 Model Description

The Polyphemus (http://cerea.enpc.fr/polyphemus/index.html) PinG model links a Gaussian puff model (Korsakissok and Mallet 2009) and the Polair3D Eulerian model (Boutahar et al. 2004; Sartelet et al. 2007, 2012). The PinG model was later extended to treat PM transport and chemistry and includes a treatment of volume sources to simulate fugitive VOC emissions (Kim et al. 2014). The treatment of gas-phase chemistry, aerosol chemistry, particle size distribution, and aqueous chemistry is identical in both the 3D Eulerian model and the Gaussian puff model. The model calculates gaseous and particulate species concentrations using the CB05 mechanism (Yarwood 2005) for gas-phase chemistry, the ISORROPIA model (Nenes et al. 1998) for inorganic aerosol species, and the H_2O model (Couvidat et al. 2012) for organic aerosol species.

47.3 Simulation Setup

The Polyphemus PinG model was applied to the Paris region in France (Greater Paris area) for the month of April 2013. Three nested domains are used with one-way coupling. The largest domain covers Europe with a horizontal resolution of 0.5°. The first nested domain covers France with a resolution of 0.1°, and the smallest domain covers the Greater Paris area with a resolution of 0.02°, corresponding to an average cell dimension of 2 km × 2 km. The vertical resolution consists of 9 levels with the top boundary of the corresponding layers at 40 m, 120 m, 300 m, 800 m, 1.5 km, 2.4 km, 3.5 km, 6 km, and 12 km. The Weather Research and Forecast model (WRF) version 3.3 with the Advanced Research WRF (ARW) dynamic solver was used to simulate the meteorological fields over the

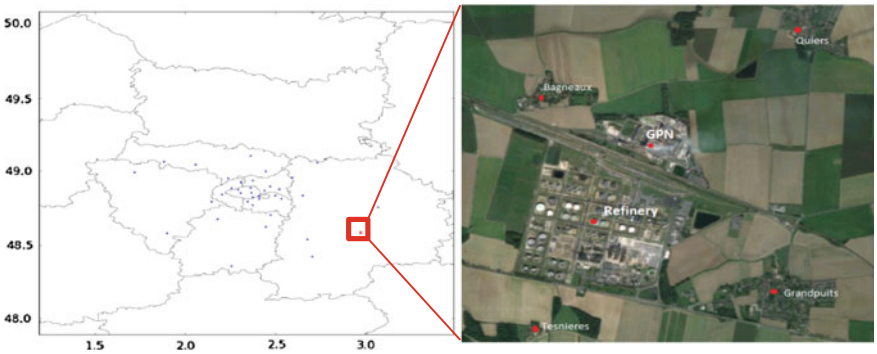

Fig. 47.1 Domain for the Greater Paris simulation (*left*) with the locations of the industrial sites (*blue dots*), the refinery (*red dot*), and the locations of the four measurement sites and the NH_3 source (GPN) around the refinery (*right*)

simulation domains. The smallest domain and the locations of all the industrial sources, which are treated as point emission sources, are shown in Fig. 47.1.

This study focuses on a refinery (Fig. 47.1), which is treated with the PinG representation for both point and volume sources, in order to evaluate its contribution to secondary PM formation and its local impacts on air pollution. The simulation results are compared to local air quality station measurements, located at about 2 km around the refinery. The location of the stations is shown in Fig. 47.1. Daily emission rates of the refinery were provided by its operator for SO_2, NO_2, mineral dust, black carbon, particulate sulfate and ammonium, volatile organic compounds (VOC) and organic matter (OM). VOC emissions are fugitive emissions and are therefore treated as a volume source encompassing the whole refinery. Two simulations were performed, one with the refinery emissions treated with the PinG representation (Simulation 1) and one without the refinery emissions (Simulation 2).

47.4 Comparison to Local Measurements and Estimated Local Contributions

The model results are compared to the measurements available at the four stations. The PM composition measurements were performed from 8 to 18 April 2013. Figure 47.2 shows the modeled and observed PM composition averaged over the measurement period. The refinery contribution corresponds to the difference between simulation 1 and simulation 2.

The PM sulfate and nitrate fractions are well represented by the model at all stations. At each station, the model overestimates the ammonium fraction and underestimates the black carbon (BC) and organic carbon (OC) fractions. It is to be

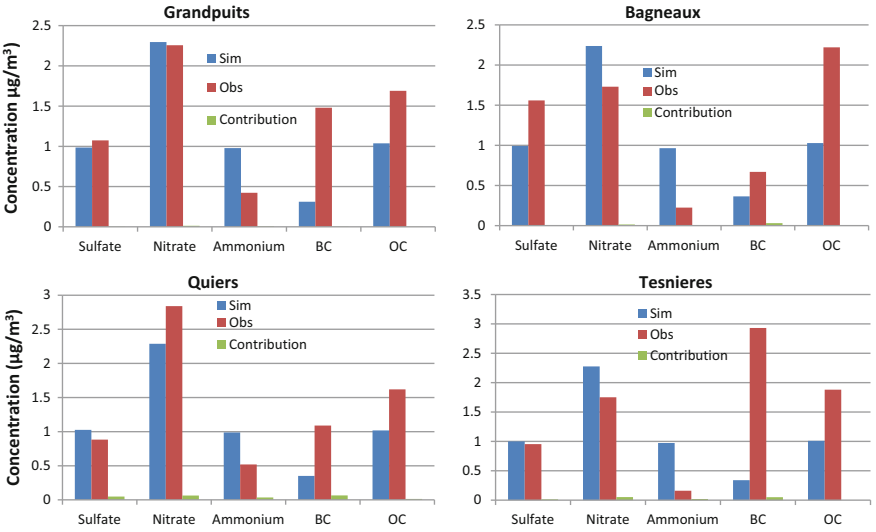

Fig. 47.2 Comparison of the model PM compositions (*blue*) to the measurements (*red*) and estimated refinery contribution (*green*), in µg/m^3

noted that the stations are located in an agricultural area, and are frequently subjected to agricultural engine emissions (e.g. tractor emissions), which are not included in the local emissions inventory. This uncertainty in the inventory leads to a large underestimation of the BC and OC fractions.

The refinery contribution at the four stations, corresponding to the difference between Simulation 1 and Simulation 2, averaged over the whole measurement period, is displayed in Fig. 47.2. The impact is negligible for the two stations closest to the refinery (Grandpuits and Bagneaux), and small for the stations of Quiers and Tesnieres. The contribution is mainly for inorganic aerosol concentrations (sulfate, nitrate, and ammonium) and BC concentrations via the refinery primary BC emissions. The contribution is more important when the distance from the refinery increases, because the puffs are emitted from elevated stacks and reach the ground only after a certain transport distance. Over the whole measurement period, the impacts of the refinery for total inorganic PM are +0.57%, +1.2%, +4.6%, 2.3% at Grandpuits, Bagneaux, Quiers, and Tesnieres, respectively. Figure 47.3 shows the evolution of sulfate, nitrate, and ammonium formation in a refinery puff.

The puff presented in Fig. 47.3 is emitted at the beginning of the measurement period. The sulfate quantity in the puff is mostly primary (0.33 kg emitted, formation of 0.13 kg during the puff lifetime). The ammonium amount is mostly secondary (0.1 kg emitted, and 0.18 kg is formed during the puff lifetime). Nitrate is exclusively secondary (no nitrate emission).

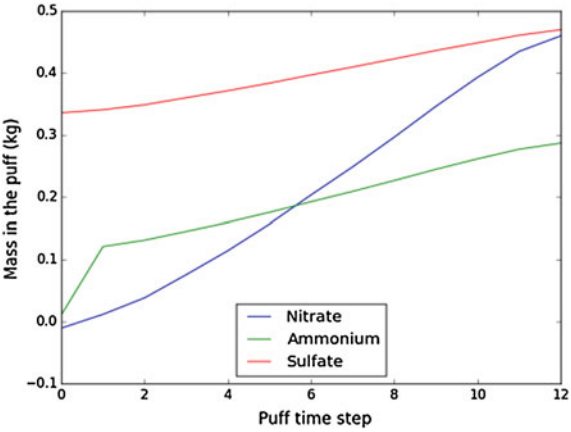

Fig. 47.3 Evolution of nitrate (*blue*), ammonium (*green*) and sulfate (*red*) mass in a refinery puff (emitted at 10:00 a.m. on 8 April 2013)

47.5 Conclusion

The Polyphemus PinG model modified to include a full treatment of PM was used over the Greater Paris area to study the contribution of a refinery to the formation of secondary PM. For the duration of the measurement campaign (8 to 18 April 2013), the averaged local impact of the refinery on the concentration of PM is small for the two stations close to the refinery (+1.5% of total modeled inorganic PM concentration at Bagneaux and Grandpuits) and becomes larger when the distance to the refinery increases (+2.3% and +4.6% of total modeled inorganic PM concentrations at Tesnieres and Quiers, respectively). The refinery contributes to the concentrations of sulfate (mostly primary) and BC, both emitted from the stacks, nitrate, via its NO_x emissions, and ammonium, via the interaction with the background NH_3 and the emitted primary ammonium. The contribution to local OC concentrations is negligible.

References

Boutahar J, Lacour S, Mallet V, Quélo D, Roustan Y, Sportisse B (2004) Development and validation of a fully modular platform for numerical modelling of air pollution: POLAIR. Int J Environ Pollut 22:17–28

Couvidat F, Debry E, Sartelet K, Seigneur C (2012) A hydrophilic/hydrophobic organic (H_2O) model: Model development, evaluation and sensitivity analysis. J Geophys Res 117:D10304. doi:10.1029/2011JD017214

Kim Y, Seigneur C, Duclaux O (2014) Development of a plume-in-grid model for industrial point and volume sources: application to power plant and refinery sources in the Paris region. Geosci Model Dev 7:569–585. doi:10.5194/gmd-7-596-2014

Korsakissok I, Mallet V (2009) Comparative study of Gaussian dispersion formulas within the Polyphemus Platform: evaluation with Prairie Grass and Kincaid Experiments. J Appl Meteor Climatol 48:2459–2473

Nenes A, Pandis SN, Pilinis C (1998) ISORROPIA: a new thermodynamic equilibrium model for multiphase multicomponent inorganic aerosols. Aquat Geochem 4:123–152. doi:10.1023/A:1009604003981

Sartelet KN, Debry E, Fahey K, Roustan Y, Tombette M, Sportisse B (2007) Simulation of aerosols and gas-phase species over Europe with the Polyphemus system: Part I-Model-to-data comparison for 2001. Atmos Environ 41:6116–6131. doi:10.1016/j.atmosenv.2007.04.024

Yarwood (2005) Update to the carbon bound chemical mechanism: CB05 final report to the US EPA, RT-0400675. http://www.camx.com/publ/pdfs/CB05_Final_Report_120805.pdf

Chapter 48
Optimization of Plume Model Calculations and Measurement Network with a Kalman Filter Approach

R. Kranenburg, J. Duyzer and A. Segers

Abstract In many industrial regions there is a strong demand for accurate monitoring of the air pollution and its sources. The Rijnmond area around Rotterdam in the Netherlands is an example of an industrial area affected by air pollution through many industrial and traffic activities as well as shipping emissions. In the area the air quality is traditionally modelled based on a Gaussian plume model using local emissions. To estimate the background concentration due to transport from non-local sources, the average difference between the model calculations and observations at three stations is taken. However, in case of local high emission events, this difference cannot be pointed to the background and the simple approach leads to false estimates of the background resulting in over or under estimation of the concentrations in the rest of the area. In this study we have developed a modeling system with a Kalman filter approach to optimize plume model concentrations using actual observations. This system is capable to adapt modelled concentrations based on the originating source of the concentrations, more accurately than using simple background estimates. We will present the system set-up and results for a testcase in the Rijnmond area for NO_x. For this testcase we have predefined the 'normal' concentrations for different meteorological situations with a Gaussian plume model. Those model calculations are put in a Kalman filter system and assimilated with actual observations. In case of a measured difference of concentration compared to the model, the system will adapt the most likely sources and in addition provide an uncertainty range of the calculation. The results show the

R. Kranenburg (✉) · J. Duyzer · A. Segers
TNO, Department of Climate, Air and Sustainability, 80015,
3508TA Utrecht, The Netherlands
e-mail: richard.kranenburg@tno.nl

C. Mensink and G. Kallos (eds.), *Air Pollution Modeling and its Application XXV*,
Springer Proceedings in Complexity, DOI 10.1007/978-3-319-57645-9_48

system is much better able to represent the NO_x concentrations than previous system. Finally we will show how the system can be used to optimise the monitoring network through minimization of the uncertainty of the model results.

48.1 Introduction

The Rijnmond area around Rotterdam in the Netherlands is an example of an industrial area affected by air pollution through many industrial and traffic activities as well as shipping emissions. In the area the air quality is traditionally modelled based on a Gaussian plume model using local emissions. To estimate the background concentration due to transport from non-local sources, the average difference between the model calculations and observations at three stations is taken. However, in case of local high emission events, this difference cannot be pointed to the background and the simple approach leads to false estimates of the background resulting in over or under estimation of the concentrations in the rest of the area.

In this study we have developed a modeling system with a Kalman filter approach to optimize plume model concentrations using actual observations. This system is capable to adapt modelled concentrations based on the originating source of the concentrations, more accurately than using simple background estimates. On top of this the Klaman filter approach also give estimates of the uncertainty interval for the concentrations.

48.2 Model Description

For this study we have used a Kalman filter approach on the Real Time URBIS model (Spaubek 2004). URBIS is a GIS tool developed by TNO which makes it possible to create detailed area wide maps of noise and air pollution in municipalities (Wesseling and Zandveld 2003). This is done on the basis of data on traffic, activities, emissions or immissions. Annual average concentration fields are calculated for 8 given meteorological conditions for each of the 11 sources used in the model.

In Fig. 48.1, we see an example of the NO_x concentration from traffic with northern wind of 1.5 m/s. For the real time modelling the actual meteorological data are used to calculate hourly concentration fields. This is done by an interpolation of the annual fields. In the Kalman filter approach in this study, we have used 9 monitoring stations in the Rijnmond area to adapt the model results on an hourly basis (Kranenburg 2010).

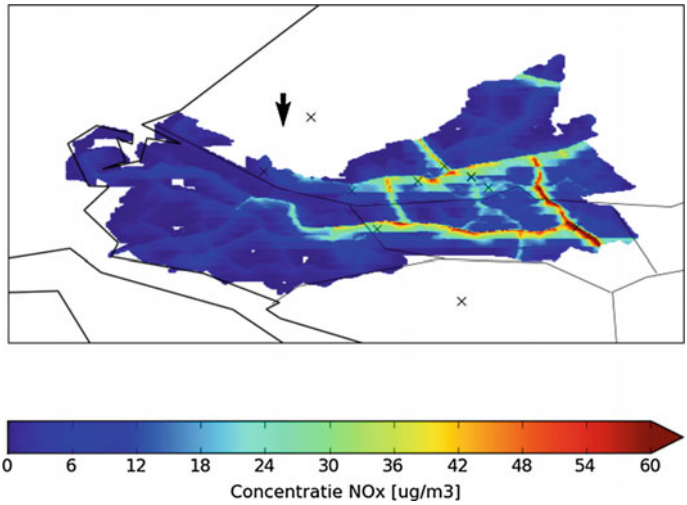

Fig. 48.1 NO_x concentration resulting from traffic with northern wind

The stations are located all around the area and also each of the important emission sources (traffic, industry, shipping and households) is covered by the stations.

Every hour the analysis step of the Kalman filter produce a correction factor of the calculated concentrations from each source, which is used over the whole domain. Further, the Kalman filter also give an uncertainy range of the concentrations.

48.3 Results

In Fig. 48.2, we see the model results for the first week of 2006 model at the station "Bentinckplein" in the center of Rotterdam. This station is located next to a busy road in the city surrounded by a high populated area. In the upper panel we see, the base result of the model. The daily cycle is captured but the high peaks at day three and seven are missed. In the lower panel we see the result after the Kalman filter and we see that we are able to match with the peak on day three, and also reach a better correlation over the rest of the week.

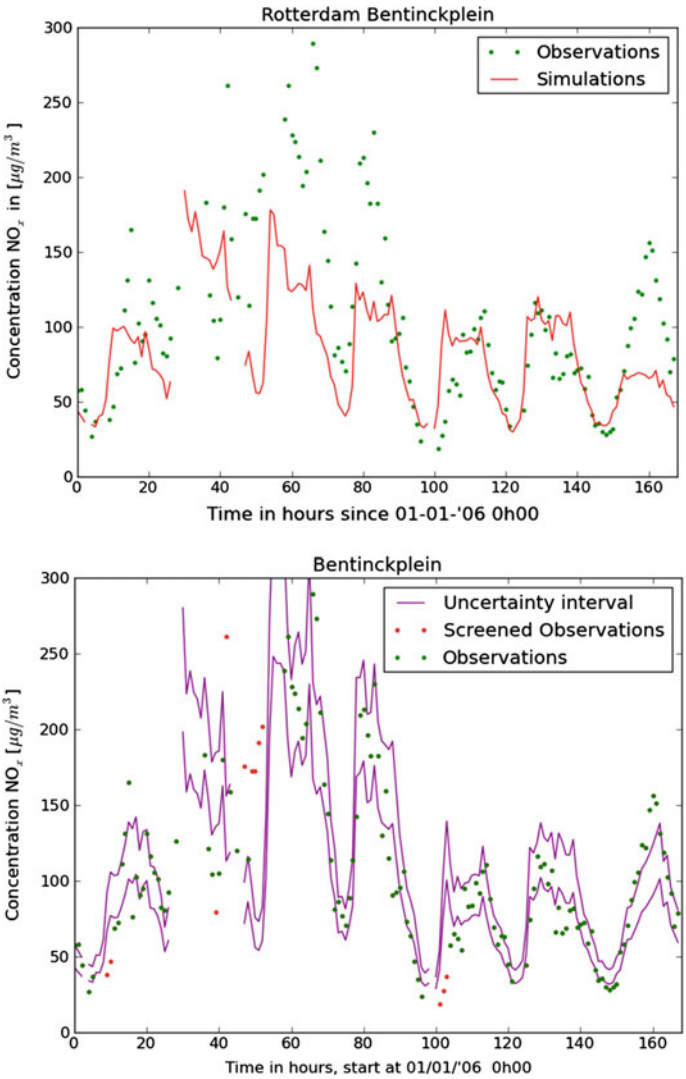

Fig. 48.2 *Upper panel* Base result of the Real Time URBIS model at Bentinckplein for the first week of 2006, *Lower panel* Uncertainty interval after the use of the Kalman filter

Questions and Answers

Questioner: Heinke Schluenzen
Question: How did you consider the spatial dependency of emissions (e.g. from ships), which are due to different positions and movements of the ships time dependent? How is this considered when combining the pre-calculated fields?

Answer: At this point, we take an annual average of the emissions, so we do not take into account the time-dependency due to shipping movements. Contrary to road traffic we have a flat temporal pattern for shipping emissions, so we do not have any timing for shipping, such that only the Kalman filter introduces the some time pattern for shipping.

Questioner: Georgios Tsegas
Question: Regarding the shipping emissions, are they composed from isolated elevated point sources?
Answer: The emissions are not constructed from isolated points, but from main shipping tracks and large harbours. According to those shipping tracks and the staying time and movements in the harbour, the emissions are calculated as an annual average.

Questioner: Luca Delle Monache
Question: What is the forecast lead time of the prediction system you have described? Is there a positive impact of the Kalman filter step beyond 1 h.
Answer: The forecast step is one hour because the measurements are on a hourly basis. After each hour the Kalman filter is applied and the current 'state' is improved. With this improved current state, we make a better forecast for the next hour, which will be again updated after an hour. So in general the impact of the Kalman filter calculation on timestep 'k' is very limited after time k + 1.

References

Kranenburg R (2010) Using a Kalman filter to improve a real time air pollution model. TNO-034-UT-2010-02193_RPT-ML

Spaubek V (2004) Opzet en test van een Real Time URBIS in de Rijnmond. TNO-Report 2004/229

Wesseling P, Zandveld PYJ (2003) URBIS Rotterdam Rijnmond. A pilot study. TNO-Report 2003/245

Chapter 49
The Impact of Emissions from Ships in Ports on Regional and Urban Scale Air Quality

Martin Otto Paul Ramacher, Matthias Karl, Armin Aulinger, Johannes Bieser, Volker Matthias and Markus Quante

Abstract Ships emit considerable amounts of pollutants, not only when sailing, but also during their stay in ports. This is of particular importance for harbor cities because ship emissions contribute to regional and urban air pollution. However, only few studies investigated the specific effect of shipping emissions on air pollution in cities. It is difficult to estimate the emissions from ships in harbors only from the technical specifications of the ships because their activities during their stay at berth differ a lot and are not well known. A multi-level approach was used to calculate the total emissions of ship activities in the port of Hamburg. The resulting emission inventory served as input for the Chemical Transport Model systems TAPM and CityChem. To investigate the impact of ship emissions on air pollution in the Hamburg area two different model runs for January and July 2013 were performed; one model run including land-based emissions and the ship emissions and a model run just including the land-based emissions. The modeling outcomes are compared with air quality data and resulted in dispersion maps of pollutants ($PM_{2.5}$ and NO_2) from harbor related ships in the Hamburg metropolitan area. On the urban scale, the highest concentrations are located in the port area of Hamburg. The monthly averaged NO_2 concentrations mostly remain within the harbor area and the southwest region of Hamburg. The regional background concentrations in the metropolitan area are only slightly increased by shipping emissions from the harbor.

49.1 Introduction

Emissions of exhaust gases and particles from ships contribute significantly to the total emissions from the transportation sector globally (Corbett and Fischbeck 1997; Eyring et al. 2005, 2010). Ships emit carbon dioxide (CO_2), nitrogen oxides (NO_x), sulfur dioxide (SO_2), carbon monoxide (CO), hydrocarbons, as well as primary and

M.O.P. Ramacher (✉) · M. Karl · A. Aulinger · J. Bieser · V. Matthias · M. Quante
Helmholtz-Zentrum Geesthacht, Institute of Coastal Research, Max-Planck-Strasse 1, 21502 Geesthacht, Germany
e-mail: martin.ramacher@hzg.de

C. Mensink and G. Kallos (eds.), *Air Pollution Modeling and its Application XXV*, Springer Proceedings in Complexity, DOI 10.1007/978-3-319-57645-9_49

secondary particles, not only when sailing, but also during their stay in-port maneuvering and hoteling. Climate effects of shipping are two-fold since emitted CO_2 and ozone formed by NO_x emissions are greenhouse gases whereas SO_2 emissions cause cooling through effects on atmospheric particles and clouds. While 70% of shipping emissions occur at sea in a range of 400 km to land (Endresen 2003), the biggest impact in terms of air pollution, contribution to climate change, harm to nature and damage to buildings and monuments happens in harbor cities (Organisation für wirtschaftliche Zusammenarbeit und Entwicklung 2014). In terms of health issues due to air pollution, international shipping is a major source for health damages throughout Europe, with about 50,000 premature deaths (Brandt et al. 2013). Nevertheless, international shipping transport is one of the least regulated anthropogenic emission sources and therefore of rising interest for scientific research (Viana et al. 2014).

When it comes to the investigation of emissions from ships in harbors, the amount and distribution of exhaust gases and particles are of particular interest. Computer based chemical transport model (CTM) systems, which take into account chemical transformation along with their atmospheric advection and diffusion, are most suited when it comes to predicting the spatial distribution of resulting concentrations and deposition fluxes. In this study, an emission inventory for ships in the port of Hamburg for 2013 was created with a bottom-up modeling approach. The main goal of this study was to quantify the effect of harbor based ships on air quality (with regard to NO_x and PM) in the region of Hamburg, Germany. To this end, the detailed port emission inventory developed in this work was employed in model simulations with two city-scale CTMs.

49.2 Ship Emissions Inventory

To calculate the ship emissions inventory, a bottom-up approached using activity data based on the Automatic Identification System (AIS) and activity based-emission factors was used (Aulinger et al. 2015). With the help of AIS data, it is possible to follow the route of a single ship and to estimate its energy demand, fuel consumption and pollutant exhaust along this route. The accurate estimation of emissions from ships at berth (including maneuvering, mooring, loading, unloading, heating, cooling, lighting etc.), which are the main source of shipping emissions in harbors (Hulskotte and Denier van der Goon 2010), requires reliable knowledge of the fuel consumption while at berth and associated fuel characteristics, which was gathered with a survey of energy consumption and fuel type in close cooperation with the Port of Hamburg (Clean North Sea Shipping 2014). The resulting functional relationships between ship size and fuel-use per hour at berth for each ship type have been combined with AIS data to calculate the fuel consumption. Using fuel specific emission factors for the most important species NO_x, SO_2, CO, CO_2, hydrocarbons (VOC), and PM, the total emissions of ships at berth were calculated. Fuel-specific emissions factors in the form of load-dependent

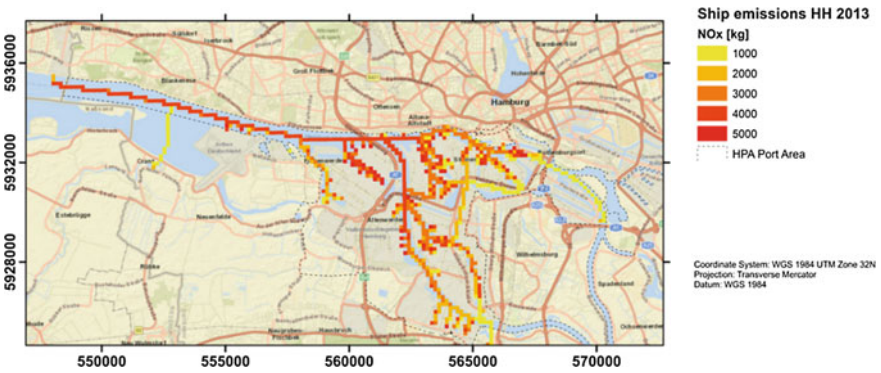

Fig. 49.1 Modeled NO_x (as NO_2) emissions in the port area of Hamburg for 2013

functions were adopted from a study by Germanischer Lloyd (Zeretzke 2013) within Interreg IVb project Clean North Sea Shipping (CNSS). They were spatially distributed on a 250 m × 250 m grid according to the ship routes inside the harbor area and temporally distributed uniformly over a year on hourly time resolution. Figure 49.1 shows the modeled annual NO_x (as NO_2) emissions in the port area of hamburg for 2013. The emissions inventory served as input for two different CTMs.

49.3 Chemical Transport Model Set-Up and Evaluation

The pollutant dispersion resulting from harbor based ship emissions was computed by two CTMs: TAPM (The Air Pollution Model, Hurley 2008) and CityChem (City-scale Chemistry Transport Model, developed recently at HZG, Karl 2016). CityChem is based on the Eulerian urban dispersion model EPISODE (Slørdal et al. 2003). The CityChem model was driven with the meteorology data, generated by the prognostic meteorology module of TAPM. The chemical transport module of TAPM was applied on the Hamburg metropolitan area with a setup of 75 × 75 grid cells of 200 × 200 m^2 each. CityChem was set-up with a main grid of 30 × 30 grid cells of 1 × 1 km^2 each and a sampling grid of 300 × 300 grid cells of 100 × 100 m^2 each. The chemistry in TAPM is based on the Generic Reaction Set (GRS) by Azzi et al. (1992). CityChem was run with detailed EMEP chemistry on the main grid, while using simple photo-stationary equilibrium close to industrial point sources and traffic sources. Emissions from traffic, industry, households were additionally fed into the two models. To investigate the impact of ship emissions on air pollution in the Hamburg area for every model, two different model runs for 2013 for the months January and July were performed; one model run including land-based emissions and the ship emissions and a model run including only the land-based emissions. The modeling outcomes are compared with air quality data from the Hamburg monitoring network (http://luft.hamburg.de/

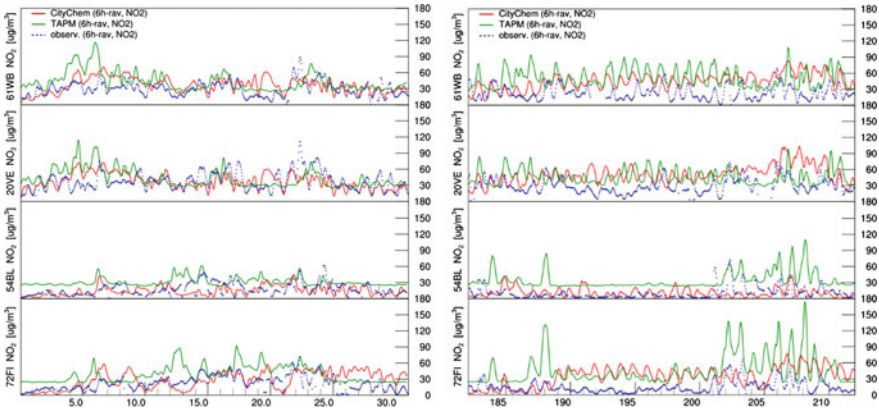

Fig. 49.2 6h running means of NO_2 concentrations for CityChem & TAPM at different urban AQ-stations in January and July 2013

). From the output of both CTMs, dispersion maps of pollutants ($PM_{2.5}$ and NO_x) from harbor related ships in the Hamburg metropolitan area were produced. The contribution of shipping to the modeled concentrations at sites of the AQ monitoring network was evaluated.

Figure 49.2 displays the measured and modeled values at the AQ stations 61WB and 20VE which are urban stations and are supposed to be influenced by shipping emissions, as well as the AQ stations 54BL and 72FL which are not influenced by shipping emissions. TAPM continually over-estimates NO_2 concentrations in comparison to measured values and in most cases compared to CityChem (Fig. 49.4). CityChem also tends to over-estimate NO_2 concentrations but is closer to the measured value range (Fig. 49.4). Nevertheless, the statistical evaluation of CityChem (Table 49.1) shows only moderate performance with higher BIAS values and lower Correlation (CORR r) values in July. Possible reasons for both models are sharp emissions of NO_x, missing CO emissions, chemical reaction mechanisms when it comes to VOC reactivity and local photochemistry. However, CityChem is able reproduce the titration of O_3 and to simulate the seasonal cycle of NO_2

Table 49.1 Statistical indicators of CityChem model runs for NO_2 at different AQ stations in January and July 2013

Station	61WB		20VE		21BI		24FL	
	Jan13	Jul13	Jan13	Jul13	Jan13	Jul13	Jan13	Jul13
MEAN Obs	30.1	23.2	38.6	30.2	29.3	19.5	23.0	16.7
MEAN Mod	36.6	44.6	37.5	50.6	34.7	37.2	28.5	27.5
RMSE	15.1	11.9	15.3	13.8	15.5	7.92	14.4	6.98
BIAS	6.56	21.4	−1.10	20.5	5.36	17.7	5.50	10.8
CORR r	0.36	0.13	0.35	0.25	0.22	0.04	0.18	0.13
SKILLr	1.02	1.73	0.82	1.35	0.97	1.04	0.95	1.36

concentrations, with higher values in winter due to domestic heating. Both models are able to predict the diurnal cycle in most of the cases. For $PM_{2.5}$ (not shown here) the models performed similarly but both models were not capable to simulate particle peak concentrations from long/short-range transportation events.

49.4 Results and Discussion

The 2D air quality maps for both CTMs with all emission sources taken into account show higher concentrations of NO_2 (Fig. 49.3) and $PM_{2.5}$ in the areas within or nearby the port area. Compared to measurements and under consideration of BIAS effects of the regional background, the concentration values tend to be too high. The most probable cause are the underlying emissions for ships or nearby industry sources. The higher over-estimation of NO_2 concentrations by TAPM in comparison to CityChem is reflected within the maps and is probably due to higher and static values for the background (boundary) conditions. The CityChem results also identify much frequented traffic areas as major source of air pollution.

Figure 49.4 shows the effect of NO_2 emissions from shipping as a result of the difference between the CityChem reference run and the CityChem run without shipping emissions. First of all, the effect of shipping emissions related to the harbor strongly depends on the meteorological variables, especially the wind direction. In case of southwesterly wind, the major wind direction in this area, the exhaust gases and particles are carried in the direction of the city center and distribute over the densely inhabited urban territory. In general, the monthly averaged NO_2 concentrations mostly remain within the harbor area and the surrounding region and the background concentrations in the metropolitan area are only slightly increased by shipping emissions from the harbor. The contribution of ship related concentrations of NO_2 and $PM_{2.5}$ in the metropolitan area of Hamburg is primarily located in the southwest area. For NO_2, maximum relative contributions from shipping are 23% in January and 45% in July. For PM2.5 maximum relative contribution from shipping are 3% in January and 16% in July. The highest concentrations for both pollutants are located in the port area of Hamburg. The impact of shipping emissions as calculated by CityChem is higher in July and affects a bigger area within the metropolitan region. The negative shares of NO_2 concentrations in the offset scenarios are due to different vertical distribution of emissions and non-linearity of the underlying chemical reaction mechanisms, when there are no ship emissions.

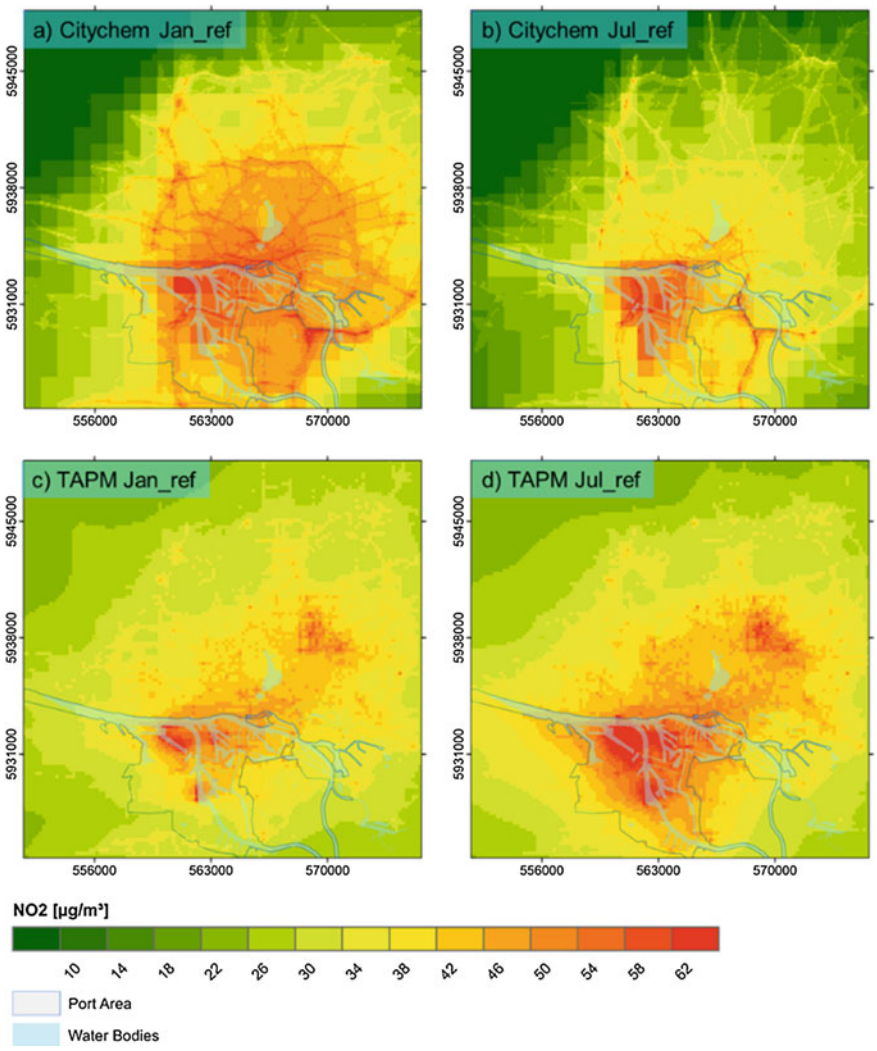

Fig. 49.3 NO_2 concentrations of the reference scenario for January and July 2013 by CityChem (**a**, **b**) and TAPM (**c**, **d**)

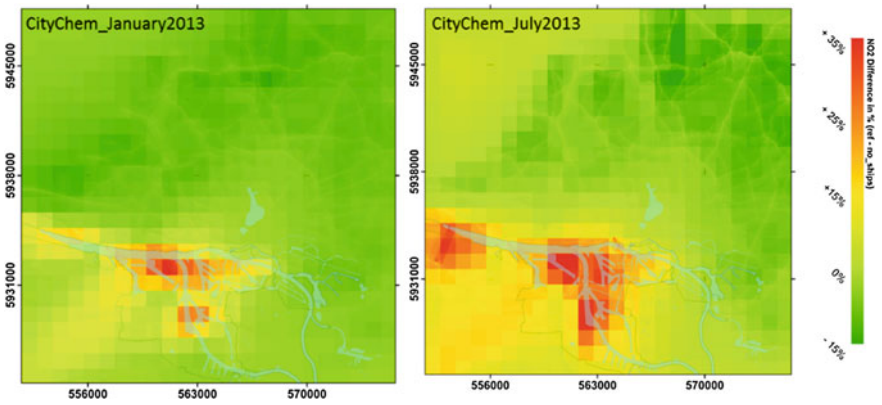

Fig. 49.4 Simulated ship contribution to NO_2 concentrations for January and July 2013 by CityChem

49.5 Conclusion

A detailed emission inventory for ship related exhaust gases and particles in the harbor of Hamburg in 2013 was calculated and fed into two CTMs. The impact of ship related emissions over the metropolitan area of Hamburg on dispersion and concentration of air pollutants was identified by the subtraction of a scenario with land-based emissions only from a scenario with all emissions including ship-related emissions. The effect of harbor based ship activities on the regional background concentration for NO_2 and $PM_{2.5}$ was identified with slight contributions. On the urban scale, the highest NO_2 concentrations are located in the port area of Hamburg and in general, the monthly averaged NO_2 concentrations mostly remain within the harbor area and the surrounding regions. Due to the gaps between modelled and measured values as reflected by poor statistical performance values particularly in July (summer conditions), a refinement of the model is necessary. Especially the NO_x emissions inventory seems to have a disproportionate high influence and requires further research. Furthermore, the chemical reaction mechanisms in CityChem will be refined and tested and dynamic background concentrations will be implemented in future TAPM simulations.

References

Aulinger A, Matthias V, Zeretzke M, Bieser J, Quante M, Backes A (2015) The impact of shipping emissions on air pollution in the Greater North Sea region—Part 1: Current emissions and concentrations. Atmos Chem Phys Discuss 15(8):11277–11323. doi:10.5194/acpd-15-11277-2015

Azzi M, Johnson GM, Cope M (1992) An introduction to the generic reaction set photochemical smog mechanism. In: Proceedings of the 11th international clean air and environment conference, Brisbane

Brandt J, Silver JD, Christensen JH, Andersen MS, Bønløkke JH, Sigsgaard T, Geels C, Gross A, Hansen AB, Hansen KM, Hedegaard GB, Kaas E, Frohn LM (2013) Contribution from the ten major emission sectors in Europe and Denmark to the health-cost externalities of air pollution using the EVA model system—an integrated modelling approach. Atmos Chem Phys 13(15):7725–7746. doi:10.5194/acp-13-7725-2013

Clean North Sea Shipping (2014) Final report—key findings and recommendations. Technical report. http://cnss.no/wp-content/uploads/2014/03/CNSS_Final_Report_web.pdf. Accessed 7 Mar 2016

Corbett JJ, Fischbeck P (1997) Emissions from Ships. Science 278(5339):823–824. doi:10.1126/science.278.5339.823

Endresen Ø (2003) Emission from international sea transportation and environmental impact. J Geophys Res 108(D17). doi:10.1029/2002JD002898

Eyring V, Isaksen IS, Berntsen T, Collins WJ, Corbett JJ, Endresen O, Grainger RG, Moldanova J, Schlager H, Stevenson DS (2010) Transport impacts on atmosphere and climate: shipping. Atmos Environ 44(37):4735–4771. doi:10.1016/j.atmosenv.2009.04.059

Eyring V, Köhler HW, van Aardene J, Lauer A (2005) Emissions from international shipping: 1. The last 50 years. J Geophys Res 110(D17305):1–12. doi:10.1029/2004JD005619

Hulskotte JHJ, Denier van der Goon HAC (2010) Fuel consumption and associated emissions from seagoing ships at berth derived from an on-board survey. Atmos Environ 44(9):1229–1236. doi:10.1016/j.atmosenv.2009.10.018

Hurley PJ (2008) TAPM V4: Part 1: technical description. CSIRO Marine and Atmospheric Research paper, vol 025. CSIRO, Aspendale, VIC

Karl M (2016) Development of the City-scale Chemistry transport model CityChem and its application to the city of Hamburg. Manuscript in preparation for Geoscientific Model Development

Organisation für wirtschaftliche Zusammenarbeit und Entwicklung (2014) Shipping Emissions in Ports: Discussion Paper No. 2014-20. http://www.internationaltransportforum.org/jtrc/DiscussionPapers/DP201420.pdf. Accessed 2 Apr 2016

Slørdal LH, Walker SE, Solberg S (2003) The urban air dispersion model EPISODE applied in AirQUIS2003. Technical description. Kjeller, Norwegian Institute for Air Research (NILU TR 12/2003)

Viana M, Hammingh P, Colette A, Querol X, Degraeuwe B, Vlieger Id, van Aardenne J (2014) Impact of maritime transport emissions on coastal air quality in Europe. Atmos Environ 90:96–105. doi:10.1016/j.atmosenv.2014.03.046

Zeretzke M (2013) Entwicklung eines Modells zur Quantifizierung von Luftschadstoffen, die durch Schiffsdieselmotoren auf See emittiert werden. Master-thesis, Technische Universität Hamburg-Harburg

Chapter 50
Influence of Ship Emissions on Ozone Concentration in a Mediterranean Area: A Modelling Approach

Rita Cesari, Riccardo Buccolieri, Adelaide Dinoi, Alberto Maurizi, Tony Christian Landi and Silvana Di Sabatino

Abstract The impact of ship emissions on the surface concentration of nitrogen oxides (NO_x) and ozone (O_3) in the Mediterranean area of the harbour of Brindisi (IT) has been investigated. Numerical simulations have been performed for a summer period of the year 2012, at different spatial scale, using the meso-scale BOLCHEM and the local-scale ADMS-Urban models. Results show that while average ground concentration of primary pollutant NO_x increases in the area surrounding the port, a decrease in O_3 concentration is observed.

R. Cesari (✉) · A. Dinoi
Institute of Atmospheric Sciences and Climate, National Research Council, 73100 Lecce, Italy
e-mail: r.cesari@le.isac.cnr.it

A. Dinoi
e-mail: a.dinoi@le.isac.cnr.it

R. Buccolieri
Dipartimento di Scienze e Tecnologie Biologiche ed Ambientali, University of Salento, S.P. 6 Lecce-Monteroni, 73100 Lecce, Italy
e-mail: riccardo.buccolieri@unisalento.it

A. Maurizi · T.C. Landi
Institute of Atmospheric Sciences and Climate, National Research Council, 40100 Bologna, Italy
e-mail: a.maurizi@isac.cnr.it

T.C. Landi
e-mail: t.landi@isac.cnr.it

S. Di Sabatino
Department of Physics and Astronomy, ALMA MATER STUDIORUM - University of Bologna, Viale Berti Pichat 6/2, 40127 Bologna, Italy
e-mail: silvana.disabatino@unibo.it

C. Mensink and G. Kallos (eds.), *Air Pollution Modeling and its Application XXV*, Springer Proceedings in Complexity, DOI 10.1007/978-3-319-57645-9_50

50.1 Introduction

Emissions from ships represent a large contribution to the total emissions from the transportation sector. Sulphur dioxide (SO_2) and nitrogen oxides (NO_x) are precursor of secondary pollutants such as ozone (O_3). The Mediterranean region is often interested by episodes of high tropospheric O_3 concentrations, especially in summer. Several model studies estimated the impact of ship emissions on pollutants concentration showing that results are dependent on emission inventories and model spatial resolution (Marmer et al. 2009; Aksoyoglu et al. 2016). Being tropospheric O_3 produced by non-linear reactions among precursors including NO_x and volatile organic compound (VOC), the impact of ship emissions on O_3 formation also depends on background concentrations (Song et al. 2010).

In the present study, we investigated the impact of ship emissions on NO_x and O_3 ground concentrations in the port of Brindisi (Italy) using the mesoscale model BOLCHEM and the local scale dispersion model ADMS-Urban for the summer period July–August 2012. A sensitivity test to the impact of the partition between NO and NO_2 ship emissions on O_3 ground concentration has been performed.

50.2 Geographical Area and Model Description

The study area is the port of Brindisi (South Eastern Italy). The port, with over 2,000 ships/year, is one of the most important of the Adriatic sea. Air pollution is monitored by stations managed by ARPA Puglia. Numerical simulations were performed using the mesoscale model BOLCHEM (Mircea et al. 2008; Colette et al. 2011) and the local scale advanced-Gaussian model ADMS-Urban (CERC 2013).

BOLCHEM comprises the meteorological model BOLAM, an algorithm for airborne transport and diffusion of pollutants, the photochemical mechanisms SAPRAC90 extended to describe the formation of condensable organic products and the aerosol dynamic model AERO3 coupled with the inorganic thermodynamic equilibrium model ISORROPIA and with the partitioning model SORGAM.

ADMS-Urban is a comprehensive system for modelling air quality in large urban areas, cities and towns. It represents source types occurring in an urban area, takes account of complex urban morphology including street canyons. ADMS-Urban models NO_x chemistry using the 8 reaction Generic Reaction Set that includes reactions with ozone and hydrocarbons.

NO_x is mostly emitted as NO. Typical molar NO_2 to NO_x emission ratio are between 10% and 40%, with a value of about 25% at the majority of the ships (Alföldi et al. 2013). The impact of different partitions between NO and NO_2 on O_3 ground concentration has been investigated with ADMS simulations.

50.3 Results and Discussion

BOLCHEM simulations were performed in a one-way nested grid configuration. The nested simulation had horizontal resolution of 0.06° × 0.06°. See Buccolieri et al. (2016) for details. Two runs were performed over the inner domain: the base simulation including anthropogenic emissions from all sources, the other one switching off the Brindisi port ship emissions. Ship emissions were calculated following the methodology Tier 3 of the European methodology EMEP/EEA emission inventory guidebook (EEA 2013), that takes into account gross tonnage and ship typology to calculate the specific fuel consumption. Emission factors were estimated as a function of the combination of engine type and fuel type. Following the zero-out method, the difference between the concentration fields produced by the two runs (thus representing ship emissions contribution) were calculated as $(C_{with\_ships} - C_{no\_ships})/C_{with\_ships}$, with C being the average concentration over the simulation period.

ADMS has been used to assess the spatial distribution of ship emission impact. Simulations were performed over a grid of 100 × 100 cells covering an area of 13 km × 7 km. Only ship-related emissions were explicitly reproduced, while back-ground data were provided by BOLCHEM (with ship emissions from port switched off). Emissions were calculated following the EMEP/EEA emission inventory guide-book. The methodology is described in Buccolieri et al. (2016).

Model results have been compared with ARPA-Puglia monitoring stations data for the whole simulation period using a molar NO_2 to NO_x emission ratio of 10% (Table 50.1). BOLCHEM overestimation of NO_x can be due to the fact that output refers to the model cell representing the harbour, where also ship emissions are located.

Figure 50.1 shows the relative contribution on NO_x and on O_3 ground concentration. To test the sensitivity to the emission ratio on O_3 concentrations, ADMS simulations were performed using values equal to 25 and 40% (Fig. 50.2). Both Figs. 50.1 and 50.2 show that due to ship emissions, NO_x concentration increases in the port area. On the other hand, O_3 decreases due to enhanced titration caused by NO_x emissions. Lower decreases on O_3 concentrations occurred at higher emission ratios values. The decrease of O_3 concentration corresponding to an increase of

Table 50.1 Averaged concentrations of NO_x and O_3 for the period July–August 2012

	NO_x (μg/m^3)			O_3 (μg/m^3)		
	Bolchem	ADMS	ARPA	Bolchem	ADMS	ARPA
Via Taranto	–	20.11	27.63	–	95.81	81.70
Casale		18.32	14.17		96.66	N/A
Via dei Mille		17.98	27.27		96.91	N/A
Terminal		24.60	21.72		93.16	94.12
Perrino		23.37	19.85		93.11	N/A
Average	*36.03*	*20.88*	*22.13*	*86.38*	*95.13*	*87.91*

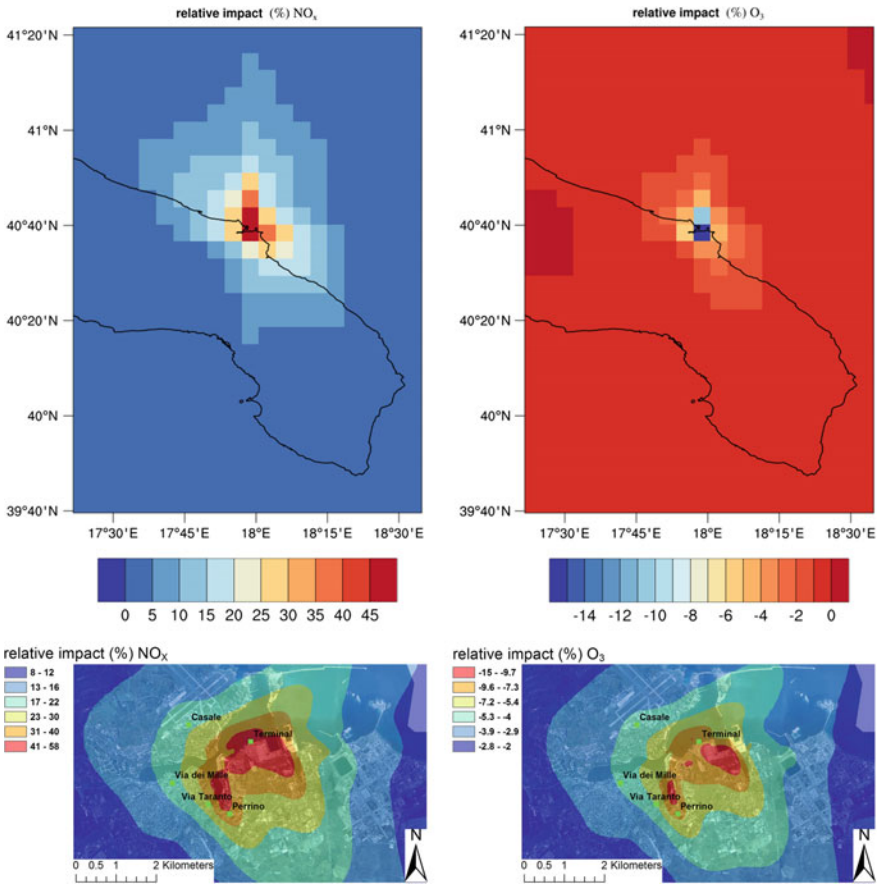

Fig. 50.1 Average relative contribution of ship emissions on NO_x an O_3 ground concentrations obtained from BOLCHEM (*top*) and ADMS-BOLCHEM (*bottom*) for July–August 2012 with NO_2 to NO_x emission ratio of 10%

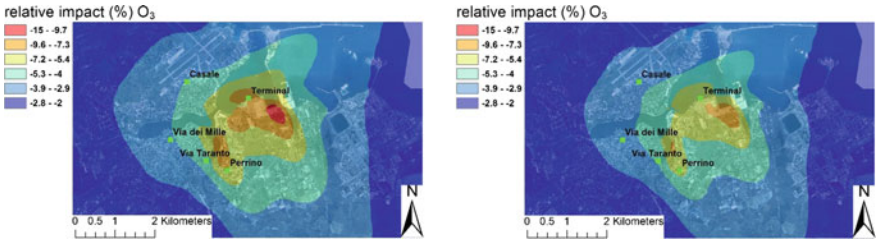

Fig. 50.2 Average relative contribution of ship emissions on O_3 ground concentrations obtained from ADMS-BOLCHEM with NO_2 to NO_x emission ratio of 25% (*left*) and 40% (*right*) for July–August 2012

NO_x emissions is in accordance with the fact that the Italian peninsula is almost entirely NO_x-sensitive, but that there are well defined VOC-sensitive regions located over urban/industrial areas and harbours (Maurizi et al. 2008). In the same area Merico et al. (2016) found a similar O_3 decrease (about 5%).

Acknowledgements This work was supported by the CESAPO project (European Territorial Cooperation Programme Greece–Italy 2007–2013) and by the POSEIDON project (MED program 2007–2013).

References

Aksoyoglu S, Baltensperger U, Prévôt ASH (2016) Contribution of ship emissions to the concentration and deposition of air pollutants in Europe. Atmos Chem Phys 16:1895–1906

Alföldi B, Lööv JB, Lagler F, Mellqvist J, Berg N, Beecken J, Weststrate H, Alfxx Duyzer J, Bencs L, Horemans B, Cavalli F, Putaud J-P, Janssens-Maenhout G, Csordás AP, Van Grieken R, Borowiak A, Hjorth J (2013) Measurements of air pollution emission factors for marine transportation in SECA. Atmos Measure Tech 6:1777–1791

Buccolieri R, Cesari R, Dinoi A, Maurizi A, Tampieri F, Di Sabatino S (2016) Impact of ship emissions on local air quality in a Mediterranean citys harbour after the European sulphur directive. Int J Environ Pollut 59:30–42

CERC (2013) ADMS-Urban Model, Cambridge Environmental Research Consultant, Cambridge. http://www.cerc.co.uk

Colette A, Granier C, Hodnebrog Ø, Jakobs H, Maurizi A, Nyiri A, Bessagnet B, D'Angiola A, D'Isidoro M, Gauss M, Meleux F, Memmesheimer M, Mieville A, Rouïl L, Russo F, Solberg S, Stordal F, Tampieri F (2011) Air quality trends in Europe over the past decade: a first multi-model assessment. Atmos Chem Phys 11:11657–11678

EEA/EMEP (2013) Air pollutant emission inventory guidebook. Technical report No 12/2013. http://www.eea.europa.eu/publications/emep-eea-guidebook-2013

Eyring V, Isaksen ISA, Berntsen T, Collins WJ, Corbett JJ, Endresen O, Grainger RG, Moldanova J, Schlager H, Stevenson DS (2010) Transport impacts on atmosphere and climate: shipping. Atmos Environ 44:4735–4771

Marmer E, Dentener F, Aardenne J, Cavalli F, Vignati E, Velchev K, Hjorth J, Boersma F, Raes F (2009) What can we learn about ship emission inventories from measurements of air pollutants over the Mediterranean Sea. Atmos Chem Phys 9:6815–6831

Maurizi A, Mircea M, D'Isidoro M, Vitali L, Monforti F, Zanini G, Tampieri F (2008) Ozone modeling over Italy: a sensitivity analysis to precursors using BOLCHEM air quality model. In: Proceedings of air pollution modelling and its application XIX

Merico E, Donateo A, Gambaro A, Cesari D, Gregoris E, Barbaro E, Dinoi A, Giovanelli G, Masieri S, Contini D (2016) Influence of in-port ships emissions to gaseous atmospheric pollutants and to particulate matter of different sizes in a Mediterranean harbour in Italy. Atmos Environ 139:1–10

Mircea M, D'Isidoro M, Maurizi A, Vitali L, Conforti F, Zanini G, Tampieri F (2008) A comprehensive performance evaluation of the air quality model BOLCHEM to reproduce the ozone concentrations over Italy. Atmos Environ 42:1169–1185

Song S, Shon Z, Kim Y, Kang YH, Oh IB, Jung CH (2010) Influence of ship emissions on ozone concentrations around coastal areas during summer season. Atmos Environ 44:713–723

Chapter 51
New Development in a Gaussian Puff Model: Consideration of Multiphase Chemical Reactivity During Atmospheric Dispersion

L. Patryl, C. Rose, L. Deguillaume, N. Chaumerliac and P. Armand

Abstract The atmospheric dispersion Gaussian puff model developed by CEA has been coupled with a new cloud chemistry model using the Kinetic PreProcessor KPP. The purpose is to take into account a more complex chemical reactivity during dispersion in order to better assess the impact in case of an accidental release. The preprocessor and chemical mechanism have also been improved by supplementary chemical reactivity (NH_3, HCN…) and by adding new photolysis calculation. The mass transfer of chemical compounds between gas phase, cloud droplet and aqueous chemical reactivity of organic and inorganic compounds has been implemented. Several sensitivity tests show the importance of the atmospheric chemical reactivity for the spatial dispersion of the release. Some of these tests are presented in this study.

51.1 Introduction

In order to take into account chemical reactivity in the atmosphere, a new off-line coupling between the Gaussian dispersion model developed by CEA and the Model of Multiphase Cloud Chemistry (M2C2) (Deguillaume et al. 2004) has been performed in 2012. A recent improvement consisted in the use of a new cloud chemistry model based on the Kinetic PreProcessing KPP module developed for 3D

L. Patryl (✉) · P. Armand
CEA, DAM, DIF, 91297 Arpajon, France
e-mail: luc.patryl@cea.fr

C. Rose · L. Deguillaume · N. Chaumerliac
Laboratoire de Météorologie Physique (LaMP), CNRS/Université Blaise Pascal,
24 av. des Landais, BP80026, 63171 Aubière Cedex, France

C. Mensink and G. Kallos (eds.), *Air Pollution Modeling and its Application XXV*,
Springer Proceedings in Complexity, DOI 10.1007/978-3-319-57645-9_51

chemistry/transport models. This cloud chemistry model is the result of the coupling between the CLEPS aqueous phase mechanism (CLoud Explicit Physico-chemical Scheme) and the gas phase Master Chemical Mechanism, MCM v3.3.1.

This model allows reproducing multiphase cloud chemistry with prescribed microphysics (Mouchel-Vallon et al. 2016). The purpose of this paper is to present these new developments through sensitivity studies. The simulations presented here are based on several environmental scenarii considering various intensities of releases, several chemical compounds and several chemical environments.

51.2 Improvements of the Chemical Module

The KPP kinetic preprocessor is a software tool that assists the computer simulation of chemical kinetic systems. The concentrations of a chemical system evolve in time according to the differential law of mass action kinetics. A numerical simulation requires an implementation of the differential laws and a numerical integration in time (Damian et al. 2002). The Rosenbock integrator is used for numerical calculations. In this study, the new chemical mechanism CLEPS for the aqueous phase reactivity is used. It has been developed recently and represents the oxidation of organic compounds up to 4 carbon atoms. The inorganic mechanism simulates the redox processes involved in the evolution of H_xO_y, sulfur, nitrogen, halogens as well as transition metals ions. The MCM gas phase mechanism also considers the reactivity of a myriad of VOCs and is widely used in other airshed modeling applications for research and regulatory applications. The model also consider a multiphase variable photolysis which is calculated by the radiative transfer model TUV developed by Madronich and Flocke (1999). A parametrization of mass transfer of chemical species into cloud droplets (Schwartz 1986) allows the dissolution of soluble gases in the aqueous phase. A simplified aqueous chemical reactivity considering only inorganic compounds in the aqueous phase have been used to validate this development. The conversion of SO_2 (sulfur) into H_2SO_4 (sulfate) in the presence of oxidants such as H_2O_2 has been followed and shows the robustness of mass transfer parametrization.

A first improvement consisted in adding in the new model the chemical reactivity of the substances that are released in the scenarii in the gas phase since they were not considered in this gas phase mechanism. Emissions and natural depositions of chemical compounds in the gas phase were also added in the mechanism; this allows re-feeding chemicals in the model throughout the whole simulation time. An accidental release is considered as a point source emission of strong intensity. Date, duration and shape are parameters which now allow for constraining the release in the new multiphase mechanism.

51.3 Effect of Multiphase Chemistry on the Accidental Release

Several chemical scenarii such as marine, remote and urban environments have been tested to evaluate the impact of the atmospheric chemistry on the release of selected pollutants (HCN, HNO_3, HCl). We performed several simulations considering or not cloud water phase. The simulation has also been performed for summertime conditions, i.e. for very efficient photolysis. For simulations considering cloud water, a constant droplet radius of 10 μm has been also considered with a liquid water content fixed at 3×10^{-7} vol/vol and a temperature at 20 °C. In this paper, we restricted our results to the marine and urban environments. Figure 51.1 shows the concentration time evolution of targeted gas chemical compounds over 4 days of simulation. In Fig. 51.1, the chemical background is instantaneously disturbed in case of 1×10^{10} molecules cm^{-3} release of ammonia (NH_3). We notice the ammonia concentration decreases very slowly for high releases. NH_3 is oxidized by the hydroxyl radical HO in the gas phase and form NH_2 for which the concentration follows a diurnal cycle, following HO concentration.

In the gas phase, the ozone cycle is also modified by the reaction of NH_2 with O_3 and HONO is strongly destroyed. The HO radical is totally consumed by the huge amount of NH_3. This impacts the oxidation efficiency of organics in the gaseous phase and also in the aqueous phase when cloud water is considered. More specifically, in the aqueous phase, since the HO source from the gaseous phase becomes negligible, the oxidation of some organics such as formic acid (HCOOH) and formaldehyde is strongly reduced. This result shows the indirect effect of the NH_3 release on the transformation in the cloud aqueous phase.

The release of ammonia leads to the modification of the chemical background. The effect is comparable for the accidental release of HCN, HNO_3, HCl or other

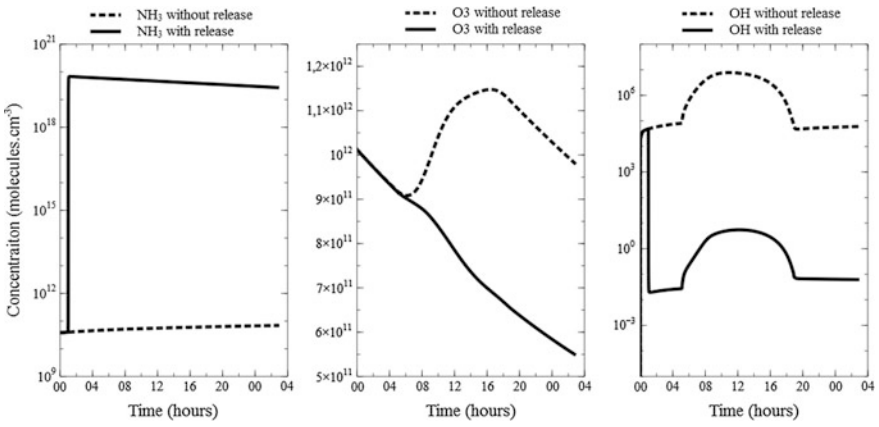

Fig. 51.1 Concentration (mg cm^{-3}) of the main chemical compounds in atmosphere for the gas phase

compounds used in industry. Duration and time (noon, midnight…) are also important parameters which can influence the chemistry reactivity. In fact, the disturbance is more or less pronounced depending on the concentration of the release.

Then, look-up tables have been calculated for each type of chemical releases (NH_3, HCN, HNO_3…) for several concentrations from 2×10^3 to 1×10^{20} molecules cm^{-3} and for several weather situations. During atmospheric dispersion, puffs are corrected by a dC/dt calculated from results of KPP according to puff concentration and time. This coupling method has been described in ITM 2012 (Patryl et al. 2012).

51.4 Chemical Dispersion

Figure 51.2a and c shows the maximum concentration at 1 pm for release respectively of NH_3 and HCL if the chemical reactivity is not taken into account. The source term is 100 kg for each compound. The wind speed varies between 1 and 3 m s^{-1}. The wind direction varies between 309° north to 59° north. The situation is unstable (class D of Pasquill). Figure 51.2b and d shows the same

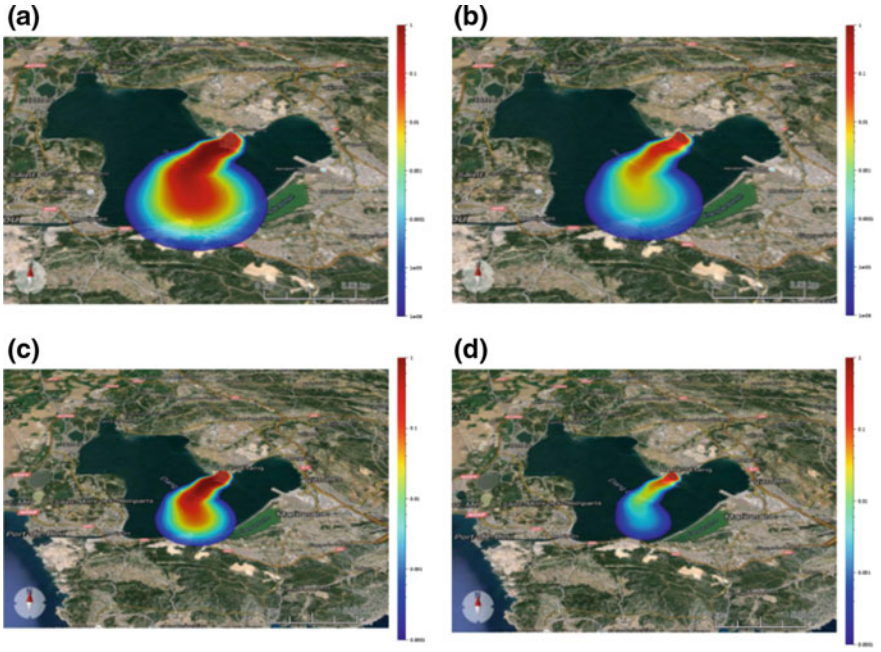

Fig. 51.2 Maximum concentration (mg m^{-3}) **a** NH_3 without chemical reactivity, **b** NH_3 with chemical reactivity, **c** HCL without chemical reactivity, **d** HCL with chemical reactivity

scenario but atmospheric dispersion is corrected with look-up tables which represent the chemical reactivity. In all scenarii, the atmospheric concentration of compounds decreases according to chemical reactivity.

51.5 Conclusion

The coupling between a Gaussian puff dispersion model developed by the CEA, and a new multiphase atmospheric chemical model using the preprocessor KPP, has been performed. The purpose was to assess with more accuracy the effect of the atmospheric multiphase chemistry on the dispersion of pollutants and the consequences on human health in case of a toxic release. Sensitivity tests show that the chemical reactivity can reduce the concentration of pollutant in the atmosphere but also can produce new compounds. The amount and effect of these secondary chemical species should be studied in future studies.

References

Deguillaume L, Leriche M, Monod A, Chaumerliac N (2004) The role of transition metal ions on HOx radicals in clouds: a numerical evaluation of its impact on multiphase chemistry. Atmos Chem Phys 4(1):95–110

Damian V, Sandu A, Damian M, Potra F, Carmichael G (2002) The Kinetic PreProcessor KPP—a software environment for solving chemical kinetics. Comput Chem Eng 26:1567–1579

Madronich S, Flocke S (1999) The role of solar radiation in atmospheric chemistry. In: Boule P (ed) Handbook of environmental chemistry. Springer, Heidelberg, pp 1–26

Mouchel-Vallon C, Deguillaume L, Monod A, Perroux H, Rose C, Ghigo G, Long Y, Leriche M, Aumont A, Patryl L, Armand P, Chaumerliac N (2016) CLEPS: a new protocol for cloud aqueous phase oxidation of VOC mechanisms, submitted to GMDD

Patryl L, Deguillaume L, Chaumerliac N, Tridon F, Armand P (2012) Extension to chemical products of the CERES platform used to evaluate the atmospheric dispersion and human health consequences of noxious releases. In: Air pollution modeling and its application XXII, Springer, pp 703–708

Schwartz SE (1986) Mass-transport considerations pertinent to aqueous phase reactions of gases in liquid water clouds. In: Jaeschke W (ed) Chemistry of multiphase atmospheric systems, NATO ASI Series, G6. Spinger, pp 415–471

Chapter 52
Validation of an Inverse Method for the Source Determination of a Hazardous Airborne Material Released from a Point Source in an Urban Environment

George C. Efthimiou, Spyros Andronopoulos, Ivan V. Kovalets, Alexandros Venetsanos, Christos D. Argyropoulos and Konstantinos Kakosimos

Abstract An improved inverse method was presented recently for the estimation of the location and the rate of an unknown point stationary source of passive atmospheric pollutant in a complex urban geometry. The inverse method was incorporated in the well-established and updated version of the ADREA-HF Computational Fluid Dynamics code. The key improvement of the proposed inverse method implementation lies in a two-step segregated approach combining a correlation and cost functions. At first only the source coordinates are analyzed using a correlation function of measured and calculated concentrations. In the second step the source rate is identified by minimizing a quadratic cost function. The validation of the new algorithm is performed by simulating the MUST wind tunnel experiment. Overall, we observed significant improvement, compared to previous implementations, on reconstructing the source information (location and rate).

G.C. Efthimiou (✉) · S. Andronopoulos · A. Venetsanos
Environmental Research Laboratory, INRASTES, NCSR Demokritos,
Patriarchou Grigoriou & Neapoleos Str., 15310 Aghia Paraskevi, Greece
e-mail: gefthimiou@ipta.demokritos.gr

I.V. Kovalets
Department of Environmental Modelling, Institute of Mathematical Machine and System Problems, National Academy of Sciences of Ukraine, Kiev, Ukraine

C.D. Argyropoulos · K. Kakosimos
Department of Chemical Engineering & Mary Kay 'O Connor Processes Safety Center, Texas A&M University at Qatar, Education City,
PO Box 23874, Doha, Qatar

C. Mensink and G. Kallos (eds.), *Air Pollution Modeling and its Application XXV*,
Springer Proceedings in Complexity, DOI 10.1007/978-3-319-57645-9_52

52.1 Introduction

The characterization of an unknown atmospheric pollutant's source following a release is a special case of inverse atmospheric dispersion problem. Such kind of inverse problems are to be solved in a variety of application areas such as emergency response (e.g. Kovalets et al. 2011; Sharan et al. 2012; Singh et al. 2013) pollution control decisions (Koracin et al. 2011) and indoor air quality (Matsuo et al. 2015).

In the urban or industrial scale, there are few researchers that have combined Computational Fluid Dynamics (CFD) with source estimation techniques (Bady et al. 2009; Chow et al. 2008; Keats et al. 2007; Kovalets et al. 2011; Kumar et al. 2016; Libre et al. 2012).

In this point it should be noticed that in some cases of inverse modeling there are some limitations. According to Dhall et al. (2006) there is a typical problem for non-linear least squares fitting due to the ill-posed minimization problem and the non-convex cost function. This problem is called 'overfitting' effect. According to this effect, the calculation errors which are introduced by the wrong source location and lead to significant underestimation of the concentration are compensated by the overestimated source rate. Thus, the resulting quadratic cost function reaches minimum for the wrong combined solution (source location and source rate). In context of data assimilation this problem is especially important when the number of measurements is insufficiently small. This 'overfitting' effect was also observed in Tsiouri et al. (2014) where the Source Inversion (SI) algorithm produced unsatisfactory results regarding the distance between the true and the estimated source location and the true to estimated source rate ratio.

Efthimiou et al. (2016) presented an integrated and innovative approach, to eliminate the 'overfitting' effect, based on two main improvements. First, we propose a non-simultaneous determination of the source location and rate, based on a two-step segregated approach combining a correlation and cost functions. Second, we suggest a correlation coefficient of measured and calculated concentrations, instead of a cost function (as in Kovalets et al. 2011). Moreover, we investigate the impact of the grid resolution, for the numerical simulations, on the determination of source characteristics. The MUST dataset has been selected for the evaluation of the proposed approach owes to its high quality data and because it has been used extensively by other similar works.

A description of the experiment and the computational simulations can be found in Kovalets et al. (2011). The present grid is slightly different than the one of Kovalets et al. (2011). It consists of 58,500 cells with minimum/maximum cell distances $dx = 4.93/9.9$, $dy = 4.95/6.2$ and $dz = 0.2/2.06$.

52.2 Method of Validation of the Predicted Source Location and Rate

In order to understand the order of magnitude of the error we have used the horizontal $r_H = \sqrt{\left(x^s - x_t^s\right)^2 + \left(y^s - y_t^s\right)^2}$ and vertical $r_V = \left|z^s - z_t^s\right|$ distances of the estimated source location (x^s, y^s, z^s) from the true source location $\left(x_t^s, y_t^s, z_t^s\right)$ where index "t" stays for the true source. We have assumed that the predicted source (x^s, y^s, z^s) is located at the center of the cell.

Concerning the source rate we have calculated the relative source rate ratio $\delta q = \max\left[\left(q^s/q_t^s\right), \left(q_t^s/q^s\right)\right]$ which is always greater than unity for both underestimated and overestimated source rates.

52.3 Computational System

The solution was performed in a Laptop with 8 GB RAM using the OpenMP protocol and all the cores (four) of the processor (Intel(R) Core(TM) i7-4700MQ CPU @ 2.40 GHz).

52.4 Results

The horizontal distance (r_H) between the real and the predicted source was found equal to 10.81 m and the vertical distance (r_V) equal to 0.54 m which are slightly better results than Kovalets et al. (2011) ($r_H = 11$ m and $r_V = 0.8$ m).

The relative source rate ratio was found equal to 2.26 which is again better result than Kovalets et al. (2011) ($\delta q = 3.1$).

52.5 Conclusions

A major change in the data assimilation code of Kovalets et al. (2011) was performed in Efthimiou et al. (2016) and included the implementation of a two-step approach:

- At first only the source coordinates were analyzed using a correlation function of measured and calculated concentrations.
- In the second step, the source rate was identified by minimizing a quadratic cost function.

The validation of the new algorithm was performed for the source location and rate by simulating a wind tunnel experiment on atmospheric dispersion among buildings of a real urban environment. Good results of source location and rate estimation have been achieved when all available measurements (244) were used to solve the inverse problem.

Acknowledgements This publication was made possible by a NPRP award [NPRP 7-674-2-252] from the Qatar National Research Fund (a member of The Qatar Foundation). The statements made herein are solely the responsibility of the authors.

References

Bady M, Kato S, Huang H (2009) Identification of pollution sources in urban areas using reverse simulation with reversed time marching method. J Asian Arch Build Eng 8:275–282

Chow FK, Kosovic´ B, Chan S (2008) Source inversion for contaminant plume dispersion in urban environments using building-resolving simulations. J Appl Meteorol Climatol 47:1553–1572

Dhall JM, Lewis S, Lakshmivarahan SD (2006) Dynamic data assimilation: a least squares approach. Cambridge University Press, p 655

Efthimiou GC, Andronopoulos S, Venetsanos A, Kovalets IV, Kakosimos K, Argyropoulos CD (2016) Modification and validation of a method for estimating the location of a point stationary source of passive non-reactive pollutant in an urban environment. In: 17th international conference on harmonisation within atmospheric dispersion modelling for regulatory purposes, 9–12 May. Budapest, Hungary

Keats A, Yee E, Lien F-S (2007) Bayesian inference for source determination with applications to a complex urban environment. Atmos Environ 41:465–479

Koracin D, Vellore R, Lowenthal DH, Watson JG, Koracin J, McCord T, DuBois DW, Chen L-WA, Kumar N, Knipping EM, Wheeler NJM, Craig K, Reid S (2011) Regional source identification using Lagrangian stochastic particle dispersion and HYSPLIT backward-trajectory models. J Air Waste Manag Assoc 61:660–672

Kovalets IV, Andronopoulos S, Venetsanos A, Bartzis JG (2011) Identification of strength and location of stationary point source of atmospheric pollutant in urban conditions using computational fluid dynamics model. Math Comput Simul 82:244–257

Kumar P, Singh SK, Feiz A-A, Ngae P (2016) An urban scale inverse modelling for retrieving unknown elevated emissions with building-resolving simulations. Atmos Environ 140: 135–146

Libre J-M, Guérin S, Castellari A, Tripathi A, Leguellec M, Mailliard T, Souprayen C (2012) Source determination in congested environment through Bayesian inference. Int J Environ Pollut 48:174–184

Matsuo T, Kondo A, Shimadera H, Kyuno T, Inoue Y (2015) Estimation of indoor contamination source location by using variational continuous assimilation method. Build Simul 8:443–452

Sharan M, Singh SK, Issartel JP (2012) Least square data assimilation for identification of the point source emissions. Pure Appl Geophys 169:483–497

Singh SK, Sharan M, Issartel JP (2013) Inverse modelling for identification of multiple-point releases from atmospheric concentration measurements. Bound Layer Meteorol 146:277–295

Tsiouri V, Kovalets I, Kakosimos KE, Andronopoulos S, Bartzis JG (2014) Evaluation of advanced emergency response methodologies to estimate the unknown source characteristics of the hazardous material within urban environments. HARMO16, Varna, Bulgaria

Part VI
Regional and Intercontinental Modeling

Chapter 53
Scavenging and Convective Clouds in the Lagrangian Dispersion Model FLEXPART

Anne Philipp and Petra Seibert

Abstract The Lagrangian particle dispersion model (LPDM) FLEXPART includes a parameterisation of wet scavenging. With FLEXPART version 8, an improved scheme was introduced which distinguishes between in-cloud and below-cloud scavenging. However, clouds are only diagnosed from grid-scale variables and thus convective clouds are neglected. Although the convection scheme of Emanuel and Živković-Rothman (1999) already implemented in FLEXPART provides this convective cloud (and precipitation) information, it is just used for convective redistribution of computational particles by deep convection. Convection parameters diagnosed from this convection scheme are investigated with the aim to improve the wet scavenging in FLEXPART by using convective cloud parameters.

53.1 Introduction

The open-source Lagrangian dispersion model FLEXPART (http://flexpart.eu/) is used by many groups worldwide, for example for investigations of radionuclide transport, pollution circulations, climatological studies and inverse modelling. It simulates the regional and global transport and dispersion using computational particles and includes processes such as dry and wet deposition. Wet scavenging depends on clouds and precipitation. It is an off-line model which requires meteorological input fields, for example from the European Centre for Medium-Range Weather Forecasts

A. Philipp (✉)
Faculty of Earth Sciences, Geography and Astronomy, Department of Meteorology and Geophysics, University of Vienna, Vienna, Austria
e-mail: anne.philipp@univie.ac.at

P. Seibert
Institute of Meteorology, University of Natural Resources and Life Sciences, Vienna, Austria
e-mail: petra.seibert@boku.ac.at

C. Mensink and G. Kallos (eds.), *Air Pollution Modeling and its Application XXV*, Springer Proceedings in Complexity, DOI 10.1007/978-3-319-57645-9_53

(ECMWF). Typically, convective clouds are grid-scale in the vertical but subgrid-scale horizontally. However, current versions of FLEXPART diagnose clouds from grid-scale parameters only. Since scavenging takes place inside or below clouds, scavenging in the upper parts or even in the whole of convective clouds is neglected.

Some time ago, it was found that under certain conditions artefacts in wet deposition fields (discontinuous fields and sharp gradients along grid lines) can appear. Inconsistent interpolation of clouds and precipitation and missing consideration of convective clouds were identified causes. A "quick fix" was implemented which rectifies the interpolation and also includes a simple assumption of cloud height and bottom if ECMWF fields indicate convective precipitation, resulting in elimination of these artefacts (Arnold et al. 2014). This drives our motivation for further improvement of convective scavenging and wet deposition quality. A possible method for enhancement is to use information already provided by the convective scheme of Emanuel and Živković-Rothman (1999, hereafter EZ99) which is implemented in FLEXPART for the simulation of convective mixing.

The first step is to check the diagnosed cloud and precipitation parameters from EZ99 for realistic height distribution and global patterns before we use them in the wet scavenging scheme.

53.2 Wet Scavenging and Convection in FLEXPART

Wet scavenging (and deposition) is implemented in FLEXPART as $m(t + \Delta t) = m(t) \exp(-\Lambda \Delta t)$, where m is the species mass on the particle, t the time and Λ the scavenging rate. The details of the parameterisation scheme evolved through three main stages (D1–D3), used in different versions of the model:

1. D1 is a bulk scheme without clouds where scavenging is applied over the whole column. The scavenging rate is parametrised with a simple power law $\Lambda = AI^B$, A being the scavenging coefficient in s^{-1}, I the precipitation rate (mm h^{-1}) and B a dimensionless exponent.
2. D2, introduced in v8, differentiates between in-cloud and below-cloud scavenging. Clouds are diagnosed from grid-scale relative humidity and it relies on parametrised cloud liquid water content (CLWC) and fraction of activated aerosol particles. The quick fix mentioned in Sect. 53.1 was developed for this version.
3. D3, the scheme of the current development version, uses cloud total water content (CTWC) from ECMWF with additional differentiation of rain, snow and ice.

In all versions, the precipitation rate is weighted by a correction factor to account for the fact that precipitation is not equally distributed over a grid cell. Further information can be found in Stohl et al. (2005, 2010).

The reasons for choosing to implement EZ99 in FLEXPART were the fact that ready-to-use Fortran code is provided by the authors, the simplicity of the input requirements (grid-scale temperature and relative humidity fields), and that it provides a displacement matrix containing all the information for vertical mixing (Forster et al. 2007). It should be noted that convective tendencies of temperature and relative humidity calculated by EZ99 are not used in FLEXPART as it is an offline model with predefined input fields of these quantities. The basic theory behind the EZ99 scheme is that supply of energy destabilises the atmosphere, and low-level convergence is rather a result of convection. Following the parcel method for conditional instability, the main conditions for convection to be triggered are the presence of convective available potential energy (CAPE), moist static energy is not monotonically increasing and the level above cloud base is unstable. The parameters of interest for our application are cloud top height (c_t, level of neutral buoyancy), cloud base height (c_b, lifted condensation level) and convective precipitation (P_{ez}).

53.3 Properties of Convective Clouds Produced by the EZ99 Convection Scheme

For examining the EZ99 diagnostics in FLEXPART we used a global set of 6-hourly ERA-Interim data from ECMWF. The data span a period of 9 years from 2002 until 2010 at a resolution of 0.75° (about 80 km) and for the lowest 43 vertical levels up to around 100 hPa.

Throughout the analysis, we found a large number of cases without or only spurious convective precipitation even if there was convective precipitation in the ERA-Interim fields (hereafter denoted by P_{ec}). Also on average, P_{ez} is significantly less than P_{ec}. Therefore, in the following, we are using only cases where both precipitation values P_{ez} and P_{ec} exceed 0.1 mm h^{-1}.

The overall maximum of cloud top heights per grid cell is shown in Fig. 53.1a. The general global distribution of convection is realistic. However, there are locations such as over the North Sea where it seems that convection is missing or underdeveloped. Even though the highest (23.5 km) and lowest cloud top maxima (1.1 km) are quite plausible, their spatial distribution is unsatisfactory. Especially over the tropic oceans and the mid-latitude continents we expected stronger deep convection. Furthermore, there are many cases of cloud top heights just reaching about 6 km, and there is a vast number of cases with very shallow convection. Figure 53.2 demonstrates such a case with convective clouds mostly extending just over one model layer, even though ERA-Interim data showed stronger convective precipitation P_{ec}.

After inspecting the EZ99 algorithm, we tested a more strict CAPE determination which is able to eliminate unrealistic shallow convection cases. Resulting maximum cloud top heights are presented in Fig. 53.1b. However, this modification leads to a big reduction of the area experiencing convection. It seems that especially in the northern mid-latitudes and over the tropic oceans almost no convection happened

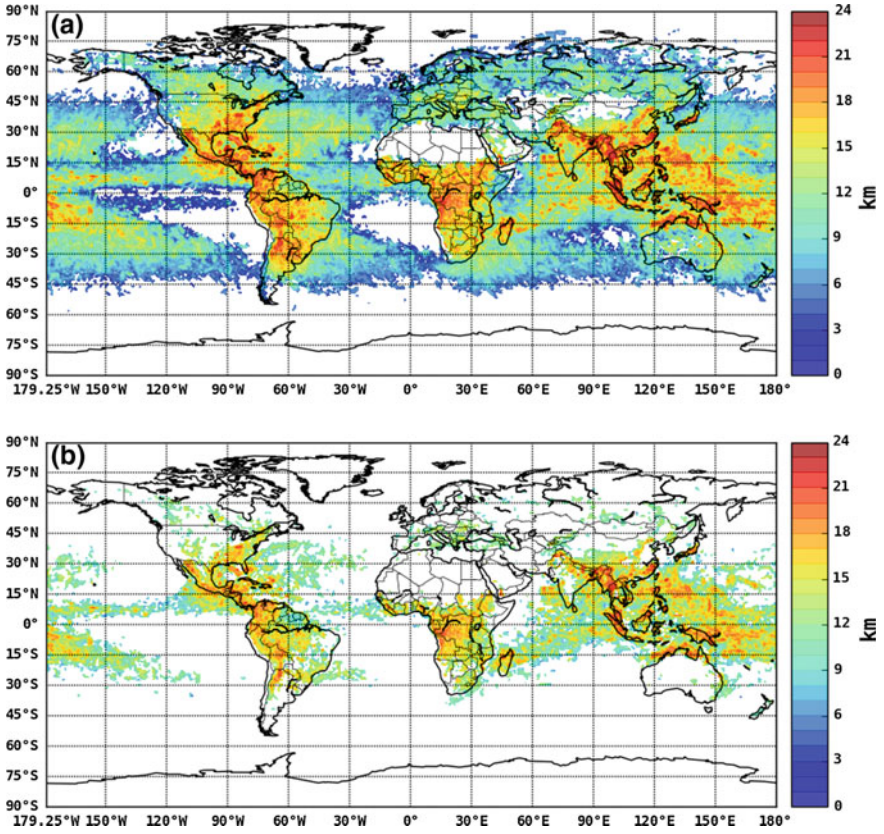

Fig. 53.1 Maximum cloud top height for each grid cell, 2002–2010. White areas: no convection triggered during the whole period. **a** Standard EZ99 scheme as implemented in FLEXPART, **b** with modified CAPE detection. All heights are above ground

over the period of 9 years, which is obviously unrealistic. The highest (22.1 km) and lowest maximum (3.1 km) values are not much different. The fact that elimination of very shallow convection leaves only few areas with convection supports our concern that strong convection is underestimated by EZ99 or, possibly, its implementation in FLEXPART.

53.4 Conclusion and Outlook

Testing the present EZ99 implementation in FLEXPART with a 9-year period globally, we found that it produces too little precipitation and too frequently very shallow convection. Deep convection in the tropics is underestimated, especially over the

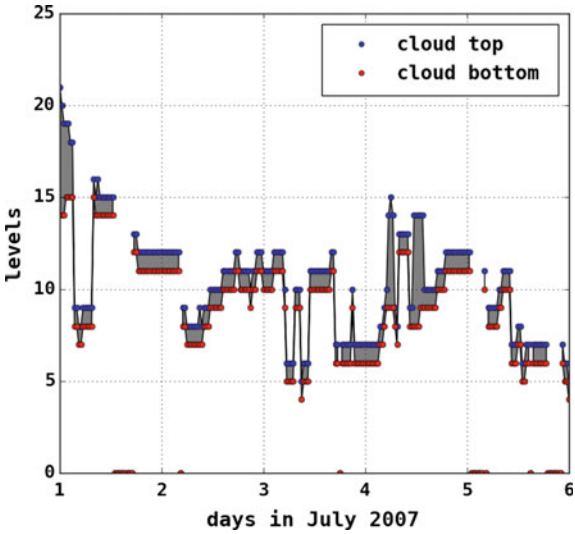

Fig. 53.2 Example of cloud top and base height diagnosed from the EZ99 scheme during a period of shallow convection in first days in July 2007. The *grey shaded area* are the clouds. Markers at level 0 mean that there is no convection. Model levels 5/10/15/20 correspond roughly to 0.16 km /0.76 km/2 km/3.9 km

oceans, and convection in mid-latitudes is too rare and too shallow. Since the vertical redistribution of computational particles in FLEXPART is done on the base of the EZ99 scheme, it is even more important to resolve these deficiencies. Only then we can also improve the wet scavenging scheme for the convective cases. Options for improving the performance of the EZ99 scheme include to test the modifications proposed by Grandpeix et al. (2004) and Peng et al. (2004).

Acknowledgements We thank ZAMG and ECMWF for access to ERA-Interim data.

References

Arnold D, Maurer C, Wotawa G, Draxler R, Saito K, Seibert P (2014) Influence of the meteorological input on the atmospheric transport modelling with FLEXPART of radionuclides from the Fukushima Daiichi nuclear accident. J Environ Radioact. doi:10.1016/j.jenvrad.2014.02.013

Emanuel KA, Živković-Rothman M (1999) Development and evaluation of a convection scheme for use in climate models. J Atmos Sci 56:1766–1782. doi:10.1175/1520-0469(1999)056<1766:DAEOAC>2.0.CO;2

Forster C, Stohl A, Seibert P (2007) Parameterization of convective transport in a Lagrangian particle dispersion model and its evaluation. J Appl Meteor 46:403–422. doi:10.1175/JAM2470.1

Grandpeix JY, Phillips V, Tailleux R (2004) Improved mixing representation in Emanuel's convection scheme. Quart J Roy Meteor Soc 130(604):3207–3222. doi:10.1256/qj.03.144

Peng MS, Ridout JA, Hogan TF (2004) Recent modifications of the Emanuel convective scheme in the Navy operational global atmospheric prediction system. Mon Wea Rev 132:1254. doi:10.1175/1520-0493(2004)132<1254:RMOTEC>2.0.CO;2

Stohl A, Forster C, Frank A, Seibert P, Wotawa G (2005) Technical note: the Lagrangian particle dispersion model FLEXPART version 6.2. Atmos Chem Phys 5:2461–2474. https://www.atmos-chem-phys.org/acp/5/2461/

Stohl A, Sodemann H, Eckhardt S, Frank A, Seibert P, Wotawa G (2010) The Lagrangian particle dispersion model FLEXPART version 8.2. https://www.flexpart.eu/downloads/26

Chapter 54
Biogenic Aerosol Particles in the Earth System Model EC-Earth

R. Schrödner, V. Phillips and E. Swietlicki

Abstract Treatments of emissions of primary biological aerosol particles (PBAP) were implemented in the global Earth System model EC-Earth. These emission schemes were improved to account for the strong peaks of PBAP concentrations in connection to precipitation events, which has been measured recently. The model is now able to treat the emission of bacteria, spores and pollen in dependency of precipitation, 10 m wind speed, relative humidity, season, vegetation type, vegetation cover, and leaf area index. Sensitivity studies on the degree of detail of the PBAP emission parameterization were conducted. The resulting concentration fields of the three PBAP were compared between the different sensitivity setups and, more generally, to the rare available measurements.

54.1 Introduction and Motivation

The reflectivity and extent of the global cloud cover is, besides meteorological parameters, depending on microphysical properties of clouds, i.e. the number and size of the cloud droplets and cloud ice particles. These depend strongly on the physical and chemical properties of the underlying particle population. Due to the release of primary biological aerosol particles (PBAP, e.g. pollen, spores, and bacteria) and the emission of gases (e.g. isoprene and terpenes) that lead to the formation of so-called secondary organic aerosol (SOA), the vegetation directly influences the number, size, and chemical composition of atmospheric particles.

R. Schrödner (✉)
Centre for Environmental and Climate Research, Lund University,
223 62 Lund, Sweden
e-mail: roland.schrodner@cec.lu.se

V. Phillips
Department of Physical Geography and Ecosystem Science, Lund University,
223 62 Lund, Sweden

E. Swietlicki
Division of Nuclear Physics, Lund University, 223 62 Lund, Sweden

C. Mensink and G. Kallos (eds.), *Air Pollution Modeling and its Application XXV*,
Springer Proceedings in Complexity, DOI 10.1007/978-3-319-57645-9_54

To date, the interactions between aerosol particles and clouds represent one major source of uncertainty of climate models (IPCC 2013). Moreover, it is a challenge to quantify how vegetation on land will respond to climate change by altering natural emissions of particles and gases. A subsequent feedback onto cloud properties, the formation of precipitation, and atmospheric radiation may further influence climate change. Thus, the aerosol-cloud-interactions provide multiple mechanisms for ecosystem-cloud-climate feedbacks. It is unclear which ones are more important.

It has been shown recently that the concentration of airborne PBAP in vegetated areas depends on meteorological variables (e.g. precipitation, 10 m wind speed, temperature) and season (e.g. Huffman et al. 2013; Manninen et al. 2014). In particular precipitation events seem to cause increased emission of PBAP resulting in locally strongly increased concentrations of airborne PBAP. To date, there exist only few global model studies that take into account PBAPs (e.g. Hoose et al. 2010; Jacobson and Streets 2009). In these, the emission rates of the considered PBAP species depend on vegetation cover, leaf area index (LAI), relative humidity, gustiness, and season. Emission rates depending on precipitation have to date not been treated.

54.2 EC-Earth and Treatment of PBAP Emissions

The conducted developments take place in the global Earth system modelling framework EC-Earth (Hazeleger et al. 2012). It can couple the atmospheric general circulation model (GCM) IFS (Integrated Forecasting System) to the atmospheric chemistry and transport model TM5 (van Noije et al. 2014), the oceanic GCM NEMO and the sea-ice model LIM3, and the dynamic vegetation model LPJ-GUESS. However for the presented study, in order to save computation time during the development phase, only the atmospheric transport part, TM5, is used driven by ERA-Interim (Berrisford et al. 2011) reanalysis data. TM5 calculates the emission, transport, microphysical and chemical conversions, and deposition of atmospheric gases and aerosol particles. The latter are described with size-resolved modal microphysics scheme M7 (Vignati et al. 2004). It uses seven log-normal size distributions of which four are soluble (nucleation, Aitken, accumulation, coarse) and three insoluble (Aitken, accumulation, coarse). The nucleation, Aitken, accumulation, and coarse mode represent particles with dry diameters smaller than 10 nm, 10–100 nm, 100–1 μm, and larger than 1 μm, respectively. The considered aerosol species are sulfate, black carbon, organic carbon, mineral dust, and sea salt. In addition, TM5 takes into account the total mass of nitrate, ammonium, and methane sulfonic acid.

For the present study, three PBAP species (bacteria, spores, pollen) have been introduced to TM5. Due to their usual size of more than 1 μm diameter they are treated in the insoluble coarse mode. In order to describe the emission of the PABP species the scheme of Hoose et al. (2010) has been implemented. Furthermore, the

scheme has been enhanced to represent the influence of precipitation events on the concentration of airborne PBAP. This parameterization is based on the measurements by Huffman et al. (2013). The PBAP emission rate of the original scheme is increased in dependence on the precipitation rate. Furthermore, precipitation causes leaf wetness, which leads to enhanced growth of microbes and increased emission for some hours after the precipitation event. However, the annual mean concentrations should stay approximately the same. Therefore, the emission rate is decreased if no precipitation occurs. The PBAP emission fluxes now can depend on precipitation, 10 m wind speed, relative humidity, season, vegetation type, vegetation cover, and LAI.

54.3 Global Simulations and Conclusions

Setup. The model is applied for a set of sensitivity studies concerning the degree of detail of the enhanced PBAP emission parameterizations. The global simulations were conducted for one year (2006) with a 3° × 2° horizontal resolution. However, the emissions are first calculated on a 1° × 1° grid and then coarsened. The resulting concentration fields were compared between the different sensitivity setups and, more generally, to the rare available measurements (summarized in e.g. Després et al. 2012).

Results. As expected, if the dependency on precipitation is included in the PBAP emission schemes, the resulting concentration fields show more variability and higher peak concentrations (Fig. 54.1). The relative difference between the original and the enhanced emission scheme is between factors of 0.5–5. The strong increase of peak PBAP concentrations could lead to a stronger local-to-regional

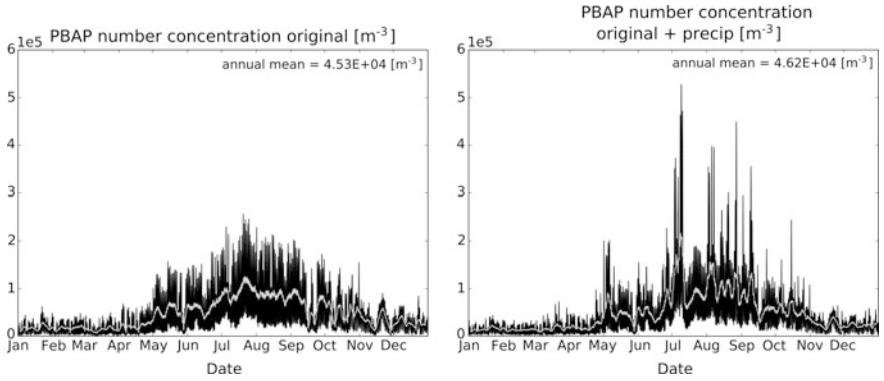

Fig. 54.1 Time series of PBAP number concentration (*black*) and its 30-day moving average (*grey*) in the lowest model layer at Colorado, USA, without (*left*) and with emission additionally triggered by precipitation (*right*)

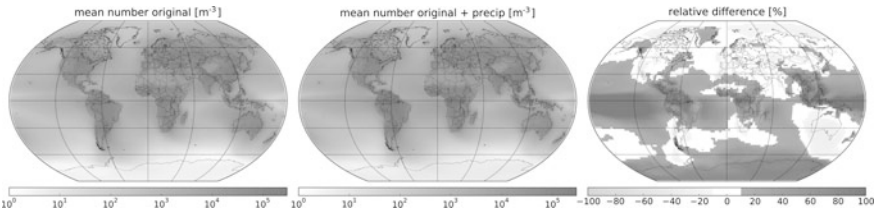

Fig. 54.2 Total PBAP number concentration without (*left*) and with emission additionally triggered by precipitation (*middle*), and relative difference between both

influence of PBAP in aerosol-cloud interactions than can be expected if more averaged emission fluxes are applied.

Overall, the modeled annual mean number concentrations in the lowest model layer do not deviate substantially from the ones resulting from the original emission formulations (Fig. 54.2), i.e. they remain in the range of the available measurements. The highest numbers occur over the densely vegetated tropical rainforests and the subpolar boreal forests, where the annual mean number concentration is up to 3×10^5 m^{-3}. Short-term (1-hourly) peaks often exceed 5×10^5 m^{-3}. The annual mean number fraction of PBAP in the coarse mode (soluble + insoluble) over vegetated land surfaces is between 0.05 and 0.6 with highest values over the tropical rain forests (peaks frequently > 0.9). The occurrence of precipitation is naturally connected with upward transport. Therefore, the increased emission of PBAP during precipitation events leads to substantially higher PBAP number concentrations in the free troposphere (factor 2–3 more) and increased long-range transport (e.g., from South America to the western tropical Pacific Ocean).

Acknowledgements This study is a contribution to the Swedish strategic research area ModElling the Regional and Global Earth system, MERGE.

Question and Answer

Questioner: Christian Hogrefe
Question: As you go into the next phase of your work, do you have sufficient measurements available to assess how your scheme is performing?
Answer: Yes, there is an increasing number of fluorescent particle measurements, which have been analyzed recently. These newer studies are expected to have a higher accuracy than earlier ones. We will use these datasets to validate the variability of the modeled concentrations and connection to meteorological parameters. In addition, there exist many long-term filter measurements providing monthly, seasonal, and annual means.

References

Berrisford P (2011) ERA report series: 1 the ERA-Interim archive version 2.0, European centre for medium range weather forecasts, Shinfield Park, Reading, United Kingdom

Després VR et al (2012) Primary biological aerosol particles in the atmosphere: a review. Tellus B 64:15589

Hazeleger W et al (2012) EC-Earth V2.2: description and validation of a new seamless earth system prediction model. Clim Dynam 39:2611–2629

Hoose C et al (2010) How important is biological ice nucleation in clouds on a global scale? Environ Res Lett 5:024009

Huffman et al (2013) High concentrations of biological aerosol particles and ice nuclei during and after rain. Atmos Chem Phys 13:6151–6164

IPCC (2013) Climate change 2013: the physical science basis. Contribution of working group I to the fifth assessment report of the intergovernmental panel on climate change. Cambridge University Press, Cambridge, United Kingdom and New York, NY, USA

Jacobson MZ, Streets DG (2009) Influence of future anthropogenic emissions on climate, natural emissions, and air quality. J Geophys Res 114:D08118

Manninen HE et al (2014) Patterns in airborne pollen and other primary biological aerosol particles (PBAP), and their contribution to aerosol mass and number in a boreal forest. Boreal Env Res 19:338–405

van Noije et al (2014) Simulation of tropospheric chemistry and aerosols with the climate model EC-Earth. Geosci Model Dev 7:2435–2475

Vignati E et al (2004) M7: an efficient size-resolved aerosol microphysics module for large-scale aerosol transport models. J Geophys Res 109:D22202

Chapter 55
Dimethylsulfide Chemistry: Annual, Seasonal, and Spatial Impacts on Sulfate

Golam Sarwar, Jia Xing, Kathleen Fahey, Kristen Foley, David Wong, Rohit Mathur, Chuen Meei Gan, Brett Gantt and Heather Simon

Abstract We incorporated oceanic emissions and atmospheric chemistry of dimethylsulfide (DMS) into the hemispheric Community Multiscale Air Quality model and performed annual model simulations without and with DMS chemistry. The model without DMS chemistry predicts higher concentrations of sulfate $\left(SO_4^{2-}\right)$ over land compared to the low concentrations over seawater. Including DMS chemistry substantially increases $\left(SO_4^{2-}\right)$ concentrations over seawater and many coastal areas. It enhances the annual mean surface $\left(SO_4^{2-}\right)$ by >0.8 μg/m^3 in some areas of the Pacific Ocean, Atlantic Ocean, Arabian Sea, and Caribbean Sea. The largest enhancement occurs in summer in which DMS chemistry increases surface SO_4^{2-} by 70% over seawater. The model without DMS chemistry underestimates the summer-time observed SO_4^{2-} in the U.S. while the model with DMS chemistry improves model performance in the U.S. coastal areas.

55.1 Introduction

Anthropogenic sources emit sulfur dioxide (SO_2) into the atmosphere which is oxidized by gas- and aqueous-phase chemical reactions to form sulfate $\left(SO_4^{2-}\right)$. Dimethylsulfide (DMS), emitted from oceans, can undergo atmospheric reactions to

G. Sarwar (✉) · K. Fahey · K. Foley · D. Wong · R. Mathur
National Exposure Research Laboratory, Environmental Protection Agency, RTP, NC, USA
e-mail: Sarwar.golam@epa.gov

J. Xing
State Key Joint Laboratory of Environmental Simulation and Pollution Control, School of Environment, Tsinghua University, Beijing 100084, China

C.M. Gan
CSC Government Solutions, RTP, NC, USA

B. Gantt · H. Simon
Office of Air Quality Planning and Standards, Environmental Protection Agency, NC RTP, USA

C. Mensink and G. Kallos (eds.), *Air Pollution Modeling and its Application XXV*, Springer Proceedings in Complexity, DOI 10.1007/978-3-319-57645-9_55

produce SO_2. Here, we study the annual, seasonal, and spatial impacts of DMS chemistry on SO_4^{2-} using the coupled hemispheric Community Multiscale Air Quality (CMAQ) model (Mathur et al. 2012).

55.2 Method

The model uses a horizontal resolution of 108 km and 44 vertical layers. Emissions and meteorological fields previously described by Sarwar et al. (2015) are also used here. Annual anthropogenic SO_2 emissions of ~54 Tg are used in the model (http://edgar.jrc.ec.europa.eu/index.php). Two model simulations are performed for 2006. One simulation uses the Carbon Bond chemical mechanism (CB05) without any DMS chemistry while the other simulation uses the CB05 with DMS. Differences in the results are attributed to DMS chemistry. In CMAQ without DMS chemistry, SO_4^{2-} can be formed via oxidation of SO_2 by one gas-phase reaction and five aqueous-phase reactions. DMS chemistry contains seven additional reactions (Sander 2011) (two reactions with hydroxyl radical and five reactions with nitrate, chlorine radical, chlorine monoxide, iodine monoxide, and bromine monoxide) for oxidation of DMS to SO_2. DMS emissions are calculated using the monthly oceanic climatological DMS concentrations and the total resistance to gas-transfer at the air/sea interface (Lana et al. 2011). We calculate an annual DMS emissions total of 16.1 Tg for the Northern Hemisphere compared to the global annual DMS emissions total of ~28 Tg reported by Kloster et al. (2006) and Lana et al. (2011).

55.3 Results and Discussion

Predicted annual-mean SO_2 and SO_4^{2-} over the seawater in the Northern Hemisphere without and with DMS chemistry are shown in Fig. 55.1. Predicted SO_2 and SO_4^{2-} concentrations generally decrease with altitude, with DMS chemistry effectively increasing SO_2 and SO_4^{2-} levels particularly near surface.

DMS chemistry enhances annual mean SO_4^{2-} over seawater by 48% compared to the simulation without DMS chemistry. It increases SO_4^{2-} by 42% in winter, 42% in spring, 70% in summer, and 43% in fall. The largest impact occurs in summer due to the combination of high DMS emission rates and high oxidant concentrations.

The spatial distribution of the predicted annual-mean surface SO_2 and SO_4^{2-} concentrations are shown in Fig. 55.2. The model without DMS chemistry predicts higher concentrations of SO_2 and SO_4^{2-} over land and small concentrations over seawater reflecting mainly the impact of anthropogenic SO_2 sources. DMS chemistry effectively enhances SO_2 and SO_4^{2-} concentrations over seawater and many

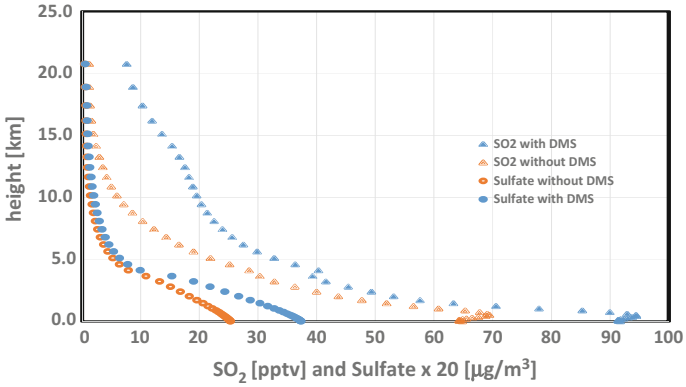

Fig. 55.1 Annual mean SO_2 and SO_4^{2-} over seawater without and with DMS chemistry

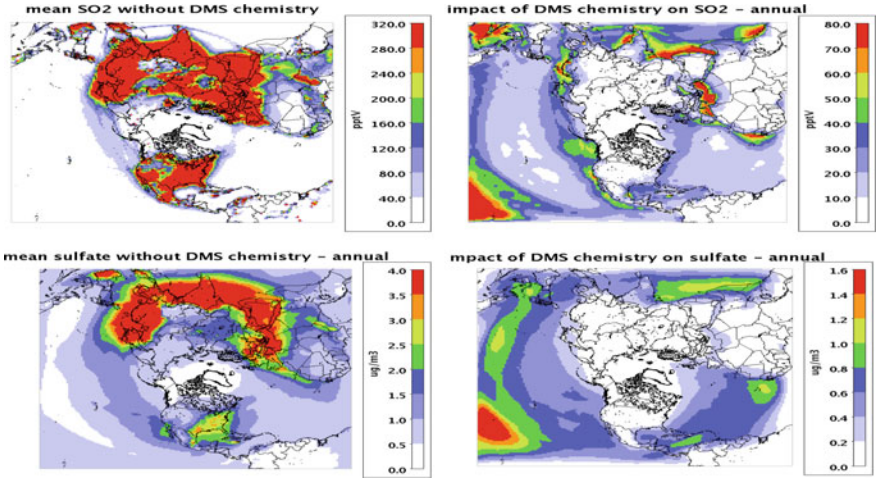

Fig. 55.2 (*Top row*) predicted annual mean SO_2 without DMS chemistry and enhancement due to DMS chemistry (*bottom row*) predicted annual mean SO_4^{2-} without DMS chemistry and enhancement due to DMS chemistry

coastal areas. Higher enhancements are predicted over seawater than over coastal areas. DMS chemistry enhances SO_2 concentrations by >40 pptv in many oceanic areas and SO_4^{2-} levels by >0.8 µg/m^3 in some areas of the Pacific Ocean, Atlantic Ocean, Arabian Sea, and Caribbean Sea.

Predicted SO_4^{2-} levels are compared to observed data from the Chemical Speciation Network (CSN) and the Interagency Monitoring of Protected Visual Environments (IMPROVE) sites in the U.S. (Fig. 55.3a). The model without DMS

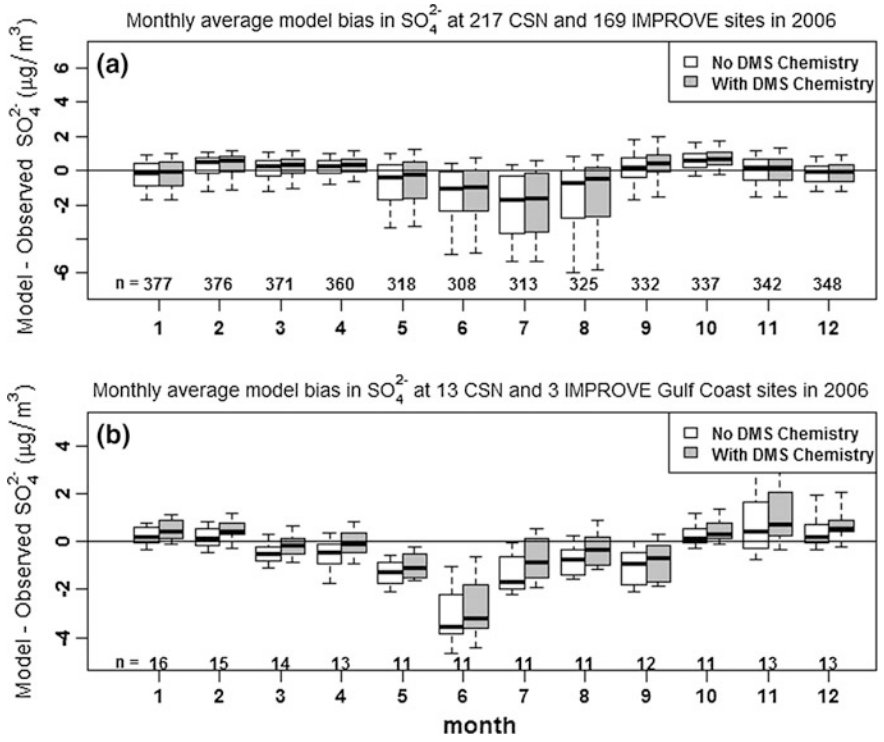

Fig. 55.3 A comparison of model predicted SO_4^{2-} with observed data from CSN and IMPROVE sites for **a** the entire U.S. and **b** sites only in the Gulf Coast areas of the U.S

chemistry underestimates the summertime observed data. DMS chemistry only marginally improves the model performance when compared to observed data from all sites. However, it affects the model performance by larger margins when compared to the observed data from coastal sites (Fig. 55.3b). It improves the model performance from March to September but deteriorates the performance in other months.

55.4 Summary

We performed annual hemispheric CMAQ model simulations without and with DMS chemistry. The model without DMS chemistry predicts only small levels of SO_2 and SO_4^{2-} over seawater. However, DMS chemistry substantially enhances SO_2 and SO_4^{2-} over seawater and coastal areas. It enhances the annual mean surface SO_4^{2-} concentrations by 48% compared to that obtained without DMS

chemistry. It enhances summertime surface SO_4^{2-} by the largest margin among all seasons. The model without DMS chemistry tends to under-predict SO_4^{2-} compared to observed data in the US. DMS chemistry only marginally affects the model performance when compared to the observed data for the entire U.S. However, DMS chemistry affects model performance for SO_4^{2-} by larger margins in U.S. coastal areas.

Disclaimer Although this paper has been reviewed by EPA and approved for publication, it does not necessarily reflect EPA's policies or views.

Questions and Answers on ITM Paper No. 6.40

1. **Questioner name**: Dick Derwent
Question: There is an oxidation product from the OH + DMS reaction which has a competitive fate between NO_2 and O_2 reactions. The NO_2 route produces NO which acts as an ozone sink in high NO_x environments. It would be interesting to see if a small increase in detail in the OH + DMS chemistry could produce this ozone sink along the coast of North America.
Answer: This reaction is not included in our current DMS chemistry. However, we can explore its impact in a future study.

2. **Questioner name**: Pavel Kishcha
Question: Could we expect any significant increase in sulfate aerosols in the future? Water temperature increases due to global warming which is followed by an increase in DMS emissions in one hand. On the other hand, anthropogenic SO_2 emissions could decrease. What factor is more effective?
Answer: Anthropogenic SO_2 emissions have decreased during the last 20 years and are likely to further decrease in the future. DMS emissions may increase in the future due to warmer water temperature. Thus, the relative importance of sulfate aerosols from DMS is likely to increase further in the future.

3. **Questioner name**: Pius Lee
Question: The enhancement plots you showed for sulfate and SO_2 production from considering DMS is much stronger in the Gulf Coast than in the Pacific Coast. It looks to me that there is a strong temperature dependency. Is it as great as halogen that is roughly dependent on water temperature (exponentially)?
Answer: Inorganic halogen (iodine) emissions depend on seawater iodide concentration, atmospheric O_3, and wind speed. Seawater iodide concentration has a strong dependency on seawater temperature. DMS emissions depends on seawater DMS concentration and transfer velocity. Seawater DMS concentrations are obtained from a global database and the Nightingale et al. (2000) parameterization is used to calculate transfer velocity. While both the wind speed and temperature affect transfer velocity, wind speed has a stronger influence on transfer velocity and DMS emissions.

References

Kloster S, Feichter J, Maier-Reimer E, Six KD, Stier P, Wetzel P (2006) DMS cycle in the marine ocean-atmosphere system—a global model study. Biogeosciences 3:29–51

Lana A et al (2011) An updated climatology of surface dimethylsulfide concentrations and emission fluxes in the global ocean. Global Biol Cycles, 25(1):1–17, GB1004

Mathur R, Gilliam R, Bullock OR, Roselle S, Pleim J, Wong D, Binkowski F, Streets D (2012) Extending the applicability of the community multiscale air quality model to hemispheric scales: motivation, challenges, and progress. In: Steyn DG, Trini S, (eds), Air pollution modeling and its applications XXI, The NATO science for peace and security programme, pp 175–179. Springer, Dordrecht, The Netherlands, Chapter 30

Nightingale PD, Malin G, Law CS, Watson AJ, Liss PS, Liddicoat MI, Boutin J, Upstill-Goddard RC (2000) In situ evaluation of air-sea gas exchange parameterizations using novel conservative and volatile tracers, Global Biogeochem Cy 14(1):373–387

Sander S et al (2011) Chemical kinetics and photochemical data for use in atmospheric studies, evaluation no. 17. Jet Propulsion Laboratory, Pasadena, CA, 10 June 2011

Sarwar G, Gantt B, Schwede D, Foley K, Mathur R, Saiz-Lopez A (2015) Impact of enhanced ozone deposition and halogen chemistry on tropospheric ozone over the Northern Hemisphere. Environ Sci Technol 49(15):9203–9211

Chapter 56
Toward a Unified National Dust Modeling Capability

Pius Lee, Daniel Tong, Youhua Tang and Li Pan

Abstract This study aims to improve the NOAA Operational Dust Forecasting Capability. NOAA has developed and is operating the U.S. Dust Forecasting Capability (DFC) in concert with one of its core missions to build a "Weather Ready Nation". The current DFC is based on the Hybrid Single Particle Lagrangian Integrated Trajectory (HYSPLIT) model (Draxler et al. 2010). The NOAA DFC has been in operations since November 2011. DFC gives dust forecast in the form of hourly surface fine particulate (particle small than 2.5 m in diameter ($PM_{2.5}$)) concentration out to 48 h covering the continental United States (CONUS). It is based on the HYSPLIT simulations made at the National Centers for Environmental Prediction (NCEP) (forecast available at http://airquality.weather.gov). The DFC real-time dust forecast is widely used to help assessing and mitigating dust storm impact on the society and the environment such as on human health (e.g., Valley Fever), air and ground transportation safety, local economy such as estate value depreciation, and climate change. This study leverages the superiority of the High Resolution Rapid Refresh (HRRR) meteorological model. HRRR is a 3 km horizontal resolution regional numerical weather prediction (NWP) model for the CONUS, run operationally at NCEP. HRRR is proposed to provide the meteorology for the DFC. We propose to develop, test, and possibly select among several wind-blown dust emission schemes for the DFC dust-emission modeling. We considered the in-line emission modules in HRRR and the FENGSHA-CMAQ (the U.S. EPA Community Multiscale Air Quality model) windblown-dust module in the operational National Air Quality Forecasting Capability (NAQFC). The FENGSHA-CMAQ version 5.1's wind-blown dust emission and diffusion module provides the initial wind-blown dust uptake and airborne suspension from the surface by using the surface wind from HRRR, and the HRRR low layer meteorology

P. Lee (✉) · D. Tong · Y. Tang · L. Pan
Air Resource Laboratory (ARL), NOAA, College Park, MD, USA
e-mail: pius.lee@noaa.gov

D. Tong · Y. Tang · L. Pan
Cooperative Institutes for Satellite and Climate, University of Maryland, College Park, MD, USA

C. Mensink and G. Kallos (eds.), *Air Pollution Modeling and its Application XXV*,
Springer Proceedings in Complexity, DOI 10.1007/978-3-319-57645-9_56

determines transport and turbulent mixing for the dust. These emission schemes are tested and evaluated over severe dust storms in the Western U.S. on May 11 2014.

56.1 Introduction

We report our effort to unify several popular dust-emission modules in various readiness levels for operational implementations, such as the in-line modules developed for HRRR and the modularized FENGSHA-CMAQ code in the operational NAQFC. We focused on a May 11 2014 storm outbreak in UT, AZ, and CA as a test case for the study. Besides the evaluation statistics we aim to rank the various wind-blown dust emission algorithms. One co-benefits from this study is its potential to better quantify dust and its impact on cloud microphysics and radiative feedback influencing the meteorology and climate.

The HRRR model is cycled on an hourly basis and forecast 18 h into the future. Because of its high temporal and spatial resolution, the HRRR is credited with providing more detailed information to decision makers than other operational mesoscale meteorological NWP models. The HRRR is based on the Weather Research and Forecasting meteorological model with the Advanced Research WRF dynamic core (WRF, Skamarock et al. 2007). With the superiority of HRRR one can anticipate good wind prediction to facilitate good modeling for dust uptake and initial suspension of dust particles as well as evolution of the dust plume due to turbulence mixing and transport.

56.2 The Fengsha-CMAQ Dust Module

The NOAA NAQFC uses the CMAQ as the chemical Transport model (CTM) (Byun and Schere 2006; Chai et al. 2013; Pan et al. 2012). The operational NAQFC equipped with the FENGSHA-CMAQ wind-blown dust emission and transport can provide a first cut testing of NAQFC's current capability to capture wind-blown dust forecast.

Dust emissions for the NAQFC's CMAQ simulations were calculated by the FENGSHA dust emission model based on a modified Owen's equation, which is a function of wind speed, soil moisture, soil texture and erodible land use types (Tong et al. 2015, Tong et al. 2012). CMAQ dust module predicts dust emission based on a modified Owen saltation equation (Owen 1964; Shao et al. 1993) with detailed parameterization of several key factors (Tong et al. 2012). These factors determine the occurrence and variation of dust emission:

$$\mathrm{F} = \sum_{i=1}^{M} \sum_{j=1}^{N} K \times A \times \frac{\rho}{g} \times S_i \times SEP \times u_* \times u_*^2 - u_{*ti,j}^2 \text{ for } \mathrm{u}_* > \mathrm{u}_{*\mathrm{t}} \qquad (1)$$

where M is the number of erodible land types, N is the number of soil types, K is the ratio of vertical to horizontal emission fluxes, A is a constant representing particle supply limitation, ρ is air density, g is gravitational acceleration (9.8 m/s^2), S_i is dust source area for land type *i, SEP* is the soil erodibility factor derived from the soil composition, u_* is the predicted friction velocity, and $u_{*ti,j}$ is the empirically-based threshold friction velocity for soil type j and land use type i. There is generally one soil texture type for a grid cell.

Dust is emitted into the air when the model calculated friction velocity exceeds the designated threshold friction velocity. Accurate estimates of all these parameters are required to improve dust forecasting performance. One of the key inputs to the FENGSHA model is the source map, which determines the areas suitable for wind erosions. We followed the method developed by Ginoux (2012) who demonstrated the use of MODIS Deep Blue Level 2 (M-DB2) aerosol products to identify dust sources in West Africa. This approach identifies dust plumes by comparing "dust optical depth (DOD)" to threshold values. An entry of DOD is found from the M-DB2 data when three criteria are met: to derive dust optical depth (DOD) from AOD, Angstrom wavelength exponent, α, and the difference in single scattering albedo, ω, between 412 and 670 nm. DOD, which represents AOD dominated by dust, is extracted when three conditions are met: 1. Angstrom wavelength exponent is negative ($\alpha < 0$); 2. Single scattering albedo, ω, is smaller than 0.95; and 3. There is positive difference in ω between 412 and 670 nm (ω 670−ω 412 > 0) If the determined DOD entry has a value smaller than 0.2, this satellite AOD record is considered a dust event.

56.3 Test Case and Evaluation

The FENGSHA wind-blown dust emission module is rather sensitive to the threshold friction velocity and the land surface texture conditions. We analyzed a readily available prediction results from the FENGSHA enabled NAQFC system that has been implemented into NCEP operations in February 2016. We used the system to retrospectively simulate the May 11 2014 dust case basing on the standard NAQFC 12 km horizontal grid (See Fig. 56.1). The NAQFC derives wind and soil moisture fields from the NCEP 12 km North American Model (NAM), the operational regional weather numerical prediction model from NCEP. NAM conducts 6 hourly data assimilation at 00, 06, 12 and 18 UTC. NAM generates hourly meteorological fields for CMAQ where the full hour values from NAM are interpolated linearly into instantaneous values correspond to the advection time steps in CMAQ. Therefore there was inherent smoothing and losing of transient features in the meteorological fields by virtue of temporal interpolation. Moreover, it is not the idea treatment for wind since he NAQFC is at 12 km horizontal resolution too coarse in describing local wind and surface texture in adequate detail critical for dust modeling. However, the operational NAQFC is a good first cut test to dive deeper into the initial uptake and suspension of the dust particles—the first two

Fig. 56.1 A MODIS visible image overlaid with high values of AOD due to dust masked identified suspended dust for May 11 2014 over CONUS

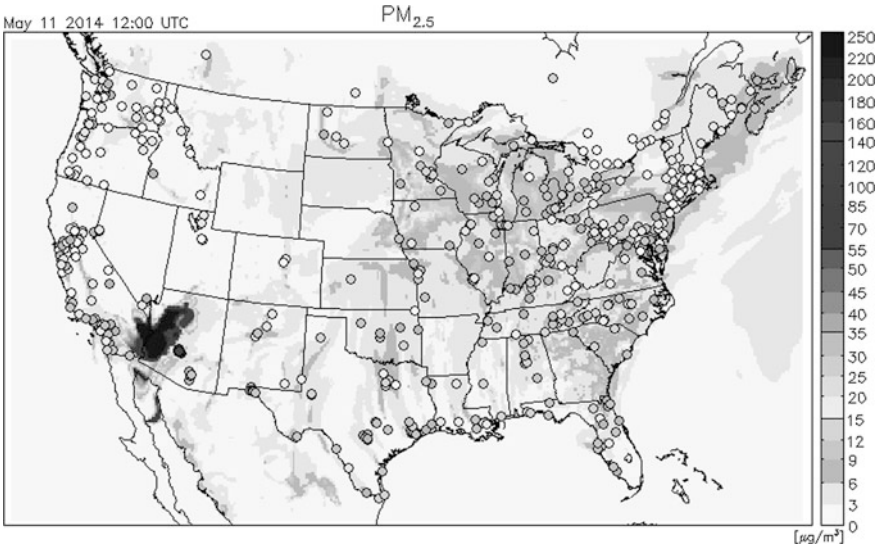

Fig. 56.2 Surface $PM_{2.5}$ (μg m^{-3}) at 12 UTC May 11 2014 depicted by a color scheme as shown in the *right-side color bar* for Prediction by the offline coupled NMMB and CMAQ as in NAQFC operations in *background shading*, and measurement by the EPA AIRNow monitoring network in *filled circles*

important processes in the chain of events defining the wind-blown dust. We evaluated the NAQFC predicted $PM_{2.5}$ forecasting skill during this dust storm and assessed the impact of dust emission on the regional air quality.

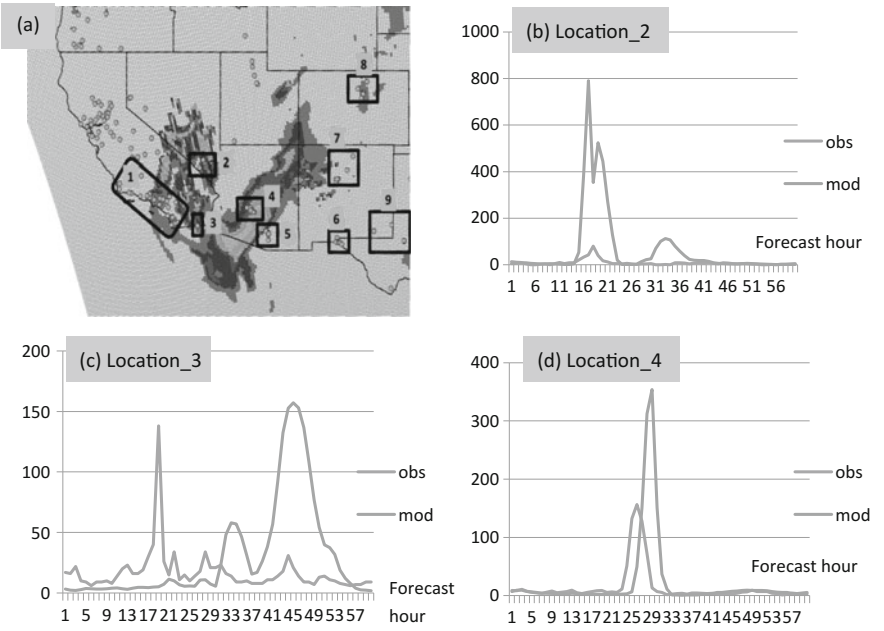

Fig. 56.3 Verification for the offline NMMB-CMAQ simulation as configured in the NAQFC against the EPA AIRNow measurements: **a** is similar to but valid for 23 UTC May 12 2014. Also shown are definitions of locations in the *emboldened rectangular boxes*; among them verification time series for locations 2, 3 and 4 were elaborated as plots (**b**), (**c**) and (**d**), respectively for hourly surface $PM_{2.5}$ concentration (μg m^{-3}) between 12 UTC May 10 and 23 UTC May 12 2014, i.e., up till 60 forecast hours

Figure 56.2 shows an instantaneous depiction of the elevated surface $PM_{2.5}$ concentration at 12 UTC May 11 2014. The predicted spatial distribution of the surface $PM_{2.5}$ concentration is roughly corresponding to what was illustrated by the satellite imagery shown in Fig. 56.1. An AIRNow monitor or monitor-cluster specific verification time series tracking the evolution of predicted concentration versus measured $PM_{2.5}$ was pursued (Fig. 56.3).

As another candidate wind-blown dust forecast potentially to be implemented as the next DFC, we leverage the superior meteorology from HRRR to couple it with the FENGSHA dust emission module and the dust transport and removal capability of CMAQ. In order to directly quantify the benefit of leveraging the 3 km resolution and the rapid hourly cycles of data assimilation in HRRR against the NAM input with a coarse grid at 12 km and 6 hourly data assimilation we also couple HRRR with FENGSHA-CMAQ offline. Again the full hour HRRR meteorological fields are written-out and accumulated in an input file for CMAQ. Similarly, the full hour HRRR fields were interpolated linearly into instantaneous values correspond to the advection time steps in FENGSHA-CMAQ. This offline coupled HRRR-FENGSHA-CMAQ system was tested and evaluated for the May 11 2014 case.

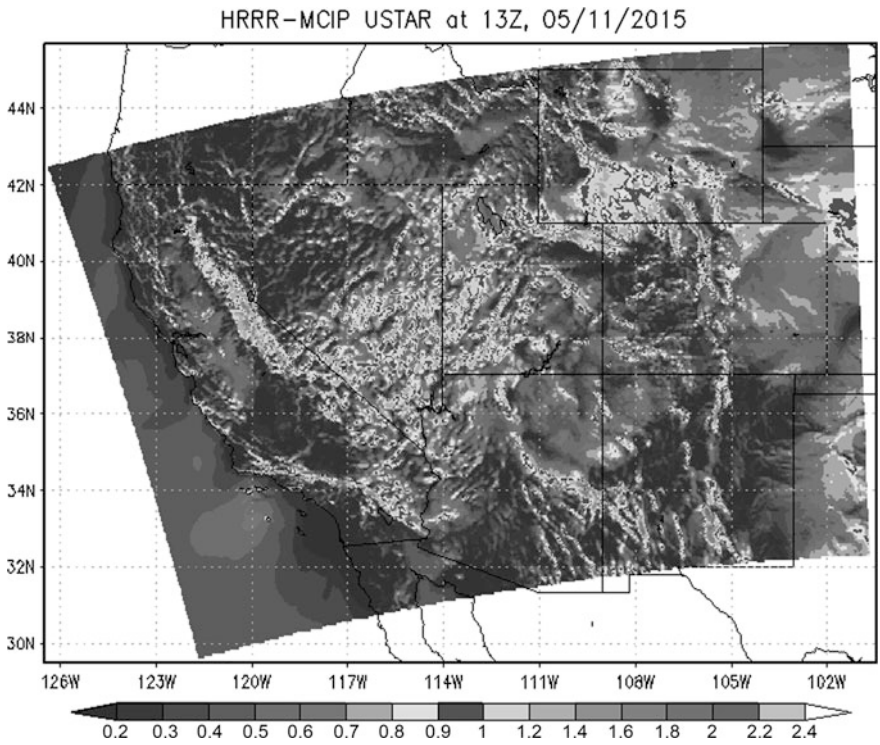

Fig. 56.4 Surface shear velocity (m s^{-1}) at 13 UTC May 11 2014 depicted by a color scheme as shown in the *bottom color bar* for the prediction by the offline coupled HRRR and FENGSHA-CMAQ in *background shading* in the diagram

56.4 Results and Summary

Figure 56.4 shows three consecutive hourly spatial plots for surface shear velocity of the offline system: HRRR FENGSHA-CMAQ system. We are embarking on running forecast for surface $PM_{2.5}$ concentration for the May 11 2014 case but realizing significant high biases in this first round of attempt. We are verifying if the surface velocity CMAQ sees is too strong at this moment.

Questions and Answers

Questioner: Marina Astitha
Question: The selection of HRRR to guide the emission of dust is based on its high spatial resolution. How will the 18 h forecast work for the dust parameterization

scheme, given the need for spin-up time for the dust emissions to be predicted with greater accuracy?
Answer: Yes. Fine resolution meteorology forecast such as HRRR reproduces fine feature and gust wind better than coarse resolution meteorology. The inclination to select HRR is exactly because of that. The current HRRR's forecast duration is 18 h. This is probably too short. But with the unification effort shown in this study, resources in software and hardware can be centralized and eventually extend the HRRR forecast to 48 h or so. The spin-up issue is primary concern as you pointed out. All the three dust emission options considered in this work used some form of climatology data to overcome this issue: e.g., soil erodible potential, soil texture used satellite-retrieved climatology compiled from the last decade. However, real-time satellite-retrieved data for soil moisture and AOD have been attempted to assist dust emission modeling. The climatology data usage was rather successful, the real-time usage for AOD was not too promising as many storms happen in the evening and night time hours and AOD are not available in those hours.

Questioner: Christian Hogrefe
Question: You mentioned that the dust scheme implemented in CMAQ5.0.2 is one of the candidate approaches you are considering. There have been substantial updates and corrections to this scheme in the upcoming CMAQ5.2 release as presented in the poster by Foroutan et al., Will you consider including the updated scheme in your testing?
Answer: Production selection of software does not usually choose the latest versions of the software. It is often a couple of versions lagged behind due to performance statistics needed to be accumulated to substantiate its accuracy and robustness. In the case of CMAQ as the Chemical transport model (CTM) of the National Air Quality Forecasting Capability (NAQFC) NOAA has tested CMAQv5.0.2 extensively. It will become the operational CTM in NAQFC rather shortly. This procedure and implementation protocol of NAQFC often delays the introduction of new science and advances of more physical based modeling for dust emission modeling such as the CMAQv5.2 dust model by Dr. Hossein Foroutan.

References

Byun DW, Schere KL (2006) Description of the models-3 community multiscale air quality (CMAQ) model: system overview, governing equations, and science algorithms. Appl Mech Rev 59:51–77

Chai T, Kim H, Lee P, Tong D, Pan L, Tang Y, Huang J, McQueen J, Tsidulko M, Stajner I (2013) Evaluation of the United States National Air Quality Forecast Capability experimental real-time predictions in 2010 using Air Quality System ozone and NO2 measurements. Geosci Model Dev 6:1831–1850. doi:10.5194/gmd-6-1831-2013

Draxler RR, Ginoux P, Stein AF (2010) An empirically derived emission algorithm for wind-blown dust. J Geophys Res 115:D16212. doi:10.1029/2009JD013167

Ginoux P, Prospero JM, Gill TE, Hsu NC, Zhao M (2012) Global-scale attribution of anthropogenic and natural dust sources and their emission rates based on MODIS Deep Blue aerosol products. Rev Geophys 50, RG3005. doi:10.1029/2012RG000388

HRRR (2016) http://www.noaanews.noaa.gov/stories2014/20140930_hrrr.html

Owen PR (1964) Saltation of uniform grains in air. J Fluid Mech 20:225–242

Pan L, Tong DQ, Lee P, Kim H, Chai T (2012) Assessment of NOx and O_3 forecasting performances in the U.S. National Air Quality Forecasting Capability before and after the 2012 major emissions updates. Atmos Environ 95:610–619. doi:10.1016/j.atmosenv.2014.06.020

Shao Y, Raupach MR, Findlater PA (1993) Effect of saltation bombardment on the entrainment of dust by wind. J Geophys Res 98:12719–12726

Skamarock W et al (2007) A time-split nonhydrostatic atmospheric model for weather research and forecasting applications. J Comput Phys

Tong DQ, Dan M, Wang T, Lee P (2012) Long-term dust climatology in the western United States reconstructed from routine aerosol ground monitoring. Atmos Chem Phys 12:5189–5205 14 June 2012

Tong DQ, Lamsal L, Pan L, Ding C, Kim H, Lee P, Chai T, Pickering KE, Stajner I (2015) Long-term NO_x trends over large cities in the United States during the 2008 Recession: Intercomparison of satellite retrievals, ground observations, and emission inventories. Atmos Environ 107:70–84. doi:10.1016/j.atmosenv.2015.01.035

U.S. EPA AIRNow (2015) Air quality guide for particle pollution. https://www3.epa.gov/airnow/air-quality-guide_pm_2015.pdf. Accessed June 2016

Chapter 57
Ozone Source Apportionment to Quantify Local-to-Continental Source Contributions to Episodic Events in Northern Iberia

Estíbaliz Sáez de Cámara, Gotzon Gangoiti, Lucio Alonso, Verónica Valdenebro, Sebnem Aksoyoglu and Emmanouil Oikonomakis

Abstract We present here a study of a number of ozone episodes in Northern Iberia (NIB) during the warm season of 2010 (April 1–September 30) using WRF and CAMx models. The episodes were selected after a detailed analysis of the ozone concentrations registered by the Air Quality Monitoring Network of the Basque Country (AQNBC), and rural background stations of the European Air Quality Database AirBase located in Northern Iberia. Preliminary results of the analysis of an early summer episode (24–26 June) are shown. For the first time during this type of episodes, it is shown that in the stations where the EU information threshold is exceeded frequently, there is an important contribution from local and regional sources, but the causative factor of high levels of ozone is the transport from medium-long range sources (France and Central Europe). Ozone production is mainly NO_x limited.

57.1 Introduction and Method

In earlier papers, we reported on the transport mechanisms and pathways behind the build-up of O_3 episodes in this region (Gangoiti et al. 2006; Valdenebro et al. 2011). However, the quantification of the contributions of local, regional, and continental of O_3 and its precursors and O_3 is still limited. The aim of this work was to quantify the influence of precursor emissions and O_3 transported from different

E.S. de Cámara (✉) · G. Gangoiti · L. Alonso · V. Valdenebro
Faculty of Engineering Bilbao, University of the Basque Country UPV/EHU, Alameda Urquijo s/n, 48013 Bilbao, Spain
e-mail: estibaliz.saezdecamara@ehu.eus

S. Aksoyoglu · E. Oikonomakis
Laboratory of Atmospheric Chemistry, Paul Scherrer Institute PSI, Villigen 5232, Switzerland

C. Mensink and G. Kallos (eds.), *Air Pollution Modeling and its Application XXV*, Springer Proceedings in Complexity, DOI 10.1007/978-3-319-57645-9_57

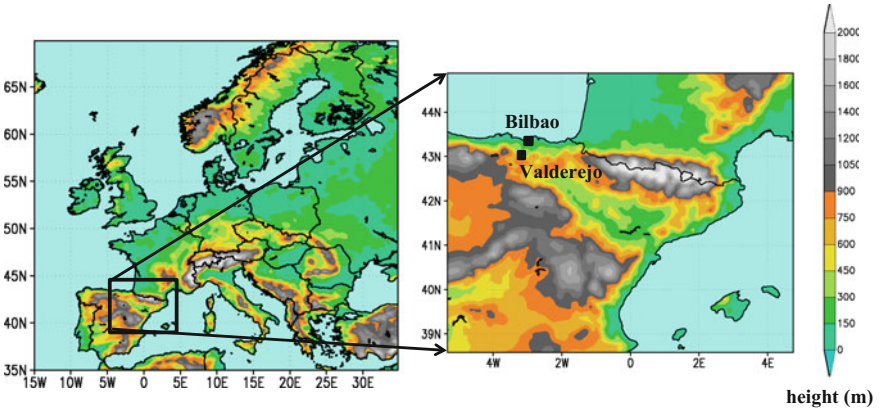

Fig. 57.1 Topographic map of the domains (*grid 1* and *2*) used by WRF and CAMx

sources on the O_3 episodes in the Basque Country. Being able to differentiate how much precursors and/or O_3 come from each source would be very helpful to develop feasible and effective O_3 control strategies. An early summer (24–26 June) episode is selected as a case study. A wider area was affected by high levels of O_3 these days: Northern Iberia (NIB) and the Western Mediterranean Basin (WMB), at the beginning of a long period of exceedances all over Europe.

Our analysis is based on the use of CAMx version 6.2 (Comprehensive Air Quality Model with extensions) and WRF version 3.7.1 (Weather Research and Forecasting Model). The model domain includes the whole Europe (with a resolution of 0.250° × 0.125°), and a nested domain with three times higher horizontal resolution over NIB and the WMB (Fig. 57.1). We used 6 h ECMWF data to provide initial and boundary conditions for WRF, whereas initial and boundary conditions for CAMx were extracted from MOZART4-GEOS5. The photolysis rates were calculated using the TUV photolysis preprocessor developed by Lee-Taylor and Madronich (2002). The required O_3 column densities were extracted from TOMS data.

Anthropogenic emissions were based on TNO/MACIII emission inventory. The data consisted of annual average emissions of CH_4, CO, NO_x, SO_x, NMVOC, PM_{10}, and $PM_{2.5}$, for 10 SNAP sectors, on a 0.125° × 0.0625° grid. Biogenic emissions were calculated using hourly meteorological data from WRF output, global USGS land use data and GlobCover2006 inventory according to the method described in Andreani-Aksoyoglu et al. (1995).

The meteorological model validation was performed using available data from monitoring networks and the high-resolution wind data recorded by a Wind Profiler Radar located near Bilbao. The predicted concentrations of O_3 and other pollutants were compared with the measurements of AQMNBC, Airbase data and hourly measurements of about 60 non-methane hydrocarbons in the natural park of Valderejo (Navazo et al. 2008).

Additionally, the Ozone Source Apportionment Technology (OSAT) was used to quantify source contributions to surface O_3 in 26 receptors during the 6-month simulation period: 15 receptors were located in urban, suburban, and rural sites of the Basque Country; the remaining are EMEP rural background stations, homogeneously distributed over NIB, Southern France, and the WMB. 9 source areas (Spain, France, Portugal, British Isles, Italy, Central Europe, Mediterranean Sea, Atlantic Ocean, and others), and initial and boundary conditions were considered.

57.2 Results and Conclusions

The 22–26 June meteorology was characterized by a blocking anticyclone located over NW France-S British Isles, forcing NE winds over the Basque Country and favoring mesoscale circulations. These conditions, together with cloudless skies and elevated temperatures, promoted O_3 formation and the transport of pollutants from regional and continental origin (Fig. 57.2). The EU long term objective for the protection of human health (120 $\mu g \cdot m^{-3}$ maximum daily 8 h mean) was exceeded on half of the AQMNBC stations: 41%, 60%, and 41% on June 24, 25, and 26, respectively. The highest concentrations were registered on the rural background stations, with an information threshold exceedance in the natural park of Valderejo. Then, the NE-E winds were replaced by N-NW ones bringing moist Atlantic 'clean' air masses over the region.

Model predictions of O_3 concentrations match the spatial and temporal variability of the observations; however, the diurnal peak is underestimated and the night-time concentrations are overestimated for in-valley stations. In addition to the graphical comparison, several statistics (MB, ME, RMSE, NMB and, NME, among others) were calculated and our results are within acceptable ranges reported in other studies.

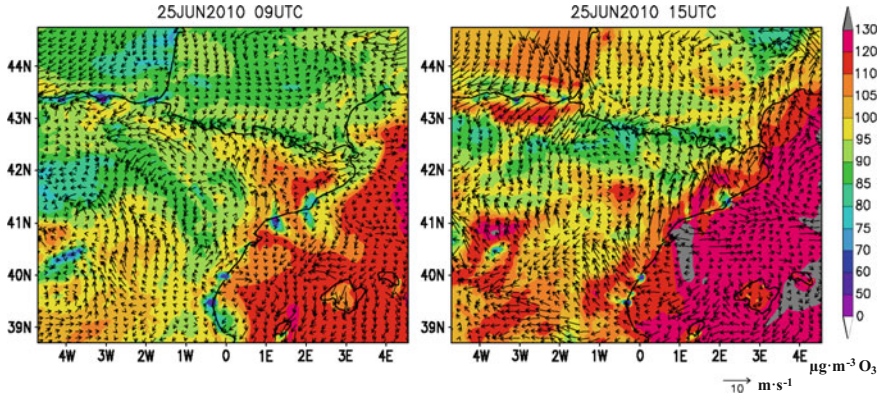

Fig. 57.2 Simulated O_3 concentrations and wind fields for June 25 at 0900 (*left*), and 1500 UTC (*right*)

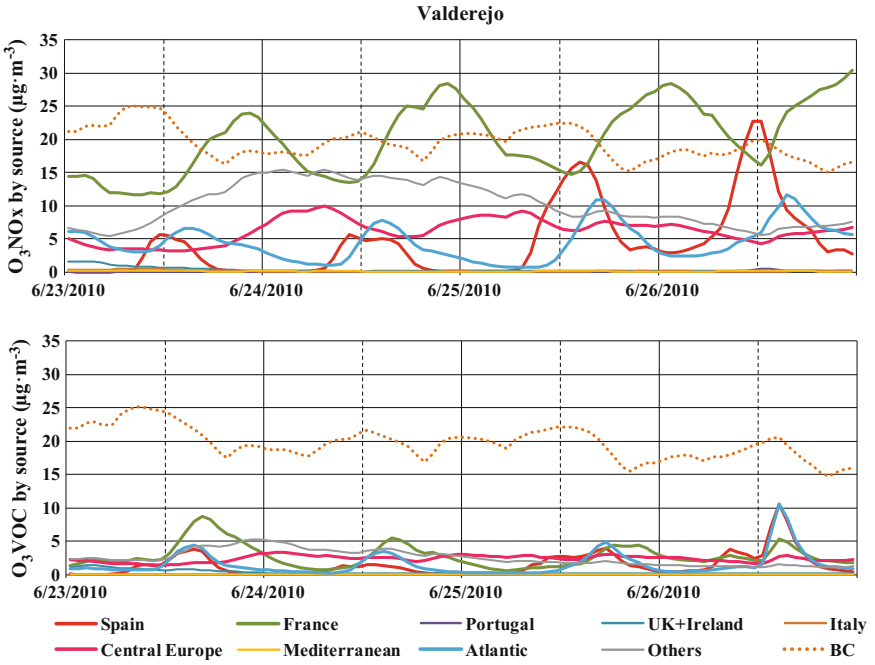

Fig. 57.3 Contribution by source area and by type -NO_x-limited conditions (*top*) or VOC-limited conditions (*down*)- to the O_3 levels registered in the natural park of Valderejo during the previous day (June 23) and peak days (June 24, 25, and 26) of the episode, according to OSAT

The dynamic of the contributions by source area and type to the O_3 level increase registered in Valderejo during the three-day the episode is characterized by: (1) the local production and transport of O_3 from other areas of Spain (Bilbao and/or SE Iberia) at midday, (2) the arrival of coastal precursors emitted from Spain and France and O_3 produced over the sea (Bay of Biscay/Atlantic) with the sea breeze, in the early afternoon, and, (3) the advection of high O_3 concentrations of continental origin (France and Central Europe) by winds with a NE-E component (Fig. 57.3). O_3 transported into or generated in Valderejo is produced under NO_x limited conditions.

The analysis of other episodes reveals significant variations in the way ozone precursors and O_3 from neighboring areas affect O_3 levels in different receptors in NIB, and that these variations depend mainly on synoptic conditions. In the Basque Country, local and regional contributions are dominant under mean O_3 conditions, but the causative factor for the onset of O_3 episodes is the concurrence of continental transport of both precursors and O_3 forced by blocking anticyclones.

Acknowledgements This work was supported by Ministry of Economy and Competitiveness through the project CTM2013-45223-P (PRORAT), UPV/EHU UFI (11/47) and Ministry of Education, Culture and Sport under the JC2015-00414 José Castillejo mobility grant to Sáez de

Cámara. The authors wish to thank the Basque Government for providing the meteorological and air quality data, the European Environmental Agency for its AirBase data, ECMWF for matero-rological data and Denier van der Goon from TNO for anthropogenic emissions.

References

Andreani-Aksoyoglu S, Keller J (1995) Estimates of monoterpene and isoprene emissions from the forests in Switzerland. J Atmos Chem 20:71–87

Gangoiti G, Albizuri A, Alonso L, Navazo M, Matabuena M, Valdenebro V, García JA, Millán MM (2006) Sub-continental transport mechanisms and pathways during two ozone episodes in northern Spain. Atmos Chem Phys 6:1469–1484. doi:10.5194/acp-6-1469-2006

Navazo M, Durana N, Alonso L, Gomez MC, Garcia JA, Ilardia JL, Gangoiti G, Iza J (2008) High temporal resolution measurements of ozone precursors in a rural background station. A two-year study. Environ Monit Assess 136:53. doi:10.1007/s10661-007-9720-4

Valdenebro V, Gangoiti G, Albizuri A, Alonso L, Navazo M, García JA, Iza J, Millán MM (2011) Build-up and decay of two ozone episodes through northern Iberia and southern France—an inter-regional transport analysis. Atmos Environ 45(8):1591–1603. doi:10.1016/j.atmosenv.2010.12.031

Chapter 58
A Comprehensive Modelling Approach for the Assessment of Global Shipping Emissions

Lasse Johansson, Jukka-Pekka Jalkanen and Jaakko Kukkonen

Abstract Emissions originating from global shipping traffic were modelled using the Ship Traffic Emission Assessment Model (STEAM), which uses Automatic Identification System (AIS) data to describe ship traffic activity. The model output can be utilized in regional air quality models on an hourly basis and can also be used to assess the impacts of miscellaneous emission abatement scenarios (e.g., changes of fuel grade, the introduction of scrubbers and slow-steaming scenarios). We present preliminary results on global shipping emissions and activities for the year 2015 and show that the presented results are qualitatively in agreement with the results presented in the 3rd IMO Greenhouse Gas Study. The main challenge for the global emission modelling of shipping is the treatment of the large number of vessels operating globally, for which it is difficult to obtain technical vessel specifications. To address this challenge we propose a solution that includes the use of a web crawler and an algorithm that can be used to complete the missing technical details. Another issue is the sparsity of satellite based AIS-data which makes it necessary to analyse individual route segments and occasionally apply advanced route generation algorithms.

L. Johansson (✉) · J.-P. Jalkanen · J. Kukkonen
Finnish Meteorological Institute (FMI), Erik Palmenin aukio 1,
00101 Helsinki, Finland
e-mail: lasse.johansson@fmi.fi

J. Kukkonen
e-mail: Jaakko.Kukkonen@fmi.fi

C. Mensink and G. Kallos (eds.), *Air Pollution Modeling and its Application XXV*,
Springer Proceedings in Complexity, DOI 10.1007/978-3-319-57645-9_58

58.1 Introduction

During the recent years AIS[1]-data has been used extensively for the assessment of shipping emissions. AIS-data describe the activities of individual vessels (e.g. speed, location) and exhaust emissions can be continuously modelled, assuming that some vessel characteristics (e.g. engine, physical dimensions) can be associated to each vessel.

An up-to-date emission inventory is essential for air quality modelling, for all sectors of anthropogenic (i.e. industry, agriculture, transport) and non-anthropogenic sources. AIS-data has been used for the assessment of shipping emissions for air quality models, but the scope of these studies have usually been limited to city-scale harbour studies or selected sea regions separately (Jalkanen et al. 2012; Johansson et al. 2013). In the 3rd IMO Greenhouse Gas Study[2] (Smith et al. 2015) global AIS-data was used to assess global shipping emissions, but the geographical and temporal variation of emissions was not considered in a level of detail that is required for air quality models.

Since the 3rd IMO Greenhouse Gas Study, both the amount of AIS satellite receivers and the amount of usable activity data for the emission modelling of shipping has increased substantially, while the cost of AIS data acquisition has decreased significantly. However, there has been no AIS-based global shipping emission modelling that could produce dynamic emission inventories for global air quality models.

58.2 Methods

The STEAM model was used to combine the AIS-based information with the detailed technical knowledge of the ships. This combined information is used to predict the resistance of vessels in water and instantaneous engine power of main and auxiliary engines on a minute-by-minute basis, for each vessel sending AIS-messages. The model then predicts as output both the instantaneous fuel consumption and the emissions of selected pollutants (Jalkanen et al. 2012; Johansson et al. 2013). In this study we have used commercial AIS messages (both terrestrial and satellite coverage) provided by Orbcomm (2015). Detailed vessel characteristics have been gathered for more than 90,000 individual ships, reported by IHS Fairplay and other ship classification societies.

[1]AIS system is globally on-board in every vessel that weighs more than 300 t. The AIS system provides automatic updates of the vessel positions and instantaneous speeds of ships at intervals of a few seconds.

[2]IMO GHG3 study is public and available at: http://www.imo.org/en/OurWork/Environment/PollutionPrevention/AirPollution/.

58.2.1 Vessel Specifications

Only a small fraction of the ships sending AIS-messages have an unique IMO identification number that can easily be used to link proper technical specifications to these vessels. However, even IMO-registered vessels can have incomplete specifications[3] and in such cases vessel type averages have commonly been used to complete the missing entries. In this work one of the main focuses is to address the issue of non-IMO registered vessels and missing technical details. Rather than using vessel type based averages, we complete missing specification entries by searching the most similar vessel (MSV) listed in the database that has the missing data entry. For the purpose of ranking the candidate ships used in this process, we calculate a similarity metric based on the vessel's length (LOA) and design speed.[4]

To address the technical specifications for ships that are not IMO-registered, we have produced an additional MMSI-linked (Maritime Mobile Service Identity) technical database using the information from several billion static[5] AIS-messages and a web crawler. The web crawler[6] uses Bing search engine by following links that contain relevant technical information. The MMSI-linked technical database offers only the rudimentary technical details for vessels, which in most cases is limited to ship type, physical dimensions and design speed. However, even such details facilitate the MSV-search and further improve the quality of associated vessel attributes.

58.2.2 Route Assessment for Data Gaps

When sparse satellite AIS-data is used, sometimes the geographical gap between two consecutive AIS-messages for a vessel can be thousands of kilometres. If such route segment passes physical feasibility checks as presented in (Johansson et al. 2013), an attempt to linearly evaluate the shipping route may result in an unrealistic situation, in which the linear route would cross over land areas. In fact, any two consecutive route points spatially close each other could imply a much longer travel route across the seas. To address this issue, a route assessment algorithm has been implemented to the STEAM model that can generate the missing route points.

---

[3]For example, information about auxiliary engines is missing.

[4]The MSV-search is only applied with the ships that represent the same vessel type. We simply sum the relative differences of length and design speed, weighting them equally.

[5]Based on Orbcomm 2015 data. A static AIS-message may contain the physical dimensions of the ship, a ship type classification and cargo information.

[6]The vessel's MMSI number is used as the search keyword. The crawler follows links to e.g., MarineTraffic.com and VesselFinder.com and parses numerical values after identified key words such as 'Length' or 'Breadth'.

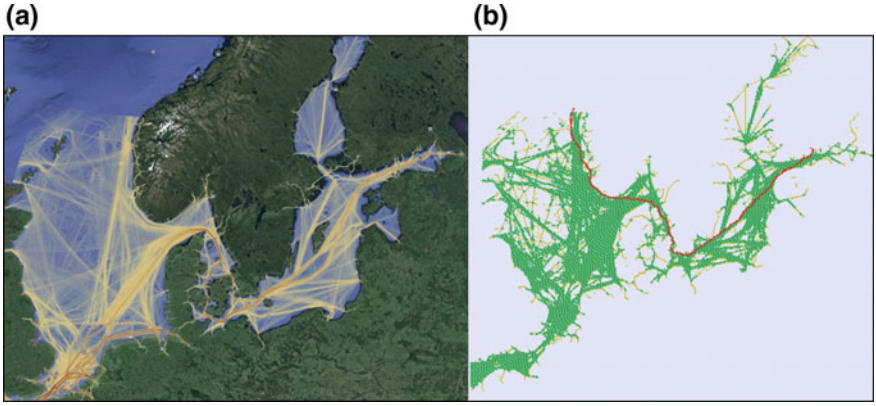

Fig. 58.1 **a–b** The route assessment algorithm and an example route network based on modelled fuel consumption. The gridded annual fuel consumption grid (**a**) has been transformed into a network of arcs and nodes (**b**). A Dijkstra algorithm can be used to assess the shortest path (*red line*) within the network

Table 58.1 Comparison of the reported statistics of IEA (Energy Information Administration) and the modelled fuel consumption for global shipping. HFO is heavy fuel oil and MDO is marine diesel oil

		IEA 2007 statistics	IEA 2011 statistics	IMO GHG3 2012 modelled	STEAM 2015 modelled
Total fuel consumption (10^9 kg)		249	254	300	266
	HFO	195	191	–	204
	MDO	54	62	–	59
Processed AIS-messages		–	–	$3{,}700 \times 10^6$	$9{,}000 \times 10^6$

For the advanced route generation we use a Dijkstra shortest path network algorithm (Cherkassky et al. 1996), visualized in Fig. 58.1. Based on a previous execution of the STEAM model, the geographical distribution of fuel consumption of IMO-registered vessels is used to cover sea area with a network of nodes and arcs. The Dijkstra algorithm can then be used to assess the shortest path between any pair of nodes in the network.

58.3 Results

The modelled fuel consumption in 2015 is shown together with IEA's reported fuel consumption statistics for 2007 and 2011 in Table 58.1. Given that the amount of global shipping activities has not increased substantially between 2011 and 2015 the results predicted in this study are qualitatively in agreement with both the

Table 58.2 Preliminary annual emissions and ship counts modelled using the STEAM model in 2015

		NO_x (10^6 kg)	SO_x (10^6 kg)	$PM_{2.5}$ (10^6 kg)	CO (10^6 kg)	CO_2 (10^6 kg)	Travel (10^6 km)	Payload (10^9 km*ton)	Ships
All ships		20,350	11,550	1,490	1,350	822,300	5,050	105,490	376,219
	IMO-registered	18,780	10,870	1,390	1,220	749,660	3,630	101,860	65,804
	Identified by MMSI	1,460	638	88	115	65,760	1,240	3,630	234,438
	Not identified	118	38	6	13	6,890	180	–	75,977

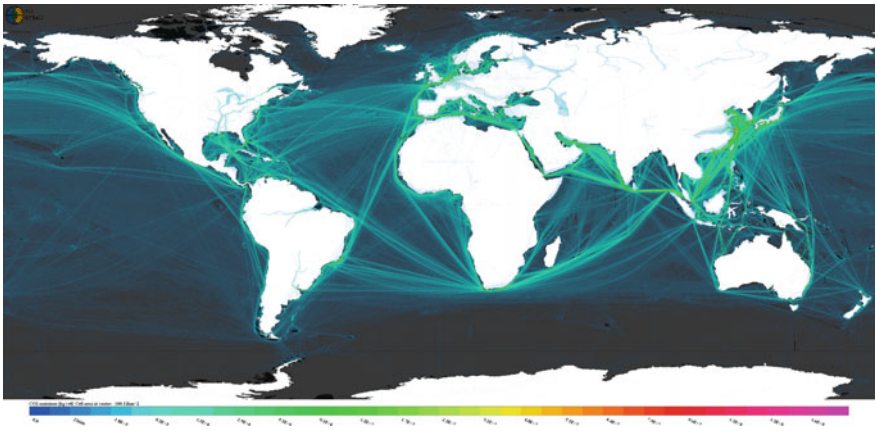

Fig. 58.2 Modelled geographical distribution of CO_2 emissions from global shipping in 2015

reported fuel consumption statistics as well as with modelled estimates presented in the 3rd IMO GHG study. The annual emissions estimated by the model are presented in Table 58.2. The global geographical distribution of CO_2 emissions has been shown in Fig. 58.2.

It can be seen from the information in Table 58.2 that IMO-registered traffic is responsible for approximately 90% of all emissions for the modelled pollutants. Only 3.5% of all travel kilometres are travelled by ships that have not been identified and associated with proper technical details.[7]

58.4 Conclusions

A refined and extended STEAM model was presented, which can be used for the assessment of global shipping activities and emissions. The model can be used to provide emission data for global-scale air quality models, using a selected temporal and spatial resolution.

The amount of used AIS messages in this study was approximately 9 billion (9×10^9), which was significantly larger than the corresponding value in the 3rd IMO GHG study for 2012. The number of satellite AIS transceivers orbiting the globe is rapidly increasing. The amount of AIS-data that will be available in future years is expected to grow further. The better availability of the AIS data is expected to result in more accurate predictions of the shipping emissions.

[7]In such cases the ships are assumed to be generic small boats with a gross tonnage of 300t (Jalkanen et al. 2012).

References

Cherkassky BV, Goldberg AV, Radzik T (1996) Shortest paths algorithms: theory and experimental evaluation. Math Program 73(2):129–174

Jalkanen J-P, Johansson L, Kukkonen J, Brink A, Kalli J, Stipa T (2012) Extension of an assessment model of ship traffic exhaust emissions for particulate matter and carbon monoxide. Atmos Chem Phys 12:2641–2659

Johansson L, Jalkanen J-P, Kalli J, Kukkonen J (2013) The evolution of shipping emissions and the costs of recent and forthcoming emission regulations in the northern European emission control area. Atmos Chem Phys 13:11375–11389. http://www.atmos-chem-phys.net/13/11375/2013/. doi:10.5194/acp-13-11375-2013, 10.5194/acpd-13-16113-2013

Smith TWP, Jalkanen J-P, Anderson BA, Corbett JJ, Faber J, Hanayama S, O'Keeffe E, Parker S, Johansson L, Aldous L, Raucci C, Traut M, Ettinger S, Nelissen D, Lee DS, Ng S, Agrawal A, Winebrake JJ, Hoen M, Chesworth S, Pandey A (2015) Third IMO GHG study 2014. International Maritime Organization (IMO), London, UK

Chapter 59
Source Apportionment of Inorganic Aerosols in Europe and Role of Biogenic VOC Emissions

S. Aksoyoglu, G. Ciarelli, I. El-Haddad, U. Baltensperger and A.S.H. Prévôt

Abstract In this study, we investigated the contribution of various source categories and regions to the secondary inorganic aerosol (SIA) in Europe with CAMx and its source apportionment tool PSAT during two measurement periods, representing cold and warm seasons. The results suggested that the main source for particulate nitrate was road transport, whereas energy industries were the most important contributor to sulfate particles. Emissions from international shipping were also found to be very important for both nitrate and sulfate particle formation. We found a large increase in secondary organic aerosol (SOA) concentrations when we doubled the biogenic volatile organic compound (BVOC) emissions during the warm season, as expected. We also found, however, a decrease in particulate inorganic nitrate and sulfate concentrations by about −35% and −12%, respectively, at different locations. The negative correlation between BVOCs and SIA indicates the importance of precursor gases and biogenic emission types. The results of further tests suggested that terpene reactions with nitrate radicals at night led to a decline in inorganic nitrate formation. Sulfate concentrations, on the other hand, decreased due to the reactions of BVOCs with OH radicals.

59.1 Introduction

Particulate matter (PM) in the atmosphere is either directly emitted or formed in the atmosphere as secondary inorganic (SIA) and organic aerosols (SOA). Observations show that SIA concentrations in Europe increase from north to south and they constitute a significant fraction of $PM_{2.5}$ in Europe especially in winter (Aas et al. 2012). Knowing the location and strength of sources contributing to $PM_{2.5}$ is essential for developing effective control strategies. Biogenic species emitted from vegetation are known as precursors of secondary pollutants like ozone and SOA

S. Aksoyoglu (✉) · G. Ciarelli · I. El-Haddad · U. Baltensperger · A.S.H. Prévôt
Laboratory of Atmospheric Chemistry, Paul Scherrer Institute (PSI), 5232 Villigen, Switzerland
e-mail: sebnem.aksoyoglu@psi.ch

C. Mensink and G. Kallos (eds.), *Air Pollution Modeling and its Application XXV*, Springer Proceedings in Complexity, DOI 10.1007/978-3-319-57645-9_59

(Boyd et al. 2015). Although there has been extensive research on formation of SOA from oxidation of BVOC (Ayres et al. 2015) information about the effects of BVOC emissions on SIA is limited.

59.2 Method

We applied the regional air quality model CAMx-v5.40 in Europe with its source apportionment tool PSAT (http://www.camx.com) for two EMEP measurement campaigns (25 Feb–26 Mar 2009 and 1–30 June 2006). Model parameterization and input data are the same as described in Ciarelli et al. (2016) except for SOA formation we used the semi-volatile equilibrium scheme SOAP (Strader et al. 1999). Biogenic VOC emissions were generated using the MEGAN v2.1 model (Guenther et al. 2012). We defined source categories based on the SNAP codes. We also investigated the contribution from various source regions to SIA concentrations in the densely populated Swiss Plateau. In order to investigate the role of biogenic emissions on the SIA formation, we doubled BVOC emissions in June 2006 and analyzed reaction rates of selected species from various reactions using the Chemical Process Analysis (CPA) probing tool.

59.3 Results and Discussions

Road transport (SNAP7) was predicted to be the most important source for particulate nitrate with the largest contribution during the cold season over northern Italy (Fig. 59.1, left). Other important sources for nitrate were ship emissions (SNAP8) along the English Channel and Benelux area and energy industries (SNAP1) in Central and Eastern Europe. The model results suggested that particulate sulfate in Europe originated from SNAP 1 sources especially in Eastern Europe (Fig. 59.1, right). The contribution of ship emissions was larger during the

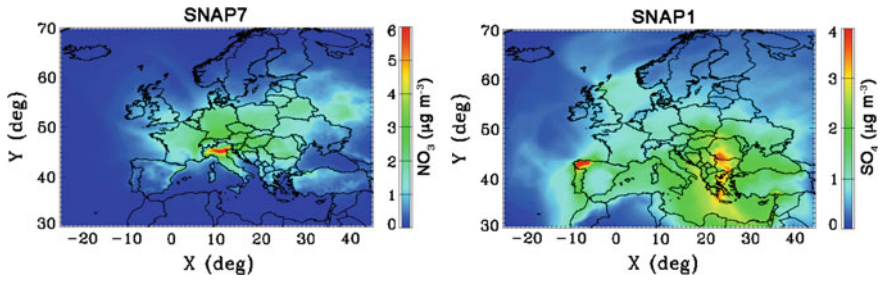

Fig. 59.1 Contribution from road transport to NO_3 in Feb–Mar 2009 (*left*) and from combustion in energy and transformation industries to SO_4 in June 2006 (*right*)

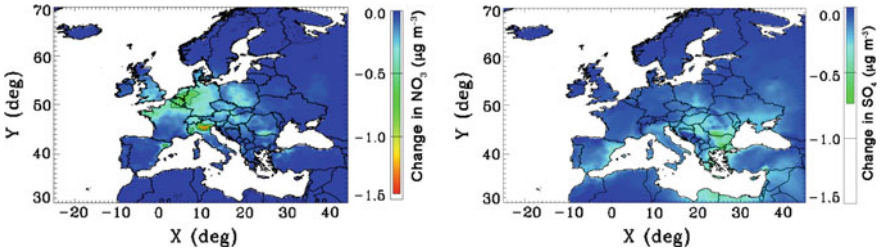

Fig. 59.2 Change in particulate nitrate (*left*) and sulfate (*right*) in June 2006 when BVOC emissions were doubled

warmer season as shown in Aksoyoglu et al. (2016). Agriculture was the dominant source for particulate ammonium, with a small contribution from road transport. A case study with the Swiss Plateau as receptor suggested that the contribution from the domestic sources to nitrate was similar to those from the neighboring countries such as Germany and France during the cold season and almost half of it was from road transport. The sources of particulate sulfate were mostly of foreign origin from SNAP1. The local agricultural activities were the main sources of particulate ammonium.

Doubling BVOC emissions led to an increase in SOA while particulate nitrate and sulfate decreased by about −35% and −12%, respectively (Fig. 59.2). Further analysis suggested that reactions of terpenes with nitrate radical at night led to a decrease in particulate inorganic nitrate formation. On the other hand, reduced availability of OH radical for gas-phase oxidation of SO_2 caused a small decrease in sulfate concentrations predicted mainly over Eastern Europe. These results indicate the importance of BVOC emissions not only for secondary organic aerosol formation but also for inorganic aerosols.

Acknowledgements Various input data were provided by INERIS, TNO, ECMWF within the EURODELTA III exercise. We thank G. Yarwood for his valuable comments. This work was funded by the Swiss Federal Office of Environment (FOEN).

Questions and Answers

Questioner's Name: Jerzy Bartnicki
Question: What method have you used for calculating contributions from individual sources and how did you take care of non-linear effects?
Answer: We used the PSAT (Particle Source Apportionment Technology) tool of CAMx model. PSAT is a reactive tracer method where a single tracer tracks the primary PM species, on the other hand, several tracers are required to track the relationships between the gaseous precursors and the resulting secondary PM species, i.e. in case of nitrogen, PSAT uses tracers such as NO_x, NO_3 radical,

HONO, N_2O_5, PAN, PNA, HNO_3, organic nitrates, particulate nitrate. This method has been compared with other methods such as brute-force and zero-out by the developers and shown to be more efficient and better able to deal with the non-linear chemistry than the other methods (Yarwood et al. 2007; Koo et al. 2009).

Questioner's Name: Rohit Mathur
Question: In the 2xBVOC experiment, did you examine the possible role of increased organic nitrate formation on reducing HNO_3 and consequently reduced PNO_3 levels?
Answer: Yes, we also investigated the organic nitrate formation in our sensitivity calculations with doubled BVOC emissions. In CB05 mechanism, organic nitrates are produced by reactions of isoprene and its oxidation products with NO_2 and NO_3 as well as from reactions of monoterpenes with NO_3. Increasing BVOC emissions led to an increase in organic nitrates and when the BVOC reactions with NO_3 radical were turned off, organic nitrate production decreased significantly at night (opposite to HNO_3 formation). These results suggest that monoterpene reactions with nitrate radicals at night are reducing the nighttime formation of HNO_3 and consequently formation of PNO_3.

References

Aas W, Tsyro S, Bieber E, Bergström R, Ceburnis D, Ellermann T, Fagerli H, Frölich M, Gehrig R, Makkonen U, Nemitz E, Otjes R, Perez N, Perrino C, Prévôt ASH, Putaud JP, Simpson D, Spindler G, Vana M, Yttri KE (2012) Lessons learnt from the first EMEP intensive measurement periods. Atmos Chem Phys 12:8073–8094. doi:10.5194/acp-12-8073-2012

Aksoyoglu S, Baltensperger U, Prévôt ASH (2016) Contribution of ship emissions to the concentration and deposition of air pollutants in Europe. Atmos Chem Phys 16:1895–1906. doi:10.5194/acp-16-1895-2016

Ayres BR, Allen HM, Draper DC, Brown SS, Wild RJ, Jimenez JL, Day DA, Campuzano-Jost P, Hu W, de Gouw J, Koss A, Cohen RC, Duffey KC, Romer P, Baumann K, Edgerton E, Takahama S, Thornton JA, Lee BH, Lopez-Hilfiker FD, Mohr C, Wennberg PO, Nguyen TB, Teng A, Goldstein AH, Olson K, Fry JL (2015) Organic nitrate aerosol formation via NO_3^+ biogenic volatile organic compounds in the southeastern United States. Atmos Chem Phys 15:13377–13392. doi:10.5194/acp-15-13377-2015

Boyd CM, Sanchez J, Xu L, Eugene AJ, Nah T, Tuet WY, Guzman MI, Ng NL (2015) Secondary organic aerosol formation from the β-pinene + NO_3 system: effect of humidity and peroxy radical fate. Atmos Chem Phys 15:7497–7522. doi:10.5194/acp-15-7497-2015

Ciarelli G, Aksoyoglu S, Crippa M, Jimenez JL, Nemitz E, Sellegri K, Äijälä M, Carbone S, Mohr C, O'Dowd C, Poulain L, Baltensperger U, Prévôt ASH (2016) Evaluation of European air quality modelled by CAMx including the volatility basis set scheme. Atmos Chem Phys 16:10313–10332. doi:10.5194/acp-16-10313-2016

Guenther AB, Jiang X, Heald CL, Sakulyanontvittaya T, Duhl T, Emmons LK, Wang X (2012) The model of emissions of gases and aerosols from nature version 2.1 (MEGAN2.1): an extended and updated framework for modeling biogenic emissions. Geosci Model Dev 5:1471–1492. doi:10.5194/gmd-5-1471-2012

Koo B, Wilson GM, Morris RE, Dunker AM, Yarwood G (2009) Comparison of source apportionment and sensitivity analysis in a particulate matter air quality model. Environ Sci Technol 43:6669–6675. doi:10.1021/es900812

Strader R, Lurmann F, Pandis SN (1999) Evaluation of secondary organic aerosol formation in winter. Atmos Environ 33:4849–4863

Yarwood G, Morris RE, Wilson GM (2007) Particulate matter source apportionment technology (PSAT) in the CAMx photochemical grid model. In: Borrego C, Norman A-L (eds) Air pollution modeling and its application XVII, Springer US, Boston, MA, pp 478–492

Chapter 60
Modelling the Atmospheric Concentration and Deposition of Pb and Cd in the UK

Anthony Dore, Ilia Ilyin, Heath Malcolm, Heather Yorston, Fiona Fordyce, Mark Cave, Harry Harmens, Małgorzata Werner, Maciej Kryza, Massimo Vieno and Stefan Reis

Abstract Two atmospheric chemistry transport models (FRAME and MSC-East) were applied to simulate the concentration and deposition of Cd and Pb in the UK. The modelled data was compared with annually averaged measured wet deposition of metals and concentrations in air. The models obtained good correlation with measurements of metal concentrations in air when estimates of wind-driven re-suspended emissions were included but large underestimates when only primary emissions were included. The results suggest that, following major reductions of heavy metal emissions in the UK, re-suspension now makes a larger contribution to total emissions than primary sources.

A. Dore (✉) · H. Malcolm · M. Vieno · S. Reis
Centre for Ecology and Hydrology, Bush Estate, EH26 OQB Penicuik, Midlothian, UK
e-mail: todo@ceh.ac.uk

I. Ilyin
EMEP/MSC-East, Moscow, Russia

H. Yorston
Edinburgh Parallel Computing Centre, Edinburgh University, Edinburgh, UK

F. Fordyce
British Geological Survey, Edinburgh, UK

M. Cave
British Geological Survey, Nottingham, UK

H. Harmens
Centre for Ecology and Hydrology, Bangor, UK

M. Werner · M. Kryza
Department of Climatology and Atmosphere Protection, University of Wrocław, Wrocław, Poland
e-mail: malgorzata.werner@uwr.edu.pl

M. Kryza
e-mail: maciej.kryza@uwr.edu.pl

C. Mensink and G. Kallos (eds.), *Air Pollution Modeling and its Application XXV*, Springer Proceedings in Complexity, DOI 10.1007/978-3-319-57645-9_60

60.1 Introduction and Model Description

The presence of trace metals in the environment, notably Cd and Pb, poses a risk to both human health and natural ecosystems. Long-term monitoring data and atmospheric chemical transport models are used to estimate concentration trends of heavy metals in the atmosphere and in precipitation. However, following reductions of heavy metal emissions over recent decades, current observations consistently report higher ambient concentrations than model estimates using existing emission inventories. The 1998 UNECE Protocol on Heavy Metals committed all participating countries to reduce their emissions of Pd and Cd to levels below those of 1990 as well as phasing out leaded petrol. As a result of this, as well as growing environmental awareness, emissions of Pb and Cd in the UK fell by 99% and 93% respectively in the UK between 1990 and 2010.

In this study, two atmospheric chemical transport models have been applied to calculate the concentration and deposition of Cd and Pb in the UK. FRAME is a Lagrangian model using annually averaged meteorology run at a 5 km resolution over the UK (Dore et al. 2013, 2014). MSC-East is a Eulerian model (Ilyin et al. 2014) which has been used to assess heavy metal pollution across Europe as part of the European Monitoring and Evaluation Programme. The model explicitly calculates the wind-driven re-suspension of heavy metals contained in surface particulate matter using dynamic meteorology. In this study the re-suspended emissions have been used to calculate metal concentrations in air with both the FRAME and MSC-East models. Here we present the preliminary results of the first application of MSC-East at a high (10 km) resolution over the UK.

60.2 Results

The modelled dry and wet deposition of Pb over the UK for the year 2012 calculated with FRAME is illustrated in Fig. 60.1. In general a strong gradient is evident, with higher concentrations found in the central and southern part of the country, due to both the long range transport of pollutants from European sources as well as the greater intensity of emissions sources in the southern part of the UK.

A rural network for monitoring the concentrations of heavy metals in air and precipitation has been in operation in the UK since the year 2004. For the year 2012 the network consisted of 14 sites at which samples of precipitation were collected every four weeks for analysis of concentrations. Measurements of the concentration of heavy metals in air using a Partisol PM_{10} sampler were also made with a weekly sample collection at 12 of these sites. Deposition of heavy metals at the sites was calculated by combining the measured concentrations in precipitation with annual precipitation measured at the sites.

Figure 60.2 illustrates the correlation with measurements of Pb concentration in air for FRAME for simulations run (i) with primary emissions only; (ii) with both

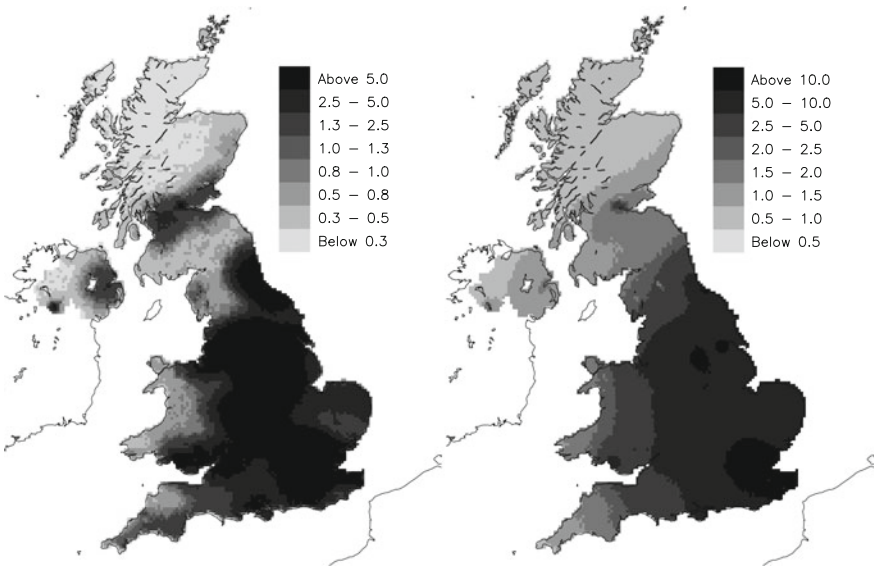

Fig. 60.1 Dry deposition of Pb (*left*); wet deposition of Pb (*right*) in gm^{-2} calculated with FRAME

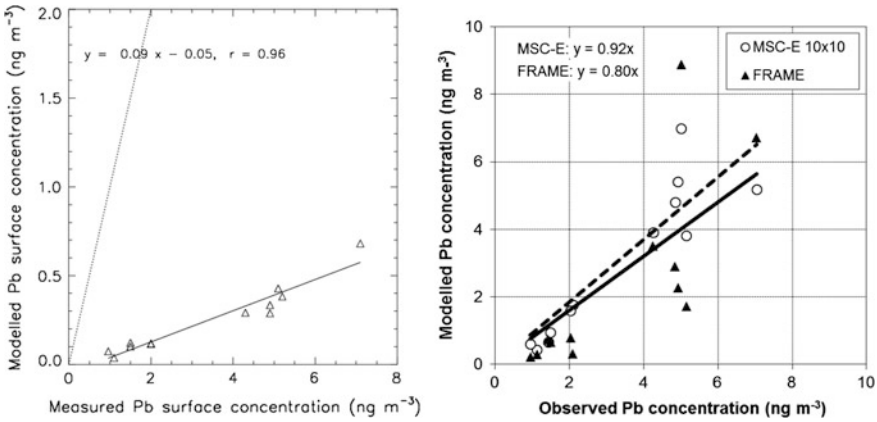

Fig. 60.2 Correlation of the model with measurements of Pb concentrations in air (ng m^{-3}) for the year 2012: *left* with primary emissions only included (FRAME); *right* with both primary emissions and re-suspension included (FRAME and MSC-east)

primary emissions and re-suspended emissions included. A significant under-estimate in modelled concentrations is apparent (normalized mean bias, NMB, of −0.93) for the simulation with primary emissions only whereas a reasonable agreement with measured values (NMB = −0.31, correlation coefficient r = 0.75) was found when re-suspended emissions were included.

Table 60.1 Estimates of primary emissions from the National Atmospheric Emissions Inventory and re-suspended emissions calculated with the MSC-east model for Cd and Pb for the UK for 2012 (Mg year^{-1})

	Cd	Pb
Primary	2.0	65.0
Re-suspended	3.5	233

The MSC-East model calculation with re-suspension included (Fig. 60.2, right side) shows better agreement with measurements of Pb air concentrations than FRAME due to the more detailed representation of transport using dynamical meteorology. For wet deposition, FRAME also obtained a reasonable correlation with measurements ($r = 0.77$, NMB $= -0.11$). For Cd FRAME obtained a correlation with air concentration of $r = 0.78$ (NMB $= -0.39$) but a poor correlation with wet deposition ($r = 0.37$, NMB $= -0.13$). Bulk collectors were used to obtain samples of precipitation and these could have been subject to dry deposition. This, combined with the difficulty of an atmospheric transport model to capture the complexity of the wet removal process could explain why correlation of model results is generally lower for wet deposition than for air concentrations.

The estimates of primary and re-suspended emissions of both Cd and Pb illustrated in Table 60.1 suggest that, following the major reductions in primary emissions of Cd and Pb in the UK, wind driven re-suspension of metals from surface soil now makes a more important contribution to concentrations in air than primary emissions.

60.3 Conclusion

Two atmospheric transport models were used to calculate the wet and dry deposition and air concentrations of Cd and Pb in the UK. Comparison with measurements from a national monitoring network revealed the large magnitude of missing emission sources when only primary emission sources were included in the simulation. Secondary 'legacy' emissions caused by the wind-driven re-suspension of surface dust were calculated using dynamic meteorology. Inclusion of re-suspended emissions led to improved agreement with measurements. Future work will use national data on metal concentrations in topsoil (Rawlins et al. 2012) with high resolution meteorological simulations to generate spatially distributed re-suspension estimates for the UK. Measurements of metal concentrations in moss have been undertaken across Europe (Harmens et al. 2011) and these represent an independent data set of the spatial distribution of Cd and Pb deposition in the UK for comparison with the atmospheric transport models.

Acknowledgements This work was funded by the Natural Environment Research Council and MSC-east.

Question and Answer

Questioner: Pius Lee
Question: You reported the encouraging news that emissions of Pb and Cd have reduced by 99% and 93%. This is a great achievement. However you gave a hint of reservation that part of the UK still has Pb critical load exceeded. What is the situation for Cd. Is it still exceeding critical loads?
Answer: Critical loads in the UK were calculated for Cd, Pb, Cu, Ni and Zn. Of these significant exceedance of the critical load occurred only for Cu, Pb and Zn, primarily in unmanaged forest in south-east UK, a region with lower critical loads due to lower leaching rates (http://www.rotap.ceh).

References

Dore AJ, Hallsworth S, McDonald AG, Werner M, Kryza M, Abbott J, Nemitz E, Dore CJ, Malcolm M, Vieno M, Reis S, Fowler D (2013) Quantifying missing sources of heavy metals in the United Kingdom with an atmospheric transport model. Sci Total Environ 479–480C:171–180

Dore AJ, Hallsworth S, Werner M, Kryza M, Nemitz E, Malcolm H, Reis S, Fowler D (2014) Modelling the concentration and deposition of heavy metals in the UK (2014) In: Steyn D, Mathur R (eds) Air pollution modeling and its application XXIII. Springer Proceedings in Complexity. Springer, Cham

Harmens H et al (2011) Mosses as biomonitors of atmospheric heavy metal deposition: spatial and temporal trends in Europe. Environ Pollut 158:3144–3156

Ilyin I, Rozovskaya O, Travnikov O, Varygina M, Aas W (2014) Heavy metal transboundary pollution of the environment. EMEP status report 2/2014

Rawlins BG, McGrath SP, Scheib AJ, Cave M, Lister TR, Ingham M, Gowing C, Carter S (2012) The advanced soil geochemical Atlas of England and Wales. British Geological Survey, Keyworth

Chapter 61
Reviving MILORD Long-Range Model for Simulating the Dispersion of the Release during Fukushima Nuclear Power Plant Accident

Marco Boetti, Silvia Trini Castelli and Enrico Ferrero

Abstract This work focuses on long range dispersion using the numerical model MILORD, a Lagrangian particle model capable of simulating transport, dispersion, removal and deposition of tracers. The chosen case study concerns the release of Caesium isotope ^{137}Cs from Fukushima Daichi nuclear plant caused by the earthquake and the subsequent tsunami in March 2011. ^{137}Cs deposition in the affected area is reproduced from 11 March until the end of that month. In order to evaluate and improve the model, simulations results are compared to station measurements and a sensitivity analysis is performed. A comparison with results of other models is briefly discussed based on a statistical analysis.

61.1 Introduction

The Lagrangian particle dispersion model MILORD (Anfossi et al. 1995) was created in 1992–93 as a tool for the long-range simulation of transport, dispersion, removal and deposition of tracers from accidental releases. MILORD was applied and validated in two case studies, the Chernobyl accident (ATMES Project) and the ETEX I field experiment. A renewed interest in long-range dispersion started after the problems related to the emissions of the volcano Eyjafjallajokull in Iceland in May 2010, and even more after the radioactive release from the Fukushima Daichi nuclear power plant in Japan in March 2011, consequent to the earthquake that

M. Boetti
Department of Physics, University of Torino, Turin, Italy

S.T. Castelli (✉) · E. Ferrero
Institute of Atmospheric Sciences and Climate, National Research Council, Turin, Italy
e-mail: s.trinicastelli@isac.cnr.it

E. Ferrero
Department of Sciences and Technological Innovation, University of Piemonte Orientale, Alessandria, Italy

C. Mensink and G. Kallos (eds.), *Air Pollution Modeling and its Application XXV*, Springer Proceedings in Complexity, DOI 10.1007/978-3-319-57645-9_61

devastated that area. Our research group was thus motivated to brush up the MILORD model and to proceed with further developments of the code. In particular, the emission module was made more flexible and adaptable to any time and space modulation and the original Reap algorithm, for calculating the deterministic part of the trajectories, was adapted to properly deal with the extreme meteorological conditions characterizing the period of the accident. A sensitivity analysis was performed varying several physical parameters. Results are discussed considering the release of Cesium isotope ^{137}Cs and simulations outputs are compared to deposition data measured at the available station measurements.

61.2 Main Model Modifications and Runs

The atmospheric transport is modelled based on two contributions given by the advection (deterministic term) and the diffusion (stochastic term). In MILORD the stochastic displacement is calculated solving the Langevin equation, the deterministic term is calculated following the Reap (1972) algorithm, based on successive iterations and computing temporary displacements subject to a convergence condition. If this last is satisfied, the algorithm allows assigning physically reasonable positions to the pollutant when dealing with coarse gridded meteorological input fields, both in time and space.

In application to Fukushima case study, we found that the algorithm convergence condition is not satisfied when the pollutant is crossing areas characterized by strong wind-velocity gradients, resulting in unrealistic particle positions. In Fig. 61.1 an example of the wind velocity fields that led to the convergence problems is reported. The divergence occurs for particles entering the area around coordinates 48.5°N latitude and 166.5°E longitude. The limitation of the algorithm emerged in these extreme meteorological conditions, which did not occur during the ATMES project and the ETEX experiment.

To enable MILORD to run properly, the Reap algorithm was modified considering appropriate convergence limits, relaxing them to less severe values, and imposing a limit to the particles displacement inside a range that was estimated as reasonable in such conditions.

Several runs were performed in order to investigate the sensitivity of the model to different quantities. The input parameters modified are the PBL height (Desiato 1992) H_{PBL}, the horizontal diffusion coefficients K_H, the number of the standard pressure levels N_L from the ECMWF input files and the integration time step Δt. In Table 61.1 the main runs are listed and detailed.

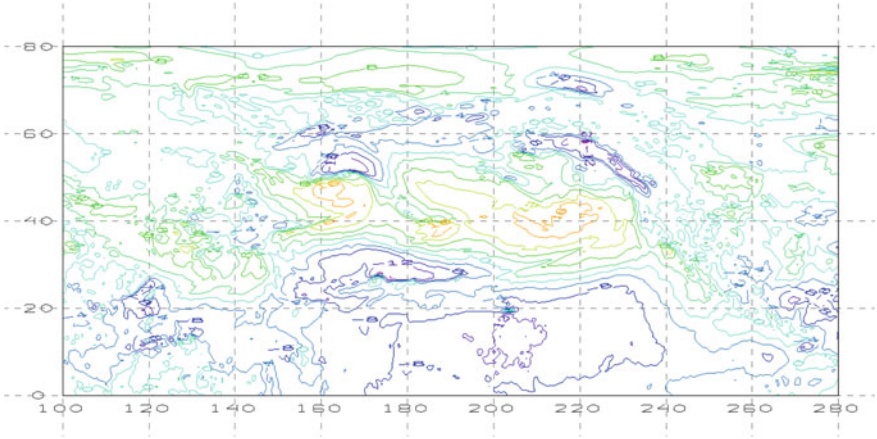

Fig. 61.1 ECMWF horizontal velocity component U [m/s] at 1000 hPa pressure level, on 15 March 2011 at 06:00 UTC; contour interval: 4.0 m/s

Table 61.1 MILORD configurations of the different Runs and statistical metrics

	H_{PBL} (m)	K_H (m^2/s)	N_L	Δt (s)	R	NMSE	FB	FA2	FA5
Run 1	Variable	50	4	2160	0.49	8.05	−0.43	0.42	0.79
Run 2	Variable	4.5×10^4	4	2160	0.56	14.90	0.29	0.57	0.96
Run 3	Fixed, 1500	4.5×10^4	4	2160	0.56	17.02	0.38	0.58	0.97
Run 4	Variable	4.5×10^4	5	2160	0.56	13.56	0.16	0.56	0.96
Run 5	Fixed, 1500	4.5×10^4	5	2160	0.53	14.57	0.22	0.59	0.95
Run 6	Variable	4.5×10^4	4	1080	0.59	16.74	0.43	0.58	0.96

61.3 Results and Conclusions

In general, the analysis showed that the variability is mainly related to the diffusivity parameters and to the variation of the integration time step. As examples of the results produced, in Fig. 61.2 the cumulated deposition is plotted for Run 1 and Run 6.

In order to evaluate the model performance, MILORD outputs have been compared to measurements from the network established by the Japan Atomic Energy Agency (JAEA). The cumulative frequency distributions for the deposition predicted and observed for Run 1 and Run 6 are shown in Fig. 61.3. The agreement between simulations and observations is clearly better for Run 6. Comparing Run 2 with Run 1 and Run 6 it was found that the dominant effect for the deposition is given by the large change in the diffusion coefficient and not by the time step.

A quantitative statistical analysis was performed calculating the correlation coefficient R, the normalized mean square error NMSE, the fractional bias FB, the Factor two FA2 and five FA5. In Table 61.1 the statistics for the different Runs are

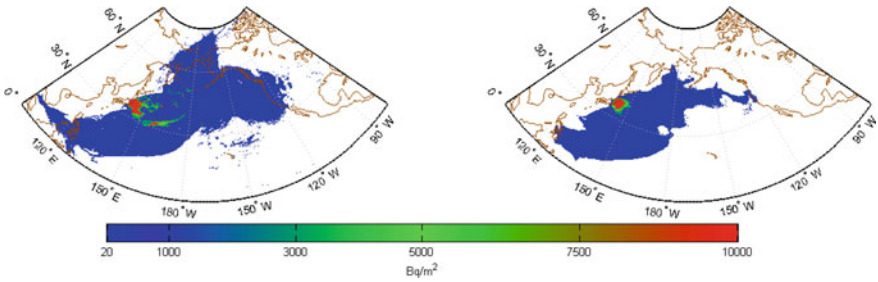

Fig. 61.2 ^{137}Cs cumulated deposition 10–31/3/2011, Run 1 (*left*) and Run 6 (*right*) setups

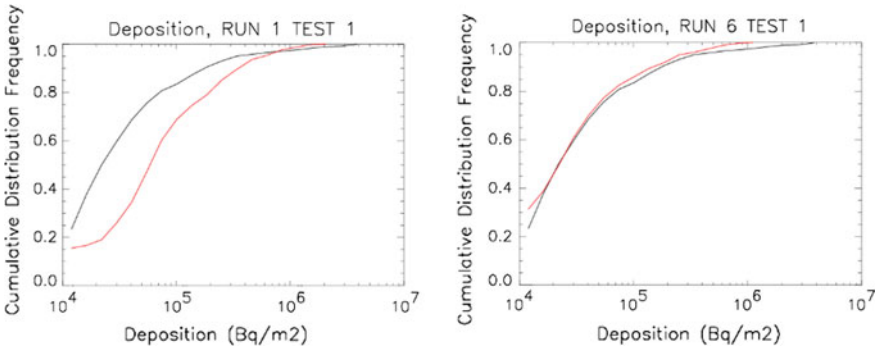

Fig. 61.3 CDF of ^{137}Cs cumulate deposition, 10–31/3/2011. Run 1 and Run 6 setups. Observed: *black line*, predicted: *red line*

Table 61.2 Statistical indices for MILORD and other dispersion models for Fukushima case

	R	NMSE	min(|FB|)	max(|FB|)
MILORD	0.49–0.59	8.05–17.02	0.16	0.43
NAME	0.69–0.88	n.a.	0.19	0.46
HYSPLIT	0.55–0.83	4.20–14.09	0.30	0.74
FLEXPART	0.78–0.83	2.55–3.84	0.08	0.13

also given, while in Table 61.2 some statistics, calculated for the JAEA deposition network data, are compared with the results of other long-range state-of-the-art dispersion models, simulating Fukushima case study (Draxler et al. 2015; Leadbetter et al. 2015). The measuring stations provided observed deposition over an area quite close to the source, thus related to spatial scales smaller than the ones MILORD was developed for. This comparison on the mesoscale was challenging for the model. Taken this into account, the statistical results are satisfactory. As a general conclusion, MILORD proved to be a reliable model also in such extreme conditions and different scale phenomena characterizing the Fukushima case study.

Question and Answer

Questioner: Christian Hogrefe
Question: Do you have plans to make further modifications to MILORD and then test it again using observations and other models?
Answer: Several developments and improvements are planned for a number of physical processes, to be then tested on the available datasets already used. For instance, implementing a modulation from the local to the long-range simulation scales in the Langevin equations, to treat more correctly the dispersion of the tracer in proximity of the source; improving the description of the plume rise, not only modulating the emission in space and time but using formulations and parameterizations from literature; introducing more physical parameterizations for the diffusion coefficients K and the PBL height; developing an interface with a mesoscale meteorological model, in order to provide more refined simulations; testing the backward trajectories receptor-source module, not yet applied.

References

Anfossi D, Sacchetti D, Trini Castelli S (1995) Development and sensitivity analysis of a Lagrangian particle model for long range dispersion. Environ Softw 10(4):263–287

Desiato F (1992) A long-range dispersion model evaluation study with Chernobyl data. Atmos Environ 26A:2805–2820

Draxler R, Arnold D, Chino M, Galmarini S, Hort M, Jones A, Leadbetter S, Malo A, Maurer C, Rolph G, Saito K, Servranckx R, Shimbori T, Solazzo E, Wotawa G (2015) World meteorological organization's model simulations of the radionuclide dispersion and deposition from the Fukushima Daiichi nuclear power plant accident. J Environ Radioact 139:172–184

Leadbetter SJ, Hort MC, Jones AR, Webster HN, Draxler R (2015) Sensitivity of the modelled deposition of Caesium-137 from the Fukushima Daiichi nuclear power plant to the wet deposition parametrization in NAME. J Environ Radioact 139:200–211

Reap R (1972) An operational three-dimensional trajectory model. J Appl Meteorol 11:1193–1201

Chapter 62
Influence of Boundary Conditions on Regional Air Quality Simulations—Analysis of AQMEII Phase 3 Results

Christian Hogrefe, Peng Liu, George Pouliot, Rohit Mathur, Shawn Roselle, Efisio Solazzo and Stefano Galmarini

Abstract Chemical boundary conditions are a key input to regional-scale photochemical models. In this study, performed during the third phase of the Air Quality Model Evaluation International Initiative (AQMEII3), we perform annual simulations over North America with chemical boundary conditions prepared from four different global models. Results indicate that the impacts of different boundary conditions are significant for ozone throughout the year and most pronounced outside the summer season while impacts for $PM_{2.5}$ are smaller and tend to be of an episodic nature with the largest impacts during summer.

62.1 Introduction

The third phase of the Air Quality Model Evaluation International Initiative (AQMEII3) is aimed at investigating the impact of intercontinental transport on regional-scale air quality by collaborating with the Task Force on Hemispheric Transport of Air Pollution (TF-HTAP). We present the results of regional-scale simulations over North America driven by different representations of large-scale atmospheric composition as simulated by global/hemispheric models participating in TF-HTAP.

C. Hogrefe (✉) · G. Pouliot · R. Mathur · S. Roselle
National Exposure Research Laboratory, Computational Exposure Division,
U.S. Environmental Protection Agency, RTP, NC, USA
e-mail: Hogrefe.Christian@epa.gov

P. Liu
National Exposure Research Laboratory, National Research Council
Fellow assigned to Computational Exposure Division,
U.S. Environmental Protection Agency, RTP, NC, USA

E. Solazzo · S. Galmarini
European Commission Joint Research Centre, Ispra, Italy

C. Mensink and G. Kallos (eds.), *Air Pollution Modeling and its Application XXV*,
Springer Proceedings in Complexity, DOI 10.1007/978-3-319-57645-9_62

62.2 Model Simulations and Observations

The 2010 annual regional air quality simulations analysed in this study were performed with version 5.0.2 of the Community Multiscale Air Quality (CMAQ) modeling system (Byun and Schere 2006). Details of the model configuration were described in Hogrefe et al. (2016). Chemical boundary conditions were prepared from global or hemispheric concentration fields simulated by (a) the European Center for Medium Range Weather Forecasts (ECMWF) Composition—Integrated Forecast System (C-IFS) model, (b) the AM3 model with coupled stratosphere-troposphere chemistry, (c) the GEOS-Chem model version 9-01-03 which includes full tropospheric chemistry and a climatological representation of stratospheric sources and sinks, and (d) CMAQ5.1 configured for hemispheric applications, hereafter referred to as H-CMAQ. The first three of these simulations were performed as part of the TF-HTAP and additional details on these simulations can be found at http://iek8wikis.iek.fz-juelich.de/HTAPWiki/WP2.3. To create boundary conditions for the regional CMAQ simulations, outputs from the global/hemispheric models were vertically interpolated and gas phase and aerosol species were mapped to the CB05TUCL/Aero6 mechanism used by CMAQ. The simulations with the four different boundary conditions are hereafter referred to as "BC C-IFS", "BC GEOS", "BC AM3", and "BC H-CMAQ", respectively. Two additional annual CMAQ sensitivity simulations were performed as follows: (a) the boundary conditions were time invariant and were set to 20 ppb for ozone and zero for all other species (these runs are referred to as "BC constant"), and (b) the boundary conditions were the same as in "BC C-IFS" but all anthropogenic emissions within the domain were set to zero (these runs are referred to as "EM zero"). Observations of ozone and $PM_{2.5}$ mass were retrieved from the U.S. Environmental Protection Agency (U.S. EPA) Air Quality System (AQS) database.

62.3 Results and Discussion

Figure 62.1 shows time series of monthly averaged daily maximum 8-h ozone from observations and the six CMAQ simulations, averaged over all AQS monitors in the modeling domain. Figure 62.2 shows the corresponding results for $PM_{2.5}$ at the location of daily AQS monitors. Figure 62.1 reveals that all simulations except "BC constant" and "EM zero" overestimate observed ozone throughout the year, the overestimation is most pronounced for "BC AM3" during spring. The spread between the "BC C-IFS", "BC H-CMAQ", "BC GEOS" and "BC AM3" is on the order of 10 ppb for most of the year, i.e. roughly 20–33% of simulated monthly mean values. However, the spread is smaller from June to September when it drops to less than 5 ppb. If the boundary conditions derived from these four models can be viewed as a reflection of the underlying uncertainty in quantifying large-scale ozone concentration fields, these results suggest that the resulting impact of this

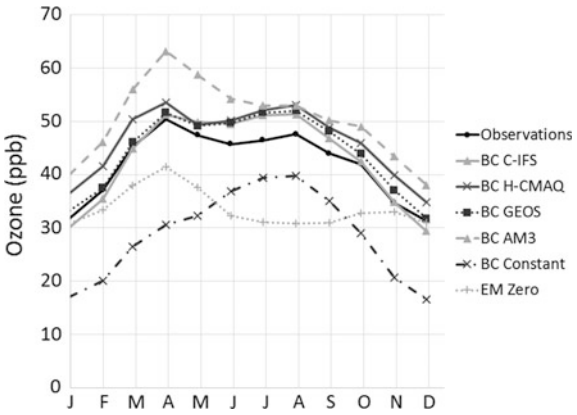

Fig. 62.1 Observed and simulated monthly averaged daily maximum 8-h ozone from observations and the six CMAQ simulations, averaged over all AQS monitors in the modeling domain

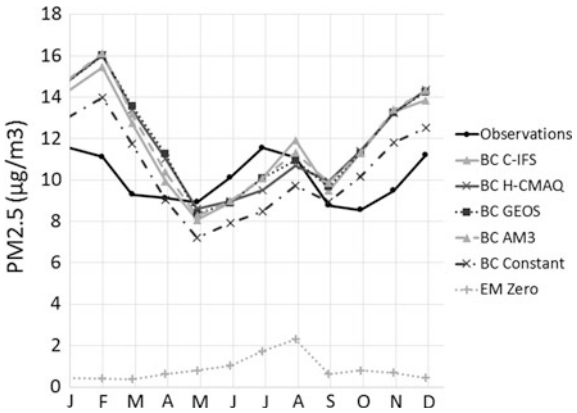

Fig. 62.2 As in Fig. 62.1 but for 24-h average $PM_{2.5}$

uncertainty on regional-scale ozone simulations is non-negligible. The results for the "BC constant" and "EM zero" sensitivity simulations indicate that during wintertime, simulated ozone concentrations are almost exclusively driven by boundary conditions, i.e. "BC C-IFS" and "EM zero" are very similar despite the lack of anthropogenic emissions in the latter, and "BC constant" is close to 20 ppb, the time-invariant value of ozone concentrations specified at the boundaries in that simulation. The "EM zero" results also indicate that the impact of boundary conditions on regional ozone is largest in springtime when free tropospheric ozone in the northern hemisphere reaches a maximum. If one views ozone from the "EM zero" simulation as the amount of regional ozone due to boundary conditions and biogenic emissions, and "BC constant" minus 20 ppb as the amount of ozone due to anthropogenic and biogenic emissions within the domain, the results indicate that the former dominates the latter even during summer (30 ppb vs. 40 ppb – 20 ppb = 20 ppb). While this is certainly an oversimplification of the non-linear system, it nevertheless reaffirms the profound impact of boundary conditions on regional-scale ozone simulations throughout the year.

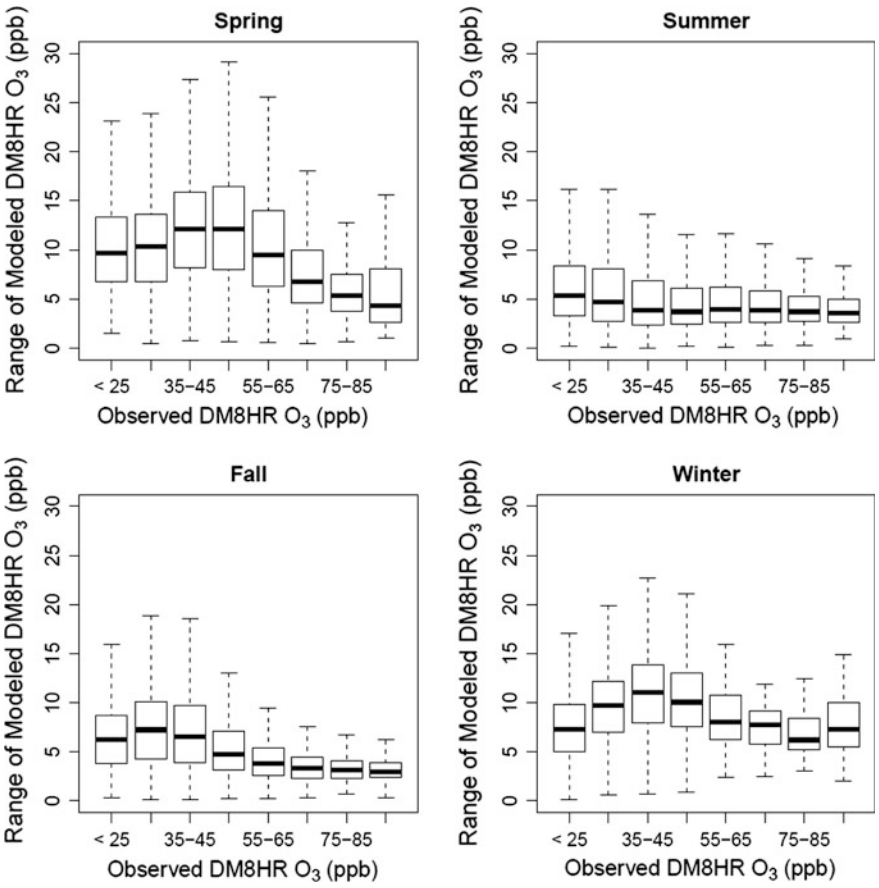

Fig. 62.3 Spread between the "BC C-IFS", "BC H-CMAQ", "BC GEOS" and "BC AM3" simulations for daily maximum 8-h ozone at AQS monitors as function of observed concentrations

The results for $PM_{2.5}$ shown in Fig. 62.2 differ from those for ozone. The spread between the "BC C-IFS", "BC H-CMAQ", "BC GEOS" and "BC AM3" is less than 1 μg/m^3 for most of the year, i.e. less than 10% of simulated monthly mean values. The only exception is summer when differences can exceed 1 μg/m^3. These findings are confirmed by the "EM zero" simulation which shows that the contribution of boundary conditions to simulated regional $PM_{2.5}$ concentrations exceeds 1 μg/m^3 only during the summer. Canadian wildfires and their different treatment in the various global/hemispheric simulation likely are a major factor for this larger contribution and the larger model-to-model spread during summer.

The time series in Figs. 62.1 and 62.2 investigate the impact of boundary conditions on monthly average concentrations. Figures 62.3 and 62.4 depict the spread between the "BC C-IFS", "BC H-CMAQ", "BC GEOS" and "BC AM3" simulations for daily maximum 8-h ozone and daily average $PM_{2.5}$ as function of

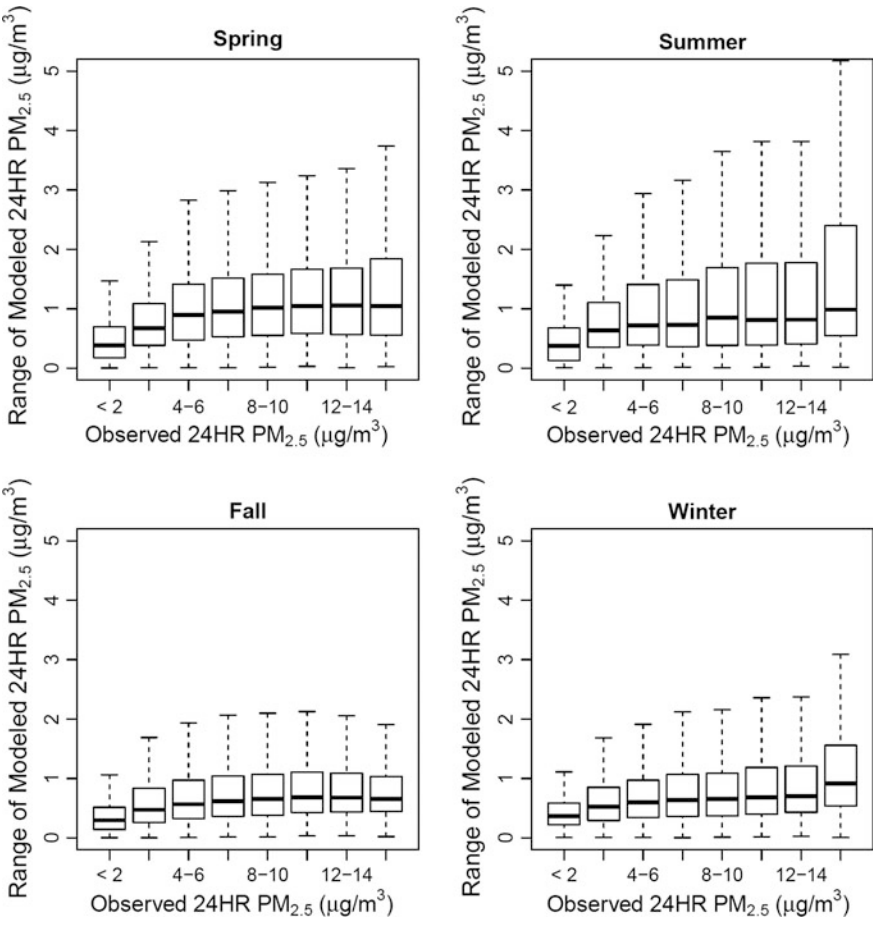

Fig. 62.4 As in Fig. 62.3 but for 24-h average $PM_{2.5}$

the observed concentrations at AQS monitors for each season. Here, the spread is defined as the difference between the two simulations with the highest and lowest simulated concentration for a given day and station. For ozone, the results show that spring has the largest spread and during all seasons the spread is larger for the mid-range of observed concentrations compared to the upper end of observed concentrations. In contrast, the spread for $PM_{2.5}$ is largest in summer and increases with observed concentrations in all seasons, indicating that episodes of elevated $PM_{2.5}$ concentrations tend to have a greater sensitivity to boundary conditions.

Acknowledgements and Disclaimer We gratefully acknowledge Johannes Flemming for providing the C-IFS fields, Rokjin Park for providing the GEOS-CHEM fields, and Meiyun Lin for providing the AM3 fields from their simulations performed for TF-HTAP. Although this work has been reviewed and approved for publication by the U.S. Environmental Protection Agency, it does not necessarily reflect the views and policies of the agency.

Questions and Answers

Questioner: Greg Yarwood
Question: This work shows how valuable tracers can be in revealing contributions of BCs. But, the BC impacts are biased high because chemical destruction was not included. So a useful improvement is to account for chemical destruction of the BC ozone tracers using a scheme such as the one published in Baker et al. (2015).
Answer: Thank you for this comment. The inert trailers used in AQMEII were not designed to be an attribution tool and as you pointed out the absolute tracer concentrations should not be interpreted to be the impact of boundary conditions on simulated ground level ozone. Instead, these tracers were designed to compare the transport and mixing of air masses from the boundaries across different models and to assess how the relative contributions of air masses originating at different vertical levels to ground level tracer concentrations varies between models.

Questioner: Heinke Schluenzen
Question: Mathematically one distinguishes boundary conditions (Diriclet/Neumann) and boundary values. Here the boundary values were changed, do all the models apply the same boundary condition? This might explain the large differences of the tracer experiments.
Answer: The different models participating in the tracer experiments used different meteorological fields and different formulations for horizontal and vertical transport. This implies that the boundary conditions indeed differed between models despite prescribing common boundary values. The resulting differences in simulated tracer concentrations reflect the impacts of different meteorological fields and process representations.

Questioner: Richard Derwent
Question: I would have appreciated a comparison with the NOAA Boulder baseline ozone observations for the Trinidad Head, California station rather that a comparison with 1210 stations.
Answer: In previous work we had compared the global models providing boundary values to CMAQ against ozonesonde observations off the California coast. This comparison showed differences in free tropospheric ozone concentrations between the global models that are consistent with the spatially averaged differences in the surface ozone fields between the various regional-scale CMAQ simulations presented here.

References

Baker KR, Emery C, Dolwick P, Yarwood G (2015) Photochemical grid model estimates of lateral boundary contributions to ozone and particulate matter across the continental United States. Atmos Environ 123:49–62

Byun DW, Schere KL (2006) Review of the governing equations, computational algorithms, and other components of the models-3 community multiscale air quality (CMAQ) modeling system. Appl Mech Rev 59:51–77

Hogrefe C, Pouliot G, Xing J, Flemming J, Roselle S, Mathur R, Galmarini S (2016) Global and regional modeling of long-range transport and intercontinental source-receptor linakges. In: Steyn DG, Chaumerliac N (eds) Air pollution modeling and its application XXIV, pp 245–250. doi:10.1007/978-3-319-24478-5_40

Chapter 63
Modelling Regional Air Quality in the Canadian Arctic: Simulation of an Arctic Summer Field Campaign

Wanmin Gong, Stephen Beagley, Junhua Zhang, Ralf Staebler, Amir A. Aliabadi, Sangeeta Sharma, David Tarasick, Julia Burkart, Megan Willis, Greg Wentworth, Jennifer Murphy, Heiko Bozem, Franziska Koellner, Johannes Schneider, Andreas Herber, W. Richard Leaitch and Jon Abbatt

Abstract Model simulations of an Arctic summer field campaign were carried out. The model results were compared with observational data from both ground-based monitoring and in situ measurements on-board multiple mobile platforms. The model was able to well capture regional sources and transport affecting the Arctic air quality. It is shown that the study area was impacted by North American (NA) regional biomass burning emissions. The model-observation comparison also corroborates previous findings on possible roles of marine-biogenic sources in aerosol production in the Arctic MBL during summertime.

W. Gong (✉) · S. Beagley · J. Zhang · R. Staebler · A.A. Aliabadi · D. Tarasick
Air Quality Research Division, Environment and Climate Change Canada, Toronto, Canada
e-mail: wanmin.gong@canada.ca

S. Sharma · W. Richard Leaitch
Climate Research Division, Environment and Climate Change Canada, Toronto, Canada

J. Burkart · M. Willis · G. Wentworth · J. Murphy · J. Abbatt
Department of Chemistry, University of Toronto, Toronto, Canada

H. Bozem
Institute for Atmospheric Physics, Johannes Gutenberg University of Mainz, Mainz, Germany

F. Koellner · J. Schneider
Particle Chemistry Department, Max Planck Institute for Chemistry, Mainz, Germany

A. Herber
Alfred Wegener Institute Helmholtz-Center for Polar and Marine Research Bremerhaven, Bremerhaven, Germany

A.A. Aliabadi
Now at Environmental Engineering, University of Guelph, Guelph, ON, Canada

C. Mensink and G. Kallos (eds.), *Air Pollution Modeling and its Application XXV*, Springer Proceedings in Complexity, DOI 10.1007/978-3-319-57645-9_63

63.1 Introduction

As the Arctic environment is changing rapidly, Environment and Climate Change Canada (ECCC) is undertaking an initiative to develop an air quality prediction capacity for the Canadian North and Arctic region, in the context of assessing the impacts of the current and future air contaminant emissions from various sources on the northern environment and human health. A major challenge in modelling the Arctic environment is the scarcity of observational data for model evaluation. In this study, model simulations were carried out for a field campaign conducted over the Canadian High Arctic during the summer of 2014. The model results were compared with detailed observational data from both ground-based monitoring and in situ measurements on-board multiple mobile platforms. Sources and processes affecting the summertime Arctic air quality and model's capability in representing them were examined.

63.2 Field Campaign and Model Simulation Setup

An intensive field study was conducted over the Canadian High Arctic in summer 2014 under a research network NETCARE (NETwork on Climate and Aerosols: Addressing Key Uncertainties in Remote Canadian Environments, http://www.netcare-project.ca). Measurements of aerosol physical and chemical properties and trace gases were made onboard the Alfred Wegner Institute (AWI) Polar 6 aircraft and the Canadian Coast Guard Amundsen icebreaker. The measurements onboard Polar 6 took place from July 4 to 21, consisting of 11 research flights based from Resolute Bay, Nunavut. The measurements onboard Amundsen took place between July 13 and August 7 as the icebreaker sailed through the eastern Canadian Archipelago. Ground-based air quality monitoring and aerosol measurements at the Canadian Aerosol Baseline Measurement station at Resolute Bay were also part of the study.

ECCC's on-line air quality forecast model GEM-MACH with a 12-bin configuration was used for the simulation. The model upgrades and adaptation for the Arctic application are as described in Gong et al. (2016). The simulation was carried out for the period of June–August, 2014. Output from a global CTM, MOZART-4 (Emmons et al. 2010) was obtained from http://www.acom.ucar.edu/wrf-chem/mozart.shtml for the chemical initial and lateral boundary conditions. The same anthropogenic emissions, as in Gong et al. (2016), and the NA wildfire emissions for the 2014 fire season, archived at the Canadian Centre for Meteorology and Environment Prediction, were used.

63.3 Results and Discussion

Figure 63.1 shows the modelled O_3 and $PM_{2.5}$ compared with the observations at the Resolute Bay ground site for the period of July 4–Aug 8, 2014, covering both Polar 6 flights and Amundsen cruise. The measurements were obtained using an integrated air quality package, airpointer® (Aliabadi et al. 2015). In general, the model tracks the observations quite well. Several high $PM_{2.5}$ episodes are shown in both observations and the simulation, which the model shows were influenced by wildfire plumes originating from Canada's Northwest Territories. These events were accompanied by a significant elevation in observed particle number density in size range >50 nm (using a scanning mobility particle sizer, SMPS) and in observed particle scattering (not shown) and absorption (using a continuous light absorption photometer, CLAP). The modelled O_3 was enhanced during these fire events, while the enhancements were less significant in the observations. The O_3 over-prediction during fire events is being investigated relating to fire representation in the model (e.g., emission factors and plume injection algorithms).

The model simulation was compared to the in situ measurements onboard the Polar 6 aircraft (see Willis et al. 2016, for a description of the instrumentations). For this comparison the 4-D model outputs were sampled along the flight path at nearest model grid points and output times. The comparison is presented in the form of vertical profiles in Fig. 63.2, grouped in two time periods of the aircraft campaign: July 4–12 (including FLT 5–10) and July 17–21 (including FLT 11–15). During the 1st time period, the study area was dominated by a high-pressure system and well insulated from the influence of air masses from lower latitudes. In contrast, during

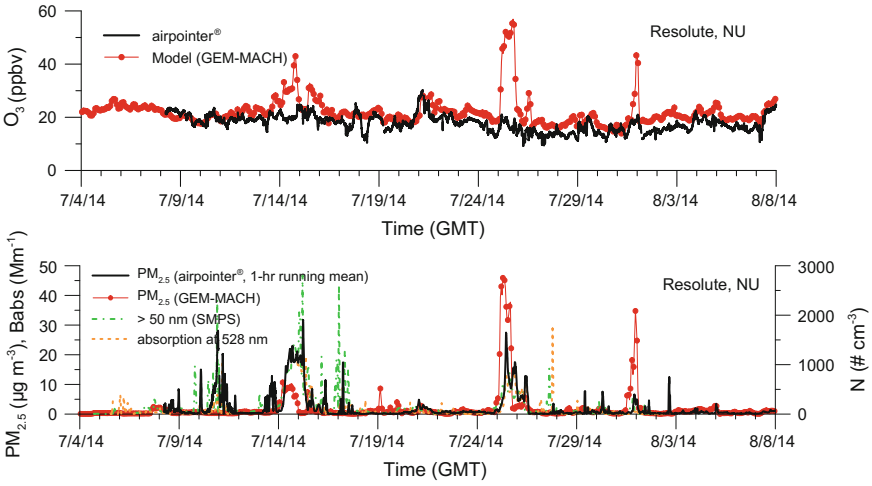

Fig. 63.1 Model-observation comparison of O_3 (*top*) and $PM_{2.5}$ (*bottom*) at resolute bay (74.71°N, 94.97°W). The bottom panel also includes the measured particle number in size range greater than 50 nm (SMPS) and particle light absorption at wavelength 528 nm (CLAP) at this site

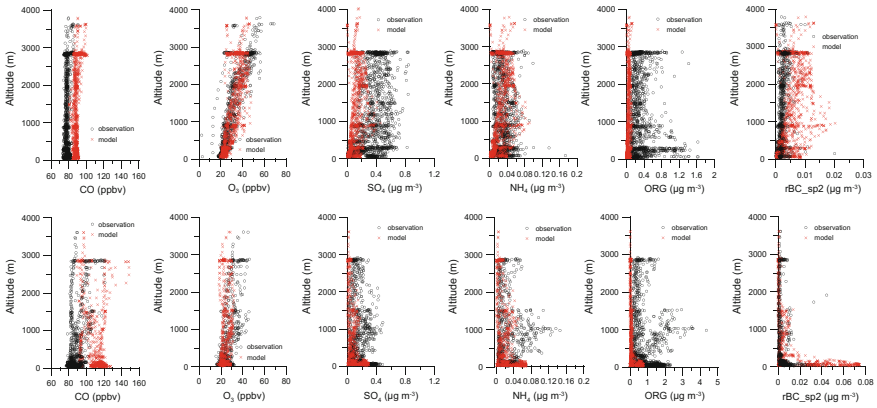

Fig. 63.2 Comparison with in situ measurements on-board Polar 6 aircraft. *Top row* period 1 (FLT 5–10, July 4–12, 2014); *bottom row* period 2 (FLT 11–15, July 17–21, 2014)

the 2nd period, the area was under an upper-level-low experiencing several frontal systems, which brought in relatively warm and moist air from lower latitudes and the influence of wildfire plumes and possibly emissions over the east coast and Arctic shipping channels.

CO and O_3: The model captured the vertical structure very well. The observed CO profiles indicated a clean, unperturbed Arctic background during the 1st period, while the latter profiles were more varied showing influence of long-range transport of more polluted air. Indications of long-range transport are also seen from the O_3 profiles of the 2nd period. These features were reproduced well by the model. However, there seems to be a systematic bias in modelled CO (~20 ppbv), which most likely is influenced by the lateral boundary conditions.

Particle mass components: The modelled particulate SO_4, NH_4, organics, and elemental carbon (EC) at 1 μm size cut were compared to measurements obtained from an Aerodyne aerosol mass spectrometer (SP-AMS) and a DMT single particle soot photometer (SP2) measuring refractory black carbon (rBC). The observed SO_4 showed relatively higher concentrations throughout the lowest 3 km during the 1st period compared to the 2nd. The model clearly under-predicted SO_4 for the 1st period. Interestingly, the modelled NH_4 compared well with the observations for this period, which could suggest that the observed excess in SO_4 was produced locally from sources not represented in the model, possibly of oceanic origin (e.g., DMS oxidation, Leaitch et al. 2013; Willis et al. 2016). The model predicted very low organics for the 1st period as the study area was free of transport from lower latitudes and the model did not represent local sources or productions. In contrast, the observations showed higher concentrations in the MBL suggesting possible marine secondary organic aerosol production (Willis et al. 2016). The modelled $EC_{1.0}$ concentrations were overall higher than rBC measurements from SP2 for the 1st period, while both model and observation showed an enhancement within the

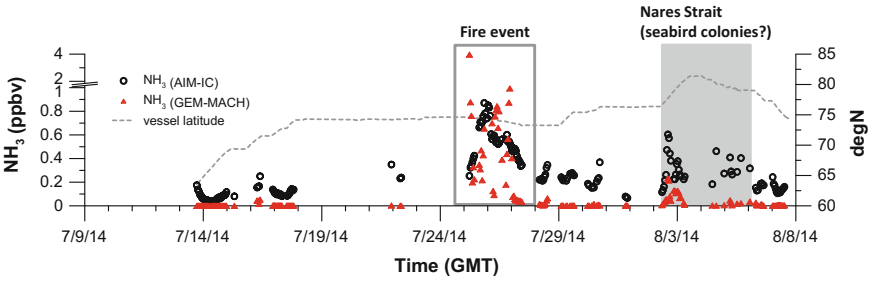

Fig. 63.3 Comparison with NH_3 measurement (AIM-IC) on-board the Amundsen icebreaker

MBL for the 2nd period. A sensitivity test is being carried out to determine the possible role of ship emissions over the east coast and Arctic shipping channels.

The modelled NH_3 was compared, in Fig. 63.3, to the Ambient Ion Monitor-Ion Chromatograph (AIM-IC) measurement onboard the Amundsen icebreaker (Wentworth et al. 2016). The measurement showed two periods of enhancement, around July 26 (in Lancaster Sound) and August 2–5 (cruising through the Nares Strait). The first enhancement was well matched by the model simulation (which was dominated by a regional biomass burning plume), while the second enhancement was not simulated by the model (other than a small contribution from a fire plume on August 3). This further supports the findings from Wentworth et al. (2016) on the role of NH_3 emissions from the seabird colonies along the coasts of Baffin Bay.

Questions and Answers

Questioner: Heinke Schlünzen
Question: Model results and aircraft measurement agree "reasonably well". Did you try to quantify the agreement by considering the measurement uncertainty and, if you did, how did you determine the measurement uncertainty?
Answer: These are initial comparisons. We plan to carry out statistical comparisons, for example by height bins, to further quantify the comparison. Regarding measurement uncertainty, it depends on the individual instrument and measurement technique. One needs to be mindful of what the instrument measures and its sensitivity when carrying out the model-observation comparison.

Questioner: Clemens Mensink
Question: In the comparison of model results and observations at the monitoring sites I see sharp peaks in ozone and $PM_{2.5}$. Can you comment on this?
Answer: The sharp peaks in measurement, particularly for $PM_{2.5}$, are often due to local sources which are not represented in the model. The major peaks in modeled time series seen here are mainly attributable to transported biomass burning plumes.

The model tends to over-predict ozone concentrations in fire plumes, which is likely (at least in part) due to the fact that the model presently does not take into account of the reduction in photolysis in fire plumes. We are currently working on addressing this issue in the model.

References

Aliabadi AA et al (2015) Air quality monitoring in communities of the Canadian Arctic during the high shipping season with a focus on local and marine pollution. Atmos Chem Phys 15: 2651–2673. doi: 10.5194/acp-15-2651-2015

Emmons LK et al (2010) Description and evaluation of the model for ozone and related chemical tracers, version 4 (MOZART-4). Geosci Model Dev 3:43–67. www.geosci-model-dev.net/3/43/2010/

Gong W et al (2016) Modelling regional air quality in the Canadian Arctic: impact of north American wildfire and Arctic shipping emissions. In: Steyn DG, Chaumerliac N (eds) Air pollution modelling and its application XXIV. Springer, Switzerland, pp 301–306

Leaitch WR et al (2013) Dimethyl sulfide control of the clean summertime Arctic aerosol and cloud. Elementa 1:00017. doi:10.12952/journal.elementa.000017

Wentworth GR et al (2016) Ammonia in the summertime Arctic marine boundary layer: sources, sinks, and implications. Atmos Chem Phys 16:1937–1953. doi:10.5194/acp-16-1937-2016

Willis MD et al (2016) Growth of nucleation mode particles in the summertime Arctic: a case study. Atmos Chem Phys 16:7663–7679. doi:10.5194/acp-16-7663-2016

Chapter 64
Evaluation of Regional Measures in order to Improve the Air Quality in the North-West European Hot Spot Region

Felix Deutsch, Wouter Lefebvre, Hans Hooyberghs, Frans Fierens and Sandy Adriaenssens

Abstract The effects of four regional emission scenarios on the concentrations of PM_{10}, $PM_{2.5}$, NO_2 and EC (elementary carbon) in the North-West European (NWE) Hot Spot region have been studied. The emission estimates were provided by TNO, regional calculations were carried out for the years 2009 and 2020 using the BelEUROS model (Deutsch et al. 2009) on a 15 × 15 km^2 grid. The effect of a highway speed limit reduction to 90 km/h on all highways in the NWE region (Belgium, France, Germany, Luxemburg, the Netherlands and the UK) showed up to 4.4% lower concentrations of EC and up to 3.5% reduction of NO_2 concentrations (mean over Belgium). The introduction of low emission zones (LEZ) in all cities in the NWE region with more than 50.000 inhabitants and more than 700 inhabitants/km^2 resulted in a reduction of 1.8% of the EC-concentrations (mean over Belgium). However, in the areas that actually make part of a LEZ the EC concentration is reduced by 19% and hence this scenario could be more effective in terms of population exposure. In the healthy diet scenario, 75% less meat production in Europe was assumed, leading basically to lower ammonia emissions (reduction of approximately 30%). This scenario results in significant reductions (4.2% as a mean over Belgium) in particulate matter ($PM_{2.5}$) concentrations due to a reduction of secondary aerosol formation. EC-concentrations are not affected by this scenario. Finally, a pellet stoves scenario was calculated in which 20% of the non-wood energy consumption (gas, oil) in the residential combustion sector had been converted to pellet stoves. This scenario resulted in considerable increases in

F. Deutsch (✉) · W. Lefebvre · H. Hooyberghs
VITO, Boeretang 200, 2400 Mol, Belgium
e-mail: felix.deutsch@vito.be

W. Lefebvre
e-mail: wouter.lefebvre@vito.be

F. Fierens · S. Adriaenssens
IRCEL/CELINE, Kunstlaan 10-11, 1210 Brussels, Belgium

C. Mensink and G. Kallos (eds.), *Air Pollution Modeling and its Application XXV*,
Springer Proceedings in Complexity, DOI 10.1007/978-3-319-57645-9_64

emissions and in an increase of EC-concentrations by up to 21% as a mean value over Belgium. $PM_{2.5}$-concentrations increase by up to 4%. Results for all scenarios are available for the whole NWE region.

64.1 Introduction

In the framework of the Joaquin (Joint Air Quality Initiative)-project (Interreg IV-B NWE-region), several emission change scenarios were calculated in order to study their effect on the air quality in North-West Europe (NWE). The NWE region is an air pollution hotspot in which reduction of the air pollution levels is strongly needed. Both local and regional measures were studied in the Joaquin-project. This abstract focusses on the regional measures.

64.2 Methodology and Scenarios

Four scenarios have been studied using the regional air quality model BelEUROS (Deutsch et al. 2009) on a 15 × 15 km^2 grid. Emissions were provided by TNO and are described in Van der Gon et al. (2014). In the first scenario a speed limit reduction to 90 km/h was implemented on the highways of the complete NWE-region. The emission reduction factors for each species were derived from Lefebvre et al. (2011a), i.e. 0.91 for NO_x, 0.87 for PM_{10} and 0.85 for $PM_{2.5}$. The second scenario implements a low emission zone in all areas in which the following criteria are met: more than 50.000 people living in the city and more than 700 inhabitants/km^2. Emission reductions in a LEZ were estimated using the emission reductions for a specific scenario studied for the city of Antwerp (Belgium). The 'healthy diet'-scenario assumed a decrease in meat production of 75% with emission changes for 2020 of about 30% for ammonia. Finally, the 'Pellet Stoves' scenario replaces 20% of the fossil fuel use by households by renewable energy in the form of wood, burned in wood pellet stoves.

64.3 Results and Conclusions

The highway reduction scenario results in moderate to rather small concentration decreases (Fig. 64.1, left). Effects are much smaller in 2020 than in 2009 because of the effects of the current legislation that will already reduce pollutant emissions by 2020. The effects of an additional speed reduction on highways in 2020 is hence smaller than the same measure applied to the 2009 emissions.

The effects of the LEZ are large in Brussels and large agglomerations in the UK as the LEZ emission reductions are applied for these locations. For instance, EC

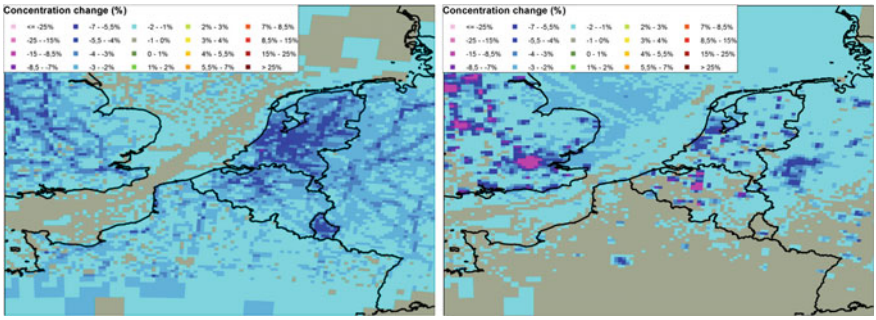

Fig. 64.1 EC-concentration changes for the 'highway speed reduction'-scenario (*left*) and the 'LEZ scenario' (*right*) in % for the year 2020

concentrations in Brussels drop by 18% in 2020 if a LEZ is introduced (Fig. 64.1, right). Reductions in the Dutch and German agglomerations seem to be comparable to the ones in Belgium, whereas the effects in the French cities are significantly smaller. Reductions outside of the LEZs are small. Generally, the effects on EC concentrations for this scenario are much larger than the effects on other pollutants, mainly because the contribution of road traffic emissions to EC concentrations is larger than the contributions to other pollutants; NO_2 and PM have also important non-traffic emission sources. It has to be noted that small influences on a regional scale can hide large differences at a local scale as shown in previous studies (e.g. Lefebvre et al. 2011b).

The healthy diet scenario results in (almost) no changes in EC- and NO_2-concentrations, but in significant reductions in $PM_{2.5}$- and PM_{10}-concentrations (Fig. 64.2, left) due to the reduction of secondary ammonium compounds caused by the NH_3 emission reduction. Note, however, that this emission reduction scenario has been assumed for the whole of Europe and not only for the NWE region, like the other emission scenarios used in this study. It becomes evident that $PM_{2.5}$-concentrations would drop significantly throughout the NWE domain by 5–6% as a

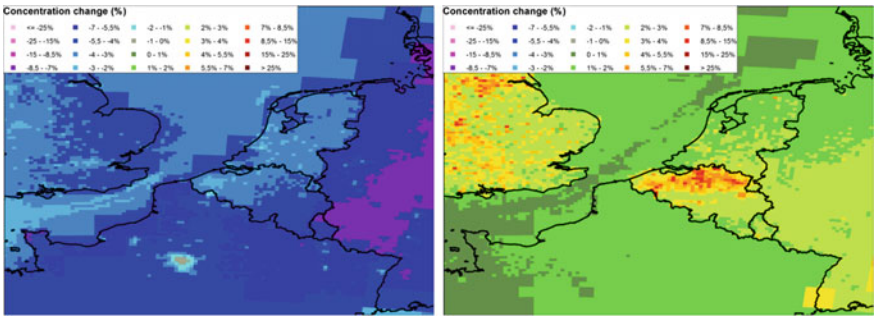

Fig. 64.2 $PM_{2.5}$-concentration changes for the 'healthy diet'-scenario (*left*) and the 'pellet stove'-scenario (*right*) in % for the year 2020

mean, however regional differences seem to be large. The reduction in parts of Germany amounts to more than 10%. Fewer 'local' differences are observed compared to scenario 3 and 4 because a secondary pollutant is affected in this scenario.

The pellet stoves scenario results in an increase of the concentrations for all investigated pollutants, especially for EC which increases drastically. The increase in EC is almost twice as large in Flanders compared to the increase in the Walloon region or in Brussels and it is much larger in 2020 than in 2009. This is because the emission reduction in the 2020 baseline scenario for other source sectors such as road transport leads to a higher contribution of residential emissions to EC concentrations in the future. However, $PM_{2.5}$- and PM_{10}-increases are larger in Brussels than in Flanders and these increases are larger in 2009 than in 2020. The EC concentrations in this scenario increase mainly on the countryside, somewhat less in the cities. We can observe a large difference in the effects for France and the effects for the other countries and regions. Whereas EC concentrations increase in France only by 3–7%, increases in Flanders can amount to more than 25%. Even $PM_{2.5}$ concentrations would increase in certain parts of Flanders by more than 15% (Fig. 64.2, right). Flanders is the region with the largest increase in EC concentrations of all regions within the NWE domain. This is on the one hand due to the differences in the origin of the EC emission inventory and on the other hand due to actual differences in the residential fuel mix by country/region.

When comparing the different emission scenarios (Table 64.1), it becomes clear that the speed reduction and the LEZ scenario have mainly effects on EC- and NO_2-concentrations. The healthy diet scenario has mainly effects on $PM_{2.5}$- and PM_{10}-concentrations and the pellet stoves scenario has (negative) effects on EC-, $PM_{2.5}$- and PM_{10}-concentrations. Hence the effects of the different scenarios can be classified to some extent. The highway speed reduction reveals significantly larger effects than the LEZ-scenario for all pollutants. However, whereas the highway reduction scenario results in larger mean concentration reductions than the LEZ scenario, the LEZ scenario results specifically in the LEZ areas (large agglomerations) in an even higher EC reduction and comparable $PM_{2.5}$ and PM_{10} reductions than the highway reduction scenario. NO_2 reductions remain smaller in the LEZ scenario, even within the LEZ areas themselves. Hence, we can assume that population exposure reduction to EC is larger in the LEZ scenario than in the highway reduction scenario as the concentration decrease takes place where most people are living. The healthy diet scenario leads to a rather large reduction in $PM_{2.5}$-concentrations, which probably cannot be reached with any other 'single' measure because this scenario makes use of the fact that a large portion of $PM_{2.5}$ is secondary $PM_{2.5}$ and originates actually from outside Belgium. The results show also very clearly that it has to be avoided that the pellet stove scenario becomes reality, as this scenario would be connected with significant increases of all pollutants, especially EC and PM.

All results and data can be found on the Joaquin-website (joaquin.eu).

Table 64.1 Comparison of the 4 regional emission scenarios for the region of Flanders (Northern Belgium) and for Belgium for the years 2009 and 2020. Numbers give the percentage of relative differences in pollutant concentrations

Pollutant	Year	Highway reduction		Low emission zone		Healthy diet		Pellet stoves	
		Flanders	Belgium	Flanders	Belgium	Flanders	Belgium	Flanders	Belgium
EC	2009	−4.63	−4.43	−1.86	−1.65	0.00	0.00	18.70	13.47
	2020	−2.74	−2.47	−2.20	−1.84	0.11	0.16	28.23	21.17
NO_2	2009	−3.21	−3.51	−0.55	−0.56	0.01	0.02	1.00	1.04
	2020	−2.59	−2.74	−0.55	−0.53	0.01	0.01	1.45	1.48
$PM_{2.5}$	2009	−0.96	−0.96	−0.31	−0.27	−4.15	−4.96	5.32	3.97
	2020	−0.63	−0.63	−0.23	−0.21	−3.62	−4.27	4.89	3.63
PM_{10}	2009	−0.69	−0.69	−0.22	−0.19	−3.23	−3.87	3.95	2.95
	2020	−0.41	−0.41	−0.15	−0.14	−2.76	−3.21	3.44	2.53

Acknowledgements The authors want to acknowledge the VMM (Vlaamse MilieuMaatschappij) who financed this study in the framework of the INTERREG IV-B NWE Joaquin project and the partners within the project.

Question and Answer

Questioner: Heinke Schluenzen
Question: Is the small impact of the low emission zones maybe a result of the difficulty to determine sufficient amounts of corresponding urban areas and, in addition, averaged out due to the 15 × 15 km^2 grid applied?
Answer: It is true that the resolution of 15 × 15 km^2 is not sufficient to determine the effect of the LEZs within the LEZs themselves. Therefore, much higher resolution is to be used. However, the goal here was to check if a more widespread use of LEZ would decrease the concentrations significantly outside of the LEZs. It is shown that this decrease is very small.

References

Deutsch F, Fierens F, Veldeman N, Janssen S, Torfs R, Buekers J, Trimpeneers E, Bossuyt M (2009) Toekomstverkenning MIRA 2009, Wetenschappelijk rapport, Thema 'Zwevend stof' (in Dutch). http://www.milieurapport.be/Upload/main/WR_Zwevend_stof_MIRA-S_2009_v18_def_TW.pdf

Lefebvre W, Fierens F, Trimpeneers E, Janssen S, Van de Vel K, Deutsch F, Viaene P, Vankerkom J, Dumont G, Vanpoucke C, Mensink C, Peelaerts W, Vliegen J (2011a) Modeling the effects of a speed limit reduction on traffic-related elemental carbon (EC) concentrations and population exposure to EC. Atmos Environ 45:197–207. doi:10.1016/j.atmosenv.2010.09.026

Lefebvre W, Schillemans L, Op't Eyndt T, Vandersickel M, Poncelet P, Neuteleers C, Dumez J, Janssen S, Vankerkom J, Maiheu B, Janssen L, Buekers J, Mayeres I (2011b) Voorstel van maatregelen om de luchtkwaliteit te verbeteren en de geluidshinder te beheersen in de stad Antwerpen (in Dutch), 2011/RMA/R/29

Van der Gon HAC, Kuenen JJP, Schaminée S, Visschedijk AJH, Manders AMM (2014) Emission data and grids for the INTERREG IVB NWE project JOAQUIN to support air quality modeling, TNO report, TNO 2015 R10357

Chapter 65
On the Relationship Between Observed NLDN Lightning Strikes and Modeled Convective Precipitation Rates: Parameterization of Lightning NO_x Production in CMAQ

Daiwen Kang, Nicholas Heath, Kristen Foley, Jesse Bash, Shawn Roselle and Rohit Mathur

In the middle and upper troposphere, lightning is the most important source of nitrogen oxides ($NO_X = NO + NO_2$), which play an essential role in the production of ozone (O_3) and influence the oxidizing capacity of the troposphere (Murray 2016). Despite much effort in both observing and modeling lightning NO_X during the past decade, considerable uncertainties still exist with the quantification of lightning NO_X (LTNOX) production and distribution in the troposphere. Further, it is challenging for regional chemistry and transport models to parameterize LTNOX production and distribution in time and space accurately. Most studies estimate global LTNOX production ranging from 2 to 8 Tg (N) $year^{-1}$ or about 10–15% of the total NO_x budget (Pickering et al. 2014). However, owing to the concerted effort to reduce anthropogenic NO_x emissions in recent decades, it is expected that the relative burden of LTNOX and its associated impact on atmospheric chemistry will increase. As a result, it is important to include LTNOX even when modeling ground level air quality and the interaction of air-surface exchange processes.

In the current version of the Community Multiscale Air Quality (CMAQ v5.1) model, for retrospective model simulations, LTNOX production is based on gridded monthly total lighting strike data from the National Lighting Detection Network (NLDN) that are then scaled by the hourly convective precipitation rate (model variable RC—rain convective) in each grid cell to estimate gridded hourly total LTNOX across the continental US. The relationship between the lightning strike totals and the modeled RC is parameterized based on Allen et al. (2012). With access to the raw NLDN

D. Kang (✉) · N. Heath · K. Foley · J. Bash · S. Roselle · R. Mathur
National Exposure Research Laboratory, Computational Exposure Division,
U.S. Environmental Protection Agency, Research Triangle Park,
Durham, NC 27711, USA
e-mail: kang.daiwen@epa.gov

R. Mathur
e-mail: mathur.rohit@epa.gov

C. Mensink and G. Kallos (eds.), *Air Pollution Modeling and its Application XXV*,
Springer Proceedings in Complexity, DOI 10.1007/978-3-319-57645-9_65

lightning strike data, retrospective model applications can use NLDN data (gridded to the model domain and aggregated to hourly totals) to more directly estimate hourly LTNOX production, avoiding the month-to-hour scaling factors. However, for modeling exercises where the observed lightning strikes are not generally available (e.g., real-time air quality forecasts), a different option is needed to provide the LTNOX estimates. We have developed a LTNOX parameterization based on the relationship between the observed NLDN lightning strikes and modeled RC from a set of Weather Research and Forecasting (WRF) simulations (the model used to create meteorological inputs for CMAQ) from 2002 to 2014 over the continental United States.

65.1 Relationship Between Lightning Strikes and Convective Precipitation

To develop a LTNOX parameterization that could be used for forecasting or other applications when NLDN data are not available, we first looked at the relationship between lightning strikes which were aggregated into hourly mean values and gridded into the modeling grid cells and the modeled hourly RC from WRF over the continental US modeling domain (12 km horizontal resolution). The results showed little to no significant correlation between the two quantities. However, when the lightning strikes and RC were each aggregated to the modeling domain average for each month in the time series, the correlation between the two quantities was clearly evident, as shown in Fig. 65.1. This indicates that even though the model-predicted RC is not a good predictor of lighting events in space and time, it does have the skill to predict overall convective activity across the domain for a given month. Further analysis of the relationship suggests unique spatial distribution patterns over the continental US through the years.

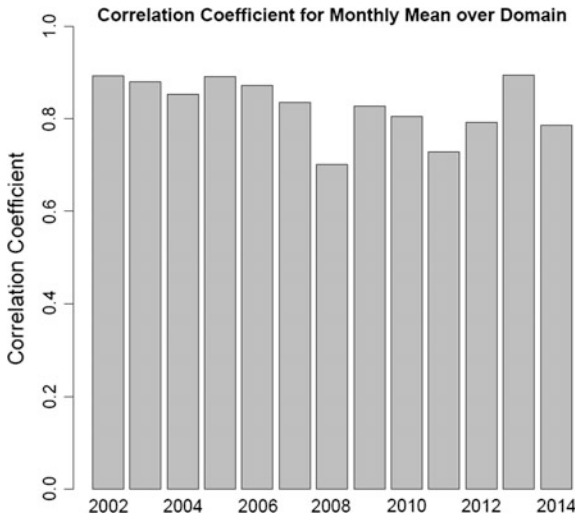

Fig. 65.1 Correlation coefficient between NLDN lightning flashes and convective precipitation rates

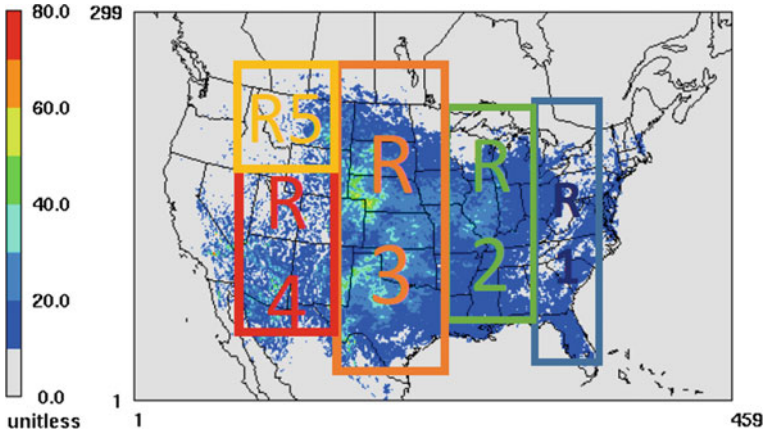

Fig. 65.2 Strike factor spatial distribution and regions for analysis

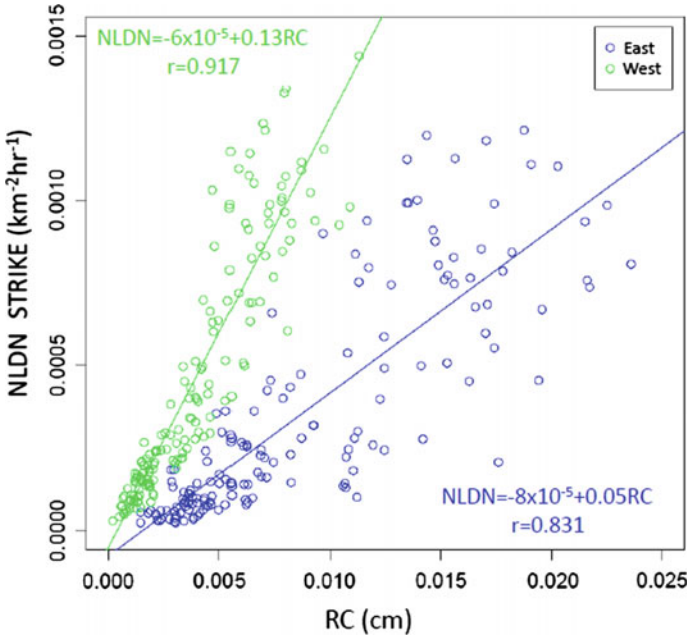

Fig. 65.3 NLDN strikes and RC for regions East (R1 in Fig. 65.2) and West (R2–R5 in Fig. 65.2)

As shown in Fig. 65.2 (background), the strike factors (the ratio between lightning strikes and RC) have larger values in the central regions of the continental US than in other areas, suggesting an examination of the relationship between lightning strikes and RC separately for different regions. Even though five regions

are arbitrarily chosen initially for the analysis, the results suggest that the correlations in Regions 2–5 can be combined as one analysis region, distinctly different from Region 1. Figure 65.3 shows the scatter plots (each point is the monthly mean value over the region) and the corresponding linear regression equations, as well as the correlation coefficients (r).

65.2 Model Parameterization

Theoretically, the above linear regression equations could be directly applied to the model grid cells depending on their location and calculate the LTNOX based on the predicted RC values. However, this direct application would cause some practical problems: (1) the analysis regions are not inclusive and neither scientifically sound; and (2) the LTNOX production would not be consistent in space (sudden changes along the bordering grid cells separating regions). As a solution to these problems, the linear regression equations are applied over an area of adjacent grid cells and the parameters interpolated onto areas that lack enough data points. Figure 65.4 shows the spatial linear regression parameters and the correlation coefficients over 3 × 3 grid cells (36 × 36 km^2 in area).

65.3 Results

Figure 65.5 presents the model-simulated monthly LTNOX column values for the years 2012 and 2013 and Fig. 65.6 shows the time series of daily total LTNOX during July for the same 2 years. For comparison, the same quantity generated using hourly NLDN lightning strike data (black) and the parameterization used in the current CMAQ model based on monthly total lightning strikes (blue) are also shown in these figures. It is evident that the linear regression parameterization (red) captures the magnitude and variability over time of the method that uses hourly NLDN strike data directly (black) and even offers an improvement over the parameterization that uses year-specific monthly total lightning data.

65.4 Summary

Based on multiyear observed NLDN lightning strike data and model-predicted convective precipitation rates, a linear regression parameterization scheme is proposed and applied in the CMAQ model to produce LTNOX over the continental United States. Preliminary results show that the LTNOX produced by this scheme is comparable to that generated by the hour-specific NLDN observed data and the current model parameterization scheme based on year-specific monthly total NLDN

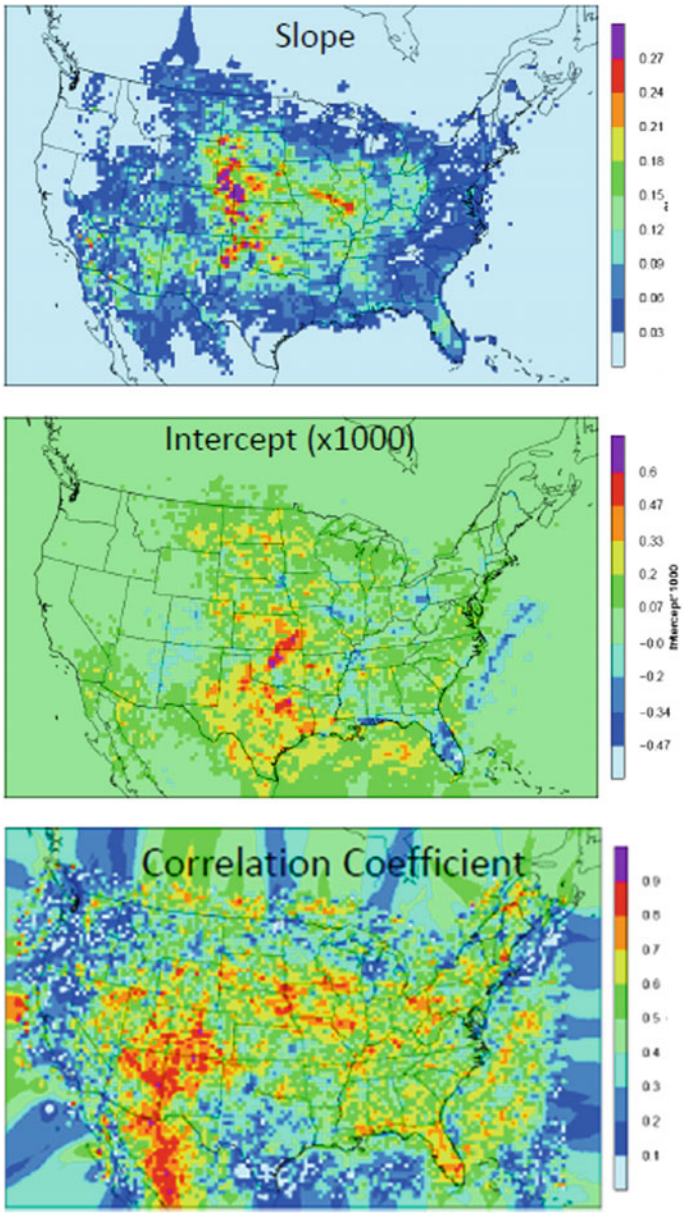

Fig. 65.4 Linear regression and correlation between NLDN and RC over adjacent grid cells (3 × 3)

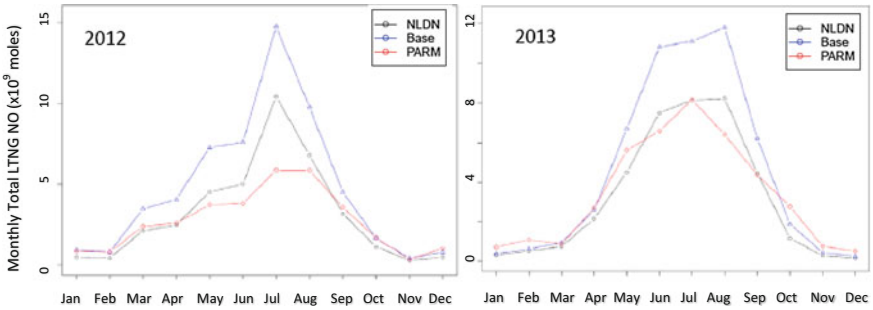

Fig. 65.5 Modeled monthly LTNOX columns using linear regression parameters (sum over the domain)

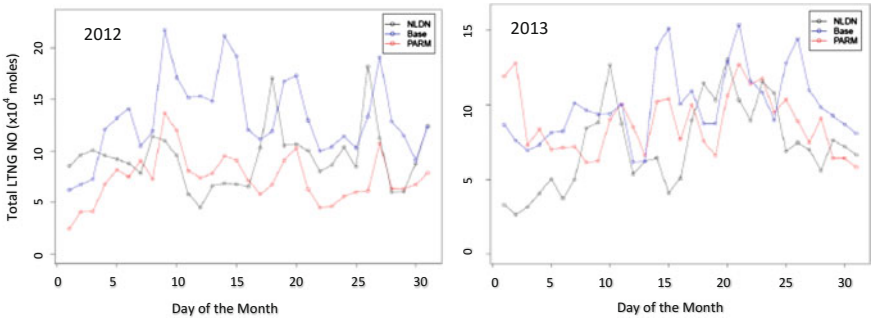

Fig. 65.6 Time series of daily total LTNOX in July (sum over the domain)

data. The advantage of the proposed scheme is that it can be applied to situations where no observed lightning data are available (such as for real time air quality forecasting and future climate studies).

Disclaimer Although this paper has been reviewed by EPA and approved for publication, it does not necessarily reflect EPA's policies or views.

Question and Answer

Questioner: Peter Viaene
Question: The lightning is oxidizing nitrogen but it must also be oxidizing oxygen. Air you including ozone emissions in your model?
Answer: NO is produced within a lightning stroke channel during the rapid heating and cooling process by N_2 and O_2. Strictly speaking, it is not an oxidizing process, but rather a physical-thermal process. During a lightning strike, O_3 may also be formed by O_2+O, but research has found that O_3 formed during a lightning strike is rather insignificant, therefore our modeling study didn't include lightning O_3 emissions.

References

Allen DJ, Pickering KE, Pinder RW, Henderson BH, Appel KW, Prados A (2012) Impact of lightning-NO on eastern United States photochemistry during the summer of 2006 as determined using CMAQ model. Atmos Chem Phys 12:1737–1758. doi:10.5194/acp-12-1737-2012

Murray LT (2016) Lightning NO_x and impacts on air quality. Curr Pollut Rep. doi:10.1007/s40726-016-0031-7

Pickering K, Allen D, Ring A, Bucsela E (2014) Lightning NO_x production per flash based on OMI NO_2 observations and ground network lightning data. In: 23rd international lightning detection conference, 18–19 Mar, Tucson, Arizona, USA

Chapter 66
LOTOS-EUROS Air Quality Simulations over China

R. Timmermans, R. Kranenburg, Limin Zeng, Lili Wang, Jianhui Bai and M. Schaap

Abstract China is suffering from high levels of air pollution due to the large increase of economic activities within recent years in combination with the large number of people living in China's megacities. The main impact on the health of the inhabitants is attributed to the high levels of particulate matter (PM). It is therefore crucial to have knowledge on the main sources of the PM pollution events. This knowledge will allow mitigation strategies for reduction of PM. In this contribution we present some results from the application of a source apportionment tool coupled to the LOTOS-EUROS model. The work is performed within the framework of the EU-FP7 project Marcopolo, a joint collaboration between Chinese and European partners. In this contribution we will show the potential of the source apportionment study to identify the main source sectors and regions responsible for PM pollution episodes in Beijing. We will additionally show some evaluation of the performance of the model. The model is underestimating the PM levels in winter a.o. due to missing sources and change physics/chemistry in high pollution and/or humidity cases.

R. Timmermans (✉) · R. Kranenburg · M. Schaap
Department of Climate, Air and Sustainability, TNO, Princetonlaan 6,
3584 CB Utrecht, The Netherlands
e-mail: renske.timmermans@tno.nl

L. Zeng
Peking University, Beijing, China

L. Wang · J. Bai
Institute of Atmospheric Physics, Chinese Academy of Sciences, Beijing, China

C. Mensink and G. Kallos (eds.), *Air Pollution Modeling and its Application XXV*,
Springer Proceedings in Complexity, DOI 10.1007/978-3-319-57645-9_66

66.1 Introduction

China is suffering from high levels of air pollution due to the large increase of economic activities within recent years in combination with the large number of people living in China's megacities. Estimates from the World Health Organization (WHO) in 2014 indicate that ambient (outdoor) air pollution was responsible for around 3.7 million premature deaths worldwide per year in 2012 (WHO 2014). The greatest burden of these premature deaths is occurring in the Western Pacific and South-East Asia regions. The mortality is mainly due to exposure to small particulate matter of 10 μm or less in diameter (PM10). These numbers underline the strong need for air pollution control with the aim to decrease the level of air pollution in China and in particular the particulate matter concentrations.

To be able to put effective air pollution policy measures in place it is crucial to pinpoint the main emission sources responsible for high pollution levels. This can be done by performing source apportionment of observed or modelled concentrations. In this study we present an application of the LOTOS-EUROS model with its source apportionment tool. The application identifies the main sources responsible for particulate matter pollution over Beijing in 2013.

66.2 Model Description

LOTOS-EUROS is a three dimensional regional chemistry transport model (CTM) conventionally used for air pollution assessments over Europe (e.g. Hendriks et al. 2015; Mues et al. 2014; Schaap et al. 2008). In this study we apply LOTOS-EUROS version 1.10 to investigate the origin of fine particulate matter across China with special emphasis on Beijing and Shanghai.

LOTOS-EUROS includes a source apportionment technique to track the origin of particulate matter components and their precursor gases (Kranenburg et al. 2013). This module uses a tagging approach tracking the contribution of a predefined set of emission categories through the model system. The labels can be defined flexibly discriminating e.g. countries/provinces, sectors or fuel type. Hence, besides the concentration of each tracer also the corresponding fractional contribution of each label is calculated.

The model was ran for the year 2010 and 2013. Through a one-way nesting procedure a simulation over East-China was performed on a resolution of 0.25° longitude by 0.125° latitude, approximately 21 by 15 km^2. We have tracked the 5 main source categories as well as the emissions from Beijing and Shanghai. To be able to assess the contributions of the regions around the cities the larger areas Tianjin-Hebei, Yangtze River Delta and Pearl River Delta were labeled separately. This resulted in 35 labels, including labels for natural emissions such as desert dust and sea-salt and for influx from outside the model domain.

66.3 Results

Figure 66.1 shows a comparison with $PM_{2.5}$ data from the (Institute of Atmospheric Physics) IAP in Beijing. In general the model is able to represent the day to day variability very well, however for January 2013 the model is showing a strong underestimation of aerosol concentrations. Figure 66.2 shows the seasonal and diurnal comparison over the entire year of 2013. It is clear the underestimation of PM is largest in winter. Possible reasons for this are: Missing secondary organic aerosols in the model, underestimation of emissions from heating in cold months, overestimated (vertical) mixing in very stable low boundary layer situations, weakening of photochemistry in high pollution and haze cases, enhanced heterogeneous chemistry during haze episodes and exponential growth of aerosols with high relative humidity. A more detailed evaluation of PM and its precursors is given in (Timmermans et al. 2017). The diurnal cycle from the model shows a distinct peak around the morning rush hour time. We have used the same diurnal temporal profiles for the emissions as used in the European applications. It is clear that this temporal profile may not be the best for application over China.

Figure 66.3 shows the source contributions to modeled PM10 concentrations from the different emission sectors and source regions for two periods in 2013. In January 2013 the main source for PM10 in Beijing is the residential combustion

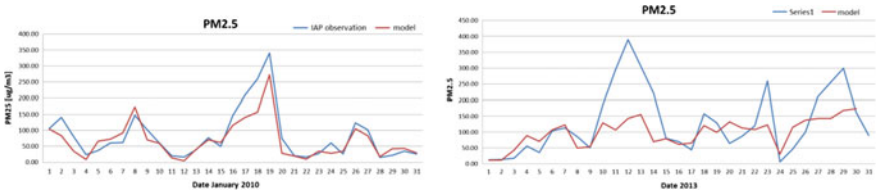

Fig. 66.1 Comparison of LOTOS-EUROS (*red line*) daily PM2.5 with in-situ observations (*blue line*) from IAP for January 2010 (*left*) and January 2013 (*right*)

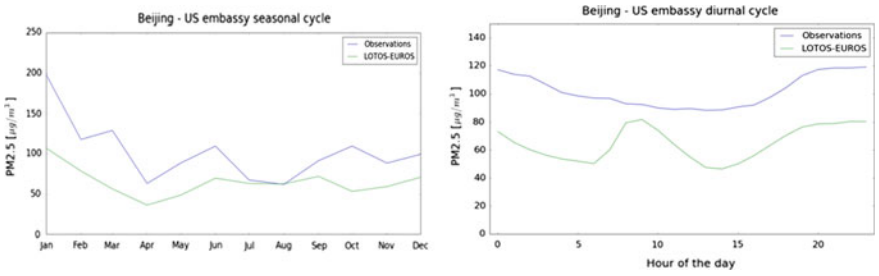

Fig. 66.2 Seasonal (*left*) and diurnal (*right*) comparison of LOTOS-EUROS (*green line*) daily PM2.5 with in-situ observations (*blue line*) from the US Embassy in 2013

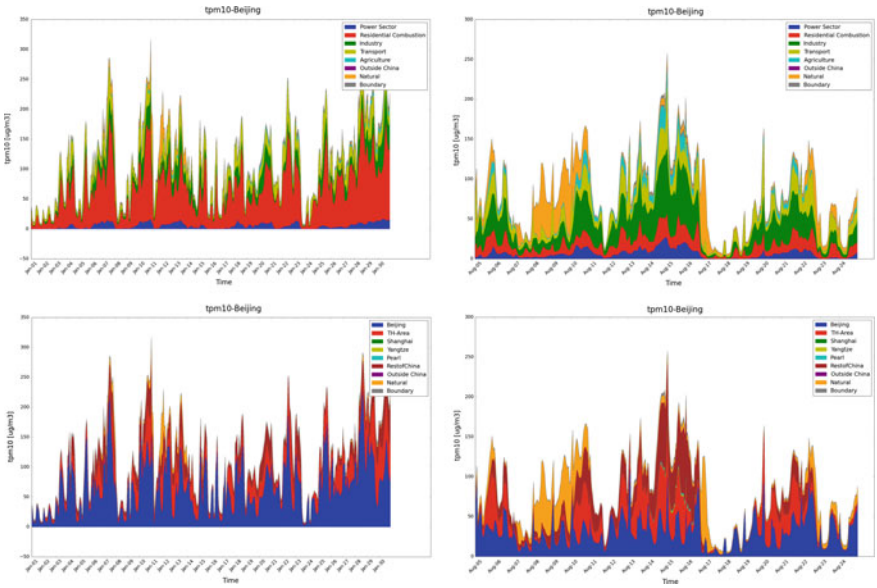

Fig. 66.3 Contribution per source category (*upper plots*) and region (*lower plots*) for PM10 for an episode in January 2013 (*left*) and August 2013 in Beijing

from local sources. In August 2013, the contributions from different sources are more evenly distributed, large contributions from industry, traffic, power sector, residential combustion and natural sources (desert dust) can be seen. In this period the contributions from outside Beijing are also larger. These plots show the potential of the system to identify main sources of pollution events for policy makers. More extended analysis of the source apportionment study is presented in (Timmermans et al. 2017).

Acknowledgements This research was partly funded by EU-FP7 project MARCOPOLO.

Questions and Answers

Questioner: Peter Viaene
Question: Did you include straw burning emissions in your model?
Answer: No we do not have these include explicitly, we do however include wild fire emissions from the operational GFAS product, this is based on thermal radiation observations from satellites. Its is unknown to us whether straw burning emissions in China are picked up by these observations.

Questioner: Pavel Kishcka
Question: The source apportionment shows that the contribution of dust is extremely low. There could be two causal factors for this result: (1) incorrect dust sources in the model and (2) problems with meteorological fields. Did you check your meteorological parameters versus measurements?
Answer: We only did a short comparison for 2013 of the meteorology versus observations from IAP, but we think that in this case the problem lies in the dust representation in the model. We are currently investigating our dust modeling in the LOTOS-EUROS model and it seems our model has a too low dust production. In this particular study however the results are also highly dependent on the dust boundary conditions from the global model, which could also be the cause of uncertainty.

References

Hendriks C, Kuenen J, Kranenburg R, Scholz Y, Schaap M (2015) A shift in emission time profiles of fossil fuel combustion due to energy transitions impacts source receptor matrices for air quality. Environ Sci Impacts 17:510–524. doi:10.1039/c4em00444b

Kranenburg R, Segers AJ, Hendriks C, Schaap M (2013) Source apportionment using LOTOS-EUROS: module description and evaluation. Geosci Model Dev 6:721–733. doi:10.5194/gmd-6-721-2013

Mues A, Kuenen J, Hendriks C, Manders A, Segers A, Scholz Y, Hueglin C, Builtjes P, Schaap M (2014) Sensitivity of air pollution simulations with LOTOS-EUROS to the temporal distribution of anthropogenic emissions. Atmos Chem Phys 14:939–955. doi:10.5194/acp-14-939-2014

Schaap M, Timmermans RMA, Roemer M, Boersen GAC, Builtjes PJH, Sauter FJ, Velders GJM, Beck JP (2008) The LOTOS EUROS model: description, validation and latest developments. Int J Environ Pollut 32:270. doi:10.1504/IJEP.2008.017106

Timmermans R, Kranenburg R, Manders A, Hendriks C, Segers A, Dammers E, Zhang Q, Wang L, Liu Z, Zeng L, Denier van der Gon H, Schaap M (2017) Source apportionment of PM2.5 across China using LOTOS-EUROS. Atmos environ, DOI:10.1016/j.atmosenv.2017.06.003

WHO (2014). http://www.who.int/mediacentre/news/releases/2014/air-pollution/en/

Chapter 67
O_3 Source Contribution During a Heavy O_3 Pollution Episode in Shanghai China

David C. Wong, Qian Wang, Roger Kwok, Jianbin Wu and Qingyan Fu

Abstract Source culpability assessments are useful for developing effective emission control strategies. The Integrated Source Apportionment Method (ISAM) has been implemented in CMAQ to track contributions from source groups and regions to ambient levels and deposited amounts of O_3. CMAQ-ISAM has been used to simulate a heavy O_3 pollution episode in Shanghai during June 2–6, 2015, to quantify the contributions of the precursor emission from different regions to O_3 concentration in Shanghai, to identify the relative importance of different ways by which regional sources affected the O_3 levels in Shanghai, and to investigate the sensitivity of O_3 formation to the precursors during the episode. The results from this study could be helpful to diagnose deficiency in the emission inputs of the air quality forecasting system which has been operating daily since 2010 World Expo.

67.1 Introduction

Shanghai Environmental Monitoring Center (SEMC) has been producing various forms of air quality products since 1997. SEMC provided 48-h air quality forecasting for the 2010 World Expo. Later in 2010, the forecasting information was in AQI format. Shanghai is one of the major cities in China and the air quality has

D.C. Wong (✉)
Computational Exposure Division, National Exposure Laboratory, US EPA, Washington, D.C., USA
e-mail: wong.david-c@epa.gov

Q. Wang · Q. Fu
Shanghai Environmental Monitoring Center, Shanghai 200235, China

R. Kwok
California Air Resources Board, Sacramento CA, USA

J. Wu
Shanghai Meteorological Bureau, Shanghai 200030, China

C. Mensink and G. Kallos (eds.), *Air Pollution Modeling and its Application XXV*, Springer Proceedings in Complexity, DOI 10.1007/978-3-319-57645-9_67

been declining in recent years, part of the growing pains in the developing country. Since the inception of the air quality forecasting system, the model was frequently not able to render accurate predictions during high ozone episodes.

In this study, we used a tool, CMAQ-ISAM (Community Multiscale Air Quality model with Integrated Source Apportionment Method) (Kwok et al. 2015) to determine potential issues in the modeling system. ISAM is an instrumental model built within CMAQ to track NOx species, NO and NO_2, and VOC carbon-bond version-5 species such as ALD2, ETHA, and XYL for their attribution to ozone formation in terms of NOx-limited and VOC-limited O_3 regimes. Tracking can be done by sectors such as energy and transportation, and by regions which are sub-domains defined by users within the simulated domain. Tracking methodology is implemented in all processes including emission, transport, deposition, cloud processing, and chemistry.

67.2 Case Study Setup

We chose an episode that occurred on 6/4 and 6/5, 2015 for this study. Figure 67.1a shows the 1-way nested domains red (27 km) and blue (9 km) and ISAM was applied to the 9 km domain only. There was a 10-day spin-up period and the actual simulation started on 6/2 for 4 days. Meteorological data that drove CMAQ was created by WRF 3.2 with the Kain-Fritsch convective cloud scheme, Purdue Lin microphysics scheme, RRTM long wave radiation scheme, Goddard short wave radiation scheme, Noah LSM, and MYJ PBL scheme. CMAQ-ISAM 5.0.2 with cb05tucl-ae6-aq and AE6 was used. Emission data was generated based on the HTAP dataset. In this application, we tracked six sectors: industrial, energy, transportation, residential, shipping, and agriculture and four regions, Fig. 67.1b (green—YRDOUT, light blue—YRD, dark blue—SHOT and red—JSFX). For model performance validation purposes, we compared with four meteorological observation sites (Fig. 67.1c, red and light blue dots) and with two sites with ozone data (Fig. 67.1c blue dots).

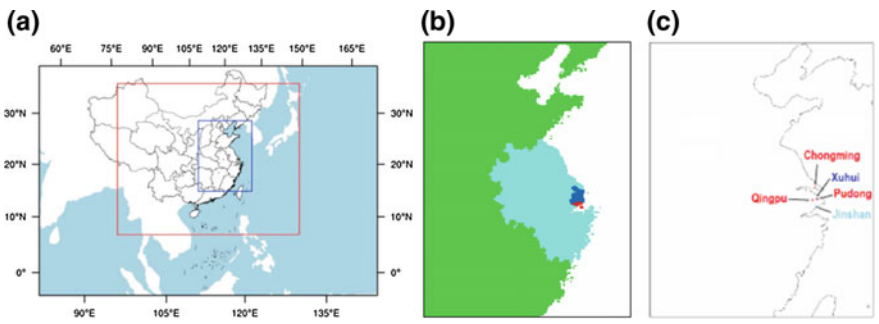

Fig. 67.1 **a** Domains of simulations, **b** Tracking regions, and **c** Observation sites

67.3 Scenario Analysis

The regular CMAQ for this study period shows at site Xuhui (Fig. 67.2a) that the model has extremely low values at night on 6/4 and 6/5 and over predicted on 6/5 during day time. At the nearby site, Jinshan (Fig. 67.2b), it showed under and over prediction but it did capture the trend and did not have the "flat line" under prediction which is the focus of the experiment, as at Xuhui.

We have examined the meteorological fields such as wind speed, wind direction, surface pressure, and surface temperature at four sites (Fig. 67.3). The model over estimated peak temperatures at Jinshan, slightly over estimated at Pudong, and

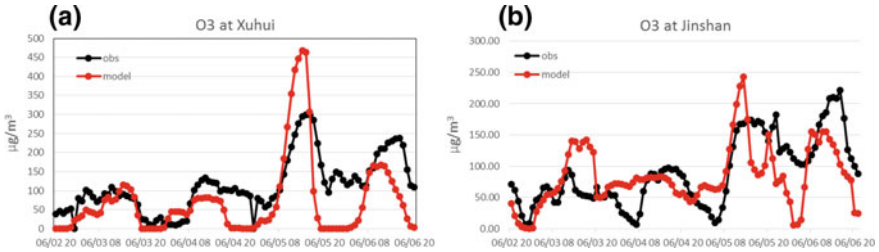

Fig. 67.2 Ozone performance at sites Xuhui (**a**) and Jinshan (**b**)

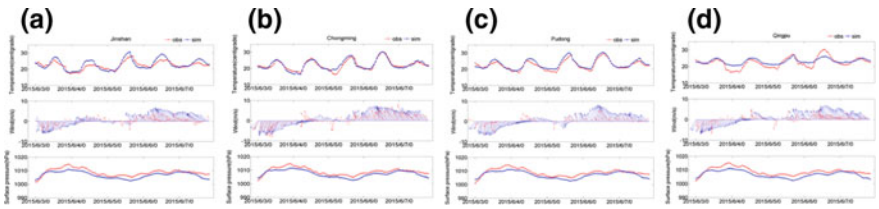

Fig. 67.3 Meteorological model performance at **a** Jinshan, **b** Chongming, **c** Pudong, and **d** Qingpu

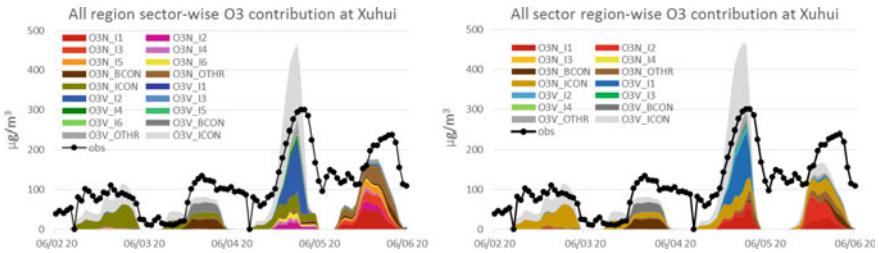

Fig. 67.4 Ozone contribution analysis at Xuhui. *Left* All regions were totaled for each of the sectors industrial(I1), energy(I2), transportation(I3), residential(I4), shipping(I5), and agriculture (I6). *Right* All sectors were totaled for each of the regions YRDOUT(I1), YRD(I2), SHOT(I3) and JSFX(I4)

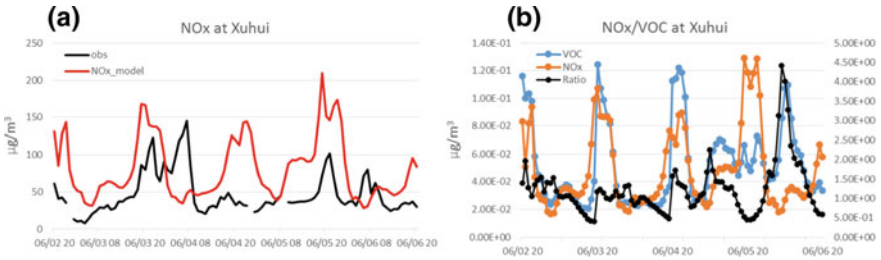

Fig. 67.5 Time series of NO_x concentration (*left*) and time series of NO_x, VOC, and their ratio (*right*) at Xuhui

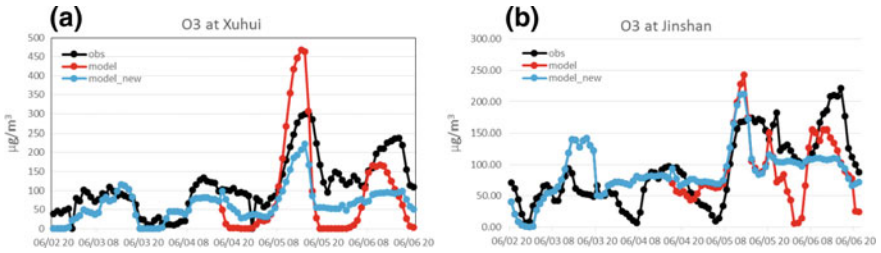

Fig. 67.6 New model results with selected NOx reduction. *Left* Xuhui (in region SHOT). *Right* Jinshan (in region JSFX)

missed high and low at Qingpu. Wind speed was over estimated at all sites most of the time. Pressure was slightly under estimated. Overall the meteorological model performed reasonable well.

Figure 67.4 shows all region sector-wise and all sector region-wise ozone contributions at Xuhui based on CMAQ-ISAM output. Simulation is dominated by the contribution from ICON (initial condition), BCON (boundary condition) and OTHR (other sources) most of the time. On 6/5 and 6/6, there were significant contributions from sectors 2, 4, and 6 and from region 1 and 2.

Figure 67.5a shows the model comparison of NO_x and clearly the model overestimated NO_x particularly at night on 6/4 and 6/5. Subsequently, the model NO_x/VOC ratio (Fig. 67.5b) renders the modeled O_3 formation regime as VOC-limited.

67.4 New Simulation

Based on all region sector-wise analyses, it showed that the impacts were from regions 1 and 2. Hence, we reran the model with NOx reduction in regions 1 and 2 and across all sectors by 50% on two separate periods: 6/4 17:00–6/5 02:00 and 6/5 17:00–23:00. Figure 67.6 shows with the proposed NOx reduction, it helps to retain

nighttime ozone level on 6/4 and 6/5 and lowered the over estimation on 6/5. At the nearby site, the change did not affect the calculation much except on 6/5 night 6/6 daytime.

67.5 Summary and Conclusion

In this exercise, we have shown the benefit of using CMAQ-ISAM as a tool to identify potential emission issues due to high uncertainty in emission processing. We have demonstrated that proposed modifications of emissions in a selective manner helps alleviate the targeted issue in the original model run, namely significantly under and over estimation of ozone at Xuhui. In turn, this will help to produce more accurate model results, in particular for the forecasting system.

Questions and Answers

Questioner: Renske Timmermans
Question: In the study the NOx emissions are reduced in the sensitivity run. Do you think the Nox emissions in the emission inventory in this region are too high, i.e. that this reduction applied is realistic for the real situation?
Answer: Based on the analysis from the contribution from regions and sectors by ISAM, it did indicate the NOx was high in Region 1 and 2. As a result of reduction of 50% of NOx, the ozone was reduced and closer to the observation level. We used this tool to determine potential errors in the emission inventory but we did not attempt to use it to provide precise amount of change in the inventory.

Questioner: Peter Viaene
Question: Why did you not include a source zone covering the sea to monitor the shipping emissions (slide 13)?
Answer: We could divide the sea into various parts if we want to track explicitly the contribution of shipping emissions impact from different part of the sea, but that will increase the computational time substantially. We ended up tracking shipping as a sector only.

Reference

Kwok RHF, Baker KR, Napelenok SL, Tonnesen GS (2015) Photochemical grid model implementation and application of VOC, NO_x, and O_3 source apportionment. Geosci Model Dev 8:99–114

Chapter 68
Modeling of Foehn-Induced Extreme Local Dust Pollution in the Dead Sea Valley

Pavel Kishcha, Boris Starobinets and Pinhas Alpert

Abstract Using high-resolution COSMO-ART model simulations, a foehn phenomenon and foehn-induced effects on extreme local dust pollution on 22 March 2013 were analyzed over the Judean Mountains (~1000 m) and over the Dead Sea valley (−420 m). The model data were supplemented with in situ meteorological measurements from a chain of stations located across the mountain ridge. Hot foehn winds created a pronounced temperature inversion over the western part of the valley. Strong foehn winds activated local dust sources, while the foehn-induced pronounced temperature inversion trapped dust particles beneath the inversion. These trapped local dust particles contributed to maximum surface dust concentration but not to dust aerosol optical depth (AOD) in the western Dead Sea valley. By contrast, in the central and eastern Dead Sea valley, in the absence of temperature inversion, the ascending airflow lifted dust particles up to 2-km altitude, contributing to the maximum local dust AOD. Thus, it was because of the temperature inversion in the western Dead Sea valley that the maximum surface dust concentration did not coincide with the maximum AOD. This lack of coincidence indicates difficulties in using satellite-based AOD for initializing dust concentration within numerical forecast systems over a region with complex mountain terrain.

68.1 Introduction

The Dead Sea valley is a unique place because of its location at ~400 m below sea level. This deep valley is flanked by relatively high mountains of ~1000 m above sea level: by the Judean Mountains to the west and by the Moab Mountains to the east. High-resolution modeling is particularly important for this area with complex terrain, unsteady winds, and frequent intrusions of Saharan dust. This study focuses on extreme local dust pollution produced by strong foehn winds in the Dead Sea

P. Kishcha (✉) · B. Starobinets · P. Alpert
Department of Geosciences, Tel-Aviv University, Tel-Aviv, Israel
e-mail: pavel@cyclone.tau.ac.il; pavelk@post.tau.ac.il

C. Mensink and G. Kallos (eds.), *Air Pollution Modeling and its Application XXV*,
Springer Proceedings in Complexity, DOI 10.1007/978-3-319-57645-9_68

valley on March 22, 2013. We simulated this foehn phenomenon, as well as its effects on dust distribution, with a comprehensive online-coupled weather forecast model COSMO-ART (Vogel et al. 2009). Reasonable agreement was found between the simulated meteorological variables and the observations (Kishcha et al. 2016a). The model also reproduced the spatiotemporal distribution of dust concentration, consistent with available measurements, in the Dead Sea valley and the surrounding areas (Kishcha et al. 2016b). Our two major findings are: first, that strong foehn winds activated local dust sources, and second, that foehn-induced pronounced temperature inversion trapped dust particles beneath the inversion. These two factors caused measured extreme dust concentrations of ~7000 μg m^{-3}, which are two orders of magnitude higher than the annual mean surface dust concentration in the Dead Sea valley (Kishcha et al. 2016a).

68.2 Method

To simulate the foehn-like phenomenon on March 22, 2013, and its effects on dust distribution over the Dead Sea valley, a comprehensive online-coupled weather forecast model COSMO-ART was used (Vogel et al. 2009; Kishcha et al. 2016b). Dust productive areas in COSMO-ART are defined by soil properties (particle size distribution, residual soil moisture and surface roughness) and environmental conditions (friction velocity, soil moisture). A data set of soil properties by Marticorena et al. (1997) and Callot et al. (2000) covering the Sahara, the Sahel, the Arabian Peninsula and the Middle East was used in the model. The emission scheme of Vogel et al. (2006) combines the formulation of White (1979) for the horizontal saltation flux of soil particles with the parameterization of Shao and Lu (2000) for the threshold friction velocity of wind erosion.

68.3 Results and Discussion

The obtained results on the foehn phenomenon and foehn-induced effects on observed extreme dust pollution in the Dead Sea valley are described in detail by Kishcha et al. (2016a, b).

The foehn phenomenon in the Dead Sea valley. On March 22, 2013, an intensive low-pressure system over the Eastern Mediterranean created favorable conditions for dust transport from the Eastern Sahara into the Eastern Mediterranean. The following shift of this cyclone eastward was accompanied by strong west winds blowing across the ridge of the Judean Mountains towards the Dead Sea valley. As shown by Kishcha et al. (2016a), both horizontal and vertical wind components significantly increased on the downwind side of the mountains, compared to the winds on the upwind side. Specifically, horizontal winds on the downwind side of

the Judean Mts. were two times stronger than horizontal winds on the upwind side. The model showed that the increase in wind speed was accompanied by air heating in the valley and by air cooling on the top of the Judean Mts.

In the Dead Sea valley, on 22 March, the air became warmer because of the adiabatic downward movement along the lee side of the Judean Mts. The temperature difference between the valley and the top of the Judean Mts. exceeded 16 °C. The significant air heating in the valley was accompanied by a considerable decrease in relative humidity from 40 to ~20%. The air-cooling on the top of the Judean Mts. was accompanied by an increase in relative humidity exceeded 90%. This suggests a possibility of some light rainfall. Available radar measurements of rainfall rate supported these model results providing observational evidence of light rainfall amounts on the upwind side of the Judean Mts. (Kishcha et al. 2016a). The adiabatic heating by the downward foehn winds in the valley caused the upward airflow there. All the above-mentioned facts are indicative of the presence of a foehn phenomenon in the Dead Sea valley. Thus, the foehn phenomenon could be significant even over the relatively low Judean Mountains of approximately 1-km height.

Foehn effects on dust. Two model experiments were conducted in order to determine separately the contribution of local dust sources to the dust distribution over the Dead Sea valley and that of remote dust sources (Fig. 68.1). In the first experiment local dust sources in the valley were excluded, while in the second experiment only local dust sources in the valley were included. Being transported by west winds from the upwind side of the Judean Mts., the remote dust was mainly responsible for the vertical dust distribution up to 7 km height over the Dead Sea valley (Fig. 68.1a). The local dust sources in the valley were mainly responsible for the extreme near-surface dust concentration and only slightly contributed to dust concentration at high altitude (Fig. 68.1b).

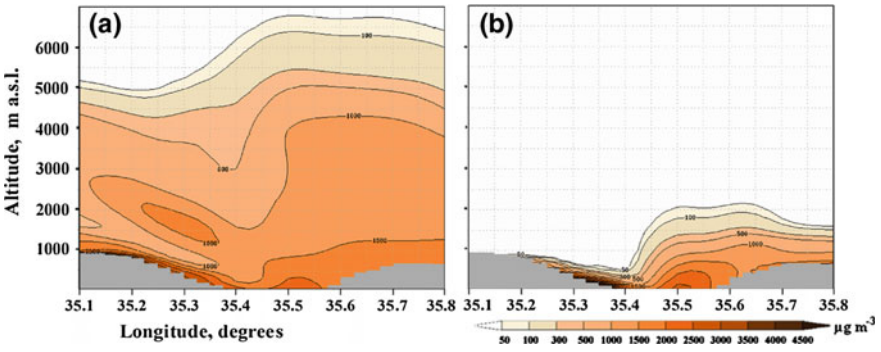

Fig. 68.1 West-east cross-sections of modeled dust concentration for two model experiments: when **a** local dust sources in the valley were excluded, and when **b** only local dust sources in the valley were included

Being associated with the foehn-like phenomenon, the strong horizontal winds on the downwind side of the Judean Mts. were capable of activating local dust sources, contributing to the strong maximum in surface dust concentration in the western the Dead Sea valley (Fig. 68.2a). The model shows that, in the western Dead Sea valley, dust was located near the surface, while, in the central and eastern Dead Sea valley, dust particles were lifted up to 2 km altitude. Such vertical distribution was determined by a foehn-induced pronounced temperature inversion in the western Dead Sea valley (Fig. 68.2b). This temperature inversion trapped dust particles beneath the inversion. This led to the extremely high near-surface dust

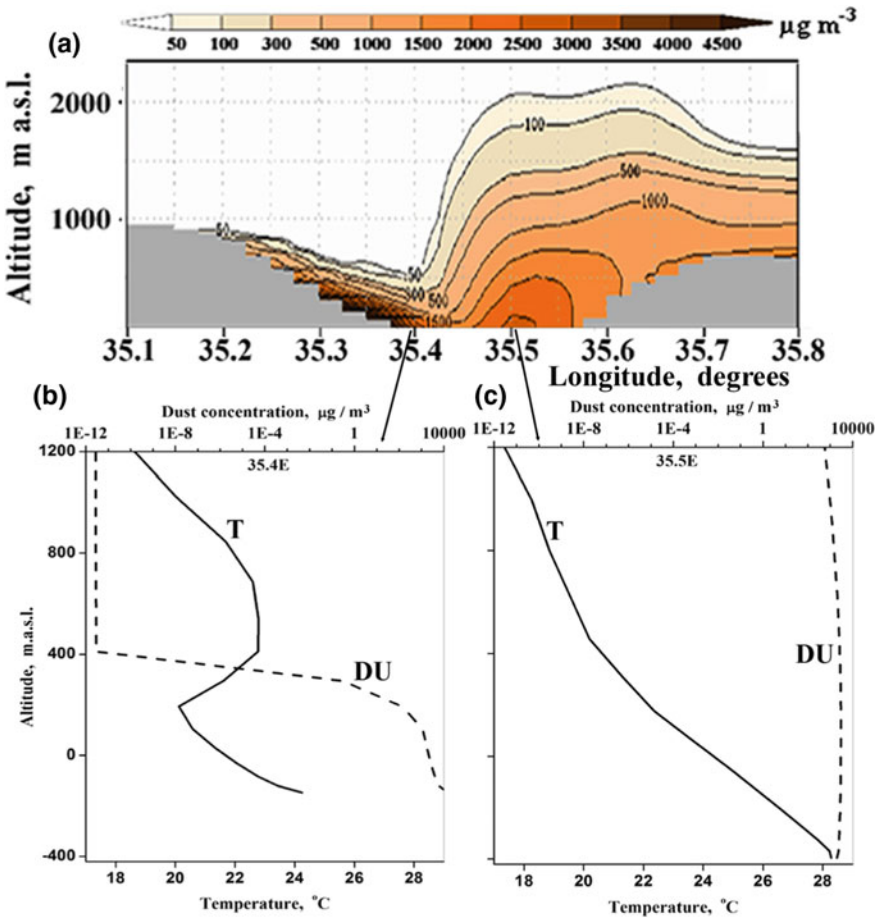

Fig. 68.2 **a** Vertical distribution of modeled dust concentration from local sources within west-east cross-section over the Dead Sea valley at 31.6°N. **b** Modeled vertical profiles of temperature (T) and dust concentration (DU) at longitude 35.4°E of maximal surface dust concentration (elevation −157 m). **c** The same as in b but for longitude 35.5°E of maximal dust AOD (elevation −405 m)

concentration in the western Dead Sea valley (Fig. 68.2b). By contrast, in the central and eastern Dead Sea valley there was no temperature inversion (Fig. 68.2c). In the absence of temperature inversion, the ascending airflow lifted local dust particles up to 2-km altitude (Fig. 68.2a), contributing to the maximum local dust aerosol optical depth (AOD). As discussed by Kishcha et al. (2016a), it was because of the temperature inversion, that maximum surface dust concentration (located in the western Dead Sea valley) did not coincide with the maximum dust AOD (located in the central Dead Sea valley). This is one of the specific effects of the foehn phenomenon on local dust pollution in the Dead Sea valley.

Acknowledgements We acknowledge support from the international Virtual Institute DESERVE (Dead Sea Research Venue), funded by the German Helmholtz Association.

References

Callot Y, Marticorena B, Bergametti G (2000) Geomorphologic approach for modelling the surface features of arid environments in a model of dust emissions: application to the Sahara desert. Geodin Acta 13(5):245–270. doi:10.1016/S0985-3111(00)01044-5

Kishcha P, Starobinets B, Alpert P, Kaplan M (2016a) Foehn-induced effects on dust pollution, frontal clouds and solar radiation in the Dead Sea valley. Meteorol Atmos Phys (submitted)

Kishcha P, Rieger D, Metzger J, Starobinets B, Bangert M, Vogel H, Schaettler U, Corsmeier U, Alpert P, Vogel B (2016b) Modeling of a strong dust event in the complex terrain of the Dead Sea valley during the passage of a gust front. Tellus B 68:29751. doi:10.3402/tellusb.v68.29751

Marticorena B, Bergametti G, Aumont B, Callot Y, N'doumé C, Legrand M (1997) Modeling the atmospheric dust cycle: 2. Simulation of Saharan dust sources. J Geophys Res Atmos 102 (D4):4387–4404. doi:10.1029/96JD02964

Shao Y, Lu H (2000) A simple expression for wind erosion threshold friction velocity. J Geophys Res Atmos 105(D17):22437–22443

Vogel B, Hoose C, Vogel H, Kottmeier C (2006) A model of dust transport applied to the Dead Sea area. Meteorologische Zeitschrift 15:611–624. doi:10.1127/0941-2948/2006/0168

Vogel B, Vogel H, Bäumer D, Bangert M, Lundgren K, Rinke R, Stanelle T (2009) The comprehensive model system COSMO-ART—radiative impact of aerosol on the state of the atmosphere on the regional scale. Atmos Chem Phys 9:8661–8680. doi:10.5194/acp-9-8661-2009

White B (1979) Soil transport by winds on Mars. J Geophys Res 84(B8):4643–4651. doi:10.1029/JB084iB09p04643

Chapter 69
Evaluation of the Impact of Air-Sea Exchange on Atmospheric Mercury Concentrations

Johannes Bieser and Corinna Schrum

Abstract Mercury is a toxic substance that is ubiquitous in the environment. In the atmosphere mercury exists mainly in the form of gaseous elemental mercury (GEM). Deposition is dominated by oxidized mercury species although they make up for only 1% of the total mercury in the atmosphere. The situation in the aquatic environment is inverse. Here, mercury exists mainly in its oxidized state Hg^{II}. Due to photolysis and biological activity mercury in the Ocean is reduced to dissolved elemental mercury (DEM). As mercury is constantly cycling between the ocean and the atmosphere it is important to include both compartments into a chemistry transport model in order to understand it's environmental fate. For this study, we coupled the atmospheric chemistry transport system CMAQ to the three dimensional Eulerian ocean-ecosystem model ECOSMO. We implemented photolysis, chemical reactions, and biologically induced transformation for elemental, oxidized, and methylated mercury species into the ocean model. Based on wind speed and temperature elemental mercury is exchanged between the ocean and the atmosphere. The model was set up for a regional domain covering the North- and Baltic Sea region and was run for a period of 14 years from 1993 to 2005. The ocean model was evaluated using DEM observations from a series of six cruises (MNB = 0.21 MNE = 0.53). Furthermore, we compared model results with and without ocean coupling to GEM observations at 5 EMEP stations. We found, that the coupled model system is able to reproduce GEM peaks which the uncoupled CTM was missing. However, the effect was limited to stations in a vicinity of 100 km to the coast (e.g. at the EMEP station DE09 in Zingst the model bias was reduced from −0.11 to 0.02 for the year 2000 and from −0.10 to −0.03 for 2005). On average, atmospheric GEM concentrations were increased by 5% in the North and Baltic Sea region.

J. Bieser (✉) · C. Schrum
Helmholtz-Zentrum Geesthacht, Institute of Coastal Research,
Max-Planck-Strasse 1, 21502 Geesthacht, Germany
e-mail: johannes.bieser@hzg.de

C. Mensink and G. Kallos (eds.), *Air Pollution Modeling and its Application XXV*,
Springer Proceedings in Complexity, DOI 10.1007/978-3-319-57645-9_69

69.1 Introduction

In order to support the implementation of the Minamata Convention on Mercury (UNEP 2013) it is important to further our understanding of the global mercury cycle. One of the major factors of uncertainty in the global mercury cycle is the exchange of Hg between ocean and atmosphere (Qureshi 2011). For this study, we coupled the atmospheric chemistry transport model (CTM) CMAQ to an ocean-ecosystem model and tested the setup for the Baltic Sea. We chose this area, as the Baltic Sea is a well confined regional Sea for which a large amount of measurement data of speciated Hg exists (Wängberg et al. 2001; Kuss and Schneider 2007). We investigate the capability of the CTM to reproduce elemental mercury concentrations in the atmosphere and the ocean as well as the air-sea flux. Finally, we quantify the range and impact of mercury evasion from the ocean on atmospheric GEM concentrations.

69.2 Model Set-Up and Domain

69.2.1 Atmospheric Model

To determine the mercury concentration in and the deposition from the atmosphere we used the chemistry transport model (CTM) CMAQ (Community Model for Air Quality). The CMAQ modelling system was developed by the U.S. EPA and is currently one of the most used CTMs worldwide. Here, we used CMAQ version 5.0.1 with the carbon bond chemistry mechanism version 5 including updated toluene chemistry and improved chlorine reactions: cb05tump, and the multi pollutant aerosol module aero6. The mercury chemistry in CMAQ is based on the implementation of Bullock and Brehme (2002) but was updated based on observations and model inter-comparisons in the course of the EU FP7 project GMOS (Global Mercury Observation System) (Bieser et al. 2014a). The outer model domain covers Europe and has a resolution of 72 × 72 km and 30 vertical layers and uses GLEMOS data for Hg boundary conditions (Travnikov and Ilyin 2009). Therein, we nested a 24 × 24 km domain over the Baltic Sea. Emissions were processed with the SMOKE-EU model (Bieser et al. 2011a, b). The model was run for the years 2000 and 2005.

69.2.2 Ocean Model

Calculations of mercury cycling in the ocean are based on the ocean-ecosystem model ECOSMO (Daewel and Schrum 2013). ECOSMO is a regional 3-d Eulerian model that considers hydrodynamics, sea ice and bio-geochemical cycling

including phyto- and zooplankton production. The ocean hydrodynamics are simulated considering time dependent surface elevation and sea ice dynamics. The hydrodynamic model is a non-linear hydrostatic z-level model, which is using semi-implicit, energy and entropy conserving numerical methods. Scalar properties are advected using a shape-preserving total variation diminishing numerical scheme. The hydrodynamic model is in detail described in Schrum and Backhaus (1999) and recent numerical updates were described by Barthel et al. (2012). The ocean bio-geochemical cycling and plankton production is resolved through simulation of 3 limiting macro-nutrient cycles, the nitrogen-, the silicon and the phosphorus cycle and oxygen. The model resolves three plankton groups, diatoms, flagellates and cyanobacteria, and two zooplankton groups. The organic matter cycling is furthermore resolved by dissolved and particulate matter groups and a simple organic surface sediment pool. A detailed model description of the bio-geochemical cycling is given by Daewel and Schrum (2013). In this model we implemented a simplified Hg chemistry scheme which includes dissolved elemental mercury, dissolved oxidized mercury, particulate oxidized mercury, dissolved methyl-mercury, and particulate methyl-mercury. This model was coupled to CMAQ with an air-sea exchange method based on the parametrizations of Nightingale et al. (2000) and Kuss (2014). A detailed description of the model and the input datasets can be found in Bieser and Schrum (2016).

69.3 Model Evaluation

Here, we focus on the models capability to reproduce dissolved elemental mercury (Hg^0) concentrations in the surface ocean, as this CMAQ setup has already been extensively evaluated for Hg concentration and deposition (Bieser et al. 2014a, b; Gencarelli et al. 2016). Typically Hg^0 makes up less than 10% of the total Hg in the surface ocean. We found, that 93% of Hg^0 concentrations were within a factor of 2 of the observations (Table 69.1). Generally, the model tends to underestimate Hg^0. This could be due to the fact, that the analysis was based on daily average concentrations, as Hg^0 concentrations are typically lower during night time.

Table 69.1 Comparison of modelled ocean surface DEM concentrations with observations from six cruises in the Baltic Sea for different seasons (Wängberg et al. 2001; Kuss and Schneider 2007)

Time of sampling	NMB	MNB	MNE	N
February and March	−0.25	−0.26	0.28	81
April	−0.41	−0.41	0.41	81
July	−0.32	−0.29	0.31	95
November	−0.06	−0.03	0.30	156
Annual	−0.27	−0.23	0.32	413

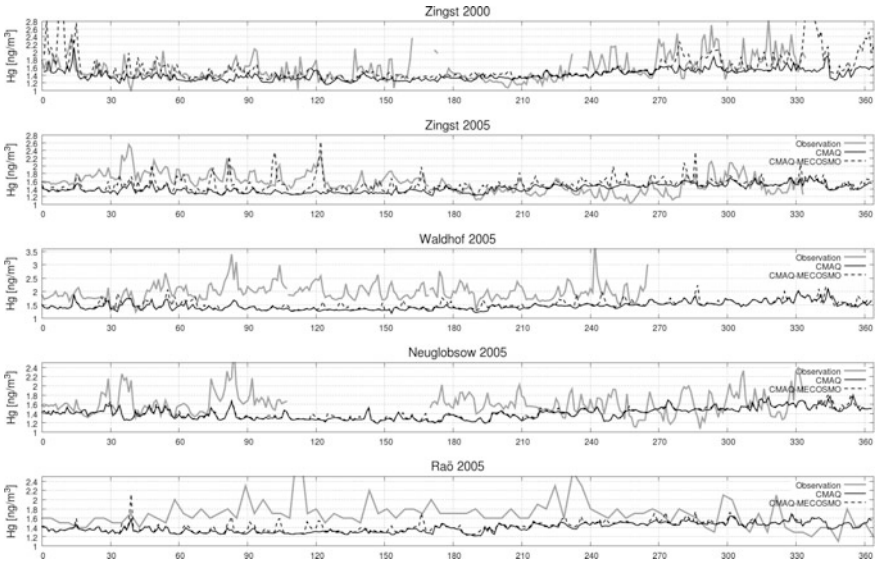

Fig. 69.1 Comparison of observed and modelled atmospheric GEM concentrations at stations around the Baltic Sea. Raö is a upwind coastal station, Zingst is a downwind coastal station, Waldhof and Neuglobsow are located 200 and 300 km south of the Batlic Sea. The black lines depict model results for atmosphere only (*full line*) and ocean coupled (*dashed line*) runs

69.4 Impact of Air-Sea Exchange on Atmospheric GEM Concentration

We found, that the air-sea exchange of Hg from the Baltic Sea has a strong impact on local downwind concentrations. At Zingst, which is located directly at the German coast, GEM concentrations were increased by 5–10% on annual average. Moreover, the coupled model setup was much better in reproducing strong GEM peaks (Fig. 69.1). At stations north and south of the Baltic Sea the impact of Hg evasion was negligible. On a regional scale the impact of the air-sea exchange was much smaller and dependent on the regional transport patterns. At the measurement station Waldhof which is located about 200 km to the south of the Baltic Sea GEM concentrations were only increased by 2–3% on annual average. However, for individual days GEM concentrations could be increased by up to 0.5 ng/m^3.

69.5 Conclusion

We coupled the atmospheric CTM CMAQ to a three dimensional Eulerian ocean-ecosystem model including mercury chemistry. The setup was tested for a regional domain over the Baltic Sea in northern Europe. The ocean model was able

to reproduce dissolved elemental mercury concentrations within a factor of 2 of observations. The air-sea exchange had a strong local and a smaller regional effect on GEM concentrations downwind of the Baltic Sea. With ocean coupling the model was able to better reproduce GEM peaks and the model was generally in better agreement with observations.

Questions and Answers

Questioner Name: R.G. Derwnet
Question: I wonder what form of chemical mechanism was used to describe oxidation of Hg^0 in the gas phase?
Answer: For this setup we used the standard CMAQ multi-pollutant mechanism (cb05tump_ae6_aq) which uses O_3, OH, and H_2O_2 as gas phase oxidants. However, I would like to point out that we performed a sensitivity study on different oxidants including Br and BrO reactions (Bieser, J. et al., Diagnostic Evaluation of Bromine Reactions on Mercury Chemistry, In: Air Pollution Modelling and its Application XXIV, Editors: Douw G. Steyn, Nadine Chaumerliac).

Moreover, there is an upcoming ACP special issue from the GMOS (Global Mercury Observation System) EU FP7 project which includes various papers with model inter-comparison studies including also the impact of different gas phase oxidants. In particular:

Travnikov, O., et al., Multi-model study of mercury dispersion in the atmosphere: atmospheric processes and model evaluation. Atmos. Chem. Phys., 17, 5271–5295, 2017

Bieser, J., et al., Multi-model study of mercury dispersion in the atmosphere: vertical and interhemispheric distribution of mercury species. Atmos. Chem. Phys., 17, 6925–6955, 2017.

Questioner Name: Jeff Weil
Question: Your ocean modeling of mercury concentrations in surface waters showed significant underestimation compared to the ship cruises. Did you account for Langmuir circulations, which are a very efficient mixing mechanism in the ocean boundary layer? This mechanism is now included in state-of-the-art ocean models.
Answer: Dissolved Hg^0 makes up only 1–10% of the total mercury in the surface ocean. It's concentration is highly dependent on the equilibrium of oxidation and reduction processes as well as the air-sea exchange. We are currently working on a more detailed representation of the Hg chemistry in the ocean and will investigate it's impact on the Hg^0 concentration. In fact, the current model performance for Hg^0 is close to the measurement uncertainty and we do not think that physical parameters are the major drivers for the model bias for individual mercury species (Together with the emissions the physical parameters do play a role for the total mercury concentrations).

That said, Langmuir circulations are not included in the ECOSMO model. Langmuir circulations occur on scales of a few meters and are thus not explicitly modelled in our setup, which has a horizontal resolution of 10×10 km^2. The model does account for wind induced vertical turbulence. Please refer to Schrum and Backhaus (1999) and Barthel et al. (2012) for more details on the ocean model.

References

Barthel K, Daewel U, Pushpadas D, Schrum C, Arthun M et al (2012) Resolving frontal structures: on the computational costs and pay-off using a less diffusive but computational more expensive advection scheme. Ocean Dyn. doi:10.1007/s10236-012-0578-9

Bieser J, Aulinger A, Matthias V, Quante M, Builtjes P (2011a) SMOKE for Europe—adaptation, modification and evaluation of a comprehensive emission model for Europe. Geosci Model Dev 4:47–68. doi:10.5194/gmd-4-47-2011

Bieser J, Aulinger A, Matthias V, Quante M, Denier van der Gon HAC (2011b) Vertical emission profiles for Europe based on plume rise calculations. Environ Pollut 159:2935–2946. doi:10.1016/j.envpol.2011.04.030

Bieser J, Matthias V, Travnikov O, Hedgecock MI, Gencarelli CN, De Simone F, Weigelt A, Zhu J (2014a) A diagnostic evaluation of modeled mercury wet deposition in Europe using atmospheric speciated high-resolution observations. Environ Sci Pollut Res 21(16)

Bieser J, Matthias V, Travnikov O, Hedgecock MI, Gencarelli CN, De Simone F, Weigelt A, Zhu J (2014b) Impact of mercury chemistry on regional concentration and deposition patterns. In: Gyring S-E, Batchvarova E (eds) Air pollution modeling and its application XXIII, pp 189–195

Bieser J, Schrum C (2016) Impact of marine mercury cycling on coastal atmospheric mercury concentrations in the North- and Baltic Sea region, ELEMENTA 111. doi:10.12952/journal.elementa.000111

Bullock OR, Brehme KA (2002) Atmospheric mercury simulations using the CMAQ model: formulation description and analysis of wet deposition results. Atmos Environ 36:2135–2146

Daewel U, Schrum C (2013) Simulating long-term dynamics of the coupled North Sea and Baltic Sea ecosystem with ECOSMO II. Model description and validation. J Mar Sys 119–120:30–49

Gencarelli CN, Bieser J, Carbone F, DeSimone F, Hedgecock IM, Matthias V, Travnikov O, Yang X, Pirrone N (2016) Sensitivity study of regional mercury dispersion in the atmosphere

Kuss J, Schneider B (2007) Variability of the gaseous elemental mercury Sea-Air flux of the Baltic Sea. Environ Sci Technol 41:8018–8023

Kuss J (2014) Water-air gas exchange of elemental mercury: an experimentally determined mercury diffusion coefficient for Hg0 water-air flux calculations. Limnol Oceanogr 59 (5):1461–146

Nightingale PD, Malin G, Law CS, Watson AJ, Liss P et al (2000) In-situ evaluation of air-sea gas exchange parameterizations using novel conservative and volatile tracers. Glob Biogl Cyc 14:373–387

Qureshi A (2011) Quantifying and reducing uncertainties in global mercury cycling. Dissertation ETH No. 19709. Zürich, Switzerland

Schrum C, Backhaus JO (1999) Sensitivity of atmosphere-ocean heat exchange and heat content in the North Sea and the Baltic Sea. Tellus A 51(4):526–549. doi:10.1034/j.1600-0870.1992.00006.x

Travnikov O, Ilyin I (2009) The EMEP/MSC-E mercury modeling system. In: Pirrone N, Mason RP (eds) Mercury fate and transport in the global atmosphere. Springer, Dordecht, pp 571–587

UNEP (United Nations Environmental Program) (2013) Minamata Convention on Mercury

Wängberg I, Schmolke S, Schager P, Munthe J, Ebinghaus R et al (2001) Estimates of air-sea exchange of mercury in the Baltic Sea. Atmos Environ 35(2001):5477–5484

Chapter 70
Regional Refined Grid Modeling of Acidic and Mercury Deposition over Northeastern US and the Contribution of New York Power Point Sources

Leon Sedefian, Michael Ku, Kevin Civerolo, Winston Hao and Eric Zalewsky

Abstract The purpose of the study was to refine the grid resolution from previous regional level assessments by reducing the latest "standard" 12 km down to a 4 km grid level in a novel application of the CMAQ modeling system on an annual timescale. The application was to determine the overall acidic and mercury deposition over New York State (NYS) and the contribution of the NY power sector point sources. To that end, the latest available EPA NEI for 2011 and WRF simulated meteorological data were generated on the 4 km grid domain over the Northeastern US centered on NYS. For mercury, emissions of the elemental, oxidized and particulate species were characterized using stack test and technology based data to allow for the proper assessment of the relative contribution from EGUs and WTE facilities using species dependent wet removal factors and dry deposition velocities. The results for mercury deposition indicate very low contributions from total NYS sources, but shows the importance of both wet and dry components. The impacts of emissions outside the modeling domain were found to clearly dominate total depositions in NYS. For acidic deposition, the importance of wet deposition for sulfate is found, while for total sulfur and nitrates, dry deposition has a significant contribution. For NYS power sector, the significant contribution of dry deposition of SO_2 is highlighted. The projected total wet depositions of sulfate, nitrate and mercury compare very favorably with observed levels at NADP sites.

L. Sedefian (✉)
SEDEFIAN Consulting, Malta, NY, USA
e-mail: lxsarkis@hotmail.com

M. Ku · K. Civerolo · W. Hao · E. Zalewsky
New York State Department of Environmental Conservation, Albany, NY, USA

C. Mensink and G. Kallos (eds.), *Air Pollution Modeling and its Application XXV*,
Springer Proceedings in Complexity, DOI 10.1007/978-3-319-57645-9_70

70.1 Introduction

As recent United States Environmental Protection Agency (USEPA) and New York State (NYS) policy and regulatory approaches have emphasized the importance of the interaction of multi-pollutants, the need has shifted to more comprehensive techniques to ascertain their impacts. Requirements to reduce toxics such as mercury from power plants and the importance of sulfate and nitrate transport in the eastern United States have taken center stage at the USEPA. Recent rules have relied heavily on regional-scale photochemical model applications and affect emissions from energy production sources such as Energy Generation Units (EGUs) and waste to energy (WTE) facilities. However, technical assessments for these requirements have not been commensurate with the latest emissions data and the techniques necessary to properly assess their implementation. That is, these assessments have relied upon outdated simulations using past emission inventories and coarse meteorological fields.

Most germane to the current study was the recognition that past modeling studies have not fully quantified current and future contributions of New York's power generation sector to the regional acidic and mercury depositions. In addition, there has been a shift in the fuel use in the EGU sector in and around NYS from coal to natural gas and the implications of this shift need to be fully understood. These issues were addressed in this study by a regional modeling assessment which has evolved considerably over the decades and the latest techniques in EPA's Community Multiscale Air Quality (CMAQ) modeling system was used to determine deposition over NYS and the contribution from NYS power sources.

Previously and noteworthy for NYS was the first in the US regulatory action on acid rain in a 1985 regulation which used a crude scale modeling analysis to determine area wide emissions contributions to impacts on NY receptors. For mercury, EPA performed regional scale modeling for all of the US in the 1997 EPA Mercury Report to Congress using RELMAP, while for NYS, the Northeast states commissioned a modeling exercise about the same time using REMSAD, with the specific goal of apportioning the contribution by source regions and major source categories.

70.2 Modeling Approach

The CMAQ modeling system (CMAS webpage, 2016) was chosen to properly account for source group attributions from inside and outside the modelling domain. It contains meteorological simulations of atmospheric parameters and wind flow conditions, an emission module for projecting man-made and natural emissions, and a chemistry module for the fate of pollutants. As expected, the smaller areas of the 4 km grid cells produced more detailed features compared to a 12 km grid for terrain and precipitation fields. Based on initial Weather Research Forecast

(WRF) simulations results, the essential importance of proper precipitation modeling in the cloud subgrid scheme was resolved by invoking the convective module for both the 12 and 4 km cases.

Through its aerosol module, CMAQ calculates condensation and evaporation of volatile inorganic gases through thermodynamic equilibrium between the gas phase and fine particle modes using the latest methods in ISORROPIA II (Fountoukis and Nenes 2007). The Sparse Matrix Operator Kernel Emissions (SMOKE) emissions processor was used to assimilate the large set of data from the 2011 National Emissions Inventory (NEI) for input to CMAQ. As part of the SMOKE processing, the set of major point sources of importance to the study were reviewed in detail resulting in about 25% adjustment to the data.

The basic deposition methods used in CMAQ rely on essentially the relationships between concentrations and the resultant deposition due to dry and wet processes and the parameters which control these processes (e.g. Wesley et al. 2002). For the dry approach, the hourly dry deposition velocity is simulated using an inverse relationship between the velocity and the various resistances to deposition. For gases, this includes aerodynamic resistance by similarity theory, surface resistance in the quasilaminar sublayer, and the resistance of the surface itself to uptake. For particles, an analogous formulation is used incorporating gravitational settling velocity. The deposition of gases and particles due to wet processes is essentially a function of the precipitation in the column through which it encounters the pollutant concentrations. It is determined using a washout ratio which represents the concentration of a specific pollutant in precipitation to air.

70.3 Results and Conclusion

Here we present samples of the overall results. CMAQ predictions of annual total (wet plus dry) sulfate (SO4) and total mercury (Hg) deposition over the domain due to the 2011 NEI (i.e. the base case) are presented in Fig. 70.1a. The SO4 results (in kg/ha) are found to be controlled by the wet component and are maximize in western Pennsylvania (PA) as a result of upwind emissions transport. The spatial variation in NY is also attributed mainly to influx of wet deposition at smaller, yet significant levels. For total Hg (in ug/m^2), which includes the elemental and oxidized forms, the same pattern is seen and is found to be controlled by the oxidized form and by both wet and dry deposition. The highest impacts are likely due to upwind coal plants, which have dominant emission. Initial modeling results had indicated the clear dominance of out of the domain sources for Hg deposition which was addressed by including these sources as boundary conditions. The relatively high impacts in the NY City area was the result of higher emissions found in the inventory due to area sources including metal processing and crematories.

An important purpose of the study was to determine the contribution from NYS power sector to the overall levels of acidic and mercury deposition. In addition to the power sector, other sources such as cement plants were also found to have large

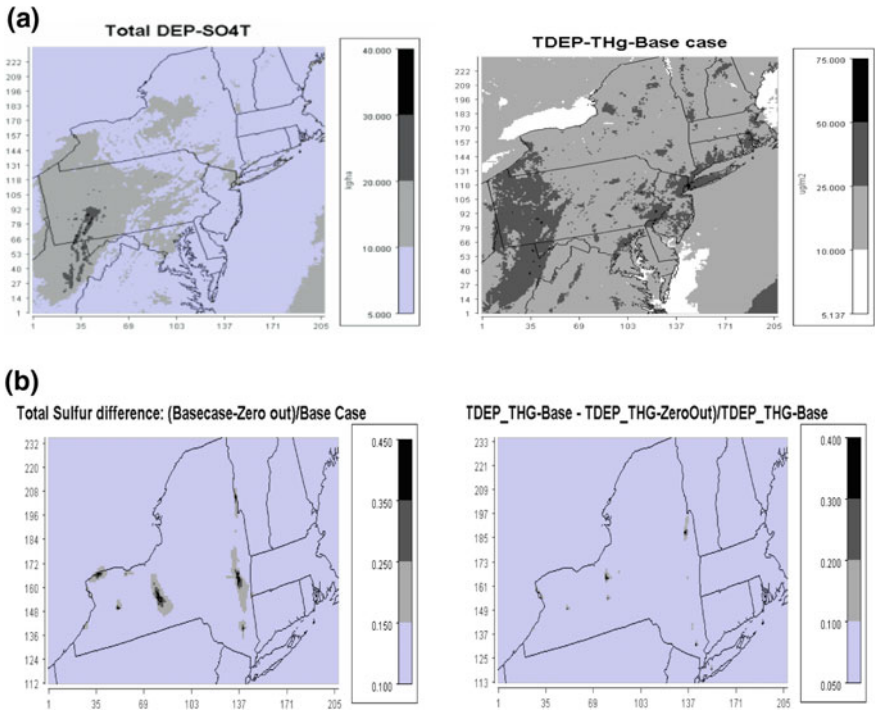

Fig. 70.1 Deposition of **a** total sulfuate (*left*) and total mercury (*right*) due to the 2011 NEI (base case) and **b** the contribution of NY power sector relative to the total sulfur (*left*) and total Hg (*right*) depositions

Hg emissions. The NYS large Hg point source impacts were determined by an additional CMAQ run where these major sources were "zeroed out" of the inventory. The difference between the base case minus the "zero out", divided by the base case represents the percent contribution of the NYS large sources including the power sector. The result for total sulfur (TS), calculated by adding 1.5 times sulfur dioxide (SO_2) to sulfate, is on the left and for total Hg is on the right in Fig. 70.1b. The incorporation of SO_2 has the effect of increasing the effect of dry deposition which is responsible for the relatively large and broad localized effects (up to one third reductions) around the NYS sources "removed" in the "zero out" case. On the other hand, these NY sources contribute little to the overall mercury impacts, with very limited areas of impacts above 10%.

Seasonal CMAQ predictions of wet deposition of sulfate and WRF simulations of precipitation are compared to available observations at monitors throughout the modeling domain from the National Atmospheric Deposition Program's (NADP) 47 sites in Fig. 70.2. The CMAQ to observed comparisons for nitrate and Hg are strikingly similar to the SO4 deposition results. These comparisons indicate a general underestimation by CMAQ for all acidic deposition and Hg species on an

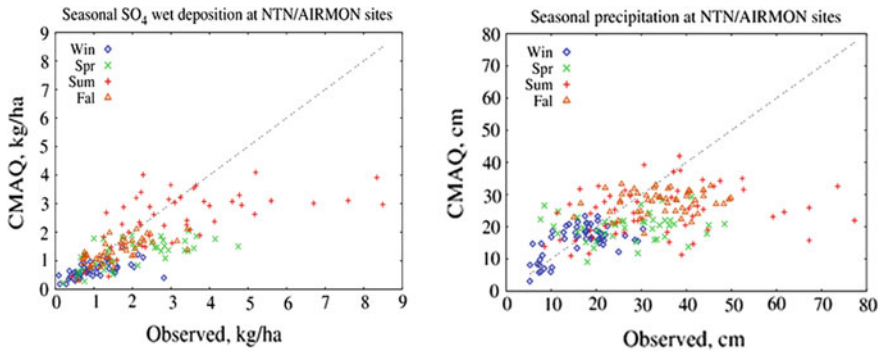

Fig. 70.2 Seasonal sulfate and precipitation comparisons of CMAQ to NADP observations

annual level which appears to be driven by the clear underestimation during the summer and, secondarily, by the spring results. Comparisons during the fall and winter seasons appear to be much better. Calculated normalized mean error (NME) and bias (NMB) indicate that on an annual basis, CMAQ simulations are all within 30% of observations, with the lowest NME and NMB for mercury (15.8 and −6.5%) which is somewhat surprising given the uncertainty in the Hg emissions inventory. From the standpoint of the modeling community, these results are remarkably good.

Acknowledgements This research was funded by a NYSERDA and supported by staff work from NYSDEC who do not necessarily endorse the study findings or conclusions.

Question and Answer

Questioner: Johannes Bieser
Question: Not a question, but wanted to point out two recent studies on mercury speciation by Mark Cohen in ELEMENTA (2016) and by A. Wedjeclt in ACP (2016).
Answer: Thanks. No answer is needed.

References

CMAS Webpage (2016) https://www.cmascenter.org/cmaq/- Accessed 9 Feb
Fountoukis C, Nenes A (2007) ISORROPIA II: a computationally efficient thermodynamic equilibrium model for K + , Cl–H2O aerosols. Atmos Chem Phys 7:4639–4659
Wesley ML, Doskey PV, Shannon JD (2002) Deposition parameterization for the industrial source complex model. http://www3.epa.gov/ttn/scram/dispersion_prefrec.htm#aermod

Chapter 71
Regional Chemical Transport Modelling with a Forest Canopy Parameterization

P.A. Makar, R.M. Staebler, A. Akingunola, J. Zhang, C. McLinden, S.K. Kharol, B. Pabla, P. Cheung and Q. Zheng

Abstract The incorporation of forest shading processes into a regional chemical transport model (Makar et al., Nat Commun 2017) greatly reduced the predicted July O_3 mean biases and root mean square errors, as well as reducing the magnitude of predicted $PM_{2.5}$ mean bias. However, the parameterization resulted in a degradation of NO_2 performance. A sensitivity study of the regional model's canopy parameterization reduced this NO_2 degradation, but suggests that the parameterization has a strong scale dependence. Grid squares with relatively low population densities influence North American ozone biases by a factor of two. Simulations at higher resolution may be required in order to simultaneously improve O_3, $PM_{2.5}$ and NO_2.

71.1 Tropospheric O_3 Models in North America: Similar Biases

Past simulations of North American surface O_3 (Solazzo et al. 2012; Chai et al. 2013; Im et al. 2015; Solazzo and Galmarini 2016) have displayed a consistent positive bias with respect to observations. These higher-than-observed predictions of average ozone maximize in specific regions: the eastern half of the USA, and the coastlines of California and the Portland through Vancouver, Canada, corridor. Previous work (Makar et al. 2017) suggested that a large portion of this bias stems from two key processes, absent in regional chemical transport models: shading by foliage (with a reduction in photolysis rates near the surface), and reductions in turbulence within the forest canopy. These two processes were shown to account for 59 to 79% of forecast ozone biases in North America (Makar et al. 2017).

P.A. Makar (✉) · R.M. Staebler · A. Akingunola · J. Zhang · C. McLinden · S.K.Kharol · B. Pabla · P. Cheung · Q. Zheng
Air Quality Research Division, Environment and Climate Change Canada, 4905 Dufferin Street, Toronto, ON M3H 5T4, Canada
e-mail: paul.makar@canada.ca

C. Mensink and G. Kallos (eds.), *Air Pollution Modeling and its Application XXV*, Springer Proceedings in Complexity, DOI 10.1007/978-3-319-57645-9_71

Here we carry out a sensitivity analysis of the forest canopy parameterization in order to attempt to improve model performance for O_3, NO_2 and $PM_{2.5}$, by focussing on the issue of sub-grid-scale variability of forest cover. The relatively low resolution of a chemical transport model, typically on the order of 1–10 km, necessitates the use of average land use categories within a grid square. Our previous work (Makar et al. 2017) uses these average values to determine whether or not to employ a forest canopy parameterization for turbulence and photolysis reduction within a given grid-square. However, anthropogenic emissions may take place on smaller scale, e.g. in small towns or along highways which take up a small fraction of a largely forested grid square, yet are un-forested at this sub-grid-scale level. We examine the potential impacts of these sub-grid-scale effects through varying the conditions under which our forest canopy parameterization is employed.

71.2 A Forest Canopy Parameterization for Regional Chemical Transport Models

Our forest canopy parameterization with Environment and Climate Change Canada's Global Environmental Multiscale—Modelling Air-quality and Chemistry (GEM-MACH) model, version 2, accounts for the attenuation of light as a function of leaf-area index, clumping index, and solar zenith angle and the reduction in vertical diffusivity expected from observations throughout multiple forest. The GEM-MACH model was split in a gather-scatter approach into "canopy" and "no-canopy" columns; the former making use of 3 additional levels to resolve light and vertical transport within the forest canopy. Further details of the parameterization may be found in Makar et al. (2017), and will be described in the oral presentation.

The previous criteria for the use of the canopy parameterization were: leaf area index >1, forest canopy height >18 m, over ½ of grid cell area must be forested, the probability of the direct downward beam of light reaching the surface must be <45%, and the human population per 10 km grid-cell must be <50,000. Here, we reduce the last criteria to 10,000 people per 10 km grid-cell. In addition, for grid-cells containing human populations between 10,000 and 3000, we assume the coefficients of vertical diffusivity are not affected by the forest canopy. These modifications attempt to characterize the extent to which chemical concentrations within towns and villages within a forested grid-cell may be influenced by sub-grid-scale variability (by turning off the parameterization for lower population densities than previous simulations, and assuming a greater degree of vertical mixing for the smallest towns).

As in our previous work, we simulate July of 2010, using the operational GEM-MACH forecast grid with 10 km resolution over North America. Our analysis makes use of hourly O_3, $PM_{2.5}$ and NO_2 observations (the last of which were

available only for Canada for the simulated time period). Table 71.1 shows the resulting mean biases, correlation coefficients, and root mean square errors for O_3 and $PM_{2.5}$ for North America, for NO_2 for Canada, and for O_3 and $PM_{2.5}$ for the four North American sub-regions of Solazzo et al. (2012). Comparisons are for the original base case and forest canopy parameterization (Makar et al. 2017), and the sensitivity study outlined above.

Table 71.1 shows that the canopy parameterization considerably improves the ozone bias (reduction by a factor of 3), as well as the $PM_{2.5}$ bias (compare columns BC vs C), but this is at the expense of increased bias and reduced RMSE performance for NO_2. The greatest improvement in O_3 and $PM_{2.5}$ bias by sub-region is usually for the original canopy parameterization, while the simulation with the best correlation coefficient and RMSE vary between sub-regions.

Figure 71.1 shows the spatial distribution of the concentration changes for July average O_3, NO_2 and $PM_{2.5}$, between the scenario carried out here versus the base case ("BC-CS"; left column of images), and versus the previous work ("CS-C"; right column of images). The canopy parameterization scenario reduces O_3 (upper left panel) with the greatest reduction in the region of greatest positive model bias (south-eastern USA), as in Makar et al. (2017), while the new scenario increases the ozone concentrations relative to that previous work (upper right panel).

Table 71.1 Evaluation metrics

	North America						Canada		
	O_3			$PM_{2.5}$			NO_2		
	BC	C	CS	BC	C	CS	BC	C	CS
MB	6.30	1.78	3.66	-3.79	-3.02	-3.32	0.92	1.81	1.38
R	0.73	0.72	0.72	0.39	0.40	0.41	0.55	0.52	0.54
RMSE	15.8	14.8	15.0	9.07	9.09	9.01	6.76	7.34	7.01

O_3 by sub-region												
	NA1			NA2			NA3			NA4		
	BC	C	CS	BC	C	CS	BC	C	CS	BC	C	CS
MB	0.95	-.99	-.36	8.08	3.42	5.19	5.18	-0.13	2.27	11.44	4.29	7.33
R	0.76	0.74	0.75	0.68	0.64	0.66	0.74	0.74	0.74	0.75	0.73	0.74
RMSE	13.6	14.4	14.0	15.7	14.7	14.9	15.4	14.24	14.5	18.5	15.5	16.6
$PM_{2.5}$ by sub-region												
	NA1			NA2			NA3			NA4		
	BC	C	CS	BC	C	CS	BC	C	CS	BC	C	CS
MB	-2.9	-2.0	-2.2	-3.7	-3.2	-3.4	-5.4	-4.6	-4.9	-3.6	-2.7	-3.2
R	0.31	0.35	0.36	0.26	0.24	0.24	0.46	0.47	0.48	0.21	0.22	0.23
RMSE	7.83	7.96	7.90	8.29	8.38	8.34	10.1	9.76	9.79	9.87	10.2	9.84

BC = Base case, C = Original canopy parameterization, CS = Canopy sensitivity scenario. Regions NA1, NA2, NA3, NA4 are shown in Fig. 71.1. The best score in each set of three scores is *shaded light grey*

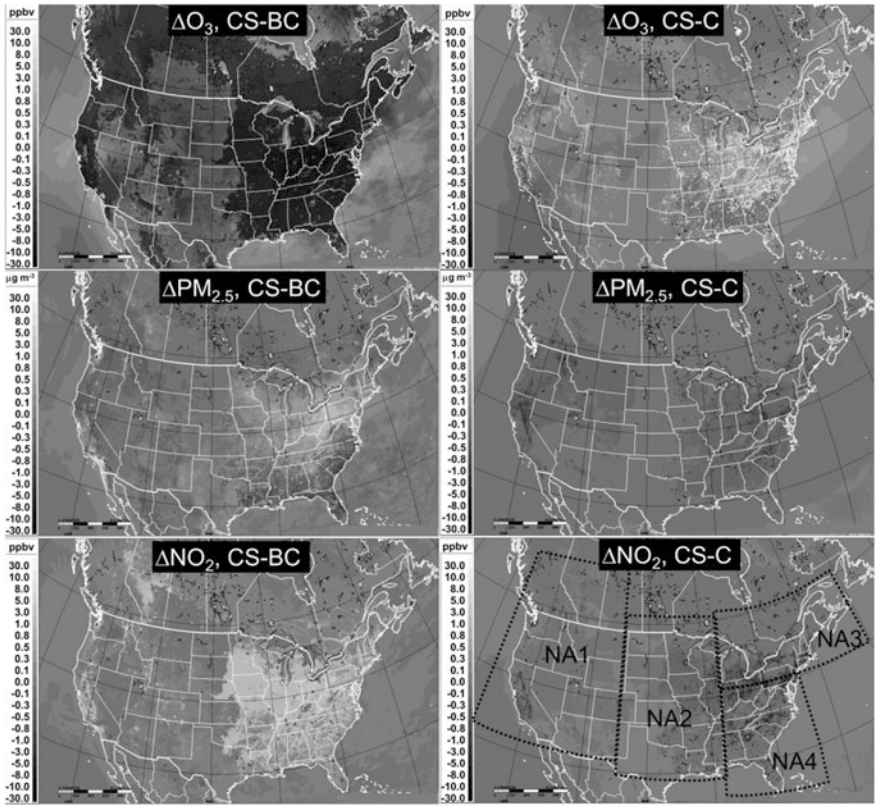

Fig. 71.1 Differences in model-predicted July 2010 average concentrations of O_3 (ppbv), $PM_{2.5}$ (μgm^{-3}), and NO_2 (ppbv), between the scenario carried out here and the base case (*left column*) and the scenario and the previous canopy simulation (Makar et al. 2017; *right column*). *Lower right panel* shows the locations of sub-regions NA1, NA2, NA3, NA4 used in the statistical analysis

$PM_{2.5}$ increases as a result of the canopy parameterization (middle left panel), though not as much as in the previous work (middle right panel). NO_2 increases (lower left panel), while not as much as in the previous work (lower right panel).

The sensitivity test carried out here shows that the impact of sub-grid-scale variability on canopy model performance is high (compare columns C and CS of Table 71.1). Treating grid squares containing small towns as "non-canopy" grid squares, and smaller villages as having vertical mixing unmodified by the canopy, reduces the overall improvements in O_3 and $PM_{2.5}$, while decreasing the magnitude of the degradation of the NO_2 performance. The "CS" strategy adopted here may thus be preferred in an operational context, if the impact of the canopy parameterization on NO_2 biases outweighs the improvements in O_3 bias and RMSE with the original strategy.

The work also highlights the importance of relatively small inhabitations towards model performance, and of sub-grid-scale emissions and transport. The choice of canopy and diffusivity treatment for grid squares with population densities between 500 and 30 inhabitants km^{-2} (small towns or villages within a large grid square) changed the North American O_3 bias by a factor of 2 (3.66 vs. 1.78 ppbv). Similar sub-grid-scale parameterizations to those carried out here, and/or simulations at higher resolution, may therefore be required to further improve model performance.

Questions and Answers

Questioner: Heinke Schlüzen
Question: Did you apply the canopy parameterization for meteorology fields (wind and temperature values within a forest as well)?
Answer: No—the intent was to construct an "add-on" parameterization which could be used for both on and off-line models, with a focus solely on turbulent transport. The parameterization could be used within the weather forecast portion of an on-line model, but that has not been attempted here.

Questioner: Hosein Foroutan
Question: What caused the increase in ozone over the ocean (especially Pacific) when you applied your parameterization?
Answer: Advection (plus chemistry). The reduction in light levels and reduced vertical transport within the forested canopy in coastal regions results in the build-up of ozone precursors there compared to the no-canopy base case. When the winds are blowing from land to ocean, this results in these precursors to ozone formation, which are higher in the canopy model than the base case, being blown offshore. This in turn results in slightly higher off-shore ozone levels in some areas such as the west coast, the Gulf of Mexico near New Orleans, and the shoreline areas of Hudson Bay. Similar effects associated with transport were also observed in some interior areas; for example, just in-land of northern Los Angeles, ozone levels increased for the canopy simulation, in non-forested regions just downwind of forests. Again, this was due to precursors not reacting due to lower light levels and reduced turbulence being transported downwind by the larger scale transport winds.

Questioner: Peter Viaene
Question: I saw that the biogenic emissions are in your model. One of the reasons the vegetation emits biogenics is to protect itself from high O_3 concentrations. Are your biogenic emissions modulated with O_3 concentrations?
Answer: The model emissions of biogenic hydrocarbons are dependent on temperature, and, in the case of isoprene, the levels of photosynthetically active radiation reaching the foliage—as has been shown in many measurement studies. In that sense, the emission rate of biogenic hydrocarbons in this model and others are

completely independent of the concentration of O_3. Both model biogenic hydrocarbon emission rates and ozone formation reactions are temperature dependent and hence may correlate, but are not necessarily causally linked.

References

Chai T et al (2013) Geosci. Model Dev 6:1831–1850
Im U et al (2015) Atmos Environ 115:404–420
Makar PA et al (2017) Nat Commun 8. doi:10.1038/ncomms15243
Solazzo E et al (2012) Atmos Environ 53:60–74
Solazzo E, Galmarini S (2016) Atmos Chem Phys Discuss. doi:10.5194/acp-2016-15

Chapter 72
Worst Case Meteorological Scenario for Norway in Case of an Accident in Sellafield Nuclear Site

Heiko Klein and Jerzy Bartnicki

Abstract Consequences for Norway in case of a hypothetical accident in Sellafield nuclear site have been of concern for Norwegian authorities for some time now. A 33-year period with meteorological data and the dispersion model SNAP was used to find out the meteorological conditions for which atmospheric transport of radioactive debris from Sellafield nuclear site to Norway is the most efficient. This was done by running the SNAP model two times each day for the entire period and selecting the situations with maximum deposition to Norwegian territory. The worst case meteorological scenario for Norway in case of a hypothetical accident in Sellafield was found on 25th of June 1989. In this meteorological situation atmospheric transport to the west coast of Norway takes only 12 h. Based on the results of the SNAP runs, the probability of reaching Norway by radioactive pollution in case of an accident in Sellafield was also analysed. Such a probability is high (25–40%) for most of the Norwegian territory, except for the northern part and very high (over 40%) for the western coast of Norway.

72.1 Introduction

In case of a real accident in the Sellafield nuclear site, the radioactive particles and gases will be released into the atmosphere and then transported in accordance with the wind pattern. In many meteorological situations, the radioactive pollution will reach the territory of Norway, sometimes very fast. In order to analyze the probability of atmospheric transport to Norway from Sellafield and to select the worst case meteorological scenario for such a transport we have used a long-term meteorological database and the dispersion model SNAP. The long-term meteorological database covers the period 1980–2012 and was originally developed at the

H. Klein · J. Bartnicki (✉)
Norwegian Meteorological Institute, Oslo, Norway
e-mail: jerzy.bartnicki@met.no

H. Klein · J. Bartnicki
Centre of Excellence for Environmental Radioactivity, Ås, Norway

C. Mensink and G. Kallos (eds.), *Air Pollution Modeling and its Application XXV*,
Springer Proceedings in Complexity, DOI 10.1007/978-3-319-57645-9_72

Norwegian Meteorological Institute for the K-27 project (Bartnicki et al. 2016). It was produced by dynamical downscaling of the ERA-Interim reanalysis (Dee et al. 2011) using the HIRLAM numerical weather prediction model (Undén et al. 2002). Its domain includes the north-eastern Atlantic and Scandinavian countries. The horizontal resolution is approximately 11 km and temporal 1 h.

The SNAP (Severe Nuclear Accident Program) model (Bartnicki et al. 2011) was the main tool for all dispersion simulations presented here. This Lagrangian dispersion model is currently operational for nuclear emergency situations and can be used both for nuclear accidents and nuclear detonations. In the model simulations the emitted mass of radioactive debris is distributed among a large number of model particles. After the release, each model particle carries a given amount of selected isotopes which can be in the form of gas, aerosol or particulate matter. During atmospheric transport, model particles are the subject of dry and wet deposition, in case of precipitation. Dry deposition is determined by atmospheric stability and includes parameterization of gravitational settling velocity, important for relatively large particles. Wet deposition parameterization has a different form for in-cloud and below cloud scavenging. Wet deposition for particles is a function of precipitation intensity and particle diameter. Radioactive decay is also calculated during the transport.

The analysis of the atmospheric transport to Norway and deposition over Norwegian territory has been performed in several steps.

In the first step we have defined a simplified source term for potential accident at Sellafield site. In reality the source term for such an accident is highly uncertain. Here we concentrated on meteorological aspects, and therefore selected the release of ^{137}Cs particles with radius 0.55 μm and density 2.3 g cm^{-3}. The size and density are a conservative approach, proper for the worst case scenario, since the lifetime for such particles in the atmosphere is relatively long, compared to other forms like gases or particles of the larger size. The release location was the Sellafield site with the coordinates (54°25′N, 3°29′E). The release rate was 2.0×10^{11} Bq s^{-1} during the first 12 h after the accident start. During the release we assumed a uniform initial distribution of model particles in vertical range 0–500 m.

In the second step the simulations with the SNAP model were performed for the entire 33-year period covered by our meteorological database. The SNAP model was run twice a day (00 and 12 UTC) with source term specified above. The simulation time was 48 h. For all model runs deposition fields were stored in the model grid system.

Next, the results of the SNAP runs were used to find out the worst case meteorological scenario for Norway in case of a potential accident in Sellafield. This scenario was selected based on the highest level of total deposition on Norwegian territory as a criterion.

Finally, statistical analysis was performed for the model results covering 33-year period. This analysis included the probability of arrival to an arbitrary grid in the model domain. The probability of arrival was calculated as a number of model runs with positive deposition to a given grid and concentration in the grid above 1000 Bq m^{-3} divided by the number of total model runs.

72.2 Results

The results of the SNAP model run with atmospheric transport to Norway and deposition on Norwegian territory were used for selection of the worst case scenario from the meteorological point of view. Such a scenario was found on 25th of June 1989.

In this scenario atmospheric transport to Norway is fast. Already after 12 h from the release start the radioactive cloud from the accident is reaching west coast of Norway. This is only half a day and does not leave much time for necessary preparations. After 30 h from the release time the radioactive cloud covers the southern and central part of Norway including the four largest Norwegian cities: Oslo, Bergen, Stavanger and Trondheim. After 50 h, deposition of cesium is visible over the entire territory of Norway.

Maps with dry, wet and total deposition of caesium for the worst case meteorological scenario are shown in Fig. 72.1. Depositions are shown 48 h from the release start.

As expected, the maximum of dry deposition can be noticed close to the sources with values between 100,000 and 300,000 Bq m^{-2}.

The pattern of wet deposition is, to a large extent, determined by the pattern of precipitation. In this case two maxima of wet deposition are visible in Fig. 72.1, one close to the source and the second on the west coast of Norway. The first one was caused by rain close to the source during the first 12 h of the simulation during the release of caesium to air. The second maximum was caused by heavy rain over the west coast of Norway meeting the radioactive cloud from the accident. The maximum of wet deposition on the west coast is over 300,000 Bq m^{-2}.

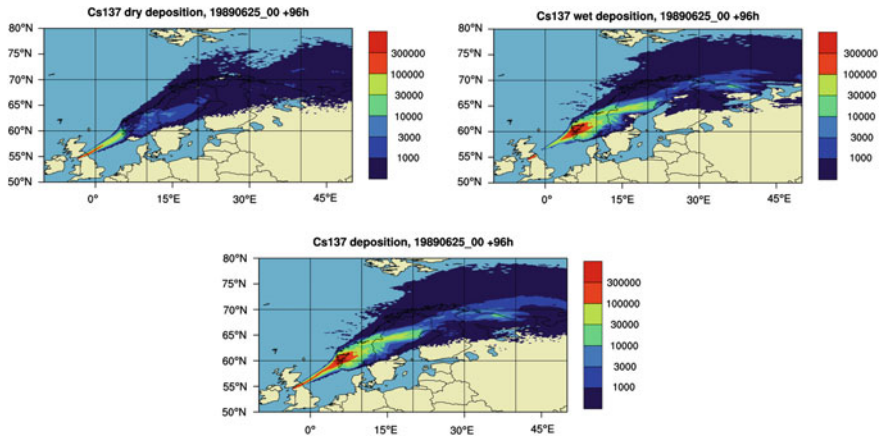

Fig. 72.1 Maps of dry (*upper-left*), wet (*upper-right*) and total (*bottom*) depositions of ^{137}Cs for the worst case meteorological scenario with the hypothetical accident start on 25th of June 1989. Units: Bq m^{-2}

Total deposition of caesium, as a sum of dry and wet deposition, shows two large maxima again, both above 300,000 Bq m^{-2}. The maximum of total deposition over the west coast of Norway is significant, both in terms of the area covered and the high value of the deposition. For this meteorological situation, high level of the total deposition can be observed in the second largest town in Norway—Bergen. Not only Norway is affected by the hypothetical accident in Sellafield in the worst case scenario, but a large part of Sweden and Finland as well. However, depositions there are much lower than in Norway and especially on the west coast of Norway.

One of the most important results of the statistical analysis of SNAP model results is a map with the probability of arrival to each model grid. This map is presented in Fig. 72.2.

Probability of arrival to Norway from a hypothetical Sellafield accident is high, higher than 25% for almost entire Norwegian territory with the exception of small northern part where probability values are between 15 and 25%.

The most likely arrival in case of the accident can be noticed for the west coast of Norway with the values exceeding 40%. It means that, on average, in one of two cases with the accident in Sellafield, the radioactive cloud will arrive to the west coast of Norway.

In addition, the map shown in Fig. 72.2 indicates also that the probability of arrival to Denmark and southern Sweden is also very high, exceeding 40%.

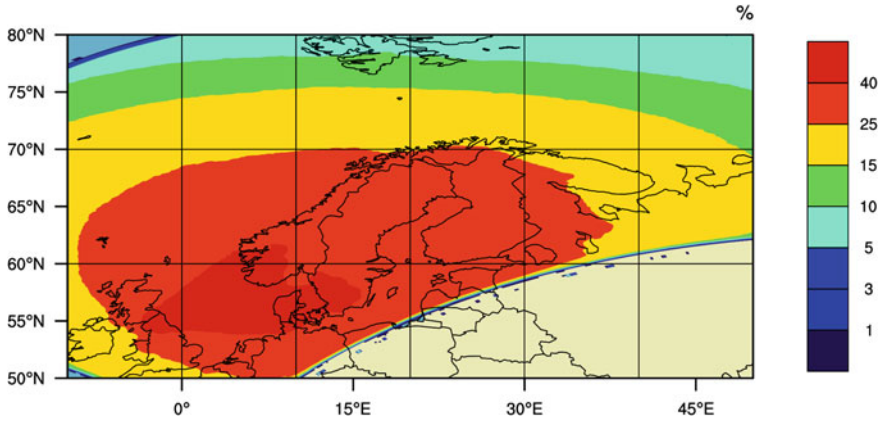

Fig. 72.2 Map with the probability of arrival calculated for the entire 33-year period of available meteorological data

72.3 Conclusions

Analysis of available meteorological data for a 33 year period indicates that in many meteorological situations atmospheric transport from Sellafield to Norway is fast, not leaving much time for the emergency response. The worst case meteorological scenario for Norway in case of a hypothetical accident in Sellafield was found on 25th of June 1989. In this meteorological situation atmospheric transport to the west coast of Norway takes only 12 h. In case of an accident in the Sellafield nuclear site there is a high probability (25–40%) of arrival of the radioactive cloud to almost the entire Norwegian territory, except the most northern part (15–25%). This probability is very high (above 40%) for the west coast of Norway.

Acknowledgements We are grateful to the Norwegian Radiation Protection Authority and to the Centre of Excellence for Environmental Radioactivity for the financial support of this. This work was partly supported by the Research Council of Norway through its Centres of Excellence funding scheme, project number 223268/F50.

Questions and Answers

Questioner: Antti Hellsten.
Question: What was the reason to use source height 0–500 m? And did you test sensitivity to this choice?
Answer: The vertical range 0–500 m was suggested to us by the experts from Norwegian Radiation Protection Authority as most likely for a hypothetical accident at Sellafield site. We have not tested sensitivity of the results to the source height in this study, but we did it in the past. The main difference in results can be notices for the source below and above mixing height.

References

Bartnicki J, Haakenstad H, Hov Ø (2011) Operational SNAP model for remote applications from NRPA. Research report no. 12, ISSN 0332-9879. Norwegian Meteorological Institute, Oslo, Norway

Bartnicki J, Amundsen I, Brown J, Hosseini A, Hov Ø, Haakenstad H, Klein H, Lind OC, Salbu B, Wendel C, Ytre-Eide MA (2016) Atmospheric transport of radioactive 644 debris to Norway in case of a hypothetical accident related to the recovery of the Russian 645 submarine K-27. J Environ Radioact 151:404–416

Dee DP, Uppala SM, Simmons AJ, Berrisford P, Poli P, Kobayashi S, Andrae U, Balmaseda MA, Balsamo G, Bauer P, Bechtold P, Beljaars ACM, van de Berg L, Bidlot J, Bormann N, Delsol C, Dragani R, Fuentes M, Geer AJ, Haimberger L, Healy SB, Hersbach H, Holm EV, Isaksen L, Kållberg P, Kohler M, Matricardi M, McNally AP, Monge-Sanz BM, Morcrette J-J, Park B-K, Peubey C, de Rosnay P, Tavolato C, Thepaut J-N, Vitart F (2011) The ERA-interim

reanalysis: configuration and performance of the data assimilation system. Quart J R Meteorol Soc 137:553–597

Undén P, Rontu L, Järvinen H, Lynch P, Calvo J, Cats G, Cuaxart J, Eerola K, Fortelius C, Garcia-Moya JA, Jones C, Lenderlink G, McDonald A, Mc-Grath R, Navascues B, Nielsen NW, Ødegaard V, Rodriguez E, Rummukainen M, Rööm R, Sattler K, Sass BH, Savijärvi H, Schreur BW, Sigg R, The H, Tijm A (2002) HIRLAM-5 scientific documentation, HIRLAM-5 project. Swedish Meteorological and Hydrological Institute, Norrköping, Sweden

Chapter 73
The Impact of Sub-hourly Meteorology on the Estimation of Odour Concentrations from an Industrial Source in Complex Terrain

V. Valdenebro, P. Uriarte, E. Sáez de Cámara, G. Gangoiti, J. Lavín, L. Alonso, J.A. García and N. García-Borreguero

Abstract Atmospheric pollutant impacts may be evaluated through the use of dispersion models, usually based on averaging times of 1 h. However, some scenarios may require shorter time lapses, as it is the case of odour impact evaluations. Version 6 of the CALPUFF modeling system, which allows the use of sub-hourly temporal resolution, coupled with the mesoscale prognostic model RAMS has been used to simulate the impacts of the odour emissions from a paper mill in a highly urbanized area located several kilometers downwind at the seaside in a moun-

V. Valdenebro (✉) · E.S. de Cámara · G. Gangoiti · L. Alonso · J.A. García
Faculty of Engineering, University of the Basque Country UPV/EHU,
Alameda de Urquijo s/n, 48013 Bilbao, Spain
e-mail: veronica.valdenebro@ehu.eus

E.S. de Cámara
e-mail: estibaliz.saezdecamara@ehu.eus

G. Gangoiti
e-mail: g.gangoiti@ehu.eus

L. Alonso
e-mail: lucio.alonso@ehu.eus

J.A. García
e-mail: joseantonio.garciaf@ehu.eus

P. Uriarte
Factor CO2, Colón de Larreategui 26, 1 A and B, 48009 Bilbao, Spain
e-mail: puriarte@factorco2.com

J. Lavín
Sociedad Española de Abastecimientos, S.A., Gran Vía Marqués del Turia, 19,
46005 Valencia, Spain
e-mail: jlavinte@aguasdevalencia.es

N. García-Borreguero
Basque Government, Environment Administration Directorate,
Donostia-San Sebastián 1, 01010 Vitoria-Gasteiz, Spain
e-mail: nicolas-garcia@euskadi.eus

C. Mensink and G. Kallos (eds.), *Air Pollution Modeling and its Application XXV*,
Springer Proceedings in Complexity, DOI 10.1007/978-3-319-57645-9_73

tainous region. A selection of consecutive days under anticyclonic conditions have been simulated using a maximum resolution of 10 min. Thirteen odour sources have been considered, including point, volume and area sources. The preliminary results show that 10 min maximum concentrations can duplicate those of the hourly simulations over wide areas of the study region. Our sub-hourly results show a better agreement with data from field olfactometry.

73.1 Introduction and Method

Atmospheric pollutant dispersion models usually employ averaging times of 1 h in meteorology, emissions and estimation of concentrations. This can significantly smooth concentration peaks registered over shorter averaging times, which could be relevant in some scenarios, such as odour impact evaluations (Nicell 2009). The capacity of the models to deal with sub-hourly temporal resolution could reduce the need of using peak-to-mean conversion ratios (Ranzato et al. 2012) that, among other factors, depend on atmospheric turbulence (Schauberger et al. 2012) but are frequently employed as a constant value.

Version 6 of the non-steady state CALPUFF modeling system coupled with the mesoscale prognostic model RAMS has been used to simulate, with sub-hourly resolution, the impacts of the odour emissions from a paper mill in a nearby area in a mountainous region near the coast during three four-day periods under

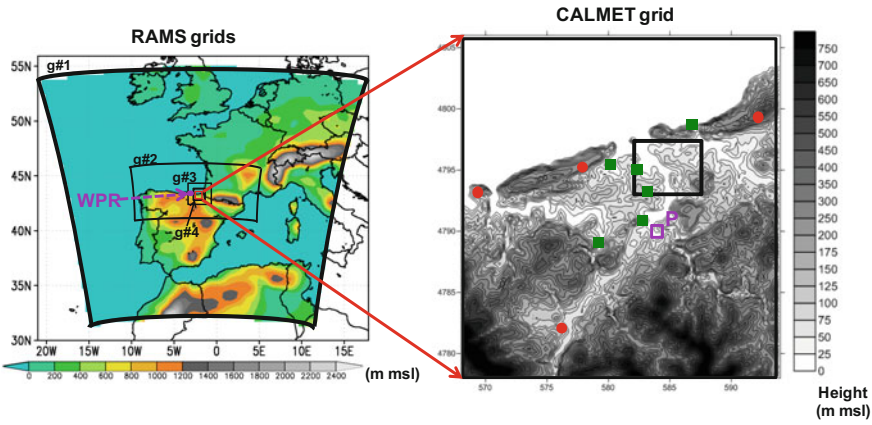

Fig. 73.1 Horizontal grids used by RAMS and CALMET-CALPUFF (RAMS' Grid #1 topography). The study area is completely included in the CALMET domain. The location of the paper mill (P), the olfactometry campaigns region (*black square* into the CALMET grid) and a selection of meteorological stations (*closed circles* and *squares*) and a wind profiler radar (WPR in RAMS Grid #3) used in the study have been marked. Data from all of the stations and the WPR have been used to validate the meteorological simulations. Besides, data from the stations marked with *green squares* have been assimilated into CALMET (hybrid mode)

anticyclonic conditions. Important daily cycles/changes in stability and wind reversals are registered almost every day in the area, making it inappropriate the use of steady-state Gaussian plume models (Millán et al. 1987). Figure 73.1 shows the grids used in the RAMS and CALMET-CALPUFF simulations. Forty-four levels have been used in RAMS up to 22.5 km and with a finer resolution near the ground; 12 levels have been used in CALMET with the cell centres at 10, 30, 60, 105, 165, 250, …, 2600 m. Thirteen odour sources belonging to the paper mill have been considered in the dispersion simulations, including point, volume and area sources. Hourly data from RAMS, 10 min data from surface stations, a time step of 10 min and constant emission rates have been used in the runs.

The simulated meteorology has been compared against data from surface stations and a wind profiler radar located in the area (see Fig. 73.1). Odour impacts have been qualitatively compared with data from field olfactometry and with a long register of citizen complaints (not shown). Results for one of the 4 day periods are shown here.

73.2 Results and Conclusions

The use of sub-hourly resolution shows more and higher peaks of concentrations, and the results are closer to the observations. This is due, to a big extent, to the assimilation of surface meteorological data with sub-hourly resolution into CALMET.

During the period 29th of July to 1st of August of 2013, depending on the location and the instant considered, concentrations may be multiplied by a factor of more than 10 inside the olfactometry region. Simulated 10 min maximum concentrations can duplicate hourly maximum values evaluated using hourly resolutions over a wide part of that area (Fig. 73.2), multiplying the latter by a factor up to

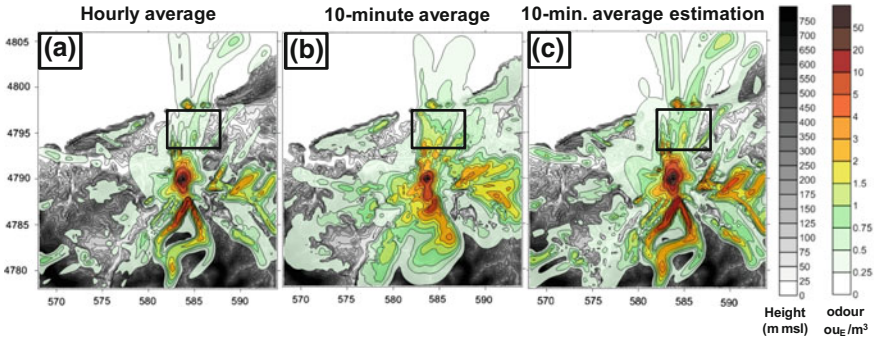

Fig. 73.2 Peak concentrations over the domain during the period 29th July to 1st August, 2013. **a** Hourly concentrations from hourly resolution simulations. **b** Direct estimation of 10 min concentrations (sub-hourly resolution simulations). **c** Ten-minute average estimation using a scaling factor (power law with exponent $p = 0.28$) applied to hourly concentrations. The *black square* in each panel frames the olfactometry campaigns region

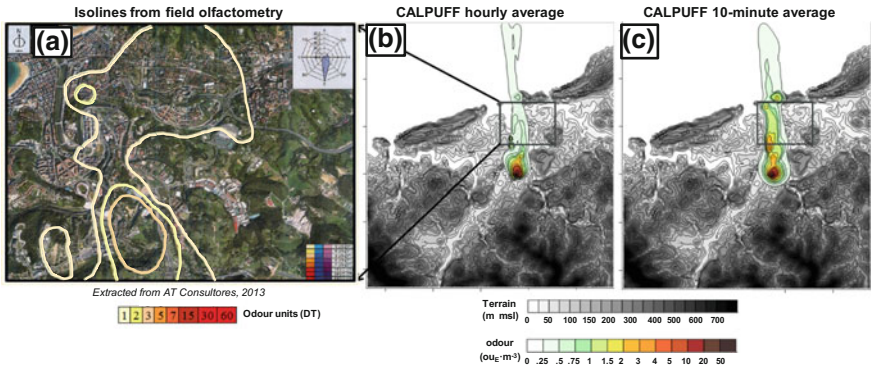

Fig. 73.3 31st July 2013, 04:00–08:00 UTC. **a** Olfactometry data (odour isopleths). **b** Simulated maximum hourly concentrations (hourly resolution simulations). **c** Simulated maximum 10 min concentrations (sub-hourly resolution simulations)

8 in some receptors. They also show a spatial pattern different from the hourly simulations and from the distribution obtained when applying a constant power law (Nicell 2009) to hourly results for the estimation of 10 min concentrations. Direct 10 min estimations agree better than hourly averages with the isopleths from field olfactometry data (Fig. 73.3).

Acknowledgements We wish to thank the Basque Government and the paper mill management staff for providing data. We also thank the Basque Government (Euskoiker Foundation Reference PT10291) and the University of the Basque Country UPV/EHU (GIA 13/03) for their financial support.

References

AT Consultores (2013) Realización de un mapa de olores en San Sebastián (Guipúzcoa) http://www.donostia.eus/info/ciudadano/ma_areas.nsf/voWebContenidosId/4453661FC9D69F-82C1257A16003CF023/$file/Informe%20olfatometrico.pdf

Millán MM, Otamendi E, Alonso L, Ureta I (1987) Experimental characterization of atmospheric diffusion in complex terrain with land-sea interactions. JAPCA 37:807–811

Nicell JA (2009) Assessment and regulation of odour impacts. Atmos Environ 43:196–206

Ranzato L, Barausse A, Mantovani A, Pittarello A, Benzo M, Palmeri L (2012) A comparison of methods for the assessment of odor impacts on air quality: field inspection (VDI 3940) and the air dispersion model CALPUFF. Atmos Environ 61:570–579

Schauberger G, Piringer M, Schmitzer R, Kamp M, Sowa A, Koch R, Eckhof W, Grimm E, Kypke J, Hartung E (2012) Concept to assess the human perception of odour by estimating short-time peak concentrations from one-hour mean values. Reply to a comment by Janicke et al. Atmos Environ 54:624–628

Part VII
Air Quality Effects on Human Health and Ecology

Chapter 74
Investigation of Current and Future Nitrogen Depositions and Their Impact on Sensitive Ecosystems in Europe

Johannes Bieser, Anna M. Backes and Volker Matthias

Abstract Eutrophication and acidification due to anthropogenic emissions is a major threat for bio diversity in vulnerable ecosystems. The combined impact of N and S deposition can be evaluated using ecosystem dependent critical load masses. Here, we used modelled N and S deposition fields from the CCLM-CMAQ chemistry transport model (CTM) to calculate the annual load. We compared the modelled loads with geo-referenced critical load (CL) maps from the Coordination Centre for Effects (CCE). We found that in central Europe around 25% of the areas defined in the CCE-CL database currently exceed their critical loads due to anthropogenic emissions. Expected NH_3 emission reductions in the agricultural sector in the next decade showed little reduction potential in the area with critical load exceedance. A source receptor study of major N and S sources in Europe gave that SO_2 emission reductions have a larger potential to decrease critical load exceedances than NH_3 emission reductions. The most effective measure was the reduction of SO_2 emissions from coal fired power plants. However, each source exhibited a different regional distribution which indicates that there is no general approach to reduce critical load exceedances. Moreover, we found a non-linear relationship between emission reductions and reductions in critical load exceedances. Furthermore, the reduction of only one of the two elements lead to diminishing returns without a reduction of the other.

J. Bieser (✉) · A.M. Backes · V. Matthias
Helmholtz-Zentrum Geesthacht, Institute of Coastal Research,
Max-Planck-Strasse 1, 21502 Geesthacht, Germany
e-mail: johannes.bieser@hzg.de

V. Matthias
e-mail: volker.matthias@hzg.de

J. Bieser
DLR – Deutsches Luft und Raumfahrtzentrum, Münchener Straße 20,
82234 Weßling, Germany

C. Mensink and G. Kallos (eds.), *Air Pollution Modeling and its Application XXV*,
Springer Proceedings in Complexity, DOI 10.1007/978-3-319-57645-9_74

74.1 Introduction

The eutrophication of terrestrial and aquatic ecosystems is a major environmental issue in Europe. In most ecosystems nitrogen is the limiting nutrient for plant growth with many species being adapted to nitrogen poor conditions. Albeit stronger national and European legislation nitrogen emissions (namely ammonia) from agriculture and animal husbandry in central Europe are still increasing, in turn leading to increased deposition.

In order to assess the environmental state of European ecosystems we evaluated exceedances of critical loads. A critical load is defined as "a quantitative estimate of an exposure to one or more pollutants below which significant harmful effects on specified sensitive elements of the environment do not occur according to present knowledge" (Nilsson and Grennfelt 1998).

For this study, we used the chemistry transport model CMAQ to determine nitrogen deposition loads for Europe. CMAQ was forced with meteorological fields from the COSMO-CLM meteorological model and emissions from the SMOKE for Europe emission model, including our newly developed ammonia emission module (Backes et al. 2016a). The study consists of two parts:

Firstly, a source apportionment study for which we investigate the impact of nitrogen and sulfur emissions from agricultural activity, power generation, and mobile sources on the area with critical loads exceedances. As the critical load is based on the amount of exchangeable cations in the soil, increasing sulfur deposition will increase the fraction of available nitrogen. Therefore, sulfur emissions from combustion processes such as coal fired power plants reduce the amount of nitrogen needed for a critical load exceedance and can have a strong impact on the affected area.

Secondly, we investigate the reduction potential of critical loads exceedances for different source sectors. Additionally, we use future emission scenarios to assess the possible development of ammonia depositions from different agricultural sectors in 2030. For this, we used a political, a technical, and a behavioral ammonia emission scenario as described in Backes et al. (2016b)

74.2 Model Set-Up and Domain

For this study we use the chemistry transport model (CTM) CMAQ v5.0.1 with the cb05tucl photochemical mechanism and the aero6_aq aerosol module to calculate the deposition fluxes of nitrogen and sulfur species. The regional CTM was set up for a domain covering the whole of Europe with a 72×72 km^2 outer domain and a nested domain over central and northern Europe with a resolution of 24×24 km^2. Boundary conditions for the chemical model were obtained from the global model TM5. Meteorological fields from the COSMO-CLM model were used

as input. The year modelled is 2008. This is exactly the same model setup used for our previous study on the impact of ammonia emissions on aerosol formation in northern and central Europe presented at the 34th ITM (Backes et al. 2016c). However, for this study we concentrate on an analysis of the wet and dry deposition fluxes. Finally, run source receptor sensitivity runs by turning off different emission sectors at a time. The emission perturbation scenarios were created with the SMOKE for Europe emission model (Bieser et al. 2011a, b). Emissions from international shipping were estimated with based on the work of Aulinger et al. (2016).

74.3 Current State of Critical Load Exceedance

We use the modelled annual sum of N and S deposition to calculate the critical load exceedance based on the Coordination Centre for Effects (CCE) critical load map (Sloothweg et al. 2015). We found, that ~30% of all vulnerable ecosystems in the CCE database exceeded their critical load in 2008, with up to 100% of area exceeded at the southern North Sea coast, the Bretagne, and parts of England (Fig. 74.1). A model run without anthropogenic emissions showed that almost 10% of the area was still exceeding their critical load simply because of oceanic sulphur deposition. However, this number could be substantially lower if the base cation deposition would have been considered. The total area exceeded was 24% when only accounting for antropogenic emissions. Furthermore, we found that most of the exceedance was due to a mixture of N and S deposition and only few areas, mostly in the south eastern part of the domain were solely S exceeded and small parts of the southern North Sea coast, England and Ireland were solely N exceeded.

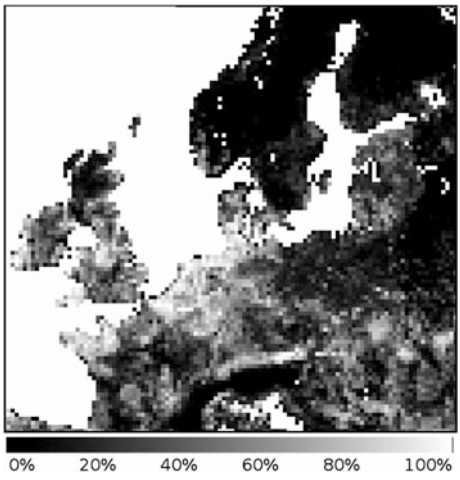

Fig. 74.1 Total % area exceeding critical load

74.4 Reduction Potential

To determine the reduction potential of agricultural sources we used three future NH_3 emission scenarios. A political scenario which is based on the European national emission ceilings for 2030 (NEC2030), a technical scenario which is based on the maximal technically feasible reduction (MTFR), and a behavioural scenario based on reduced meat consumption (RCAP). These scenarios are described in further detail in Backes et al. (2016b). Figure 74.2 depicts the reduction potential of % area exceeded for the three emission scenarios. It can be seen, that all scenarios exhibit a similar spatial pattern with the largest reductions found in the RCAP scenario and the lowest reductions in the NEC2030 scenario. The largest impact of agricultural sources was found for France, mainly in the north-west (Bretagne) but also in the south at the Swiss border (Jura). In the MTFR and the RCAP scenario the % area exceeding the critical load can be reduced by up to 50% points. However, in regions with large sulfur deposition loads a reduction in nitrogen deposition did not led to a reduction of exceedances. These regions are mainly located the southern North Sea coast and eastern Europe.

To identify the major contributors to critical loads exceedances in northern and central Europe, we run CMAQ with major emission sectors turned off. For this study we looked at emissions from power generation which makes up 45% of the total S and 15% of the total NOx emissions, mobile sources which are responsible for 30% of the NOx emissions, and international shipping which is responsible for 10% of the S and 15% of the NOx emissions inside the model domain. The S emissions from power plants had by far the largest impact and led to a significant reduction of % area exceeded (Fig. 74.3a). The effect was particularly strong in Germany and eastern Europe, and England. Mobile sources had the largest impact in central England and southern Germany (Fig. 74.3b). Finally, shipping emissions were the only source sector that led to a strong exceedance reduction in coastal areas (Fig. 74.3c).

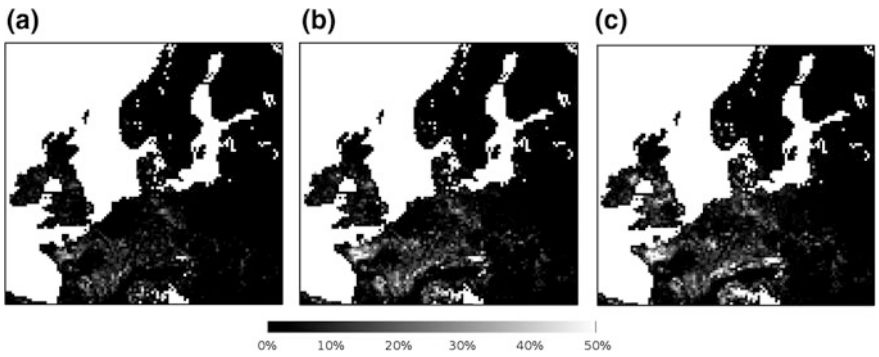

Fig. 74.2 Reduction potential for agricultural NH_3 emission reduction scenarios **a** NEC2030 **b** MTFR **c** RCAP. Shown is the reduction in percentages points

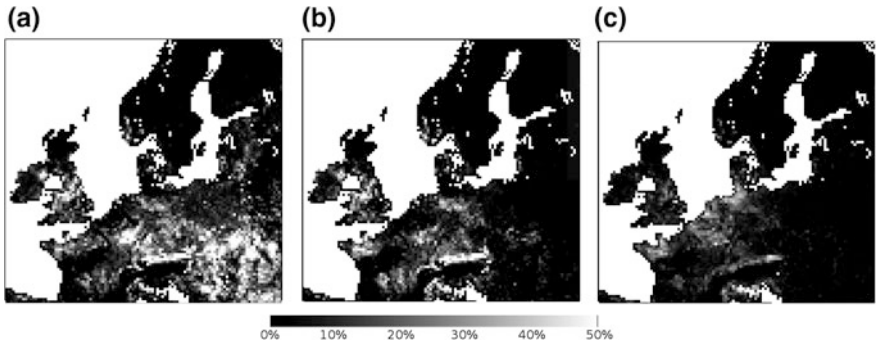

Fig. 74.3 Reduction potential for anthropogenic emission sources: **a** power generation, **b** mobile sources, **c** shipping emissions

Finally, we investigated the response of a gradual reduction of emissions. Here we found that the reduction of S emissions from power plants showed mostly a linear response in exceedance reductions. The reduction of NH_3 emissions from agricultural sources, on the other hand, gave diminishing returns with each further reduction step.

74.5 Conclusion

In this study we used modelled N and S deposition from the SMOKE-EU/CCLM/CMAQ air quality modelling system to determine the % area exceeding their critical loads. We found that about 25% of the vulnerable ecosystems in the model domain have critical load exceedances due to anthropogenic emissions.

The exceedances were generally due to a mixture of N and S deposition which means that a combined reduction of both species holds the largest potential to reduce the % area exceeded. However, reduction of S emissions was found to be more effective than the reduction of N emissions. S deposition reductions were especially impactful in the eastern part of the domain, which can be explained by large SO_2 emissions from coal fired power plants in the area as well as long range transport due to the prevailing westerly winds.

The foreseeable NH_3 emission reductions in the agricultural sector based on the NEC2020 had only little influence and were mostly limited to France.

In this model set-up sulfate emissions from sea salt contributed another 10% non-anthropogenic critical loads exceedances. However, we did not account for the alkaline effect of base cations. Dependent on the treatment of sea salt emissions, SO_2 emissions from international shipping had a strong impact on the North Sea coast.

Questions and Answers

Questioner Name: Tony Dore
Question: As critical loads are 'threshold' values, calculations of exceedance may not show reductions in % area exceeded in high deposition areas for future scenarios. Have you considered using alternative statistics for exceedance, such as average accumulated exceedance which could take into account the load of exceedance above the critical load?
Answer: This is a very important issue. Especially as policy makers might not understand that an emission reduction will not affect the % area exceeded and might be inclined to neglect any further attempts on emission reduction. Thus, for policy counseling the reduction in accumulated exceedance might be a suitable measurement to express the gradual benefit of emission reductions. From a scientific viewpoint, however, the accumulated exceedance is no suitable factor because of the very nature of this indicator. The critical loads are based on habitat suitability indices which means that at a certain exceedance level plants of a certain type will not be able to grow no matter how large the exceedance is. I think another way of expressing the gradual benefit of emission (and thus deposition) reductions could be to use different threshold levels for the critical load exceedance (e.g. habitat suitability 90, 75, 50, 25%). To my knowledge a methodology for this has not been developed yet, but in the end instead of % aera of exceedance we could have an indicator which states the % of plants able to grow. This index could be more responsive to emission reductions. But in areas with very high deposition, small emission reductions might still show no effect.

Questioner Name: Stefano Galmarini
Question: For this study and your model chain list 5 critical points that would benefit from a model inter-comparison or evaluation phase.
Answer: The five main sources of uncertainty in this study are: (1) precipitations fields, (2) dry deposition velocities, (3) spatio-temporal distribution of ammonia emissions, (4) treatment of surface bi-directional ammonia flux, (5) organic nitrogen chemistry (including heterogenous reactions).

Questioner Name: Peter V
Question: How did you do the source apportionment?
Answer: We used a brute force method reducing one emission sector at a time by a certain amount. As we were looking on annual total depositions the model response showed to be mostly linear. We think that a brute force method is suitable if the scientific question is what effect would the reduction of a certain source by a certain factor have on future pollution levels. Opposed to this a labelling approach would have been more suitable if the scientific question was which fraction of the current pollution is due to a certain source.

References

Aulinger A, Matthias V, Zeretzke M, Bieser J, Quante M, Backes A (2016) The impact of shipping emissions on air pollution in the greater North Sea region—Part I: Current emissions and concentrations. Atmos Chem Phys (2):739–758. doi:10.5194/acp-16-739-2016

Backes AM, Bieser J, Aulinger A, Quante M, Matthias V (2016a) Ammonia emissions in Europe, Part I: Development Of a dynamical ammonia emission inventory. Atmos Environ 131:55–66

Backes AM, Bieser J, Aulinger A, Quante M, Matthias V (2016b) Ammonia emissions in Europe, Part II: How ammonia emission abatement strategies affect secondary aerosols. Atmos Environ 126

Backes AM, Bieser J, Aulinger A, Quante M, Matthias V (2016c) Influence of ammonia emissions on aerosol formation in Northern and Central Europe. In: Douw SG, Chaumerliac N (eds) Air pollution modeling and its application XXIV, pp 29–36

Bieser J, Aulinger A, Matthias V, Quante M, Builtjes P (2011a) SMOKE for Europe—adaptation, modification and evaluation of a comprehensive emission model for Europe. Geosci Model Dev 4:47–68. doi:10.5194/gmd-4-47-2011

Bieser J, Aulinger A, Matthias V, Quante M, Denier van der Gon HAC (2011b) Vertical emission profiles for Europe based on plume rise calculations. Environ Pollut 159:2935–2946. doi:10.1016/j.envpol.2011.04.030

Nilsson J, Glennfelt P (eds) (1998) Critical loads for sulphur and nitrogen: report from a workshop, March. Skolaster, Sweden, Copenhagen, Denmark, Nordic Council of Ministers

Slootweg J, Posch M, Hettenlingh JP (eds) (2015) Modelling and mapping the impacts of atmospheric deposition of nitrogen and sulphur: CCE status report 2015. RIVM Report 2015-0193, Coordination Centre for Effects, Bilthoven, Netherlands, 182 pp. http://www.wge-cce.org

Chapter 75
Changing Agricultural NH_3 Emissions Since 1979: The Impact on N Deposition and Health Effects Across Europe and the Potential for Further Reductions in the Future

Camilla Geels, Thomas Ellermann, Ole Hertel, Jørgen Brandt, Carsten A. Skjøth, Wilfried Winiwarter, Ulas Im, Kaj M. Hansen and Jesper H. Christensen

Abstract The Danish Eulerian Hemispheric Model (DEHM) has been used to study the development in air quality in Europe from 1979 to 2015. The large changes in anthropogenic emissions both within and outside Europe—especially since the beginning of the 1990s—led to a decrease in many air pollutants. The model analysis captured this observed trend. Using the EVA system (Economic Valuation of Air pollution) we were able to derive health impacts, showing (for the

C. Geels (✉) · T. Ellermann · O. Hertel · J. Brandt · U. Im · K.M. Hansen
J.H. Christensen
Department of Environmental Science, Aarhus University, Roskilde, Denmark
e-mail: cag@envs.au.dk

T. Ellermann
e-mail: tel@envs.au.dk

O. Hertel
e-mail: oh@envs.au.dk

J. Brandt
e-mail: jbr@envs.au.dk

U. Im
e-mail: ulas@envs.au.dk

K.M. Hansen
e-mail: kmh@envs.au.dk

C.A. Skjøth
National Pollen and Aerobiological Research UnitInstitute of Science and the Environment, University of Worcester, Worcester, UK
e-mail: c.skjoth@worc.ac.uk

W. Winiwarter
IIASA—International Institute for Applied Systems Analysis, Laxenburg, Austria
e-mail: winiwart@iiasa.ac.at

C. Mensink and G. Kallos (eds.), *Air Pollution Modeling and its Application XXV*,
Springer Proceedings in Complexity, DOI 10.1007/978-3-319-57645-9_75

European modelling domain) that premature deaths in 2010 were less than half of the 1980 value. While the decrease was also determined for nitrogen compounds in general, the share of reduced nitrogen (NH_3 and NH_4^+) increased—a result of both emission trends and atmospheric behavior. An experimental emission scenario applied to the model suite demonstrated further health improvements are possible for technically feasible measures to reduce ammonia emissions.

75.1 Introduction and Study Setup

A number of international agreements have through the years aimed at limiting the emissions of air pollutants and the related negative effects. As a result, European emissions of NO_x and SO_x have since 1990 (EEA) been reduced by about 40 and 70%, respectively. The abatement policy has been less successful for NH_3 emissions from the agricultural sector. Here the emissions have decreased by about 25% over the same time period. There are, however, large differences in the national abatement policies, affecting the overall developments in the national emissions (Sutton et al. 2011). NH_3 is an important air pollutant as it contributes both to the nitrogen load on sensitive nature areas as well as to the formation of particulate matter ($PM_{2.5}$) with potential negative impacts on the human health (e.g. Stevens et al. 2010; Sutton et al. 2011; Brandt et al. 2013). As NO_x and SO_x emissions have been decreasing at a faster rate, the relative importance of NH_3 is increasing. Studies have even described a climate penalty on NH_3 emissions, with a potential for increasing emissions in a future warmer climate (Skjøth and Geels 2013). This makes it relevant to evaluate the temporal variation in impacts of NH_3 emissions throughout the latest decades in relation to both air quality and its impact.

We will have special focus on the Danish case, as Denmark is one of the countries in Europe, where strong regulations of farming activities and new technologies have resulted in a significant decrease (>30%) in NH_3 emissions. Despite the documented positive environmental effects of e.g. advanced agricultural technologies, these are not commonly used in many regions of Europe. Moreover, effects of extending Danish regulations to all of Europe have not been analyzed before. In an illustrative model approach we have therefore constructed a hypothetical experimental scenario of how the NH_3 emissions would be if typical emissions factors related to agricultural activities in Denmark were applicable in all of Europe.

Simulations of air quality for the time period 1979 to 2015 have been carried out with the DEHM model. DEHM is a 3D chemistry-transport model covering the Northern Hemisphere and including several nests with higher and higher resolution over Europe and Denmark (e.g. Brandt et al. 2012 and references therein). Anthropogenic emissions are based on a combination of different inventories like ECLIPSEv5.0 for the largest domain, EMEP emissions for European domains, and a national emission inventory with high a high spatial resolution for the domain over Denmark.

Besides the 37 year model run, an additional calculation for the NH_3 emission scenario mentioned above has been made. The experimental scenario is constructed by applying the emission factors related to agricultural activities in Denmark for the same activities in the other countries in Europe. National emission factors and activity data for 2010 are extracted from the GAINS model (Amann et al. 2011), and the final scenario is obtained by scaling the EMEP emissions within the DEHM model domain. For EU28 as a whole, the NH_3 emissions in this hypothetical experiment are reduced about 33%. In countries with a high level of regulation (like the Netherlands), smaller reductions are obtained, while significantly higher reductions are seen for other countries (e.g. Germany, France, and Slovenia).

Impact of air quality is carried out with the EVA (Economic Valuation of Air pollution) model (Brandt et al. 2013), which has been applied to assess the development in the human health impacts related to air-quality. EVA use gridded concentration fields from the European part of the DEHM domain with a resolution of 50 km × 50 km (this domain also includes parts of Russia). Currently the air-quality components related to health effects included in the EVA system are: gaseous O_3, CO, and SO_2, and particulate SO_4^{2-}, NO_3^-, as well as the primary emitted part of $PM_{2.5}$. NH_4^+ contributes to the particle mass when NH_3 has reacted with sulfate or nitrate to form e.g. ammonium nitrate.

75.2 Results and Discussion

The DEHM results have been evaluated against measurements from the EMEP network, which in general shows a fair agreement for most pollutants. The general decreasing trend is captured for both gasses and deposition of the main N- and S-components, whereas the overall $PM_{2.5}$ level is underestimated. Part of the underestimation can be explained with the fact that Secondary Organic Aerosols (SOA) is not included in the current version of the model. In Fig. 75.1 the development in NH_3 and NH_4^+ concentrations at a monitoring site in Denmark is shown as an example. A positive bias is seen for NH_3, which is a well-known limitation for regional scale modelling of NH_3 (Geels et al. 2012). The development in NH_4 is, however, captured well. We thus conclude, that is reasonable to use the DEHM simulations in combination with EVA to study the overall developments in air-quality related health effects across Europe. It will nevertheless be a conservative estimate due to the lack of SOA.

Nitrogen deposition: The modeled total deposition of nitrogen within the European domain show a clear decreasing trend as expected from the developments in emissions. From 1980 to 2010 the total N load decreases by ca 28% on average, but this number includes large regional differences that can be subject to further analyses. The NH_3 experimental scenario for 2010 gives an additional decrease of 12%, but with large regional differences. On average, the fraction of the N load

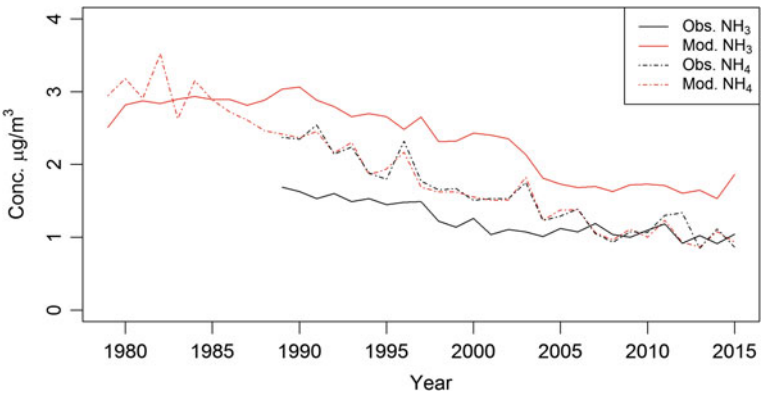

Fig. 75.1 The inter-annual variation of the NH_3 and NH_4 concentrations (µg NH_3–N and NH_4–N pr. m^3)—at the measurement station Tange in Denmark (Tange: 56°21'N, 9° 36'E). The Tange site is located within an agricultural area

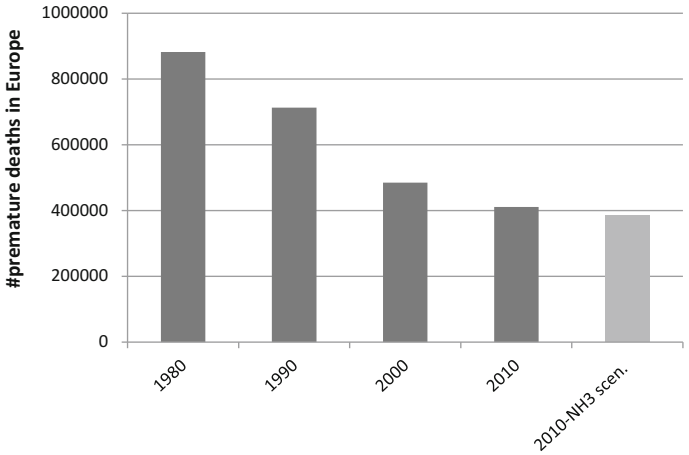

Fig. 75.2 The number of premature deaths linked to air pollution, as estimated by the EVA system for a number of selected years. For the years up to and including 2000, population data for year 2000 is used, while population data for 2010 is used in the estimates for 2010

coming from NH_3 increases from ca. 15% in 1980 to about 29% in 2010. This is due to the smaller decrease in NH_3 emissions than in NO_x emissions, but also due to changes in the residence time of N components in a less acidic atmosphere (Fagerli and Aas 2008). This could be relevant to investigated further, e.g. by using scenarios with constant SO_x emissions.

Health impacts: The EVA system includes a number of health effects, but here we focus on the number of premature deaths for simplicity. As seen in Fig. 75.2 there is a significant decrease in the total number of premature deaths linked to air pollution within the European model domain (the population data covers EU28 and Norway). The number is reduced from ca. 880.000 in 1980 to ca. 410.000 in 2010

and further reductions are seen towards 2015. Applying the experimental NH_3 scenario in 2010 brings the number of premature deaths down by ca. 25.000 (6%), highlighting the importance of the agricultural sector. This further supports a previous EVA study for year 2000 that showed that ca. 23% of the health impacts can be related to the agricultural sector. Additional model calculations are therefore needed in order to extend this analysis back and forth in time.

75.3 Conclusion

A 37-year long simulation with the DEHM model has been used to assess the impact of air pollution and to demonstrate the effect of the successful reduction of many air pollutants. We show that there is a potential to reduce the NH_3 emissions further, if existing agricultural technologies and regulations are widely applied in Europe. Based on an experimental scenario, we find that up to 25.000 premature deaths could then be avoided, and the atmospheric nitrogen load on the environment could be reduced by 12%.

Acknowledgements This study was mainly funded through the Nordforsk NordicWelfAir project (75007). Developments made as part of the EU project ECLAIRE (project no: 282910) has also been included.

Questions and Answers

Questioner: Tony Dore
Question: You showed the importance of NH_3 as a pollutant important for both human health and natural ecosystems. Why have most European countries been unable to significantly reduce NH_3 emissions, where they have successfully tackled NO_x and SO_2?
Answer: The "polluter pays" principle has been the basis for a large part of the national and international regulation of air pollution. But for some reason this principle does not (fully) apply, when it comes to regulation of the agricultural sector. I am guessing that it is caused by a combination of issues like: food security, strong and influential farmers unions as well as traditions.

Questioner: Peter Viaene
Question: This is an AQ conf. and people focus on the AQ aspect. Injection of nitrogen (N) into the soil is not really a solution to the problem.
Answer: I agree, AQ is certainly not the only problem related to N. A more holistic approach is needed in order to study the full effect of e.g. introducing new abatement techniques limiting the emissions to the atmosphere, but leading to more N within the soil-plant system. Please see our Poster/chapter on this (Geels et al., this book).

Questioner: Ted Russell
Question: Did you look at how well the model captures the spatial and temporal variation of the $[NH_4^+]/(2[SO_4^{2-}] + [NO_3^-])$ (based on equivalents)? As Dick Derwent said, it has remained very constant. This would be an interesting assessment of the system.
Answer: No, we have not looked at this so far. But thanks for the suggestion—it will be an interesting way to test if the model describes the processes related to these species correct. Especially because we now have a simulation covering so many years with large decreases in the emissions and hence with changes in the chemical regimes in the atmosphere.

Questioner: Wouter Lefebvre
Question: You showed that for 60% of the areas in Europe the critical loads for N were exceeded. The pervious speaker (Johannes Bieser) showed only 25%.
Answer: The numbers shown here were based on assessments made by the Coordination Centre for Effects (note—this plot was showed in the oral presentation, but is not included in this chapter). Johannes Bieser had estimated the exceedances based on own model results. Comment by Johannes Bieser: It is probably strongly influenced by the model domain.

References

Amann M, Bertok I, Borken-Kleefeld J, Cofala J, Heyes C, Hoeglund-Isaksson L, Klimont Z, Nguyen B, Posch M, Rafaj P, Sandler R, Schoepp W, Wagner F, Winiwarter W (2011) Cost-effective control of air quality and greenhouse gases in Europe: modeling and policy applications. Environ Model Softw 26:1489–1501

Brandt et al (2012) An integrated model study for Europe and North America using the Danish Eulerian Hemispheric Model with focus on intercontinental transport. Atmos Environ 53: 156–176

Brandt J et al (2013) Contribution from the ten major emission sectors in Europe and Denmark to the health-cost externalities of air pollution using the EVA model system—an integrated modelling approach. Atmos Chem Phys 13:7725–7746

Fagerli H, Aas W (2008) Trends of nitrogen in air and precipitation: model results and observations at EMEP sites in Europe, 1980–2003. Environ Pollut 154:448–461

Geels C, Andersen HV, Ambelas Skjøth C, Christensen JH, Ellermann T, Løfstrøm P, Gyldenkærne S, Brandt J, Hansen KM, Frohn LM, Hertel O (2012) Improved modelling of atmospheric ammonia over Denmark using the coupled modelling system DAMOS. Biogeosciences 9:2625–2647. doi:10.5194/bg-9-2625-2012

Skjøth, Geels (2013) The effect of climate and climate change on ammonia emissions in Europe. Atmos Chem Phys 13:117–128

Sutton et al. (2011). The European Nitrogen Assessment. Cambridge University Press

Stevens et al (2010) Nitrogen deposition threatens species richness of grasslands across Europe. Environ Pollut 158(9):2940–2945

Chapter 76
Improved Modelling of Ammonia by Using Manure Transport Data

R. Kranenburg, C. Hendriks, J. Kuenen and M. Schaap

Abstract Accurate representation of ammonia emission patterns from agriculture in chemistry transport models (CTMs) is important for the evaluation and prediction of particulate matter episodes. The temporal variability of ammonia emissions from manure application is currently not well represented in CTMs. In this study we examine the use of Flemish manure transportation data to model the temporal variability in ammonia emissions from manure application and assess the impact on the LOTOS-EUROS model performance for ammonia and secondary inorganic aerosols (SIA). Manure transport data reflect national regulations as well as meteorological conditions influencing temporal manure application patterns. We used manure transport data from Flanders (Belgium) as a proxy to derive the emission variability of emissions from manure application. The temporal variability for livestock housing and mineral fertilizer is improved based on Skjøth et al. (2011). With the improved emission variabilities air quality simulations for north-western Europe for the period 2007–2011 were performed with the CTM LOTOS-EUROS at 7×7 km^2 resolution. Model performance was evaluated using two-weekly passive sampler data from 20 locations in Flanders. Model performance for ammonia improved by using meteorologically dependent temporal variability for ammonia, mainly by a better representation of the spring maximum. The improved performance is reflected in a smaller bias and 15–20% higher temporal correlation for all stations. Both improvements in temporal variability (livestock housing/fertilizer, and manure application) are important to increase the agreement between model and measurements. The impact on model performance for secondary inorganic aerosols (SIA) is negligible. Although the use of manure transport data as proxy for emissions from manure application comes with quite large uncertainties and simplifications, the developments provide a good starting point to improve representation of temporal variability of this source.

R. Kranenburg (✉) · C. Hendriks · J. Kuenen · M. Schaap
TNO, Department of Climate, Air and Sustainability, P.O. Box 80015
3508TA Utrecht, The Netherlands
e-mail: richard.kranenburg@tno.nl

C. Mensink and G. Kallos (eds.), *Air Pollution Modeling and its Application XXV*,
Springer Proceedings in Complexity, DOI 10.1007/978-3-319-57645-9_76

76.1 Introduction

Accurate representation of ammonia emission patterns from agriculture in chemistry transport models (CTMs) is important for the evaluation and prediction of particulate matter episodes. The temporal variability of ammonia emissions from manure application is currently not well represented in CTMs. In this study we examine the use of Flemish manure transportation data to model the temporal variability in ammonia emissions from manure application and assess the impact on the LOTOS-EUROS model performance for ammonia and secondary inorganic aerosols (SIA).

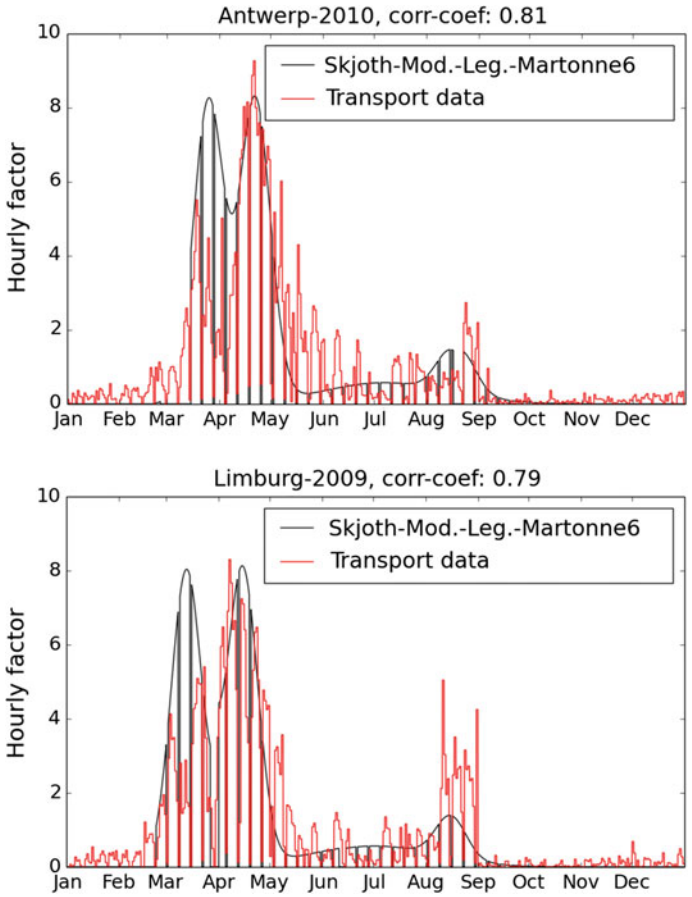

Fig. 76.1 Timing of ammonia emissions based on transport data and on the parametrization. *Upper panel* Antwerp-2010, *Lower panel* Limburg 2009

76.2 Method

In this study we made an improved temporal variation profile for ammonia emissions from manure applications. The basis of these profiles is based on Skjøth et al. (2011) with on top of that improvements with local regulations and extended use of meteorological conditions. For the Flanders situation we will validate the results with manure transport data from the Flemish government.

We have improved the method of Skjoth in three steps. (1) redistribute the peak emission moments over the year, (2) include local regulations, (3) use 'de Martonne' index to describe wet periods with no spreading of fertilizer.

In the method based on Skjoth, four emission peak moments are described (early spring, late spring, summer, autumn). Based on the manure transport data, we have defined the weights of each of those four peaks for the Flanders region. Second we have included that it is restricted to use fertilizer on Sundays and also between November 1st and February 15th. Last we have defined a weekly de Martonne index, which is the amount of rain in the last week divided by the (average temperature + 10). Analysis of the transport data, shows that if 'de Martonne' index is over 5, the spreading of fertilizer is postponed.

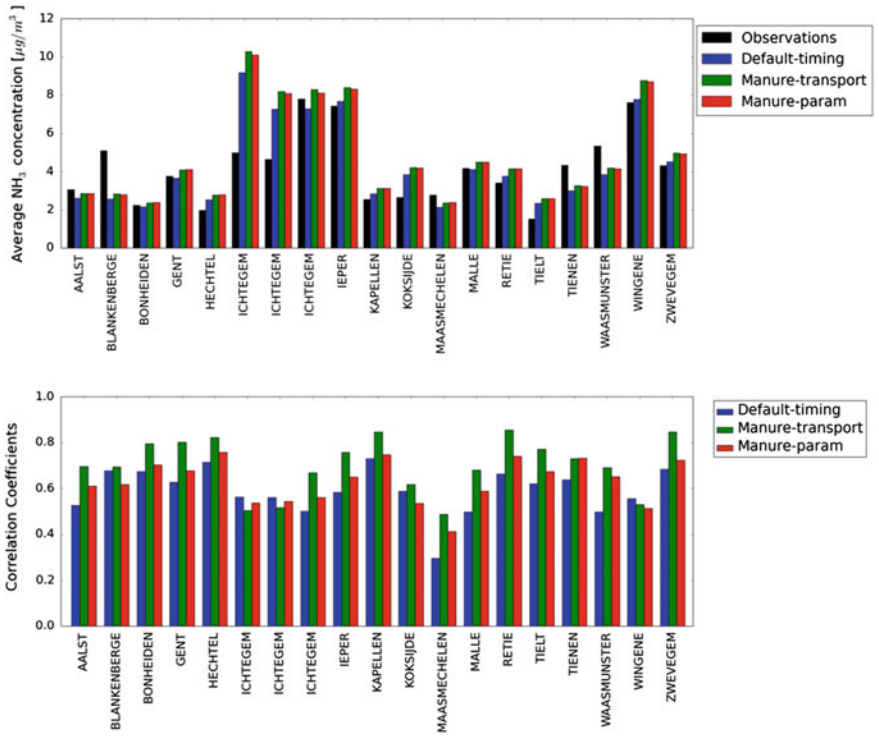

Fig. 76.2 Average concentrations (*upper panel*) and temporal correlations (*lower panel*) for ammonia in Flanders

In Fig. 76.1, we see for the province Antwerp in 2010 and for province Limburg in 2009, the timing of ammonia emissions based on the transport data and on the described parametrization. The timing of the peaks are well captured but sometimes we miss the full amplitude.

76.3 Results

With those new timings we have run our CTM-model LOTOS-EUROS. We did three runs, (1) a base run with default emission timing, (2) emission timing following transport data, (3) emission timing following the described parametrization. For 19 monitoring stations in Flanders we have calculated the annual average concentration and the temporal correlation coefficient between the measurements and the model results (see Fig. 76.2). In general we can see that the parametrization has a better correlation than the base model. The run with the transport data give, as expected, the best correlation but we cannot use this uniformly for every year or for other areas in Europe. The upper panel of the figure shows that he annual average concentration do not have any large differences between the three runs.

Acknowledgements The work presented here was financed by the Flemish Government, Department of Environment, Nature and Energy (reference: LNE/OL201200017).

Questions and Answers

Questioner: Peter Viaene

Question: (comment) You could probably improve the modelling of manure spreading by not only considering the rainfall, but also soiltypes. As the spreading is very different for different soiltypes depending on the amount of water in the soil type.

Answer: It will be a good idea to improve the timing of the manure emissions by taking care of the different soiltypes. As we know that due to rain the spreading will be delayed, it will be useful to investigate those delays for different soiltypes.

Reference

Skjøth CA, Geels C, Berge H, Gyldenkærne S, Fagerli H, Ellermann T, Frohn LM, Christensen J, Hansen KM, Hansen K, Hertel O (2011) Spatial and temporal variations in ammonia emissions —a freely accessible model code for Europe. Atmos Chem Phys 11:5221–5236. doi:10.5194/acp-11-5221-2011

Chapter 77
Airborne Emissions from Livestock Farms and Exposure of Nearby Residents using an Atmospheric Dispersion Model

H.A.M. Sterk, A.N. Swart, J.P.G. van Leuken, J.F. Schijven, A.J.A. Aarnink, I.M. Wouters, I. Janse, R.J. Wichink Kruit and W.A.J. van Pul

Abstract To estimate the exposure of local residents to substances emitted by livestock farms, we applied a dispersion model to calculate the air concentrations in the surroundings following from these emissions. At several livestock farms, indoor air measurements were performed to determine emission strengths, while ambient measurements were carried out to compare with model results. Measured substances were particulate matter (PM), endotoxins and micro-organisms. The dispersion model only simulated PM concentrations, which were used as a proxy to determine the dispersion concentrations of endotoxins and micro-organisms. For the living micro-organisms, the process of inactivation has to be taken into account. Here we describe the followed methodology and preliminary results.

77.1 Introduction

Since several years, there is an increased interest in the health of people living near livestock farms. Livestock farms emit particulate matter (PM) which may be accompanied by endotoxins and micro-organisms. Endotoxins (cell wall substances of micro-organisms) and PM are linked to respiratory health effects, such as

H.A.M. Sterk (✉) · A.N. Swart · J.P.G. van Leuken · J.F. Schijven · I. Janse · R.J. Wichink Kruit · W.A.J. van Pul
RIVM (National Institute for Public Health and the Environment), PO Box 1, 3720 BA Bilthoven, The Netherlands
e-mail: marina.sterk@rivm.nl

A.J.A. Aarnink
Wageningen Livestock Research, PO Box 338, 6700 AH Wageningen, The Netherlands

I.M. Wouters
IRAS (Institute for Risk Assessment Sciences, Utrecht University), PO Box 80178, 3508 TD Utrecht, The Netherlands

C. Mensink and G. Kallos (eds.), *Air Pollution Modeling and Its Application XXV*, Springer Proceedings in Complexity, DOI 10.1007/978-3-319-57645-9_77

pneumonia, asthma and COPD. Pathogenic micro-organisms could potentially cause infectious diseases, such as Q fever and avian flu. In the current research, we aim to estimate the exposure of residents near livestock farms through airborne emissions. We used the atmospheric dispersion model OPS (Operational Priority Substances, Sauter et al. 2016), developed by the National Institute for Public Health and the Environment (RIVM, The Netherlands).

As a first step, individual animal houses and surrounding concentrations are studied. Measurements of PM, endotoxins, and micro-organisms have been carried out in and nearby livestock farms. From the measured indoor concentrations and ventilation rates in animal houses, the emission strength was estimated. Subsequently, based on this emission, we calculate PM concentrations in the areas around the livestock farm with the OPS short-term (OPS-ST) dispersion model. This is a Gaussian plume model based on hourly meteorological data such that concentrations per hour can be simulated. As the dispersion of endotoxins and micro-organisms cannot be modelled directly, concentrations of endotoxins and micro-organisms are derived from the dispersion of PM. For this purpose, measured size fraction distributions of PM and the measured distribution of endotoxins and micro-organisms over PM are used. The derived concentrations of endotoxins and micro-organisms are compared with the results of field measurements. The process of inactivation will be included in the model to account for die-off of micro-organisms.

77.2 Methodology

77.2.1 Measurements

For this research, concentrations of PM, endotoxins and micro-organisms were studied at individual animal houses and their direct surroundings. Micro-organisms were studied by using cultivation-based techniques for the detection of viable bacteria (expressed as colony forming units: CFU) and PCR-based techniques for the detection of DNA derived from both living and dead bacteria. As livestock farming indicator micro-organisms, *Escherichia coli* and *Staphylococcus spp.* were selected. These micro-organisms serve as indicators to estimate potential spread of other, more pathogenic, micro-organisms which have similar properties relevant for their dispersal. Regarding the animal housing types; laying hen, broiler, sow, and growing-finishing pig farms were selected, as these farm types produce the largest emissions (Maassen et al. 2016).

Outside measurements took place on fixed distances from the livestock farms at approx. 100 m upwind (as indicator for the background concentrations), and approx. 25, 50 and 100 m (and occasionally 200 m) downwind. Measurements were also performed near the air exhaust of the animal houses to gain insight in the concentration levels inside the animal houses and to determine the emission strength. The emission strength was obtained by multiplying the concentrations with the actual ventilation rates.

Additionally, for some days, the particle size distribution of PM was determined as well as the distribution of micro-organisms (living plus dead material) and endotoxins over the different particle size classes.

77.2.2 OPS-ST Dispersion Model

The OPS-ST model is a short-term Lagrangian transport and deposition model, in which relations between individual sources and specific receptors are described by Gaussian plumes using hourly meteorological data (Sauter et al. 2016). Contrary to the long-term model, which uses long-term averaged meteorological data, the short-term model is highly suitable to compare output with short measurement campaigns, or to study the diurnal variation.

The main purpose of OPS is to calculate the concentration and deposition of pollutants such as PM, and acidifying compounds as SO_2, NO_x and NH_3 in the Netherlands. For each individual source, OPS calculates the concentrations due to dispersion and transport and by taking into account the chemical conversion and dry and wet deposition. For a certain location, the contributions of individual sources are summed to obtain the total concentration at that site.

77.2.3 Inactivation

The concentrations of particulate matter as calculated by OPS are influenced by the dispersion, transport, and deposition. In the case of airborne micro-organisms, the inactivation (or die-off) should be considered as well. This process is affected by environmental and meteorological conditions, mainly temperature, humidity and ultra violet radiation (Tang 2009).

To calculate concentrations including inactivation (C_{incl_inact}), this process is combined with the Gaussian plume equations as a first-order rate process with an exponential function of the distance (x), wind speed (u) and the inactivation rate λ with $C_{incl\_inact} = C \cdot \exp\left(-\lambda \frac{x}{u}\right)$, where C is the concentration after dispersion and transport (Van Leuken et al. 2016).

77.2.4 PM Particle Size Distribution and Conversion to Micro-Organisms and Endotoxins

In the OPS model, six particle size classes are taken into account for PM, namely: <0.95, 0.95–2.5, 2.5–4, 4–10, 10–20 and 20–50 (all in μm). The amount of PM is divided over these classes according to their mass fraction in each class. These particle size distributions (psd) differ per animal type and depend on the farm

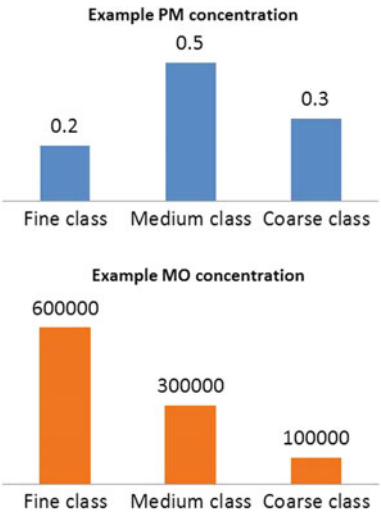

Fig. 77.1 Arbitrary example of the PM concentration (μg/m^3) and the according micro-organisms (MO) concentrations (organisms/m^3) for 3 size classes

housing type and feed as studied by Lai et al. (2014). For the moment, similar particle size distributions are assumed in this study, where the 30 classes studied by Lai et al. (2014) are clustered into the six particle size classes of OPS.

For some measurement days, the psd and the distribution of the micro-organisms and endotoxins over this PM were measured. At the time of writing this extended abstract, these data still need to be analyzed for further use.

A conversion needs to be made from the PM concentrations at a certain location to the concentrations of micro-organisms and endotoxins. As the OPS model keeps track of the individual concentrations per PM size class, we can use the relative fraction of micro-organisms as distributed over the PM psd measured in the farm. When, for instance (see example in Fig. 77.1) in the farm 0.2 μg/m^3 PM is measured in the finest class and 600000 micro-organisms are found in this class, this means we can use a conversion factor of 600000/0.2 = 3000000 micro-organisms/μg PM. Then we calculate the micro-organisms concentrations using the PM concentration field, assuming that the distribution of micro-organisms does not change over the PM distribution. Of course, the psd of PM does change after emission as particularly the heavier particles are more prone to deposition caused by sedimentation and are not as easily transported in air. Furthermore, inactivation of micro-organisms can now be implemented in OPS as a first order removal rate of PM.

77.3 Results

Some preliminary results of the comparison of one of the sampling days regarding the *Staphylococcus spp.* concentrations at a poultry farm are shown. For now we assumed a uniform distribution of the micro-organisms over the PM psd.

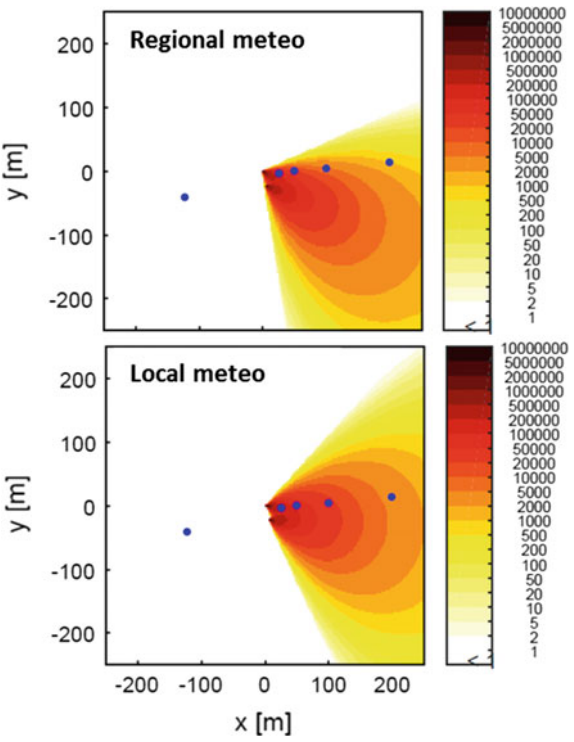

Fig. 77.2 Modelled plume of *Staphylococcus spp.* concentrations (CFU/m^3) at 1.5 m height for one of the sampling days at one particular hour. The dots indicate the location of the measurements. The *top figure* is with regional meteorology, the *bottom figure* with meteorology measured at the site

Figure 77.2 gives an example of the *Staphylococcus spp.* concentrations at a single time point for the area surrounding the farm. At this particular farm, two animal houses were present for which similar emissions are assumed. As such, an overlap of two plumes is visible. The importance of including local meteorology is also shown by the different direction of the plume when either regionally averaged meteorology is taken into account (top figure) or the meteorology as measured at that site (bottom figure).

Figure 77.3 shows the measured and modelled concentrations for the individual measurement sites for the case in Fig. 77.2. Three sets of simulations are shown: (a) without inactivation (these can be considered as maximum values), (b) including a first estimate of inactivation, and (c) including local measurements of meteorology on top of b. Regarding the measurements, it is clear that the background values were substantially lower than the downwind concentrations. Although concentrations decrease with distance from the animal houses, even at 200 m downwind concentrations are obviously elevated compared to the background values.

Regarding the model results, we see the stronger effect of inactivation with increasing distances due to that micro-organisms have been airborne for a longer time. When comparing the simulations with regional meteorology, this results in a stronger underestimation of the measurements compared to results without inactivation. Including the local measurements in the meteorological field enhances the

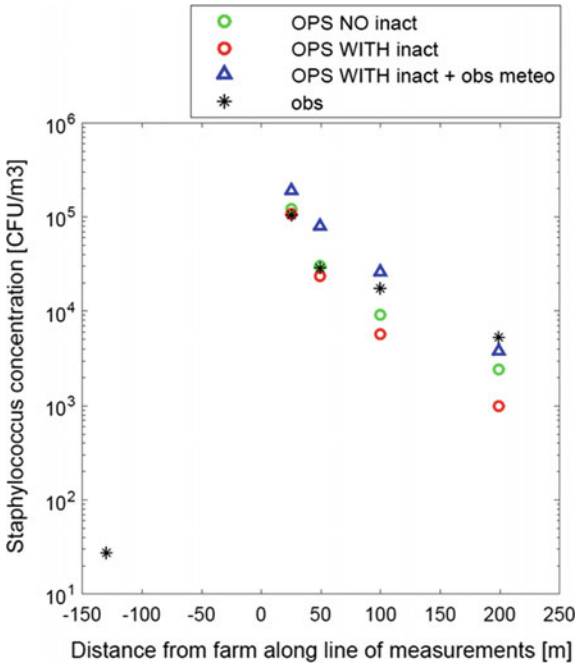

Fig. 77.3 Measured and modelled viable *Staphylococcus spp.* concentrations (CFU/m^3) at the different distances for the case as in Fig. 77.2. Modelled results are for **a** excluding inactivation, **b** including inactivation, and **c** including inactivation and meteorology as observed at the site

modelled concentrations, which now results in stronger overestimations near the source. In general though, the model results (note: still preliminary) agree reasonably well with the observations, yet model input parameters need to be evaluated.

77.4 Conclusions and Outlook

Measured and modelled concentrations of *Staphylococcus spp.* clearly decreased with distance from the animal house. Although there was a strong decrease in concentration with distance from the source, at 200 m distance substantially higher *Staphylococcus spp.* concentrations were found compared to the background observations. This was also found for other poultry farms. Preliminary simulations indicate the importance of including the inactivation of living micro-organisms, as well as the usage of accurate meteorology.

Further analyses regarding the comparison of the model with measurements have yet to be carried out, as well as for the other sampling days and other components (e.g. PM, micro-organisms and endotoxins).

As a next step, the simulations will be scaled up to create regional exposure maps. Furthermore, a QMRA (Quantitative Microbial Risk Assessment) model will be developed. This QMRA model takes several factors into account, such as the

human behavior (e.g. light/heavy activity), age, inhalation and the dose-response relation. By coupling the QMRA model with the concentrations in the ambient air (the exposure) as determined by the dispersion model OPS, an estimation of the health risks is obtained for the residents living nearby animal houses.

Acknowledgements This research is funded by the Ministry of Health, Welfare and Sport, the Ministry of Economic Affairs, and a subsidy of the Long fund (Longfonds, 3.2.11.022).

Questions and Answers

Questioner: Douw Steyn
Question: Your model evaluation approach, using a log concentration scale, seems unreasonably demanding. How much better (visually at least) would the model appear if you used a linear scale?
Answer: Indeed I also had to get used to using a log concentration scale, but this is actually very common in the science of micro-biology. As the amount of micro-organisms can decrease very rapidly, a linear scale would only show distinguishable output for very small distances close to the emission point, while we are also interested in concentrations further away.

Questioner: Heinke Schlünzen
Question: How did you consider the impact of the building on this close-to-scale dispersion and did you consider the heat emission resulting from the densely packed animal stock?
Answer: We do not consider the impact of the buildings as this is currently not available in the model, though we agree that this might impact the dispersion at these local scales. Therefore, for now, measurements were only performed on days with a certain wind direction criterion where the direction of the emissions had to be aligned with the wind direction to avoid a large influence of the building.

We also did not include the heat emission resulting from the densely packed animal stock. Though this is an option in the model, the actual heat emission was unknown, while furthermore we expect this to be more important for industrial sources with significantly higher temperatures.

Questioner: Jaakko Kukkonen
Question: Regarding the transport of micro-organisms in the atmosphere, it is challenging to model their viability, due to the large number of possible micro-organisms. There are millions of different species of micro-organisms, viruses and bacteria, some of which are harmless, some extremely hazardous. Would you like to comment, please?
Answer: Indeed, there are many, many micro-organisms with each different behavior regarding inactivation for example. In this study, several pathogenic micro-organisms were selected for which their presence in livestock farms was investigated. As indicator micro-organisms, which can occur in higher

concentrations and are therefore more easily measured, *Staphylococcus spp.* and *E. coli* were chosen. These represent two groups of bacteria, namely the gram positive (*Staphylococcus spp.*) and gram negative (*E. coli*) bacteria which have quite distinct characteristics. Gram positive bacteria have a thicker cell wall for instance and are therefore less easily inactivated.

To determine the inactivation rate, a literature study was carried out after which several results from literature were combined on which a regression analysis was performed to determine the function for the inactivation rate. This is hence based on more micro-organisms than just *Staphylococcus spp.* and *E. coli*, though of course not all existing micro-organisms can be included as there are simply way too many while additionally they may be difficult to measure. But by distinguishing between gram positive and gram negative bacteria, we do take into account an important characteristic of the micro-organism species. As such, the inactivation rate is also a function of the bacteria type, besides for example temperature.

References

Lai HTL, Aarnink AJA, Cambra-López M, Huynh TTT, Parmentier HK, Groot Koerkamp PWG (2014) Size distribution of airborne particles in animal houses. Agric Eng Int CIGR J 16(3):28–42

Maassen K, Smit L, Wouters I, Van Duijkeren E, Janse I, Hagenaars T, IJzermans J, Van der Hoek W, Heederik D (2016) Veehouderij en gezondheid omwonenden. RIVM, Bilthoven

Sauter F, Van Zanten M, Van der Swaluw E, Aben J, De Leeuw F, Van Jaarsveld H (2016) The OPS-model, description of OPS 4.5.0. http://www.rivm.nl/media/ops/OPS-model.pdf

Tang JW (2009) The effect of environmental parameters on the survival of airborne infectious agents. J R Soc Interface. doi:10.1098/rsif.2009.0227.focus

Van Leuken JPG, Swart AN, Havelaar AH, Van Pul A, Van der Hoek W, Heederik D (2016) Atmospheric dispersion modelling of bioaerosols that are pathogenic to humans and livestock—A review to inform risk assessment studies. Microbiol Risk Anal 1:19–39

Chapter 78
Air Quality Model-Based Methods for Estimating Human Exposures: A Review and Comparison

Haofei Yu, Armistead G. Russell, James A. Mulholland, Cesunica E. Ivey, Josephine T. Bates, Mariel D. Friberg, Ran Huang, Jennifer L. Moutinho and Heather A. Holmes

Abstract Determining estimates of human exposure is increasingly relying on the use of air quality models and satellite observations to provide spatially and temporally complete pollutant concentration fields. Air quality models, in particular, are attractive as they capture the emissions and meteorological linkages. Additionally they can provide source impact information and concentration fields for a range of species not currently provided from satellite-based observations (e.g., MODIS and MAIAC), and are not subject to cloud interference. Multiple methods based on air quality modeling (including using CMAQ and/or RLINE) with and without data fusion, have been developed and are being used in health studies as part of the EPA-funded Southeastern Center for Air Pollution and Epidemiology Clean Air Research Center. The methods include CMAQ-Data Fusion where concentrations fields are blended with observations to provide spatially and temporally complete pollutant concentrations fields of $PM_{2.5}$, EC, CO, and NO_2. To improve the spatial resolution, this method was extended to include RLINE fields for fine scale (250 m) exposure assessment. Another method was developed to estimate spatial exposure estimates of emissions source categories using CMAQ-derived source impacts for 16–32 sources, along with observations of individual PM species. Each of these

H. Yu · A.G. Russell (✉) · J.A. Mulholland · C.E. Ivey · J.T. Bates · M.D. Friberg · R. Huang · J.L. Moutinho
School of Civil and Environmental Engineering, Georgia Institute of Technology, Atlanta, GA, USA
e-mail: ted.russell@ce.gatech.edu; ar70@ce.gatech.edu

J.T. Bates
e-mail: jbates2019@gatech.edu

R. Huang
e-mail: rhuang48@gatech.edu

J.L. Moutinho
e-mail: jennifer.moutinho@gatech.edu

H.A. Holmes
Department of Physics, University of Nevada Reno, Reno, NV, USA

C. Mensink and G. Kallos (eds.), *Air Pollution Modeling and its Application XXV*, Springer Proceedings in Complexity, DOI 10.1007/978-3-319-57645-9_78

approaches have individual strengths and weaknesses. The methods that use a data fusion approach to blend observations and air quality model fields are found to best capture the spatiotemporal trends in the observations, reducing the standard error in the exposure estimates. In the past, such methods were limited by the availability of air quality model fields over long periods, but such fields are becoming more routinely available from air quality forecasting activities.

78.1 Introduction

Air pollution has been found to be linked with approximately 6.5 million premature deaths every year, and is considered to be the largest environmental health risk worldwide and a leading risk factor for global burden of disease (International Energy Agency (IEA) 2016). To appropriately quantify and effectively mitigate adverse health effects due to air pollution, human exposure to air pollution needs to be properly characterized.

Evolving from purely observational approaches, recent studies on air pollution exposures have relied on mechanistic air quality models to provide pollution concentration fields for exposure estimation purposes. Comparing with direct measurement and remote sensing based methods, air quality models are cost-effective, and do not suffer from non-retrieval issues due to cloud cover or instrument malfunctions, though suffer from other limitations. A wide range of air quality models have been applied in past studies, ranging from simple, zero-dimensional box model, to sophisticated three-dimensional models that incorporated complex physical and chemical algorithm. Among these models, two types of models have received the most attention: Gaussian dispersion models and Eulerian Chemical Transport Models (CTMs). In dispersion models, pollutant concentrations are generally estimated using the Gaussian plume equation, or similar formulation. Examples of dispersion models include AERMOD, RLINE and CALPUFF. Due to the nature of Gaussian plume equation, dispersion models are normally applied in small region. They are relatively easy to implement, and are capable of generating pollutant concentration fields that are highly resolved (down to dozens of meters). CTM models, on the other hand, are generally applied in regional to continental domains with grid size usually exceed 4 km. Examples of commonly used CTM models in the US including CMAQ and CMAx. Unlike dispersion models, which generally include none or limited chemistry reactions, CTM models have detailed representation of atmospheric chemistry built in which makes them ideal for the modeling of reactive or secondary pollutants.

Each air quality model has its own strengths and weaknesses. When applied in exposure estimation, the outcomes may be different and would reflect the models used. Hence, comprehensive cross-comparisons among different models are needed to better inform users regarding the appropriate choices of models. Furthermore, despite the usefulness of air quality models, caution should be taken before directly applying raw air quality model outputs in exposure estimation due to errors and

biases, which may vary by modeled species, season, and region of the modeling domain. The errors and biases are introduced in several ways, including emission data, and simplified mathematical formulations of both meteorological and air quality models. Substantial exposure misclassification may occur if air quality model results were not carefully evaluated. To address this issue, as part of the EPA-funded South-eastern Center for Air Pollution and Epidemiology Clean Air Research Center, three data fusion methods based on air quality models were developed. Results from the three data fusion methods, along with raw outputs from RLINE and CMAQ model, were evaluated and compared with each other. Strengths and weakness of different air quality model-based methods regarding their application in exposure assessments are discussed.

78.2 Methods

The focus area of this study is the metro-Atlanta region in the State of Georgia, USA (Fig. 78.1). The pollutants of interests are $PM_{2.5}$, EC, CO, and NO_2. The time period of this study is the entire year of 2011. Five methods were included here: RLINE, CMAQ, and three data-fusion methods. RLINE is a Gaussian stead-state dispersion model designed for near-road air pollution assessments. Hourly input meteorological data to the RLINE model were collected at Hartsfield-Jackson Atlanta International Airport, and input emission data at roadway link level were provided by Atlanta Regional Commission. Only on-road mobile emission sources were included in RLINE modeling. CMAQ is a CTM model commonly used for regulatory air quality modeling practices in the US and the modeling results are provided by the US Environmental Protection Agency with 12 km spatial resolution. The three data fusion methods adopted here including (1) A CMAQ-obs method that strategically blend air quality model outputs with observational data to correct for model errors and biases; (Friberg et al. 2016) (2) A CMAQ-RLINE-obs method that further blend CMAQ-obs results with RLINE results to improve spatial

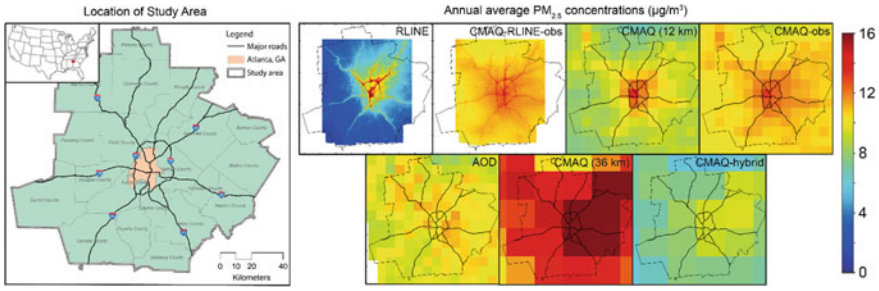

Fig. 78.1 The study area of Atlanta, Georgia. USA, and annual average $PM_{2.5}$ concentrations from the five selected methods

resolution of modeled pollutant concentrations; (Bates 2015) and (3) A CMAQ-hybrid method that simultaneously adjust source impact fields obtained from CMAQ simulations using observations of individual PM species (Ivey et al. 2015). Due to data availability, source impact fields from 36 km CMAQ modeling results were used, and 16 source categories and 37 species were included. Further details of each method are described in corresponding references.

78.3 Results and Discussion

Figure 78.1 also provides spatial plots of annual average $PM_{2.5}$ concentrations from the five selected methods (Results for EC, CO and NO_2 not shown). For comparison purposes, the results from satellite AOD and 36 km CMAQ modeling results used in CMAQ-hybrid method are also presented in Fig. 78.1. Additionally, results from the five methods were evaluated using 10 statistical metrics at one monitoring site located near downtown Atlanta area, and the results are shown in Table 78.1.

Table 78.1 Statistical evaluations of the five method included in this study

Metrics[a]	RLINE	CMAQRLINEobs[a]	CMAQ (12 km)	CMAQobs[a]	CMAQ (36 km)	CMAQhybrid[b]
MB ($\mu g/m^3$)	−6.82	1.93	2.61	2.14	5.32	−1.68
ME ($\mu g/m^3$)	6.82	1.96	3.96	2.28	7.58	3.96
RMSE ($\mu g/m^3$)	7.96	2.30	5.24	2.93	9.36	5.33
MNB (%)	−62	17	31	21	66	−5
MNE (%)	62	18	40	22	80	35
NMB (%)	−65	17	24	19	48	−15
NME (%)	65	18	36	21	68	36
MFB (%)	−94	16	21	18	35	−15
MFE (%)	94	16	31	19	53	38
R^2	0.17	0.96	0.43	0.87	0.09	0.14

[a]*MB* mean bias; *ME* mean error; *RMSE* root mean squared error; *MNB* mean normalized bias; *MNE* mean normalized error; *NMB* normalized mean bias; *NME* normalized mean error; *MFB* mean fractional bias; *MFE* mean fractional error; R^2 correlation coefficient between modeled and measure concentrations

[b]Leave-one-out assessment results

The impact of on-road mobile sources on $PM_{2.5}$ concentrations are apparent from RLINE and CMAQ-RLINE-obs results (Fig. 78.1), but not captured as well by other methods with large grid sizes (12 and 36 km). Such results are expected given the high spatial resolution of RLINE results (500 m). In addition, CMAQ-RLINE-obs results show generally elevated $PM_{2.5}$ concentrations compared with raw RLINE results. This is because only on-road mobile source emissions were included in RLINE modeling, while in CMAQ modeling, all source categories were included. The CMAQ-RLINE-obs fusion method also significantly increased statistical performances of either RLINE or CMAQ model for all 10 metrics (Table 78.1. e.g., R^2 increased from 0.17 (RLINE) to 0.96). For the purpose of exposure estimation, high resolution concentration data are generally preferred. Dispersion models such as RLINE are able to generate pollution fields in high resolution, but lack the capability of accounting for critical atmospheric chemistry processes, which can be addressed using CTM models such as CMAQ. The CMAQ-RLINE-obs method successfully integrated the strengths of both models by fusing their results and also corrected biases and errors associated with raw modeling outputs.

Between CMAQ and CMAQ based data fusion methods (12 km CMAQ and CMAQ-obs, 36 km CMAQ and CMAQhybrid), spatial concentration patterns are similar but concentration levels are different (Fig. 78.1). This finding is also expected since data-fusion method essentially adjust raw CMAQ concentration levels to correct for biases and errors. Between 12 and 36 km CMAQ results, however, $PM_{2.5}$ concentration levels and spatial patterns are different. Lower resolution results (36 km) show overall higher annual average $PM_{2.5}$ concentrations in the study domain, while the locations for the highest concentrations also shifted from downtown Atlanta region (12 km CMAQ) to right side of the domain (36 km CMAQ). Such disparities are likely due to differences in input emission and meteorological data, as well as model configurations. Data fusion methods (CMAQ-obs and CMAQ-hybrid) also improved performance of raw CMAQ outputs, even when using leave-one-out assessment (Table 78.1). Furthermore, spatial patterns of $PM_{2.5}$ concentrations of the AOD method are somewhat similar with results of CMAQ and CMAQ based data fusion methods, though missing data are likely to occur in AOD method as the results of non-retrievals. It is also worth mentioning that, compared to other methods, one of the unique strengths of the CMAQ-hybrid method is the capability of simultaneously adjusting concentrations of many species (37 in this case) from multiple emission source categories (16 in this study) while considering mass balance. Such capability are useful for identifying and controlling important emissions sources for regulatory purposes.

Acknowledgements This work was funded, in part, by the Electric Power Research Institute and the U.S. Environmental Protection Agency (Grant RD834799). Its contents are solely the responsibility of the grantee and do not necessarily represent the official views of the funding entities. Further, the funding entities do not endorse the purchase of any commercial products or services mentioned in the publication. Observational data and logistical support were provided by Atmospheric Research Associates.

Questions and Answers

Questioner: Heinke Schlunzen
Question: How did you avoid double counting of emissions? How did you avoid to completely adjust to the measured data and thus have no independent measurement to compare with?
Answer: The fields are "calibrated" to the observations, so the resulting fields are used as informed (i.e., consistent with our estimates of emissions, the meteorology, and chemistry) interpolations, providing information between observation sites. The general magnitude of the base field is captured by the observations themselves. Calibration removes the direct link to the specific magnitude of the emissions. In terms of not using the observations in both the calibration and evaluation, we used leave-one-out cross validation, which is very common in the exposure science field. The method being tested is applied totally leaving one measurement out. The pollutant exposure field is developed, and the value at the monitor location is compared with the withheld value. This is done exhaustively (all monitors) and statistical evaluation is conducted for the resulting set of observed concentrations to those developed without using that observation at all. As discussed in a prior talk by Ran et al. (2016), you can extend this approach to account for spatial groupings of monitors.

Questioner: Ari Karppinen
Question: Would be interested in knowing some details of the model connecting AOD and surface level $PM_{2.5}$, as it seems to be working extremely well.
Answer: The AOD-based methods used in the health communities are very evolved. The regression analysis used allows for regression coefficients that are spatially and temporally varying, and they also use the observations and other inputs (observed meteorology). Thus, it is not like a typical approach used in atmospheric sciences where the relationship is based on PM levels and aerosol characteristics alone. More details on various AOD approached can be found in a variety of publications including Chang et al. (2014) (used here), Lv et al. (2016) and Schwartz et al. (2015):

Chang, H. H., Hu, X., & Liu, Y. (2014). Calibrating MODIS aerosol optical depth for predicting daily PM2.5 concentrations via statistical downscaling. J Expos Sci Environ Epidemiol, 24(4), 398–404. doi:10.1038/jes.2013.90.

Lv, B., Y. Hu, H. H. Chang, A. G. Russell and Y. Bai (2016). "Improving the Accuracy of Daily PM2.5 Distributions Derived from the Fusion of Ground-Level Measurements with Aerosol Optical Depth Observations, a Case Study in North China." Environmental Science & Technology 50(9): 4752–4759.

Kloog I, Koutrakis P, coull BA, Lee HJ, Schwartz J. Assessing Temporally and Spatially Resolved PM2.5 Exposures for Epidemiological Studies using Satellite Aerosol Optical Depth Measurements. Atmospheric Environment 2011; 45: 6267–6275.

References

Bates (2015) Comparison of two downscaling techniques going from 12-km to 250 M resolution. Paper presented at the 14th annual community modeling and analysis (CMAS) conference, Chapel Hill, NC

Friberg et al (2016) Method for fusing observational data and chemical transport model simulations to estimate spatiotemporally resolved ambient air pollution. Environ Sci Technol 50(7):3695–3705

International Energy Agency (IEA) (2016) World energy outlook special report 2016: energy and air pollution. International Energy Agency, Paris, France

Ivey et al (2015) Development of PM 2.5 source impact spatial fields using a hybrid source apportionment air quality model. Geosci Model Dev 8(7):2153–2165

Chapter 79
Source Impacts on and Cardiorespiratory Effects of Reactive Oxygen Species Generated by Water-Soluble $PM_{2.5}$ Across the Eastern United States

Josephine T. Bates, Rodney J. Weber, Joseph Abrams, Vishal Verma, Ting Fang, Cesunica Ivey, Cong Liu, Mitchel Klein, Matthew J. Strickland, Stefanie E. Sarnat, Howard H. Chang, James A. Mulholland, Paige E. Tolbert and Armistead G. Russell

Abstract It is hypothesized that $PM_{2.5}$ with high oxidative potential (OP) can catalytically generate reactive oxygen species (ROS) in excess of the body's antioxidant capacity, leading to oxidative stress. Therefore, two advanced methods for conducting source apportionment, along with field experiments characterizing air quality, are used to identify the sources of $PM_{2.5}$ with high OP and relate them to acute health effects. The field study measured OP of ambient water-soluble $PM_{2.5}$ using a dithiothreitol (DTT) assay at four sites across the Southeastern United States from June 2012 to June 2013. Source apportionment was performed on collocated

J.T. Bates (✉) · C. Ivey · C. Liu · J.A. Mulholland · A.G. Russell
School of Civil and Environmental Engineering, Georgia Institute of Technology, Atlanta, GA, USA
e-mail: jbates2019@gatech.edu

A.G. Russell
e-mail: ar70@ce.gatech.edu

R.J. Weber · T. Fang
School of Earth and Atmospheric Sciences, Georgia Institute of Technology, Atlanta, GA, USA

J. Abrams · M. Klein · M.J. Strickland · S.E. Sarnat · P.E. Tolbert
Department of Environmental Health, Rollins School of Public Health, Emory University, Atlanta, GA, USA

H.H. Chang
Department of Biostatistics and Bioinformatics, Rollins School of Public Health, Emory University, Atlanta, GA, USA

V. Verma
Department of Civil and Environmental Engineering, University of Illinois at Urbana-Champaign, Champaign, IL, USA

C. Liu
School of Energy and Environment, Southeast University, Nanjing, China

C. Mensink and G. Kallos (eds.), *Air Pollution Modeling and its Application XXV*, Springer Proceedings in Complexity, DOI 10.1007/978-3-319-57645-9_79

speciated $PM_{2.5}$ samples using the Chemical Mass Balance Method with ensemble-trained profiles in Atlanta, GA and CMAQ-DDM for Atlanta and all other measurement sites (Yorkville, GA, Centerville, AL, and Birmingham, AL). Source-OP relationships were investigated using least squares linear regression. The model for Atlanta, GA was applied to $PM_{2.5}$ source impacts from 1998–2010 to estimate long-term trends in ambient $PM_{2.5}$ OP for use in population-level acute epidemiologic studies. Biomass burning contributes the largest fraction to total historical OP in Atlanta, followed by light-duty gasoline vehicles and heavy-duty diesel vehicles (43%, 22% and 17%, respectively). Results find significant associations between estimated OP and emergency department visits related to congestive heart failure and asthma/wheezing attacks, supporting the hypothesis that $PM_{2.5}$ health effects are, in part, due to oxidative stress and that OP is a useful indicator of $PM_{2.5}$ health impacts. Finally, controlling $PM_{2.5}$ sources with high OP, like biomass burning, may help prevent acute health effects.

79.1 Introduction

$PM_{2.5}$ mass concentration has been linked to a variety of cardiorespiratory effects (Pope et al. 2009). However, due to the heterogeneity of mixture of species arising from various sources and complex chemistry, the underlying biological mechanisms driving the association between $PM_{2.5}$ and health are not known. This work investigates the hypothesis that $PM_{2.5}$ can induce oxidative stress by catalytically producing reactive oxygen species (ROS) in excess of the body's antioxidant capacity after inhalation by using population-level analyses of acute health effects on a novel measure of $PM_{2.5}$ oxidative potential (OP), or ROS-generating potential. Further, this study expands upon previous research that identified bulk species, like organic carbon, to have high OP by investigating the relationship between emissions sources and OP. Identifying these sources and providing better health indicators for $PM_{2.5}$ facilitates the optimization of air pollution control strategies aimed at minimizing acute health effects.

79.2 Methods

$PM_{2.5}$ samples were collected at four locations (Jefferson street (JST) in Atlanta, GA, Yorkville, GA, Birmingham, AL, and Centerville, AL) using a HiVol, Thermo Anderson, nondenued sampler with prebaked $8 \times 10''$ quartz filters. JST represents a fixed site with 196 23 h integrated samples (midnight to 11 a.m.) from June 2012 to April 2013, while a trailer rotated between the other measurement sites each month between June 2012–June 2013 taking 23 h integrated samples. A semi-automated acellular dithiothreitol (DTT) assay was used to measure the OP of water-soluble filter extracts from these samples (Verma et al. 2014). The water-soluble fraction was used because it is believed to be more biologically available. In brief, an extract is

combined with 100 μM of DTT. Then the concentration of DTT is measured at specific time steps. DTT acts as an acellular surrogate to NADPH, so as DTT reacts to form a byproduct, ROS are formed; therefore, the rate of DTT destruction (in nmol min^{-1} m^{-3}) is proportional to the rate of ROS generation, or OP. A linear slope parameter created from the DTT measurements over time represents the OP (nmol min^{-1} m^{-3}) of the sample (Cho et al. 2005).

Source apportionment was performed using the Chemical Mass Balance Method (CMB) with ensemble-based profiles at JST (Balachandran et al. (2012). The CMB profiles require total concentrations rather than water-soluble fractions, so collocated measurements taken at the same time as the DTT filter measurements of 24 h integrated total $PM_{2.5}$ concentration, organic carbon, elemental carbon, sulfate, nitrate, ammonium, and metals were used. Details on measurement methods can be found in Hansen et al. (2003, 2006), and Edgerton et al. (2005). The CMB sources and species identified include light-duty gasoline vehicles (LDGV), heavy-duty diesel vehicles (HDDV), soil dust (SDUST), biomass burning (BURN, mostly prescribed burning in Atlanta (Tian et al. 2009)), ammonium sulfate (AMSULF), ammonium bisulfate (AMBSULF), ammonium nitrate (AMNITR), and not otherwise apportioned organic carbon (OTHER_OC), most likely related to aged biogenic emissions. Furthermore, 15 CMAQ-DDM3D/PM sources were created using a hybrid chemical transport-receptor model approach for JST and all other measurement sites (Hu et al. 2014).

Sources were related to OP using correlation analyses and least squares linear regression with sources as the independent variables and measured OP as the dependent variable. Using a backward selection approach, any source with a coefficient with a p-value of the F-statistic >0.05 was removed from the regression to prevent overfitting from sources that do not significantly contribute to total OP (Bates et al. 2015). Further, lab experiments showed that AMSULF is not significantly DTT active, so it was also removed from the OP regression (Bates et al. 2015).

The final model was applied to simulated daily CMB source impacts in Atlanta, GA from August 1998–December 2009 to estimate historical ambient OP and seasonal trends in source contribution to OP. Furthermore, time series analyses were used with this historical estimation to characterize the relationship between emergency department visits related to cardiorespiratory distress and ambient estimated OP and measured $PM_{2.5}$. Methods on these analyses can be found in Strickland et al. (2010), Winquist et al. (2015), and Gass et al. (2015).

79.3 Results and Discussion

The following regression relates CMB source impacts and measured OP in Atlanta, GA:

$$\mathrm{OP} = 0.066 + 0.12 * \mathrm{LDGV} + 0.061 * \mathrm{HDDV} + 0.074 * \mathrm{BURN}$$

$$R^2 = 0.49;\ \text{mean squared error} = 0.013\ \text{nmol}\ \text{min}^{-1}\ \text{m}^{-3}\ (4.0\%\ \text{of mean of measurements})$$

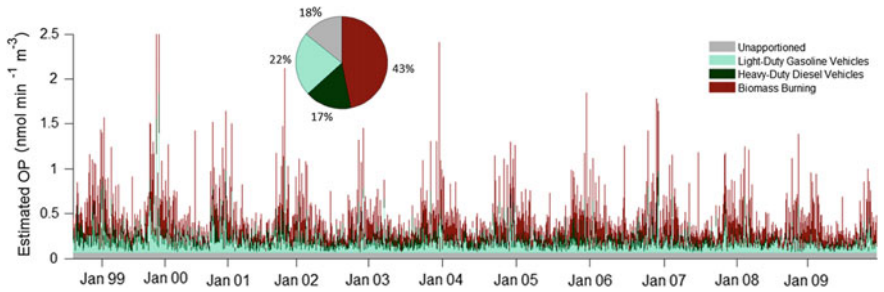

Fig. 79.1 Source contributions to daily estimated ambient OP in Atlanta, GA from 08/1998 to 12/2009

OP acts as a multipollutant, multisource indicator with the coefficients in the model representing intrinsic OP in nmol min^{-1} μg^{-1}_{source}. LDGV exhibits the highest intrinsic activity, mostly likely driven by metals (like copper) and organic carbon, followed by BURN, which has a high oxygenated organic carbon fraction, and HDDV, which also contains metals and organic carbon. The exclusion of sulfate and biogenic species suggests that these sources do not significantly contribute to total OP. The high intercept could be related to missing sources or organic carbon artifacts present on the nondenuded DTT filters but not on the denuded filters used for measurements for CMB source apportionment.

Figure 79.1 illustrates the historical trend in daily ambient OP in Atlanta, GA as estimated using the regression. This time series shows a strong seasonal trend in estimated OP, which is also apparent in the measurements, with higher values in the winter driven by prescribed burning and lower values in the summer, when prescribed burning is illegal. Additionally, the overall contributions of each source over the entire time period are 43%, 22%, and 17% (standard deviations: 16%, 11% and 11%) for BURN, LDGV, and HDDV, respectively, further illustrating the importance of BURN for OP.

Figure 79.2 illustrates the estimated risk ratios for lag 0–7 exposure (exposure over 8 days) to estimated OP and measured $PM_{2.5}$ in the 5-county Atlanta area from January 1999 to December 2009. These graphs show elevated risk for congestive heart failure and asthma/wheezing attacks after being exposed to $PM_{2.5}$ with high OP. Additionally, in two-pollutant models with exposure to both OP and $PM_{2.5}$, used to estimate the effect of one pollutant while controlling for the other, OP remains significantly associated with these acute health effects while $PM_{2.5}$ does not. These results support the hypothesis that oxidative stress is a plausible biological mechanism driving, in part, health effects due to $PM_{2.5}$ exposure. Additionally, this work supports the use of OP, as measured using a DTT assay, as a useful multipollutant, multisource health indicator complimentary to $PM_{2.5}$ mass. Future health studies will be performed at other locations across the Eastern United States using OP estimates from a regression developed using CMAQ-DDM source impacts. Controlling and understanding sources with high OP, such as biomass

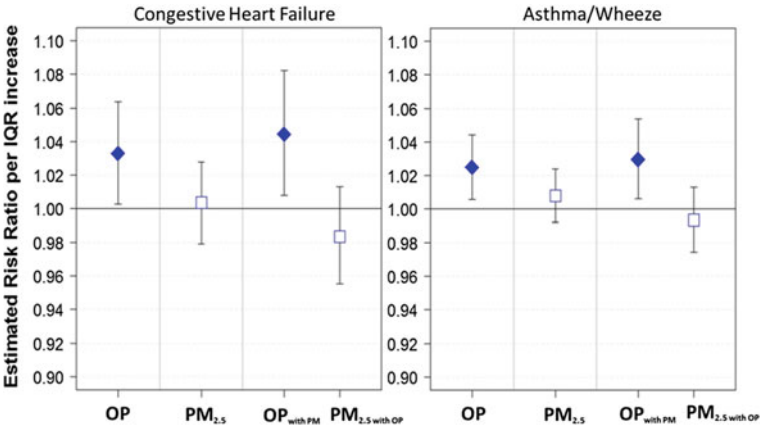

Fig. 79.2 Lag 0–7 risk ratios for estimated OP and measured $PM_{2.5}$ in Atlanta, GA

burning and vehicle emissions, may be critical for preventing acute cardiorespiratory effects from $PM_{2.5}$.

Acknowledgements This work was funded, in part, by U.S. Environmental Protection Agency under Grants RD834799, RD83096001, RD83107601 and RD83215901. Its contents are solely the responsibility of the grantee and do not necessarily represent the official views of the US EPA. Further, the US EPA does not endorse the purchase of any commercial products or services mentioned in the publication. Observational data and logistical support was provided by Atmospheric Research & Analysis, Inc.

Questions and Answers

Questioner: Peter Viaene.
Question: Is there any specific reason why you couldn't/didn't include all source types? Isn't there a risk of missing indirect effects these other sources could have on your results?
Answer: For the source apportionment step, we used all available sources with profiles for CMB in Atlanta and 15 relevant sources developed for CMAQ-DDM. In the regression modelling, there are two main reasons that sources were removed from the model, one statistical and one physical. First, we wanted to avoid overfitting of the model by removing coefficients that were not statistically significant. Second, we wanted to investigate which sources contributed the most to OP and thus be used to simulate OP of ambient $PM_{2.5}$ by removing sources without significant impact and analyzing how the results changed. Removing these sources did not change the R^2 of the model significantly.

References

Balachandran et al (2012) Ensemble-trained source apportionment of fine particulate matter and method uncertainty analysis. Atmos Environ 61:387–394

Bates et al (2015) Reactive oxygen species generation linked to sources of atmospheric particulate matter and cardiorespiratory effects. Environ Sci Technol 49(22):13605–13612

Brunekreef B, Holgate ST (2002) Air pollution and health. Lancet 360(9341):1233–1242

Cho et al (2005) Redox activity of airborne particulate matter at different sites in the Los Angeles Basin. Environ Res 99(1):40–47

Delfino et al (2005) Potential role of ultrafine particles in associations between airborne particle mass and cardiovascular health. Environ Health Perspect 113(8):934–946

Edgerton et al (2005) The southeastern aerosol research and characterization study: Part II. Filter-based measurements of fine and coarse particulate matter mass and composition. J Air Waste Manage Assoc 55(10):1527–1542

Fang T, Verma V, Guo H, King LE, Edgerton ES, Weber RJ (2015) A semi-automated system for quantifying the oxidative potential of ambient particles in aqueous extracts using the dithiothreitol (DTT) assay: results from the southeastern center for air pollution and epidemiology (SCAPE). Atmos Meas Tech 8(1):471–482

Gass et al (2015) Ensemble-based source apportionment of fine particulate matter and emergency department visits for pediatric asthma. Am J Epidemiol 181(7):504–512

Hansen et al (2003) The southeastern aerosol research and characterization study: Part 1-overview. J Air Waste Manage Assoc 53(12):1460–1471

Hansen et al (2006) Air quality measurements for the aerosol research and inhalation epidemiology study. J Air Waste Manage Assoc 56(10):1445–1458

Hu Y, Balachandran S, Pachon JE, Baek J, Ivey C, Holmes H, Odman MT, Mulholland JA, Russell AG (2014) Fine particulate matter source apportionment using a hybrid chemical transport and receptor model approach. Atmos Chem Phys 14(11):5415–5431

Pope et al (2009) Fine-particulate air pollution and life expectancy in the United States. N Engl J Med 360 (4):376–386

Strickland et al (2010) Short-term associations between ambient air pollutants and pediatric asthma emergency department visits. Am J Respir Crit Care Med 182(3):307–316

Tian et al (2009) Assessment of biomass burning emissions and their impacts on urban and regional PM2.5: a Georgia case study. Environ Sci Technol 43(2):299–305

Verma et al (2014) Reactive oxygen species associated with water-soluble PM2.5 in the southeastern United States: spatiotemporal trends and source apportionment. Atmos Chem Phys 14(23):12915–12930

Winquist et al (2015) Impact of ambient fine particulate matter carbon measurement methods on observed associations with acute cardiorespiratory morbidity. J Expo Sci Environ Epidemiol 25(2):215–221

Chapter 80
The Dust Cycle in the Arabian Peninsula and Its Role in the Urban Air Quality

P. Patlakas, J. Kushta, E. Drakaki, J. Al Qahtani, I. Alexiou, N. Bartsotas, C. Spyrou and G. Kallos

Abstract The dust cycle plays an important role in the atmospheric processes. The levels of dust concentration in the Arabian cities are quite high, a fact that affects air quality. A better understanding of this phenomenon may lead in reduced impacts. Towards this direction, an integrated modeling approach has been selected and applied in SW Saudi Arabia. More specifically, we discuss the characteristics of the dust production processes using the RAMS/ICLAMS multiscale model. A series of very high resolution simulations have been performed and potential mitigation actions are discussed. A reduction in dust concentration is evident by changing the landscape characteristics. Extreme dust events affect the study areas despite the tested activities and changes. A characteristic example is the "haboobs".

80.1 Introduction

It is well known that dust affects air quality because it increases dramatically the particulate concentrations. The levels of dust concentration in the Arabian cities are quite high during most of the days of the year. The most important factor affecting dust production is the soil characteristics (soil composition, physical and chemical properties, water content, temperature etc.). The most known, small-scale, production mechanism is saltation-bombardment. This mechanism governs the uptake of dust particles up to about 10 μm. The other controlling factors are wind speed

P. Patlakas · J. Kushta · E. Drakaki · N. Bartsotas · C. Spyrou · G. Kallos (✉)
School of Physics, University of Athens, University of Athens Campus,
Bldg. Phys-V, 15784 Athens, Greece
e-mail: kallos@mg.uoa.gr

J. Al Qahtani · I. Alexiou
Saudi Aramco, Dhahran, Saudi Arabia

C. Mensink and G. Kallos (eds.), *Air Pollution Modeling and Its Application XXV*,
Springer Proceedings in Complexity, DOI 10.1007/978-3-319-57645-9_80

and turbulence. Weather conditions affecting dust production/transport/deposition are of multi-scale, ranging from small surface inhomogeneities to mesoscale and large-scale systems.

The main objective of this work is to study the perturbations of the locally-producing dust mechanisms and the potential mitigation actions for an area under consideration. The tool used for this study is the RAMS/ICLAMS multiscale modeling system (Solomos et al. 2011; Kushta et al. 2014) with a fully coupled dust sub-model. The area under consideration is the SW Saudi Arabia. A series of very-high resolution simulations have been performed and potential mitigation actions are discussed.

80.2 Soil and Vegetation Impact on Dust Concentration Over a Limited Area

The study area is in the SW part of the Kingdom of Saudi Arabia—the Jizan Region. The selection is made for its characteristics. It is a coastal area with a salted soil strip of 1–2 km followed by a high-dust productivity area and then by a mountainous range. The area is also affected by meso-γ scale phenomena such as the haboobs (Solomos et al. 2011) and meso-β scale ones like the "Tokar Gap Jet" (Davis et al. 2015).

Several configurations were tested to assess the potential impact of urbanization and landscape change procedures (e.g. vegetation cover) in the selected area. The simulations were performed for selected cases during the warm period of the year.

- Case 1 represents the Control Run.
- Case 2 represents patches of urban (70%) and desert characteristics (30%).
- Case 3 has the same characteristics as in second but with more vegetation (evergreen shrub).
- Case 4 is the same as case 3 but the vegetation is trees.
- Case 5 is a larger area covered with patches of urban (90%) and semi-desert (10%) surrounded by patches of desert (90%) and semi-desert (10%).
- Case 6 has the same core as case 5 but the surrounding area is covered by vegetation (shrub, 100%) (Fig. 80.1).

As seen in Fig. 80.2, the reduction in dust concentration over the area of interest is negligible near the coast (that has no local production of dust) but very significant a few kilometers inland (nearly 100%). The changes in land use will impact distant areas also according to the wind flow. No major changes were observed using different types of vegetation.

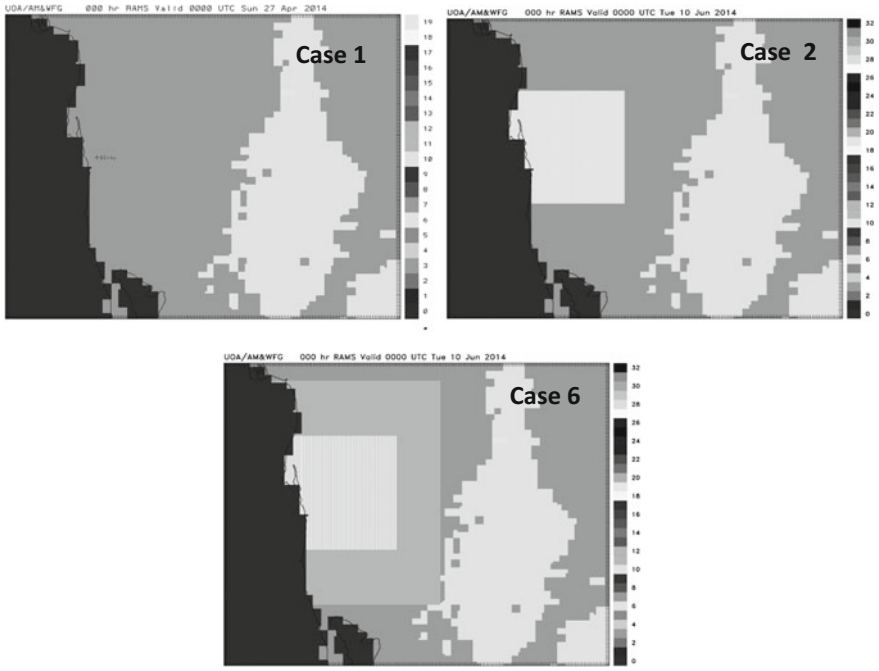

Fig. 80.1 The model setup for case studies 1, 2 and 6 which was used for the estimation of the impact of urbanization

80.3 Locally-Produced/Long-Range Transported Dust

In the second part of this study, the contribution of African Dust over KSA has been assessed with the use of two simulations: one including dust sources in Africa (RUN1) and the second excluding them (RUN2). The domain used has a spatial resolution of 9 km. Six months have been simulated: March, April, June, July, August and September of 2014. The contribution of mineral dust from East Africa on the West Coast of KSA is quantified by the difference in the two runs. In Fig. 80.3 this difference is assessed in the vertical; showing the contribution of African sources on dust concentration up to 7 km height.

During March and April the African dust seems to dominate in the area of interest while during June it plays a significant role only during the last days. A mechanism explaining these dust outbreaks is the "Tokar Gap Jet". This behavior is stretched over July and August as the contribution is enhanced and is reversed again in September. In September the sources of dust that affect the area of interest are rather inland KSA sources. As seen in Table 80.1 the contribution of African sources to Jazan Province dust concentration has a seasonal variation.

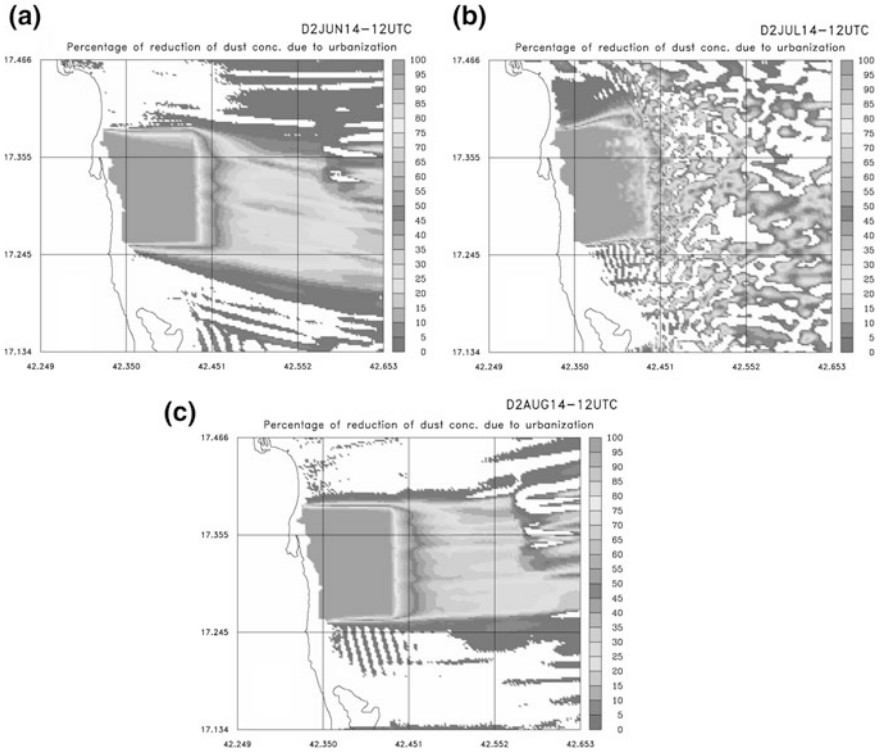

Fig. 80.2 Difference in near surface dust concentration between the control run and the second case for June (**a**), July (**b**) and August (**c**)

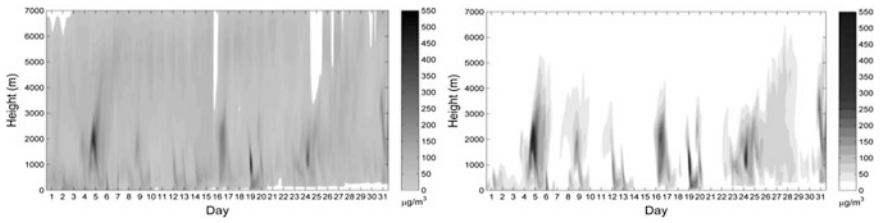

Fig. 80.3 Time-height distribution of dust concentration over the study area on July 2014 (*left plot*) and relative contribution of African dust sources calculated as Dust with African—Dust without African Sources (*right plot*)

The contribution of KSA versus non—KSA dust sources has been assessed and quantified in a similar way. The integrated dust concentration from the surface to the top of the atmosphere (dust load) has been calculated. The contribution from the external sources is significant in the coastal areas of the Arabian Peninsula,

Table 80.1 Contribution in percentage of African sources on the dust concentration over JEC

Month of simulation	Mean monthly local dust (μgm^{-1})	Mean monthly LRT dust (μgm^{-1})	Mean monthly total dust (μgm^{-1})	Contribution of African sources (%)
March	15.4	69.4	84.8	71
April	20.4	39.9	60.3	52
June	39.3	18.2	57.5	34
July	22.8	48.3	71.1	66
August	14.5	57.7	72.2	78
September	30.9	14.2	45.1	32

especially in the eastern part. In the central and western parts 20% of the total dust load can be attributed to sources outside SA.

Dust particles follow the synoptic weather patterns and general atmospheric circulation. For example, in August the area is affected mostly by dust originating from Iran, whereas in May it remains almost unaffected by external sources. However, the seasonal variability of the dust load seems to be more intense in the eastern part of the Peninsula.

In order to better understand the seasonal variability of dust concentration, the monthly-average dust load contribution in Jazan, Dhahran, Riyadh and Jeddah have been estimated and displayed in Fig. 80.4. The biggest values are observed during the summer season, due to the increased activity of neighboring sources. The eastern regions are most affected, but with high seasonal variability. For example, the maximum contribution is around 90% in the area of Dhahran on September and the minimum is ~15% during November. On the contrary, there is less influence from external sources on the western regions (Jazan, Jeddah) reaching a maximum value of 40%. The contribution is weaker on the transitional periods and peaks on the summer and winter periods.

80.4 A Haboob Case in SW Arabian Peninsula

In this part, a dust mobilization mechanism that can cause severe dust events over our region is studied. This mechanism, named 'density current', results from the downdrafts of convective storms and it is usually associated with a pressure rise, a shift in wind direction, and an increase in wind speed. This combination can lead to boundary layer convergence. The warm and moist air in the lower tropospheric levels is lifted above the edge of cool air and a line of severe but shallow convection occurs above the surface intrusion. Intense turbulence near surface enhances dust production. When dust events rise from such density currents the resulting dust front is usually referred to as 'haboob'.

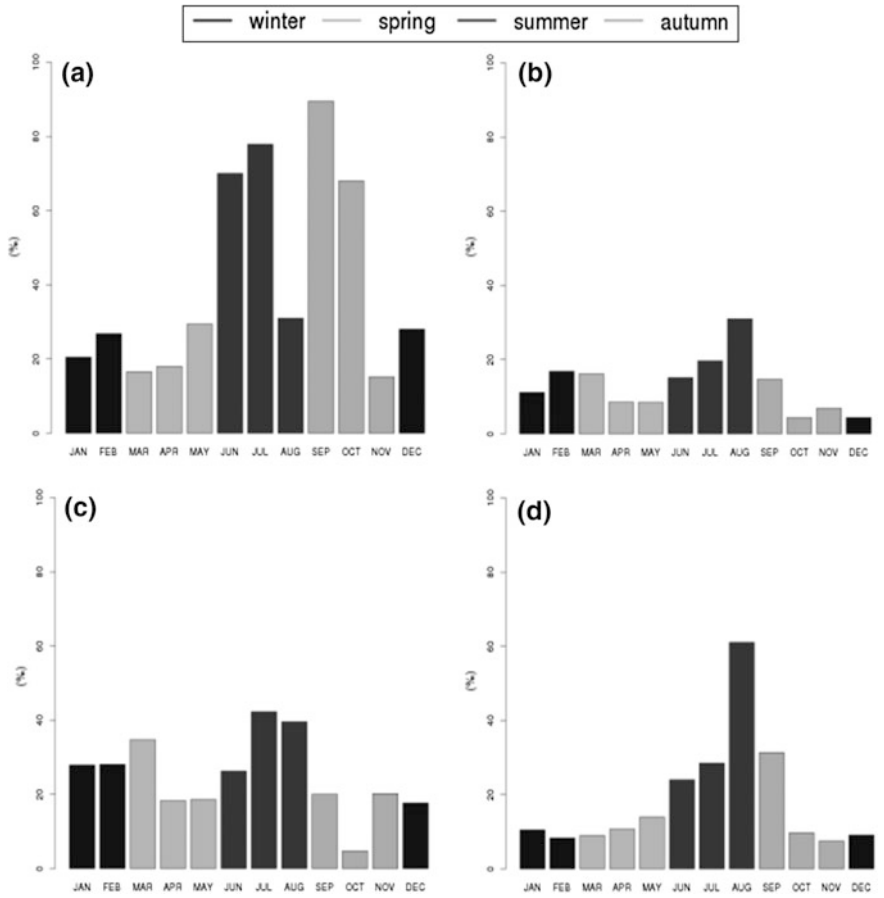

Fig. 80.4 Monthly average dust load contribution for Dhahran (**a**), Jazan (**b**), Jeddah (**c**) and Riyadh (**d**)

On 25–26 May, 2015, high dust concentrations occurred over the study area. The simulation using the same configuration, revealed the presence of the aforementioned mechanism (density current—haboob). The model simulations captured the haboob generation and its fast propagation on 26th of May, 2015 on a very accurate way (shown in Fig. 80.5).

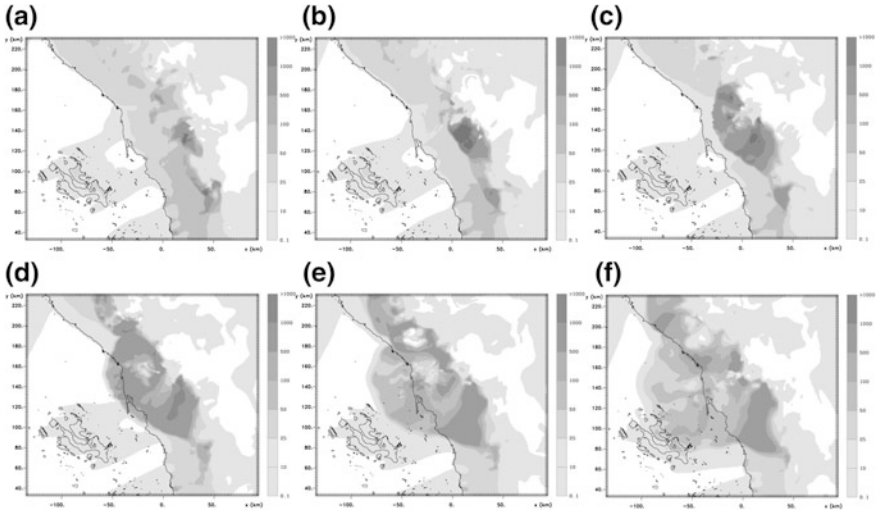

Fig. 80.5 Evolution (half hour frames) of a haboob event in the West Coast of the Arabian Peninsula (26 May 2015, 12:00–14:30—Frames **a**–**f**)

80.5 Conclusions

Proper changes in landscape characteristics can lead to the reduction of local dust production and therefore to the improvement of air quality in neighboring areas and especially in residential or industrial regions. However, long range transported dust and especially extreme dust events continue to affect local microclimate.

The model simulations discussed here illustrate the impact of different scenarios, concerning landscape cover, on dust production and dust concentrations in neighboring urban areas. This change refers mainly to dust production affected by local characteristics such as sea breezes and other mesoscale weather events. However, depending on the time of the year, long range transported dust may have a significant contribution. For example the Tokar Gap Jet can be responsible for high concentrations of dust during summer period. At the same time extreme dust events such as density currents affect areas under consideration despite the mitigation policies. Even though such events cannot be restricted, mitigation activities can be applied while a warning system would be able to minimize the problems produced by such extreme events.

Questions and Answers

Questioner: Pavel Kischa
Question: Long-Range dust transport from the eastern Sahara brings dust, which is mainly distant from the surface. So, could we ignore its effect on human "health" in Saudi Arabia?
Answer: First of all, transport of dust from East Sahara to the Arabian Peninsula does not occur very often especially during summer where ITCZ is shifted to the North and Easterlies dominate. East African dust produced near the west coast of Red Sea is quite possible to be transported towards the area of study. These areas are included within the model domain.

References

Davis SR, Pratt LJ, Jiang H (2015) The Tokar Gap jet: regional circulation, diurnal variability, and moisture transport based on numerical simulations. J Clim 28(15):5885–5907. doi:10.1175/JCLI-D-14-00635.1

Kushta J, Kallos G, Astitha M, Solomos S, Spyrou C, Mitsakou C, Lelieveld J (2014) Impact of natural aerosols on atmospheric radiation and consequent feedbacks with the meteorological and photochemical state of the atmosphere. JGR. doi:10.1002/2013JD020714

Solomos S, Kallos G, Kushta J, Astitha M, Tremback C, Nenes A, Levin Z (2011) An integrated modeling study on the effects of mineral dust and sea salt particles on clouds and precipitation. Atmos Chem Phys 11:873–892. doi:10.5194/acp11-873-2011

Chapter 81
Nearly Zero-Energy Buildings in Finland: Legislation Alternatives for Residential Wood Combustion and the Impact on Population Exposure to Fine Particles

Mikko Savolahti, Maija Mattinen, Ville-Veikko Paunu and Niko Karvosenoja

Abstract Wood combustion is being promoted as an environmentally friendly energy source in the residential sector, although it's fine particle emissions and consequential detrimental effects on human health has been clearly shown in recent scientific literature. In Finland, supplementary wood heating is common, and the popularity of masonry heaters in new detached buildings has been on the rise. Finnish legislation concerning EU's requirements on nearly zero-energy buildings is in preparation, and possibly includes a component that may have an increasing effect on the need of supplementary wood heating. This study demonstrates that the potential increase would cause notable fine particle emissions in the future. We studied several wood consumption scenarios and the resulting $PM_{2.5}$ concentrations in 2050. In the scenario with the biggest increase in wood consumption, the masonry heaters in new detached buildings would cause an additional 10% rise in the current background concentrations in some suburban areas. Increasing the share of wood heating would also be somewhat counterproductive to the purpose of the Energy Performance of Buildings directive, since the legislation won't improve the actual energy efficiency of these houses.

81.1 Introduction

Exposure to fine particles in ambient air is the most significant environmental hazard for human health in Finland (Pekkanen 2010), and residential wood combustion (RWC) is the biggest domestic source of primary $PM_{2.5}$ emissions

M. Savolahti (✉) · M. Mattinen · V.-V. Paunu · N. Karvosenoja
Finnish Environment Institute SYKE, P.O. Box 140, 00251 Helsinki, Finland
e-mail: mikko.savolahti@ymparisto.fi

V.-V. Paunu
e-mail: ville-veikko.paunu@ymparisto.fi

C. Mensink and G. Kallos (eds.), *Air Pollution Modeling and its Application XXV*,
Springer Proceedings in Complexity, DOI 10.1007/978-3-319-57645-9_81

(Savolahti et al. 2015). RWC appliances include central heating boilers, masonry heaters or other room heaters, sauna stoves and fireplaces used for recreational purposes. The majority of the emissions comes from appliances that are not used as the primary heating method of a house.

The European Commission's Energy Performance of Buildings directive (2010/31/EU) requires all new buildings to be nearly zero-energy by the end of 2020. These buildings are described as having "very high energy performance, and the low amount of energy they require comes mostly from renewable sources". Member states can determine their own national legislation to achieve this goal in a cost-efficient way. Biomass is being promoted as a carbon free and environmentally friendly energy source, but the harmful impact of RWC on air quality has been shown to be a major issue (WHO 2013). Due to the selected calculation formula of the energy efficiency rate of buildings, increasing the share of wood combustion in heating may appear to also increase the energy efficiency in some cases. Currently the formula includes a maximum allowed amount of net heating energy from a masonry heater, but the government is planning a possible increase to it. Masonry heaters are the most common biomass-fired room heaters in Finland. The have a high efficiency and relatively low emissions, compared to the typical iron stoves in many European countries (Savolahti et al. 2016).

In this study, we estimate the resulting $PM_{2.5}$ emissions and impact on population exposure in Finland, if the use of masonry heaters is increased in new detached houses. Using an integrated assessment model, we study the concentrations and population exposure in 2050, assuming a linear growth for the new building stock.

81.2 Methodology

In Finland, the energy efficiency rate (E-value) of a building is calculated as:

$$Evalue = kWh_{purchased\ energy} \times ec \tag{81.1}$$

where *ec* is the energy coefficient factor. These coefficients are country-specific and defined in the national legislation. Energy coefficient factors for Finland are presented in Table 81.1. For masonry heaters the factor is lower than for most other heating methods. With residential combustion of fuels, however, the efficiency of the heating appliance needs to be taken into account. This means that for masonry heaters, *ec* is

Table 81.1 Energy coefficient factors in current finnish legislation

Heating method	Energy coefficient factor
Fossil fuel boiler	1
Biofuel boiler	0.5
Electric heating	1.7
District heating	0.7

similar to district heating. The Finnish legislation currently has a 2000 kWh/a maximum allowance for net heating energy from masonry heaters, which is close to our estimation for the current average wood use in new detached houses.

We assume that 90% of the new detached houses include a masonry heater. In the baseline scenario these houses gain 2000 kWh/a of net heating energy from the heater. This is converted to purchased energy using a coefficient of 1/0.6, as instructed in the National building code (ME 2013). In this study, we assume that the increases in the maximum allowance increase the actual wood use accordingly.

We assessed new detached houses between 2012 (when the E-value was introduced) and 2050. The number of annually built detached houses was estimated to be approximately 11 500 on average, and the number of houses with a masonry heater was thus 10 300. We calculated four emission scenarios according to the net heating energy a single house gets from its masonry heater: (1) 2000 kWh/a in all houses (Baseline), (2) additional 1000 kWh/a in all houses, (3) additional 2000 kWh/a in houses with electric heating and (4) additional 2000 kWh/a in all houses. $PM_{2.5}$ emission factor for masonry heaters was 48 mg/MJ. This value is used for modern masonry heaters in the Finnish emission scenarios model and it is based on measurements by the University of Eastern-Finland (Savolahti et al. 2016).

The spatial allocation of the emissions was based on the locations of new detached buildings from the last 10 years. This means that we assume future houses to be built in areas with a similar population density than what has been the case in recent years. The fine particle concentrations resulting from the use of masonry heaters are modelled in a 1 km × 1 km grid, as explained in Karvosenoja et al. (2010). These are then compared with the population densities in the corresponding grid cells.

81.3 Results and Discussion

The masonry heaters in the studied houses are estimated to produce 225–450 t of $PM_{2.5}$ emissions in 2050 (Table 81.2). The upper end of the range is equivalent to 5% of all $PM_{2.5}$ emissions from Finnish RWC in 2014. Future emissions from RWC are highly dependent on the prevalence of wood combustion, which has had major fluctuations in the past. Savolahti et al. (2016) estimated that if wood consumption stays at the level of 2010, the emissions in 2030 would decrease by 18%. Thus, due to the constant renovation of the appliance stock, total emissions in 2050 will probably be notably lower than now.

Table 81.2 Annual fine particle emissions in 2050

Scenario	PM2.5—emissions (t/a)
Baseline, 2000 kWh/a in all buildings	225
Additional 1000 kWh/a in all buildings	338
Additional 2000 kWh/a in buildings with electric heating	273
Additional 2000 kWh/a in all buildings	450

The modelled impact on ambient fine particle concentrations is shown in Fig. 81.1. The concentrations are mostly <0.5 μg/m^3 in case a) and <1.3 μg/m^3 in case c). Currently the measured background concentrations in Finland are typically 7–10 μg/m^3. The modelled concentrations appear mostly on the outskirts of major population centers, and would increase the background concentrations in these areas by 1–10%. As most of the new detached houses are located near population centers, the impact to population exposure is higher than the current average in wood heating (Paunu 2012).

Exposure to fine particles has been estimated to cause 1800 annual deaths in Finland (Pekkanen 2010). The use of masonry heaters in the new detached buildings notably increase local concentrations in many suburban areas and thus inevitably result in detrimental health impacts. If the maximum allowance for a masonry heater's net heating energy is increased, this doesn't translate directly to actual wood use, since the particular E-value requirement is only checked when a new house is built. However, this could increase the amount of buildings where supplementary heating is necessary. The actual consumption of wood is then determined by price, outside temperatures and the energy efficiency of the house. In addition to health effects, RWC is the biggest contributor to Finnish black carbon emissions (Savolahti et al. 2016), which are seen as a potential factor in global warming (Bond et al. 2013).

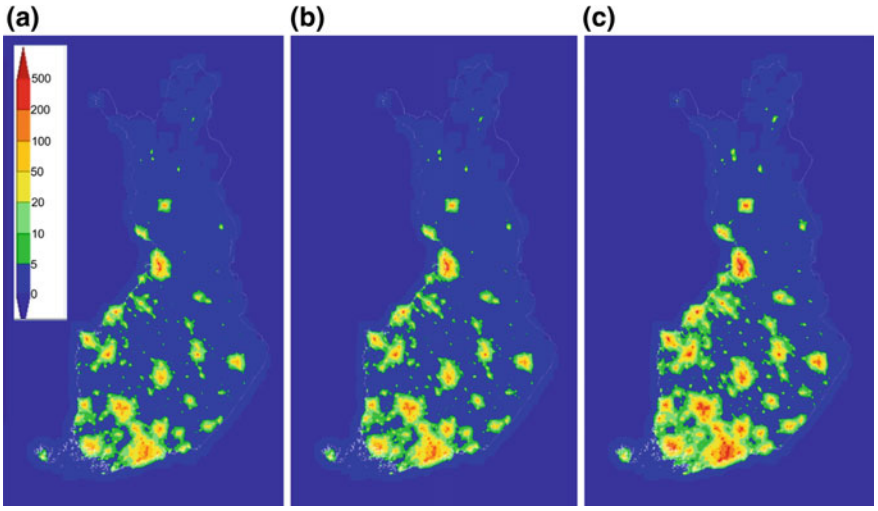

Fig. 81.1 Modelled increase in $PM_{2.5}$ concentrations (ng/m^3) in 2050 from masonry heaters with net heating energies of **a** 2000 kWh/a, **b** additional 2000 kWh/a in detached residential buildings with electric heating and **c** 4000 kWh/a in all detached residential buildings

81.4 Conclusions

This study demonstrates that with the current prevalence of supplementary wood heating, even the efficient, modern masonry heaters produce emissions that have an impact on the air quality in many suburban areas. Supplementary wood heating of new detached buildings causes a notable increase in local ambient $PM_{2.5}$ concentrations and population exposure already in the baseline. The potential increase in wood consumption, due to planned changes in the national legislation, would bring additional detrimental health effects. Since wood combustion also produces greenhouse gases and black carbon, increasing it's share in heating is not justifiable on environmental grounds, especially if it results in less ambitious energy efficiency improvements.

References

Bond TC, Doherty SJ, Fahey DW, Forster PM, Berntsen T, DeAngelo BJ, Flanner MG, Ghan S, Kärcher B, Koch D, Kinne S, Kondo Y, Quinn PK, Sarofim MC, Schultz MG, Schulz M, Venkataraman C, Zhang H, Zhang S, Bellouin N, Guttikunda SK, Hopke PK, Jacobson MZ, Kaiser JW, Klimont Z, Lohmann U, Schwarz JP, Shindell D, Storelvmo T, Warren SG, Zender CS (2013) Bounding the role of black carbon in the climate system: A scientific assessment. JGR Atmos 118(11):5380–5552. doi:10.1002/jgrd.50171

Directive 2010/31/EU of the European Parliament and of the Council of 19 May 2010 on the energy performance of buildings

Karvosenoja N, Kangas L, Kupiainen K, Kukkonen J, Karppinen A, Sofiev M, Tainio M, Paunu V-V, Ahtoniemi P, Tuomisto JT, Porvari P (2010) Integrated modeling assessments of the population exposure in Finland to primary PM2.5 from traffic and domestic wood combustion on the resolutions of 1 and 10 km. Air Qual Atmos Health. DOI 10.1007/s11869-010-0100-9

Ministry of the environment (2013) D5 Suomen rakentamismääräyskokoelma. Rakennusten energiankulutuksen ja lämmitystehontarpeen laskenta. Ohjeet 2012

Paunu V-V (2012) Emissions of residential wood combustion in urban and rural areas of Finland. Master's thesis

Pekkanen J (2010) Elin- ja työympäristön riskit Suomessa. Ympäristö ja Terveys-4 lehti 3:2010

Savolahti M, Karvosenoja K, Kupiainen K, Paunu V-V (2015) Pienpolton päästövähennyskeinojen kustannustehokkuus ja vaikutukset väestöaltistukseen. Suomen ympäristökeskus

Savolahti M, Karvosenoja N, Tissari J, Kupiainen K, Sippula O, Jokiniemi J (2016) Black carbon and fine particle emissions in Finnish residential wood combustion: Emission projections, reduction measures and the impact of combustion practices. Accepted manuscript, Atmos Environ 11 Jun 2016. doi:10.1016/j.atmosenv.2016.06.023

WHO (2013) Review of evidence on health aspects of air pollution—REVIHAAP Project. Technical report

Chapter 82
Characterization of Traffic Emissions Exposure Metrics in the Dorm Room Inhalation to Vehicle Emissions (DRIVE) Study

Jennifer L. Moutinho, Donghai Liang, Rodney Weber, Jeremy Sarnat and Armistead G. Russell

Abstract Detailed measurements and dispersion modeling was conducted to develop more accurate integrated or biologically-relevant metrics to assess exposure to potentially high pollutant levels of primary traffic emissions.

Detailed measurements and dispersion modeling was conducted to develop more accurate integrated or biologically-relevant metrics to assess exposure to potentially high pollutant levels of primary traffic emissions. A 13-week intensive sampling campaign was conducted at six ambient and two indoor monitoring sites surrounding one of the busiest highway segments in the US with the study area focusing on the Georgia Institute of Technology campus to capture the heterogeneity of primary traffic emissions. Fifty-four college students living in dorms near (20 m) or far (1.4 km) from the highway were recruited for personal exposure monitor sampling and biomonitoring. A dispersion model (RLINE) was used to develop spatial concentration fields at a 25 m resolution over the area of primary exposures. Initial RLINE results were biased, due either to errors in the emissions or the model. Analysis suggests that both may be important, depending upon species. To correct for high bias in the near-road environment, the RLINE results were calibrated using measurement observations after the urban background was removed. Both the measurement observations and dispersion modeling results show that the highway has a substantial impact on primary traffic pollutant (particularly elemental carbon and carbon monoxide) concentrations and capture the prominent spatial gradients across the campus domain, though the gradients were highly species dependent. These results, along with other exposure metrics, were used to identify which metrics

J.L. Moutinho (✉) · R. Weber · A.G. Russell
Georgia Institute of Technology, Atlanta, GA, USA
e-mail: jennifer.moutinho@gatech.edu

D. Liang · J. Sarnat
Emory University, Atlanta, GA, USA

C. Mensink and G. Kallos (eds.), *Air Pollution Modeling and its Application XXV*,
Springer Proceedings in Complexity, DOI 10.1007/978-3-319-57645-9_82

are most predictive of biologically-relevant responses to primary traffic exposures that could be used for large panel-based epidemiologic studies.

82.1 Introduction

Highly trafficked roads are major emission sources that lead to high levels of localized pollution in urban areas due to tailpipe exhaust, road dust, and break and tire wear (U.S. EPA 2001). Tail pipe emissions can lead to a range of primary and secondary pollutants including carbon monoxide, nitrogen dioxide, particulate matter, and ozone. While it tends to be easier to sample and link individual pollutants to adverse health effects, near-road pollution tends to be highly heterogeneous which has prompted studying traffic air pollution with a more multipollutant perspective (HEI 2010). Further, there is recognition that populations are never exposed to a single pollutant at one time. Numerous studies have investigated the suitability of using proximity-based or single-species tracers of primary traffic pollution. Relatively few have examined associations among these metrics at multiple steps along an emissions-to-dose pathway. The potentially high pollutant levels and related human exposures are of concern, and in response, a combined field experiment and modeling study was designed with the study area focusing on the Georgia Institute of Technology campus in Atlanta. This framework allows for new opportunities when assessing exposure and adverse health effects of primary traffic emissions (Yan et al. 2009).

82.2 Methods

A 13-week intensive sampling campaign (September 2014–December 2014) was conducted at six ambient and two indoor monitoring sites surrounding Atlanta's busiest highway. The study area focused on the Georgia Institute of Technology campus, which is in the geographic core of Atlanta, Georgia with its eastern edge bordering a major highway. This stretch of highway is one of the most traveled highways in the United States and serves as a classic traffic emission hotspot with an average of 320,000 vehicles and 16,000 trucks per day (GA DOT 2012). Traffic-related contaminant indicators were selected to capture the heterogeneity of primary traffic emissions and were sampled using a highly instrumented stationary roadside site located 10 m from the major highway. A roof site was located in the middle of the campus 500 m west of the highway and two additional locations collected measurements alternating between indoor and outdoor air from dormitory rooms located in the two groups of dormitories on campus. One is in close proximity (20 m) to the highway and the other is removed from major roads (1.4 km from the highway). Finally, two existing monitoring sites provided sampling results to better assess pollutant gradients over the sampling area before and after the sampling campaign: an EPA Near-road Monitoring Network site located 70 m north

of the roadside site and an urban background site located 2.3 km west of the highway. The Rollins School of Public Health at Emory University also followed 54 college students living in the dormitories during the sampling period for personal exposure monitor sampling and biomonitoring. The personal monitor sampling included continuous $PM_{2.5}$ and 48 h integrated nitrogen dioxide measurements, as well as GPS tracking to determine exposure and behavioral differences between the students living in the two different dorms.

In order to quantify primary vehicle emissions exposure, hourly on-road dispersion modeling concentrations were linked to the personal exposure GPS location tracking. RLNE (Research LINE source model), an EPA developed steady-state, Gaussian plume dispersion model, was used to provide the hourly mobile source impacts on the carbon monoxide (CO), nitrogen oxides (NOx), and fine particulate matter ($PM_{2.5}$) concentrations across the whole study domain at a 25 × 25 m grid resolution (Snyder, Venkatram et al. 2013). Emission inputs used were link-based, on-road mobile source emissions for 2010 in the 20-county region surrounding metro Atlanta developed by the Atlanta Regional Commission (ARC) using their traffic demand and mobile source emissions modeling (D'Onofrio 2015). ARC estimated the emissions, in g/m/s, of CO, NOx, and $PM_{2.5}$ for 43,712 links based on modeled traffic volume, vehicle speed, and fleet demographics. The hourly meteorological input data was developed with AERMET (Cimorelli et al. 2005). The surface meteorological data measurements were from the National Weather Service at the Hartsfield-Jackson Atlanta International Airport (ATL) and preprocessed using AERMINUTE. The upper air data measurements were from the Peachtree City Falcon Field Airport (FFC).

Raw RLINE results were corrected by using an annual and diurnal adjustment to emissions, and replacing wind speed hours less than 1 ms^{-1}. The 2010 ARC link emissions were scaled to 2014 using the mobile emissions ratio of 2014 to 2010 from the Motor Vehicle Emission Simulator 2014 (US EPA 2014). The average diurnal emissions profile was used to provide hourly link-based emissions. Accounting for the diurnal variation in emissions is important because in the evening when the boundary layer is low, if the annual average traffic volume is used, the estimated pollutant concentrations are biased high. Further, since steady-state dispersion models tend to overestimate concentrations during calm air conditions, the US EPA suggests resetting any wind speed less than 1 ms^{-1} to 1 ms^{-1} (EPA 2000). In order to correct for unreasonably high concentrations in the RLINE output, ground-level measurements were used to scale the results. Linear regression was applied to the RLINE results and the local background was removed. This process reduced unrealistically high concentrations that were observed on and very near the main highway emissions source and led to concentration levels that more accurately represent pollutant concentrations due to the direct impact of traffic emissions across the study domain.

82.3 Results and Discussion

While RLINE captures the spatial variation and the fine texture of the exposure fields, the raw simulated concentrations were unreasonably high (Fig. 82.1a). The adjusted RLINE results remove all low wind speed events, which also lead to unrealistic simulated concentration fields, and included the annual and diurnal corrections (Fig. 82.1b). The resulting simulated values are then calibrated with observations to develop linear regressions to correct the RLINE results (Fig. 82.1c). The final calibrated fields simulate realistic species correlations and still capture the spatial variation.

The average simulated impact of on-road mobile sources on $PM_{2.5}$, NOx, and CO concentrations over the fine-scale domain was 0.57 ug m^{-3}, 4 ppb, and 24 ppb, respectively (Fig. 82.1c). The fields for all the directly simulated pollutant concentrations are similar showing high levels over and very near the freeway. Levels on the campus are generally low. Higher concentrations are found on the other side of the freeway where more trafficked surface streets are found. However, the generally easterly winds still led to emissions from the highway impacting the campus. The highest levels are predicted when winds are low, such that the averages are dominated by concentrations occurring when winds and dispersion are both low (e.g., at night), even if the emissions are low. The presence of major surface streets surrounding the campus are seen, though at much lower levels that near the freeway (including at the near dorm).

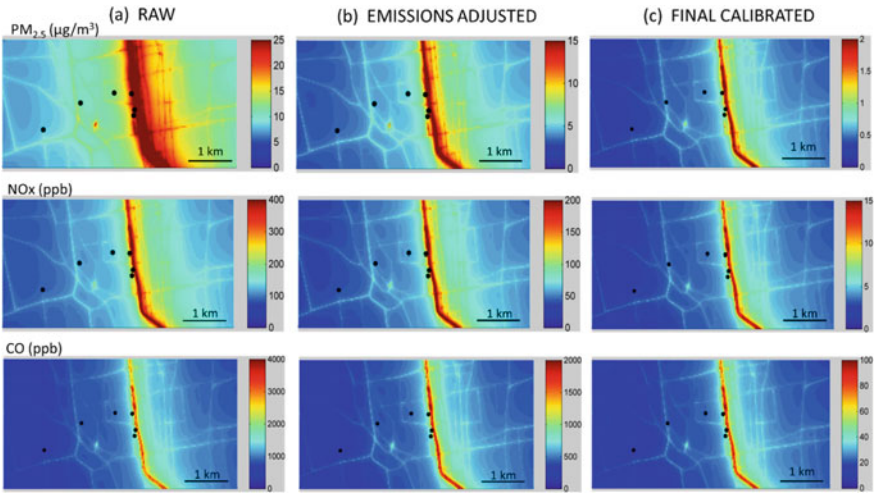

Fig. 82.1 RLINE fine scale dispersion modeling: hourly simulated $PM_{2.5}$, NOx, and CO concentrations (September–December 2014). **a** Raw RLINE output; **b** Raw RLINE outputs adjusted using annual and diurnal ratios, and replacing wind speed hours less than 1 ms^{-1}; **c** Final calibrated fields scaled by observations using a linear regression correlation to provide more accurate model outputs. *Black dots* represent the sampling locations. Resolution: 25 × 25 m

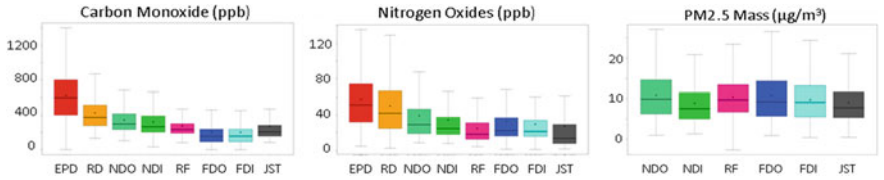

Fig. 82.2 Observed spatial gradients for CO, NOx, and $PM_{2.5}$ at the sampling sites arranged in order of increasing distance from the highway source: EPD—Georgia Department of Natural Resources Near-road Network Monitor (5 m), RD—Near-roadway stationary site (10 m), NDO—Near Dorm outside (20 m), NDI—Near Dorm inside (20 m), RF—Rooftop lab (500 m), FDO—Far Dorm outside (1.4 km), FDI—Far Dorm inside (1.4 km), JST—urban background (2 km)

Measurements from the sampling sites (Fig. 82.2) were compared to RLINE dispersion modeling results to understand how the primary vehicle emissions effect the overall concentrations across the domain. These results have also helped determine the driving factors, traffic count and/or metrological conditions, for elevated concentrations over the study domain.

This study aims to identify which exposure metrics are most predictive of biologically-relevant primary traffic exposures for panel-based epidemiologic studies by assessing traditional exposure indicators and multipollutant traffic exposure metrics. Using hourly fine-scale dispersion modeling results linked to location-tracking was one of the metrics assessed in this study. The Georgia Institute of Technology campus location and the numerous sampling sites enabled a clearer understanding of near-road pollutant spatial distribution and emission-to-exposure pathways.

Acknowledgements Research described in this article was conducted under contract to the Health Effects Institute (HEI), an organization jointly funded by the United States Environmental Protection Agency (EPA) (Assistance Award No. R-82811201) and certain motor vehicle and engine manufacturers. The contents of this article do not necessarily reflect the views of HEI, or its sponsors, nor do they necessarily reflect the views and policies of the EPA or motor vehicle and engine manufacturers. Additional measurement data was provided by Atmospheric Research and Analysis, Inc. and Georgia Department of Natural Resources.

Questions and Answers

Questioner: Peter Viaene

Question: If I understand correctly, during the calibration you are only changing the emissions that are input into the R-LINE. This implies that you attribute the model error solely to the emissions input. Isn't that a problem?

Answer: The emissions data used as input are not changed during the calibration process. The RLINE output is adjusted using an annual ratio and a diurnal ratio for more accurate results. Applying these constant adjustments before or after the model run results in the same concentration change since RLINE is a steady state, Gaussian plume model. For the linear calibration using the observed measurements, the adjusted RLINE output was used to generate the linear regression.
Questioner: Jeff Weil

Question: Was the high bias in R-LINE due to the predicted/ assumed stable conditions and low winds and were stable conditions not observed? What were the typical low wind speeds measured?

Answer: The meteorological data used as input for RLINE was observed wind speed measurements, not predicted or assumed conditions. A wind speed less than 1 ms^{-1} was considered a low wind speed measurement as suggested by the US EPA.

References

Cimorelli AJ, Perry SG, Venkatram A, Weil JC, Paine RJ, Wilson RB et al (2005) AERMOD: a dispersion model for industrial source applications. Part I: General model formulation and boundary layer characterization. J Appl Meteorol 44:682–693

D'Onofrio D (2015) Atlanta roadside emissions exposure study

Georgia Department Of Transportation (2012) Traffic data. http://www.dot.ga.gov/. Accessed Sep 2013

HEI (2010) Traffic-related air pollution: a critical review of the literature on emissions, exposure, and health effects. Special report 17, Boston, MA

Snyder MG, Venkatram A, Heist DK, Perry SG, Petersen WB, Isakov V (2013) RLINE: a line source dispersion model for near-surface releases. Atmos Environ 77:748–756

U.S. EPA (2000) Meteorological monitoring guidance for regulatory modeling applications

U.S. EPA (2001) Control of emissions of hazardous air pollutants from mobile sources: final rule. 66(61)

U.S. EPA (2014) Motor vehicle emission simulator (moves). http://www.epa.gov/otaq/models/moves/

Yan B et al (2009) Roadside, urban, and rural comparison of primary and secondary organic molecular markers in ambient PM2.5. ES&T 43:4287–4293

Chapter 83
A Global-Scale Multi-resolution Study of Surface Air Quality Impacts from Commercial Aircraft Emissions

Saravanan Arunachalam, Alejandro Valencia, Raquel A. Silva, Jiaoyan Huang, Mohammad Omary and Lakshmi Pradeepa Vennam

Abstract The Model for Ozone and Related chemical Tracers, version 4 (MOZART-4), an offline global-scale chemistry-transport model was applied to assess air quality impacts focusing on ground-level O_3 and $PM_{2.5}$ due to full-flight (during cruise (CRZ) mode, and landing/take-off (LTO) activities) commercial aircraft emissions. MOZART-4 was run at two different horizontal resolutions—the first at 2.4 × 1.9°, which is typical of most global-scale models, and a second at a much finer resolution of 0.67 × 0.5°, and using 56 and 72 vertical layers, respectively, for the year 2005. Overall, emissions during LTO modes cause higher impacts on surface $PM_{2.5}$ concentrations than CRZ. Full flight impact on surface $PM_{2.5}$ concentration was ~0.018–0.023 μg/m^3 which is in the range of estimates reported by previous studies. However, we saw that CRZ mode had higher contribution on surface O_3 than from LTO; totally, aircraft attributed global annual average surface O_3 was ~2.0–2.4 ppbv, higher than previously reported values.

83.1 Introduction

Global commercial aircraft emissions are expected to grow 4% per year (Wilkerson et al. 2010) in coming decades. This could enhance global air pollution from aviation contribution, while emissions from other sectors are projected to decline in North America and Europe. Because of the unique 4-D profile of aircraft activity (from surface to ~15 km), its impacts include local, regional, and global scales and affect air quality, climate change, and public health (Lee et al. 2010). However, recent studies have disagreements on global premature mortalities contributed from aircraft emissions for $PM_{2.5}$ (310–13,920), and the surface air quality impacted by cruise emissions (Barrett et al. 2010; Jacobson et al. 2013; Kapadia et al. 2016; Lee et al. 2013; Yim et al. 2015). The goal of this study is to understand the contribution from landing/take-off (LTO) and cruise (CRZ) modes of commercial flight opera-

S. Arunachalam (✉) · A. Valencia · R.A. Silva · J. Huang · M. Omary · L.P. Vennam
The University of North Carolina, Chapel Hill, NC, USA
e-mail: sarav@email.unc.edu

C. Mensink and G. Kallos (eds.), *Air Pollution Modeling and its Application XXV*,
Springer Proceedings in Complexity, DOI 10.1007/978-3-319-57645-9_83

tions on surface air quality. In this study, impacts on surface O_3 and $PM_{2.5}$ from LTO and CRZ emissions were investigated using MOZART-4 global at two different horizontal resolutions. We compare our results with previous global-scale studies that assessed surface air quality impacts due to aircraft emissions.

83.2 Methodology

MOZART-4 was used in this study (Emmons et al. 2010) with anthropogenic, biogenic, and aircraft emissions from intergovernmental Panel on Climate Change (IPCC) fifth Assessment Report (AR5) Representative Concentration Pathways (RCP) 4.5, Model of Emissions of Gases and Aerosols from Nature (MEGAN), and Aviation Environmental Design Tool (AEDT) (Guenther et al. 2006; Riahi et al. 2011; Wilkerson et al. 2010). Two horizontal resolutions are 2.5 × 1.9 and 0.67 × 0.5° for coarse and fine resolutions, respectively (detailed information can be found in Silva et al. 2016). The vertical layers of coarse and fine resolutions are 56 (48 km) and 72 (78 km), respectively, which are identical in the lowest 56 layers. In order to investigate impact of aircraft emissions from LTO and CRZ, four different scenarios are simulated, including full flight (full), no aircraft emissions below 3 km (noairc_below_3 km), above 3 km (noairc_above_3 km), and no aircraft emissions (base). Full (FUL = full−base), CRZ (full−noairc_above_3 km), and LTO (full−noairc_below_3 km) impacts are calculated by subtraction of modeled fields. All scenarios were run for 2005 with 6-month spin-up in each case.

83.3 Results

83.3.1 Vertical Profile Evaluation

O_3 concentrations simulated from MOZART (FUL + all emission sectors) in both resolutions were compared with measurements from the Intercontinental Chemical Transport Experiment (INTEX) in July 2005 (Fig. 83.1). Similar O_3 vertical profiles from both resolutions were observed, and compared well with INTEX observations.

83.3.2 Surface $PM_{2.5}$ and O_3 Variations

Aircraft-attributed global average surface $PM_{2.5}$ concentrations are high from LTO than CRZ (~0.7 and 0.5% (~0.01 and ~0.008 μg/m^3), respectively) in both resolutions, and the numbers are similar to results from coupled CAM5 (Table 83.1).

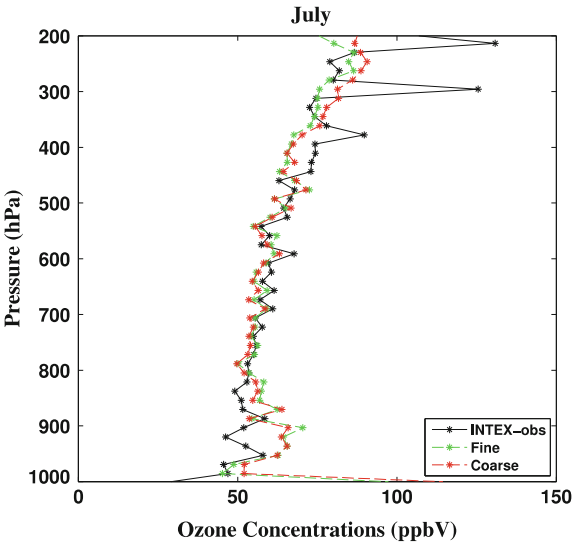

Fig. 83.1 Evaluation of O_3 vertical profiles with INTEX observations

Table 83.1 Global averaged O_3 and $PM_{2.5}$ contributed from aircraft emissions, MOZART data are from this study and other model results are from Jacobson et al. (2015)

Model	Average O_3 (ppbv)	Average $PM_{2.5}$ (μg/m^3)
GATOR-GCMOM	0.046 (0.36%)	0.0834 (0.45%)
GEOS-5	0.52, 0.28–1.60 (1.92%)	−0.17 (−1.86%)
NASA GISS Model2	0.17, 0.13–0.22 (0.53%)	0.0062 (0.42%)
CAM5 fixed	0.48, 0.32–0.67 (1.80%)	0.0034 (0.21%)
CAM5 coupled	0.37, 0.12–0.83 (1.38%)	0.0133 (1.18%)
GEOS-Chem	0.43, 0.27–0.65 (1.63%)	0.007 (0.14%)
MOZART Coarse FUL	1.98 (7.19%)	0.023 (1.01%)
MOZART Coarse CRZ	1.46 (5.30%)	0.009 (0.41%)
MOZART Coarse LTO	0.48 (1.73%)	0.013 (0.58%)
MOZART Fine FUL	2.4 (7.56%)	0.018 (1.30%)
MOZART Fine CRZ	1.7 (5.52%)	0.008 (0.54%)
MOZART Fine LTO	0.5 (1.78%)	0.010 (0.71%)

$PM_{2.5}$ contributions from LTO and CRZ are higher in coarse than in fine resolutions by 0.005 μg/m^3. However, when we analyzed population-weighted $PM_{2.5}$ concentrations, higher numbers were found in fine than coarse resolutions. This indicates that when population exposure is considered, spatial population patterns becomes important, and are associated with spatial variations of aircraft attributed $PM_{2.5}$ concentrations. Hot spots of LTO-attributed $PM_{2.5}$ concentrations are located in the Eastern U.S., Europe, Northern India, and Eastern China. In addition to these regions, CRZ impacts on surface $PM_{2.5}$ were also seen in Tibet due to terrain

elevation. A decrease in surface $PM_{2.5}$ related to CRZ emissions was found in Southern China, and attributed to decrease in sulfate aerosols.

Surface O_3 concentrations increased ~1.8 and 5.5% (0.5 and ~1.5 ppbv) due to LTO and CRZ respectively, in both resolutions. This is probably due to high NOx emissions in CRZ altitude, related gas-phase chemistry in upper troposphere, and downwelling in regions close to tropics in Northern Africa and Middle East or with high elevation terrain, such as the Tibet, Western U.S., and Greenland. However, population-weighted O_3 concentrations due to aircraft are still seen to be high in densely population regions in the finer resolution modeling. Overall, globally averaged aircraft attribution of O_3 concentrations calculated using MOZART is higher than numbers in previous studies (Table 83.1). The uncertainties might come from previously stated concerns with MOZART-4 in the dynamic-chemical coupling in the UTLS region (Emmons et al. 2010; Grewe et al. 2002).

83.3.3 Vertical Profiles of O_3 and $PM_{2.5}$

CRZ attributed $PM_{2.5}$ zonal vertical profiles show a modest impact on surface air quality; a large fraction of $PM_{2.5}$ generated from CRZ emissions stays at CRZ altitude in high latitudes regions. High contribution from LTO emissions on surface $PM_{2.5}$ concentrations were seen which is consistent with our summary of global average. CRZ impacts on zonally averaged $PM_{2.5}$ vertical profiles are related to sulfate aerosols, whereas LTO impacts are mainly associated with nitrate aerosols. O_3 zonal vertical profiles show similar patterns; however, CRZ impacts in vertical pattern show a far southern and deeper vertical convection. This is due to atmospheric conditions in tropical areas enhancing O_3 production and strong downwelling related to global circulation in the 30° longitude region, as also discussed in Barrett et al. (2010). Our findings related to limited transport from CRZ altitude to surface are similar to conclusions made by Lee et al. (2013).

83.4 Conclusions

We quantified surface O_3 and $PM_{2.5}$ impacts due to commercial aircraft emissions during CRZ and LTO modes at two different horizontal resolutions using MOZART-4, and a high resolution globally chorded full-flight aircraft emissions inventory. We find that surface $PM_{2.5}$ impacts were mainly due to LTO unlike some of the previous studies. However, using population-weighted $PM_{2.5}$ concentrations, cruise mode becomes more important, especially at fine resolution, highlighting that some of the LTO impacts of $PM_{2.5}$ are in relatively less or non-populated areas of the globe. Global domain-ave O_3 impacts are higher with fine than coarse resolution, whereas, for $PM_{2.5}$, global impacts are higher with coarse than fine resolution by 128%. However, on population-weighted basis, coarse is only 88% of fine grid

impacts, highlighting significance of population patterns. Surface O_3 fields due to CRZ are higher when using MOZART-4, which points to directions for additional investigation in the future, specifically in model improvements focusing on UTLS and coupling of dynamics with chemistry, and looking at sub-grid scale processes.

Questions and Answers

Questioner Name: Greg Yarwood

Question: Could chemistry occurring in concentrated exhaust plumes from aircraft at cruise influence impacts on ozone?

Answer: Yes, NOx emissions from aircraft at cruise altitude are high. NOx not only im-pact ozone at upper troposphere and lower stratosphere, but also influences OH and CH_4. However, for grid-based models, once the emissions occur in grids, they will be directly diluted to grid size, which might not represent plume-scale chemical processes. Using plume-in-grid model can improve ozone chemistry and better representation of ozone concentrations in plumes.

Questioner Name: Pavel Kischa

Question: Using model data, you estimated a strong impact of aviation emissions on surface $PM_{2.5}$ concentrations. Could you prove your model results by any measurements of chemical composition of $PM_{2.5}$ aerosols?

Answer: Overall chemical composition of aerosols can be evaluated through ambient air monitoring networks, e.g. IMPROVE in the United States. Model evaluations of MOZART due to all emissions sources were done for various chemical species (CO and O_3) and optical depth for aerosol (Emmons et al. 2010). However, there is no data available to evaluate chemical composition of aerosol from aviation contribution at regional and global scales. After evaluating total baseline $PM_{2.5}$, we quantified incremental changes in $PM_{2.5}$ and its chemical composition due to aircraft emissions, which is a standard approach for source attribution in the literature. Chemical species of aerosols from aviation contribution were analyzed and dominated by secondary components of $PM_{2.5}$, which are consistent with results from previous studies.

Questioner Name: Hosein Foroutan

Question: Could you comment on the impacts of the model treatments in the topmost layer including the location of the model-top, grid resolution, and tropospheric-stratospheric interactions on your results?

Answer: In these two resolutions, the topmost layers are different. There are 56 (48 km) and 72 (78 km) layers for coarse and fine resolution, respectively. In this study, we only focus on cruise altitude, which is in the region of 10–15 km (model layers 30–35) around the tropopause. In MOZART only O_3, NOx, HNO_3, N_2O_5, CO, and CH_4 were constrained in stratosphere. Our source attribution results from the two resolutions are generally similar which indicates impact from topmost layer

could be minor and ignorable. We do acknowledge that MOZART-4 has limitations on the dynamic-chemical coupling in the UTLS region that needs to be explored further in future work.

References

Barrett et al (2010) Environ Sci Technol 44:7736–7742
Emmons et al (2010) Geosci Model Dev 3:43–67
Guenther et al (2006) Atmos Chem Phys 6:3181–3210
Grewe et al (2002) Chemosphere 74:851–861
Jacobson et al (2013) Faraday Discuss 165:369–382
Jacobson et al (2015) FAA-AEE report
Kapadia et al (2016) Atmos Chem Phys 16:10521–10541
Lee et al (2010) Atmos Environ 44:1–57
Lee et al (2013) Atmos Chem Phys 13:5505–5522
Riahi et al (2011) Clim Change 109:33–57
Silva et al (2016) Environ Health Perspect 124:1776–1784
Wilkerson et al (2010) Atmos Chem Phys 10:6391–6408
Yim et al (2015) Environ Res Lett 10. doi:10.1088/1748-9326/10/3/034001

Chapter 84
Testing a New Holistic Management Tool for Nitrogen—Environmental Impacts of Using Manure Acidification in the Danish Agricultural Sector

Camilla Geels, Steen Gyldenkærne, Tavs Nyord, Kaj M. Hansen, Hans Estrup Andersen, Hans Thodsen, Dennis Trolle, Karsten Bolding, Berit Hasler and Karen Timmermann

Abstract The fate of anthropogenic reactive nitrogen (N) is often described as a cascade of different nitrogen forms and effects throughout the environment. In order to describe the fate in detail, a holistic approach covering the flow between the main environmental compartments is needed. Therefore a new management tools has

C. Geels (✉) · S. Gyldenkærne · K.M. Hansen · B. Hasler
Department of Environmental Science, Aarhus University, Aarhus, Denmark
e-mail: cag@envs.au.dk

S. Gyldenkærne
e-mail: sgy@envs.au.dk

K.M. Hansen
e-mail: kmh@envs.au.dk

B. Hasler
e-mail: bh@envs.au.dk

H.E. Andersen · H. Thodsen · D. Trolle · K. Bolding · K. Timmermann
Department of Bioscience, Aarhus University, Aarhus, Denmark
e-mail: hea@bios.au.dk

H. Thodsen
e-mail: hath@bios.au.dk

D. Trolle
e-mail: dtr@bios.au.dk

K. Bolding
e-mail: bolding@bios.au.dk

K. Timmermann
e-mail: kt@bios.au.dk

T. Nyord
Department of Engineering, Aarhus University, Aarhus, Denmark
e-mail: tavs.nyord@eng.au.dk

C. Mensink and G. Kallos (eds.), *Air Pollution Modeling and its Application XXV*,
Springer Proceedings in Complexity, DOI 10.1007/978-3-319-57645-9_84

been setup for an area in Denmark. A holistic approach is attempted by linking models for the main compartments (atmosphere, watershed and aquatic) and including a common emission scenario. The scenario describes a new technique for reducing ammonia emissions and at the same time increase N availability for crops using acidification of liquid manure and use of air cleaners in pig and poultry houses. Here the first results from a pilot study in Northern Jutland, Denmark, will be presented.

84.1 Introduction and Study Setup

National and international targets for ammonia (NH_3) emission, urge the agricultural sector to apply new technologies. Both from animal houses and during field application the NH_3 loss to the atmosphere can be high. Air cleaning from mechanical ventilated animal houses like pig and poultry houses and lowering pH of liquid manure by acidification are abatement technologies that can reduce NH_3 emission to the atmosphere. More reactive nitrogen (Nr) will then be available for the plants, but more Nr could potentially be transferred to the watershed instead and hence lead to increased eutrophication in the aquatic environment.

A system to lower pH of liquid manure, by adding concentrated sulphuric acid (H_2SO_4) shortly before field application, is a common technology in Denmark. The idea behind this method is that a lower pH level will limit the dissociation of NH_4^+ to $NH_3 + H^+$ and thus suppresses the volatilization of NH_3. Field scale experiments using such a system (see Fig. 84.1) has been carried out at two different locations (Seidel et al. 2015). The resulting NH_3 emissions were measured by combining calibrated chamber measurement and passive flux samplers.

Fig. 84.1 The white box in front of the tractor contains the sulphuric acid. The acid is pumped into a tube that runs underneath the tractor and all the way down along the slurry tanker. At the rear of the wagon the acid is added to the slurry just before the slurry flows into the hoses and applied on the field. Foto: Tavs Nyord

As part of the national monitoring and assessment program for the Aquatic and Terrestrial Environment in Denmark, a detailed NH_3 emission inventory is updated each year. The inventory is based on detailed information from the main agricultural databases. The final inventory hence includes, the total annual ammonia emission coming from e.g. animal houses and storages, at the exact locations of these in Denmark and from fields due to grown crops as well as emission due to application of manure and mineral fertilizer. The emission from fields is distributed within a 100 m × 100 m map covering all of Denmark (Plejdrup and Gyldenkærne 2011). The emission inventory for 2012 has been used as the base case representing the current emissions. Emission factors for air cleaning (BAT, EPA 2016) and the new emission factors from the acidification experiment have been used to construct a scenario for Denmark. Here it is assumed that all pig and poultry houses are provided with air cleaners and that acidification is used on all fields receiving surface applied liquid manure.

These emission inventories are in the next steps used at input to the different models included in the holistic model chain. First model in the chain is the atmospheric chemistry-transport model DEHM (Christensen 1997; Geels et al. 2012a). DEHM covers the Northern Hemisphere and zooms in on Europe and Denmark with higher and higher resolution (5.6 km × 5.6 km over Denmark). This setup secures that the inflow of long-rang transported components is included and the components influenced more directly by local sources (e.g. NH_3) also are reasonably well resolved over Denmark. The model is continuously improved and evaluated and has been used for a number of nitrogen assessments (Geels et al. 2012a, b; Hertel et al. 2012). Two model simulations have been made based on meteorology for year 2009 and national/international anthropogenic emissions for year 2012. The only difference between the two simulations is the NH_3 emissions, which are based on the two inventories described above. The outcome of the two simulations is maps of the concentration and depositions (both wat and dry) of the main NH_x and NO_x components.

This will be used as input to the next models in the model chain: a watershed biophysical SWAT model (e.g. Lu et al. 2015) describing hydrology as well as nutrient and sediment dynamics within the catchment area and the GOTM-FABM-PCLake model that is an aquatic lake-ecosystem model. These models require detailed information on a number of parameters describing the specific area. They are therefore typically setup for a specific catchment area, where the necessary information on e.g. sub-basin configurations, soil types, land use and slope classes can be collected. Finally the cost minimization model (TargetEconN, Hasler et al. 2016) has been updated to include the cost associated with the use of acidification. Thereby the best combination of abatement measures to reach a specific environmental objective (e.g. a freshwater quality) at the lowest possible cost can be identified. In the current study the full system will be tested for the Limfjord in northern part of Denmark. It is a 180 km long inlet connecting the North Sea and Kattegat.

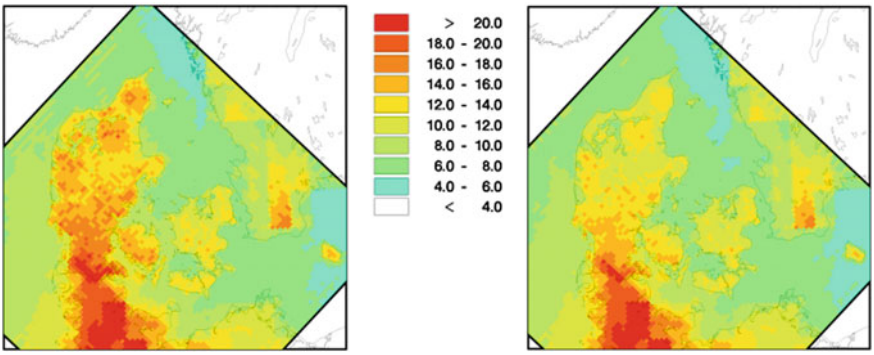

Fig. 84.2 The total N deposition across Denmark for the simulations with NH_3 emissions representing the current production (*left*) and the acidification/air cleaners scenario (*right*). In Kg N/ha/year

84.2 Results and Discussion

Atmospheric emissions: The base case representing the present agricultural praxis within the agricultural sector leads to a total annual emission of 59 K tonnes NH_3 in 2012. Using the new emission factors and hence including acidification gives a total annual emission of 35 K tonnes NH_3 in the scenario.

Atmospheric deposition: The total N deposition in Denmark decreases with ca. 11% if acidification and air cleaners are applied at the national scale. As seen on Fig. 84.2. the decrease is modelled to be largest in the agricultural areas in Jutland (western part of Denmark). The atmospheric deposition to Limfjorden decreases by ca. 16% and of this the largest decrease is seen in the dry deposition of NH_x.

84.3 Conclusion

The effect of new abatement technologies based on air cleaning and acidification of liquid manure will be accessed by a novel holistic model tool. Based on field experiments, a new emission scenario for Denmark has been made and used in an atmospheric model. The simulated change in depositions of N components will be used as input to the next models in the holistic model chain. Thereby the possible effects of increasing the nutrient load in the aquatic systems can be evaluated. The first results demonstrate that air cleaners and acidification has the potential to limit the loss of NH_3 to the atmosphere and the following deposition of N to e.g. sensitive terrestrial and aquatic nature areas.

Acknowledgements This study was mainly funded by DCE—Danish Center for Environment and Energy through the DEEMON project. Part of the model developments has been supported by the dNmark alliance funded by the Danish InnovationFund and the national NOVANA programme.

References

Christensen JH (1997) The Danish Eulerian hemispheric model—A three-dimensional air pollution model used for the Arctic. Atmos Environ 31:4169–4191

EPA 2016, Miljøteknologi. BAT: http://mst.dk/virksomhed-myndighed/landbrug/miljoeteknologi-og-bat/

Geels C, Andersen HV, Ambelas Skjøth C, Christensen JH, Ellermann T, Løfstrøm P et al (2012a) Improved modelling of atmospheric ammonia over Denmark using the coupled modelling system DAMOS. Biogeosciences 9:2625–2647

Geels C, Hansen KM, Christensen JH, Skjøth CA, Ellermann T, Hedegaard GB, Hertel O, Frohn LM, Gross A, Brandt J (2012b) Projected change in atmospheric nitrogen deposition to the Baltic Sea towards 2020. Atmos Chem Phys 12:2615–2629

Hasler B, Hansen LB, Konrad M, Estrup Andersen H, Termansen M (2016) Spatial modelling of non-point nitrogen loads to fulfill water quality policies. Paper presented at the 22nd EAERE (European Association of Environmental and Ressource Economics) conference, Zurich

Hertel O, Geels C, Frohn LM, Ellermann T, Skjøth CA, Løfstrøm P, Christensen JH, Andersen HV, Peel RG (2012) Assessing atmospheric nitrogen deposition to natural and semi-natural ecosystems—Experience from Danish studies using the DAMOS system. Atmos Environ

Lu S, Kronvang B, Audet J, Trolle D, Andersen HE, Thodsen H et al (2015) Modelling sediment and total phosphorus export from a lowland catchment: comparing sediment routing methods. Hydrol Process 29(2):280–294

Plejdrup MS, Gyldenkærne S (2011) Spatial distribution of emissions to air—the SPREAD model. Report no. 823

Seidel A, Pachplski A, Nyord T, Kage H (2015) Reduction of ammonia emissions by acidification and injection of cattle slurry applied to perennial grassland. In: RAMIRAN 2015—16th international conference rural-urban symbiosis: proceedings book, pp 85–88, ISBN: 978-3-946094-02-9

Part VIII
Aerosols in the Atmosphere

Chapter 85
Human Driven Changes in Atmospheric Aerosol Composition

M. Kanakidou, S. Myriokefalitakis and N. Daskalakis

Abstract A set of global 3-dimensional model simulations have been performed to investigate the changes in atmospheric composition driven by humans. Sensitivity simulations using past, present and future anthropogenic emissions of pollutants are analyzed to derive the importance of human-driven emissions of pollutants for aerosol composition, including aerosol water, and for dust aerosol aging. The results show that applied emission control has significantly limited air pollution levels compared to a hypothetical uncontrolled situation. They also point out that human activities have increased atmospheric acidity and as a result the solubility of nutrients, like iron and phosphorus, in atmospheric deposition.

85.1 Introduction

Atmospheric aerosols are ubiquitous components of the atmosphere with variable shape, size and chemical composition that depending on their sources and atmospheric aging. This determines their properties and their impact on human health and climate. In the atmosphere they scatter or absorb radiation and affect the water cycle. They also impact on ecosystems because aerosols can contain nutrients or toxic components. Aerosols and aerosol water also serve as media for multiphase chemistry that changes both atmospheric oxidant levels and aerosol properties.

M. Kanakidou (✉) · S. Myriokefalitakis · N. Daskalakis
Environmental Chemical Processes Laboratory, Chemistry Department,
University of Crete, Heraklion, Greece
e-mail: mariak@chemistry.uoc.gr

S. Myriokefalitakis
Department of Physics and Astronomy, Institute for
Marine and Atmospheric Research (IMAU), Utrecht University,
Utrecht, The Netherlands

N. Daskalakis
LATMOS/IPSL, CNRS, Paris, France

C. Mensink and G. Kallos (eds.), *Air Pollution Modeling and its Application XXV*,
Springer Proceedings in Complexity, DOI 10.1007/978-3-319-57645-9_85

The composition and thus properties of atmospheric aerosol have been changed due to anthropogenic emissions of pollutants into the atmosphere. Interactions of desert dust, the most abundant aerosol originating from natural continental sources with acidic compounds of anthropogenic origin increase dust's solubility and solubilize nutrients carried by dust, such as Fe and P. Water soluble organic di-acids, acting as ligands, present in aerosol water and in cloud droplets can form Fe-complexes, changing dust solubility as well as organics' chemical properties.

85.2 Methods

The well documented model TM4-ECPL (Daskalakis et al. 2015; 2016; Myriokefalitakis et al. 2016a, b; Kanakidou et al. 2016, and references therein) has been used for the present study. The model accounts for multiphase chemistry, including Fenton reactions and oxalate formation as well as all major aerosol components, including secondary organic aerosol, aerosol aging in the atmosphere, atmospheric transport and deposition. Secondary inorganic aerosols like sulphate (SO_4^{2-}), nitrate (NO_3^-) and ammonium (NH_4^+) are calculated using ISORROPIA II thermodynamic model (Fountoukis and Nenes 2007).

TM4-ECPL is driven by the ECMWF (European Centre for Medium—Range Weather Forecasts) Interim re–analysis project (ERA—Interim) meteorology. The model has a horizontal resolution of 3° in longitude by 2° in latitude and 34 hybrid vertical layers, from surface up to 0.1 hPa. Two different categories of simulations have been performed for the present study. First, a set of 30-years simulations using year specific meteorology and natural emissions (Daskalakis et al. 2016) and second a set of simulations with meteorology and natural emissions for the year 2008 and anthropogenic emissions representative for past, present and future atmosphere. A spin-up time of one year has been used for all simulations. The historical Atmospheric Chemistry and Climate Model Intercomparison Project (ACCMIP) dataset has been used for the anthropogenic (including ships and aircraft emissions) and biomass burning emissions for the year 1850 (hereafter PAST), while those for the years 2008 (hereafter PRESENT) and 2100 (hereafter FUTURE) come from the Representative Concentration Pathway 6.0 (RCP 6.0) emission scenario. For the 30-years of simulations an additional alternative anthropogenic emissions scenario has been developed by Daskalakis et al. (2016) that neglects any technology development since 1980 and assumes constant per capita emissions as those in 1980 (BA1980) accounting for population increase and large scale geographic shift. Figure 85.1 shows the computed annual mean trends in SO_2 emissions for the studied period from 1980 to 2010 for these two scenarios. Figure 85.1a shows that SO_2 emissions have decreased globally due to technological improvements and legislation with strongest reductions over US and Europe but increased over the Arabian Peninsula, India and south east Asia. In the BA1980 scenario (Fig. 85.1b) emissions are assumed to have increased almost everywhere.

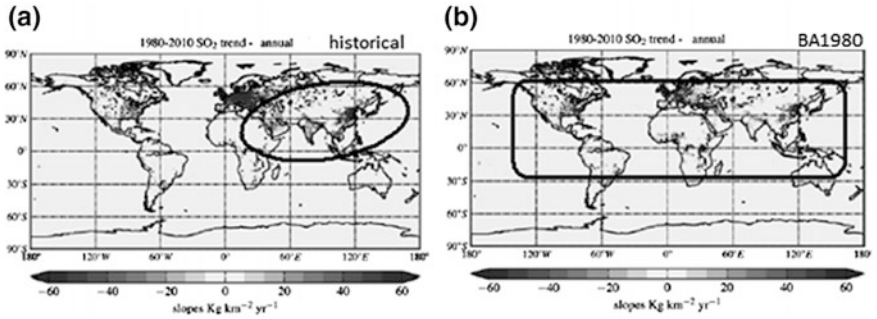

Fig. 85.1 Annual mean trends in the emissions of SO_2 for the period 1980–2010 **a** for the ACCMIP historical emissions **b** for the hypothetical BA1980 anthropogenic emission scenario. In **a** trends are negative except over the *circled areas* in Asia where they are positive; while in **b** most of the trends are positive (*inner box*)

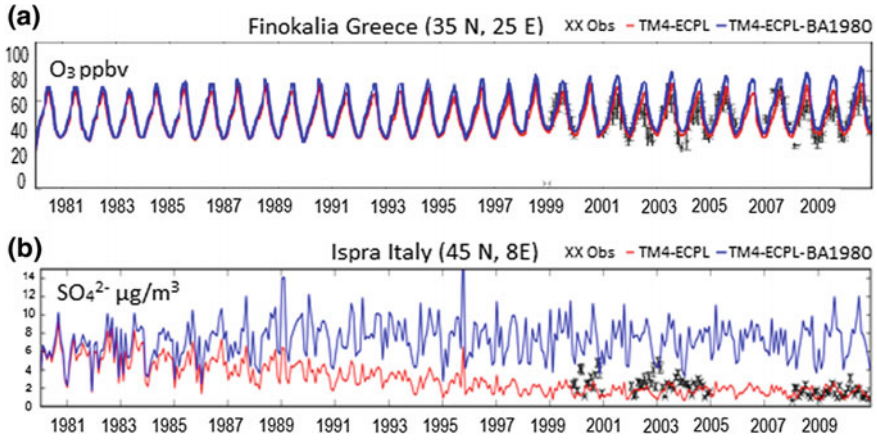

Fig. 85.2 Surface concentrations as computed by the model for the ACCMIP base case simulation (*lower line*) and using the AE1980 anthropogenic emission scenario (*upper line*). Observations are marked with symbols (monthly mean and standard deviation). **a** ozone at Finokalia (35 N, 25 E) in Greece **b** sulfates at Ispra (45 N, 8 E) in Italy

85.3 Changes in Atmospheric Concentrations Due to Human Activities

During the past years air quality legislation has been applied, forcing to a technology development in several sectors, and globalization of the economy led to geographic shift in human economic activities. These changes are accounted in the ACCMIP historical anthropogenic emissions here used for the base simulations. The 30-year base case simulation performs reasonable against global surface observations (Fig. 85.2 for O_3 and SO_4^{2-}, more details in Daskalakis et al. 2016).

The results of the alternative anthropogenic emissions scenario (BA1980) are also depicted in this figure. This is the only difference between the simulations that also account for the year-to-year observed variability in the meteorology and changes in natural emissions issued from the meteorological changes. This alternative anthropogenic emissions scenario shows larger improvements in air quality than calculated by assuming constant anthropogenic emissions of the year 1980 (as usually done) compared to the base case simulation. Significant reductions in concentrations of all air pollutants but ozone are calculated for the base case when compared to the BA1980 simulation. They show a clear imprint of the effect of anthropogenic emission mitigation measures to the pollutant levels. This hypothetical anthropogenic emissions scenario is also not able to reproduce the observed trends in surface concentrations, showing the effectiveness of technological advances and applied legislation the past years in limiting air pollution. Furthermore, accounting for the disproportional increase in energy demand over China and India, the comparison of simulated and observed surface pollutant levels also indicates that the explosive increase in local population and the industrial activities globalization have masked the environmental benefit from technological advances.

85.4 Changes in Atmospheric Acidity

We have further investigated the changes in the atmospheric acidity due to emissions changes. For this purpose we focus on the simulation performed for the year 2008, using PAST, PRESENT and FUTURE anthropogenic emissions. The increase in anthropogenic emissions since preindustrial period has led to increased sulfuric and nitric acid formation in the atmosphere and thus to increased atmospheric acidity (changing the pH of both clouds and aerosols). Figure 85.3a shows the present day pH of fine aerosols as calculated by TM4-ECPL using the coupled to the model ISORROPIA module (Fountoukis and Nenes 2007) with values lower

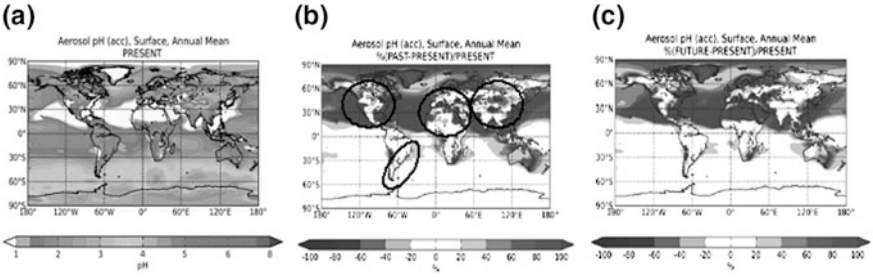

Fig. 85.3 **a** pH of the fine aerosol water as computed by ISORROPIA in TM4-ECPL (all below 2 except in the southern band around 60S where values are between 3 and 5, **b** changes in pH in the PAST (pH was higher except in *circled areas* that was lower), **c** projected changes in the FUTURE (all positive) due to anthropogenic emissions changes

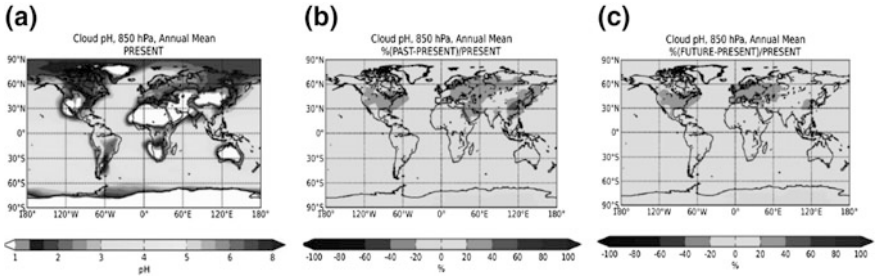

Fig. 85.4 **a** Annual mean cloud water pH at 850 hPa for the PRESENT atmosphere, **b** changes in annual cloud water pH in the PAST (pH was higher) and **c** projected for the FUTURE (pH is expected to be higher)

than 2 in most areas but the southern ocean where sea-salt aerosol dominates and increases fine aerosol pH to values above 3. Figure 85.3b, c also show how this pH has changed, and will change, due to human activities.

Similarly, Fig. 85.4a depicts the cloud water pH computed based on ion balance accounting for CO_2, SO_2, NH_3, ions of strong acids and oxalate, and its changes in the PAST and to the FUTURE (see details in Myriokefalitakis et al. 2016a). As expected, cloud water is a more diluted and less acidic media than aerosol water. According to our calculations, PRESENT cloud water is more acidic than has been in the PAST and is expected to be in the FUTURE.

85.5 Impact of Changes of Atmospheric Acidity on Nutrient Deposition

Global model simulations of the atmospheric cycles of iron (Fe) and phosphorus (P) performed by Myriokefalitakis et al. (2016a) and Myriokefalitakis et al. (2016a, b) took into account the above discussed changes in atmospheric acidity as well as the enhancement of solubilization flux of Fe and P present in mineral dust aerosols, i.e. the rates at which Fe and P are converted into soluble forms. These rates are a function of acidity and of ligand presence. The simulations show that a 3 times increase in dust-Fe solubilization and a 75% increase in dust-P solubilization may have occurred in the past 150 years due to the human-driven increase in atmospheric acidity. They also show that emission control in the near future will reduce the dust-Fe solubilization flux by about half and by about 30% the dust-P solubilization flux relative to present day. These findings are important for the marine ecosystems that are affected by atmospheric deposition of nutrients and show the strong links of atmospheric chemistry and biogeochemical cycles.

85.6 Conclusions

Our results indicate the efficiency of past air quality legislations and technology developments in limiting the rapid degradation of the atmospheric environment. They provide an alternative to the traditionally used way of evaluating the environmental benefit from human actions to protect the environment. They show that this benefit is larger than thought and that in some cases like over China and India air quality would have been worse if measures were not take. However, due to the large increase in energy demand to these regions resulting from the globalization in the economy and the rapid increases in the local population and its standards of life this beneficial impact is not seen. Because of human driven emissions, atmospheric fine aerosol water is more acidic nowadays compared to both the preindustrial period and will be in the future with significant implications for solubilization fluxes of nutrients present in dust and thus on the marine ecosystems.

Questions and Answers

Questioner: Dick Derwent
Question: It is not an easy task to produce historic global emission inventories. Have you checked your predictions of ozone as surface sites with the baseline ozone observations collected by NOAA Boulder (Parrish et al. 2014) showing the growth from 1950 to 2000s followed by a levelling OH?
Answer: Indeed, historic emission inventories are difficult to be constructed. Therefore, in our study we use what is widely used by the modeling community, the anthropogenic emissions inventories: the historical Atmospheric Chemistry and Climate Model Intercomparison Project (ACCMIP) database for the year 1850 and for the years 1980–2000 that has been constructed by Lamarque et al. (Geosci. Model Dev., 6, 179–206, 2013). For the years after 2000, we use the Representative Concentration Pathway 6.0 (RCP 6.0) emission scenario developed by van Vuuren et al. (Clim. Change, 109, 5–31, 2011). With regard to model evaluation we have compared with all available surface data without however selecting only the baseline conditions as done in the Parrish et al. (JGR, doi:10.1002/2013JD021435, 2014) paper. The purpose of the comparison to observations was to evaluate the ability of the model to reproduce realistically the atmospheric concentrations. In this case a comparison with "baseline" measurements would not provide any additional information.
Questioner: Wanmin Gong
Question: Is your scenario where you keep per-capital energy consumption at 1980 level the worse-case scenario? It is difficult to untangle the increase in energy demand, new technology, and legislation impacts.

Answer: It should not be considered as the worst-case because it does not account for the increase in energy demand per capita since 1980. The worst-case scenario should account for stagnant technology i.e. for the same energy demand same constant per capita emissions and in addition account for the increase in energy demand per capita. While, there are statistics for the energy demand per capita, it is indeed very difficult to distinguish the impact of new technologies from that of legislation. The concept of our modeling study does not allow separating between new technology and legislation. However, it provides an alternative way to investigate the effectiveness of emission mitigation legislation.

References

Daskalakis N, Myriokefalitakis S, Kanakidou M (2015) Sensitivity of tropospheric loads and lifetimes of short lived pollutants to fire emissions. Atmos Chem Phys 15:3543–3563

Daskalakis N, Tsigaridis K, Myriokefalitakis S, Fanourgakis GS, Kanakidou M (2016) Large gain in air quality compared to an alternative anthropogenic emissions scenario. Atmos Chem Phys 16:9771–9784

Fountoukis C, Nenes A (2007) ISORROPIA II: a computationally efficient thermodynamic equilibrium model for K^+–Ca^{2+}–Mg^{2+}–NH_4^+–Na^+–SO_4^{2-}–NO^{3-}–Cl^-–H_2O aerosols. Atmos Chem Phys 7:4639–4659

Kanakidou M, Myriokefalitakis S, Daskalakis N, Fanourgakis G, Nenes A, Baker AR, Tsigaridis K, Mihalopoulos N (2016) Past, present and future atmospheric nitrogen deposition. J Atmos Sci 73:2039–2047

Myriokefalitakis S, Daskalakis N, Mihalopoulos N, Baker AR, Nenes A, Kanakidou M (2016a) Changes in dissolved iron deposition to the oceans driven by human activity: a 3-D global modelling study. Biogeosciences 12:3973–3992

Myriokefalitakis S, Nenes A, Baker AR, Mihalopoulos N, Kanakidou M (2016b) Bioavailable atmospheric phosphorous supply to the global ocean: a 3-D global modeling study. Biogeosciences 13:6519–6543

Parrish DD et al (2014) Long-term changes in lower tropospheric baseline ozone concentrations: comparing chemistry-climate models and observations at northern midlatitudes. J Geophys Res Atmos 119:5719–5736. doi:10.1002/2013JD021435

Chapter 86
Aerosols in the Mediterranean Region and Their Role in Cloud Formation

G. Kallos, A. Nenes, P. Patlakas, E. Drakaki, M. Koukoula, D. Rosenfeld and N. Mihalopoulos

Abstract The physical and chemical characteristics of aerosols are considered as critical for nucleation processes, cloud formation and evolution. The Mediterranean Region is well known for the mixture of aerosols from different origins such as desert dust, sea salt and anthropogenic and biomass burning. Sea salt is in relatively small quantities compared to dust amounts during episodes but its constant presence plays a key role in cloud formation, especially concerning the initial stage. In this work we discuss modeling results related to nucleation processes and cloud formation in the Eastern Mediterranean. Emphasis is given in the impact of sea salt on Marine Boundary Layer (MBL) and orographic cloud formation. The role of other sources of aerosols is also discussed. The modeling tool used for the simulations is the RAMS/ICLAMS fully-coupled modeling system. Satellite data and in situ measurements have been also used for a more comprehensive analysis.

86.1 Introduction

The Mediterranean Region is characterized by a mixture of aerosols of various origins and sources. The most important sources are desert dust, sea salt, biomass burning and anthropogenic releases from industrial and urban activities. The composition of this mixture exhibits seasonal variability and affects the nucleation

G. Kallos (✉) · P. Patlakas · E. Drakaki · M. Koukoula
School of Physics, University Campus, University of Athens, Bldg. Phys-V, 15784 Athens, Greece
e-mail: kallos@mg.uoa.gr

A. Nenes
Department of Earth and Atmospheric Sciences, Georgia Institute of Technology, Atlanta, GA, USA

D. Rosenfeld
Institute of Earth Sciences, The Hebrew University of Jerusalem, Jerusalem, Israel

N. Mihalopoulos
Department of Chemistry, University of Crete, Heraklion, Greece

C. Mensink and G. Kallos (eds.), *Air Pollution Modeling and its Application XXV*, Springer Proceedings in Complexity, DOI 10.1007/978-3-319-57645-9_86

processes, cloud formation and evolution (Kallos et al. 2007). The characteristic paths and time scales of transport and transformation in the Mediterranean are discussed in this publication. The temporal scales for gas to particle conversion are of the order of hours depending on the season. As it was discussed in previous work, the spatial and temporal distribution of precipitation is affected by the aerosol characteristics (Solomos et al. 2011). The main objective of this work is to better understand the nucleation processes and the role of sea salt and other aerosols on the marine boundary layer characteristics and orographic cloud formation. Emphasis is given in the eastern part of the Mediterranean and particularly in Crete and East Mediterranean Coast. Particular emphasis is given in the role of sea salt as CCN. The work is performed with the aid of the fully-coupled modeling system RAMS/ICLAMS. Cloud characteristics retrieved from satellite data are used for comparison with the model results. In situ data from the remote location station of Finokalia were used for the microphysical parameterization.

86.2 Cloud Formation in Crete

The phenomenon under consideration is a case of low cloud formation in Crete and the sea north of it. It occurred on 13–14 September 2015. The winds are moderate to strong from North. As the air masses are lifted over the landscape of Crete, the clouds are thick very close to the ground and touching the orographic peaks at the center of the island. Orographic cloud formation just over land is a phenomenon that occurs frequently. This cloud formation either starts diluting when the air masses start descending at the southern part of the island or advect southerly at higher altitudes. This cloud formation does not always precipitate. Although, large droplets fall very often when the orographic lifting starts and later they are converted into light rain at higher altitudes. During winter, snow is also frequently observed in higher altitudes.

The island of Crete is characterized by complex terrain and mountains reaching the height of ~2500 m. The distance between the shore and the mountain peaks varies from 2 to 20 km. The orientation of the island is East–West and acts as a barrier to the prevailing winds that are from northern directions. Southerly flow always carries warm and dry air masses associated with Saharan dust. Descending to the North, after passing over the mountains, results in very high temperatures. Under such conditions, cloud formation is not frequent in Crete except in specific cases as described in Spyrou et al. (2010).

The case under consideration is 13–14 September 2015. During this period, moderate to strong northerly winds persisted along the Aegean Sea reaching the northern coast of Crete where the air masses started to be lifted over the Cretan orographic features (Fig. 86.1). Low clouds started to form (mixed stratiform and low-level CB). The cloud formation started South of the Cyclades Islands intensifying to the South over the sea as illustrated in the satellite pictures of Fig. 86.2a, c. Figure 86.2a is in visible while Fig. 86.2c illustrates the cloud formation with the

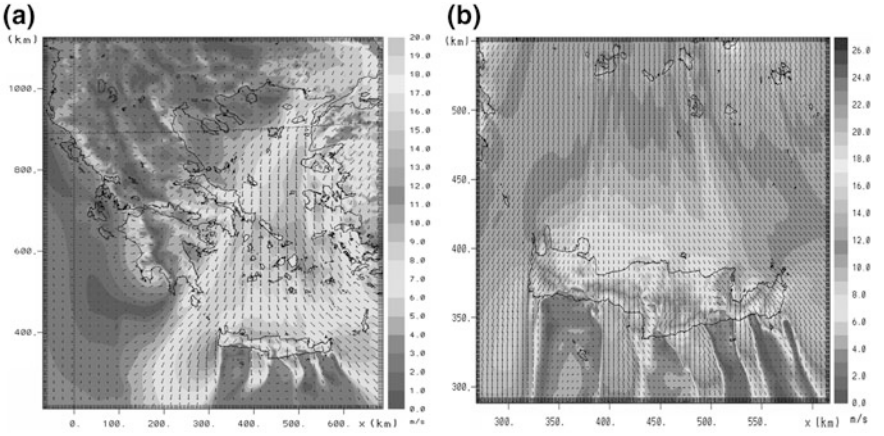

Fig. 86.1 Flow fields over the Aegean Sea and Crete **a** near the surface (10 m AGL) and **b** at the *top* of the MBL (250 m AGL) for 13 September 2015, 11:00 UTC

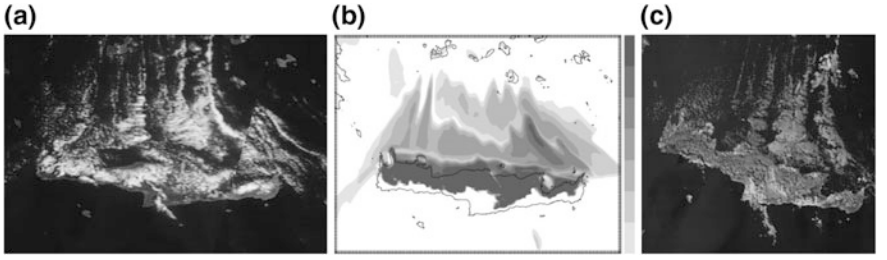

Fig. 86.2 Satellite images for 13 September 2015, 11:20 UTC **a** visible, **b** model simulated cloud fraction, **c** processed indicating the CCN concentrations

colors illustrating the areas with high CCN concentrations. The satellite retrievals of CCN (based on the NPP/VIIRS data from 13/9/2015 11:19 UT) showed that warm clouds generated on the north of the island of Crete. The CCN reached the number of 313/cm^2 at supersaturation of 0.25% over the sea in the area North of Crete.

The concentrations tend to become higher as approaching Crete where it was reaching the amounts of 451 and 529 (at S = 0.21%) over Central and East Crete respectively. Similar behavior but in higher Supersaturation is observed downwind, to the southern part of the island.

A number of sensitivity tests has been carried out in order to explore the role various types of aerosols. In this particular case it was found that the anthropogenic-origin aerosols were around the regular background while there is no desert dust at considerable amount. The main origin of aerosols and CCN is sea salt from the Aegean Sea. The relatively strong winds generated waves with white caps that favor the sea spraying. In addition, the wave breaking over the northerly coasts

of the Aegean islands enhances further its production. Sea spraying in an unsaturated environment (northerly winds with relatively low water content) leads in quick evaporation and release of salt particles. Most of the salt particles remain within the MBL while a considerable amount is injected above it with the aid of the updrafts generated over the Aegean islands, mainly during the day hours (chimney effect). Sea salt particles are highly hygroscopic and assist in the warm cloud formation at the top of the MBL and above it. The coarse fraction of salt particles acts as GCCN and leads to the quick formation of larger droplets and precipitation.

In this section we discuss the results from two model configurations: (1) sea salt is entering the nucleation processes as CCN and GCCN (basic case) and (2) sea salt is not entering the nucleation processes and nucleation is done only by the background quantity of aerosols (no indirect effects). For the first case the number of CCN is the background (300 #/cm3) plus the activation from the CCN and GCCN while for the second is only the background.

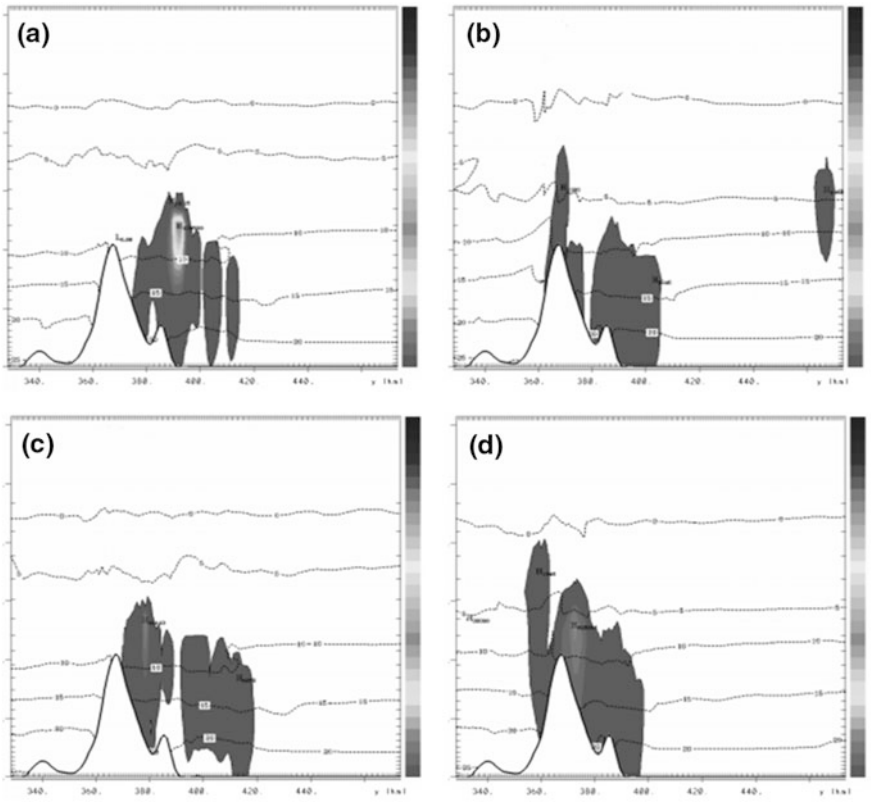

Fig. 86.3 Rain droplet concentration from the basic run (**a**, **b**) and the run without the indirect effects of sea salt (**c**, **d**), at (i) 14/9/2015 13:00 UTC (**a**, **c**) and (ii) 14/9/2015 21:00 UTC (**b**, **d**)

Figure 86.2b illustrates the simulated by the RAMS/ICLAMS model cloud fraction (case 1) at the same time as in Fig. 86.2a, c. As illustrated in this figure, the model was able to simulate successfully the cloud formation in the area south of Cyclades and over the island of Crete. No significant differences are seen between the two cases.

In order to investigate the impacts of sea salt on the vertical structure of the cloud systems cross-sections N-S have been created for various parameters. As seen in Fig. 86.3 the number of rain droplets is higher in the first case. This is something expected because the number of CCN and GCCN is higher in this case and the hydroscopicity of the salt helps on fast droplet growth. The distribution of the cloud droplet size is skewed to the right when the sea salt indirect effects on the formation of CCN and rain droplets is activated (Fig. 86.4a, b). On the other hand smaller droplet sizes are observed when the indirect effects of sea salt are not taken into consideration (Fig. 86.4d, e). This is due to the fact that sea salt is highly hydroscopic. It forms both CCN and GCCN and that leads to the formation of more cloud droplets as soon as the air mass moisture is adequate. This can lead to different results, during the evolution of the event. At the early stage of the event, when there are strong updrafts due to orographic lifting, the rich in seasalt air masses become saturated rather quickly. The droplets grow fast with large diameters and start precipitating. The rain is highly localized as seen in Fig. 86.3a. This is not happening without the indirect impact of sea salt particles as illustrated in Fig. 86.3c.

When the event becomes mature enough, the contribution of the sea salt particles in cloud droplet diameter is not so important. The background of CCN is adequate to condense the available water vapor. The presence of seasalt in some cases can cause superseding conditions as more particles are available for droplet formation. In these cases, the cloud droplet concentration is higher.

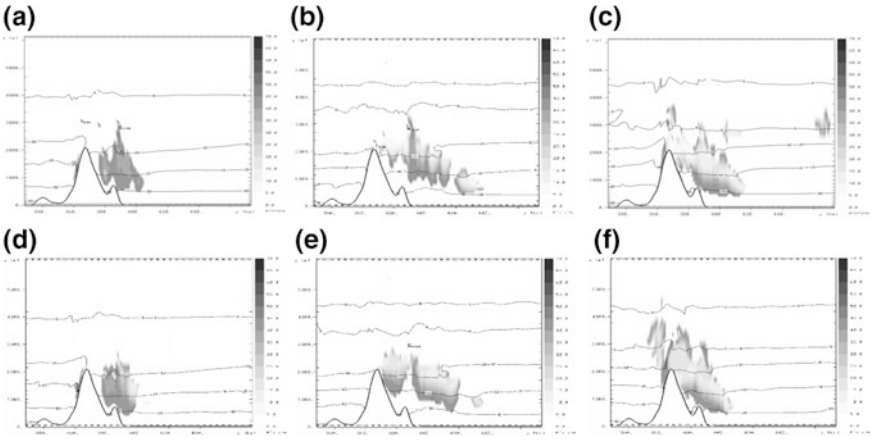

Fig. 86.4 Cloud droplet diameter from the basic run (**a**, **b**, **c**) and the run without the indirect effects of sea salt (**d**, **e**, **f**) at (i) 14/9/2015, 01:00 UTC (**a**, **d**), (ii) 14/9/2015, 13:00 UTC (**b**, **e**) and (iii) 14/9/2015 21:00 UTC (**c**, **f**)

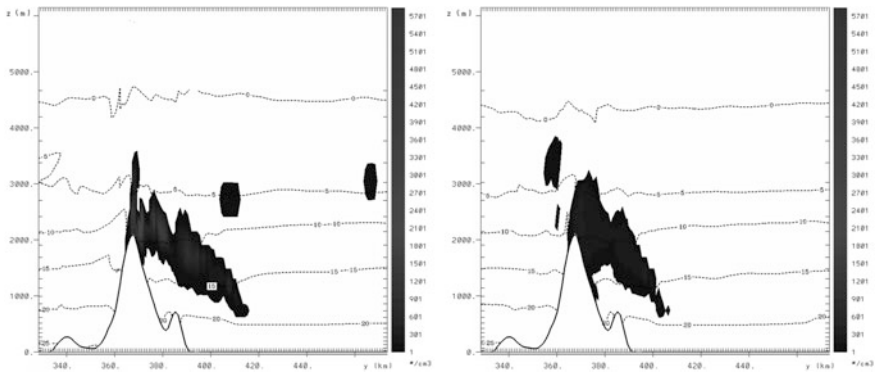

Fig. 86.5 Cloud droplet concentration basic run (*left*) and without the indirect effects of sea salt (*right*), at 14/09/2015, 21:00 UTC

The growth of the droplet inside the cloud is a highly competitive procedure. For this reason despite the fact that sea salt tends to form bigger particles, the high concentration of CCNs will result to a high concentration of droplets with smaller sizes than expected as shown in Fig. 86.4. In fact, the sizes are quite similar to the case without the impact of sea salt as can been seen in Fig. 86.4c, f. In almost all the cases the larger cloud droplets are in the bottom of the cloud deck (Fig. 86.5).

86.3 Conclusions

The simulations show that in areas with relatively high sea salt amounts such as Southern Aegean and Eastern coast of the Mediterranean, low cloud formation, enhanced with orographic lifting is frequent. Desert dust in combination with sea salt can lead in deep convection through orographic lifting and activation of ice nucleation processes. In such cases, the contribution of aerosols from anthropogenic origin is limited. In cases where the lifting is slow and made due to thermal updrafts the sea salt does not play a significant role in the cloud droplet size distribution but mainly in the cloud droplet concentration. Discussion of the cases with other sources of CCN and particularly from dust and anthropogenic sources is not included due to limited space.

Questions and Answers

Questioner: Peter Viaene
Question: What model are you using for the seasalt production (Monahan?)
Answer: Yes, it is the Monahan scheme.

References

Kallos G, Astitha M, Katsafados P, Spyrou C (2007) Long-range transport of anthropogenically and naturally produced particulate matter in the Mediterranean and North Atlantic: current state of knowledge. JAMC 46(8):1230–1251. doi:10.1175/JAM2530.1

Spyrou C, Mitsakou C, Kallos G, Louka P, Vlastou G (2010) An improved limited area model for describing the dust cycle in the atmosphere. JGR 115:D17211. doi:10.1029/2009JD013682

Solomos S, Kallos G, Kushta J, Astitha M, Tremback C, Nenes A, Levin Z (2011) An integrated modeling study on the effects of mineral dust and sea salt particles on clouds and precipitation. Atmos Chem Phys 11:873–892. doi:10.5194/acp-11-873-2011. http://www.atmos-chem-phys.net/11/873/2011/

Chapter 87
Kinetic Modeling of SOA Formation for α- and β-Pinene

K. Gatzsche, Y. Iinuma, A. Mutzel, T. Berndt, L. Poulain, A. Tilgner and R. Wolke

Abstract In the last years, two major findings concerning secondary organic aerosol (SOA) were reported. Firstly, the aerosol particles formed by the organic compounds are higher viscous than previously thought. Up to now, SOA formation modeling has mostly based on gas-particle equilibrium partitioning of semi-volatile species. This approach implicates sufficient diffusion of the organic compounds into the particle phase to keep the condensed phase in equilibrium with the gas phase, thus the phase state of the particle phase is important for SOA modeling. Secondly, highly oxidized multifunctional organic compounds (HOMs) are found to influence the early aerosol growth. In order to investigate both aerosol phase state and HOMs in detail in the SPACCIM model framework, a kinetic partitioning approach was implemented in the box model and the gas-phase chemistry mechanism was updated by HOMs. Finally, the insights of the performed box model studies have been utilized to improve SOA modeling within a 3D model and first results are shown in the present study.

87.1 Introduction

Secondary organic aerosol (SOA) is the major burden of the atmospheric organic particulate matter with 140–910 TgC year^{-1} (Hallquist et al. 2009). SOA particles are formed via the oxidation of volatile organic carbons (VOCs), where the volatility of the VOCs is lowered. Accordingly, gaseous compounds can either nucleate to form new particles or condense on existing particles. The framework of SOA formation under natural conditions is very complex because there are a multitude of gas-phase precursors, atmospheric degradation processes, and products after oxidation. Up to

K. Gatzsche (✉) · A. Mutzel · T. Berndt · L. Poulain · A. Tilgner · R. Wolke
Leibniz Institute for Tropospheric Research (TROPOS), Permoserstraße 15,
04318 Leipzig, Germany
e-mail: gatzsche@tropos.de

Y. Iinuma
Instrumental Analysis Section, Okinawa Institute of Science and Technology
Graduate University (OIST), 1919-1 Tancha, Onna-son, Kunigami,
Okinawa 904-0495, Japan

C. Mensink and G. Kallos (eds.), *Air Pollution Modeling and its Application XXV*,
Springer Proceedings in Complexity, DOI 10.1007/978-3-319-57645-9_87

now, simulations predominantly underestimate measured SOA mass (Volkamer et al. 2006). Thus, the present study has the aim to improve the understanding of SOA formation processes.

Firstly, SOA formation from chamber studies have been investigated with the box model SPACCIM (SPectral Aerosol Cloud Chemistry Interaction Model, Wolke et al. 2005) to gain a better understanding of the key chemical and physical processes. Therefore, SPACCIM has been further developed concerning the gas-to-particle mass transfer by implementing a kinetic partitioning approach established by Zaveri et al. (2014).

Additionally, the formation and immediate partitioning of highly oxidized multifunctional organic compounds (HOMs) which were found in the gas phase during lab and field studies (Mutzel et al. 2015; Jokinen et al. 2015; Berndt et al. 2016) have been considered in the advanced SPACCIM. Additionally, the regarding compounds can have a low volatility and their importance for the early aerosol growth makes them indispensable in SOA modeling. Thus, the measured HOM yields have been incorporated in the utilized gas-phase chemistry mechanism.

After evaluating the sensitivity and impact of the partitioning model parameters in SPACCIM, a stepwise implementation in COSMO-MUSCAT (COnsortium for Small-scale MOdelling and MUlti-Scale Chemistry Aerosol Transport) is conducted. First results of the impact of HOMs on SOA formation has been achieved with the 3D model.

87.2 Model Frameworks and Recent Developments

Box model framework: SPACCIM is an adiabatic air parcel model incorporating a complex size-resolved cloud microphysical model and a multiphase chemistry model (Wolke et al. 2005). Interaction between both models is performed by a coupling scheme, whereby both models run as far as possible independently and apply their own time step control. However, the partitioning of organic gases towards the particle phase was not considered in the original SPACCIM model code and therefore, the kinetic partitioning approach, established by Zaveri et al. (2014), has been implemented. The kinetic partitioning is based on Fick's second law, which describes the diffusive flux of a solute in the particle phase. Additionally, this relation is extended by a particle phase reaction of the solute Zaveri et al. (2014):

$$\frac{\partial A_i(r,t)}{\partial t} = D_{\mathrm{b},i}\frac{1}{r^2}\frac{\partial}{\partial r}\left(r^2\frac{\partial A_i(r,t)}{\partial r}\right) - k_{\mathrm{c},i}A_i(r,t). \tag{87.1}$$

Therein, i means the particle-phase concentration of the solute i depending on the particle radius r and the time t, the bulk diffusion coefficient of the individual solute in the particle phase $D_{\mathrm{b},i}$, and the chemical rate constant for reactions of the solute within the particle phase $k_{\mathrm{c},i}$. Equation (87.1) utilizing the fundamental simplification of a constant bulk diffusion coefficient $D_{\mathrm{b},i}$. Zaveri et al. (2014) provides a special

solution of Eq. (87.1) applicable to general systems treated with 3D Eulerian models, which has been implemented in SPACCIM.

The basic gas-phase chemistry mechanism for α- and β-pinene has been adapted from Chen and Griffin (2005) and measured HOM yields (Jokinen et al. 2015; Berndt et al. 2016) have been incorporated. The vapor pressures of the semi-volatile and low volatile organic compounds has been estimated by the group contribution method of Compernolle et al. (2011).

3D model framework: COSMO-MUSCAT is the state-of-the-art multiscale model system developed at the modeling department of TROPOS (Wolke et al. 2012), which is qualified for process studies in local and regional areas. The model system consists of two online-coupled codes. The non-hydrostatic and compressible meteorological model COSMO (Schättler et al. 2013) as meteorological driver and the chemistry transport model MUSCAT for atmospheric transport as well as chemical transformations of gas-phase and particle-phase species.

Biogenic VOC emission estimates are derived by the emission scheme provided by Steinbrecher et al. (2009). The gas-phase chemistry mechanism is composed of RACM (Regional Atmospheric Chemistry Mechanism, Stockwell et al. 1997) and MIM2 (Mainz Isoprene Mechanism 2, Karl et al. 2006). SOA formation is described by the SORGAM modul (Secondary Organic Aerosol Model, Schell et al. 2001), which has been implemented in the updated version of Li et al. (2013). The HOM yields have been incorporated in the existing gas-phase chemistry mechanism for α- and β-pinene, limonene, mycrence (Jokinen et al. 2015; Berndt et al. 2016), and for three sesquiterpenes (α-cedrene, β-caryophyllene, and α-humulene, Richters et al. 2016).

87.3 Results

Box model results: Sensitivity studies have been examined to characterize the influence of the different model parameters on the SOA formation. As a result of this investigation, the diffusion coefficient of the particle phase D_b and the chemical rate constant for particle-phase reactions k_c have found to be the key parameters for the kinetic partitioning. For liquid particles and highest pseudo-first-order rate constants, the SOA formation is most effective. Around $D_b = 10^{-15}\ m^2 s^{-1}$, the transition between liquid and semi-solid particles occur. Therefore, SOA mass is markedly reduced for values $D_b \leq 10^{-15}\ m^2 s^{-1}$. A more detailed description of the results from the parameter sensitivity studies and the chamber simulations is given Gatzsche et al. (2017).

Additionally, the influence of the considered HOM yields on SOA formation has been investigated. For α-pinene ozonolysis, SOA formation occurs earlier and 50% more organic mass is formed in comparison to the base case (see Fig. 87.1). HOMs partition almost immediately into the particle phase and therefore, serve as absorbing

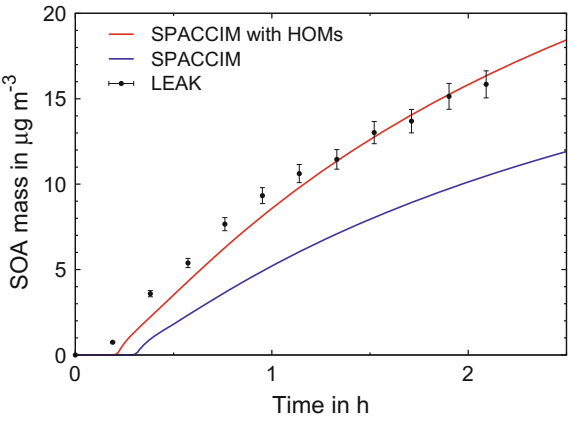

Fig. 87.1 Results of the box model SPACCIM for α-pinene ozonolysis: Simulated SOA mass with (*red*) and without (*blue*) consideration of HOMs. Measured SOA mass (*black dots*) from a chamber experiment for α-pinene ozonolysis in LEAK (**Le**ipziger **A**erosol**k**ammer) are shown for comparison

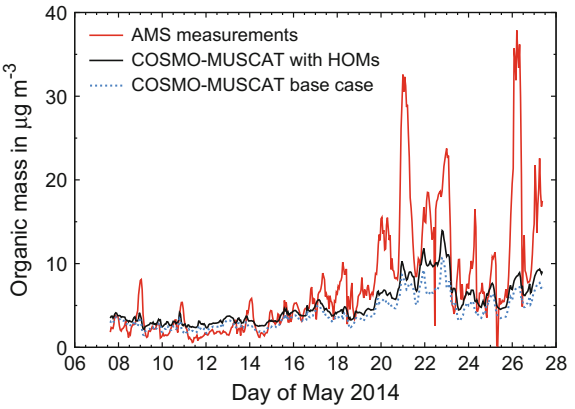

Fig. 87.2 Results of the 3D model COSMO-MUSCAT for the TROPOS field site Melpitz (51° 32′N, 12° 54′E, 87 m asl); Hourly AMS measurements of organic mass (PM1) and hourly model results of organic mass calculated from SOA and POA with HOMs (*solid black line*) and without HOMs (*dotted blue line*)

mass for the remaining semi-volatile compounds. Overall, HOMs contributes with about 30% to the total SOA mass.

3D model results: In Fig. 87.2 a comparison between the hourly measured and simulated organic aerosol mass concentrations at the TROPOS field site Melpitz is shown with and without consideration of HOMs. Online measurements of the particle composition at Melpitz have been conducted with an Aerodyne High-327 Resolution Time-of-Flight Aerosol Mass Spectrometer (HR-TOF-AMS, Aerodyne, Inc., DeCarlo et al. 2006), to derive the organic aerosol mass. For comparison, simulated SOA and POA (primary organic aerosol) were added up to derive the organic mass concentration from the model. The temporal trend of the simulated organic aerosol mass is in good agreement with the measured organic mass. However, some characteristic concentration peaks are not reproduced by the model. Overall, the simulation including HOMs provides more organic mass and, therefore, fits better to the measurements.

87.4 Conclusions

The advanced framework including the kinetic partitioning approach and a gas-phase chemistry mechanism updated by HOMs has been applied in the box model SPACCIM. The comparison with α-pinene chamber experiments have shown a strong improvement for the simulated SOA mass. Sensitivity studies have revealed that in particular the particle phase diffusion coefficient and the rate constant for particle phase reactions affect the simulated SOA. For the 3D modeling, the consideration of HOMs leads to increased SOA mass and consequently higher total organic mass concentrations, which are in better agreement with available field measurements.

Question and Answer

Questioner: Peter Viaene.
Question: Have you considered changes in reaction surface which would affect the kinetics by introducing a $k_c(r_p)$?
Answer: The reactivity of the surface can be influenced by the partitioning of organic compounds. However, we did not consider changes of k_c in our simulations. Since, no measurement values of k_c are available to us, we initially have to estimate this parameter from simulations. We will consider the idea for further investigations.

References

Berndt T, Richters S, Jokinen T, Hyttinen N, Kurtén T, Otkjær RV, Kjaergaard HG, Stratmann F, Herrmann H, Sipilä M, Kulmala M, Ehn M (2016) Hydroxyl radical-induced formation of highly oxidized organic compounds. Nat Commun (in press)

Chen J, Griffin RJ (2005) Modeling secondary organic aerosol formation from oxidation of α-pinene, β-pinene, and d-limonene. Atmos Environ 39(40):7731–7744. doi:10.1016/j.atmosenv.2005.05.049

Compernolle S, Ceulemans K, Müller JF (2011) Evaporation: a new vapour pressure estimation methodfor organic molecules including non-additivity and intramolecular interactions. Atmos Chem Phys 11(18):9431–9450. doi:10.5194/acp-11-9431-2011

DeCarlo PF, Kimmel JR, Trimborn A, Northway MJ, Jayne JT, Aiken AC, Gonin M, Fuhrer K, Horvath T, Docherty KS, Worsnop DR, Jimenez JL (2006) Field-deployable, high-resolution, time-of-flight aerosol mass spectrometer. Anal Chem 78(24):8281–8289. doi:10.1021/ac061249n

Gatzsche K, Iinuma Y, Tilgner A, Mutzel A, Berndt T, Wolke R (2017) Modeling studies of SOA formation from -pinene ozonolysis. Atmos Chem Phys Discuss 1–33. doi:10.5194/acp-2017-275

Hallquist M, Wenger JC, Baltensperger U, Rudich Y, Simpson D, Claeys M, Dommen J, Donahue NM, George C, Goldstein AH, Hamilton JF, Herrmann H, Hoffmann T, Iinuma Y, Jang M, Jenkin ME, Jimenez JL, Kiendler-Scharr A, Maenhaut W, McFiggans G, Mentel TF, Monod A, Prévôt ASH, Seinfeld JH, Surratt JD, Szmigielski R, Wildt J (2009) The formation,

properties and impact of secondary organic aerosol: current and emerging issues. Atmos Chem Phys 9(14):5155–5236. doi:10.5194/acp-9-5155-2009

Jokinen T, Berndt T, Makkonen R, Kerminen VM, Junninen H, Paasonen P, Stratmann F, Herrmann H, Guenther AB, Worsnop DR, Kulmala M, Ehn M, Sipilä M (2015) Production of extremely low volatile organic compounds from biogenic emissions: measured yields and atmospheric implications. Proc Natl Acad Sci 112(23):7123–7128. doi:10.1073/pnas.1423977112

Karl M, Dorn HP, Holland F, Koppmann R, Poppe D, Rupp L, Schaub A, Wahner A (2006) Product study of the reaction of oh radicals with isoprene in the atmosphere simulation chamber saphir. J Atmos Chem 55(2):167–187. doi:10.1007/s10874-006-9034-x

Li YP, Elbern H, Lu KD, Friese E, Kiendler-Scharr A, Mentel TF, Wang XS, Wahner A, Zhang YH (2013) Updated aerosol module and its application to simulate secondary organic aerosols during impact campaign May 2008. Atmos Chem Phys 13(13):6289–6304. doi:10.5194/acp-13-6289-2013

Mutzel A, Poulain L, Berndt T, Iinuma Y, Rodigast M, Böge O, Richters S, Spindler G, Sipilä M, Jokinen T, Kulmala M, Herrmann H (2015) Highly oxidized multifunctional organic compounds observed in tropospheric particles: a field and laboratory study. Environ Sci Technol 49(13):7754–7761. doi:10.1021/acs.est.5b00885

Richters S, Herrmann H, Berndt T (2016) Highly oxidized RO_2 radicals and consecutive products from the ozonolysis of three sesquiterpenes. Environ Sci Technol 50(5):2354–2362. doi:10.1021/acs.est.5b05321

Schättler U, Doms G, Schraff C (2013) A description of the nonhydrostatic regional cosmo-model. Part vii: user's guide. Deutscher Wetterdienst, Offenbach. http://www.cosmo-model.org

Schell B, Ackermann IJ, Hass H, Binkowski FS, Ebel A (2001) Modeling the formation of secondary organic aerosol within a comprehensive air quality model system. J Geophys Res Atmos 106(D22):28,275–28,293. doi:10.1029/2001JD000384

Steinbrecher R, Smiatek G, Koeble R, Seufert G, Theloke J, Hauff K, Ciccioli P, Vautard R, Curci G (2009) Intra- and inter-annual variability of VOC emissions from natural and semi-natural vegetation in Europe and neighbouring countries. Atmos Environ 43(7):1380–1391. doi:10.1016/j.atmosenv.2008.09.072

Stockwell WR, Kirchner F, Kuhn M, Seefeld S (1997) A new mechanism for regional atmospheric chemistry modeling. J Geophys Res Atmos 102(D22):25,847–25,879. doi:10.1029/97JD00849

Volkamer R, Jimenez JL, San Martini F, Dzepina K, Zhang Q, Salcedo D, Molina LT, Worsnop DR, Molina MJ (2006) Secondary organic aerosol formation from anthropogenic air pollution: rapid and higher than expected. Geophys Res Lett 33(17):1944–8007. doi:10.1029/2006gl026899

Wolke R, Sehili A, Simmel M, Knoth O, Tilgner A, Herrmann H (2005) SPACCIM: a parcel model with detailed microphysics and complex multiphase chemistry. Atmos Environ 39(23–24):4375–4388. doi:10.1016/j.atmosenv.2005.02.038

Wolke R, Schröder W, Schrödner R, Renner E (2012) Influence of grid resolution and meteorological forcing on simulated european air quality: a sensitivity study with the modeling system COSMO-MUSCAT. Atmos Environ 53:110–130. doi:10.1016/j.atmosenv.2012.02.085

Zaveri RA, Easter RC, Shilling JE, Seinfeld JH (2014) Modeling kinetic partitioning of secondary organic aerosol and size distribution dynamics: representing effects of volatility, phase state, and particle-phase reaction. Atmos Chem Phys 14(10):5153–5181. doi:10.5194/acp-14-5153-2014

Chapter 88
Evaluation of Organic Aerosol and Its Precursors in the SILAM Model

Marje Prank, Julius Vira, Riinu Ots and Mikhail Sofiev

Abstract Volatility basis-set (VBS) was implemented in the atmospheric chemistry and transport model SILAM for modelling organic aerosol (OA). We present the evaluation of the concentrations of OA and its precursors against observations available in the EBAS database. SILAM simulations with biogenic and anthropogenic emissions from different inventories and different assumptions about the chemical composition of the VOC emissions and OA volatility are analyzed. The contributions of different precursors to the total OA are evaluated.

88.1 Introduction

Secondary organic aerosol (SOA) makes up the majority of organic particles in the atmosphere, especially during warm periods, indicating an important role of the biogenic volatile organic compounds (VOCs), but also in winter, originating from biomass burning. Large uncertainties exist in modelling the organic carbon emission, formation of SOA and its partitioning between the gas and aerosol phases.

We present the evaluation of the concentrations of organic aerosols and their pre-cursors from SILAM (http://silam.fmi.fi/) simulations with biogenic and anthropogenic emissions from different inventories and different assumptions about the chemical composition of the VOC emissions and organic aerosol (OA) volatility against the observations available in the EBAS database.

M. Prank (✉) · J. Vira · M. Sofiev
Finnish Meteorological Institute, Helsinki, Finland
e-mail: marje.prank@fmi.fi

J. Vira
e-mail: julius.vira@fmi.fi

M. Sofiev
e-mail: mikhail.sofiev@fmi.fi

R. Ots
School of Chemistry, University of Edinburgh, Edinburgh, UK

C. Mensink and G. Kallos (eds.), *Air Pollution Modeling and its Application XXV*,
Springer Proceedings in Complexity, DOI 10.1007/978-3-319-57645-9_88

88.2 Modelling SOA with SILAM

The volatility basis-set (VBS) scheme (Donahue et al. 2006) was implemented in the SILAM model for modelling OA. The oxidation of the gas-phase precursors is simulated with the CBM-IV chemical scheme, using updated reaction rates from IUPAC (http://iupac.pole-ether.fr) and JPL (http://jpldataeval.jpl.nasa.gov). Terpenes oxidation has been added from the CB05 reaction list. SOA production is computed from toluene, xylene, isoprene and monoterpenes using the NO_x dependent yields of Lane et al. (2008). VBS in SILAM has 1 non-volatile bin and 4 semivolatile bins (1–1000 μg/m^3 saturation concentrations), separately for SOA from biogenic and anthropogenic precursors, and additionally 3 intermediate volatility bins (1e4–1e6 μg/m^3) for anthropogenic IVOC emissions.

The model setup followed the AQMEII3 specifications. The four considered cases are shown in Table 88.1. In the base case we used the volatility distribution of Shrivastava et al. (2011) for the anthropogenic emissions. The Biogenic Emission Model (BEM, Poupkou et al. 2010), implemented online in SILAM, was used for the biogenic VOCs emission. Wildfire emissions originated from IS4FIRES and were assumed nonvolatile, as the emission calibration already partly includes secondary species. We compare the base case with simulations with (i) full VOC and IVOC emissions from fires, (ii) using MEGAN biogenic emissions instead those of BEM, and (iii) including SOA formation from IVOCs from diesel exhaust following Ots et al. (2016), where n-pentadecane (C15H32) is introduced as a surrogate for the intermediate volatility compounds and is emitted proportionally to NMVOCs from diesel engines. The MEGAN-MACC inventory, downloaded from http://eccad.sedoo.fr, has monthly temporal resolution, and the diurnal emission variations were computed as a function of the solar zenith angle.

Table 88.1 Model setups for the computed cases

	Base	FullFire	MEGAN	Diesel
Anthropogenic IVOC	6.5 * OA (Shrivastava et al. 2011)	6.5 * OA	6.5 * OA	6.5*OA for residential heating (S2), other sectors OA non-volatile. C15H32 from diesel vehicles (S72, S8) emitted proportionally to NMVOC * 12.25
BioVOC emission model	BEM	BEM	MEGAN-MACC	BEM
Wildfire emission	Non-volatile	6.5 * OA + gaseous precursors	Non-volatile	Non-volatile

88.3 Results and Discussion

The base case simulations showed large underestimation of OA in winter, while the summertime concentrations were well reproduced (Fig. 88.1, left). During the summer, OA was dominated by biogenic compounds, mostly originating from monoterpenes. In winter, the largest contribution was attributed to residential heating.

The wintertime OA concentrations computed with the volatility distribution of Shrivastava et al. (2011) did not exceed the values obtained by emitting all anthropogenic OA as nonvolatile and not accounting for SOA formation. Adding up the concentrations of OA and condensable gases brings the model quite close to the observed OC (Fig. 88.1, right), but due to slow wintertime oxidation the gases in the intermediate volatility range do not reach low enough volatility to partition to the aerosol phase. This indicates that the reasons for the winter time underestimations are both in missing emissions and too slow aging processes in the model.

Table 88.2 summarizes the model skill for the simulations. While including the full wildfire organic emissions or using the diesel emissions of Ots et al. (2016) reduces noticeably the model bias, the temporal correlation for these cases is low. The reason for this behavior is that they both mainly contribute to OA in summer—the fires because of larger emissions and the diesel surrogate because of faster

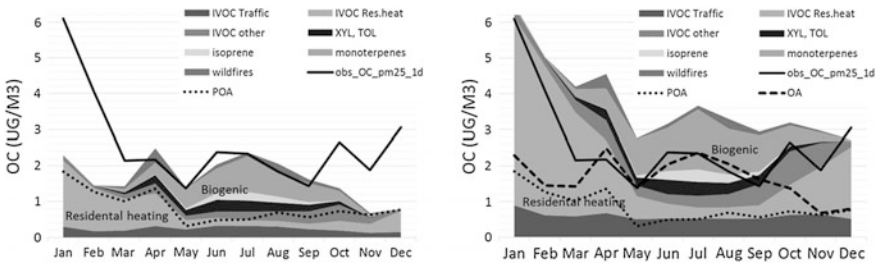

Fig. 88.1 Modelled OC composition by sources and precursors, monthly mean, average over stations. *Left*—aerosol phase, *right*—aerosol and condensable gases, EMEP OC measurements (*solid black line*) and model results for primary OC assumed nonvolatile (*dotted line*) and modelled OA (*dashed line*)

Table 88.2 Model-measurement comparison of OC for different model setups

OC	NMB (%)	Stdev ratio	Correlation (temporal)	Correlation (spatial)
Base	−41.87	0.71	0.40	0.70
MEGAN	−42.78	0.67	0.41	0.82
Diesel	5.34	1.21	0.35	0.81
FullFire	−29.98	1.03	0.36	0.59
POA NV	−63.28	0.50	0.49	0.74

oxidation—and further emphasize the wrong seasonal variation in the modelled OA.

Using MEGAN instead of BEM improves the spatial correlation noticeably. Large discrepancies were found between the biogenic VOC emissions from different models. Figure 88.2 compares the isoprene and monoterpene emissions from BEM, MEGAN-MACC and EMEP models. BEM shows the highest isoprene emissions, also the monoterpene emissions are substantially higher than those of MEGAN-MACC inventory. The emission patterns also differ considerably between the inventories.

The concentrations of isoprene were heavily overestimated by SILAM (Table 88.3). With BEM SILAM overestimated isoprene 4.4 times and with MEGAN-MACC 2.5 times. The isoprene simulated with the MEGAN emissions had spatial correlation of 0.88 for the annual average values, while BEM simulations failed to reproduce the spatial pattern. The temporal correlation was better for the BEM simulation (0.62 vs. 0.46), probably due to the monthly temporal

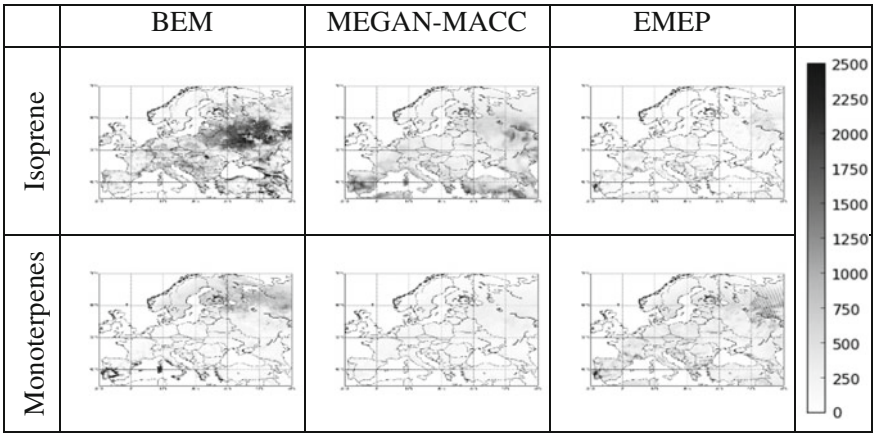

Fig. 88.2 Emission maps of isoprene and monoterpenes for July 2010

Table 88.3 Model-measurement comparison for SOA precursors

	Emission	NMB (%)	Stdev ratio	Correlation (temporal)	Correlation (spatial)
XYL	MACC	−8.46	1.18	0.34	0.20
TOL	MACC	−47.98	0.41	0.32	0.43
ISOP	BEM	338.91	3.56	0.62	−0.20
	MEGAN-MACC	153.04	1.70	0.46	0.88
MNTERP	BEM	−20.95	0.83	0.52	
	MEGAN-MACC	−79.92	0.24	0.00	

resolution of the MEGAN data, while BEM was called every SILAM time-step with the current meteorology.

The errors in modelled monoterpene concentration could not be reliably estimated, as the observations were available only at the Birkenes station. Simulations with BEM emissions underestimated there by about 30% and with MEGAN-MACC about 80%. The model showed almost no monoterpenes in winter, while the observed values were 5–8 times lower than summer but still noticeable.

Toluene was underestimated about twice and xylene reproduced with small negative bias. Large underestimation was present for both in summer, while the winter values were overestimated, indicating too strong oxidation in summer and too slow in winter.

The simulated contributions from isoprene, xylene and toluene to the OA were small, making the model not sensitive to the errors in those species. Due to the large impact of monoterpenes, more observations would be beneficial to evaluate the model for that species.

Question and Answer

Questioner: Paul Makar
Question: How well does the VBS temperature dependence capture the observed temperature dependence of IVOC-like compounds?
Answer: A wide range of IVOC vaporization enthalpies has been reported in literature (30–150 kJ mol^{-1}) and noticeable model sensitivity to this value was shown by Farina et al. (2010), although mainly for the upper layers of the atmosphere. However, the values used in this study are the same as used by Tsimpidi et al. (2010), and these are already at the higher end of the reported range (64–112 kJ mol^{-1}, depending on the VBS bin).

Also, there is evidence from the AMS measurements that the missing part of the winter SOA is aged aerosol. So the gap between the observations and model cannot be fully explained by wrong temperature dependence of the partitioning, but rather some emissions of organic compounds are still missing from the anthropogenic emission inventories the models are missing wintertime aging processes.

References

Donahue NM, Robinson AL, Stanier CO, Pandis SN (2006) Coupled partitioning, dilution, and chemical aging of semivolatile organics. Environ Sci Technol 40:2635–2643. doi:10.1021/es052297c

Farina SC, Adams PJ, Pandis SN (2010) Modeling global secondary organic aerosol formation and processing with the volatility basis set: implications for anthropogenic secondary organic aerosol. J Geophys Res Atmos 115:1–17. doi:10.1029/2009JD013046

Lane TE, Donahue NM, Pandis SM (2008) Effect of NOx on secondary organic aerosol concentrations. Environ Sci Technol 42:6022–6027

Ots R, Young DE, Vieno M, Xu L, Dunmore RE, Allan JD, Coe H, Williams LR, Herndon SC, Ng NL, Hamilton JF, Bergström R, Marco C Di, Nemitz E, Mackenzie IA, Kuenen JJP, Green DC, Reis S, Heal MR (2016) Simulating secondary organic aerosol from missing diesel-related intermediate-volatility organic compound emissions during the Clean Air for London (ClearfLo) campaign. Atmos Chem Phys 16:6453–6473. doi:10.5194/acp-2015-920

Poupkou A, Giannaros T, Markakis K, Kioutsioukis I, Curci G, Melas D, Zerefos C (2010) A model for European biogenic volatile organic compound emissions: software development and first validation. Environ Model Softw 25:1845–1856. doi:10.1016/j.envsoft.2010.05.004

Shrivastava M, Fast J, Easter R, Gustafson WI, Zaveri, RA, Jimenez JL, Saide P, Hodzic A (2011) Modeling organic aerosols in a megacity: comparison of simple and complex representations of the volatility basis set approach. Atmos Chem Phys 11:6639–6662. doi:10.5194/acp-11-6639-2011

Tsimpidi AP, Karydis VA, Zavala M, Lei W, Molina L, Ulbrich IM, Jimenez JL, Pandis SN (2010) Evaluation of the volatility basis-set approach for the simulation of organic aerosol formation in the Mexico City metropolitan area. Atmos Chem Phys 10:525–546. doi:10.5194/acp-10-525-2010

Chapter 89
Development, Implementation, and Evaluation of a Physics-Based Windblown Dust Emission Model

Hosein Foroutan, Jeff Young, Peng Liu, Limei Ran, Jonathan Pleim and Rohit Mathur

Abstract A physics-based windblown dust emission parameterization scheme is developed and implemented in the CMAQ modeling system. A distinct feature of the present model includes the incorporation of a newly developed, dynamic relation for the surface roughness length, which is important in correctly predicting both the friction velocity and the roughness correction factor used in the dust emission model. Careful attention is paid in integrating the new dust module within the CMAQ to ensure the required input parameters are correctly configured. The model is evaluated for two test cases including the continental United States and the Northern hemisphere, and is shown to be able to capture the occurrence of the dust outbreak and the level of the soil concentration.

89.1 Introduction

Windblown dust, emitted from surface of the earth to the atmosphere, has significant impacts on atmospheric phenomena and air quality. It contributes to the alteration of solar radiative budgets, reduction of the atmospheric visibility, and long-range transport of organic chemicals, airborne bacterial species, and trace metals. Considering these strong impacts, quantifying and modeling the factors that control windblown dust emission are important. Nevertheless, several studies (Uno et al. 2006; Todd et al. 2008; Huneeus et al. 2011) demonstrated considerable differences in the dust generation between model predictions and observations, pointing to a need to improve windblown dust emission modeling.

The high level of uncertainty in modeling dust emission is attributed to two issues. First, windblown dust emissions involve several complex and nonlinear processes that are governed by meteorology, land surface characterization, and soil

H. Foroutan (✉) · J. Young · P. Liu · L. Ran · J. Pleim · R. Mathur
Computational Exposure Division, National Exposure Research Laboratory, U.S. Environmental Protection Agency, Research Triangle Park, NC, USA
e-mail: foroutan.hosein@epa.gov

C. Mensink and G. Kallos (eds.), *Air Pollution Modeling and its Application XXV*, Springer Proceedings in Complexity, DOI 10.1007/978-3-319-57645-9_89

texture. A second source of uncertainty is related to the implementation of windblown dust emission schemes into atmospheric modeling systems. In particular, the parameters and physics packages used by mesoscale models should be consistent with the input data required by the dust emission schemes.

In this work, we present the development of a physics-based windblown dust model, and its integration within the Community Multiscale Air Quality (CMAQ v5.1) modeling system. We put more emphasis on the aspects of the model and its implementation that may be of interest within other modeling systems as well.

89.2 Model Development

In formulation of the newly developed model, the main mechanism behind the windblown dust emission is considered to be the saltation (sand blasting). The physics of saltation can be summarized as follows: The wind shear over a surface can result in uplifting the sand particles. However, the gravity force on the particles ultimately exceeds the uplifting force carrying them back to the surface. The striking of these returning particles to the surface, known as the saltation, can overcome the inter-particle cohesive forces and result in vertical emission of smaller dust particles.

These processes are mathematically formulated in the present model. The friction velocity, representing the surface shear stress exerted by the blowing wind, is calculated at the surface of the earth. The aerodynamic lifting of surface particles can occur only above a certain threshold velocity. Here, we first calculate the ideal threshold friction velocity on a dry, smooth, and bare surface through a particle size dependent relation (Shao and Lu 2000). The idea behind this approach is that the soil particles with diameters from around 60–200 μm are most likely to be picked up by the wind, resulting in saltation and vertical dust emission. For smaller particles, cohesive forces prevent the saltation, while larger particles are harder to move due to the gravity force. The actual threshold friction velocity is obtained through two correction factors incorporating the effects of soil moisture (Fecan et al. 1999) and non-erodible surface roughness elements (Xi and Sokolik 2015). Both these factors suppress the dust emission, therefore, they are both formulated such that they increase the threshold friction velocity and decrease the likelihood of saltation. Once the friction velocity exceeds its threshold value, saltation (horizontal movement) is allowed to happen and the corresponding horizontal flux (White 1979) is calculated. Finally, the vertical flux of the dust is calculated based on a sandblasting efficiency formulation (vertical-to-horizontal dust flux ratio). A physics-based sandblasting efficiency formulation developed by Lu and Shao (1999) is used in the present dust emission model which includes the effect of soil plasticity, texture, and density. Figure 89.1 shows a schematic diagram of the steps in the present windblown dust model.

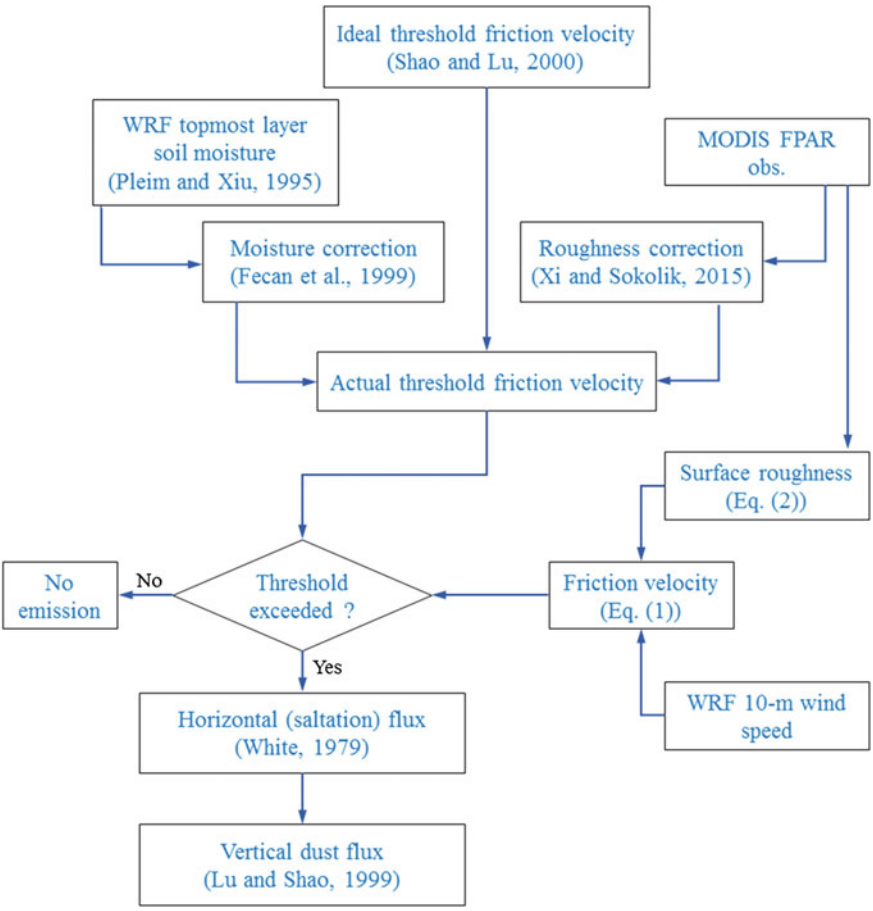

Fig. 89.1 Schematic diagram of the present windblown dust model

89.3 Model Implementation

The present windblown dust model is briefly discussed in the previous section. It should be noted, however, that the integration of the model within a mesoscale atmospheric chemistry model is equally important. In this model (or any other physics-based windblown dust model), the phenomena involved in the dust emission are formulated through analyses of microphysical phenomena in a controlled environment. Therefore, attention needs to be paid in implementing these fully "microphysical" schemes into mesoscale models. In particular, the model-driven parameters should be consistent with those relevant to the dust generation mechanisms. Here, we implement our windblown dust scheme into the CMAQ modeling system (CMAQ v5.1) driven by meteorological fields from WRF (WRF v3.7).

Nevertheless, the discussion in principle is valid for any mesoscale atmospheric or air quality model.

The friction velocity is a critical parameter in all dust emission schemes, and models are shown to be most sensitive to its value. The atmospheric models (WRF in this case) usually provide the friction velocity u_* as an output variable. However, we argue that this modeled friction velocity should not be used as an input to dust emission parameterization since it represents the surface roughness length that is significantly larger than that relevant to the "microscopic" dust generation phenomena. Here, we recalculate (see Fig. 89.1) the friction velocity using the modeled 10 m wind speed (U_{10}) as:

$$u_* = \frac{\kappa U_{10}}{\ln(10/z_0)} \tag{89.1}$$

where, κ is the von Karman constant, and z_0 is the surface roughness length relevant to "microscopic" phenomena involved in the dust generation. In order to develop a relation for z_0 applicable to our model, we have collected the surface roughness length data from several field and laboratory measurements including those summarized by King et al. (2005) and Hébrard et al. (2012). From a linear fitting of data, we estimate the surface roughness length z_0 relevant to the small-scale aeolian processes as:

$$z_0/h = \begin{cases} 0.96\lambda^{1.07}, & \lambda < 0.2 \\ 0.083\lambda^{-0.46}, & \lambda \geq 0.2 \end{cases} \tag{89.2}$$

where, h is the seasonal effective height of roughness elements and λ is the total roughness density, which is a function of the vegetation coverage (Xi and Sokolik 2015). It should be noted that z_0 in Eq. (89.2) is variable both spatially and temporally since the roughness density λ changes with the vegetation coverage fraction. The fraction of absorbed photosynthetically active radiation (FPAR) from Moderate Resolution Imaging Spectroradiometer (MODIS) is used to represent more realistic time-varying vegetation coverage in the present model.

Another important parameter in the dust emission parameterization is the level of soil moisture which affects the threshold friction velocity through a correction factor. The formulation of the soil moisture correction factor (Fecan et al. 1999) has been developed by altering the moisture representative of the topmost ~1 cm of the soil. Therefore, attention should be paid in using the model-driven soil moisture as an input to the dust emission model, especially if the land surface model has a significantly thick surface layer. In that case, higher level of soil moisture can considerably suppress the dust generation. In the present study, we configure CMAQ with the Pleim and Xiu (1995) land surface model (PX LSM), where the topmost layer has a thickness of 1 cm.

89.4 Model Evaluation

The CMAQ v5.1 model with the new windblown dust scheme is used for two simulations: (1) a one-month (March 2011) simulation of a domain covering the continental U.S. (CONUS), and (2) simulation of an African dust storm in early March 2006 on a domain covering the Northern hemisphere.

89.4.1 The CONUS Test Case

For this test case, model simulations are performed over a 12 km horizontal resolution grid covering the CONUS, and portions of Mexico and Canada. More details of the CMAQ model setup and configurations can be found in Appel et al. (2015). Figure 89.2 shows a spatial plot of mean bias for the fine (PM2.5) soil as defined by the Interagency Monitoring of Protected Visual Environments (IMPROVE; http://vista.cira.colostate.edu/improve) network. The IMPROVE network sites are typically located in rural areas, therefore, the value of soil from these sites is a good indication of the dust outbreak. It can be seen that the modeled soil concentrations are in relatively good agreement with the IMPROVE observations with the mean bias generally in the range of ± 1 μgm^{-3}. There are some underpredictions in the southwest U.S. (Arizona and New Mexico), and some overpredictions in the states located just east of the Rocky Mountains. The domain-wide soil mean bias in March 2011 is 0.12 μgm^{-3} (with median bias of 0.11 μgm^{-3}) over 1326 observations.

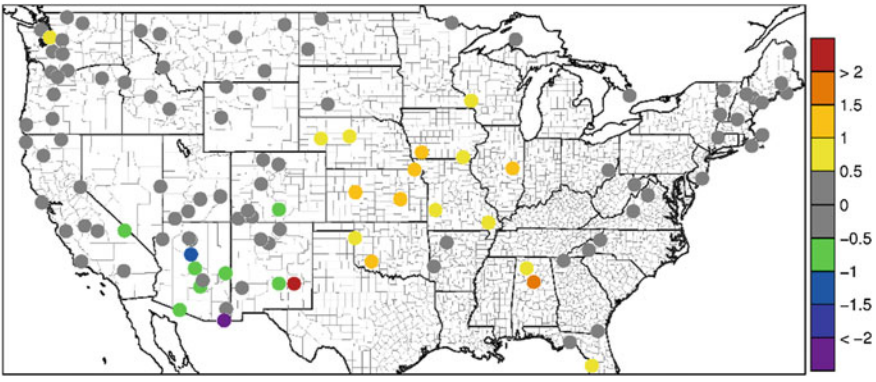

Fig. 89.2 Soil mean bias (μgm^{-3}) at the IMPROVE network sites in March 2011

89.4.2 The Hemispheric Test Case

In order to evaluate the model performance in simulating major dust storms, a hemispheric scale domain covering the Northern hemisphere with a 108 km grid resolution is considered. Simulations are performed for March 2006 with the focus being on a strong Saharan dust storm that occurred in early March. A strong northerly wind started a wide front of dust in northern Algeria on March 5 that affected the air quality across a considerable part of the northwest Africa during the period of March 6–13, 2006. The event is well-documented in Thomas et al. (2009). Figure 89.3 presents the daily Aerosol Optical Depth (AOD) at 550 nm wavelength for March 6 and 7, 2006. For each day, the CMAQ-modeled AOD is compared to the MODIS Terra optical depth at 550 nm extracted from the NASA Reverb/ECHO data system (http://reverb.echo.nasa.gov/reverb/). Although the level of AOD is slightly underestimated by CMAQ, the timing and geographical pattern of the dust event is in quite good agreement with the satellite observations showing the

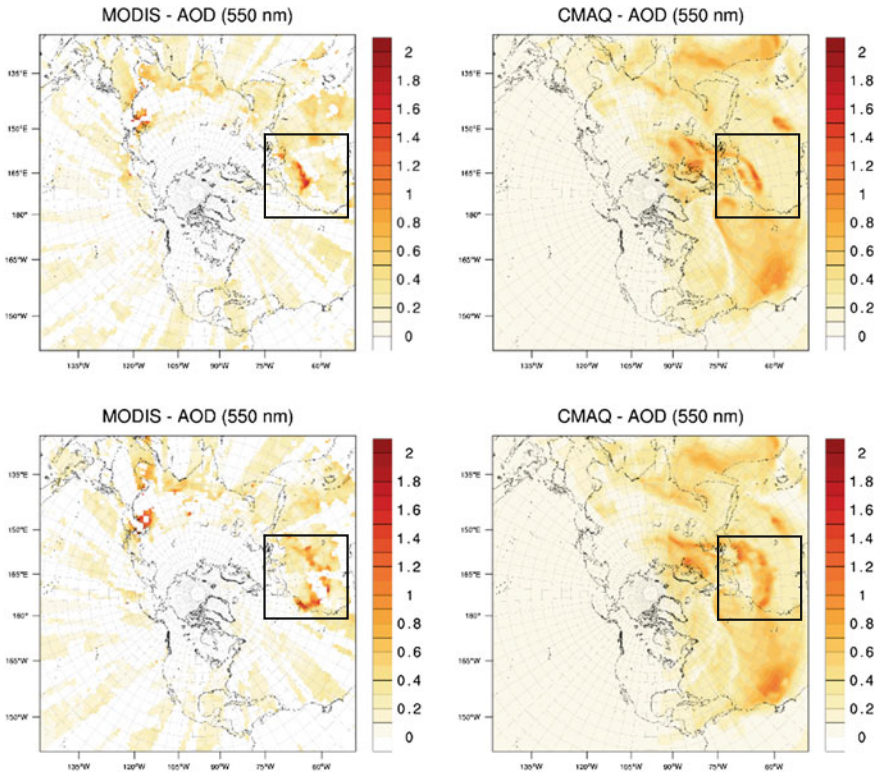

Fig. 89.3 Daily AOD at 550 nm for March 6 (*top*) and March 7 (*bottom*) 2006; comparison between the CMAQ-modeled values and MODIS Terra observations. The box marks the location of the African dust storm

capability of this new dust emission model in capturing major dust outbreaks even on relatively coarse grids. It should be noted that the there is no "tuning" parameter in the newly developed windblown dust module and the same model is used for both cases of the CONUS and hemispheric.

As a summary, the present evaluations indicate an overall agreement of the newly developed windblown dust model in CMAQ and surface and satellite observations. Additional detailed assessment of the model for other test cases is currently underway.

References

Appel KW, Napelenok S, Hogrefe C, Foley KM, Pouliot G, Roselle SJ, and Pleim JE (2015) Evaluation of the community multiscale air quality model version 5.1. In: 14th annual CMAS conference, Chapel Hill, NC, Oct 5–7

Fecan F, Marticorena B, Bergametti G (1999) Parameterization of the increase of the aeolian erosion threshold wind friction velocity due to soil moisture for arid and semi-arid areas. Ann Geophys 17:149–157. doi:10.1007/s005850050744

Hébrard E, Listowski C, Coll P, Marticorena B, Bergametti G, Määttänen A, Montmessin F, Forget F (2012) An aerodynamic roughness length map derived from extended Martian rock abundance data. J Geophys Res 117:E04008. doi:10.1029/2011JE003942

Huneeus N et al (2011) Global dust model intercomparison in AeroCom phase I. Atmos Chem Phys 11:7781–7816. doi:10.5194/acp-11-7781-2011

King J, Nickling WG, Gillies JA (2005) Representation of vegetation and other nonerodible elements in Aeolian shear stress partitioning models for predicting transport threshold. J Geophys Res 110:F04015. doi:10.1029/2004JF000281

Lu H, Shao Y (1999) A new model for dust emission by saltation bombardment. J Geophys Res 104:16827–16842. doi:10.1029/1999JD900169

Pleim JE, Xiu A (1995) Development and testing of a surface flux and planetary boundary layer model for application in mesoscale models. J Appl Meteorol 34:16–32. doi:10.1175/1520-0450-34.1.16

Shao Y, Lu H (2000) A simple expression for wind erosion threshold friction velocity. J Geophys Res 105:22437–22443. doi:10.1029/2000JD900304

Thomas M, Gautier C, Ricchiazzi P (2009) Investigations of the March 2006 African dust storm using ground-based column-integrated high spectral resolution infrared (8–13 μm) and visible aerosol optical thickness measurements: 1. Measurement procedures and results. J Geophys Res 114:D11202. doi:10.1029/2008JD010928

Todd MC et al (2008) Quantifying uncertainty in estimates of mineral dust flux: an intercomparison of model performance over the Bodélé depression, Northern Chad. J Geophys Res 113:D24107. doi:10.1029/2008JD010476

Uno I et al (2006) Dust model intercomparison (DMIP) study over Asia: overview. J Geophys Res 111:D12213. doi:10.1029/2005JD006575

White BR (1979) Soil transport by winds on Mars. J Geophys Res 84:4643–4651. doi:10.1029/JB084iB09p04643

Xi X, Sokolik IN (2015) Seasonal dynamics of threshold friction velocity and dust emission in Central Asia. J Geophys Res Atmos 120:1536–1564. doi:10.1002/2014JD022471

Chapter 90
Highly Hygroscopic Particulate in Cloud Environment

Eleni Drakaki, Stavros Solomos, Christos Spyrou, Jonilda Kushta and George Kallos

Abstract Highly hygroscopic aerosols, such as sodium chloride or sulphates are often present in the atmosphere. They can be produced through several natural or anthropogenic processes (ocean spray, fires, volcanoes, anthropogenic emissions). Their hygroscopicity depends on their chemical properties and thus some of them can serve as cloud condensation nuclei (CCN) easier than others having different impacts on the cloud formation. While the interactions of hygroscopic aerosols with water in the atmosphere is more clearly understood, the impact of aerosols in the resulting precipitation remains inconclusive (Rosenfeld et al. 2008). The thermodynamic state, the background aerosol composition of the atmosphere and the topographical variation of the region can modify these impacts. In this study we use a fully coupled modeling system (atmospheric and chemical—RAMS/ICLAMS) in order to study the impact of highly hygroscopic particles in a cloud system, representing the average thermodynamic conditions of winter convective clouds in the eastern Mediterranean. Of particular interest is the analysis of the level of background pollution in such sensitivity studies. For this reason we applied the material dispersion processes to two characteristic air masses with different pollution levels: clean air masses and highly polluted. This study focuses on the contribution of the material dispersion on the size and number of cloud droplets as well as the liquid and ice mass of the respective cloud system. The dispersion of NaCl (Material 1) resulted in decrease of the amount of ground precipitation, while the background pollution affected the distribution of liquid and ice masses as well as the size of the

E. Drakaki · C. Spyrou · J. Kushta · G. Kallos (✉)
Atmospheric Modeling and Weather Forecasting Group, School of Physics, University of Athens, University Campus, Bldg PHYS-V, 15784 Athens, Greece
e-mail: kallos@mg.uoa.gr

S. Solomos
National Observatory of Athens, IAASARS, I. Metaxa & Vas. Pavlou St, 15236 Penteli, Greece

J. Kushta
The Cyprus Institute, EEWRC, 20 konstantinou Kavafi Street, 2121 Aglantzia Nicosia, Cyprus

C. Mensink and G. Kallos (eds.), *Air Pollution Modeling and its Application XXV*, Springer Proceedings in Complexity, DOI 10.1007/978-3-319-57645-9_90

hydrometeors. In respect to the time of cloud development the effect of the material dispersion was more evident in the mature phase of the cloud system.

90.1 Introduction

Aerosols from various sources in the atmosphere, affecting directly and indirectly the atmospheric composition, cloud droplets and ice crystals formation, influence the radiate balance and modify the initiation and evolution of precipitation in time and space (Rosenfeld et al. 2008). The thermodynamic state and the background aerosol composition of the atmosphere are some of the factors that can modify these impacts. The explicit representation of the cloud droplets and ice crystals condensations improves the simulation accuracy of precipitation distribution as well as the onset and severity of precipitation. Beyond, the configuration factors, mainly vertical and horizontal resolution that influence the model performance and the inclusion of the aerosol effects in the microphysical processes are essential. In order to study such interactions, the fully coupled modeling system RAMS/ICLAMS has been used. The state-of-the-art model includes online natural and anthropogenic aerosol cycles, photochemistry and various chemical processes. Mineral dust, sea salt and several anthropogenic aerosol are also considered as condensation nuclei (Solomos et al. 2011; Kushta et al. 2014; Kallos et al. 2014). The main objective of this study is to investigate the impact of giant sea salt particles on a winter convective cloud system in the eastern Mediterranean that develops in different background pollution levels (clean—polluted).

90.2 Model Configuration and Data Used

The case examined here is a Mediterranean convective cloud system (Levin et al. 2005). Its initial temperature and humidity profile is show in Fig. 90.1. Since aerosol interactions are associated with processes in the microphysics scale, 2-D cloud-resolving simulations, with 65 vertical levels were performed. During these, NaCl with lognormal number median diameter of 0.2 μm, released in a layer at 200 m height and dispersed all over the domain by the atmospheric circulation. In order to simulate the near surface sea salt emission rate, the injection rate assumed to be 1 $\mu g m^{-3} s^{-1}$. According to observation data, 500 and 800 units/cm^3 aerosol particles concentration was assumed, for the clean and polluted background respectively (Rosenfeld et al. 2008). The different conceptual scenarios are shown at Table 90.1.

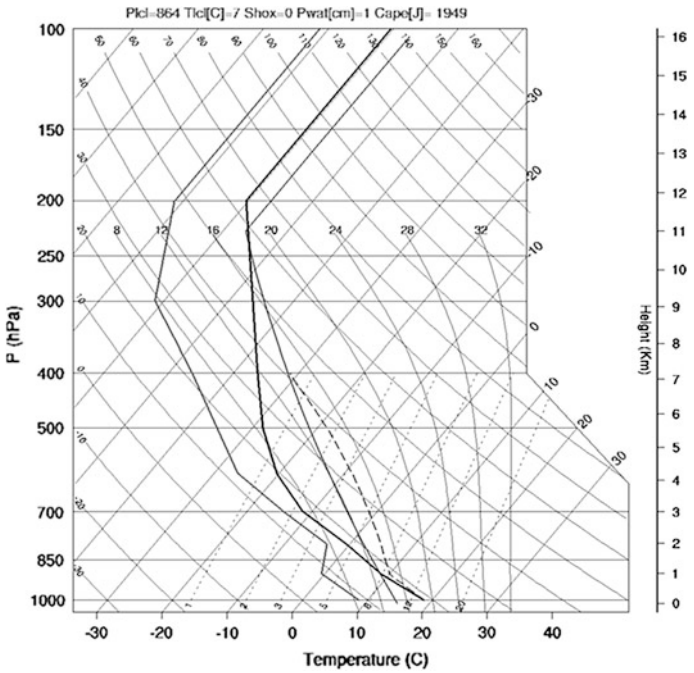

Fig. 90.1 Initial atmospheric temperature and humidity profile at 12:00 UTC

Table 90.1 Conceptual scenarios under study

Pollution level	Sodium chloride dispersion on 200 m layer at 200 m height	Scenarios name
Clean	No	Control-Clean
Polluted	No	Control-Polluted
Clean	Yes	Material 200 cl
Polluted	Yes	Material 200 pol

90.3 Results

For both clean and polluted atmospheric conditions the total amount and the fraction of ice precipitation decreased as it is seen in Table 90.2. However, in the polluted atmosphere scenario the percentage reduction is smaller. This implies that there is a limit on the amount of the available CCN that can affect the resulting precipitation depending on the system potential.

In Fig. 90.2 (right) the distribution of total precipitation has two picks around 13:30 and 14:00 UTC. In material dispersion cases, there is a lag in the presence of the second maximum. The fraction of solid precipitation is only present at the

Table 90.2 6 h accumulated precipitation and ice fraction of 6 h accumulated precipitation

Scenarios	6 h accumulated precipitation (mm)	Ice fraction of 6 h accumulated precipitation (mm)
Control-Clean	102.5	2.0
Material 200 cl	56.5	0.3
Control-Polluted	77.6	1.7
Material 200 pol	55.0	0.3

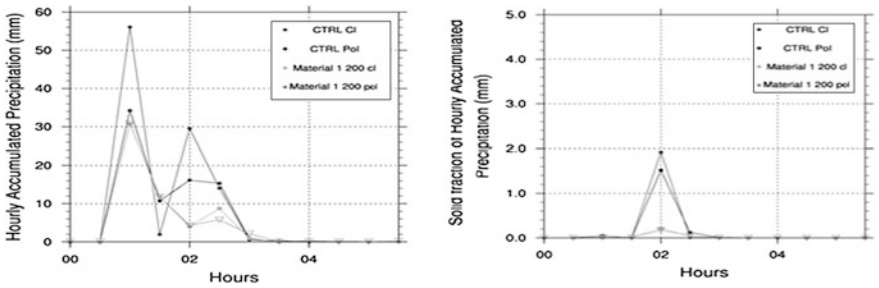

Fig. 90.2 30 min accumulated precipitation in mm (*left*), solid fraction of 30 min accumulated precipitation in mm (*right*)

second peak, implying that ice processes are slower. However, the peak value is decreasing with the CCN availability, in agreement with the precipitation.

In Fig. 90.3, the role of NaCl particles as condensation nuclei, due hygroscopicity, is successfully captured by the model. There is only a small increase in cloud droplets mixing ratio with the CCN availability. On the other hand, the number density of cloud droplets increases significantly from the beginning of the simulation. This indicates that the number and the size of cloud droplets increases as there are more available particles for CCN activation.

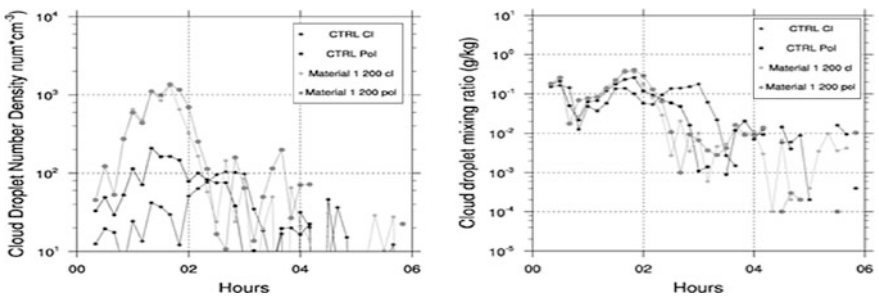

Fig. 90.3 Cloud droplet number density in number/cm^3 (*left*) and cloud droplets mixing ration in g/kg (*right*)

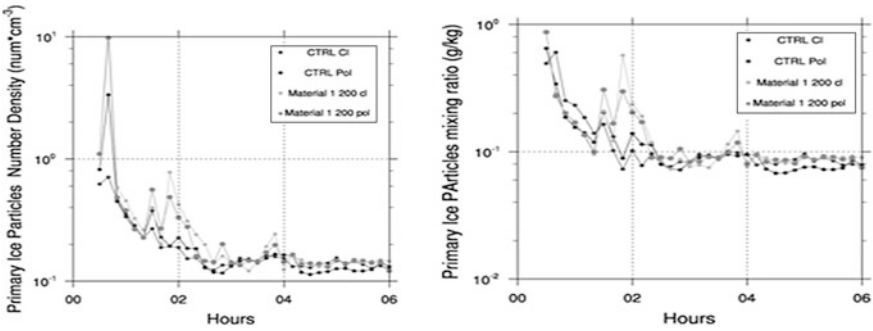

Fig. 90.4 Primary ice crystals number density in number/cm^3 (*left*) and primary ice crystals mixing ration in g/kg (*right*)

It is of high interest how cloud condensates affect the ice formation processes. For this purpose the distribution of the primary ice particles, the ones that form by vapor deposition only, is presented in Fig. 90.4. We can easily see that the impact of the material dispersion is more evident just before the peaks in precipitation are occurred as well. This fact implies that changes in ice formation have direct impact on precipitation. In cases with additional aerosol particles, more small ice crystals are formed around 12:30 UTC (before the first maximum of precipitation around 13:00 UTC). Then, around 13:30 the number of ice crystals increases, and so does their size.

Since temperatures are below 0 °C, supercooled cloud droplets and ice crystals are co-existing. (Figure 90.5). The ambient environment is subsaturated for liquid water and supersaturated for ice.

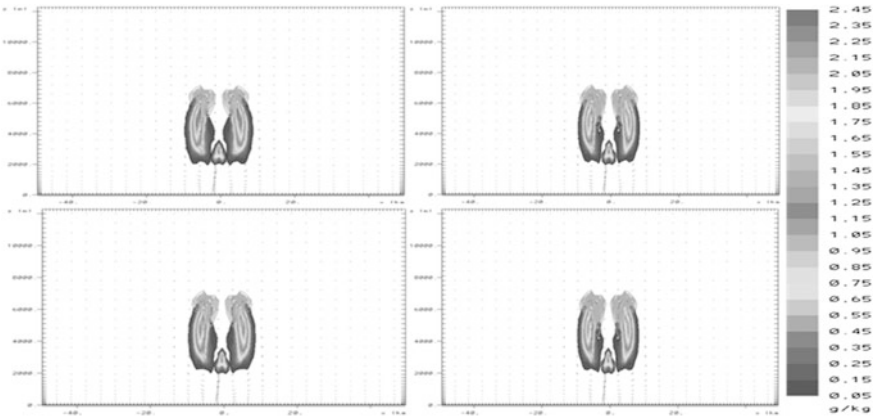

Fig. 90.5 liquid mixing ratio (*blue*) in g/kg and ice mixing ratio (*green*) for the control-clean (*left-top*) and NaCl-clean (*right-top*), control-polluted (*left-bottom*) and NaCl-polluted (*right-bottom*) scenarios respectively at 12:30 UTC

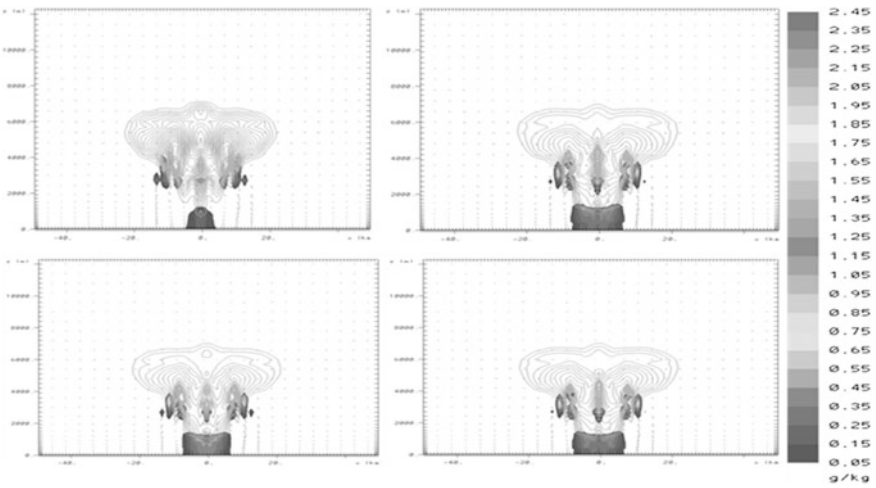

Fig. 90.6 liquid mixing ratio (*blue*) in g/kg and ice mixing ratio (*green*) for the control-clean (*left-top*) and NaCl-clean (*right-top*), control-polluted (*left-bottom*) and NaCl-polluted (*right-bottom*) scenarios respectively at 13:00 UTC

This fact, according to Wegener–Bergeron–Findeisen, leads to evaporation of supercooled cloud droplets and ice crystal growth through vapor deposition, which is depicted well at Fig. 90.6. The bigger part of the cloud, after 30 min contains mostly ice crystals, that will grow enough to sediment and be precipitated as water by melting in temperatures over 0 °C.

90.4 Conclusions

Precipitation is a physical process that shows great correlation with the different characteristics of aerosols present in the atmosphere. This correlation is particularly evident at the "mature" stage of a cloud. More specifically, the response time of the cloud system ranges from 30 to 90 min with different results depending on the case. The level of background pollution has the potential to change the spatiotemporal distribution of precipitation, as well as its onset, duration and composition. The presence of available CCN intervention on the condensation processes affects both cloud droplet and ice crystal formation. However, this is not a linear process, and there is a limit to the impact of cloud condensation nuclei, set by the dynamics of the individual cloud system.

References

Kallos G, Solomos S, Kushta J, Mitsakou C, Spyrou C, Bartsotas N, Kalogeri C (2014) Natural and anthropogenic aerosols in the Eastern Mediterranean and Middle East: possible impacts. Sci Total Environ. doi:10.1016/j.scitotenv.2014.02.035

Kushta J, Kallos G, Astitha M, Solomos S, Spyrou C, Mitsakou C, Lelieveld J (2014) Impact of natural aerosols on atmospheric radiation and consequent feedbacks with the meteorological and photochemical state of the atmosphere. JGR. doi:10.1002/2013JD020714

Levin Z, Teller A, Ganor E, Yin Y (2005) On the interactions of mineral dust, sea-salt particles and clouds: a measurement and modeling study from the Mediterranean Israeli dust experiment campaign. J Geophys Res 110:D20202. doi:10.1029/2005JD005810

Rosenfeld D, Lohmann U, Raga GB, O'Down CD, Kulmala M, Fuzzi S, Reissel A, Andreae MO (2008) Flood or drought: how do aerosols affect precipitation?

Solomos S, Kallos G, Kushta J, Astitha M, Tremback C, Nenes A, Levin Z (2011) An integrated modeling study on the effects of mineral dust and sea salt particles on clouds and precipitation. Atmos Chem Phys 11:873–892. doi:10.5194/acp11-873-2011

Chapter 91
Modelling Multiphase Aerosol-Cloud Processing with the 3-D CTM COSMO-MUSCAT: Application for Cloud Events During HCCT-2010

Roland Schrödner, Ralf Wolke, Andreas Tilgner, Dominik van Pinxteren and Hartmut Herrmann

Abstract The online-coupled 3-D chemistry transport model COSMO-MUSCAT was enhanced by a detailed description of aqueous phase chemical processes. The aqueous phase chemistry is represented by the detailed chemical mechanism CAPRAM 3.0i reduced (C3.0RED). In addition, the deposition schemes were improved in order to account for the deposition of matter incorporated in cloud droplets of ground layer clouds and fogs. The extended model system was applied for real 3-D case studies connected to the field experiment HCCT-2010 (Hill Cap Cloud Thuringia, 2010). Process and sensitivity studies were conducted and the results were compared to the available measurements during HCCT-2010. The studies indicate the requirement to consider chemical cloud effects in regional CTMs because of their key impacts on e.g., oxidation capacity in the gas and aqueous phase, formation of organic and inorganic particulate matter, and droplet acidity.

R. Schrödner (✉) · R. Wolke · A. Tilgner · D. van Pinxteren · H. Herrmann
Leibniz Institute for Tropospheric Research (TROPOS), Permoserstrasse 15,
04303 Leipzig, Germany
e-mail: roland.schrodner@cec.lu.se

R. Wolke
e-mail: wolke@tropos.de

R. Schrödner
Centre for Environmental and Climate Research, Lund University,
Sölvegatan 37, 223 62 Lund, Sweden

C. Mensink and G. Kallos (eds.), *Air Pollution Modeling and its Application XXV*,
Springer Proceedings in Complexity, DOI 10.1007/978-3-319-57645-9_91

91.1 Introduction and Motivation

Clouds play a major role in the atmosphere due to their influence on the Earth's radiative budget, on the hydrologic cycle and on the chemical composition of the gas phase and particles in the troposphere (e.g. Ramanathan et al. 2001). Due to the presence of the gaseous, liquid and solid phase, clouds favor the development of "multiphase chemistry". The multiphase cloud processing (i.e., multiphase chemical processes within clouds) of the tropospheric aerosol affects the physico-chemical properties of the gas and the particle phase on a wide range of time and spatial scales. Furthermore, the radiative and microphysical properties as well as the lifetime of clouds are driven by the dynamics of the atmosphere and by microphysical processes, which are influenced by the physico-chemical properties of the particles and cloud droplets.

The interaction of clouds with gases and aerosol particles is one major source of uncertainty of air quality models (Gong et al. 2011). Hence, an adequate description and understanding of interactions between gaseous, liquid and solid components of the atmosphere as well as their connection to atmospheric dynamics is crucial for further improvement of the performance of atmospheric models.

The field experiment HCCT-2010 (Hill Cap Cloud Thuringia, 2010, van Pinxteren et al. 2012) took place in autumn 2010 at Mt. Schmücke, Germany. The main goal of HCCT-2010 was to investigate the physico-chemical aerosol-cloud processing. Therefore, the chemical composition and physical properties of the air, of the particles, and of the cloud droplets have been measured upwind, within, and downwind of the passage of an air parcel through an orographic cloud. For the prevailing south-westerly wind directions the airflow roughly passes the measurement sites one after the other. Measurements of the aerosol-cloud processing have only been performed under suitable conditions, i.e., amongst others, a cloud with LWC > 0.1 gm^{-3} is present at the summit, no fog at the valley measurement sites, no precipitation at any site, south-westerly wind direction at the summit (200–250°), and wind speed at the summit between 2 and 12 ms^{-1} (Tilgner et al. 2014). Such episodes are so-called full-cloud events (FCEs).

91.2 The Model System COSMO-MUSCAT

The multiscale model system COSMO-MUSCAT (Wolke et al. 2012) consists of two online-coupled model codes: the CTM MUSCAT, which calculates the dispersion and chemical processing for several gas phase and particulate species based on meteorological fields provided every time step by the forecast model of the German Weather Service (DWD) COSMO (Schättler et al. 2014).

The model has been extended to consider explicit cloud-chemical processes (chemical aqueous phase reactions and phase transfer) on the regional scale. This included the adaptation of the numerical schemes in order to ensure a robust

integration for the use in real atmospheric 3-D scenarios with dynamic, prognostic meteorology. In addition, the deposition schemes were extended in order to account for the deposition of cloud droplets of ground layer clouds and fogs by applying the scheme for dry deposition of particles (Zhang et al. 2001) to the droplets of clouds in the lowermost model layer.

Setup. The simulations were performed using a nesting approach. The runs in the outer nests cover the full 6-week measurement period, but do not consider aqueous phase chemistry. In order to save computational resources, aqueous phase chemical processes were only switched on in the innermost domain that spans 92 × 72 grid cells with a horizontal resolution of 0.7 km and a vertical depth of the lowest model layer of ~20 m. Furthermore, runs in the innermost domain were only carried out for short periods (up to 48 h) around chosen FCEs. These are FCE1.1 (14 Sep 2010, 09:00–23:50 UTC) and FCE11.2 + 11.3 (1 Oct 2010 18:50–2 Oct 2010 22:30 UTC).

For the gas phase chemistry, the state-of-the-art gas chemical mechanism RACM–MIM2ext (Stockwell et al. 1997; Tilgner 2009) was used. Aqueous phase chemical processes are described by the detailed reduced aqueous phase chemistry mechanism CAPRAM 3.0i reduced (C3.0RED) (Deguillaume et al. 2010), or the much more simplified inorganic aqueous phase mechanism INORG (Sehili et al. 2005), or they were neglected for sensitivity purposes. In addition to the simple sulfate, nitrate, and acidity production described by INORG, C3.0RED treats also a complex HO_x and transition metal ion chemistry (TMI), organics up to C4, and a more detailed sulphate and nitrate chemistry.

91.3 3-D Simulation of HCCT-2010

Previously conducted studies of an artificial 2-D scenario (Schrödner 2016) revealed that in comparison to the simple aqueous phase chemistry by INORG, the detailed aqueous phase chemistry in C3.0RED leads to decreased gas phase oxidant concentrations, increased night-time nitrate mass, decreased night-time pH, and differences in produced sulfate mass. Moreover, the treatment of detailed aqueous phase chemistry enables the investigation of the formation of aqueous secondary organic aerosol (SOA) mass.

In general, the model is able to follow the variability of the LWC (Fig. 91.2a). However, sometimes deviations of more than 0.1 gm^{-3} are observed. Furthermore, there are some periods, where the modeled cloud disappears, but still considerably high LWCs have been measured.

The results of the 2-D–studies could be confirmed by the 3-D–simulations. Figure 91.1a shows the differences between C3.0RED and INORG for day-time gas phase OH during FCE1.1 (lowest ~1000 m). The gas phase concentrations of the main oxidants OH and NO_3 are substantially decreased within and after a cloud. The net reduction ~20 km after the mountain top is 5–20% for OH and 60–99% for NO_3. Corresponding to the cloud extent (within the 12 layers), the modeled

decrease can cover large parts of the model domain. The reduction of gas phase OH is mainly due to the decrease of HO_2, and gas phase NO_3 is lost via phase transfer of itself and of N_2O_5 followed by formation of nitrate, which are not considered in INORG. The photolytically driven reproduction of OH after the cloud passage is considerably slowed down due to the clouds shading large parts of the domain throughout the simulation. Overall in comparison to INORG (or no aqueous phase chemistry), the lower gas phase oxidant concentrations modeled by C3.0RED lead to longer lifetimes and, therefore, higher concentrations of gas phase VOCs.

The production of sulfate and differences in produced sulfate mass in the lowest model layer during the night can be seen in Fig. 91.1b, c. The cloud processing at the mountain ridge can be clearly seen in the simulations. As INORG lacks of the acidity production by the formation of organic acids (mainly formic acid) and nitrate via N_2O_5, the modeled pH using C3.0RED is slightly lower (up to 0.2) during the day and substantially lower during the night (up to 1.2), respectively. Due to the low night-time pH in C3.0RED, the sulfate formation via O_3 becomes unimportant, which, hence, leads to ~20% lower night-time sulfate mass concentrations compared to INORG. However, during the day the additional sulfate formation via HNO_4, which is not present in INORG, results in locally up to ~10% higher sulfate mass concentrations in C3.0RED. However during FCE11.2 + 11.3, often already cloud processed air reaches the Thuringian Forest as in the model cloudy air is often present between the inflow edges (west and south) and the mountain ridge.

The measured daytime concentration of HO_2 in the gas phase tends to be overestimated by the model. However, if C3.0RED is used, this overestimation is substantially reduced and model values lie within a factor of 2 of the measured concentrations (Fig. 91.2b).

Whereas the agreement between model and measurement is mostly within a factor of ~3 for the inorganic mass (Fig. 91.2c), larger uncertainties occur for the modeled organic cloud water concentrations with a factor of 1.2–5 for formate and >10 for glycolate.

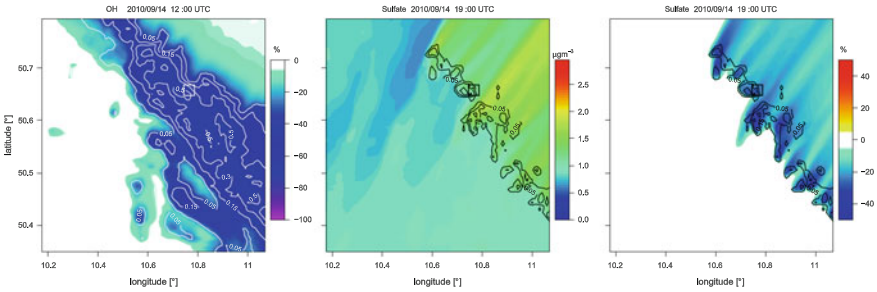

Fig. 91.1 *Left* relative difference C3.0RED-INORG of the gas phase concentrations of OH within the lowermost ~1000 m. *Middle* sulfate mass in the lowest model layer. *Right* relative difference C3.0RED-INORG of the sulfate mass

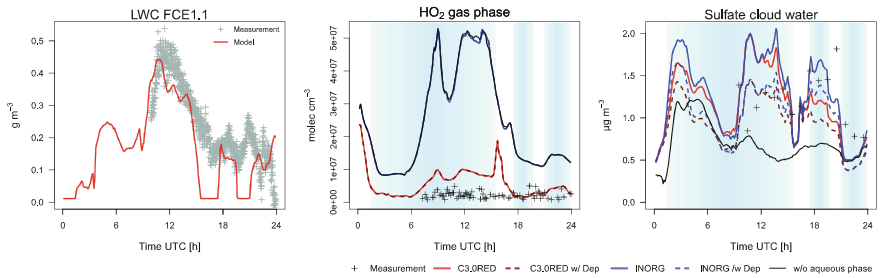

Fig. 91.2 Timeseries of liquid water content (LWC), gas phase concentration of HO_2, and sulfate mass in cloud water at the summit station of Mt. Schmücke

The treatment of cloud droplet deposition does not imply any changes to the modeled gas phase concentrations, but with up to 30% a substantial fraction of the particulate mass is lost (e.g. sulfate, Fig. 91.2c). This leads to a better agreement between and model and measurement during FCE1.1.

91.4 Summary and Conclusions

The CTM COSMO-MUSCAT was enhanced by a detailed description of aqueous phase chemical processes. It was applied for 3-D–simulations connected to the field experiment HCCT-2010. For this purpose, the complex aqueous phase chemical mechanism C3.0RED was used. Overall, the conducted studies showed the 3-D applicability of C3.0RED and the spatial effects of clouds have been demonstrated and investigated. The simulation results were compared to selected measurements conducted at the Mt. Schmücke measurement site (in-cloud). For the two considered periods, the model showed both agreements and disagreements. The discrepancies for the inorganic mass are at least partly due to uncertainties of the modeled concentrations of the sulfate precursor SO_2, and the ammonium precursor NH_3 influencing the pH of the cloud droplets. The treatment of cloud droplet deposition of the ground layer clouds at the coniferous forest canopy increased the agreement between model and measurements.

Acknowledgements This work was gratefully funded by the scholarship program of the German Federal Environmental Foundation (DBU). This work is part of RS's PhD Thesis (Schrödner 2016). Furthermore, the NIC Jülich and ZIH Dresden supported this work. We gratefully acknowledge the DWD Offenbach for good cooperation.

References

Deguillaume L et al (2010) J Atmos Chem 64(1):1–35

Gong W et al (2011) Atmosphere 2(4):567–616
Ramanathan V et al (2001) Science 294:2119–2124
Schättler U et al (2014) Deutscher Wetterdienst, Offenbach, 2013. http://www.cosmo-model.org
Schrödner R (2016) Modeling the tropospheric multiphase aerosol-cloud processing using the 3-D chemistry transport model COSMO-MUSCAT, Doctoral thesis, 172 pp. University of Leipzig, Leipzig, Germany
Sehili AM et al (2005) Atmos Environ 39(23–24):4403–4417
Stockwell WR et al (1997) J Geophys Res-Atmos 102(D22):25847–25879
Tilgner A (2009) Modelling of the physico-chemical multiphase processing of tropospheric aerosols, Doctoral thesis, 215 pp. University of Leipzig, Leipzig, Germany
Tilgner A et al (2014) Atmos Chem Phys 14(17):9105–9128
van Pinxteren D et al (2012) Biennial report 2010/2011, 30–39, Leibniz Institute for Tropospheric Research, Leipzig
Wolke R et al (2012) Atmos Environ 53:110–130
Zhang LM et al (2001) Atmos Environ 35(3):549–560

Chapter 92
Application of Trajectory Clustering for Determining the Source Regions of Secondary Inorganic Aerosols Measured at K-puszta Background Monitoring Station, Hungary

Zita Ferenczi, Kornélia Imre and László Bozó

Abstract Understanding the formation process of atmospheric particles is vital because of the significant impact of particulate matter on human health and climate change. Atmospheric particles can be formed by nucleation process via a number of different mechanisms, such as binary nucleation (involving H_2SO_4 and water vapour), ternary nucleation (involving NH_3, H_2SO_4 and water vapour) and ion-induced nucleation for charged particles, depending on the environmental conditions. Particle formation increases the total number concentration of ambient submicron particles and contributes thereby to climate forcing. The transformation processes of new particle formation (NPF) and secondary organic aerosol have been studied. It was found that gaseous sulphuric acid, ammonia, and organic compounds are important precursors to NPF events and H_2SO_4-NH_3-H_2O ternary nucleation is one of the important mechanisms. Using cluster analysis on the backward trajectories makes it possible to identify the most relevant types of air mass transport routes, and the directions from where precursor gases are transported. The influence of synoptic-scale atmospheric transport patterns on observed levels of sulphate, nitrate and ammonium has been examined.

92.1 Introduction

Atmospheric particulate matter (PM) can have both a natural and an anthropogenic origin that influences its composition and size. The effect of local meteorological conditions and in addition, long-range transport can have a significant influence on

Z. Ferenczi (✉) · L. Bozó
Hungarian Meteorological Service, P.O. Box 39, Budapest 1675, Hungary
e-mail: ferenczi.z@met.hu

K. Imre
MTA-PE Air Chemistry Research Group, Egyetem ut 10, Veszprém 8200, Hungary

C. Mensink and G. Kallos (eds.), *Air Pollution Modeling and its Application XXV*,
Springer Proceedings in Complexity, DOI 10.1007/978-3-319-57645-9_92

PM concentration levels recorded at a specific site (Abdalmogith and Harrison 2005), but this is not currently well documented in many European geographical areas. Secondary inorganic aerosols (SIA)—SO_4^{2-}, NO_3^-, NH_4^+—constitute a dominant part of particulate matter in Europe. They are called secondary because they are not emitted directly into the atmosphere but produced as a result of chemical reactions concerning sulphur dioxides, nitrogen oxides and ammonia. These gases are emitted by transport, industry and agriculture. During the last decades their emissions decreased considerably in Europe and this resulted in lower ambient concentrations for SIA.

New particle formation and subsequent growth of atmospheric particles have been observed in different environments: from sub-arctic Lapland and remote boreal forest to urban and suburban environments. Results showed that H_2SO_4 is the key compound affecting the NPF. However, before NPF, sulphuric acid clusters have to be stabilized by other compounds. The most proper candidates could be amines, ammonia and extremely low volatile organics (Tao et al. 2016).

Combining advanced particle formation theories with cluster and backward trajectory analyses contributes to better understanding of the relevant atmospheric processes, and provides a useful tool for preparing effective air quality management strategies.

92.2 Methods

K-puszta is a background monitoring station, located in a clearing in a mixed forest on the Hungarian Great Plain in the middle of the Carpathian Basin. The nearest big city is Kecskemét located about 20 km to the southeast, opposite to the prevailing wind direction. In the direction of the prevailing wind being northwesterly the nearest anthropogenic source is Budapest the capital of Hungary located 80 km from the station, The Hungarian Meteorological Service performs the measurement of gaseous components and the analysis of precipitation, furthermore provides data for EMEP and WMO-GAW networks. The evaluated data are from K-puszta.

The commonly used Hybrid-Single Particle Lagrangian Integrated Trajectory (HYSPLIT) model (Stein et al. 2015) developed by the National Oceanic and Atmospheric Administration's Air Resources Laboratory was applied. HYSPLIT uses archived 3-dimensional meteorological fields generated from observations and short-term forecasts. Three-day, hourly back trajectories for January 2007 to December 2015, arriving at the sampling location K-puszta at 1200 UTC and 800 m above ground level were calculated.

Trajectory clustering is a time series clustering problem. Time series clustering methods can be categorized into three main categories: feature-based, model-based, and raw-data-based (Liao 2005). In the feature based methods, time series data are converted to static data and traditional clustering techniques, such as k-means, fuzzy c-means, and hierarchical clustering methods, are applied to the static data. Effectiveness of the feature-based methods highly depends on the effectiveness of

two processes: conversion of the time series to a static value and clustering the static values. In model-based methods, a probabilistic model is assumed for the time series data, and the time series data is evaluated by its fitness degree to the applied model. The nature of the trajectory clustering problem is not suitable for model-based approaches, especially when the clusters are unknown. In raw-data-based methods time series data are given to the model as they are, without reducing to several features. Each time series data from the beginning to the end are considered as a sample for the model, and clustering is performed based on the output of the model. Several different raw-data-based methods exist in the literature, such as Dynamic Time Warping (DTW), Self Organizing Map (SOM) and various similarity/dissimilarity measures (Karaca and Camci 2010). Among the mentioned methods, the traditional clustering, k-means technique has been selected in this work. Nevertheless it has to be recognized that the k-means cluster analysis is sensitive to the selection of the initial cluster centers.

92.3 Results

The influence of synoptic-scale atmospheric transport patterns on observed levels of sulphate, nitrate and ammonium has been analysed. First the cluster centers had to be determined. The trajectory with the smallest total distance from the cluster center was is assigned to the cluster. Every cluster center is the arithmetic mean of all members of a cluster. Figure 92.1 shows the finally specified cluster centers which are used for the examination of SIA origins. It can be seen that there are 8 dominant paths of air masses reaching Hungary.

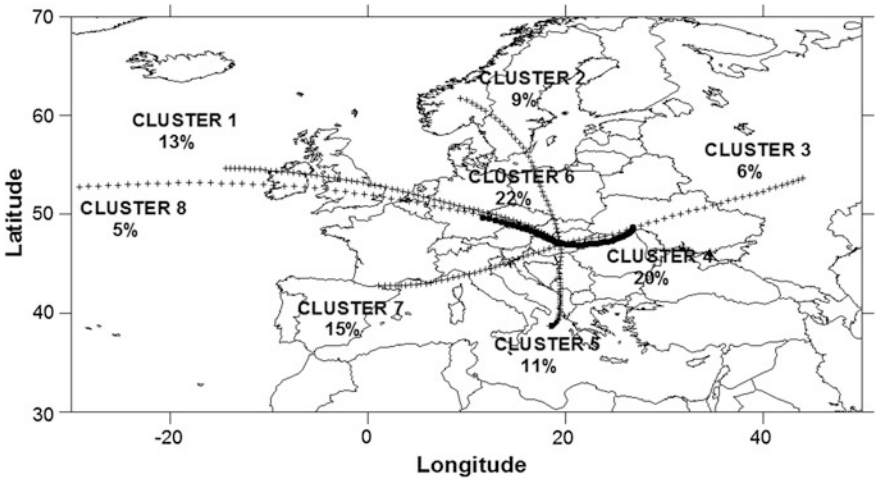

Fig. 92.1 Cluster centers for the time interval 2007–2015

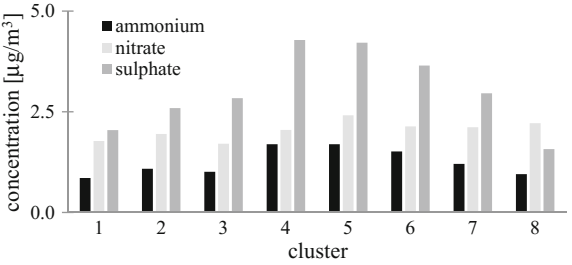

Fig. 92.2 Mean ammonium, nitrate and sulphate concentrations by trajectory clusters for 2007–2015

Annually, the most frequent patterns of the clusters coincided with cluster 6 and cluster 4, representing 22% and 20% of the days, respectively (see Fig. 92.1). These directions represent the main continental source areas of the precursor gases of SIA in east and west. According to the results, three potential source areas were identified as having important contributions to SIA in Hungary (see Fig. 92.2). Trajectory class mean NH_4^+ concentration ranged from 0.86 to 1.69 μgm^{-3}. The highest concentrations were strongly associated with air originated from eastern Europe (cluster 4) and a slow marine flow (cluster 5). The highest (2.41 μgm^{-3}) and lowest (1.7 μgm^{-3}) nitrate concentrations at K-puszta were associated with cluster 5 (southern) and cluster 3 (from Russia), respectively, whereas the highest (4.28 μgm^{-3}) and lowest (1.57 μgm^{-3}) sulphate concentrations were associated with the same clusters as the ammonium concentrations (see Fig. 92.2). Based on the sulphate and ammonium concentration ratios we can assume that sulphate mainly exist as $(NH_4)_2SO_4$ in K-puszta. Relatively high SIA concentrations were associated with eastern, southern and western pathways (cluster 4, 5 and 6). Probably these three continental paths were responsible for picking up air pollution over the continent of Europe and transporting them to the K-puszta station Malcolm et al. (2000) concluded that the concentrations are highest when air parcels pass over the European source region. These trajectories have short transport patterns, indicative of slow-motion air masses and represent the effect of continental air masses passed over countries, where industries are concentrated.

92.4 Conclusion

In this study, air mass backward trajectory cluster analysis was used to investigate the transport pathways and potential source of SIA in K-puszta monitoring station. Eight clusters were generated from backward trajectory cluster analysis for the period 2007–2015. Among them, two air mass trajectories originated from the continental region with a total occurrence frequency of 41% of the SIA concentration at K-puszta. The largest daily contribution to annual SIA concentration was observed for the continental clusters (clusters 4, 5 and 6). Based on our preliminary results we can conclude, that the main SIA sources are in the continental regions in Europe.

Acknowledgements The authors gratefully acknowledge the NOAA Air Resources Laboratory (ARL) for the provision of the HYSPLIT transport and dispersion model website (http://www.ready.noaa.gov) used in this publication.

References

Abdalmogith SS, Harrison RM (2005) The use of trajectory cluster analysis to examine the long-range transport of secondary inorganic aerosol in the UK. Atmos Environ 39:6686–6695

Karaca F, Camci F (2010) Distant source contributions to PM_{10} profile evaluated by SOM based cluster analysis of air mass trajectory sets. Atmos Environ 44(7):892–899

Liao TW (2005) Clustering of time series data—a survey. Pattern Recogn 38(11):1857–1874

Malcolm AL, Derwent RG, Maryon RH (2000) Modelling the long-range transport of secondary PM10 to the UK. Atmos Environ 34:881–894

Stein AF, Draxler RR, Rolph GD, Stunder BJB, Cohen MD, Ngan F (2015) NOAA's HYSPLIT atmospheric transport and dispersion modeling system. Bull Am Meteorol Soc 96:2059–2077. doi:10.1175/BAMS-D-14-00110

Tao Y, Ye X, Jiang S, Yang X, Chen J, Xie Y, Wang R (2016) Effects of amines on particle growth observed in new particle formation events. J Geophys Res Atmos 121. doi:10.1002/2015JD024245

Chapter 93
Impact of Aerosol Microphysical Properties on Mass Scattering Cross Sections

V. Obiso, M. Pandolfi, M. Ealo and O. Jorba

Abstract We assessed the sensitivity of simulated mass scattering cross sections (α_{λ}^{sca} [m^2/g]) of three aerosol species to different particle microphysical properties and derived constraints on these microphysical properties for the north-western Mediterranean basin, by means of a comparison between code calculations and observations. In particular, we calculated α_{λ}^{sca} of mineral dust, organic carbon and sulfate at three wavelengths in the visible range with a T-matrix optical code, considering ±20% perturbations on size distribution, refractive index and mass density, and oblate/prolate spheroids with two different axial ratios as shape perturbations. Then, we compared the simulation results with a set of observed α_{λ}^{sca} of mineral dust, aged organics and ammonium sulfate sources provided by the IDAEA-CSIC of Barcelona (Spain) and representative of the north-western Mediterranean basin.

93.1 Introduction

Atmospheric aerosols can scatter and absorb electromagnetic radiation, causing a redistribution of the radiative energy in the atmosphere (Boucher et al. 2013). The Aerosol-Radiation Interaction (ARI) radiative forcing still contributes to dominate the uncertainty associated with the anthropogenic contribution to the climate change (Myhre et al. 2013). Also the role of the natural aerosols in affecting the Earth's radiative balance is poorly constrained (Rap et al. 2013). The ARI parameterization mainly consists in the characterization of the aerosol optical properties. Errors in

V. Obiso (✉) · O. Jorba
Earth Sciences Department of Barcelona Supercomputing Center (BSC-ES),
Nexus II Building, c/ Jordi Girona 29, 08034 Barcelona, Spain
e-mail: vincenzo.obiso@bsc.es

M. Pandolfi · M. Ealo
Institute of Environmental Assessment and Water Research (IDAEA-CSIC),
c/ Jordi Girona 18-26, 08034 Barcelona, Spain

M. Ealo
Department of Astronomy and Meteorology, Faculty of Physics,
University of Barcelona, c/ Martí i Franquès 1, 08028 Barcelona, Spain

C. Mensink and G. Kallos (eds.), *Air Pollution Modeling and its Application XXV*,
Springer Proceedings in Complexity, DOI 10.1007/978-3-319-57645-9_93

their estimation, indeed, can have an important impact on the estimates of the ARI radiative effects (Yu et al. 2006; Zhang et al. 2016). The optical properties in turn depend on the microphysical properties of the particles (Boucher et al. 2013; Hand and Malm 2007). The uncertainty affecting the optical properties, indeed, is caused above all by an incomplete knowledge concerning the microphysical properties of the particles (Yu et al. 2006). Hence, different assumptions on the microphysical properties can affect the calculation of the optical properties and so the assessments of the ARI radiative effects. In order to better understand the relationship between aerosol microphysical and optical properties, we carried out the experiment which we present in this paper.

93.2 T-Matrix Code

The T-matrix method is a powerful exact technique to compute electromagnetic scattering by homogeneous non-spherical particles (Mishchenko and Travis 1998). For this work, the T-matrix code by Mishchenko and Travis (1998) has been used. It allows calculating integrated optical properties of poly-disperse, non-spherical (rotationally symmetric), homogeneous particles.

93.3 Observations

We used a set of observed aerosol α_{λ}^{sca} provided by the Institute of Environmental Assessment and Water Research of Barcelona (IDAEA-CSIC: http://www.idaea.csic.es). Pandolfi et al. (2011) collected measurements of aerosol mass concentrations and optical properties, in the period 2010–2014, at the Montseny regional background station (middle altitude emplacement located within the Montseny Natural Park, Spain: 41°46′45, 63″N–02°21′28, 92″E; 720 m a.s.l.; ACTRIS/GAW). From these data, Ealo et al. (2017) derived α_{λ}^{sca} at 3 wavelengths in the visible range ($\lambda_1 = 0.450\,\mu m$; $\lambda_2 = 0.525\,\mu m$; $\lambda_3 = 0.635\,\mu m$) through Multilinear Regression (MLR) analysis, using scattering measurements of dry ($RH < 40\%$) particles and PM_{10} mass concentrations. The MLR has been performed considering the possible sources of the particles, detected in the PM mass 24 h filter chemical speciated data (Querol et al. 2009) through the application of the Positive Matrix Factorization (PMF) model (Paatero 1997) For our work we used three sources detected using the PMF model at the Montseny station: mineral dust (traced by typical crustal elements), aged organics (traced mainly by organic carbon) and ammonium sulfate (traced mainly by SO_4^{2-} and NH_4^{+}) (Pandolfi et al. 2016). These data can be considered representative of the regional background of the north-western Mediterranean basin but they fall within the quite extended range of experimental estimates available in literature (Hand and Malm 2007).

93.4 Experiment Setup

We defined the reference aerosol microphysical properties following the aerosol parameterization of the GOCART model (Chin et al. 2002), for organic carbon and sulfate, and the NMMB-MONARCH model (formerly known as NMMB/BSC-CTM) (Pérez et al. 2011), for mineral dust. Both these parameterizations have been mainly derived from the OPAC database (Hess et al. 1998). We performed bulk (PM_{10}) calculations of α_{λ}^{sca} of mineral dust, organic carbon and sulfate, using the following formula (Tegen and Lacis 1996):

$$\alpha_{\lambda}^{sca} = \frac{\beta_{\lambda}^{sca}}{M} = \frac{3 < Q_{\lambda}^{sca} >_s}{4 \rho r_{eff}}$$

being β_{λ}^{sca} the scattering coefficient, M the mass concentration, $< Q_{\lambda}^{sca} >_s$ the mean scattering efficiency, ρ the mass density and r_{eff} the effective radius. The calculations have been performed at three wavelengths in the visible range ($\lambda_1 = 0.450\,\mu m$; $\lambda_2 = 0.525\,\mu m$; $\lambda_3 = 0.635\,\mu m$): the wavelengths at which the observations were available. In order to generate variability in the microphysical assumptions for the particles, we gave as inputs to the T-Matrix code the reference microphysical properties independently perturbed: this means that when a property was perturbed the other ones were not. In particular, for each aerosol species, we considered perturbations of $\pm 20\%$ on the size distribution (separately for the geometric radius r_g and the geometric standard deviation σ_g), on the refractive index (separately for the real n_R and the imaginary n_I parts) and on the mass density ρ; as shape perturbations we considered two types of spheroid: moderate and extreme, averaging for each axial ratio χ the oblate and the prolate options.

93.5 Data Analysis

We compared the simulated α_{λ}^{sca} with the observation data, associating mineral dust with the mineral dust source, organic carbon with the aged organics source and sulfate with the ammonium sulfate source. At first, we analyzed the sensitivity of the α_{λ}^{sca} values and spectral dependence to the different perturbed microphysical properties. Regarding the α_{λ}^{sca} values, for each species and microphysical property we evaluated the importance of the variability range of the simulated value at $\lambda_2 = 0.525\,\mu m$ against the uncertainty affecting the observed value at the same wavelength. Regarding the α_{λ}^{sca} spectral dependence, instead, we estimated the importance of the variability range of the logarithmic spectral dependence linear slope of the simulated values with respect to the uncertainty affecting the slope of the observed values. Hence, in order to integrate and complete the comparison analysis, we performed also linear fits of the logarithmic spectral dependence of both the simulated and the

observed α_{λ}^{sca} and then, in order to constrain the perturbed microphysical properties, we performed a compatibility test on the best fit parameters. The test has been performed on the best fit parameters of all the code calculations with respect to those of the observation data.

93.6 Results

We found that the mineral dust α_{λ}^{sca} values are affected mainly by the size distribution and also, but with a lower impact, by the mass density perturbations. On the other hand, no microphysical properties seem to have any impact on the α_{λ}^{sca} spectral dependence. So, it seems that, due mainly to the size of the particles larger than the visible wavelengths, the dust α_{λ}^{sca} are quite stable with respect to the microphysical perturbations (in the spectral range of the experiment). For mineral dust, in the north-western Mediterranean basin, the prescriptions derived from our analysis are:

Size distribution	Refractive index	Mass density	Shape
$r_g = 3.583 \times 10^{-1}$ μm	$n_R = (1.530; 1.530; 1.530)$	$\rho = 2.506 \times 10^3$ kg/m^3	*Sphere*
$\sigma_g = 1.600$	$n_I = (8.500; 6.650; 4.500) \times 10^{-3}$		
$r_{eff} = 6.221 \times 10^{-1} \mu m$			

The organic carbon α_{λ}^{sca} values are affected mainly by refractive index (real part), size distribution and also, but with a lower impact, by mass density and shape perturbations. The α_{λ}^{sca} spectral dependence, instead, is significantly affected only by the size distribution perturbations. So, the organic carbon α_{λ}^{sca} seem to be more sensitive than the mineral dust α_{λ}^{sca} to the microphysical perturbations, due mainly to the size of the particles smaller than the visible wavelengths. For organic carbon, in the north-western Mediterranean basin, the prescriptions derived from our analysis are (being the refractive index values relative to λ_1, λ_2 *and* λ_3, respectively):

Size distribution	Refractive index	Mass density	Shape
$r_g = 1.696 \times 10^{-2}$ μm	$n_R = (1.377; 1.377; 1.377)$	$\rho = 1.800 \times 10^3$ kg/m^3	*Sphere*
$\sigma_g = 2.200$	$n_I = (5.000; 5.500; 6.700) \times 10^{-3}$		
$r_{eff} = 8.024 \times 10^{-2}$ μm			

The sulfate α_{λ}^{sca} values are mainly affected by the refractive index (real part) and also, but with a lower impact, by size distribution, mass density and shape perturbations. On the other hand, the α_{λ}^{sca} spectral dependence is mainly affected by the size distribution and also by the refractive index perturbations. So, it seems that the sulfate α_{λ}^{sca} are the most unstable with respect to the microphysical perturbations, due to the particle size close to the visible wavelengths. For sulfate, in the

north-western Mediterranean basin, the prescriptions which we provide from this analysis are (being the refractive index values relative to λ_1, λ_2 *and* λ_3, respectively):

Size distribution	Refractive index	Mass density	Shape
$r_g = 8.340 \times 10^{-2}$ μm $\sigma_g = 1.624$ $r_{eff} = 1.501 \times 10^{-1}$ μm	$n_R = (1.547; 1.545; 1.543)$ $n_I = (1.000; 1.000; 1.610) \times 10^{-8}$	$\rho = 1.700 \times 10^3$ kg/m^3	*Sphere*

93.7 Future Work

In the future, we will carry out other radiative and atmospheric simulations in order to study the impact of the particle microphysical perturbations on the ARI radiative effects and on meteorological variables.

Funding Sources & Acknowledgements This work is funded by the Spanish Ministry of Economy and Competitiveness [grant: CGL2013-46736-R]. Further support has been provided by the Severo Ochoa Program, awarded by the Spanish Government [grant: SEV-2011-00067]. Vincenzo Obiso is funded by the Spanish Ministry of Economy and Competitiveness ['FPI-SO' grant: SVP-2013-067953]. Marco Pandolfi is funded by the Spanish Ministry of Economy and Competitiveness ['Ramón y Cajal' grant: RYC-2013-14036]. We thank Noemi Pérez for providing the PM chemical speciated data for the Montseny station.

References

Boucher O, Randall D, Artaxo P, Bretherton C, Feingold G, Forster P, Kerminen V-M, Kondo Y, Liao H, Lohmann U, Rasch P, Satheesh SK, Sherwood SBS, Zhang, XY (2013) Clouds and aerosols. In: Stocker TF, Qin D, Plattner G-K, Tignor M, Allen SK, Boschung J, Nauels A, Xia Y, Bex V, Midgley PM (eds) Climate change 2013: the physical science basis. Contribution of working group I to the fifth assessment report of the intergovernmental panel on climate change. Cambridge University Press, Cambridge, United Kingdom and New York, NY, USA

Chin M, Ginoux P, Kinne S, Torres O, Holben BN, Duncan BN, Martin RV, Logan JA, Higurashi A, Nakajima T (2002) Tropospheric aerosol optical thickness from the GOCART model and comparisons with satellite and sun photometer measurements. J Atmos Sci 59:461–483

Ealo M, Alastuey A, Pérez N, Reche C, Ripoll A, Querol X, Pandolfi M (2017) From air quality to climate: impact of aerosol sources on optical properties at urban, regional and continental levels in the north-western Mediterranean. Atmos Chem Phys Discuss (in review)

Hand JL, Malm WC (2007) Review of aerosol mass scattering efficiencies from groud-based measurements since 1990. J Geophys Res 112:D16203

Hess M, Köpke P, Schult I (1998) Optical properties of aerosols and clouds: the software package OPAC. Bull Am Met Soc 79:831–844

Mishchenko MI, Travis LD (1998) Capabilities and limitations of a current FORTRAN implementation of the T-matrix method for randomly oriented, rotationally symmetric scatterers. J Quant Spectro Radiat Transf 60:309–324

Myhre G, Shindell D, Bréon F-M, Collins W, Fuglestvedt J, Huang J, Koch D, Lamarque J-F, Lee D, Mendoza B, Nakajima T, Robock A, Stephens G, Takemura T, Zhang H (2013) Anthropogenic and Natural Radiative Forcing. In: Stocker TF, Qin D, Plattner G-K, Tignor M, Allen SK, Boschung J, Nauels A, Xia Y, Bex V, Midgley PM (eds) Climate change 2013: the physical science basis. Contribution of Working Group I to the fifth assessment report of the intergovernmental panel on climate change. Cambridge University Press, Cambridge, United Kingdom and New York, NY, USA

Paatero P (1997) Least squares formulation of robust non-negative factor analysis. Chemometr Intell Lab Syst 37:23–35

Pandolfi M, Alastuey A, Pérez N, Reche C, Castro I, Shatalov V, Querol X (2016) Trends analysis of PM source contributions and chemical tracers in NE Spain during 2004–2014: A multiexponential approach. Atmos Chem Phys 16:11787–11805

Pandolfi M, Cusack M, Alastuey A, Querol X (2011) Variability of aerosol optical properties in the Western Mediterranean Basin. Atmos Chem Phys 11:8189–8203

Pérez C, Haustein K, Janjic Z, Jorba O, Huneeus N, Baldasano JM, Black T, Basart S, Nickovic S, Miller RL, Perlwitz JP, Schulz M, Thomson M (2011) Atmospheric dust modeling from meso to global scales with the online NMMB/BSC-Dust model—Part 1: model description, annual simulations and evaluation. Atmos Chem Phys 11:13001–13027

Querol X, Alastuey A, Pey J, Cusack M, Pérez N, Mihalopoulos N, Theodosi C, Gerasopoulos E, Kubilay N, Koçak M (2009) Variability in regional background aerosols within the Mediterranean. Atmos Chem Phys 9:4575–4591

Rap A, Scott CE, Spracklen DV, Bellouin N, Forster PM, Carslaw KS, Schmidt A, Mann G (2013) Natural aerosol direct and indirect radiative effects. Geophys Res Lett 40:3297–3301

Tegen I, Lacis AA (1996) Modeling of particle size distribution and its influence on the radiative properties of mineral dust aerosol. J Geophys Res 101(D14):19237–19244

Yu H, Kaufman YJ, Chin M, Feingold G, Remer LA, Anderson TL, Balkanski Y, Bellouin N, Boucher O, Christopher S, DeCola P, Kahn R, Koch D, Loeb N, Reddy MS, Schulz M, Takemura T, Zhou M (2006) A review of measurement-based assessments of the aerosol direct radiative effect and forcing. Atmos Chem Phys 6:613–666

Zhang Z, Meyer K, Yu H, Platnich S, Colarco P, Liu Z, Oreopoulos L (2016) Shortwave direct radiative effects of above-cloud aerosols over global oceans derived from 8 years of CALIOP and MODIS observations. Atmos Chem Phys 16:2877–2900

Author Index

C. Mensink and G. Kallos (eds.), *Air Pollution Modeling and Its Application XXV*,
Springer Proceedings in Complexity, DOI 10.1007/978-3-319-57645-9